Thèse de doctorat

Presentée à l'Université Paris Diderot (UPD)

Spcialité: Physico-chimie de l'environnement

Evolution de la composition chimique de l'atmosphère au-dessus du bassin Méditerranéen: Forçages, mécanismes et scénarios

soutenue le 17 décembre 2018 par:
Arineh Cholakian

Jury

Karine Sartelet (CEREA) :	Rapporteure
Michael Gauss (MET):	Rapporteur
Eric Villenave (EPOC) :	Examinateur
Fabien Solmon (LA) :	Examinateur
Nathalie Poisson (ADEME) :	Invitée
Matthias Beekmann (LISA) :	Directeur de thèse
Isabelle Coll (LISA) :	Co-directrice de thèse
Augustin Colette (INERIS) :	Co-directeur de thèse

Ecole Doctorale des Sciences de l'Environnement d'Ile de France (ED129)

Acknowledgements

Before starting the serious business of atmospheric chemistry and physics, I would like to take a moment and thank the many (many) people who have helped me during the four previous years. Of course, having the memory of a goldfish, chances are I am going to forget many people, to whom I offer my sincere apologies.

First of all, I would like to thank the reporters for this thesis, Karine Sartelet and Michael Gauss for accepting to be in the jury, I would also like extend my sincere gratitude to Eric Villenave, Nathalie Poisson and Fabien Solmon for accepting to be a part of the jury as well. I would like to thank ADEME, INERIS and the ChArMEx project, for funding my thesis and to LISA for having me for the duration of my thesis. I would like to thank the administrative part of LISA and Genèvieve specifically for drafting many contracts for me.

I would be remiss if I don't start by thanking Matthias from the bottom of my heart, my PhD director who was there for me the whole four years (despite being very busy himself) and even before for my masters, giving excellent suggestions, taking the time to have many lively debates with me and offering advice whenever he could. I would like to thank Isabelle and Augustin as well, my co-directors, who also had many helpful ideas and were extremely helpful whenever I approached them.

I passed the past four years in the modelisation department of LISA with the most wonderful people: Mathieu (the best office-mate i could've asked for), Arthur (who kills more plants than he would like to admit), Ines (who finally signed her contract, yay!), Richard (who should've become a professional motivational speaker), Giancarlo (who likes to put sound on atmospheric simulations), Victor (my INERIS neighbor whom I never met at INERIS), Marie (the now "ex" coffee dealer for the group), Guillaume (problem solver extraordinaire), Adriana, Christel and Beatrice (my morning coffee partners), Gil and Gilles, Benoit (the only person that calls us on the office number), Bernard (who people say has a cupboard full of gazpacho cartons in his office),Boutheina (sorry for your bottle that i threw away), all the people who I was lucky enough to meet at LISA but left before I finished my PhD: Audrey, Vincent, Julie, Stéphanie, Hervé, Alice, Charlotte, Lorenzo and all the other people who helped in many ways.

Before finishing, I would like to thank my parents, who have always been there for me and have helped me throughout my life whenever they could. I would also like to thank my friends who have suffered through many lectures on how biogenic organic aerosols can be considered air pollutants (and what biogenic organic aerosols actually are). I would also pause here to give an honorable mention to my ps4, just because it has entertained me whenever I needed it for the past four years. After that last sentence I would like to deny being a geek.

Thank you everyone.

Contents

Contents iii

List of Figures viii

List of Tables xii

List of equations and reactions xiii

Abstract 1

Résumé 3

Introduction 5

I Scientific context 11
1 Earth's atmosphere . . . 14
2 Atmospheric gas-phase chemistry . . . 19
2.1 Formation of radicals in the atmosphere . . . 19
2.2 Nitrogen oxides . . . 20
2.3 Volatile organic compounds . . . 21
2.4 Ozone cycle . . . 21
3 Atmospheric aerosol sources and chemical composition . . . 22
3.1 Formation of inorganic aerosols . . . 23
3.2 Formation of organic aerosols . . . 26
3.3 Health effects of atmospheric aerosols . . . 28
3.4 Effects of aerosols on climate . . . 29
4 Fine aerosol atmospheric observations . . . 31

4.1 Measurements related to fine aerosols . . . 31
4.2 Spatial variability of fine aerosols . . . 32
5 The Mediterranean region . . . 33
5.1 Atmospheric characteristics . . . 34
5.2 The ChArMEx campaign . . . 37
6 Thesis goals . . . 39
6.1 Model evaluation and amelioration for the western Mediterranean basin . . . 40
6.2 Future conditions of the Mediterranean basin in different scales . . . 40

II Atmospheric modeling **43**
1 Fundamental basis of chemistry transport models . . . 45
2 The CHIMERE chemistry transport model . . . 48
2.1 Inputs and outputs . . . 48
2.2 Physical processes and chemical mechanisms in CHIMERE . . . 51
2.2.1 Horizontal and vertical transport and turbulent mixing . . . 51
2.2.2 Deposition . . . 52
2.2.3 Gaseous chemistry . . . 55
2.2.4 Aerosol module . . . 55
3 Simulation of organic aerosols in atmospheric models . . . 58
3.1 Two-product schemes . . . 59
3.2 Volatility basis set . . . 61
3.3 Carbon number - polarity grid (np+mP scheme) . . . 66
3.4 Statistical oxidation model . . . 66
3.5 Molecular schemes . . . 68
4 Simulation of organic aerosols in CHIMERE . . . 69

III Evaluation of simulations for the Mediterranean basin **71**
1 Specific modelisation chain for the Mediterranean region . . . 73
2 Meteorological input simulations . . . 74
3 Anthropogenic emission inputs . . . 84
4 Orographic representativeness error for Cap Corse . . . 86
5 Simulation of dimethyl sulfide in CHIMERE . . . 91
5.1 Physical dependencies of dimethyl sulfide flux into the atmosphere 91
5.2 Chemical processes . . . 95
5.3 Simulated DMS fields and its oxidation products . . . 98

IV Simulation of OA in western Mediterranean **99**
1 Summary of article . . . 101
2 Simulation of organic aerosols in the western Mediterranean basin . . . 103
3 Abstract . . . 104
4 Introdution . . . 105
5 Model setup . . . 106

5.1 Organic aerosol simulation . . . 107
5.1.1 CHIMERE standard scheme . . . 107
5.1.2 Volatility basis set scheme . . . 108
5.1.3 Modified volatility basis set scheme . . . 108
6 Experimental data set . . . 109
6.1 ChArMEx measurements . . . 109
6.2 Other measurements . . . 111
7 Model validation . . . 111
7.1 Orographic representativeness error . . . 111
7.2 Meteorology evaluation . . . 113
7.3 Gaseous species . . . 113
7.4 Particulate species . . . 115
8 Organic aerosol simulation . . . 116
8.1 Comparison of PM_1 total organic aerosol concentration . . . 117
8.2 Total cabonaceous particle origins based on ^{14}C measurements . . . 117
8.3 Volatility and oxidation stat comparison with PMF results . . . 119
9 Budget of organic aerosols . . . 120
10 Conclusion and discussion . . . 121
11 References . . . 125

V Effects of future drivers on PM_{10} concentration **131**
1 Summary of article . . . 133
2 Future climatic drivers and their effect on PM_{10} components in Europe and the Mediterranean Sea . . . 135
3 Abstract . . . 136
4 Introdution . . . 137
5 Methods . . . 138
5.1 Modeling framework . . . 138
5.2 CHIMERE chemistry transport model . . . 139
5.3 Climate scenarios . . . 139
5.4 Air pollutant emissions . . . 140
6 Climate impacts . . . 140
6.1 Meteorological parameters . . . 140
6.2 PM_{10} concentrations . . . 142
6.3 Distribution of PM_{10} chemical components . . . 143
6.4 Dependence of PM_{10} components to meteorological parameters . . . 146
6.4.1 Inorganic PM components . . . 146
6.4.2 Biogenic secondary organic aerosols . . . 148
6.4.3 Dust and salt particles . . . 151
6.4.4 Total PM_{10} and $PM_{2.5}$ dependencies to meteorological components . . . 151
7 Impacts of boundary condition and anthropogenic emissions . . . 151
7.1 Boundary conditions . . . 152

7.2 Anthropogenic emissions . . . 152
7.3 Cumulative impacts . . . 154
8 Conclusion and discussion . . . 155
9 References . . . 157

VI OA simulation scheme effects on future scenarios 163
1 Summary of article . . . 164
2 Importance of organic aerosol simulation scheme for particulate matter concentrations in climate projections . . . 166
3 Abstract . . . 167
4 Introdution . . . 167
5 Simulations . . . 169
5.1 CHIMERE chemistry transport model . . . 169
5.2 OA schemes used for the simulations . . . 169
5.3 Choice of years . . . 170
6 Scheme validation . . . 170
7 Analysis of the simulations . . . 172
7.1 Changes in biogenic emissions . . . 172
7.2 European region . . . 173
7.2.1 Changes in BSOA concentration . . . 173
7.2.2 Changes in the origins of OA . . . 174
7.3 Mediterranean region . . . 175
7.3.1 Changes in concentration . . . 176
7.3.2 Changes in the origin and volatility state of organic aerosols 176
7.3.3 Spatial distribution of future changes . . . 177
8 Sensitivity of different schemes to temperature changes . . . 177
9 Conclusions . . . 178
10 References . . . 181

VII. Population exposure in PACA region 185
1 Summary of article . . . 187
2 Population exposure in south of France to atmospheric pollutant in future scenarios . . . 189
3 Abstract . . . 190
4 Introdution . . . 191
5 Materials and methods . . . 192
5.1 CHIMERE CTM . . . 192
5.2 Simulations . . . 192
5.3 Anthropogenic emissions . . . 193
5.4 Current and future population for the PACA domain . . . 193
6 Results . . . 195
6.1 Meteorological parameters . . . 195
6.2 Changes in chemical species . . . 196

6.3 Population exposure to atmospheric components in future scenarios 198
6.4 Exposure analysis for the entire PACA region 199
6.5 Spatial analysis of the simulated exposure tendencies 200
6.6 Localization of main risks 200
6.7 County per county analysis 201
7 Summary and conclusions 204
8 References 205

VIII Conclusions and perspectives **207**
1 Model evaluation and amelioration for the western Mediterranean basin . 208
2 Future conditions of the Mediterranean basin in different scales 211
3 Perspectives 214

Bibliography **217**

A Acronyms **251**
1 Acronyms 251

B Supplementary materials for articles **255**
1 OA simulation schemes in CHIMERE article - SI 256
2 Climate scenarios and PM concentration changes in CHIMERE article - SI . 265

C MELCHIOR2 chemical scheme **277**
1 MELCHIOR2 Chemical scheme and meteorological parameters used in CHIMERE 277

List of Figures

I.1 Major components of the Solar system planets . . . 15
I.2 Life-times of different atmospheric gases and aerosols . . . 16
I.3 The temperature change projected by RCP scenarios . . . 18
I.4 The ozone cycle . . . 22
I.5 Formation processes and size modes of atmospheric aerosols . . . 23
I.6 Simplified schematic of SIA and SOA formation . . . 27
I.7 Health impacts of aerosols . . . 29
I.8 Direct, semi-direct and indirect interactions of aerosols with solar radiation . . . 30
I.9 Composition of PM_1 concentrations in Cap Corse, Mallorca and Paris . . . 32
I.10 Anthropogenic characteristics of the Mediterranean Sea . . . 33
I.11 Natural characteristics of the Mediterranean Sea . . . 34
I.12 Anthropogenic emission sources of some species around the Mediterranean Sea 35
I.13 RCCI factor for future climatic sensitivity . . . 36
I.14 *MISTRALS axes* . . . 37
I.15 *ChArMEx project work packages* . . . 38
I.16 *SAFMED SOP 1b measurements* . . . 39

II.1 Simplfied schematic of a CTM . . . 46
II.2 Inputs needed, the major processes and outputs in CHIMERE . . . 49
II.3 Example of nesting in a CTM . . . 51
II.4 Simplified schematic of a two-product scheme . . . 59
II.5 Simplified schmeatic of the volatility basis set scheme . . . 61
II.6 VBS-1D scheme including fragmentation and non-volatile SOA formation . . . 63
II.7 Schematic of VBS-2D . . . 65
II.8 Representation of a np+mP scheme . . . 66
II.9 Representation of a statistical oxidation model . . . 67

III.1 Coarse and nested domains used in this study . . . 73
III.2 Vertical levels and their distribution in the simulations . . . 75
III.3 2D maps of wind speed and direction in all tested parameterizations in the WRF model for the 19th of July . . . 77
III.4 Stations used for the evaluation of different WRF parameterizations . . . 79
III.5 An example of radio-sounding comparisons for the midnight balloon of 19th of July at Nîmes . . . 79
III.6 Comparison of the chosen parameterization to in-situ measurements . . . 80
III.7 Boxplots showing the comparison of all radiosounding launches available in the period of 10th to 30th of July . . . 83
III.8 Comparison of shipping emissions in HTAP-V2 and MACC-III for SO_2 . . . 85
III.9 3D representation of the Cap Corse as seen in the model in the DEMO1 (1km) domain . . . 86
III.10 Real orography, simulated DEMO10 orography and DEMO1 orography . . . 87
III.11 The cell containing the measurements site and its neighbouring cells . . . 88
III.12 Non-linear regressions performed using concentration of OA and altitude of sites shown in figure III.11 . . . 89
III.13 Time series of all confidence intervals for all converged equations for OA . . . 90
III.14 Sea surface concentration of DMS for the month of July . . . 94
III.15 Piston velocities calculated for a range of temperatures . . . 96
III.16 Simulated DMS concentrations in DEMO30 and DEMO10 . . . 97
III.17 Changes of some components in the four tested parameterizations for DEMO30 and DEMO10 . . . 97

IV.1 Domains used in this study . . . 107
IV.2 Schemes used in this study . . . 109
IV.3 Experimental data sites . . . 110
IV.4 Orographic representativeness error calcultations . . . 112
IV.5 Time series for simulated gaseous species compared to observations . . . 115
IV.6 Time series for simulated aerosol species compared to observations . . . 116
IV.7 Time series for simulated total organic aerosol compared to observations in different schemes . . . 117
IV.8 Simulation-observation comparisons for ^{14}C measurements in different schemes in average . . . 119
IV.9 Simulation-observation comparisons for ^{14}C measurements in different schemes for different filters . . . 119
IV.10 Simulation-observation comparisons for PMF results in different schemes for different volatility bins . . . 120
IV.11 Simulation-observation comparisons for PMF results in different schemes in average . . . 121
IV.12 2D average organic aerosol concentration maps from different sources and different altitudes in absolute values . . . 122

IV.13 2D average organic aerosol concentration maps from different sources and different altitudes in relative values . . . 123

V.1 Domains and sub-domains used in this study . . . 138
V.2 Meteorological time series for historic and future scenarios: temperature, precipitation amount and number of rainy hours . . . 141
V.3 Meteorological time series for historic and future scenarios: wind speed, wind direction and height of the boundary layer . . . 142
V.4 Time series for PM_{10} in historic and future scenarios in the EUR and MED subdomains . . . 143
V.5 2D average maps for PM_{10} in historic and future scenarios in different seasons 144
V.6 Seasonal boxplots for PM_{10} in historic and future scenarios . . . 145
V.7 Concentrations and relative changes of PM_{10} in historic and future scenarios . 146
V.8 BSOA, sulfates, nitrates and dust concentrations in historic and future scenarios in all studied subdomains . . . 147
V.9 2D average maps for BSOA, sulfates, nitrates and dust concentrations in historic and future scenarios . . . 148
V.10 Correlation coefficients between all tested meteorological parameters to BSOA, sulfates, nitrates and dust . . . 149
V.11 Correlation coefficients between all tested meteorological parameters to ammonium, salt, PM_{10} and $PM_{2.5}$ . . . 149
V.12 Relative impact of climate, boundary conditions and anthropogenic emissions on aerosol components . . . 152
V.13 Emission scenario comparisons . . . 153

VI.1 Simulation chain used in this study . . . 170
VI.2 Changes in BSOA concentration and choice of years . . . 171
VI.3 Comparison of the three tested schemes to experimental data . . . 173
VI.4 Comparison of concentration and percentage of changes of BSOA in future scenarios . . . 174
VI.5 Comparison of oxidation state and origins of OA in future scenarios in all tested schemes for European and the Mediterranean regions . . . 175
VI.6 2D maps of changes in the concentration of BSOA, terpenes, isoprene and temperature in historic simulations compared to future scenarios . . . 176
VI.7 Normalized changes of BSOA concentration to temperature in different scenarios for summer in European and the Mediterranean regions . . . 177

VII.1 Domains used in the this study . . . 193
VII.2 The procedure of preparation of anthropogenic emissions for the PACA region 194
VII.3 Population change (in %) in all SSP scenarios for France, compared to 2005 . 194
VII.4 Re-gridded population for 2005 and its changes in future SSP scenarios for 2030s and 2050s for the PACA region . . . 195

VII.5 Changes of meteorological parameters in future scenarios compared to historic simulation for 2005 196
VII.6 Seasonal concentration change seen in future scenarios for a number of components (in %) 197
VII.7 2D representations of ozone, PM_{10}, $PM_{2.5}$, dust and BSOA for the PACA region 198
VII.8 Population-weighted exposure in the reference simulation and its changes (in %) compared with the reference simulation for the SSP3 and SSP5 demographic scenarios 199
VII.9 2D representations of exposure to ozone, PM_{10}, $PM_{2.5}$, dust and BSOA for the PACA region for historic and future case studies 201
VII.10 Counties of the PACA region and associated population density 201
VII.11 Population-weighted exposure in different departments for the SSP3 scenario 202
VII.12 Population-weighted exposure in different departments for the SSP3 scenario 203

List of Tables

II.1 Anthropogenic and biogenic precursors of schemes coded in CHIMERE 69
II.2 Lumped surrogate species in SOA simulation schemes in CHIMERE 70

III.1 Simulation chain, domains and their resolution and input data for simulations used for the Mediterranean area 74
III.2 Tested parameterizations for the WRF model in order to simulate the meteorological fields 76
III.3 Statistical information for radio-sounding stations in three domains, compared to the four parameterizations 82
III.4 Comparison of DEMO30 and DEMO10 simulations with four parameterizations to E-OBS data 84
III.5 Simulated altitude of the Ersa site in Cap Corse, as seen in different domains and their difference with the real altitude 87
III.6 Orographic representativeness errors (ORE) calculated for different chemical components and meteorological parameters 91
III.7 Four parameterizations for the calculation of piston velocity, all depending on wind speed and temperature 95

IV.1 Gas and aerosol and meteorological measurements 110
IV.2 Relative orographic representativeness error values for some species 114
IV.3 Statistical information for comparisons of gaseous species 114
IV.4 Statistical information for comparisons of aerosol species 116
IV.5 Statistical information for comparisons for total organic aerosol to observations of different schemes 118

V.1 Series of historic and future scenarios used in this study and their inputs . . . 140

List of equations and reactions

I.1 OH radical formation 1 . . . 19
I.2 OH radical formation 2 . . . 19
I.3 OH radical formation 3 . . . 19
I.4 OH radical formation 4 . . . 19
I.5 HO_2 radical formation 1 . . . 20
I.6 HO_2 radical formation 2 . . . 20
I.7 HO_2 radical formation 3 . . . 20
I.8 NO_3 radical formation 1 . . . 20
I.9 Nitrogen oxides 1 . . . 20
I.10 Nitrogen oxides 2 . . . 20
I.11 Titration of O_3 . . . 20
I.12 Transformation of NO to NO_2 . . . 21
I.13 Termination reactions for the O_3 cycle 1 . . . 22
I.14 Termination reactions for the O_3 cycle 2 . . . 22
I.15 Termination reactions for the O_3 cycle 3 . . . 22
I.16 Inorganic aerosol formation 1 . . . 24
I.17 Inorganic aerosol formation 2 . . . 24
I.18 Inorganic aerosol formation 3 . . . 24
I.19 Formation of sulfates 1 . . . 24
I.20 Formation of sulfates 2 . . . 24
I.21 Formation of sulfates 3 . . . 24
I.22 Reactions of ammonium with sulfates 1 . . . 24
I.23 Reactions of ammonium with sulfates 2 . . . 24
I.24 Reactions of ammonium with sulfates 3 . . . 24
I.25 Reactions of DMS 1 . . . 24
I.26 Reactions of DMS 2 . . . 25

I.27 Formation of nitrates 1 . . . 25
I.28 Formation of nitrates 2 . . . 25
I.29 Formation of nitrates 3 . . . 25
I.30 Formation of nitrates 4 . . . 25
I.31 Formation of nitrates 5 . . . 25
I.32 Reaction of nitrates with ammonium . . . 25
I.33 Reaction of nitrates in maritime environments 1 . . . 26
I.34 Reaction of nitrates in maritime environments 2 . . . 26
I.35 Reaction of nitrates in maritime environments 3 . . . 26
I.36 Reaction of nitrates in maritime environments 3 . . . 26
I.37 Reaction of nitrates with ammonium 3 . . . 26
II.1 Mass conservation equation . . . 45
II.2 Turbulent mixing flux . . . 52
II.3 Equivalent turbulent vertical velocity . . . 52
II.4 Dry deposition of gases . . . 52
II.5 Dry deposition of aerosols . . . 53
II.6 Wet scavenging in gases inside rain droplets . . . 53
II.7 Wet scavenging of aerosols by nuclei formation . . . 54
II.8 Wet scavenging in aerosols by rain out . . . 54
II.9 The size distribution of aerosols . . . 56
II.10 Aerosol coagulation in process . . . 56
II.11 Aerosol absorption flux . . . 56
II.12 Aerosol absorption characteristic time . . . 57
II.13 Mass equation for absorption . . . 57
II.14 Mean absorption coefficient . . . 57
II.15 Mean absorption coefficient for organic aerosols . . . 57
II.16 Partitioning coefficient for organic aerosols . . . 58
II.17 Oxidation of VOCs . . . 59
II.18 Raoult's law . . . 59
II.19 Partitioning of SVOCs in gaseous/particulate phases . . . 60
II.20 Partitioning constant for SVOCs . . . 60
II.21 Partitioning constant for SVOCs combined with equation II.18 . . . 60
II.22 Yield of SOA formation from SVOCs . . . 60
II.23 VBS-1D representation equations . . . 62
II.24 VBS-1D representation equations including fragmentation and formation of non-volatile SOA . . . 63
II.25 Average oxidation state . . . 64
II.26 Simplified average oxidation state . . . 64
II.27 Partitioning constant for SVOCs used in VBS-2D . . . 64
III.1 Equations used for the orographic representativeness error calculation . . . 89
III.2 DMS sea-air flux before simplifications . . . 92
III.3 Difference of concentration between the air-sea interface before simplification 92
III.4 Difference of concentration between the air-sea interface after simplification . 92

III.5 DMS sea-air flux after simplifications 92
III.6 Schmidt number 94
III.7 DMS chemistry scheme 1 96
III.8 DMS chemistry scheme 2 96
III.9 DMS chemistry scheme 3 96
III.10 DMS chemistry scheme 4 96
III.11 DMS chemistry scheme 5 96

Abstract

Subject to numerous anthropogenic (gaseous and particulate atmospheric pollution burden) and natural (desert dust events ...) forcings, but also heavily populated on its shores, the Mediterranean is recognized as a region particularly sensitive to the evolution of atmospheric pollutants and climate change. Today, the assessment of the future composition of the atmosphere in the Mediterranean is a major environmental and health issue. In particular, the simulation of the secondary organic aerosol (SOA) in the western basin remains little discussed in the literature, particularly because of the complexity of the subject. The ChArMEx (Chemistry-Aerosol MEditerranean Experiment) intensive campaign, which aims to scientifically evaluate the current and future state of the Mediterranean atmospheric environment, has given us the opportunity to improve our understanding of the organic fraction as well as total aerosols over the Mediterranean, using a 3D modeling approach.

As a first step, different simulation schemes of organic aerosols (OA) taking into account the evolution of the semi-volatile organic compounds in the atmosphere (functionalization versus fragmentation), as well as the formation of the non-volatile SOA, have been implemented in the CHIMERE model. The comparison of these schemes with the measurements make it possible to highlight the main sources of OA formation in the western basin of the Mediterranean and to define the configuration of the most appropriate scheme for the simulation of this aerosol. We found that the scheme that takes into account the non-volatile SOA fragmentation and formation processes fits best to the mass cocnentration, oxidation state, and origin of the OA measured in the ChArMEx project, especially in Cap Corse and Mallorca.

Subsequently, we utilized the CHIMERE model in order to present a detailed look at the future conditions of the Mediterranean basin. Future scenarios proposing different intensities for climate change have been investigated. In particular, the isolated effects of different drivers (regional climate, anthropogenic emissions and long-distance transport) have been identified, and the share of each in the evolution of the composition of the atmosphere for the main components of particulate matter has been estimated. In order to quantify the effect of the change of the scheme used for the simulation of the OA on future scenarios, 15 years of historic simulations and 15 years of future simulations were performed with three different OA simulation schemes. The results show that the percentage change in biogenic SOA can be underestimated by a factor of 2 in a simple scheme for the simulation of the SOA, compared to a scheme taking into account the functionalization, fragmentation and formation of non-volatile SOA.

In order to bring a more regional perspective on the Mediterranean coasts, 5 years of simulations have been carried out on the PACA region on the south-eastern coasts of France, in order to study the exposure of the population to atmospheric pollutants, as well as the combined impact of demographic evolution (population change) and future atmospheric scenarios on this exposure in two case studies at the 2030 and 2050 horizons. The results show that the individual exposure as well as the cumulative exposure of the population decreases for most atmospheric compounds. On the other hand, the risk associated with the exposure of the entire population to ozone, biogenic SOA and desert dust could increase over large parts of the region, particularly in urban areas with high levels of population growth.

Résumé

Soumise à de nombreux forçages anthropiques (charge en polluants atmosphériques gazeux et particulaires) et naturels (recirculations côtières, évènements de poussières désertiques...), mais aussi fortement peuplée sur l'ensemble de ses rives, la Méditerranée est reconnue comme une région particulièrement sensible à l'évolution des émissions de polluants et au changement climatique. Aujourd'hui, l'évaluation de la composition future de l'atmosphère en Méditerranée constitue un enjeu environnemental et sanitaire majeur. En particulier, la simulation de l'aérosol organique secondaire (AOS) dans le bassin occidental reste un volet peu abordé dans les travaux de recherche, notamment en raison de la complexité du sujet. La campagne intensive ChArMEx (Chemistry-Aerosol MEditerranean Experiment), qui vise à l'évaluation scientifique de l'état actuel et futur de l'environnement atmosphérique méditerranéen, nous a offert l'opportunité d'améliorer notre compréhension de la fraction organique des aérosols de l'atmosphère au-dessus de la Méditerranée, par une approche de modélisation 3D.

Dans un premier temps, différents schémas de simulation d'aérosol organique (AO) prenant en compte l'évolution de la matière organique semi-volatile dans l'atmosphère (fonctionnalisation versus fragmentation), ainsi que la formation de l'AOS non-volatile, ont été implémentés dans le modèle CHIMERE. La comparaison de ces schémas avec les mesures a permis de mettre en évidence les principales sources de formation de l'AO dans le bassin ouest de la Méditerranée et de définir la configuration du modèle la plus appropriée pour la simulation de cet aérosol. Nous avons constaté que le schéma qui prend en compte les processus de fragmentation et de formation de l'AOS non-volatile correspondait le mieux avec la masse, l'état d'oxydation et l'origine de l'AO mesurés dans le projet ChArMEx, notamment au Cap Corse et à Majorque.

Dans un deuxième temps, nous avons mis en œuvre le modèle CHIMERE dans sa version améliorée afin de proposer une analyse future du bassin Méditerranéen. Des scénarios futurs proposant différentes intensités pour le changement climatique ont été investigués. Notamment, les effets isolés des forçages (climat, émissions anthropiques, transport longue-distance) ont été identifiés, et la part de chacun dans l'évolution de la composition de l'atmosphère a été estimée, pour les principaux composants de la matière particulaire. Afin de quantifier l'effet du changement de schéma sur l'évolution de l'AO sur les scénarios futurs, 15 années de simulations historiques et 15 années de simulations futures ont été effectuées avec trois schémas distincts. Les résultats montrent que le pourcentage de changement d'AOS biogénique peut être sous-estimé d'un facteur 2 dans avec un schéma simple pour la simulation de l'AOS d'origine biogénique, par rapport à un schéma prenant en compte la fonctionnalisation, la fragmentation et la formation de l'AOS non-volatile.

Avec la volonté d'apporter un regard plus régional sur les côtes de la Méditerranée, 5 années de simulations ont été effectuées sur la région PACA, dans le but d'étudier l'exposition de la population aux polluants, ainsi que l'impact combiné de l'évolution démographique et de scénarios atmosphériques futurs sur cette exposition dans deux cas d'étude aux horizons 2030 et 2050. Les résultats montrent que l'exposition individuelle ainsi que le cumul d'exposition de la population diminue pour plupart des composés atmosphériques. En revanche, le risque lié à l'exposition de l'ensemble de la population à l'ozone, aux AOS biogéniques ainsi qu'aux poussières désertiques pourrait augmenter sur de larges parties du territoire, en particulier dans les zones urbaines montrant de forts taux de croissance démographique.

Introduction

Mechanisms for the formation of atmospheric gaseous species are now well known, particularly thanks to the extensive research work carried out over the last three decades. The better understanding of these processes now allows for a more robust approach to assess their impacts on air quality and human health. Conversely, the processes of formation and aging of atmospheric aerosols (also called particles or particulate matter - PM) are not yet fully understood, particularly with regard to the organic fraction that composes them.

Atmospheric particulate matter has received a large amount of attention in the recent years because of its particularly harmful effects on human health, accounting for around 7 million premature deaths both due to indoor and outdoor air pollution (World health organisation 2018). Among the best-known effects are those related to cardiovascular and pulmonary diseases, especially in vulnerable age groups (children and the elderly, Kurt et al. 2012). The degree of particulate matter perilousness is highly dependent to its size, as smaller particles can penetrate deeper into the pulmonary system, and even into the blood circulatory system (Tie et al. 2009).

It has also been shown in recent studies that PM can have direct, indirect or semi-direct effects on the Earth radiative balance: by reflecting or absorbing solar and terrestrial radiations, and by interacting with clouds changing their properties and their life-times (Kurt et al. 2012). Quantitatively, the IPCC reports that aerosols play an important role in climate change scenarios, with negative or positive forcings, depending on the type of aerosol (Edenhofer, Elgizouli, et al. 2014).

Understanding the problems related to atmospheric aerosols requires a good knowledge of their physical and chemical properties. But one main issue about PM is its high temporal and spatial variability, and the size dependency of this variability. PM can be directly emitted into the atmosphere, or they can be formed in the atmosphere by chemical or physical processes. The sources for the formation of both cases (directly emitted or formed in the atmosphere) can be natural, such as deserts, directly emitting dust particles or vegetation emissions acting as a precursor in the formation of aerosols in the atmosphere. PM sources can also be anthropogenic, road traffic or factory emissions resulting in the formation of both primary and secondary types of aerosols. Therefore, the spatial variability of aerosols depends on the proximity of the source - or precursor sources in the case of aerosol formation. Temporally, differences in its concentration is seen in diurnal, week-day/weekend, monthly and seasonal observations. For example, changes in week-to-weekend concentrations can be observed for aerosols with anthropogenic sources, as human activity during the weekend is less than the week. Diurnal cycles can also be observed in light-sensitive aerosol formation, such as aerosol formation from plant-based biogenic precursors. The same goes for monthly and seasonal changes, as plant activity is reduced during the cooler periods or since the use of domestic heating is very dependent on the season. In addition, PM covers different size ranges, from small particles with a diameter of some nanometers (from nucleation) to bigger ones with diameters around some micrometers (from mechanical abrasion). Atmospheric processes

such as coagulation and condensation which occur during the life cycle of atmospheric particles act further on the size distribution.

Aerosols are a mixture of organic and inorganic components. Indeed, while the processes of formation of inorganic aerosols are almost entirely known, the mechanisms of formation of organic aerosols (OA) are still very uncertain. This is in the first place because of the sheer enormity of the number of organic compounds in the atmosphere that are or can result in the formation of organic aerosols. The secondary reason is the general complexity of organic chemistry that can occur in the atmosphere. Secondary organic aerosols result from oxidation of volatile organic compounds (VOC) in the atmosphere and are in their majority in the fine fraction of PM. The spatial variability explained above for total PM is even more pronounced for OA. Their distribution in the fine aerosol fraction around the world can be between 20% to 50% and can reach as high as 90% according to Kanakidou et al. (2005). J. Jimenez et al. (2009) created a database of measurements for fine aerosols in about 30 sites around the world, showing a high disparity for OA both in seasonality and also spatially. They also show that a considerable amount of this OA is of the secondary type.

The Mediterranean Sea shows a high burden of organic aerosol background levels. This area has many characteristics that explain this particular aerosol exposure. First, because of its location and climate, high temperatures and large amounts of solar radiation contribute throughout the year to maintaining active photochemistry in the basin. Then, geographically, the sea is surrounded by orographically high lands, which creates marine recirculations over the basin that make the residence times of the air masses longer than usual over the sea. Finally, the basin is located at the confluence of air masses coming from Europe, Asia, North America and North Africa (Lelieveld et al. 2002). Therefore, abundant sources of anthropogenic and biogenic particles can be transported to this region, where they contribute to the pollution levels locally. Also, local emission sources such as shipping routes increase the burden of the existing pollution in the area. For all these reasons, the Mediterranean Sea is a highly interesting region to study, especially regarding the interactions of the aforementioned sources on formation of the Mediterranean pollution burden. In addition, it could be among the most sensitive regions to climate change. Giorgi (2006) estimated climate change hotspots using precipitation and temperature changes in different regions in a set of climate scenarios. They concluded that the Mediterranean Sea and northeastern Europe were the most sensitive regions of the world, according to the global simulations studied. But it is important to note that the issue of air quality in this region is becoming more important, given that there is a high population density around the basin that is potentially affected by the harmful effects of air pollutants.

Despite all the reasons cited above, few measurement campaigns investigating PM issues have been conducted in the Mediterranean region. This is especially true for the western basin. To address the problem mentioned above and also to fill the gap due to lack of measurements in the region, the ChArMEx (CHemistry AeRosol Measurement

EXperiment) project was organized, along with its sister projects forming the MISTRALS (Mediterranean Integrated Studies at Regional and Local Scales) program, starting at 2010 and to be continued up to 2020. The general goals of this project are to better understand the current atmospheric conditions and chemical state of the western Mediterranean region, and to predict its future conditions. These objectives suggest the need to use a numerical model in the project to give researchers the ability to understand current chemistry and predict future conditions in the Mediterranean basin.

Atmospheric numerical models give us the capability to test, understand and evaluate the processes resulting in the formation of different atmospheric components. For this purpose and also for the prediction of future atmospheric conditions, atmospheric models are an indispensable tool. Chemistry-transport models can take into account all atmospheric phenomena, including emissions, chemistry, deposition and vertical or horizontal transport of different atmospheric pollutants by discretizing the desired region into small cubes. Of course, it is impossible for these models to include the entire atmospheric chemistry containing millions of compounds. Therefore, reduced chemistry schemes are used in which chemically and thermodynamically similar compounds are grouped together in order to reduce the number of species to be treated by the model. This approach is especially useful for organic compounds, since they cover a spectrum of 10^4 to 10^5 species (Goldstein and Galbally 2007). On the other hand, this approach opens up a large number of possibilities in the classification, grouping and organization of similar organic compounds. This, along with the fact that multiple formation processes can be taken into account (or not) in atmospheric models for the simulation of OAs, enable researchers in proposing several different schemes for the formation of OA in atmospheric models. When exploring climate change, atmospheric models become an indispensable tool. Many hypothesis can be made about the extent of changes made to meteorological parameters due to climate change and the degrees of mitigation put into place in order to combat it. Therefore, several scenarios exist with different degrees of severity that can be tested in atmospheric models for the Mediterranean region. While the climate scenarios present an interesting topic themselves, the effects of changing the way OA is simulated in the model is of interest as well. We are uncertain about the extent of effects of climate change on the mechanisms involving the formation of OA, therefore, different eventualities can be tested in order to quantify the amount of changes in the simulation of this aerosol in future scenarios.

The objectives of the present thesis focus on the problem of OA modeling to better describe current and future atmospheric composition over the Mediterranean basin, and their impacts on sensitive environments. The first goal is to achieve a better understanding and quantification of the sources and formation processes of OA in the western Mediterranean area. For this purpose, a version of the regional chemistry-transport model CHIMERE, aiming at improving OA modeling, will be evaluated against intensive and detailed measurements from the ChArMEx campaign. In particular, several model configurations - including changes in the functionality of the aerosol chemical scheme -

will be tested, in order to better take into account the peculiarities of the Mediterranean and the complexities associated with the simulation of OA.

The second goal is to assess the future conditions of the Mediterranean basin. Several underlying objectives lie inside this goal: first, analyzing the different drivers (mainly climate and emission changes) of future air quality and quantifying the effects of each one on future PM concentration and composition in the western Mediterranean area, but then also to provide an analysis of future air quality at a refined scale, focusing on the Southeastern coasts of France, and exploring the exposure of current and future population in this region to atmospheric pollutants. In order to achieve this second goal, several series of future climate scenarios will be set up and analyzed for our Mediterranean domain, each of them being different from the others by a single driver, in order to quantify its role on future simulations. The explored drivers here are anthropogenic emissions, regional climate and long-range transport. The effects of changing the OA simulation scheme are quantified as well. Finally, a regional focus on the Mediterranean coasts of France is included, which proposes a discussion on the effects of climate and demographic changes on the risk associated with the exposure of individuals to air pollutants.

The thesis is divided into 8 chapters. A brief scientific context is presented in chapter 1, where a summary of the state of the art of atmospheric chemistry knowledge - regarding both gaseous and particulate phases - is included, as well as a short presentation of health and climate impacts of atmospheric PM. An analysis of the atmospheric characteristics of the Mediterranean region is also conducted, including the description of the ChArMEx campaign. Finally, the goals and methodology of this thesis are presented.

The second chapter discusses atmospheric modeling, briefly introducing chemistry-transport models. A detailed description to the CHIMERE chemistry-transport model, the model used in this thesis, is also presented in this chapter.

The third chapter concerns some of the atmospheric modeling peculiarities regarding the Mediterranean region. Starting from this chapter, tests, simulations performed for the present thesis and results obtained from each one are discussed. It presents explanations on the simulation of dimethyl sulfide from bodies of water, discusses orographic representativeness of the Cap Corse area - where most measurements of the ChArMEx campaign were performed - and finally includes a comparison of the different parameterizations used for the simulation of the complex meteorology of the Mediterranean region.

Chapter 4 compares several schemes implemented in the CHIMERE model for the simulation of OA in the western basin to measurements of not only the OA concentration, but also other concerned species (isoprene, mono-terpenes, etc.) and for properties of OA such as oxidation state and origins.

Chapter 5 and onward revolve around the second goal of the thesis:

- Chapter 5 explores the effects of anthropogenic emissions, regional climate change and long-range transport on the concentration changes of PM and its components in future scenarios.
- The changes induced in future scenarios by changing the OA simulation scheme are presented in chapter 6.
- Chapter 7 focuses on a regional analysis of the Southeastern coasts of France - the PACA region - exploring the effects of climate change in 2030s and 2050s. This chapter also discusses future population changes for this region - as predicted by different population scenarios - and calculates the population exposure to future gas and PM concentrations.

A conclusion of the results achieved in this thesis is provided in chapter 8.

CHAPTER

I Scientific context

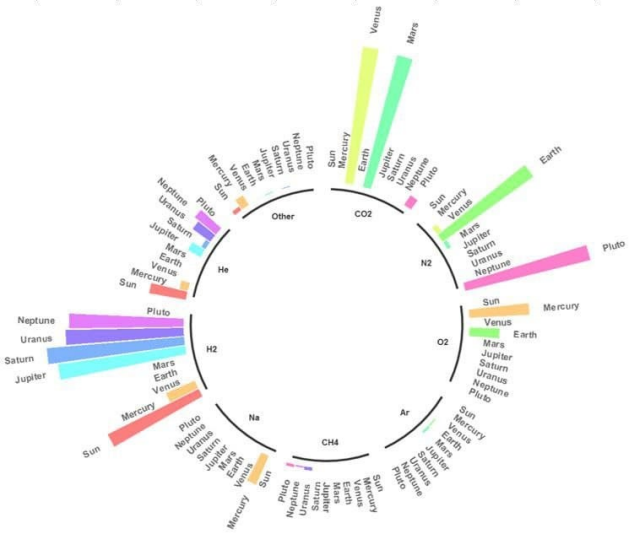
Contents

1 Earth's atmosphere **14**
2 Atmospheric gas-phase chemistry **19**
2.1 Formation of radicals in the atmosphere 19
2.2 Nitrogen oxides 20
2.3 Volatile organic compounds 21
2.4 Ozone cycle 21
3 Atmospheric aerosol sources and chemical composition **22**
3.1 Formation of inorganic aerosols 23
3.2 Formation of organic aerosols 26
3.3 Health effects of atmospheric aerosols 28
3.4 Effects of aerosols on climate 29
4 Fine aerosol atmospheric observations **31**
4.1 Measurements related to fine aerosols 31
4.2 Spatial variability of fine aerosols 32
5 The Mediterranean region **33**
5.1 Atmospheric characteristics 34
5.2 The ChArMEx campaign 37
6 Thesis goals **39**
6.1 Model evaluation and amelioration for the western Mediterranean basin 40

6.2 Future conditions of the Mediterranean basin in different scales 40

Summary. The earth's atmosphere is what makes life possible on earth. It contains multiple layers each with their own behavior. Its composition changes in time and in space. It contains a high number of chemical species, with different lifetimes and chemical characteristics. An example of these species are a group of components called greenhouse gases (GHGs), which help the planet keep survivable temperatures for human beings. After the industrialization era, the emissions of these gases has increased drastically, causing the average temperature of the earth to increase, leading to a man-made rapid climate change. Particulate matter, or aerosols, defined as liquid or solid particles in suspension in the air can exist in our atmosphere as well and they can be of different types: primary aerosols are emitted directly into the atmosphere, while secondary aerosols are formed in the atmosphere by the means of chemical reactions. Among them, secondary organic aerosols (SOAs) are formed in the atmosphere from organic compounds. The concentration of SOA is highly variable spatially and temporally, showing high summertime concentrations in the Mediterranean basin, which is the focus of this thesis. The Mediterranean basin has some peculiarities: it has a high population density living around it, strong anthropogenic and biogenic emission sources in or around the basin, high residence times for atmospheric compounds in this region, particular meteorological regimes and finally high sensitivity to climate change. These reasons are why the ChArMEx project was organized and also are the motivations behind the current thesis. The goals of the thesis are to better understand the sources and origins of high PM (particulate matter) concentrations in the Mediterranean basin, and also to provide an estimation of what the conditions of the basin might be in the future. To achieve these goals, a 3D chemistry-transport model is used in order to simulate the PM concentration in the region, compare these simulations to measurements obtained during the ChArMEx project and improve the model, making it more adapted to the particular characteristics of the basin. The second step is to use this improved model in future scenarios to estimate the future characteristics of the basin regarding particulate matter. In this concise introduction into the scientific context of this thesis, first, we will be discussing the physical properties of the atmosphere (section 1). A brief explication of gaseous chemistry is given (section 2), followed by a more detailed look at the aerosol chemistry, physics, health effects (section 3) and its atmospheric dispersion regarding to the region (section 4). In the part that ensues, a look at the natural and human-dependent characteristics of the Mediterranean basin is given (section 5). At the end, the goals of this thesis are discussed in detail (section 6).

The atmosphere is a layer or a set of layers of gases surrounding a planet, held into place by the gravitational force provided by the planet itself. The density of this atmosphere depends on the mass of each planet; the higher the mass of the planet, the higher the gravitational force produced, therefore the thicker the layer of gas that it can hold into place. For example, Jupiter with a mass around 300 times more than the Earth, creates a gravitational force of around 23.1m.s^{-2}, which holds the thickest atmosphere in the solar system. On the other hand, Mercury, with a mass 5.5% of mass of the Earth, cannot sustain an atmosphere because of its low gravitational force (around 3.7m.s^{-2}). This, among other various reasons, can explain the differences between the composition and density of the atmosphere in different planets. Looking at our own solar system, an impressive variety of chemical compositions can be seen in different planets. Figure 1.1 shows the atmospheric composition of different planets in our solar system. Some of these planets have kept their primordial nature from when they were formed, like Jupiter and Saturn, made up of nearly 100% hydrogen. Others have changed in time, but not in the direction that would make life possible, for example, Venus' atmosphere is made up of 96% carbon dioxide, making the clouds in this planet to be made up of sulfuric acid. Only the earth's atmosphere has evolved in a way that is capable of containing and sustaining life.



CO_2	93.5305	CO	0.0059
Ne	4.3157	Xe	0.0021
He	1.2439	O_3	0.0012
CH_4	0.4249	NO_2	0.0012
Kr	0.2706	NH_3	0.0002
H_2	0.1258	SO_2	0.0007
N_2O	0.0772	H_2S	0.0000

Figure I.1 – *Major composition of different planets in the solar system (left image) and percentage of some trace gases in earth's atmosphere (right table, Grey: stable species, orange: variable species, pink: highly variable species).*

1 Earth's atmosphere

The atmosphere on earth makes life as we know it possible since it provides multiple conditions: oxygen for respiration, carbon dioxide for plant photosynthesis, greenhouse gases (GHGs) which keep the earth temperature at survivable levels, and the ozone layer which provides protection against UV rays. Its major contributors are 78.1% nitrogen, 20.9% oxygen, around 0.93% argon and a large amount of water vapor (which is not counted in the percentages given before). The remaining 0.04% corresponds roughly to the concentration of carbon monoxide in our atmosphere, leaving an extremely small percentage for the other components. It is fair to say that the whole science of the atmospheric chemistry is focused on this 0.04%, corresponding to millions of compounds, in gaseous or particulate phase.

The atmosphere is divided into five major layers: troposphere, stratosphere, mesosphere, thermosphere and exosphere. The ones that concern major events in atmospheric chemistry are the first and the second layers, the troposphere and the stratosphere. The troposphere contains most of the mass of the atmosphere, albeit being the layer with the smallest thickness. Each of these layers has a specific thermal profile. The planetary boundary layer (PBL, or atmospheric boundary layer, ABL) is the part of the troposphere that is immediately in contact with the earth's surface. The planetary surface characteristics, such as its radiative forcing, have direct impacts on the behavior of this layer. Therefore, since the radiative forcing over the bodies of water is different than that of continental areas, the PBL characteristics differ in these two, as described below. Strong vertical mixing and rapid turbulences in temperature, humidity, wind speed, etc. are some of the characteristics of the PBL.

The clear weather continental PBL can be either convective, typically during day-time when solar insolation heats the surface, and creates a negative (potential) temperature gradient or stable, typically during night time, when radiative heat loss cools the surface. It thus results in strong daily temperature cycles. Its height can vary between 200m (at night) and 1500 (during daytime) on average, while it can get to a few kilometers as well. In addition, a neutral PBL often presents cloudy weather and strong winds limiting the daily temperature and wind cycles. The average height of this kind of PBL is around 1000m. The marine PBL has a smaller daily cycle, because of the slow temperature change of the water surface. The height of the PBL for the ocean surface is lower in general, somewhere between a few hundred meters to 2km (Garratt 1994), but in average mostly around 500m. The atmosphere above the PBL, where the wind becomes quasi-geostrophic and the atmosphere is more or less non-turbulent (but not yet strongly stratified) is called the free atmosphere.

The chemical compounds that exist in our atmosphere (except the major ones cited above) can be emitted directly into it, either by anthropogenic or biogenic processes, or can be formed there by the means of chemical reactions. These two are called primary and secondary compounds, respectively. Some of these compounds are chemically inert,

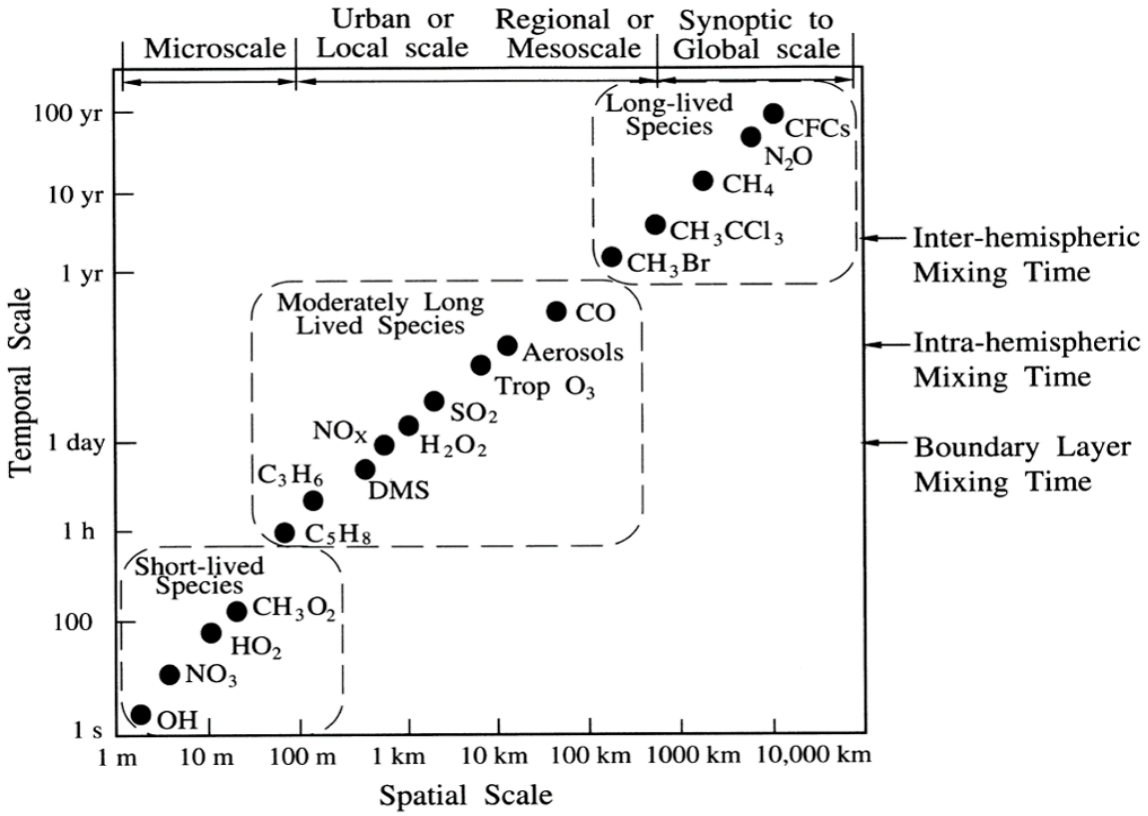


Figure I.2 – *Life-times of different atmospheric gases from very short-lived species (radicals, etc.) to very long-lived (methane, CFCs). The image is taken from Seinfeld et Pandis 2016.*

such as CO_2, therefore they do not participate in chemical reactions; however, this does not in any way mean that they do not or did not in the past participate in the formation and evolution of our current atmosphere. Figure I.2 shows the life-times of some gases in our atmosphere, where CO_2, methane (CH_4) and CFCs (with atmospheric life-times of 5 years, 10 years and around 100 years respectively) are classified as long-lived species. On the other end of the reactivity scale, short-lived species also exist in the atmosphere; an example of these are radical species which play an important role in the atmospheric chemistry, albeit having low concentrations and short life times. Hydroxyl radical (OH), hydroperoxyl radical (HO_2) and atomic chlorine (Cl^-) are examples of these species, which have atmospheric lifetimes of 1 second to 1 minute, so they are in steady-state equilibrium with more stable compounds. Other species, such as sulfur oxide, hydrogen peroxide, etc. have an a lifetime between the short-lived species and the inert ones. These species can stay in the atmosphere for an intermediate time scale (like a day for both species mentioned above). Normally these are the species that can have adverse impacts on the human health.

The composition of the atmosphere changes in time and in space, meaning that a spatial disparity as well as an important temporal evolution can be seen in the concentration of trace species, not only at short time scales, but also at climatological time scales (decades or more). The importance of inert species comes into play when discussing our atmospheric climate. Species such as methane, carbon dioxide, water vapor, etc. are regarded as GHGs. While being (at least most of them) almost inert themselves, they absorb and emit radiative energy, heating our atmosphere and producing the greenhouse effect. This effect is beneficial for our survival, since without these gases, the temperature of the Earth's surface would have been too low. It was first identified by Joseph Fourier in 1827 (Joseph Fourier 1827). However, anthropogenic emissions have increased their concentration in our atmosphere in recent times, having huge consequences.

With increasing GHG concentrations, the radiative forcing and the greenhouse effect increases as well, raising the surface temperature and resulting in climate change. We started experiencing this effect since the start of the industrial revolution (around 1800s) in a lesser degree, when large amounts of GHGs were emitted into the atmosphere because of industrialization. Still, the GHG emissions back then were a fraction of what we emit into the atmosphere today. After the discovery of the greenhouse effect in the early 1800s, Svante Arrhenius in 1896, presented the hypothesis that if the amount of GHGs in the atmosphere were high enough, they would result in increasing surface temperatures, in other words global warming (Arrhenius 1896). The idea was immediately disregarded by his peers as to be too improbable. The scientific proof for global warming was found in late 1930s to 1940s by Guy Callendar, who, while proving the link between CO_2 and temperature increase (Callendar 1938), thought it to be a beneficial side-effect of the industrialization era since it would prevent future ice ages. The research on climate change has continued since then to this day, gaining a lot of traction in recent years.

Since then we have understood that this is not a beneficial effect and thus climate scenarios have been developed in order to estimate the effects of climate change on different aspects (local and global meteorology, rising water levels, water scarcity, etc.) by the intergovernmental panel on climate change (Edenhofer, Elgizouli, et al. 2014) using estimations on GHG gas emission changes, land use changes, population changes and in some cases, expected changes in CO_2 removal technology from the atmosphere (IPCC, 2014). The IPCC proposes 4 climatic scenarios in its latest report, called Representative Concentration Pathways (RCPs): RCP2.6, RCP4.5, RCP6 and RCP8.5. The number after each RCP refers to the maximum ratiative forcing reached at the end of the century (e.g. 8.5 $W.m^{-2}$ for RCP8.5). Depending on the severity of the scenario (from the extremely optimistic to the very pessimistic), the amount of GHG emission changes which consequently induces temperature changes differ until the end of the century. For scenarios covering GHG emissions from 430ppm eq-CO_2 (RCP2.6) to more than 1000 ppm eq-CO_2 (RCP8.5) with an average of 500-700 ppm eq-CO_2 for intermediary scenarios, temperatures are likely to increase (till the end of the century) to between $1\,°C$ (RCP2.6) and $4.6\,°C$ (RCP8.6) (figure I.3b) with an average increase of around $2\,°C$ for RCP4.5

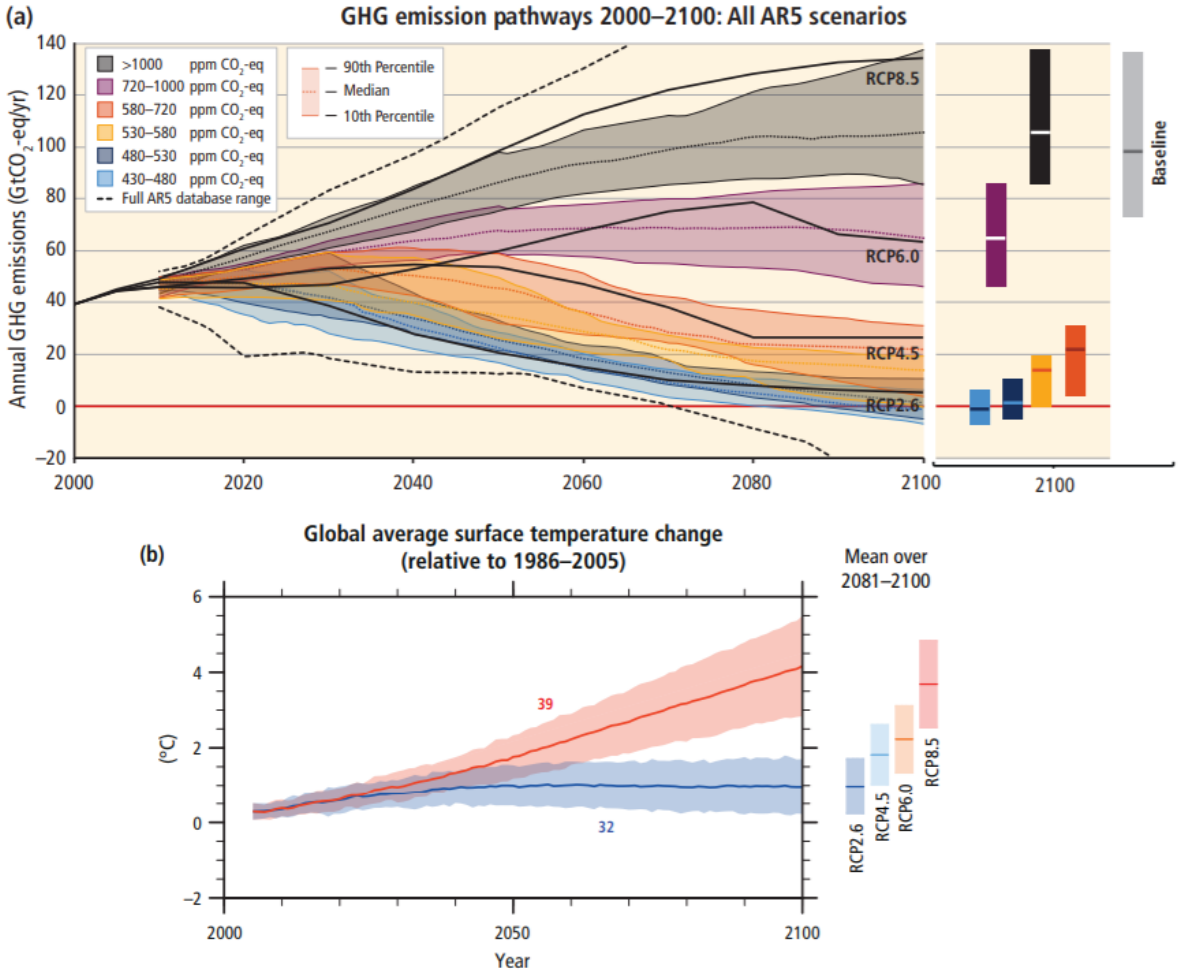


Figure I.3 – *The RCP (representative concentration pathways) scenarios in IPCC (intergovernmental panel on climate change). The number after each RCP represents the radiative forcing by each scenario in W.m^{-2}. (a): changes in GHG emissions in different scenarios compared to a historical period of 1986-2005. (b): changes in global temperature in each scenario compared to a historical period of 1986-2005 (IPCC, 2014).*

and RCP6 (the intermediary scenarios) compared to a historical period of 1976 to 2005, according to IPCC (Edenhofer, Elgizouli, et al. 2014).

While GHGs contribute to climate change, other gaseous species can have important impacts, either directly or indirectly on our atmosphere, therefore it is important to study the chemistry involving these species. Since most of the atmospheric chemistry happens in the troposphere, the focus of the next section will be the chemistry of trace gases in the Earth's troposphere.

2 Atmospheric gas-phase chemistry

As mentioned before, most of the chemical components emitted into our atmosphere are consumed in the troposphere, except those with very long life-times (around decades which were discussed before) that can make it into the stratosphere. The gas-phase chemistry of the troposphere mostly revolves around the oxidation of organic compounds (e.g. methane, VOCs) in the presence of nitrogen oxides (NO_x, sum of NO and NO_2) in a chain of free radical reactions under the action of sunlight (J. Seinfeld and S. Pandis 2016). The production and the photolysis of ozone plays a central role in reaction cycles. The presence of sunlight is indispensable to this chemistry since it provides the necessary energy allowing the formation of reactive radical species, initiating and propagating reaction chains. Most of these reactions happen in the presence of radicals, making OH radical (in daytime) and nitrate radical (NO_3, mostly during the night) important oxidants in the atmosphere, albeit their low concentrations. In the following section, a brief introduction to the gas-phase chemistry in the troposphere is given.

2.1 Formation of radicals in the atmosphere

Formation of the OH radical can be considered as the key background reaction in the troposphere which happens due to photolysis of ozone:

$$O_3 + h\nu \longrightarrow O_2 + O \tag{I.1}$$

$$O_3 + h\nu \longrightarrow O_2 + O(^1D) \tag{I.2}$$

$$O(^1D) + M \longrightarrow O + M \tag{I.3}$$

$$O(^1D) + H_2O + h\nu \longrightarrow 2OH^{\cdot} \tag{I.4}$$

In many cases, the fate of O(^{1}D) is being quenched by colliding with most commonly O_2 or N_2 and forming oxygen atom (Reaction I.3), which then reforms ozone, creating a null cycle. Occasionally, O(^{1}D) collides with water molecules instead of O_2 or N_2, resulting in the formation of an OH radical. The formation of OH from O(^{1}D) at room temperature and at 50% relative humidity happens only 2 out of 10 times (J. Seinfeld and S. Pandis 2016). The reaction presented above is globally the major source of production of OH, however, other sources can exist for the formation of this radical as well, i.e. nitrous acid (HONO) and recycling of peroxy radicals (in low-NO_x environments).

The hydroperoxyl radical (HO_2) is formed by the dissociation of HCHO in the presence of sunlight or by oxidation of hydrogen peroxide by OH:

$$HCHO + h\nu \longrightarrow HCO^{\cdot} + H^{\cdot} \tag{I.5}$$

$$HCO^{\cdot} + O_2 \longrightarrow CO + HO_2^{\cdot} \tag{I.6}$$

$$H_2O_2 + OH^{\cdot} \longrightarrow HO_2^{\cdot} + H_2O \tag{I.7}$$

HO_2 is another radical species, which has an important role in the oxidation of organic compounds and also in the ozone cycle. Reactions which form new radicals from stable species are called initiation reactions. The sum of HO_2 and OH is sometimes referred to as HO_x. Additional OH and HO_2 sources which transform OH into HO_2 and vice versa, (keeping the HO_x balance unchanged) will be presented a little further. This type of reactions is called *propagation reaction*.

As seen above, the production of the OH radical needs sunlight. Therefore, it happens only during the day. During the night, the main radical allowing chemistry in the atmosphere is the nitrate radical, which is formed from the reaction of ozone and nitrogen dioxide (NO_2):

$$O_3 + NO_2 + M \longrightarrow NO_3^{\cdot} + M \tag{I.8}$$

During daytime, NO_3 is rapidly destroyed by photolysis forming back NO_2 and O or NO and O_2. Thus during daytime, OH is the most important oxidant agent, but during the night NO_3 is considered as the most important oxidant in the atmosphere, together with ozone. Other radicals of course exist in the atmosphere, however, these three are the most important ones.

2.2 Nitrogen oxides

Nitrogen oxides are emitted into the atmosphere mostly because of human activities during combustion: road transport, industrial activities, household activities, etc. They can also be emitted naturally because of lightning, however, the amount of lightning-related NO_x emissions is negligible compared to emissions due to human activities. On the sea surface, shipping emissions can be a big source of NO_x emissions, while natural emissions of NO from the sea surface can occur as well, however in much lower quantities. Nitrogen oxides are the only source of production of ozone in the atmosphere:

$$NO_2 + h\nu \longrightarrow NO + O \tag{I.9}$$

$$O_2 + O + M \longrightarrow O_3 + M \tag{I.10}$$

M is commonly N_2 or O_2. After its formation, ozone can react with NO to form NO_2:

$$O_3 + NO \longrightarrow NO_2 + O_2 \tag{I.11}$$

Reactions I.9 to I.11 form a reaction cycle with a zero balance. Reaction I.11 is called titration reaction, because it rapidly removes ozone in environments with large NO concentrations.

2.3 Volatile organic compounds

Volatile organic compounds (VOCs) are organic gaseous species in the atmosphere composed of carbon, hydrogen and addition of oxygen, nitrogen, sulfur, halogens to the

existing carbon-hydrogen chain. This class, includes an enormous number of species, as mentioned before. They enter the atmosphere from being emitted from natural or anthropogenic sources, therefore they can be regrouped into anthropogenic VOCs (AVOCs) and biogenic VOCs (BVOCs). The ratio of emission of BVOCs to AVOCs is around 90% to 10% globally. AVOCs are emitted from human activities such as road transport, biomass burning, industrial processes, etc. While BVOCs are mostly emitted by plant activities. For example, Isoprene (C_5H_8) is emitted by photosynthetic activities in a large variety of plants, therefore it presents high sensitivity to solar radiation. Another example of BVOCs are terpenes, which depend on biophysical activities in plants, therefore their emission is not strongly light dependent and can continue overnight, however, they depend strongly to temperature. There are multiple sinks for the removal of VOCs from the atmosphere: oxidation reactions with major atmospheric radicals, photolysis by solar radiation and deposition into the surface are among these sinks, the oxidation reactions being the most important removal process. BVOCs especially are highly reactive to said oxidants because of their characteristic olefinic double bonds in their chemical structure. For example, the isoprene life-time towards OH is around 1.4 hours, while that of some mono-terpenes is around a few minutes. The lifetimes of AVOCs are more variable and usually longer than that of BVOCs. The oxidation of VOCs in the atmosphere can result in the formation of Secondary Organic Aerosol (SOA)s (see section 3).

2.4 Ozone cycle

Ozone is a purely secondary compound, meaning that it is formed in the atmosphere and is not emitted into it. The tropospheric ozone cycle is summarized in figure I.4. This cycle is what combines the two cycles explained above, the NO_x and the VOC cycles. In the VOC cycle, the reactions of RO_2 and HO_2 radicals with NO create NO_2, while recycling RO and OH radicals:

$$RO_2 + NO \longrightarrow RO + NO_2 \tag{I.12a}$$

$$HO_2 + NO \longrightarrow OH + NO_2 \tag{I.12b}$$

Transformation of NO to NO_2 without consuming ozone allows net formation of ozone by reactions I.9 and I.10.

This cycle, which functions principally using radical species, initiates with reactions that form radicals (reaction I.4 and I.6), and finishes by reactions that form more stable species (called *termination reactions*):

$$NO_2 + OH^{\cdot} \longrightarrow HNO_3 \tag{I.13}$$

$$HO_2^{\cdot} + HO_2^{\cdot} \longrightarrow H_2O_2 \tag{I.14}$$

$$RO_2^{\cdot} + HO_2^{\cdot} \longrightarrow ROOH + O_2 \tag{I.15}$$

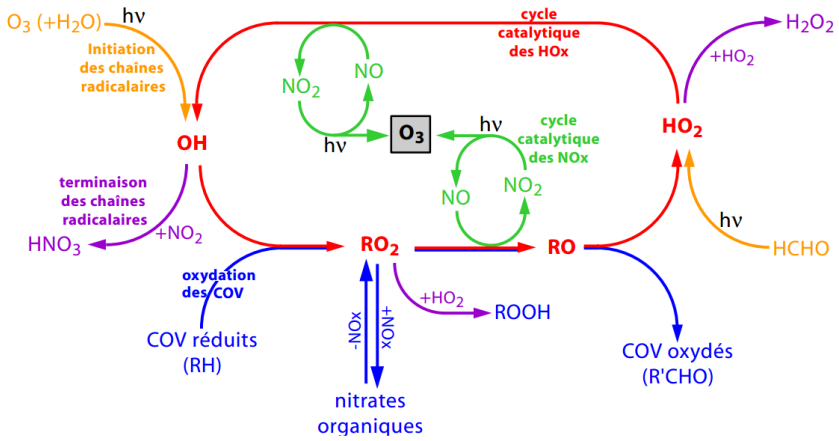


Figure I.4 – *ozone cycle in the troposphere. This cycle includes parts of the carbon cycle and the carbon as well. Image is taken from Camredon and Aumont, 2007.*

For high concentration of NO_x, (reaction I.13) on the left side of figure I.4 becomes the terminating reaction. If concentration of existing NO_x is low, the top and down sides of figure I.4 become the ending reactions (reaction I.14 and I.15), each combining two peroxy radicals. This cycle gives meaning to low-NO_x and high-NO_x regimes, where, the formation and evolution of the concentration of ozone depends on the existing concentration of NO_x. In the low-NO_x regime, more NO_x leads to more ozone formation, because of the reactions of peroxy radicals with NO, forming NO_2 and recycling OH. In the high-NO_x regime, more NO_x decreases ozone formation, because it removes OH from the system. In this regime, a competing effect for OH is present between VOC and NO_x as seen in figure I.4 (Camredon and Aumont 2007). Increasing VOC concentrations always increase ozone formation.

3 Atmospheric aerosol sources and chemical composition

Particulate matter (PM) or aerosols denote liquid or solid particles suspended in the atmosphere with the exception of all kinds of hydrometeors (clouds, rain, snow, etc.). These aerosols can be classified in different ways, but mainly by their origin and by their size. Primary aerosols are those emitted directly into the atmosphere from natural sources (volcanic eruptions, sea-salt emissions, desert dust emissions, etc.) or human activities (wood burning, shipping and traffic emissions, etc.); while secondary aerosol are formed from precursor gases, implying a chain of physico-chemical processes of precursor gases in the atmosphere. Secondary aerosols are divided into two groups: secondary inorganic aerosols (SIA) and SOA.

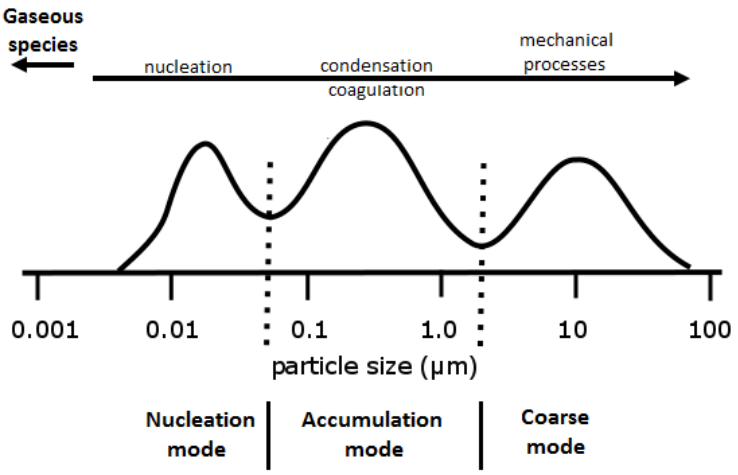


Figure I.5 – *Formation processes and size modes of atmospheric aerosols.*

The formation processes of aerosols depend on their size range. Size wise, aerosols are classified depending on their aerodynamic diameter (D_p) into three groups: Nucleation mode ($Dp < 0.1\,\mu\mathrm{m}$), accumulation mode ($0.1\,\mu\mathrm{m} < D_p < 1\,\mu\mathrm{m}$) and coarse mode ($D_p > 1\,\mu\mathrm{m}$). The formation of aerosols in the accumulation and nucleation modes is usually a result of chemical processes such as nucleation, condensation and coagulation, while that of coarse mode usually follows mechanical mobilization and emission into the atmosphere. Figure I.5 shows the typical atmospheric size distribution of aerosols. Examples for coarse mode aerosols are mineral dust, sea salt and pollen which can be produced by mechanical processes such as erosion, sea spray and resuspension. The composition of these aerosols depends directly on their source, e.g. for the case of mineral dust, the mineral composition of the surface. In the scientific literature, particulate matter is classified regarding its size as PM_1, $PM_{2.5}$, PM_{10} which corresponds to particles with a diameter less than $1\,\mu\mathrm{m}$, less than $2.5\,\mu\mathrm{m}$ and less than $10\,\mu\mathrm{m}$ respectively. Particles can both be solid or liquid, with both organic and aqueous phases.

3.1 Formation of inorganic aerosols

The main types of inorganic aerosols are ammonium, nitrate and sulfate. Sulfates are mainly formed in the atmosphere as secondary particles from the oxidation of SO_2 into sulfuric acid, either in gaseous or aqueous phases. The fastest pathway for the formation of sulfates in the gaseous phase is by oxidation with the OH radical (radicals are denoted by a circle above them in the reactions that follow):

$$SO_2 + \dot{OH} + M \longrightarrow HOSO_2 + M \tag{I.16}$$

$$HOSO_2 + O_2 + M \longrightarrow SO_3^- + \dot{HO_2} \tag{I.17}$$

$$SO_3^- + H_2O \longrightarrow H_2SO_4(g) \tag{I.18}$$

The third reaction (reaction I.18) happens in the presence of water vapor. Sulfuric acid has a very low vapor pressure and high solubility, and thus passes into the particulate phase in order to form sulfates. The formation of sulfates in the gaseous phase by this mechanism is slower than the mechanism given below for the aqueous phase.

The aqueous phase production of sulfates is initiated by the solution of SO_2 in water, where SO_2 starts to dissociate and the products of this dissociation depend on the pH of the aqueous environment:

$$SO_2(g) + H_2O + M \longleftrightarrow SO_2.H_2O(aq) \quad (pH < 2) \tag{I.19}$$

$$SO_2.H2O(aq) \longleftrightarrow HSO_3^- + H^+ \quad (2 < pH < 7) \tag{I.20}$$

$$HSO_3^- \longleftrightarrow SO_3^{2-} + H^+ \quad (pH > 2) \tag{I.21}$$

Oxidation of these products results in the formation of S (VI), the major oxidant depends also on the pH level of the aqueous environment (H_2O_2, O_3 or OH if pH≈6 or H_2O_2 if pH<3). As said before, S (VI) has a very low volatility, therefore it can easily condense into existing particles or nucleate with other compounds with low vapor pressure, resulting in the formation of sulfates. For example, it can nucleate with ammonium to form ammonium sulfate ($(NH_4)_2SO_4$) which is the resultant of neutralization of sulfuric acid. The resulting product can be formed in the aqueous phase or in the aerosol phase depending on the relative humidity (see below).

$$NH_3(g) + H_2SO_4(aq) \longrightarrow NH_4HSO_4 \quad (aq\ or\ s) \tag{I.22}$$

$$2NH_3(g) + H_2SO_4(aq) \longrightarrow (NH_4)_2SO_4 \quad (aq\ or\ s) \tag{I.23}$$

$$3NH_3(g) + 2H_2SO_4(aq) \longrightarrow NH_4HSO_4.(NH_4)_2SO_4 \quad (aq\ or\ s) \tag{I.24}$$

A secondary source for the formation of sulfates is the emission of dimethyl sulfide (DMS) in marine environments. The biologic activities of planktons in the oceans and seas indeed results in the formation of DMS, which is then emitted into the atmosphere. The flux of DMS emission into the atmosphere depends on the amount of DMS available in the first layers of the water, and also on the velocity of the wind interacting with the sea surface. The emitted DMS in the atmosphere can be oxidized by OH radical by the means of abstraction or addition reactions to, in the end, form mostly methanosulfonic acid (MSA), SO_2 and other minor products:

$$Abstraction: \quad DMS + OH^{\cdot} \rightleftarrows aMSA + bSO_2 + cSO_3 + ... \tag{I.25}$$

$$Addition: \quad DMS + OH^{\cdot} \rightleftarrows dDMSO + eDMSO_2 + fSO_2 + ... \tag{I.26}$$

The abstraction path is more active at higher temperatures and the addition path at lower temperatures (J. Seinfeld and S. Pandis 2016). MSA and SO_2 then can form sulfate aerosols. The flux of DMS emitted from the sea surface to the atmosphere has

been estimated in multiple studies, using techniques such as piston velocity (Elliott 2009) or the sea surface chlorophyll concentrations (Albert et al. 2012), but it still stays an uncertain topic. The formation of sulfates from DMS has been estimated to be 6-22% of the total sulfates globally (Ganor et al. 2000).

The formation of nitrates is related to the formation of nitric acid in gaseous or aqueous phases. The gaseous phase reactions (especially during the day) include oxidation of NO_2 by the OH radical:

$$NO_2 + OH^{\cdot} + M \longrightarrow HNO_3 \tag{I.27}$$

Or oxidation of NO_2 by:

$$NO_2 + O_3 \longrightarrow NO_3 + O_2 \tag{I.28}$$

$$NO_3 + RH \longrightarrow HNO_3 + R \tag{I.29}$$

$$NO_3 + NO_2 \longrightarrow N_2O_5 \tag{I.30}$$

$$N_2O_5(g) + H_2O(s) \longrightarrow 2HNO_3(g) \tag{I.31}$$

The neutralization of sulfuric acid occurs first before that of nitric acid (J. Seinfeld and S. Pandis 2016), the neutralization of nitric acid occurring if ammonia is still present in the atmosphere once H_2SO_4 is neutralized, to form ammonium nitrate in the aqueous or solid phase:

$$HNO_3(g) + NH_3(g) \longleftrightarrow NH_4NO_3(s) \quad or \quad NH_4^+(aq) + NO_3^-(aq) \tag{I.32}$$

The phase in which the products are formed depends on atmospheric conditions and mainly relative humidity. Not all aerosols share the same affinity to water: each aerosol's hygroscopicity is the deciding factor for the amount of water vapor it can take in. The amount of water that can be absorbed by an aerosol depends on the ambient relative humidity following a hysteresis function. If the relative humidity passes a certain limit for each aerosol, the aerosol finds itself in a state of saturated aqueous solution, the aforementioned limit being called the deliquescence point (DRH). From the other side, if the relative humidity is lower than a certain point, the aerosol stays in solid state. This point is called the efflorescence point (ERH). Both these points have a strong dependence upon the chemical composition of the aerosol. For example, for the reaction mentioned above (reaction I.32), the DRH for ammonium nitrate is around 62%.

In certain atmospheric environments, other elements enter these equations. For example, in maritime conditions, salt particles can interact with sulfuric or nitric acids, liberating hydrochloric acid (HCl):

$$HNO_3(g) + NaCl(s) \longrightarrow NaNO_3(s) + HCl(g) \tag{I.33}$$

$$H_2SO_4(g) + NaCl(s) \longrightarrow NaHSO_4(s) + HCl(g) \tag{I.34}$$

$$H_2SO_4(g) + 2NaCl(s) \longrightarrow Na_2SO_4(s) + 2HCl(g) \tag{I.35}$$

Or in areas with dust emissions, the dust particles can contain calcium which can react with nitrates:

$$HNO_3(g) + CaCO_3(s) \longrightarrow Ca(NO_3)_2 \tag{I.36}$$

Or in anthropogenic areas:

$$HNO_3(g) + NH_3(g) \longrightarrow NH_4NO_3(g) \tag{I.37}$$

The production of these species can depend greatly on different factors, such as gaseous precursor concentration, levels of atmospheric oxidants, air temperature and humidity and also the characteristics of preexisting aerosols. A simplified scheme for the processes involving SIA formation is shown in figure I.6.

3.2 Formation of organic aerosols

Formation of SOA generally results from the oxidation of volatile organic compounds (VOCs). To put it simply, the VOCs in the atmosphere are oxidized to semi-volatile organic compounds (SVOCs), and these SVOCs can subsequently be oxidized again and again on their way to form carbon monoxide or carbon dioxide. In the meanwhile, SVOCs, in any of their multiple stages of oxidation, can transfer to the particular phase to form SOAs. SOA can be regrouped into anthropogenic SOA (ASOA) and biogenic SOA (BSOA). SVOCs can oxidize a number of times before passing into particulate phase, meaning that, for example, first generation SVOCs can react with oxidants to form second generation SVOCs, which are more oxidized and thus less volatile; causing what is called “aging” processes. When a VOC is oxidized, in most cases, the oxygen to carbon (O:C) ratio of the product becomes higher and therefore its volatility becomes lower. This is called functionalization. Another factor that can affect the volatility of SVOCs is the carbon chain length. The longer the carbon chain for the SVOC is, the lower its volatility gets. Longer carbon chain SVOCs can break in the atmosphere, causing a phenomena called “fragmentation”. If an SVOC with a long C chain is broken in the atmosphere, the resulting molecules are more volatile than the original SVOC. While this is the general scheme in which SOA is produced, there are other processes that have to be taken into account as well. For example, recent studies (C. Cappa and J. Jimenez 2010; Ehn et al. 2014) show that SVOCs, after their formation, can pass into a state of such low volatility that they cannot become volatile after that and stay in particulate phase, this is called the “nonvolatile SOA formation” processes.

It is important to bear in mind that what is called SVOC includes a range of 10^4 to 10^5 species, most of them having different thermodynamic and chemical characteristics (Goldstein and Galbally 2007); the sheer enormity of the number of species that can participate in the formation of SOA, the uncertainty of formation pathways, yields and reaction speeds for each of these species makes them difficult to study and to model.

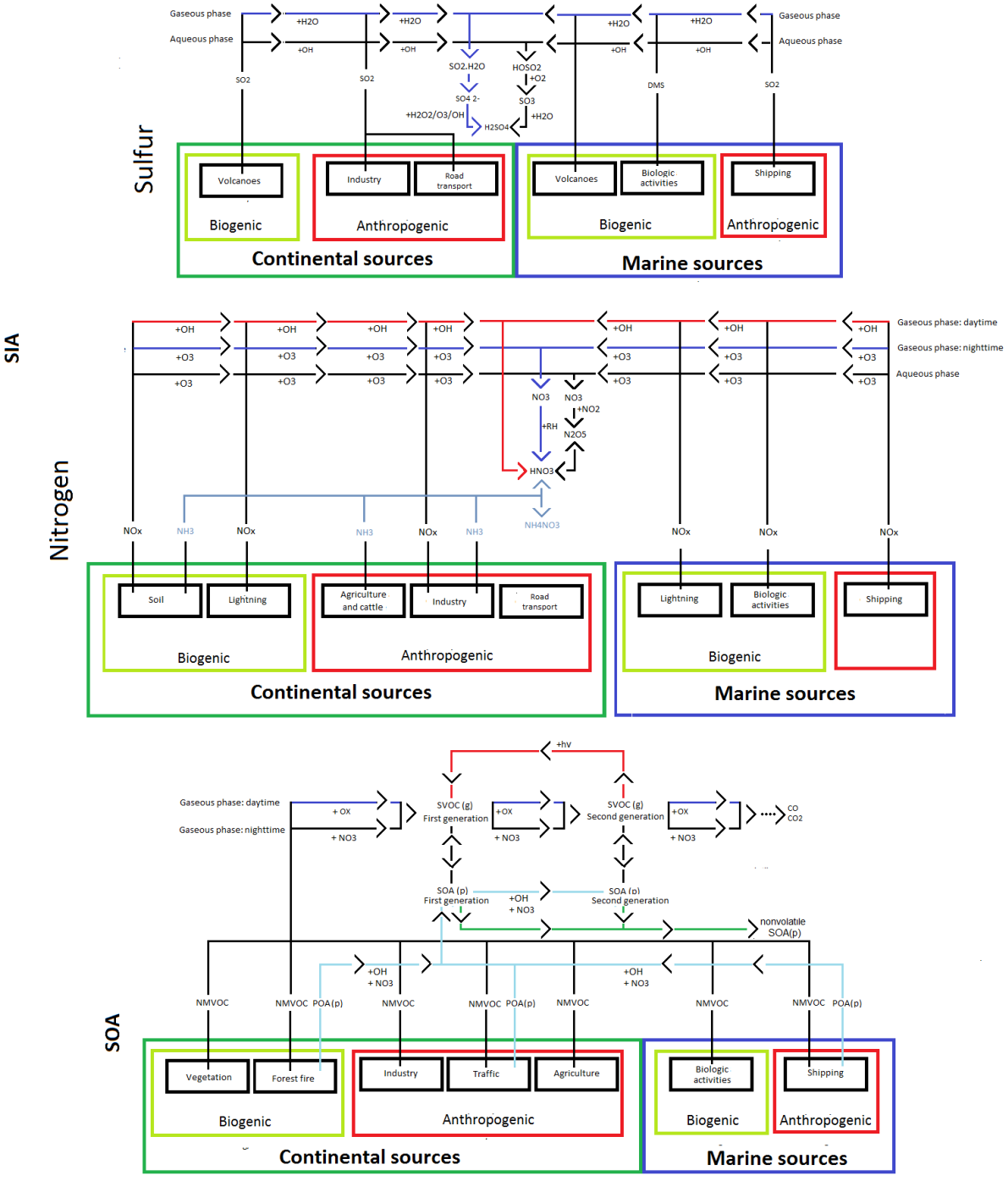


Figure I.6 – *Simplified schematic of formation of secondary inorganic aerosols and secondary organic aerosols in the atmosphere.*

Examples of VOC precursors for the formation of BSOA include isoprene, monoterpenes and sesqui-terpenes, which are emitted by plants. The formation of SOA from these sources greatly depends on the dominant species of a region, for example, the needle-leaf forests produce monoterpenes, while in broad-leaf forests are more susceptible in producing isoprene. ASOA production precursors include xylenes and toluene, which normally are produced by human activities such as road traffic and industries. A simplified schematic of SOA formation is presented in figure I.6.

3.3 Health effects of atmospheric aerosols

Multiple studies show that particulate matter affects human health through the toxic properties of its compounds, causing mainly cardiovascular and respiratory diseases resulting in premature deaths (R. M. Harrison and Yin 2000; Pöschl 2005; Mauderly and Chow 2008; Tie et al. 2009). The extent of these effects depends on their composition and size. According to world health organization (WHO, 2018), ambient air pollution causes 4.2 million premature deaths per year globally, from which around 40% corresponds to respiratory diseases caused by PM pollution. On the other hand, indoor air pollution causes 3.8 million deaths per year globally, where again particulate matter is of special concern. Brunekreef and Holgate (2002) calculated the mortality caused by PM_{10}, $PM_{2.5}$, ozone and nitrogen oxides, concluding that $PM_{2.5}$ represents more mortality risk compared to PM_{10}. The smaller the particles are, the more they can penetrate into the human respiratory system; ultrafine ($PM_{0.1}$) particles are particularly dangerous in this regard, since they are small enough to enter the blood stream through respiratory tract membranes (figure I.7). It is important to bear in mind that $PM_{0.1}$ particles have in a large extent anthropogenic sources, while particles with diameters superior to $2.5\,\mu\mathrm{m}$ have more natural origins. Therefore, while naturally occurring particles can also cause health issues, it is in fact particles with anthropogenic sources that are more dangerous for human health. Albeit an increasing amount of awareness and research in this area, the relationship between particulate matter and human health is still subject of intense research. The links between PM exposition and many other illnesses (allergies, neurogenerative, psychiatric) yet have to be better assessed. Also, PM components are not equally toxic. Especially reactive oxygen compounds are known to foster oxidative stress and inflammatory processes, poly-aromatic compounds adsorbed at the surface of dust particles are mutagenic (Cassee et al. 2013).

The only way to reduce the mortality caused by particulate matter air pollution, is to control its emission and formation in the atmosphere, by limiting anthropogenic pollutant emissions into the atmosphere. Such emission reduction policies have been carried out to a degree in certain parts of the world, but the countries with higher risk factor for such diseases, i.e. countries with high population and uncontrolled air pollution have not yet reduced their emissions to an acceptable degree.

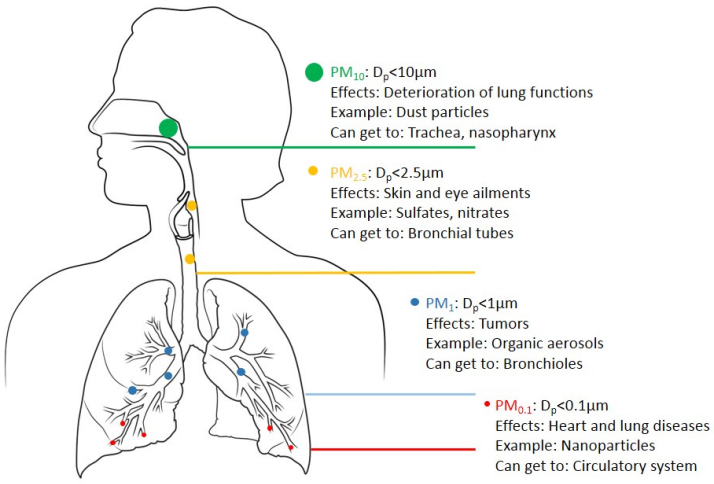


Figure I.7 – *Health impacts of aerosols and their penetration distance into the respiratory system by size.*

3.4 Effects of aerosols on climate

Atmospheric aerosols affect our climate in different ways:

- They can reflect or absorb the incoming solar radiation
- They can reflect or absorb the terrestrial radiation (to a much lesser degree)
- They can interact with clouds in complex ways leading to changes in cloud reflectivity and albedo, cloud lifetime, cloud height and cloud precipitation
- They can also change the soil albedo, but this effect is marginal compared to the others.

These effects are categorized in IPCC report (Edenhofer, Elgizouli, et al. 2014) as irradiance changes from Aerosol-Radiation Interactions (ari) and from Aerosol-Cloud Interactions (aci). Therefore, effective radiative forcing from aerosol-radiation interactions (ERFari) includes radiative forcing caused by direct and semi-direct interactions of solar radiation with aerosols and effective radiative forcing from aerosol-cloud interactions (ERFaci) includes radiative forcing from changes made by aerosols in cloud properties (figure I.8). Direct interaction of aerosols with solar radiation is when radiation is intercepted directly by a particle and this interaction results in either absorption or scattering of radiation, respectively causing heating and cooling effects for the atmosphere.

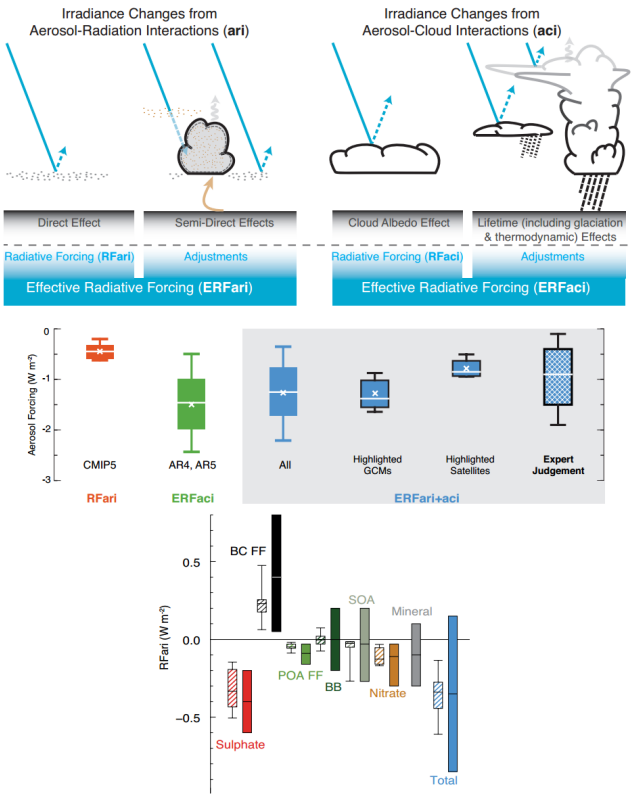


Figure I.8 – *Definition of direct, semi-direct and indirect interactions of aerosols with solar radiation and radiative forcing caused by direct, semi-direct and indirect interactions caused by total aerosols and different components (IPCC, 2014).*

Aerosol absorption may also decrease cloud cover since it heats the air, and as a consequence reduces relative humidity (known as the semi-direct effects), leading to a positive radiative forcing. The indirect effects include an increase in droplet number associated with increases in aerosols, leading to an increase in cloud albedo (reflectivity), and a decrease in precipitation efficiency associated with increases in aerosols.

The aforementioned interactions coupled with GHG increases cause the global climate to change. While the effects of GHGs is more straight-forward to calculate, the radiative forcing from aerosols is still one of the most uncertain parts related to climate change (Boucher et al. 2013). While GHGs in general cause warming of our atmosphere, aerosols, in their totality, are believed to have a cooling effect, counterbalancing a part of this warming. Figure I.8-a shows the ERFari and ERFaci and their sum (ERFari+ERFaci) for pre-industrial to present day period (1750-2011) calculated using global simulations, satellite data and expert predictions, showing a radiative forcing of around $-0.5\,\mathrm{W\,m^{-2}}$, $-1.5\,\mathrm{W\,m^{-2}}$ and $-1.3\,\mathrm{W\,m^{-2}}$ on average, respectively. For comparison, radiative forcing caused by carbon dioxide, well-mixed GHGs and ozone for the same period are around

$1.8\,\mathrm{W\,m^{-2}}$, $1.1\,\mathrm{W\,m^{-2}}$ and $0.4\,\mathrm{W\,m^{-2}}$ respectively. It is also important to bear in mind that while we already know that clouds can strongly affect climate, their effect on a future and thus warmer climate is not yet certain (meaning that the extent of its retroactions with climate are uncertain). For future climate studies, global models are used to simulate the cloudiness, but due to their too coarse resolution, cannot fully resolve these cloud fields. Therefore, the uncertainty of these models for future scenarios is high. This uncertainty results in the scatter of climate model ensemble results delivered by IPCC together with best estimates (Edenhofer, Elgizouli, et al. 2014).

While the totality of radiative forcing caused by aerosols seems to point to a cooling effect, it can be different if each aerosol component were to be analyzed separately. Figure I.8-b shows the RFari caused by different components of anthropogenic aerosols for the same period. The RF caused by almost all components points to a cooling effect except for black carbon (BC) and dust from arid regions (Johnson et al. 2004) which shows a warming one. BC, contrary to the other aerosols seems to have a heat absorbing property. The RFari for individual aerosol components is more uncertain than the total RFari.

The complexity of processes regarding aerosol formation and their uncertain effects on climate mean that studying these components in more detail is necessary, especially in a climatic context, where their complexity becomes two-fold (effect of aerosols on climate, effects of climate on atmospheric composition) because of the uncertainties involved.

4 Fine aerosol atmospheric observations

4.1 Measurements related to fine aerosols

Fine aerosols in the atmosphere include aerosols with an aerodynamic diameter less than $2.5\,\mu\mathrm{m}$ ($PM_{2.5}$). The chemical composition of fine aerosol fraction can be determined with different online or offline instruments. To determine the chemical composition of submicron particles for a long period of time, usually on-line methods such as aerosol mass spectrometers (AMS) are used, high resolution time of flight AMS (HR-ToF-AMS, Ng et al. (2011)) and quadrupole aerosol speciation monitors (Q-ACSM, Decarlo et al., 2006) are the most used in speciation of atmospheric submicron aerosol speciation. The main difference between these instruments is the system that each utilizes to separate ions, the ACSM uses electric fields accelerated by four cylindrical metal rods arranged symmetrically around the ion beam and the HR-ToF-AMS functions on the premise that after ionization, all ions (ideally) have the same kinetic energy and therefore smaller ions reach the detector in shorter flight times than larger ions. Whatever the method, they both measure the concentration of different ions present in submicron aerosols using the obtained mass spectra and its standard deviation. Using these data, a receptor modeling analysis can be performed to obtain different factors determining the true dimensional-

ity of the obtained data. This method called positive matrix factorization (PMF, Paatero (1997)) in the atmospheric scientific community allows to determine the origin (traffic, marine, etc.) of different components of PM_1, but it also enables the estimation of the oxidation state of submicron OA. In the classic utilization of the PMF method, three factors are identified for the oxidation state of OA: HOA (hydrogen-like organic aerosol, not oxidized), SVOOA (semi-volatile oxygenated organic aerosols) and LVOOA (low-volatility oxygenated organic aerosols) which correspond to newly emitted OA (POA, primary OA), newly formed SOA and aged SOA respectively. J. Jimenez et al. (2009) examined these factors for different parts of the world and showed, once again, a strong spatial variability in this aspect as well. Each of these factors can be highly variable depending on the region where the measurements are performed, for example, urban or marine areas show different characteristics, which will be discussed below.

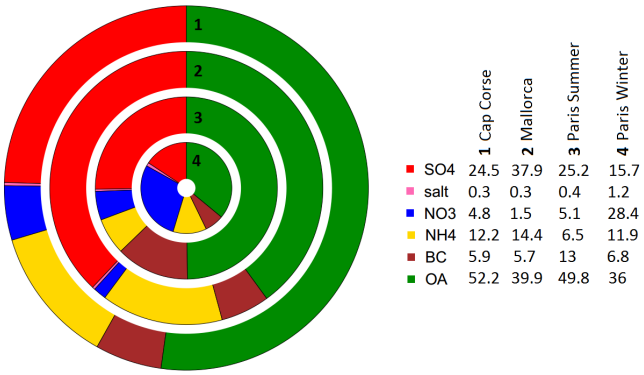


Figure I.9 – *Composition of PM_1 concentrations in Cap Corse, Mallorca and Paris.*

4.2 Spatial variability of fine aerosols

Fine PM show high spatial and temporal variations in the atmosphere, as well as high variability in sources and origins. To explain more, in figure I.9, the distribution of different components for PM_1 size fraction is shown for three measurement sites of the SAFMED campaign in Ersa and Es Pinar for the summer of 2013 and Sirta, Paris in 2009. The Es Pînar and Ersa stations will be discussed in more detail later, the Sirta station values is taken from Crippa, Haddad, et al. (2013) and Crippa, Decarlo, et al. (2013). As seen here, the distribution of different components in PM_1 changes between sites and seasons. The two Mediterranean sites show similar distributions with some minor differences, while the Parisian station shows a different structure. However, whatever the differences, it is visible that OA has an important contribution to the PM_1 concentration.

The total concentrations of PM_1 in these sites show strong variations as well, showing averages of $3.71\,\mu g\,m^{-3}$, $2.88\,\mu g\,m^{-3}$, $4.5\,\mu g\,m^{-3}$ and $14\,\mu g\,m^{-3}$ for Ersa, Es Pînar, Paris

summer and Paris winter respectively, attesting to the high spatial and temporal variability. If absolute values are compared, in the case of BSOA in summertime, the concentrations correspond to $1.93\,\mu g\,m^{-3}$, $1.125\,\mu g\,m^{-3}$, $1.62\,\mu g\,m^{-3}$ and $5.5\,\mu g\,m^{-3}$. If these values were compared to other sites in the world, this fact becomes more tangible. J. Jimenez et al. (2009) shows this fact for multiple sites globally, finding average concentrations of as high as $80\,\mu g\,m^{-3}$ (Beijing, China) with high variation in PM_1 components.

The high contribution of organic aerosols in the Mediterranean area shown in the previous section, justifies the need of studying this region in more detail. Alongside the organic fraction, the total aerosol burden in the area is high as well and the region has unique characteristics which will be explained in the following section.

5 The Mediterranean region

The Mediterranean Sea is the largest body of water in Europe, almost entirely enclosed by land, connecting to the Atlantic Ocean by the strait of Gibraltar, to the Black Sea by the strait of Bosporus and to the Red Sea by the artificially made Suez Canal. The Mediterranean Sea is enclosed by southern Europe from the north, the Middle East at the east, northern Africa in the south. It shares coasts with 22 countries in total. The surface of this sea is around 2.5 million km^2. The average depth of the Mediterranean is around 1,500 meters, with a maximum recorded depth of 5,267m in the Calypso deeps. A total of 10,000 islands exist in the Mediterranean Sea, including Corsica and Mallorca islands which will be discussed in more detail in the sections that follow, because they offer possibilities for remote atmospheric observations.

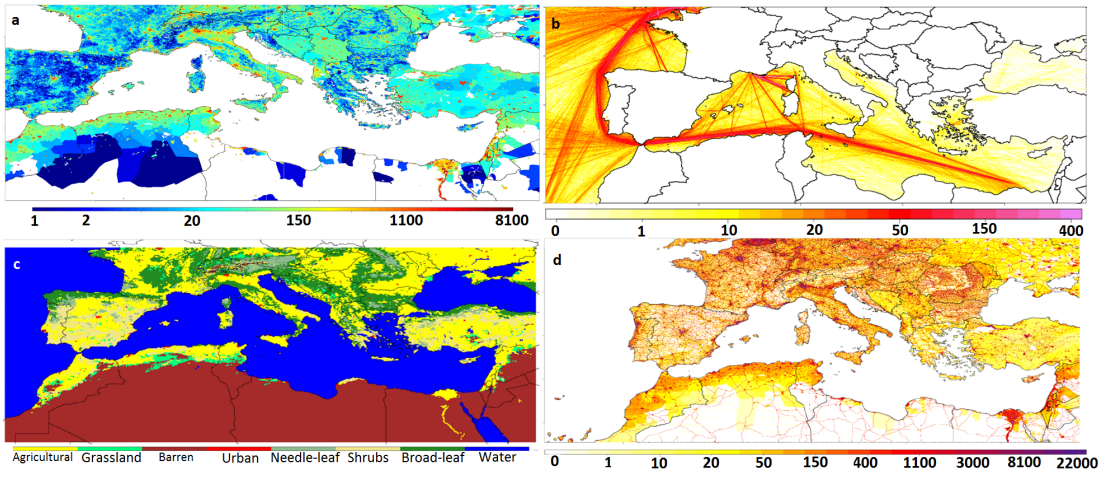


Figure I.10 – *Anthropogenic characteristics of the Mediterranean Sea: a: population density(person/m2), b: shipping routes, c: land use around the basin, d: roads around the basin.*

The density of population living in the Mediterranean coasts is quite high with a high spatial variability (figure I.10-a), from 1000 people.km^{-2} around the Nile delta to 20 people.km^{-2} around the coasts of Libya; the population growing from 95 million in 1979 to 143 million in 2000 and it is estimated to reach 174 million by 2025. Also, the basin counts 33% of the worldwide tourism, counting 306 million travelers out of 980 million worldwide in 2013. A 25-30% increase in this tourism is estimated till the year 2030 (Lanquar 2011). Apart from the anthropogenic emissions caused by a high density of population around the basin (I.10-d as an example for road traffic), the shipping emissions in the basin itself are important as well (figure I.10-b). The burden of merchant shipping traffic for the Mediterranean Sea is around 30% of the world-wide amount , the burden of emissions of nitrogen oxides, sulfur oxides and particulate matter is 3.5%, 3.9% and 3.7% respectively for the year 2015, of global emissions, all sectors confounded (Johansson et al. 2017). Land use for the Mediterranean region is highly diverse spatially (figure I.10-c), the European coasts, Turkish coasts and North West African coasts mostly contain agricultural lands, urban sites as anthropogenic sources and broadleaf forests and shrubs as natural uses; while north eastern African coasts mainly contain barren lands, with the exception of some areas like the Nile delta.

5.1 Atmospheric characteristics

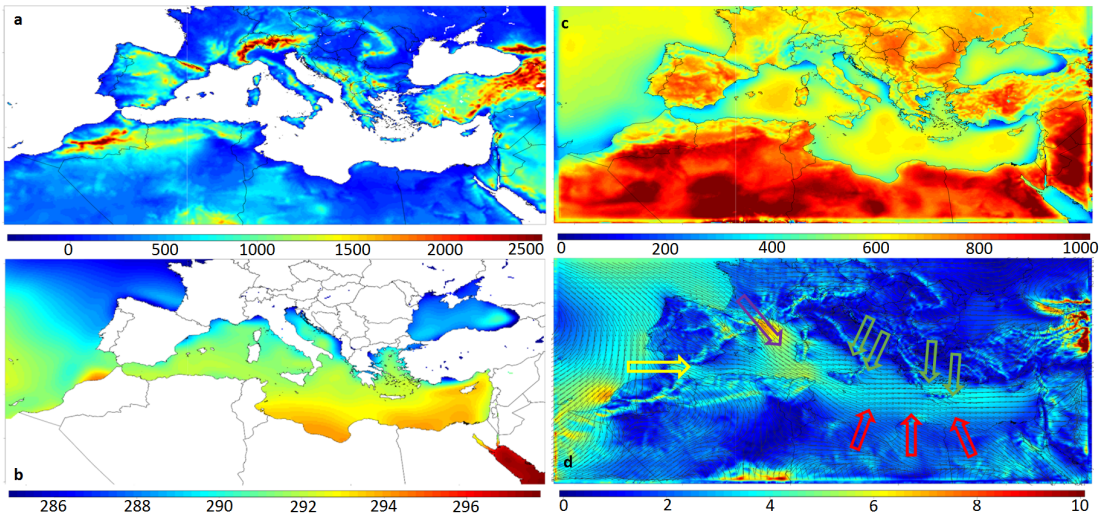


Figure I.11 – *Natural characteristics of the Mediterranean Sea: a: orography (m), b: planetary boundary layer height (m), c: sea surface temperature (k), d: wind speed (m/s), wind direction and major wind systems.*

The basin, especially the western part, is enclosed by land with elevated orography (figure I.11-a), creating barriers for the movement and transport of air masses and therefore keeping the air circulating within the basin. Like other bodies of water, on average, low boundary layer height is observed (figure I.11-b), the average being around 500m

for the basin (compared with around 800m for the European continent). The average 10m height wind speed is around $4m.s^{-1}$, with wind systems such as the Mistral, the Bora and the Etesian which can transport air masses from the European continent towards the basin, the Sirocco transporting African air masses, and the Westerly transporting western air masses (figure I.11-d). With these strong wind systems transporting pollutants towards the basin and the high altitude lands enclosing the basin, the chances of an air mass staying in the basin and circulating locally within the basin are quite high, resulting in high residence times for pollutants in the region.

The sea surface temperature (SST) is on average around $20\,°C$ (figure I.11-c); two quite different profiles are seen for the SST in the northern and southern parts of the basin (and in consequence western and eastern parts as well) for the SST. The Mediterranean climate consists of hot dry summers and rainy winters. This region is at the crossroads of the descending branches of both large-scale convective motions, Hadley and Walker cells, resulting in lower than usual mixing depths which prevent efficient dispersion of pollutants, especially in the eastern part of the basin (Dayan et al., 2017). The western part is affected by the transport of air masses from the northern American as well. Moreover, high solar radiation during summer provides the conditions for high photochemical activity. It is also important to take into account that deposition is generally less favored over the water for compounds with low solubility like ozone than over vegetation. These factors result in high ozone concentrations during the summer period for the whole basin, as well as increased PM concentration. This is contrary to what is seen in central Europe, where PM concentrations are maximum during winter because of lower boundary layer heights, more SVOCs and inorganic compounds (such as nitrates and ammonium) in the particulate phase due to of lower temperatures.

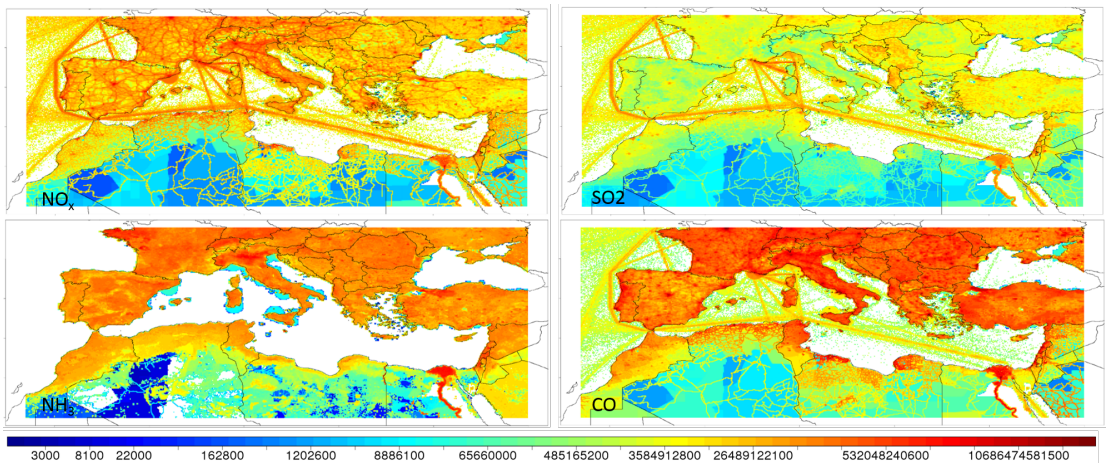


Figure I.12 – *Anthropogenic aerosol emission sources that affect the Mediterranean basin for NO_x, SO_2, NH_3 and CO in molecules.cm^{-2}*

The Mediterranean Sea is subject to multiple aerosol sources (emission sources of

pollutants in figure I.12), both natural and anthropogenic, making the aerosol burden in general in this area quite high (Lelieveld et al. 2002). Biogenic aerosol sources are mainly transported from Europe (K. N. Sartelet et al. 2012), while anthropogenic sources are transported both from Europe and Africa; dust particles enter the area mainly from the African coasts (Bouchlaghem et al. 2009; Vincent et al. 2016); and biomass burning generates aerosols that come from Spain, Europe and Africa to the basin especially during the summer period (M. O. Andreae and Merlet 2001; Korontzi et al. 2006). In addition, local emissions such as shipping emissions (Marmer et al. 2009), sea salt and other marine aerosols (Schwier et al. 2017) also contribute to the aerosol burden in the area (figure I.12).

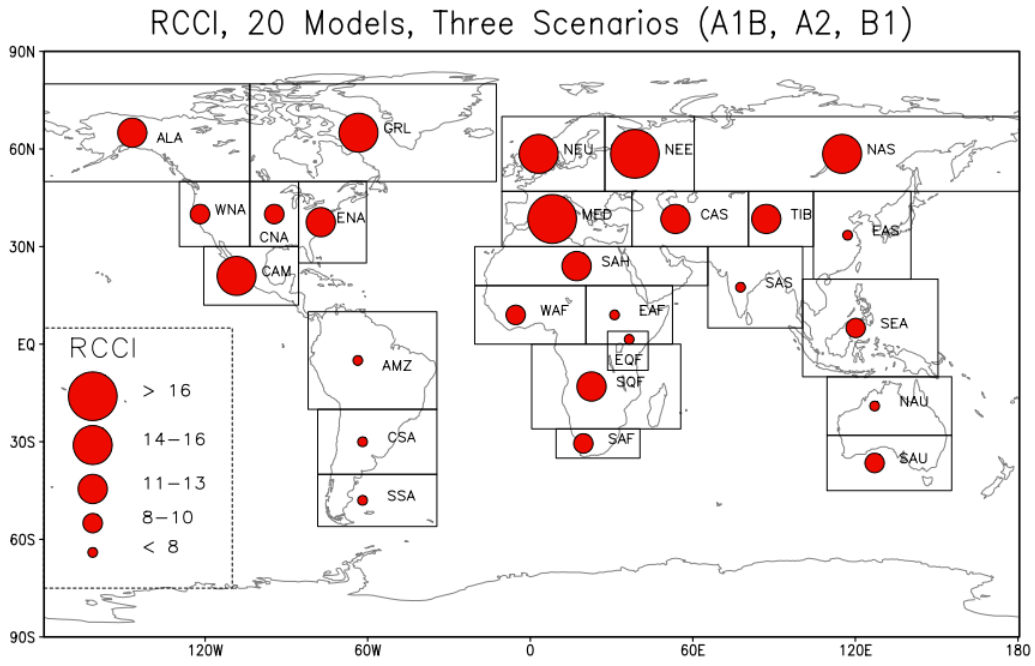


Figure I.13 – *RCCI (regional climate change index) value calculated using 20 global climate models for three SRES scenarios: A2, B1 and A1B. Image is taken from Giorgi, 2006.*

The Mediterranean region is identified as one of the hotspots for climate change, meaning that it shows high sensitivity to changes of climate in future scenarios (Giorgi 2006). Giorgi, using an ensemble of global climate models and three climatic scenarios (A1B, A2 and B1 IPCC-SRES scenarios, Ipcc 2000; Bernstein et al. 2007), calculates a regional climate change index (RCCI) based on regional mean precipitation change, regional mean surface temperature change and changes in inter-annual variability of precipitation and temperature. This index was calculated for 26 different regions of the world, to estimate the most responsive regions to climate change. Giorgi then concludes

that the Mediterranean and North Eastern Europe are the principal hotspots (figure I.13). Other studies were performed by other researchers concluding high sensitivity for the Mediterranean region (Adloff et al. 2015; Ciardini et al. 2016).

In light of all these factors, studying the Mediterranean region becomes interesting and necessary. This is true for both occidental and oriental sides of the basin, but the amount of literature existing for the eastern basin is much more than that of the western region area (Lelieveld et al. 2002 ; Bardouki et al. 2003 ; Sciare, Oikonomou, Cachier, et al. 2005 ; Koçak et al. 2007 ; Koulouri et al. 2008 ; Sciare, Oikonomou, Favez, et al. 2008). Among the research done for the western basin, studies focusing on gaseous species and their reactivity seems to prevail and not much attention has been given to the aerosol formation in the area, especially when speaking of organic aerosols.

To summarize, the Mediterranean basin is impacted by multiple sources for aerosols in and around the basin, intense photo-chemical processes, high population density and high climate sensitivity; these reasons make studying the Mediterranean interesting and they also underline the importance of measurement campaigns and measurement-simulation comparisons for this basin.

5.2 The ChArMEx campaign

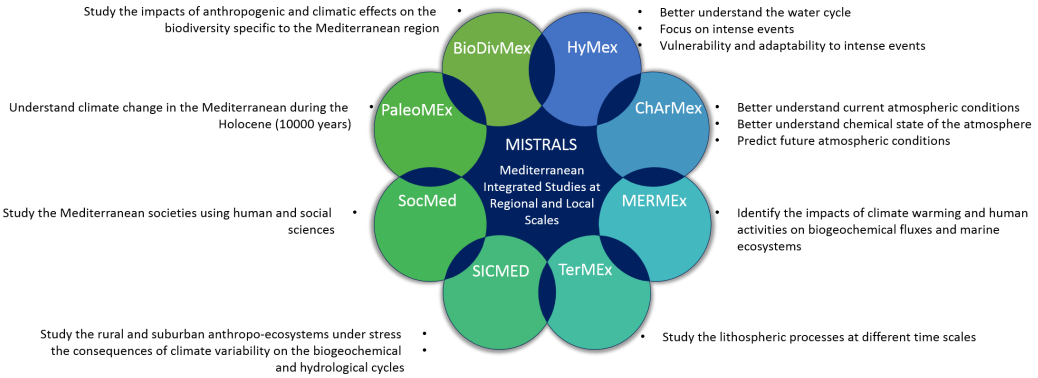


Figure I.14 – *MISTRALS axes*

The MISTRALS (Mediterranean Integrated Studies at Regional and Local Scales, http://www.mistrals-home.org) program was initiated, with the aim of focusing the efforts of the international environmental research communities in different fields around the Mediterranean basin. The program started in 2010 and is to continue its activities for 10 years, covering 8 different axes: HyMeX (Hydrological cycle in the Mediterranean eXperiment, https://www.hymex.org), ChArMEx (Chemistry-Aerosol Mediterranean Experiment, http://charmex.lsce.ipsl.fr), MERMEx (Marine Ecosystems Response in the Mediterranean Experiment, https://mermex.mio.univ-amu.fr), SocMed (Sociétés en Méditerranée), TerMEx (the Terra Mediterranean earth science Experiment), SICMED

(Surfaces et Interfaces Continentales Méditerranéennes), PaleoMEx (Paleo Mediterranean Experiment) and BioDivMEx (BioDiversity of the Mediterranean Experiment). The principal goals of each of these axes is shown briefly in figure I.14.

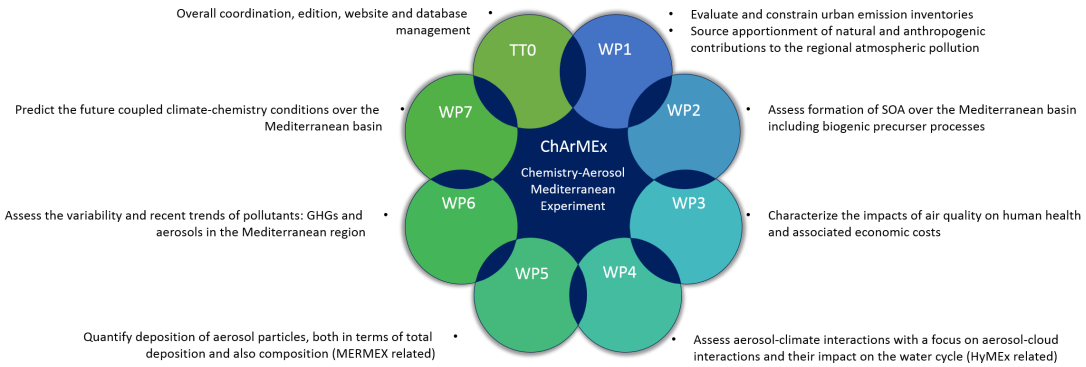


Figure I.15 – *ChArMEx project work packages*

The current thesis is a part of the ChArMEx project, which aims to evaluate the current and future state of the Mediterranean atmosphere and to understand the impacts of the atmospheric conditions in the basin on the regional climate, air quality, human health and marine biogeochemistry. To achieve these goals, the project was divided into seven work packages (WPs): source apportionment, chemical processes, health impacts, aerosol properties and climate impacts, deposition, variability/trends and future (figure I.15). While there is some overlap between different work packages, this thesis is mainly based on the goals aimed to be achieved by WP2 and WP7: to understand and to quantify the formation processes of secondary compounds over the Mediterranean basin with regards to the unique conditions of this basin and to estimate future changes in the basin. In particular, one of the main goals of WP2 is to use the measurements obtained during the different observational periods of the ChArMEx campaign to better understand the atmospheric conditions especially regarding the production of photo-oxidant and organic aerosol production in the western Mediterranean basin. The second objective of this WP is to evaluate atmospheric models by comparing simulated concentrations of different components to measurements and to identify necessary improvements taking into account the specific conditions of the Mediterranean basin. Such atmospheric models can then be used in WP7 to predict future changes in the basin.

Many different observation periods were performed during the ChArMEx campaign. One period that interests this work is the SAFMED (Secondary Aerosol Formation in the MEDiterranean) SOP 1b (Special Observation Period 1b) sub-campaign. This campaign took place during the summers of 2013 and 2014 (the results obtained during the summer of 2013 are used in this work). The general goal of SAFMED is to understand the origins of high SOA concentrations observed over the western Mediterranean during the summer. While the ChArMEx campaign covers the whole Mediterranean, the SAFMED

part of this campaign only concerns the western basin of the Sea. Since the focus of this thesis is the western Mediterranean as well, the data from this project will be used in this work. Figure I.16 shows the location and type of measurements performed during the SAFMED SOP 1b campaign in 2013, during this campaign, the Ersa supersite, located in the northern Corsica was decided to be chosen as a representative site for the whole western Mediterranean basin.

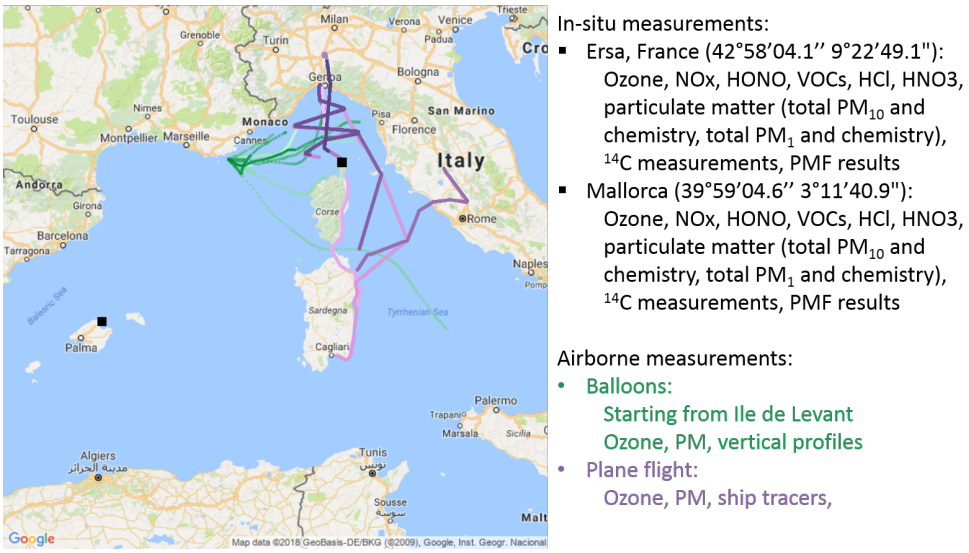


Figure I.16 – *SAFMED SOP 1b measurements*

6 Thesis goals

The Mediterranean region, as mentioned before, presents its own particular characteristics. High aerosol burden, high pollutant transfer towards the basin, high solar radiation which results in high oxidant levels, and on the other hand, an important population density and high climatic sensitivity makes this region an essential object to study. As explained before, the studies covering the western Mediterranean basin focusing on the chemical composition of this region are scarce, which is why this work is focused on the aerosols in the western basin. In light of these facts, the general goals of the current thesis are the following:

- Goal 1: Achieve a better understanding and quantification of sources and formation processes of OA (and also other particles) in the western Mediterranean basin
- Goal 2: Study the impacts of climate change on the atmospheric conditions and air quality of the western Mediterranean basin on different scales

The first goal is important on its own, since it answers many of the issues raised in this introduction about the Mediterranean atmosphere, therefore it is necessary to achieve the goals assigned in this part in order to be able to proceed to the second part. The two goals are intertwined when it comes to understanding the performance of the model in this region: without a good grasp on the performance of the model and without finding the most appropriate parameterization for the simulation of the Mediterranean basin (e.g. the results of goal 1), the second goal could not be achieved. The two goals each follow a different methodology which will be discussed in the following sections:

6.1 Model evaluation and amelioration for the western Mediterranean basin

The focus of this part is to characterize the aerosol composition in the western Mediterranean basin, by the means of a 3D chemistry-transport model (CTM, in the case of this thesis the CHIMERE model). This study is based on the measurements achieved during the ChArMEx project, which gives the opportunity of precise and rigorous observation-simulation comparisons. Because of the aforementioned particularities of this region, improvements to the model might be necessary in order to fully represent the western Mediterranean basin. Among the studied components, a special focus has to be given to organic aerosols, which have a high concentration in this region and also their simulation is more difficult in CTMs.

The methodology of achieving this goal is to first, effectuate a thorough evaluation of the CHIMERE model. This evaluation is done by first, preparing the model for an initial simulation, and then comparing the resulting simulations with observations obtained for the same period. As a consequence of this step, the weak points of the model for this specific region of the world can be pinpointed. The second step is to implement changes in the model in order to mend the weak points identified in the previous step. An important attention is given to OA simulation when these modifications are performed. This modified version of the model can be further used in the other parts of the thesis, identification of sources and origins of aerosols is done using the modified model.

6.2 Future conditions of the Mediterranean basin in different scales

The second part of the thesis envisions to understand the changes and their intensity in future scenarios for the Mediterranean basin. The focus of this part is on the PM and organic aerosols because of the problematic explained before. Because of the importance of OA in this region, special attention is given to this type of aerosol, both in regards to its future concentrations and also the changes that its concentration can show because of different forcings. This goal applies not only to the basin on its entirety, but also to a more local scale (PACA region in the south-eastern coasts of France), where the exposure of the population living around the basin is explored in future scenarios to find the extent of the effects on the increasing population due to changing climate.

The approach taken in this phase is to in the first place, study the conditions of the Mediterranean basin in different future scenarios. In this part, a thorough comparison of different future scenarios to historic simulations is performed for the whole basin and then compared to the European region, in order to identify the differences between the two areas. The goal of the thesis is to study PM and especially the OA, therefore, an analysis of the changes of PM in total and different PM components is performed, including OA. Certain factors contributing to PM concentration changes in future scenarios are identified and the amount of the impact of each one is calculated. Using the modified model obtained from the first phase, the effect of changes in OA simulation methods is also studied.

Second part of this phase, is to focus on local air quality changes in future scenarios for the Mediterranean basin. In this part, the simulations from the previous part are used as boundary conditions for a smaller domain focused on the southern coasts of France with the Mediterranean Sea. The air quality of these regions is studied for 2030s and 2050s using future anthropogenic emissions corresponding to each period and the impact of climate change on the population of these areas is calculated.

As a summary, the goals of the two phases are to:

- Phase 1
  - Evaluate the CHIMERE model for the Mediterranean area (chapter III)
  - Modify the model taking into account the specific conditions of the Mediterranean basin (chapter III)
  - Identify the sources and origins of OA in this region (chapter IV)
- Phase 2
  - Study future scenarios with a focus on PM concentrations (chapter V)
  - Identify and quantify factors contributing to the changes in PM concentrations in future scenarios (chapter V)
  - Quantify the effects of changes in the OA simulation scheme used in future scenarios (chapter VI)
  - Study the effects of climate change on the air quality of southern coasts of France and its consequences on the population of this area (chapter VII).

CHAPTER

II

Atmospheric modeling

Contents

1 Fundamental basis of chemistry transport models **45**
2 The CHIMERE chemistry transport model **48**
2.1 Inputs and outputs 48
2.2 Physical processes and chemical mechanisms in CHIMERE . . . 51
3 Simulation of organic aerosols in atmospheric models **58**
3.1 Two-product schemes 59
3.2 Volatility basis set 61
3.3 Carbon number - polarity grid (np+mP scheme) 66
3.4 Statistical oxidation model 66
3.5 Molecular schemes 68
4 Simulation of organic aerosols in CHIMERE **69**

Summary.3D modeling of the chemical composition of the atmosphere is a relatively new science. The simulations done with these models can be global with less horizontal resolution and less details on the chemical composition or they can be regional with higher resolution and more simulated species. Of course, given that the atmospheric chemistry and physics are complicated topics, in order to afford the computational needs necessary, simplifications have to be done both in chemistry and in the solving of equations regarding physical processes. Numerous chemistry-transport models (CTMs) exist that are used for this purpose, the basis for which are discussed in this chapter (section 1). The focus of this thesis is on the CHIMERE CTM, therefore the explications on the different modules of a CTM will be presented for the CHIMERE model (section 2). The simulation of OA is what we want to improve in the Mediterranean basin, therefore a detailed review of different schemes implemented in different CTMs has been included (section 3). At the end, a short discussion about OA simulation schemes that have been added and tested in CHIMERE has been included (section 4).

3D modeling of the atmospheric composition is performed by global chemistry models or rCTMs. Global chemistry transport models simulate the concentrations of multiple atmospheric components for the globe, they may be coupled with an online general circulation model or use the information produced by one in an off-line fashion. rCTMs, however, only simulate a chosen region, but with a better horizontal resolution and often with a larger number of simulated species and included reactions. In this work, an rCTM is used, which will be introduced shortly.

History of atmospheric modeling is intertwined with efforts to create a method for meteorological forecast. The basis of most of the early models in this area was Bjerknes' theorem which was developed late 1800s and early 1900s (Bjerknes 1902). He actually proposed the idea that using his theorem, it would be possible to predict what the atmospheric meteorological conditions would be in a few hours (Thorpe et al. 2003). Using his theorem, Richardson developed a primitive meteorological prediction model, which was supposed to predict one day of meteorological conditions, using a room full of people as 'calculators' who did calculations manually and each passed their calculations to the next person. Like Peter Lynch says in his book (Lynch 2006) his model failed to do what it was supposed to, while he also explains that the reason for the failure was not in the physical processes used, but because of not applying smoothing techniques to the data. This was the first effort in simulating atmospheric conditions. In 1940s when computers were invented, weather forecasting became feasible. After the suggestion of Von Neumann in 1946, a project was started to dedicate a recently developed computing system (the ENIAC) to weather forecasting. Charney in 1949 performed the first successful numerical weather prediction using a 1D model (Charney and Eliassen 1949). Since then, weather forecast models have come a long way. After first successful attempts in meteorological modeling, atmospheric modeling was extended to chemistry, first treating a limited number of chemical reactions in order to see the chemical evolution of certain species. The first global chemistry-transport models were developed in the 1970s (Holloway et al. 1971; Arakawa and A. 1972; etc.), although the complexity of the chemical scheme followed the available computational power directly. The first rCTM, was developed in 1980s (Robbins et al., 1980; Eliassen et al. 1982; Garcia and Solomon 1983; Owens et al. 1985; etc.).

1 Fundamental basis of chemistry transport models

A CTM uses the mass conservation equation for each component used in the model to determine the changes in its concentration:

$$\frac{\partial C_i}{\partial t} = (\frac{\partial C_i}{\partial t})_{chemistry} + (\frac{\partial C_i}{\partial t})_{emissions} + (\frac{\partial C_i}{\partial t})_{advection} + (\frac{\partial C_i}{\partial t})_{diffusion} + (\frac{\partial C_i}{\partial t})_{deposition} \quad \text{(II.1)}$$

Equation II.1, called the mass conservation equation, contains all the source and the sink terms for each chemical component in the model; therefore, solving this equation

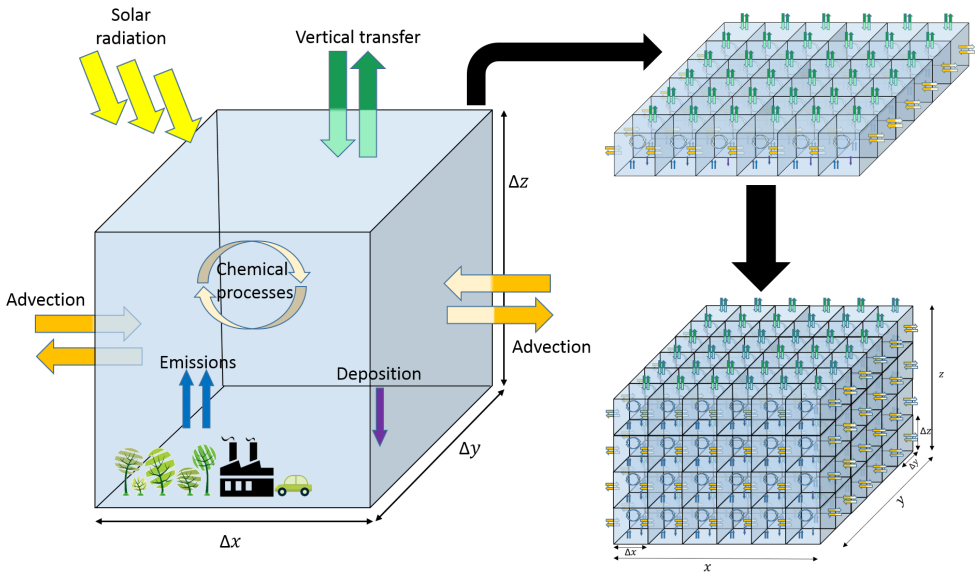


Figure II.1 – *A simplified representation of what a CTM looks like: In each cube, the time evolution of chemical species is calculated taking into account different processes, then the interaction between horizontal and vertical cubes covering the simulation domain is simulated.*

would give the concentration of a given species for a given time. However, solving this equation analytically is possible only for extremely simplified cases. These cases, obviously do not in majority of circumstances comply with the complexity of the atmospheric physics and chemistry. Therefore, it should be solved numerically.

One way to achieve that goal is to discretize in time and space, cutting the desired simulation domain into small cubes both horizontally and vertically (figure II.1). For each cube, the sources and sinks are calculated, and the interactions between neighboring cubes are taken into account. Generally, the hypothesis is made that the concentration of each species in each cube is homogenous. If n variables are considered and the domain has m cubes, a system of n×m equations with n×m unknowns should be solved in order to provide the necessary output for each time-step. As an example, a domain covering the European continent with a horizontal resolution of 0.44° and 9 vertical levels would have around 70000 cubes (m=70000). If around 100 species were to be simulated (n=100, which is a relatively low number of species for rCTMs), the number of unknowns would be around 7×10^6. Solving this number of differential equations has to be done using numerical methods. Numerical solvers used in chemistry-transport models can be divided into two types: explicit and implicit ones. An explicit solver implies that a direct computation of the desired unknown is possible and the variable is not dependent to other variables, while in an implicit solver coupled sets of equations or a matrix based solution has to be used, since variables are dependent to each other and

have to be solved simultaneously. Implicit methods use an iterative approach to function, while semi-explicit solvers combine both explicit and implicit methods. In iterative methods, an initial guess is used, and then the equation is solved multiple times, each time improving the solution (in a stable case) with the number of iterations decided by the user. As it can be guessed, the higher the requested number of iterations, the higher the time necessary to solve the equation and in most cases, the higher the accuracy of the resulting solution. In this way, the aforementioned equation is solvable in each cube.

To solve the mass conservation equation, some input information needs to be provided to the CTM. An rCTM does not cover the whole globe, therefore, boundary conditions are necessary, which are provided either by global chemistry models or by bigger-domain simulations with the same rCTM. This technique, imbricating smaller and spatially better resolved ones in a larger domain is called grid-nesting. Initial conditions are also used in order to provide information about the existing atmospheric chemical conditions of the region, which are fed to the model the same way as boundary conditions only for the first time-step. Anthropogenic and biogenic emissions of different components have to be presented in the model as inputs. In addition, the rCTM needs information about the land use types of the simulation domain. Each CTM contains information about chemical and thermodynamic properties of different species, reactions types and their speeds, which are normally obtained from dedicated laboratory experiments, such as atmospheric chamber studies.

Each CTM has several modules, treating chemistry, transport, deposition, etc. processes. Some of them provide additional information as well, for example the size distribution of aerosols can be calculated in some CTMs, while others only give the total amount of aerosols. The chemistry module in each CTM revolves around a chemical mechanism, which is an essential part of the inner working of the model. A chemical scheme represents the reactions and species that exist in our atmosphere and it can be divided into two types: explicit and reduced schemes. Explicit mechanisms contain a detailed chemistry of reactions and species. For example, Generator for Explicit Chemistry and Kinetics of Organics in the Atmosphere (GECKO-A, **Aumont2005a**) is a box-model that is used to generate explicit chemical schemes for different atmospheric species. While the mechanism created by these types of models is very complete, it is too heavy to be implemented directly into CTMs because of the high number of species and reactions contained in them. That's why reduced schemes are created, where species with similar chemical and thermodynamic properties are grouped (lumped) together in order to reduce the number of the reactions and components in the model. This grouping of species especially concerns VOCs, since their numbers are high and their chemical properties can be close to each other. The lumped species can be decided in two fashions, either by the properties of a real species, meaning that all species close to that component are lumped together, or by a fictive average species, meaning that an average of a group of species is assigned to a lumped group.

It is important to mention that each CTM is different. They normally have their own

specific modifiable options. For each CTM (sometimes even for different versions of one CTM) the input information has to be provided in a specific format. The thermodynamic and chemical information used by each CTM can be unique to that CTM. The coding (language, functions, order of functions, etc.) is generally specific for each CTM. This is why we see comparisons of different CTMs to each other in inter-comparison studies (for example EURODELTA project, Bessagnet, Pirovano, et al. 2016), especially when all the input information are kept the same in order to compare these models.

The main processes used in the CHIMERE CTM, the model used in this thesis, is explained in the section that follows.

2 The CHIMERE chemistry transport model

CHIMERE is an offline Eulerian rCTM which can be used for physical and chemical processes research, climatological and future scenario runs and operational air pollution forecasts (Menut, Bessagnet, et al. 2013). Like other atmospheric models, it needs external forcings to function: meteorological fields, boundary conditions and information on emissions of atmospheric pollutants. Using this information, CHIMERE can simulate the concentrations of a chosen list of species in a continental or regional scale over a range of horizontal resolutions from 1km to 100km. The first version of the model was released in 1997, covering just gas-phase chemistry. First studies performed with this model aimed at better understanding the photo-oxidant chemistry around Paris area (Cécile Honoré et al. 2000; Menut, Vautard, et al. 2000; Robert Vautard et al. 2000). In 2004, a module was added to the scheme making it capable of simulating aerosol components as well as gaseous species (Bessagnet, Hodzic, et al. 2004). Since then, it has grown and (as of the writing of this thesis) its last version is the CHIMERE2017b. In this work, two different versions of the model are used: 2013b and a modified version of 2014b. The inputs needed, the major processes and outputs are shown in figure II.2.

2.1 Inputs and outputs

First step in running CHIMERE is choosing the horizontal and vertical resolutions of the domain of the simulations. The horizontal domain can be rectangular or it can be quasi-rectangular with a small increment in order to take into account the surface changes in higher and lower latitudes.

The vertical domain is defined by hybrid sigma-p coordinates, meaning that the surface pressure scales the levels. The number of vertical layers can be chosen by the user. The algorithm allows layer thickness to change exponentially in the lowest 200hPa of the atmosphere, and have constant thickness (in pressure coordinates) from 200hPa to the top of the atmosphere.

The land use data is then extracted using the horizontal domain. Two options are available for land use data inputs: GLCF (http://glcf.umd.edu/data/) or Globcover

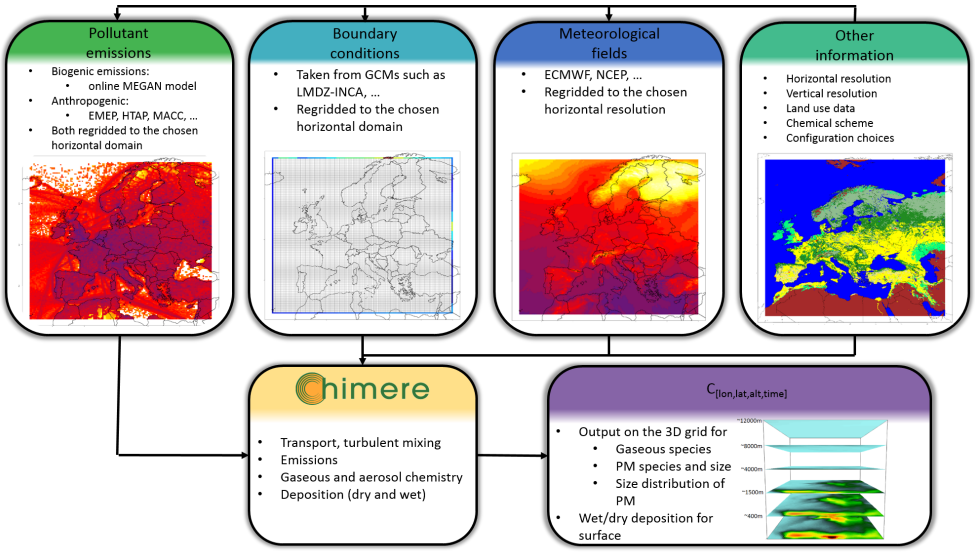


Figure II.2 – *Inputs needed, the major processes and outputs in CHIMERE.*

(Arino et al. 2008; Bicheron et al. 2011). The resolution of these two databases are 1km×1km and 300m×300m respectively. Globcover originally contains 22 classes and is derived from satellite data, the version used in CHIMERE has 8 classes: Agricultural lands, glass lands, Barren lands, inland water, urban, shrubs, needle leaf forests, broadleaf forests and oceans.

CHIMERE, in its standard chemical scheme, uses anthropogenic emissions of 23 species, which have to be provided as an input. Although this data can be delivered by different emission inventories, specific factors, such as the coverage area, the resolution, the species, etc. should be considered when choosing the emissions inventory. The default anthropogenic emissions in CHIMERE is the EMEP (European Monitoring and Evaluation Programme, Vestreng et al. 2007; http://www.ceip.at/) emissions inventory which provides annual data for NO_x, Non-Methanic Volatile Organic Compounds (NMVOCs), SO_x, CO, $PM_{2.5}$ and PMcoarse for 10 activity sectors (SNAP, Selected Nomenclature for Air Pollution). This annual data is distributed into monthly emissions for species used in the model by passing through an aggregation table using (most commonly) the emiSURF interface. The same aggregation table is used to distribute NMVOC emissions into individual species, then to group them again according the lumped species used in the model. Any other emission inventories such as edgar-HTAP (Hemispheric Transport of Air Pollution; http://edgar.jrc.ec.europa.eu/htap_v2/index.php), MACC-TNO (Kuenen et al. 2014), ECLIPSE (http://www.iiasa.ac.at/), etc. can also be used in the model if they have annual data for these activity sectors for at least species mentioned above and the desired region. It is important to mention that these emission inventories might have major differences with each other, either because of the method used in their construction (top-down, bottom-up) or the raw information

used by the developer, therefore inter-comparison studies exist for different emission inventories (Granier et al. 2011; Pouliot et al. 2012). Almost each of these inventories has a different horizontal resolution. Although in emiSURF means for downgrading emissions to finer resolutions has been provided, it is better to use anthropogenic emissions with higher default horizontal resolution for finer domains. Fire emissions can be prepared for the model as well, using another interface called APIFLAME (Turquety et al. 2014).

Biogenic emissions in CHIMERE are taken from an online module implemented inside CHIMERE called Model of Emissions of Gases and Aerosols from Nature (MEGAN, Guenther et al. 2006). MEGAN provides emission factors for isoprene, limonene, α-pinene, β-pinene, ocimene, and some other monoterpenes with a horizontal resolution of 0.008×0.008. In calculating biogenic emissions, meteorological parameters such as wind speed, solar radiation, actinic flux and monthly leaf area index (LAI) are taken into account. Bear in mind that the MEGAN implemented in CHIMERE is a reduced version of this model and some of its options are not available (as an example CO_2 attenuation, O_3 effects on isoprene emissions, effects of humidity on emissions).

Salt emissions from the sea surface in the model are optionally calculated using the parameterization proposed by Monahan (1986). Sea salt can be likewise treated as inert species not interacting with other species in the atmosphere, or as reactive species (Na^+, Cl^-, SO_4^{2-}) interacting with others.

Dust emissions also can be activated in the model. The parameterization is different for emissions originating from Africa or Europe. For African dust emissions the scheme from S. C. Alfaro and Gomes (2001) and the optimizations from Menut, Schmechtig, et al. (2005) are used. The model proposed by S. C. Alfaro and Gomes (2001) is the combination of saltation flux calculation proposed by Marticorena and Bergametti, (1995) and sandblasting model by S. Alfaro et al. (1998). The dust emissions over Europe follow a simplified version of the same scheme, close to what is proposed by Zender et al. (2003). Since dust emissions from continental Europe are not comparable in their intensity with those of African area, a simplified scheme was deemed to be sufficient.

Modules capable of treating and regridding meteorological information from two sources are implemented in CHIMERE: the ECMWF data (https://www.ecmwf.int) or outputs of the WRF model (Weather research and forecast, Wang et al. 2015). The ECMWF data can be used directly in CHIMERE, while in order to prepare WRF data, the WRF model has to be used separately. In other words, the WRF model has to simulate a domain a little bigger than what is going to be used in CHIMERE using NCEP data (National Centers of Environmental Predictions) reanalysis meteorological data (http://www.ncep.noaa.gov) with a base resolution of 1°. The WRF model includes an impressive list of modifiable parameters for meteorological simulations.

Boundary conditions are taken from global chemistry model simulations in case of a domain covering the whole Europe in CHIMERE. For example, LMDZ-INCA (Hauglus-

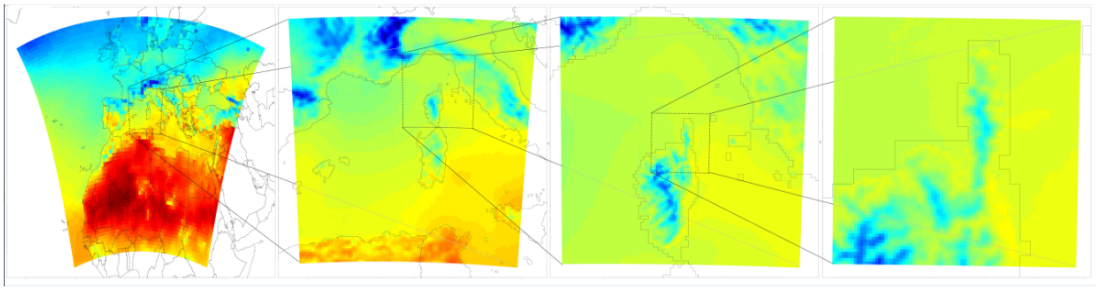


Figure II.3 – *The process of nesting smaller domains inside a continental domain: The domain on the left side uses global chemistry transport simulation results as boundary conditions, the rest use the results from the previous bigger domain as boundary conditions.*

taine et al. 2014), GOCART (Ginoux et al. 2004) or C-IFS from the CAMS project (https://atmosphere.copernicus.eu/) global models can provide this information; modules of extracting and regridding this information are already present in CHIMERE. For smaller domains, it is preferred to use the simulations from a bigger domain with lower resolutions for the same period as boundary conditions. Sometimes a higher resolution for a specific part of the domain is desired, in this case "nested" domains can be used in order to use a bigger but coarser domain as boundary conditions for the smaller one. The bigger domain still has to use data from global chemistry models as boundary conditions. Figure II.3 shows the nesting process for a coarse domain with three nested domains inside.

With all the input information provided, CHIMERE can simulate the concentrations of a list of gaseous and particulate species depending on what options were activated in the model. Hourly time steps are provided for all output species; for dry and wet deposition, 12 hour sums are provided for each component.

2.2 Physical processes and chemical mechanisms in CHIMERE

2.2.1 Horizontal and vertical transport and turbulent mixing

Three parameterizations are available for horizontal transport:

- First order upwind scheme: A simple scheme that does not need much computational power, in return it is not very accurate.
- Second order Van Leer scheme (Leer 1979): More complex and more accurate than the upwind scheme, in return it needs more computational sources.
- Third order parabolic piecewise method (PPM, Colella and P. R. Woodward 1984) scheme, accurate, little diffusive, but time consuming.

Vertical transport advection is calculated in a way that vertical wind speed balances horizontal divergence/convergence. For the first layer, the lateral incoming and outgoing fluxes for each cell are calculated and this value is balanced with an incoming/outgoing flux from the upper border of each cell. After the first layer, the calculation is repeated for all cells of the second layer, using all lateral fluxes and those to the first layer. This is repeated in a recursive manner until the top layer. Vertical transport is represented by the two first mechanisms presented for horizontal transport (the upwind and the Van Leer schemes). The Van Leer scheme used by default is on the second order, therefore, the necessary information cannot be assured for the first and the last layers of the simulation, since a second order scheme requires information from at least the previous and the next layers. Therefore, the scheme is changed automatically to the upwind scheme for these two levels even if the Van Leer scheme is activated.

At each layer change, a turbulent mixing flux for that layer (layer k) is calculated using:

$$Flux = V_k \frac{C_{k+1}(\frac{D_k}{D_{k+1}} - C_k)}{H_k} \tag{II.2}$$

Where,

$C \rightarrow$ Concentration

$H \rightarrow$ Layer thickness

$D \rightarrow$ Density

$V_k \rightarrow$ Equivalent turbulent vertical velocity

The density dependent ratio is used in this equation since the mass should be conserved between the two layers. The same equation is repeated for the upper layer. And V_k is calculated by:

$$V_k = \frac{K_z}{\frac{1}{2}(H_k + H_{k+1})} \tag{II.3}$$

Where K_z is the vertical turbulent diffusivity which is calculated using the Troen and Mahrt (1986) method.

2.2.2 Deposition

The dry deposition of gases is treated with an analogy of resistances (Wesely 1989), corresponding to the inverse sum of aerodynamic resistance, laminar boundary layer resistance and surface resistance:

$$\nu_d^i = \frac{1}{R_a + R_b^i + R_c} \tag{II.4}$$

Where,

$\nu_d^i \rightarrow$ Deposition speed for the gaseous species i

$R_a \rightarrow$ Aerodynamic resistance

$R_b^i \rightarrow$ Quasi-laminar boundary layer resistance

$R_c \rightarrow$ Surface resistance

The aerodynamic resistance is the resistance to vertical transfer from a given level in the surface layer to near the surface. Quasi-laminar resistance depends on the atmospheric turbulence as well the molecular diffusion of gas i. Surface resistance is a combination of parallel resistances itself, each corresponding to soil, plant surface, plant stomata, plant mesophyll, etc. Aerodynamic and boundary limit resistances are calculated using meteorological parameters (friction velocity, u^* and the Obukov length, L).

Dry deposition for aerosols is calculated with the same analogy, but the sedimentation velocity (J. Seinfeld and S. Pandis 2016) has been added to the equation:

$$\nu_d = \nu_s + \frac{1}{r_a + r_b + r_a r_b \nu_c} \tag{II.5}$$

Where,

$\nu_d \rightarrow$ Deposition speed

$r_a \rightarrow$ Aerodynamic resistance

$r_b \rightarrow$ Quasi-laminar boundary layer resistance for particles

$\nu_s \rightarrow$ Sedimentation velocity

Over vegetal canopies, corrections have been added, including a dependence to leaf area index (LAI) for different seasons, and more realistic treatment of resistances in winter (depending on ice, water, etc., L. Zhang et al. 2003). The dry deposition of aerosols follows two processes: a Brownian motion process which is efficient for small particles and a sedimentation process efficient for large particles. For the intermediate size range of aerosols (the accumulation mode), dry deposition is very slow and therefore particles accumulate in this size range.

Wet scavenging has also been taken into account in the model, in clouds or rain droplets and for aerosols or gases, each with a different parameterization. Gases can be scavenged in non-raining clouds. Since the clouds can evaporate and therefore the captured gases can be released again, the scavenging of gaseous species in clouds is considered to be a reversible process. The parameterization of this process is taken from J. Seinfeld and S. Pandis (2016). On the other hand, gases can be scavenged inside rain droplets under clouds as well, which then fall onto the ground. This irreversible process is expressed by:

$$\Gamma = \frac{pD_g}{6 \times 10^5 u_g D^2}(2 + 0.6 Re^{\frac{1}{2}} Sc^{\frac{1}{3}}) \tag{II.6}$$

Where,

$\Gamma \rightarrow$ Scavenging coefficient

$p \rightarrow$ Precipitation rate

$D_g \rightarrow$ Molecular diffusion coefficient

$u_g \rightarrow$ Raindrop velocity

$Re \rightarrow$ Reynolds number of droplet

$Sc \rightarrow$ Scmidt number of droplet

For aerosols, the interactions of particles with clouds can be two-fold: They can be scavenged by coagulation with clouds or they can act as nuclei for the formation of new droplets. The latter process is more efficient in clouds. The flux of this process is expressed by Tsyro (2002):

$$[\frac{Q_l^k}{dt}] = -\frac{\epsilon_l P_r}{w_l h} Q_l^k \tag{II.7}$$

Where,

$P_r \rightarrow$ Precipitation rate per grid cell

$w \rightarrow$ Liquid water content

$h \rightarrow$ Cell thickness

$\epsilon \rightarrow$ Empirical uptake coefficient (between 0-1)

Aerosols can also be captured and rained out to the ground by falling rain droplets, the flux for this process follows:

$$[\frac{Q_l^k}{dt}] = -\frac{\alpha p E_l}{u_g} Q_l^k \tag{II.8}$$

Where,

$E \rightarrow$ Collision efficiency coefficient

$\alpha \rightarrow$ Empirical coefficient

$p \rightarrow$ Precipitation rate per grid cell

$u_g \rightarrow$ Raindrop velocity

Resuspension of particulate species is parameterized following what was suggested by Vautard, Honoré, et al. (2005). This process involves freshly deposited small particles by turbulent wind which are really easy to mobilize shortly after their deposition. For the sake of simplicity, resuspension of secondary components is ignored. A simple resuspension rate depending on the friction velocity and the time after start of resuspension is used for this process (Loosmore and Cederwall 2004).

2.2.3 Gaseous chemistry

As explained before, reduced chemical mechanisms are used in CTMs in order to reduce the number of reactions and species existing in the model and thus reducing the computational time. CHIMERE contains three chemical mechanisms:

- MELCHIOR1 (Lattuati 1997) containing 300 reactions and 80 gaseous species. The principal goal of this scheme was to study the evolution of the ozone in the atmosphere.
- MELCHIOR2 (Derognat et al. 2003) which is a reduced version of MELCHIOR1 containing 120 reactions and 40 gaseous species in order to reduce computing times. This scheme's principal goal was to study boundary layer atmospheric chemistry. It follows the chemical operators concept (W. P. Carter 1990; Aumont, Jaecker-Voirol, et al. 1996). This scheme is commonly used in most studies done by the CHIMERE model.
- SAPRC-07A (W. Carter 2010) which contains 275 reactions and 85 species. It is the most recent chemical mechanism added to CHIMERE. It was compared to MELCHIOR2 (Menut, Bessagnet, et al. 2013) and for common atmospheric species, good agreement was seen between the two schemes (Mailler et al. 2017).

Different types of reactions are used in the model, but most of the reaction kinetics follow the Arrhenius law. The chemical species and reactions existing in the default MELCHIOR2 scheme are presented in annex C.

2.2.4 Aerosol module

The gaseous chemical mechanism explained above is coupled with a sectional aerosol module containing several species: PPM (primary particle material), nitrate, sulfate, ammonium, several BSOA and ASOA species, salt (dry salt or sodium and chloride as well), dust, black carbon, elemental carbon and water. The usage of many of these aerosol species is activated by options in the model. Particles are distributed into logarithmic sectional size bins, which can be modified by the user by choosing the number of bins, the finest and the coarsest bin. For example, in this work, a 10 bin distribution is used, with bins ranging between $40\,\mathrm{nm}$ to $40\,\mu\mathrm{m}$. In this way, each bin covers a size fraction of a factor of 2.

For the simulation of inorganic aerosols the ISORROPIA model is used as explained before.

Physical processes taken into account for aerosol formation are coagulation, absorption and nucleation. The mathematical representation of aerosols in the model is dependent of composition and size distribution of aerosols. The density distribution of aerosols is discretized in a finite number of bins, so, all particles in section l have the

same composition characterized by their mean diameter dl (for each aerosol type). This representation sums up to:

$$Q_l = \sum_k Q_l^k \tag{II.9}$$

Where,

Q_l (μg m^{-3}) $\rightarrow$ Total mass concentration in section l

Q_l^k (μg m^{-3}) $\rightarrow$ Mass concentration of component k in section l

For coagulation, the classical theory of Gelbard and J. H. Seinfeld (1980) has been used. Assumption is made that the coagulation involves binary collision, therefore the mass balance is written as:

$$\begin{aligned}\frac{dQ_l^k}{dt} = \frac{1}{2}\sum_{i=1}^{l-1}\sum_{j=1}^{l-1}({}^{1a}\beta_{i,j,l}Q_i^kQ_j + {}^{1b}\beta_{i,j,l}Q_j^kQ_i) \\ -\sum_{i=1}^{l-1}({}^{2a}\beta_{i,l}Q_l^kQ_i - {}^{2b}\beta_{i,l}Q_l^kQ_l) \\ -\frac{1}{2}({}^{3}\beta_{l,l}Q_l^kQ_l) - Q_l^k\sum_{i=l+1}^{m}({}^{4}\beta_{i,l}Q_i)\end{aligned} \tag{II.10}$$

Where,

${}^{1,2,3,4}\beta \rightarrow$ Sectional coagulation coefficients

The first term on the right side of this mass balance equation represents the flux of coagulation of component k into the section l, from the collision of two aerosols from all the sections below l. The second term shows the sink flux of difference between a particle larger than section l, formed from coagulation of a particle within section l and section lower than l, and a particle within section l and a section lower than l. The third and the forth terms are the out flux of coagulation of particles from the section l into another one and the coagulation of particles from section l into higher sections. The sectional coefficients for coagulation depend on composition of particles, their physical characteristics and also to meteorological data such as temperature, pressure and turbulence (Fuch, N. 1964). The major phenomena controlling coagulation for sub-micron particles is the Brownian movement and for coarse particles is the sedimentation.

For absorption, the absorption flux J is calculated by:

$$J = \frac{1}{\tau}(G - G_{eq}) \tag{II.11}$$

Where,

$G \rightarrow$ Gas phase concentration

$G_{eq} \rightarrow$ Equilibrium concentration

$\tau \rightarrow$ Characteristic time

If the gas phase concentration is higher than the equilibrium concentration condensation happens. On the other hand, evaporation of the particulate phase will happen if the gas phase concentration is lower than the equilibrium concentration. The characteristic time is:

$$\tau = \frac{1 + \frac{8\lambda}{\alpha d}}{2\pi\lambda c d N} \tag{II.12}$$

Where,

$\lambda \rightarrow$ Free path of molecules

$\alpha \rightarrow$ Accommodation coefficient

$c \rightarrow$ Mean molecular velocity

$d \rightarrow$ Diameter

$N \rightarrow$ Particle number

Two things to notice about the characteristic time equation: first, it depends on the particle number, so molecules in the model are assumed to be internally mixed. Second, in clean conditions, the characteristic time increases, therefore, the absorption flux decreases. The characteristic time for rather clean conditions ($N < 10^4 cm^{-3}$), for SVOC with a diameter of $0.1\mu m$ and an accommodation coefficient of 0.2 is around 5 minutes. The mass equation for absorption for the species k in the section l is:

$$(\frac{dQ_l^k}{dl})_{absorption} = H_l^k Q_l \tag{II.13}$$

Where,

$H_l^k \rightarrow$ Mean absorption coefficient

This variable is calculated by the equation II.11 represented above, resulting in:

$$H_l^k = \frac{12\lambda c_k}{\rho_p d_l^2 (\frac{1+8\lambda}{\alpha_k d_l})} (G^k - G_{eq,l}^k) \tag{II.14}$$

For inorganics, the equilibrium concentration is calculated by the processes included in ISORROPIA, which also calculates the water content in the particles. For organics, the equilibrium concentration is temperature dependent and is calculated by (Pankow 1987):

$$G_{eq,l}^k = \frac{Q_l^k}{OM_l K_k^p} \tag{II.15}$$

Where,

$K_k^p \rightarrow$ Partitioning coefficient

$OM_l \rightarrow$ Absorbent organic matter concentration

And K_k^p is expressed by (considering thermodynamic equilibrium between gas and particulate phases):

$$K_k^p = \frac{10^{-6} RT}{MW_{OM} \zeta_k p_k} \tag{II.16}$$

Where,

$R \rightarrow$ Ideal gas constant

$T \rightarrow$ Temperature

$MW_{OM} \rightarrow$ Mean molecular weight

$\zeta_k \rightarrow$ Activity coefficient in bulk aerosol phase

$p_k \rightarrow$ Vapor pressure of i as a pure liquid

The activity coefficient is difficult to calculate, so it is assumed constant and equal to 1. It is also important to mention that the interactions between organic and inorganic compounds are not taken into account since they are not well known.

For nucleation, the parameterization of Kulmala et al. (1998) is used for sulfuric acid. Sulfuric acid/water vapor homogeneous nucleation occurs in cold and humid regions with weak particle load as this process is in competition with absorption. In addition, the effect is on the ultrafine particles and the calculated nucleated aerosols are added to the lowest bin. The nucleation rate is parameterized as a function of temperature, relative humidity and sulfuric acid vapor concentration. Although nucleation of organic aerosols has been already proven to be important (Kavouras et al. 1998), no parameterization exists for its simulation, so it is not considered in the model.

3 Simulation of organic aerosols in atmospheric models

The simulation of OA in CTMs follows the same logic as explicit and lumped chemistry mechanisms: because of the sheer enormity of the number of components that can participate in their simulation, implementation of an explicit chemical scheme in CTMs for the simulation of organic aerosols is not possible. Therefore, simplified chemical schemes that can characterize the complex nature of OA and numerous phenomena that can participate in their formation are necessary. So, many different parameterizations exist for their simulation in CTMs, each of which have advantages and drawbacks. We will try to discuss the basis and the positive and negative points for some of these schemes in this section.

3.1 Two-product schemes

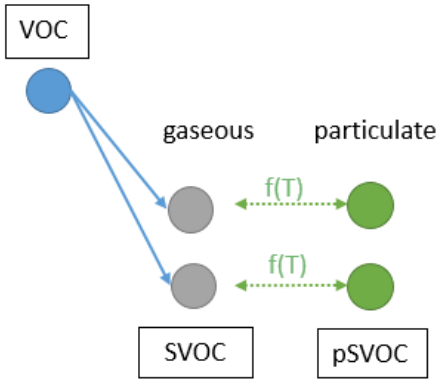


Figure II.4 – *Simplified schematic of a two-product scheme.*

This SOA scheme is based on the method proposed by Odum et al. (1997). The authors performed several laboratory studies on species such as α-pinene and m-xylène, observing an increase in the yields of SOA formation when more organic mass is formed. They proposed a mass dependent yield with the hypothesis that the condensation of SOA on preexisting OA occurs mostly by absorption. Odum et al. (1997) considered that the oxidation of a precursor VOC will result in n semi-volatile products:

$$VOC + OH \rightarrow \sum_{i=1}^{n} \alpha_i SVOC_{g,i} \tag{II.17}$$

α_i is the yield to be determined for each SVOC. It is assumed that each VOC can only pass one oxidation state. It is also assumed that there is a perfect miscibility between all components of OA and the mixture is homogenous, therefore the Raoult's law applies:

$$P_i = \lambda_i x_i P_i^{sat} \tag{II.18}$$

Where (i corresponds to each SVOC component),

$P_i \rightarrow$ Partial vapor pressure

$x_i \rightarrow$ Molar fraction

$\lambda_i \rightarrow$ Activity coefficient

$P_i^{sat} \rightarrow$ Saturation vapor pressure of i

Each SVOC can enter particulate phase following Pankow's theorem (Pankow 1987, see above) using a partitioning constant ($k_{OM,i}$):

$$SVOC_{g,i} \overset{k_{OM,i}}{\longleftrightarrow} SVOC_{p,i} \tag{II.19}$$

And $k_{OM,i}$ is:

$$k_{OM,i} = \frac{C_{p,i}}{C_{g,i}C_{OA}} \tag{II.20}$$

Where (i corresponds to each SVOC component),

$C_{p,i} \rightarrow$ Concentration of i in the particulate phase

$C_{g,i} \rightarrow$ Concentration of i in the gaseous phase

$C_OA \rightarrow$ Total OA concentration

Combining equations II.18 and II.20 gives:

$$K_{OM,i} = \frac{10^{-6}RT}{MW_{OM}\lambda_i p_i^{\circ}} \tag{II.21}$$

If all these hypothesis are taken into account, the SOA formation yield can be expressed as:

$$Y_{SOA} = C_{OA}\sum_{i=1}^{n}\frac{\alpha_i k_{OM,i}}{1 + C_{OA}k_{OM,i}} \tag{II.22}$$

Where:

$Y_{SOA} \rightarrow$ SOA formation yield

$\alpha_i \rightarrow$ Yield from each SVOC

$k_{OM,i} \rightarrow$ Partitioning constant for each SVOC

$C_{OA} \rightarrow$ Total concentration of OA.

Odum et al. (1997) then calculated α_i and $k_{OM,i}$ for a certain number of SVOCs. They concluded that in the limits of the observed species, formation of two SVOCs ($i = 2$) is necessary to reproduce the measured concentration (hence a "two-product" scheme). They then optimize the parameters $\alpha_{1,2}$ and $k_{OM,1,2}$ for the tested species. Figure II.4 shows a simplified schematic for the two-product scheme.

The advantage of this scheme is the fact that it contains a minimal number of species and reactions for the simulation of SOA, therefore it is light and less demanding numerically. It was also very convenient for expressing the available laboratory data within a model. The negative point is that in many cases, it cannot represent either the concentration of OA or its characteristics (oxidation state) since it has an extremely simplistic look at a very complex issue (J. Jimenez et al. 2009). In addition, the SOA concentration simulated by this scheme can show a strong underestimation (depending on the region that is simulated), since the experiments performed to develop this scheme were not long enough to take into account multiple oxidation steps for SVOCs (Volkamer et al. 2006).

Also, the concentrations of OM (Organic Matter) used in the laboratory experiments in order to calculate the SOA production yields were too high, therefore are not realistic for the atmospheric concentrations of this component.

Many CTMs use this scheme (or a scheme close to this one with minor modifications) in order to simulate the concentration of OA. The secondary organic aerosol model (SORGAM, Schell et al. (2001)) which is an Odum-based module has been used in many atmospheric models such as RCG (Stern and Yamartino 2006), CMAQ (Byun et al. 2006; Matthias et al. 2008), MINNI (Calori et al. 2014), EURAD (Memmesheimer et al. 2004) and WRF-chem (Grell et al. 2005).

3.2 Volatility basis set

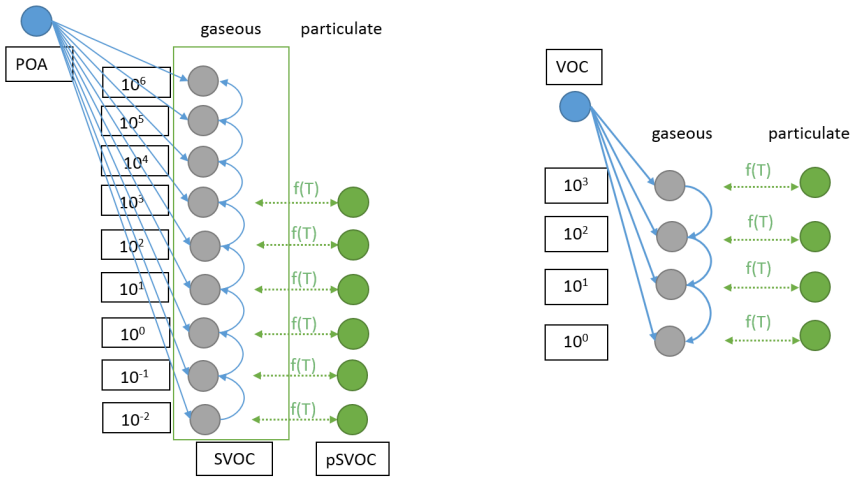


Figure II.5 – *Simplified schmeatic of the volatility basis set scheme.*

The Volatility Basis Set (VBS) was introduced by Donahue, Robinson, et al. (2006). They proposed that the organic compounds could be classified according to their volatility calculated in terms of saturation concentration (or C^*) for each component. So, they created a set of groups of volatility (bins) and distributed organic aerosols in said bins according to their volatility range.

They continued this work in Robinson, Donahue, M. K. Shrivastava, et al. (2007), where they distributed POAs in bins covering the range of $10^{-2}\,\mu g\,m^{-3}$ to $10^{6}\,\mu g\,m^{-3}$. They considered that these volatility bins cover three larger groups: non-volatile organic compounds with C*$<0.1\,\mu g\,m^{-3}$, SVOCs covering the range of $0.1\,\mu g\,m^{-3}$ <C*$<10^{3}\,\mu g\,m^{-3}$ and Intermediate-volatility Organic Compounds (IVOCs) covering the range of $10^{3}\,\mu g\,m^{-3}$ <C*$<10^{6}\,\mu g\,m^{-3}$ (Robinson et al., 2007). In this scheme, IVOCs cannot pass to the particulate phase and the formation of particulate OA occurs in the range of $0.1\,\mu g\,m^{-3}$ <C*$<10^{3}\,\mu g\,m^{-3}$. For normal atmospheric concentrations of OA, SVOC can exist both

in gaseous and aerosol phases, but IVOCs are always in gaseous phase. This parameterization for POA is used in other works as well, defining the volatility distribution of different sources of POA emissions from chamber experiments. For example, Grieshop, Logue, et al. (2009) and Grieshop, Donahue, et al. (2009) explore the volatility bins by emissions from flaming and smoldering of hard- and soft-wood fires under plume-like conditions, Robinson, Donahue, M. K. Shrivastava, et al. (2007) explored POA emissions from traffic; Shrivastava et al. (2008) proposed aging processes to be added to POA oxidation reactions. After aging processes were added into the scheme, IVOCs started to be able to pass to lower volatility bins, therefore, there is a possibility for IVOCs to enter the particulate phase after long enough processing.

What was discussed until now concerned POAs, but a similar approach was taken for VOC precursors, which can be both biogenic and anthropogenic (BVOC and AVOC respectively). Instead of 9 volatility bins, only 4 volatility bins in the range of $1\,\mu\mathrm{g\,m^{-3}}$ <C*<$10^3\,\mu\mathrm{g\,m^{-3}}$ are used for both ASOA and BSOA with yields dependent on NO_x availability (high-NO_x or low-NO_x conditions, Lane, Donahue, and S. Pandis 2008; Lane, Donahue, and S. N. Pandis 2008; Murphy and S. Pandis 2010; Tsimpidi et al. 2010). In these works, only the volatility of SVOCs is taken into account. This approach is called the VBS-1D.

$$\begin{aligned} VOC + OH &\xrightarrow{k_{OH}} \sum_{i=1}^{4} \alpha_i SVOC_{g,i} \\ POA + OH &\xrightarrow{k_{OH}} \sum_{i=1}^{9} \alpha_i SVOC_{g,i} \\ SVOC_{g,i} &\rightarrow bSVOC_{g,i-1} \end{aligned} \tag{II.23}$$

The VBS-1D scheme can be and has been implemented and compared to observational data. For example, it was tested for PMCAMx-2008 CTM (Karydis et al. 2007) and also in other CTMs many times (M. Shrivastava, Lane, et al. 2008; Murphy and S. Pandis 2010; Tsimpidi et al. 2010; Hodzic and J. Jimenez 2011; Q. J. Zhang et al. 2013). The underestimation problem encountered for the two-product scheme has been solved here by adding aging processes, however, the most common result that is seen when using VBS-1D with the aging option turned on is an overwhelming overestimation of BSOA. When the BSOA aging option is turned off, the scheme seems to represent the OA concentrations seen in the atmosphere better, albeit showing a slight overestimation on the ASOA side, since turning BSOA aging off and leaving ASOA aging on can create an imbalance in the distribution of these two. A simplified version of the VBS-1D scheme is shown in figure II.5.

Other processes have been added to VBS-1D as well, for example, strongly oxidized heavier and less volatile SVOCs can be broken in the atmosphere to form smaller and more volatile SVOCs (fragmentation processes). Also, recent studies have shown that, after its formation, the SOA can become non-volatile and hence, stay constantly in the particulate phase (formation of non-volatile SOA). For this reason, Shrivastava et al. (2011, 2013, 2015) added these two processes in the VBS version of WRF-CHEM, CAM5 (5th

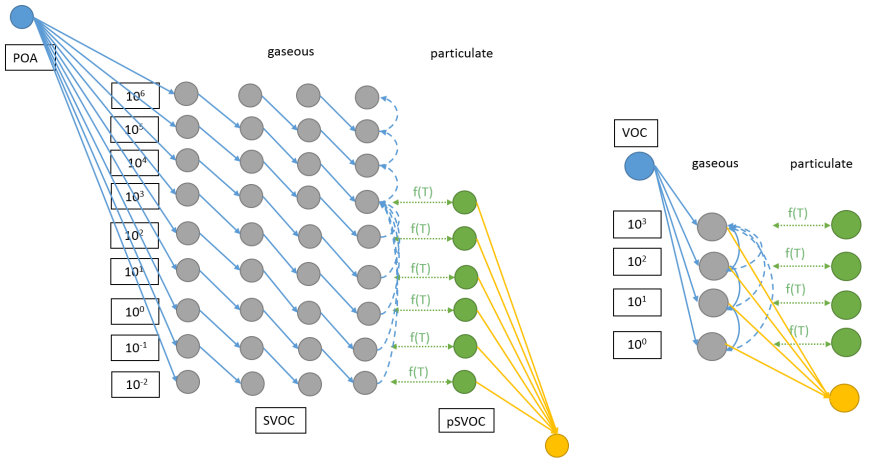


Figure II.6 – *Simplified schematic of the volatility basis set scheme including fragmentation and formation of non-volatile SOA.*

version of CAMx) and CMAQ respectively. A simplified version of the VBS-1D scheme with these processes included is shown in figure II.6.

$$\begin{aligned} VOC + OH &\xrightarrow{k_{OH}} \sum_{i=1}^{4} \alpha_i SVOC_{g,i} \\ POA + OH &\xrightarrow{k_{OH}} \sum_{i=1}^{9} \alpha_i SVOC_{g,i} \\ SVOC_{g,i} &\rightarrow bSVOC_{g,i-1} + cSVOC_{g,i+1} + dNVSOA \end{aligned} \tag{II.24}$$

It is possible to add another dimension to the VBS scheme, in order to include the oxidation state of OA in more detail (Donahue, Epstein, et al. 2011; Murphy, Donahue, Fountoukis, et al. 2011; Donahue, J. Kroll, et al. 2012). The addition of a second dimension is to improve the ability of the model to predict thermodynamic properties, including organic mixing and polarity and with a goal of ultimately describing oxidation chemistry (Donahue, Epstein, et al. 2011). The logic behind adding the second dimension is that the age and oxidation states of different types of OA should be better presented in a scheme that is dependent on O:C ratio as well as volatility of the particles. The reason for which oxidation state is chosen as a second dimension is because of the almost interchangeable definition of oxidation and oxygenation in OA. What is meant by oxygenation here is the O:C ratio in OA, which is, as shown by C. L. Heald, J. H. Kroll, et al. (2010) highly correlated with the oxidation of OA. The aforementioned oxidation level is calculated by the ratio of oxygen to carbon atoms (O:C) in each compound which then results in the calculation of the average oxidation state ($\overline{OS}_C$, J. Kroll et al. 2011). The approach is to determine O:C and H:C values for OA using experimental instruments

such as the HR-ToF-AMS, then calculate $\overline{OS}_C$ using equation II.25:

$$\overline{OS}_C = -\sum_i^n OS_i \frac{n_i}{n_C} \tag{II.25}$$

Where:

OS_i: Oxidation state associated with element i

$\frac{n_i}{n_C}$: Molar ratio of element i to carbon

$\overline{OS}_C$: Average oxidation state.

The summation in equation II.25 is done over all non-carbon elements in OA, which in the atmosphere, consists primarily of hydrogen ($OS_H = +1$) and oxygen ($OS_O = -2$), therefore II.25 becomes:

$$\overline{OS}_C \approx 2(O:C) - (H:C) \tag{II.26}$$

Using this formula and the distribution of C^* constrained from SOA growth, emission dilution measurements or volatility based chromatography, Donahue et al. (2011, 2012) proposed a 2D distribution between these two dimensions that is in presented in figure II.7. The probability of functionalization over fragmentation is also derived from $\overline{OS}_C$ in this scheme (which is called the VBS-2D) and it becomes higher as $\overline{OS}_C$ is higher. Figure II.7 shows the naming convention proposed in Murphy, Donahue, Robinson, et al. (2014) which is quite frequently used in OA simulation articles. The reaction constant K_{OH} for the reaction of each of VBS-2D species with OH has to be determined in order to be able to use this scheme. Donahue, Chuang, Ye, et al. (2013) propose using an empiric equation based on the number of oxygen and carbon elements:

$$K_{OH} = 1.2 \times 10^{-12}(n_C + 9n_O - 10(O:C)^2) \tag{II.27}$$

Where,

n_C : Number of carbon atoms

n_O: Number of oxygen atoms

This equation, takes into account the increase of reaction constant both with increasing carbon elements, and an initial increase with increasing oxygen functional groups. For highly oxidized molecules which thus contain less hydrogen elements, the constant decreases. Chuang and Donahue (2016) further modified this scheme to account for the production and aging of organonitrates in high-NO_x conditions, but as far as we know, this modifications were tested only in a box model and were not implemented into a CTM.

The VBS-2D was implemented in CTMs, though not as much as the 1D version of this scheme since the 2D version is extremely demanding numerically. For example, Zhao

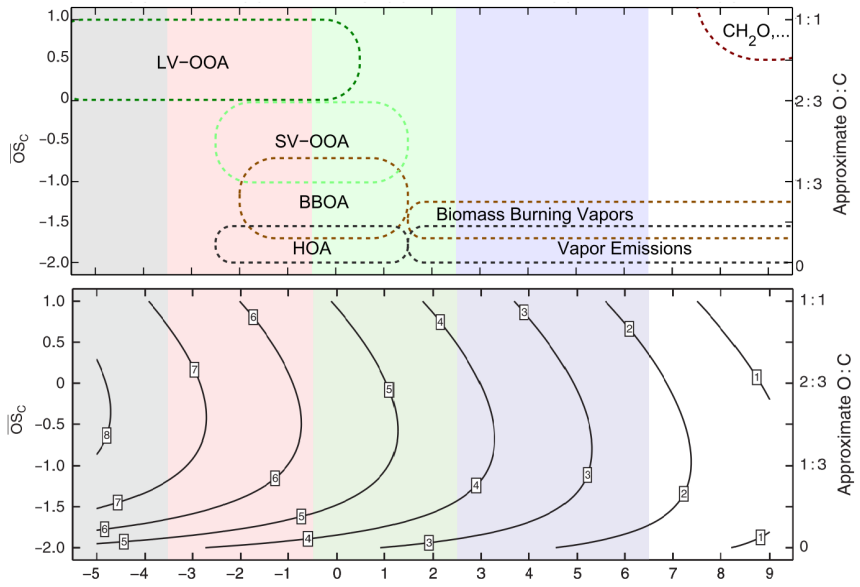


Figure II.7 – *The representation of the two dimensions (volatility and oxidation state) taken into account in a VBS-2D scheme. Image is taken from Donahue et al. 2012.*

et al., (2016) uses the VBS-2D scheme in CMAQ CTM to simulate the effects of organic aerosol aging and IVOC emissions on the formation of OA over China. They find that these two factors contribute 40% and to a factor of 10 respectively for Chinese urban areas, the factor of 10 being the sum of effects of aging and IVOC emissions.

In addition, a simplified version of the VBS-2D (called the VBS-1.5) has been developed more recently and tested in CTMs. The difference between the VBS-1D, VBS-2D and VBS-1.5D is the fact that in the first one, no dependence to O:C ratio is coded in the scheme, in the second, a full scale two-dimensional dependence is added and in the third case, a number of species with constant O:C ratios and C^* (for each one) have been added to the scheme, therefore limiting the depth of the second dimension while keeping its functionality for lumped species. The VBS-1.5D was added to CMAQ and CAMx (Koo et al. 2014). Ciarelli et al. (2016) tested VBS-1.5D as well for comparisons on Europe. Comparisons between VBS-1D and VBS-2D have been performed using the CMAQ-VBS (Zhao et al. 2015). Other models such as CMAQ (Zhao et al. 2015) , LOTOS-EUROS (Manders-Groot et al. 2016), EMEP (Bergström et al. 2012) and WRF-CHEM (Ahmadov et al. 2012) have been modified to include VBS-1.5D as well. The VBS-1.5D shows promising results, while it is not as numerically demanding as the VBS-2D for CTMs, it adds a new layer of complexity to the simulation of SOA. In most cases, the VBS-1.5D can be compared to the VBS-1D accompanied with fragmentation and formation of non-volatile SOA processes, both taking into account aging of different types of OA, their oxidation state and formation of non-volatile SOA.

3.3 Carbon number - polarity grid (np+mP scheme)

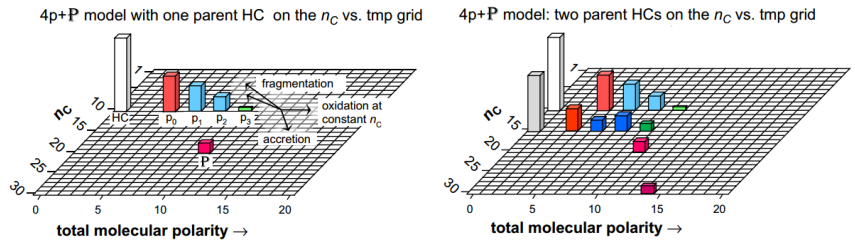


Figure II.8 – *Representation of a np+mP scheme. Image is taken from Pankow and Barsanti (2009).*

This approach was developed by Pankow and Barsanti (2009) with the goal of developing a scheme that contains more details than a two-product scheme and is simpler than the VBS-2D scheme. For the authors, in both the VBS scheme and the two-product scheme, temperature is the only non-kinetic variable taken into account. However, it was shown that the polarity of organic compound in the presence of water especially when the concentration of organic compounds is low can have important impacts on the formation of OA (Pankow and Chang 2008; Pun and Seigneur 2008). They therefore propose the np+mP scheme. It is based on the two product scheme, but the number of products is more than two (n>2, therefore "np" in the name instead of "2p") and the formation of m non-volatile compounds is taken into account (corresponding to "mP" in the name). The values and characteristics of n and m can be variable in different time steps in this scheme. So in summary, it is a 2D scheme like the VBS-2D, but instead of volatility and oxidation state as the two dimensions it uses carbon number and polarity (Barsanti et al. 2011).

The scheme was tested in the chemically explicit GECKO model (Camredon, Hamilton, et al. 2010), but was not implemented in its actual format in CTMs as far as we know.

3.4 Statistical oxidation model

The statistical oxidation model (SOM) uses number of oxygen atoms compared to number of carbon atoms in order to simulate the behavior of SOA (C. D. Cappa and Wilson 2012; C. Cappa, X. Zhang, et al. 2013). This scheme can be called a hybrid of the oxidation state proposed by J. Kroll et al. (2011), the VBS-2D of Donahue et al. (2011, 2012, 2013a, 2013b) and the N_C-polarity grid of Pankow and Barsanti (2009). It is based on consequent reactions of each species with OH which could result in addition of an oxygen atom to aforementioned component. It uses a two-dimensional grid with N_C-N_O as the two dimensions in order to predict the evolution and properties of gas- and particle-phase organic precursors and their products; it can also decide the ratio of frag-

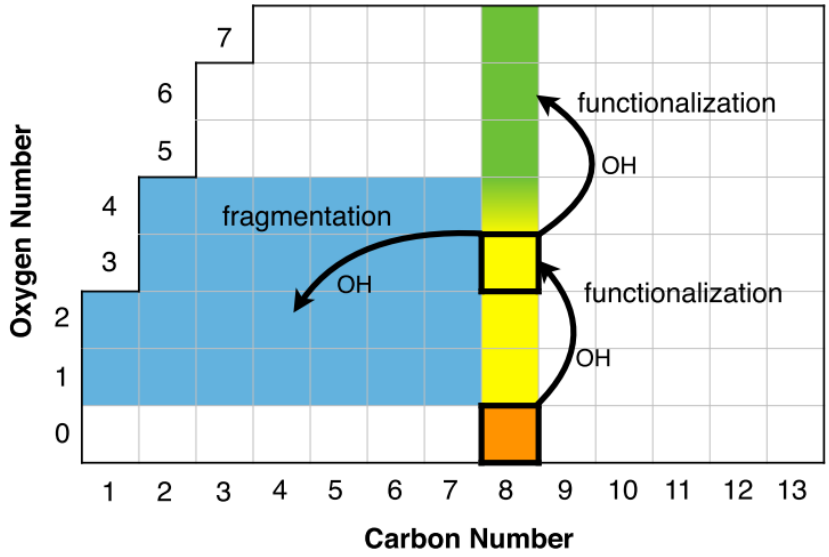


Figure II.9 – *Representation of the statistical oxidation model (SOM). Image is taken from Jathar et al. 2015.*

mentation to functionalization processes. Each N_C-N_O pair is considered a component in this scheme (called a SOM species), which reflects the average properties (e.g., vapor pressure, reactivity, etc.) of actual species with the same N_C-N_O. The reaction constants and the SOA precursors are the same used in SAPRC-11 chemical scheme (W. Carter 2015).

Six parameters determine the fate of a SOM species: Four functionalization probabilities, p1-p4 which correspond to the probability of addition of 1, 2, 3 or 4 oxygen atoms to the SOM species; a fit parameter presenting the fragmentation probability; the fragmentation probability and at the end the decrease in volatility because of addition of an oxygen atom. These values are optimized using either atmospheric chamber studies or chemically explicit GECKO model (Aumont, Szopa, et al. 2005; Camredon and Aumont 2007). The difference of this scheme with respect to the VBS-2D scheme is that no volatility bins are used in this scheme (but precise vapor pressures).

This scheme was implemented and tested in CMAQ (Jathar et al. 2016; C. D. Cappa, Jathar, et al. 2016) and compared to measurements. The former reference found that the concentration simulated by this scheme is close to what was simulated by the two-product scheme when using the same yields, however, the contribution of anthropogenic precursors is stronger for the SOM than for the two-product scheme. Also, the SOA simulated by SOM has much lower volatility than the two-product scheme, therefore it consists more of aged SOA.

3.5 Molecular schemes

The goal of a molecular model is to represent precursors and their products of oxidation using thermodynamic and chemical properties. For this purpose, the procedure is to identify all the precursors, their properties and their oxidation products and then group them according to their chemical and thermodynamic characteristics in order to reduce the number of species by proposing surrogate species with the same properties. The aforementioned characteristics can be the chemical structure or physico-chemical parameters such as molar mass, polarity, solubility, etc.). This approach was proposed by (Pun, R. J. Griffin, et al. 2001, Pun, Seigneur, and Lohman 2006; Pun and Seigneur 2007).

The molecular models use either chemically explicit models such as GECKO or atmospheric chamber experiment data, in order to determine the properties of species and lump them into groups. This approach is used in models like Polyphemus (Couvidat, Kim, et al. 2013; Chrit, K. Sartelet, Sciare, Pey, et al. 2017, CMAQ (Pun, Wu, et al. 2003). There are different versions of this scheme available implemented in a variety of modules, AEC (Kim 2011; Kim et al. 2011), H^2O (Couvidat, Debry, et al. 2012; Couvidat, Kim, et al. 2013) and SOAP (Couvidat and K. Sartelet 2015) are examples of modules using this approach. As an explanation, H^2O contains six surrogate species from the oxidation of isoprene:

- Surrogate 1 (hydrophilic, oxidation by OH and low-NOx conditions, high-volatility)
- Surrogate 2 (hydrophilic, oxidation by OH and low-NOx conditions, high-volatility)
- Surrogate 3 (hydrophilic, oxidation by OH and low-NOx conditions, medium-volatility)
- Surrogate 4 (hydrophilic, oxidation by OH and high-NOx conditions, medium-volatility)
- Surrogate 5 (hydrophobic, oxidation by OH and high-NOx conditions, medium-volatility)
- Surrogate 6 (hydrophobic, oxidation by NO3, high-volatility)

The example shows the grouping processes used for a precursor, here, for isoprene, in regards to their properties, where different combinations of thermodynamic and chemical characteristics are formed as surrogates to take into account all types of possible species. This scheme was tested for the Mediterranean region for the ChArMEx period, using the POLYPHEMUS (V. Mallet et al. 2007) model and the SOAP scheme (mentioned above), showing a good agreement between measurements and simulations for the Cap Corse area, both for 2013 and 2014 campaigns (Chrit, K. Sartelet, Sciare, Pey, et al. 2017; Chrit, K. Sartelet, Sciare, Majdi, et al. 2018).

	SOA1-SOA2-SOA3		VBS	
Anthropogenic	TOL	Toluene (L)	TOL	Toluene (L)
	TMB	Trimethylbenzene (L)	TMB	Trimethylbenzene (L)
	NC4H10	n-butane (L)*	NC4H10	n-butane (L)*
			OLE1	C4-C13 terminal alkenes (L)
			OLE2	C4-C13 internal alkenes (L)
			ARO1	Toluene (L)
			ARO2	Xylenes (L)
			ALK4	Branched C5-C6 alkanes (L)
			ALK5	C7-C13 n-alkanes
Biogenic	APINEN	α-pinene	APINEN	α-pinene
	BPINEN	β-pinene	BPINEN	β-pinene
	LIMONEN	Limonene	LIMONE	Limonene
	OCIMEN	Ocemene (L)	OCIMEN	Ocemene (L)
	C5H8	Isoprene	C5H8	Isoprene
	HUMULE	Humulene (L)	HUMULE	Humulene (L)

Table II.1 – *Anthropogenic and biogenic precursors of schemes coded in CHIMERE.*

4 Simulation of organic aerosols in CHIMERE

CHIMERE uses the molecular scheme with a parameterization introduced by Bessagnet, Menut, et al. (2008). It contains three different levels of complexity (which will be called SOA1, SOA2 and SOA3 from here on) with different number of reactions and simulated species. The chosen approach is to create different groups of lumped species according to their physical and chemical properties. For example, hydrophilic and hydrophobic SOA are separated since the former is more likely to dissolve into aqueous inorganic particles and the latter is more likely to be absorbed into organic particles. In the first case, the dissolution processes is governed by Henry's law and in the second case by Raoult's law. Both the Henry's constant and the saturation vapor pressure of the surrogate species are derived from the average properties of the group. Other properties are estimated using the structure of each surrogate compound. The approach is based on Odum et al. (1997) for anthropogenic compounds and R. J. Griffin et al. (1999) for biogenic species and was tested and compared to in-situ observational data by Pun, Seigneur, and Kristen (2006). Anthropogenic and biogenic precursors and surrogate species are shown in table II.1 and II.2 respectively. Species starting with An or Bi in this table are respectively of anthropogenic or biogenic origins; species names finishing with D or P show hydrophilic or hydrophobic species; i or m in the species name shows low or intermediate saturation vapor pressure; and finally 0, 1 or 2 shows non-dissociative, once-dissociative or twice-dissociative species. In the simplest scheme only one SOA species exists in the model: a lumped SOA representing all species that

Molecular scheme			**VBS**		
Species	**C***	**M**	**Species**	**C***	**M**
$AnA0D^{3}$	10	142	$(O-O2-O3)POA1$	0.01	250
$AnA1D^{2,3}$	10	168	$(O-O2-O3)POA2$	0.1	250
$AnA2D^{3}$	10	186	$(O-O2-O3)POA3$	1	250
$AnBIP^{2,3}$	0.03	167	$(O-O2-O3)POA4$	10	250
$AnBmP^{2,3}$	150	152	$(O-O2-O3)POA5$	100	250
$BiA0D^{3}$	10	168	$(O-O2-O3)POA6$	1000	250
$BiA1D^{2,3}$	10	170	$(O-O2-O3)POA7$	10^{4}	250
$BiA2D^{3}$	10	186	$ASOA1$	1	150
$BiBmP^{2,3}$	41	236	$ASOA2$	10	150
$ISOPA1^{2,3}$	260	177	$ASOA3$	100	150
$ISOPA2^{3}$	1.5	177	$ASOA4$	1000	150
SOA^{1}	0.001	250	$BSOA1$	1	180
			$BSOA2$	10	180
			$BSOA3$	100	180
			$BSOA4$	1000	180

Table II.2 – *Lumped surrogate species in SOA simulation schemes in CHIMERE, Saturation concentration (C^{*}) is in $\mu g.m^{-3}$ and molar mass (M) is in* $\mathrm{g\,mol^{-1}}$.

this aerosol can contain.

The VBS-1D version has also been added to CHIMERE in multiple studies (Hodzic and J. Jimenez 2011; Q. J. Zhang et al. 2013) and has been compared to observational data from the MILAGRO (Stone et al. 2010) and MEGAPOLI (Petetin et al. 2014) campaigns for the Paris region respectively. Anthropogenic and biogenic precursors are shown in table II.1 and surrogate species are shown in table II.2. In the standard version of VBS added to CHIMERE, the POA is only oxidized for one generation.

The VBS-1D including fragmentation and formation of non-volatile SOA was not tested in the CHIMERE model until now. The addition of this modified version of VBS-1D is added to CHIMERE in this thesis.

The last scheme that was recently implemented in CHIMERE is the SOAP model (Secondary Organic Aerosol Processor, Couvidat and K. Sartelet 2015). This is a molecular model, meaning that it functions with surrogates for species according to their chemical and thermodynamic properties. A complete explanation and validation of this model is presented in Couvidat, Bessagnet, et al. (2018).

CHAPTER

III

Evaluation of the atmospheric simulations for the western Mediterranean basin

Contents

1 Specific modelisation chain for the Mediterranean region **73**
2 Meteorological input simulations **74**
3 Anthropogenic emission inputs **84**
4 Orographic representativeness error for Cap Corse **86**
5 Simulation of dimethyl sulfide in CHIMERE **91**
5.1 Physical dependencies of dimethyl sulfide flux into the atmosphere 91
5.2 Chemical processes 95
5.3 Simulated DMS fields and its oxidation products 98

Summary. The Mediterranean Sea has specific particularities. In order for a simulation to be close to the real conditions of this region, these peculiarities have to be introduced in the model. Thus the general purpose of this chapter is to describe the work performed to set–up a model configuration specific for the Mediterranean region, and to perform a first evaluation. This includes adding some new modules. One of these issues concerns the complex meteorology of the Mediterranean region. In this work, the WRF model used for the meteorological simulations has been tested with several parameterizations and compared to meteorological observations in order to find the set of parameterizations that best represent the region. Radio sounding data, in-situ stations and E-OBS (a dataset containing gridded daily stations for the European and North African regions) data have been compared to different WRF simulations (section 2). This model also provides orographic outputs that can affect the quality of observation-simulation comparisons. For example, the Cap Corse supersite is located in a region with a steep altitude gradient. Therefore, there are some discrepancies in the orographic simulation of this region compared to the real amtitude. In order to address this issue, a method of calculating an orography induced error was put into place, which shows that the orographic representativeness error for most secondary pollutants is low, while it is high for primary components (section 4). A brief introduction of anthropogenic emissions used in this thesis is presented as well (section 3). Another peculiarity that is normally not taken into account in CTMs is the biogenic emissions originating from the sea surface. Dimethyl sulfide is an example of these emissions, which could then affect the formation of SO_2 and subsequently sulfate particles. Different parameterizations for the simulation of DMS emissions from sea surface have been implemented and tested in CHIMERE (section 5). This model configuration will be used in the next chapter (IV) for a detailed evaluation of organic aerosol schemes.

1 Specific modelisation chain for the Mediterranean region

The purpose of this chapter is to set-up an appropriate simulation chain that corresponds well to the characteristics of the Mediterranean Sea, and perform some preliminary analysis on the simulations ran using these parameters. Domains, used input information and other modifications added to the model in order to better catch the specificities of the Mediterranean region are presented in this chapter. These information and modifications will be then used for the simulation of OA which will be discussed in the next chapter.

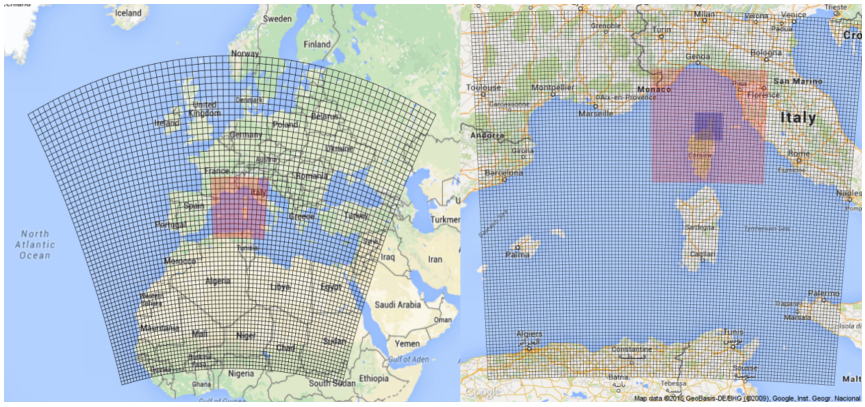


Figure III.1 – *Coarse and nested domains used in this study, the horizontal resolution of the coarse domain is 30km, three nested domains were used, zommed on the western Mediterranean (10km), Corsica (3km) and CapCorse (1km).*

First step into starting the simulations is to decide the domain or domains that are going to be used in these simulations: a large domain was chosen that covers the whole Europe and the Northern Africa, in order to take into account all sources that can be transported to the Mediterranean Sea from farther away. For this purpose, not only Europe, but also Saharian Africa (to take into account dust sources) was included in the domain. Because of the large size of this domain, its horizontal resolution is only 30km. This resolution is in no ways enough for a successful representation of the northern part of Corsica (where a ChArMEx supersite is located) with a geometry of 40km in length and 15km in width (in other words, 1.5 cells by 0.5 cells in the simulation domain described above). In order to address this issue, nested domains were added for a focus on the western basin of the Mediterranean and on the Cap Corse itself. Figure III.1 shows the domain grids used for this purpose, table III.1 shows the horizontal resolution of these domains along with other input information used. The number of vertical layers and their level of coverage can be chosen as well. For this purpose, we chose to use 15 vertical levels, starting from the surface and covering the altitude of about 12km (figure

	Domains			
	DEMO30	DEMO10	DEMO3	DEMO1
Nested	No	Yes	Yes	Yes
Meteorology	WRF-NCEP	WRF-NCEP	WRF-NCEP	WRF-NCEP
Anthropogenic emissions	HTAP-MACC-III	HTAP-MACC-III	HTAP-MACC-III	HTAP-MACC-III
Biogenic emissions	MEGAN	MEGAN	MEGAN	MEGAN
Vertical levels	15	15	15	15
Resolution	30km	10km	3km	1km

Table III.1 – *Simulation chain, domains and their resolution and input data for simulations used for the Mediterranean area.*

III.2). The vertical resolution changes in specific areas of the atmosphere: resolution is 50 meters near the surface, 400m within the CBL on average and 1km above it. After deciding the simulation domains and resolution, description of some of the input information follows, meteorological data fields and anthropogenic emissions leaving most of choices.

The simulations performed for this purpose cover the period of the SAFMED project, starting from 10th of July 2013 for a month. The coarse domain simulations start 10 days earlier while smaller domain simulations start 5 days earlier, in order to provide the necessary spin-up time (time needed for the model to get independent from the initial conditions). The characteristics of the simulations used in this part have been shown in table III.1.

2 Meteorological input simulations

The WRF (weather research and forecasting,Wang et al. 2015) regional meteorological model has been used with the NCEP (National Centers of Environmental Predictions) reanalysis meteorological data (http://www.ncep.noaa.gov) with a base resolution of 1○. The WRF model is used in order to interpret the NCEP data into regional grids and using parameters needed for the CTM. It offers a large number of options, many of them can be tested for the Mediterranean domain in order to find the parameterization that is more suitable for the Mediterranean region. This is performed by first, running multiple series of simulations with different parameters, comparing the resulting simulations with meteorological data and deciding which series corresponds better with the measurements. For simulating the meteorological fields, for each domain, the same domain with the same resolution is used, containing around 20 more cells larger on each side in order to exclude the relaxation factor used in the WRF model.

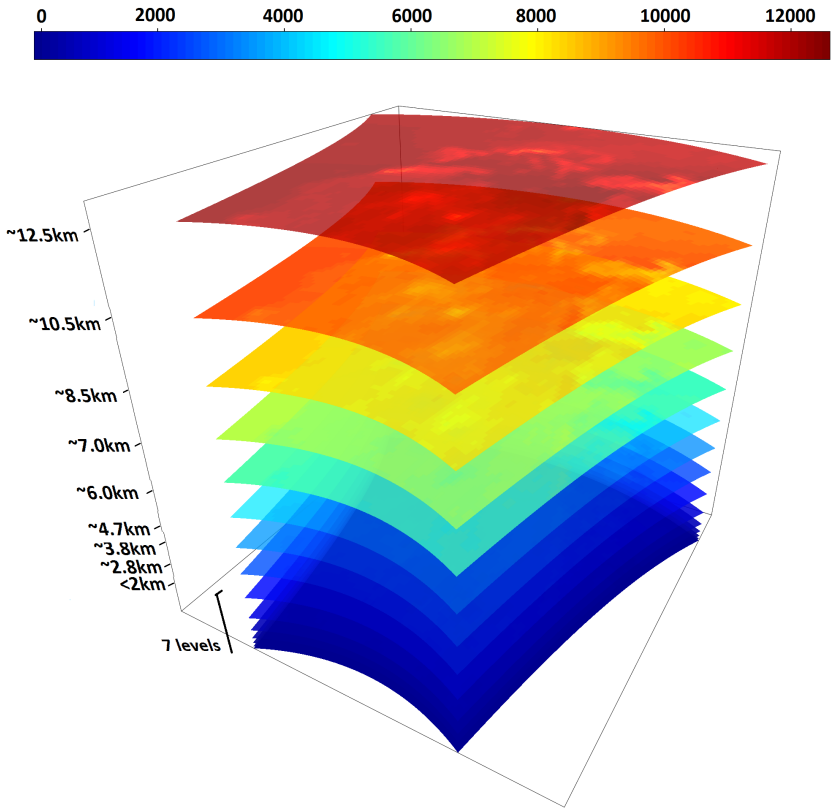


Figure III.2 – *Vertical levels and their distribution in the simulations.*

Table III.2 shows the six more stable parameterizations tested for the WRF domain. Other configurations were tested as well, which were either not stable or did not show major differences with a parameterization that is already explored in table III.2. Each of the configurations aim to explore a specific option, for example parameterizations 1, 2 and 3 aim to see the differences caused by nudging, while the other parameters stay on the default value. The fourth parameterization is meant to explore the feedback option effects compared to parameterization 2. Parameterization 5 aims to explore SST update and microphysics effects, (these two were explored separately in other configurations, but are not presented in here). Parameterization 6 uses radiation, land surface and surface layer schemes used by Menut, Rea, et al. (2015), the other options are kept at values that have already been explored in this work. The aforementioned article was used for these parameters for two reasons: (i) the authors tested the parameters for the western Mediterranean region specifically and (ii) the number of available options in the WRF model for these three parameters are 9 each, testing each one of these options would have taken too much time and numerical resources.

The nudging option in table III.2 entails that the simulated values are “nudged” to-

	Parameterizations					
	Par 1	**Par 2**	**Par 3**	**Par 4**	**Par 5**	**Par 6**
Nudging	0	1	2	1	1	1
Feedback	1	1	1	0	1	1
SST update	1	1	1	1	0	1
Microphysics	3	3	3	3	1	4
surface layer scheme	1/1	1/1	1/1	1/1	1/1	2/4
Radiation	1	1	1	1	1	4
Options	For all parameterizations,topographic wind, ocean physics,cumulus and PBL options have been activated.					

Table III.2 – *Tested parameterizations for the WRF model in order to simulate the meteorological fields.*

wards the measurements during the simulations (using a type of data assimilation in the model), it provides three options: no nudging used, nudging used only for the surface level and nudging used for all the levels.

Feedback option (also called two-way-nesting) means that the domains can communicate with each other, meaning that the simulated meteorological fields in the smaller domain can affect the fields simulated in the bigger domain. Of course, this is in case all domains are simulated at the same time and not separately.

SST update refers to the sea surface temperature update performed during simulations, varying in time. Meaning that, if the option is activated, an input file containing time-varying SST measurements is used in the simulations, otherwise, monthly constant fields are used instead.

The microphysics module in the WRF model contains the options for simulating the removal of moisture from the air, based on thermodynamic and kinetic parameters simulated in the model. In III.2, three options are explored for the simulation of this parameter: the Kessler scheme (option denoted as 1), the WRF Single-Moment 3-class scheme (noted as 3, Hong et al. 2004) and WRF Single-Moment 5-class scheme (noted as 4). The Kessler scheme is a simple warm-rain scheme that does not take into account ice, while the other two tested schemes take into account in the first case ice and snow, and in the second case, ice, snow and super cooled water as well as multi-phase interactions between them.

The land surface option refers to the thermodynamic and kinetic relations between the land surface and the atmosphere, here for the option 1, a 5-layer thermal diffusion scheme is used, which takes into account only soil temperature; option 4 for the same processes denotes the Pleim-Xiu land surface scheme.

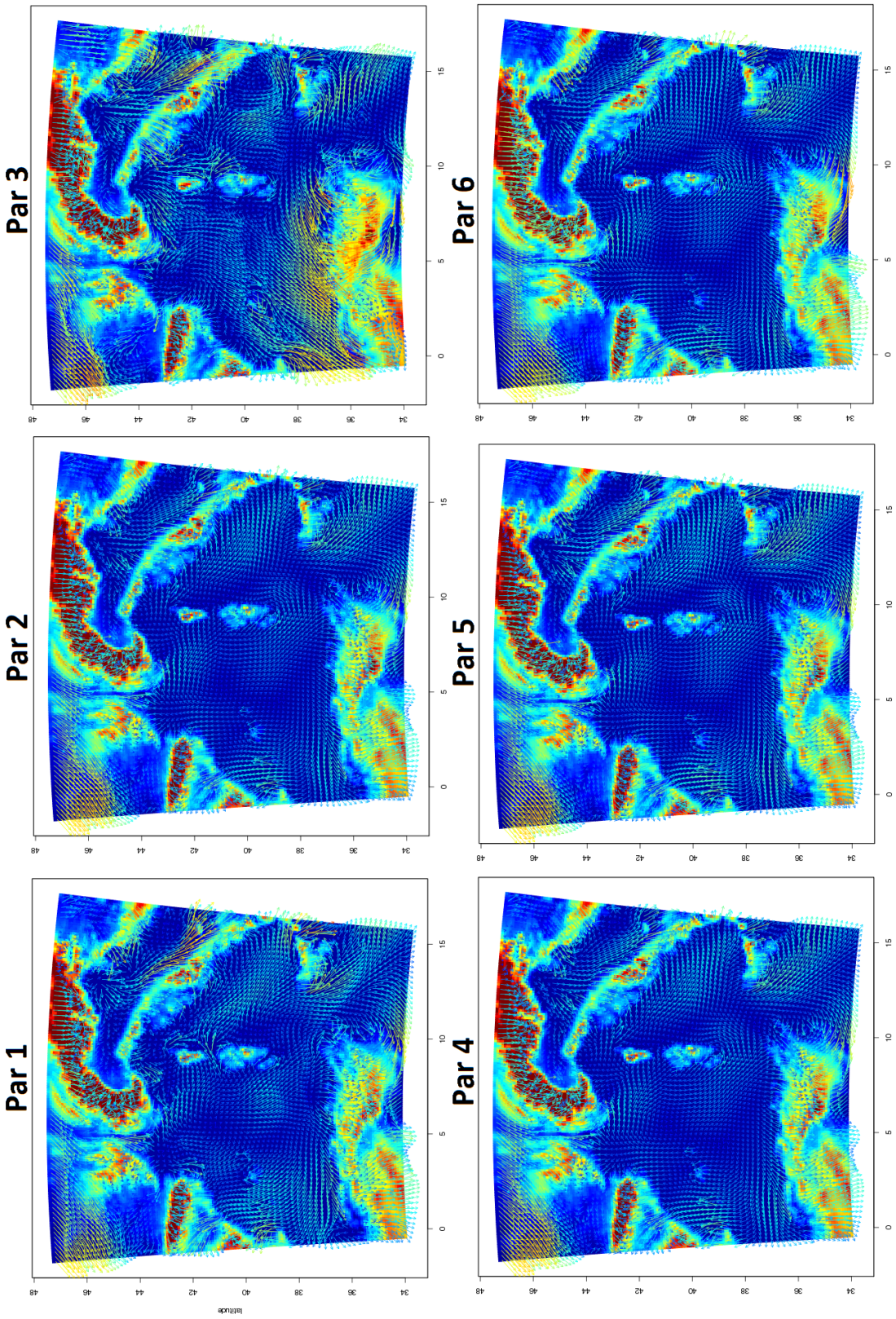


Figure III.3 – *Maps of wind speed and wind direction in the six parameterizations tested in the WRF model. The background of each map shows the simulated orography. The fields were prepared for the 19th of July at midnight.*

The surface layer option relates to the surface temperature prediction schemes, where option 1 is a simple thermal diffusion scheme based on the Monin-Obukhov surface layer scheme (Janjic 2003), while option 4 uses more evolved Noah-MP land surface model.

The radiation scheme refers to how shortwave radiation is treated in the model, the options here used are the Dudhia scheme (Dudhia 2011) and the RRTMG scheme (Mlawer et al. 1997).

A good explication and comparison of different WRF physics and microphysics schemes is given in Dudhia (2010) and Dudhia (2011).

Changing some of the options presented in table III.2 results in negligible changes in the meteorological fields, while some others show visible effects. Figure III.3 shows the results of these tests for the same parameterizations shown in III.2 for the DEMO10 domain for one time-step corresponding to the 19th of July at midnight for wind speed and direction. As mentioned, while for some of the images (for example par 1, par 2 and par 3) visible differences are seen between the simulations, for others (par 6 with par 5 and par 4 in most areas) no major differences are seen, at least between the given series. Some configurations seem to be more unstable than the others regarding to wind speeds in the basin, for example, par 3 shows high wind speeds at the northern coasts of Africa, northern Africa itself and around the Corsica island which is not reproduced in other schemes. Par 1 shows a strong wind regime passing between the Corsica and Sardinia, and around the southern Italian coasts not seen in other configurations. Par 2 seems like a stable simulation, no high wind regimes in the basin are seen. Par 6 presents something in between par 2 and par 1. The point being, there are visible and palpable differences between these simulations, which means a procedure is necessary in order to choose between them.

The problem now is to find a way to choose between these configurations, which are all plausible physically speaking. In order to do so, the simulations were compared to a set of measurements. The observations used here are from radio-sounding data for three stations: Ajaccio, France (41 °55'5", 8 °47'38"), Nîmes, France (43 °51'22", 4 °24'22") and Palma, Spain (39 °36'21", 2 °42'24") which are all within or near the Western Mediterranean basin. These measurements cover the period of two months (July and August 2013), two balloons for each day one at midnight and the other one at midday (in rare cases, only one balloon a day). The data covers basic meteorological parameters such as temperature, relative humidity and wind speed on a vertical column.

In addition, E-OBS data network (surface datasets provided by European Climate Assessment & Dataset (ECAD) project for monitoring and analyzing climate extremes, Haylock et al. 2008; Hofstra et al. 2009) was also compared to these series. E-OBS dataset covers the period of 1950s to 2015 (updated each year to add the data for the previous year), presenting daily values for minimum, maximum and average temperature, precipitation, relative humidity and wind speed and direction. The total number of stations in this dataset is almost 7000, covering the whole European continent and

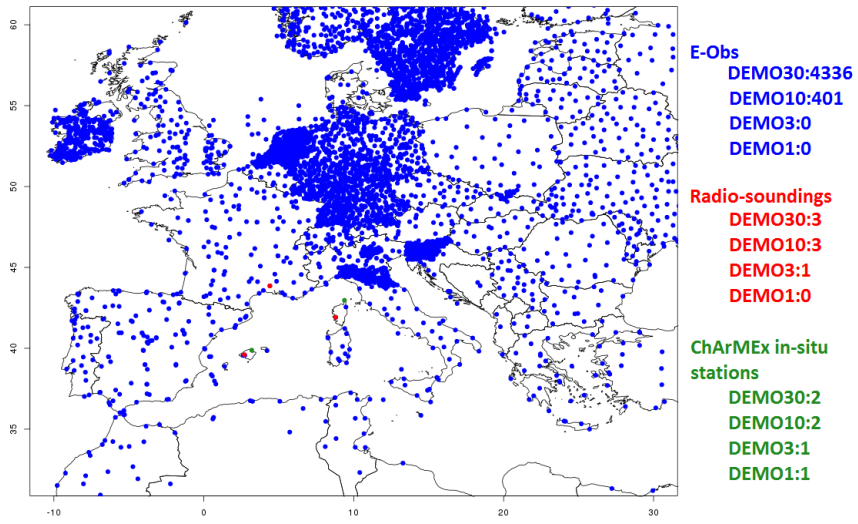


Figure III.4 – *All E-OBS (blue), radio-sounding (red) and in-situ (green) measurements used for the evaluation of the different tested WRF parameterizations.*

also the northern coasts of Africa. However, not all these stations are in the simulation domain, reducing the number of compared stations to around 4300 for DEMO30 and 400 for DEMO10.

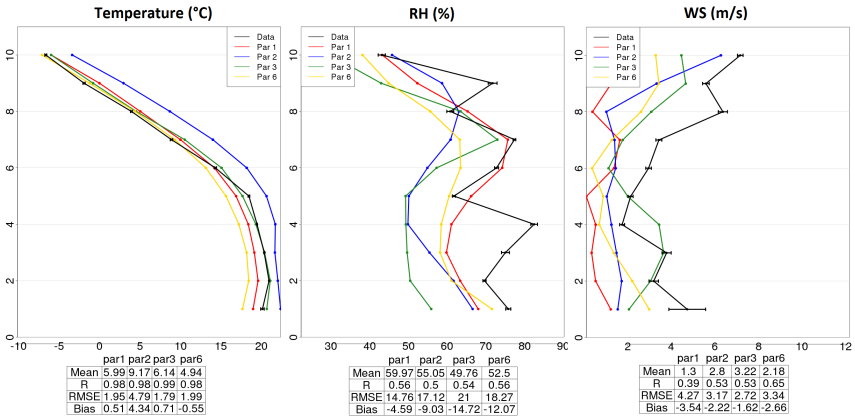


Figure III.5 – *An example of radio-sounding comparisons for the midnight balloon of 19th of July at Nîmes, compared to four parameterizations. Vertical axis shows the different levels in the model, and the horizontal axis shows temperature, relative humidity and wind speed from left to right respectively. For the measurements error bars were calculated using the multiple measurements done in each model level.*

Also, some in-situ measurements were performed during the ChArMEx campaign which have been added to the data pool for these comparisons. Two stations are the

most notable: Ersa, Cap Corse and Es Pînar, Mallorca stations where hourly temperature, relative humidity, wind speed and direction and precipitation were provided.

For the data pool introduced above, all available stations in all domains were compared to simulations. It is important to bear in mind that for some domains, no data was available from the E-OBS stations (DEMO3 and DEMO1). For these two domains, only radio-sounding data from the Ajaccio station and also in-situ meteorological measurements were compared. All stations, the number of data points and their distribution is shown in III.4. In the parts that follow, each of these datasets will be compared to the meteorological simulations showing the most differences: par 1, par 2, par 3 and par 6. Of course the other parameterizations were compared to measurements as well, but will not be presented in here. A comparison of the midnight radio-sounding of 19th of July is

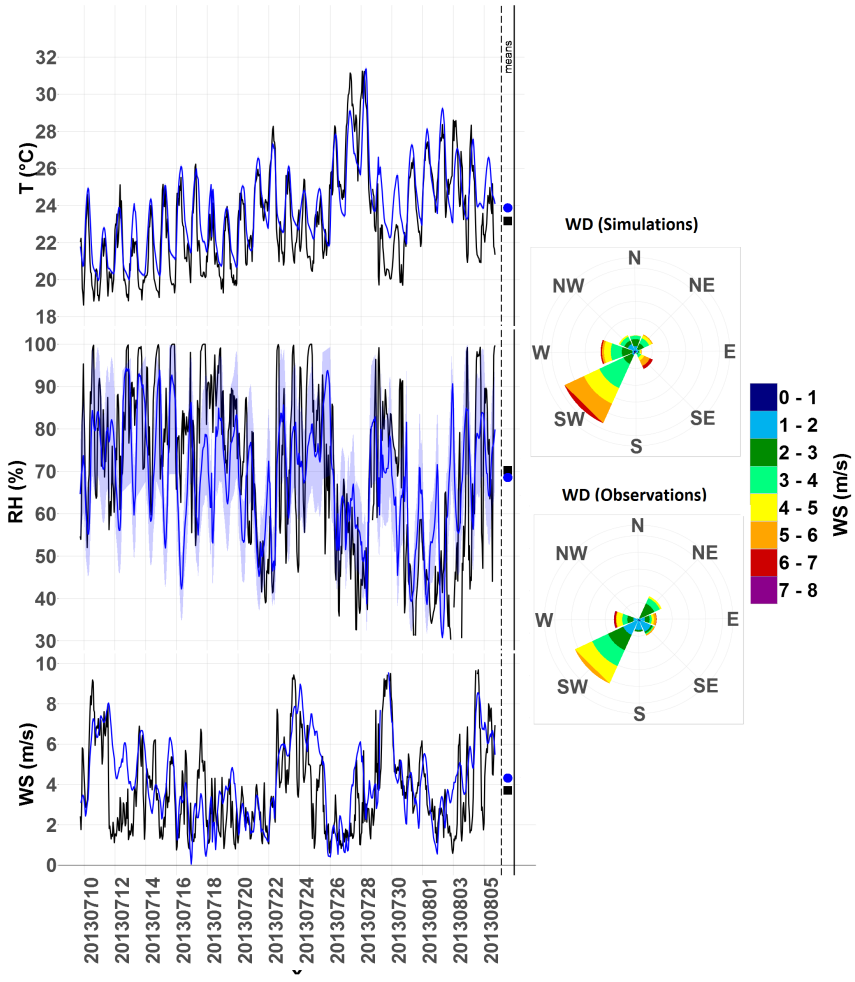


Figure III.6 – *Comparison of the chosen parameterization to in-situ measurements in the Ersa station for temperature, relative humidity, wind speed and wind direction.*

presented in III.5, it shows the comparisons of the four of the parameterizations shown

above for the Nîmes station, for temperature, relative humidity and wind speed. The vertical axis shows the vertical levels in the model, while the horizontal axis shows the three aforementioned meteorological variables. While the balloon provides several measurements for each interval representing a layer in the model, the model output gives us only one value corresponding to that layer. These multiple measurements were averaged (the black point shown in each plot for each level) using the ensemble of the points to calculate an error bar (shwon by a black bar for each level). There is a table below each parameter that shows the statistical information for this radio-sounding. Judging from these images, among the tested configurations, in average, par 2 and par 6 are more comparable to the data than the other two parameterizations. While it is important to look at balloons each separately, one balloon is not representative for the whole domain, therefore a comparison of the average statistical values was prepared for these measurements shown in table III.3.

The E-OBS comparisons were also compared to the simulations for the two bigger domains. These comparisons were done station by station, however, because of the high number of stations only the averaged statistical information has been provided in table III.4. The tables III.3 and III.4 show that, on average, the performance of the sixth tested parameterization is better that the other ones (concerning average biases and correlations). Same results are obtained when individual in-situ comparisons are analyzed to meteorological measurements. The comparison of this parameterization specifically to all the radio-sounding measurements and the ChArMEx in-situ stations is shown in figure III.7 (for DEMO10 and DEMO3) and III.6 (for DEMO1) respectively. Figure III.6 shows that there is a good correlation between different parameters for DEMO1 in Ersa for in-situ measurements for this parameterization (correlation of 0.86, 0.54, 0.66 and 0.37 and bias of 3%, -2.4%, 16.4% and 13% for temperature, relative humidity, wind speed and wind direction respectively).

In figure III.7, vertical profiles of the same variables shown in figure III.5 are presented, but for a total of 32 balloon launches at each site in the period of 10 july to 30 july (32 ballons for each site when data was available for all three sites). In addition, for each vertical level of simulations, two boxplots show the variability of the 32 measurements (in red) and corresponding simulations (in blue, for Ajaccio D10 in dark blue and D3 in light blue). The small white dot on the boxes shows the average for each level. The altitudes correspond to the average altitude represented in each vertical level. For temperature, bias at different sites and altitude levels is in general small, being on average -1.16, -0.61 and -0.39$^{\circ}C$ over the different altitudes for Palma, Nîmes and Ajaccio respectively. Correlation (with respect to sounding time), is on average 0.65, 0.80 and 0.80, for Palma, Nîmes and Ajaccio respectively. Looking at the box plots for each altitude, there is a lot of variability in the values seen in each level both in the model and in observations. This is normal since all balloons regardless of being midnight or midday launches have been used to produce the boxplots.

The analysis provided here for the different parameterizations helped us to determine

			Stations											
			Ajaccio				Nîmes				Palma			
			1	2	3	6	1	2	3	6	1	2	3	6
DEMO10	T	R	0.96	0.97	0.96	0.96	0.98	0.98	0.98	0.98	0.98	0.98	0.98	0.98
		Mean	15.1	12.6	15.8	15.1	7.0	10.9	7.2	6.7	16.5	16.4	17.5	16.4
		RMSE	7.8	5.3	8.0	7.8	2.6	4.7	2.7	2.8	4.8	4.7	5.5	4.7
		Bias	-1.7	-4.2	-1.1	-1.7	0.2	4.1	0.4	-0.1	2.7	2.6	3.7	2.6
	RH	R	0.19	0.44	0.02	0.27	0.22	0.26	0.17	0.33	0.3	0.4	0.2	0.4
		Mean	34.7	48.7	34.6	35.9	62.9	51.0	47.4	56.9	35.6	40.2	34.0	39.8
		RMSE	25.8	19	26.7	23.2	24.5	20.0	24.1	22.8	20.5	18.6	23.8	18.5
		Bias	-9.5	4.4	-9.7	8.3	8.1	-3.8	-7.4	2.1	-3.9	0.7	-5.5	0.3
	WS	R	0.16	0.37	0.03	0.3	0.3	0.36	0.17	0.35	0.5	0.7	0.4	0.7
		Mean	6.8	4.1	6.5	5.0	5.6	5.1	7.1	5.4	4.1	4.0	4.6	4.0
		RMSE	4.8	3.7	5.7	4.7	3.8	3.8	4.4	3.8	4.2	3.8	4.9	3.8
		Bias	0.7	-2.0	0.4	-1.1	6.8	-0.5	1.5	-0.2	-1.5	-1.6	-1.0	-1.6
DEMO3	T	R	0.98	0.98	0.98	0.98								
		Mean	13.0	13.3	13.9	13.2								
		RMSE	5.5	5.4	6.1	5.4								
		Bias	-0.6	-0.3	-0.3	-0.4								
	RH	R	0.41	0.44	0.42	0.46								
		Mean	48.1	45.2	46.4	45.0								
		RMSE	19.8	20.5	20.2	20.3								
		Bias	5.5	2.6	3.8	2.4								
	WS	R	0.36	0.38	0.34	0.39								
		Mean	6.1	6.3	6.5	6.0								
		RMSE	3.7	3.8	3.5	3.7								
		Bias	-1.8	-2.0	-2.2	-1.7								
DEMO1		R	0.98	0.98	0.98	0.98								
		Mean	10.8	11.0	11.1	11.0								
		RMSE	3.2	3.2	3.3	3.1								
		Bias	-0.8	-0.6	-0.5	-0.6								
		R	0.46	0.48	0.42	0.48								
		Mean	40.8	46.7	44.1	46.9								
		RMSE	3.2	3.2	3.2	3.1								
		Bias	-3.0	2.9	0.3	3.1								
		R	0.32	0.38	0.38	0.39								
		Mean	6.1	6.2	5.9	5.7								
		RMSE	3.7	3.7	3.6	3.7								
		Bias	-1.7	-1.8	-1.5	-1.3								

Table III.3 – *Statistical information for radio-sounding stations in three domains, compared to the four parameterizations, bear in mind that DEMO3 and DEMO1 are small domains and Palma and Nîmes are not in them.*

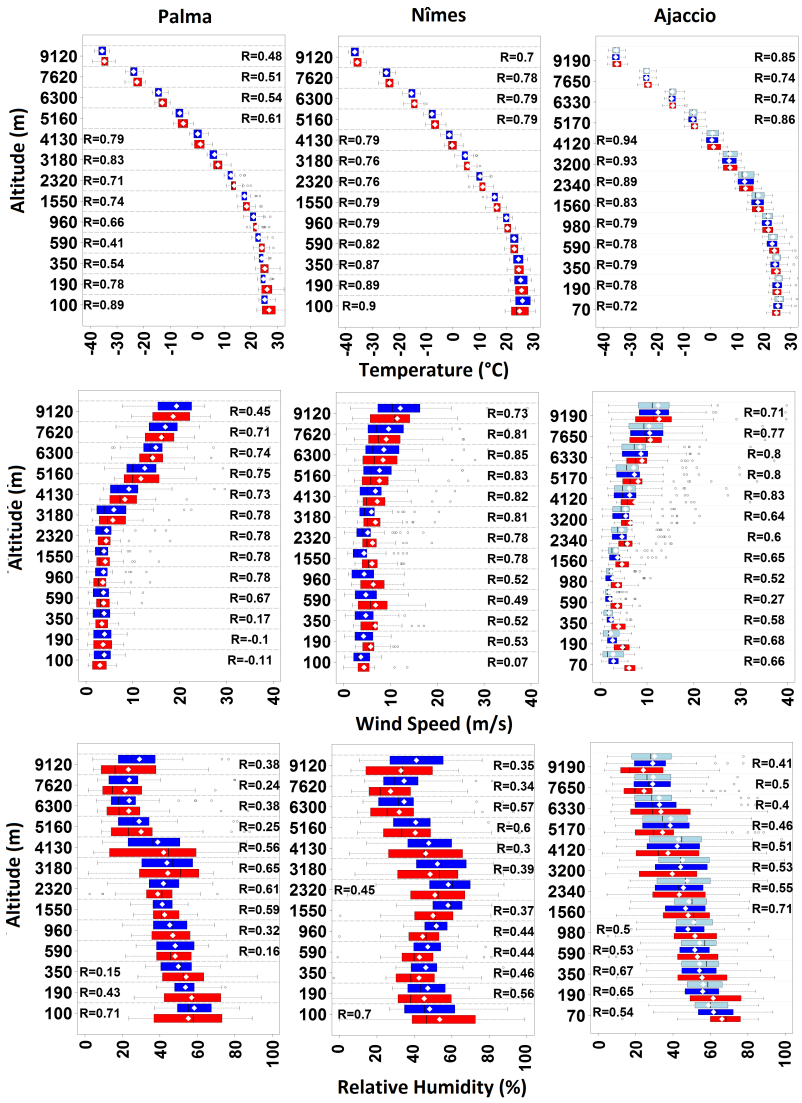


Figure III.7 – *Boxplots showing the comparison of all radiosounding launches available (total of 32 balloons for each site) in the period of 10th to 30th of July. Each row of figure represents a parameter, each column a station. The Y axis shows the altitude and the X axis shows temperature (∘C), wind speed (m.s^{-1}) and relative humidity (%). The blue box shows the simulations and the red box the observations. If possible, both D10 (dark blue) and D3 (light blue) simulations are displayed, else only the D10 one. On each box the white dot shows the average over 32 soundings, the bars the variability (minimum and maximum with outliers shown with dots). R values represent the correlation coefficient between measurements and observation for each level.*

that one of them corresponds better on average, both taking into account the correlation and bias of comparisons to radio-sounding and E-OBS datasets. This parameterization

		Parameterizations											
		Par 1			Par 2			Par 3			Par 6		
		R	RMSE	Bias	R	RMSE	Bias	R	RMSE	Bias	R	RMSE	Bias
DEMO30	Tmax(°C)	0.87	2.8	1.5	0.87	2.9	1.9	0.78	3.4	1.7	0.87	3.3	2.6
	Tmin(°C)	0.7	2.9	-1.8	0.7	2.9	-1.7	0.6	3.4	-1.8	0.7	2.5	-0.6
	Tmean(°C)	0.9	1.8	-0.1	0.9	1.7	-0.3	0.8	2.3	-0.3	0.9	1.7	0.7
	RH(%)	0.8	14.0	9.5	0.7	10.9	5	0.4	16.1	10.2	0.7	8.9	-3.1
	WS(m/s)	0.7	1.7	-1.0	0.7	1.4	-0.7	0.4	2.2	-1.5	0.7	1.5	-0.7
	WD(°)	0.4	98.2	4.0	0.4	97.1	5.1	0.4	102.0	4.2	0.4	97.1	6.6
	P(mm)	0.5	47.0	17.1	0.5	47.0	17.1	0.3	47.0	17.1	0.5	47.0	17.1
DEMO10	Tmax(°C)	0.7	4.4	2.3	0.8	3.7	2.4	0.6	4.1	1.7	0.8	4.2	3.2
	Tmin(°C)	0.3	3.1	-1.9	0.5	3.2	-2.7	0.4	3.2	-2.4	0.5	2.9	-1.9
	Tmean(°C)	0.5	2.6	1.4	0.8	1.4	0.5	0.7	2.0	0.7	0.8	1.8	1.3
	RH(%)	0.4	14.0	2.3	0.6	11.0	-4.3	0.2	14.6	8.8	0.6	12.9	-4.4
	WS(m/s)	0.5	1.5	-0.7	0.6	1.1	-0.2	0.3	1.8	-1.1	0.6	1.1	-0.1
	WD(°)	0.3	76.5	23.6	0.4	73.1	14.0	0.1	95.1	46.0	0.4	73.1	10.7
	P(mm)	0.3	5.1	2.0	0.2	5.1	2.0	0.1	5.1	2.0	0.2	5.1	2.0

Table III.4 – *Comparison of DEMO30 and DEMO10 simulations with four parameterizations to E-OBS data for maximum, minimum and average temperature, relative humidity, wind speed and wind direction and precipitation. The number of stations were shown in figure III.4.*

(par 6) was then compared in more detail to in-situ measurements obtained during the ChArMEx campaign showing good results (presented above). In all the following simulations presented in this chapter, this parameterization is used for the simulation of meteorological fields (par 6 representing nudging to 1, feedback to 1, WRF single-momentum 5-class microphysics, Noah-MP land surface, Monin-obukhov surface layer and RRTMG radiation schemes with SST update, topographic winds, ocean physics and cumulus options turned on).

The meteorological inputs presented here provide the orographic data to CHIMERE as well. A simple comparison between the altitudes simulated for the Ersa site and the real one shows us that a discrepancy exists in the simulation of Cap Corse orography because of steep gradients of altitude, that are not reproduced in the model even at high horizontal resolution of 1km. Therefore, in a later section (section 4), a detailed analysis of this problem is presented and a method for analyzing the errors caused by this issue is implemented.

3 Anthropogenic emission inputs

The HTAP-V2 emissions (Hemispheric Transport of Air Pollution-V2) are used for most of the SNAP (Selective Nomenclature for Air Pollution) sectors in these simulations (table III.1, http://edgar.jrc.ec.europa.eu/htap_v2/index.php). The base resolution of this emission inventory is 10km×10km and it covers the northern hemisphere globally.

The MACC-III emissions (Monitoring Atmospheric Composition and Climate, Kuenen et al. 2014) cover the European area and have a base resolution of 7km×7km. Both of these inventories are good candidates as anthropogenic emission inputs for the European area, but since our coarse domain covers the northern Africa as well as the European continent we decided that it was more pertinent to the study to use the HTAP-V2 emissions instead of the MACC-III emissions in order to cover this area. However, the shipping sector in this inventory was judged to overestimate ship traffic around the Cap Corse area, especially on the shipping lines between Marseilles and the Corsica Island, due to overweighing ferries with respect to cargos (Van der Gon, personal communication). This, could be explained by the fact that the boat traffic description is based on voluntary information. The raw data used for this sector in the MACC-III emissions was re-distributed in order to address this issue. Therefore for all SNAP sectors, the HTAP-V2 emissions are used, while the shipping emissions sector is replaced in this inventory by the emissions proposed by MACC-III inventory because of the importance of the shipping emissions around the Corsica and the Gulf of Geneva in this study. Figure III.8 shows the comparison of the shipping emissions in HTAP-V2 and MACC-III for the 10km domain for SO_2, where it is visible that the emissions proposed by HTAP-V2 are much more than what is presented by MACC-III.

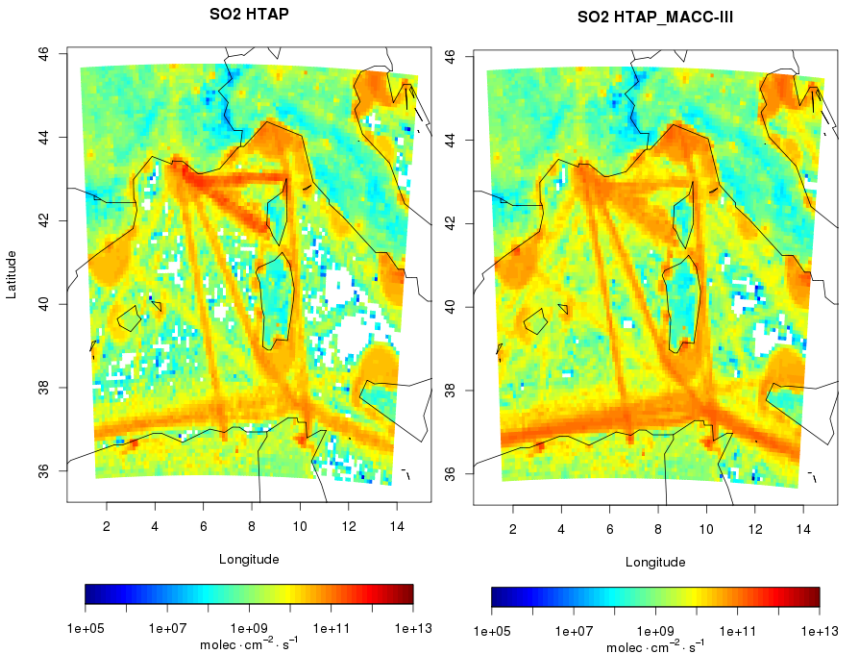


Figure III.8 – *Comparison of shipping emissions in HTAP-V2 (left) and MACC-III (right) emission inventories for SO_2.*

4 Orographic representativeness error for Cap Corse

Before describing the observation-simulations comparisons in chapter IV, it is important to assure that the model grid cell is representative of the measurement site. In urban areas, one has to assure that a measurement site is not affected by local emissions which might not be represented by the model. In case of a strong orography, one of the key parameters that can affect representativeness of the comparisons to measurements is the altitude of the in-situ site which might not be correctly represented in the model. In our case, this orography is simulated by the meteorological inputs (WRF) that is afterwards used in CHIMERE. It is important to bear in mind that a CTM functions in cells, meaning that the domain is cut into several hundred small cubes. For each cell, the altitude in the model is calculated by averaging the altitudes of the area inside the cell. For areas where the altitudinal gradient changes too abruptly, this averaged altitude can be far from the altitude of some of the points in the same cell as it can be imagined. This is what happens when simulating the Corsica region, being an island with high orographic points, the altitude of a small region can change quite suddenly, making the simulated altitude far from what it is in reality. The altitude in Cap Corse does not reach as high as high as the highest point in Corsica itself, but compared to the size of this region, it presents nevertheless a strong altitudinal gradient from three directions (western, eastern and northern directions, figure III.9).

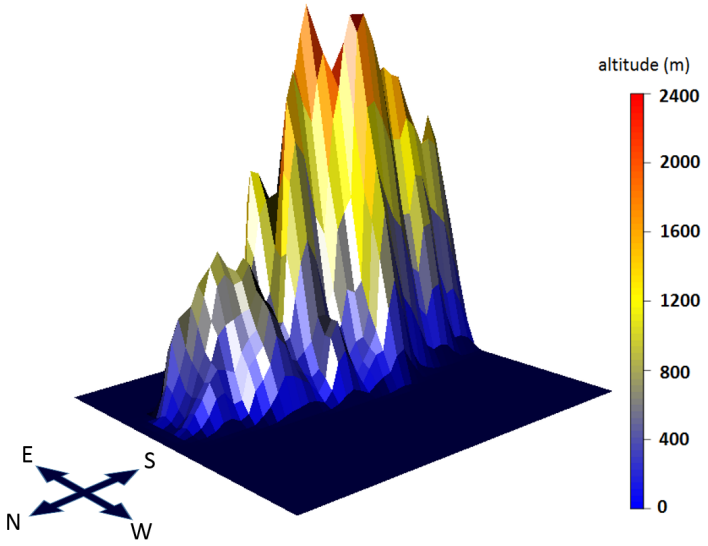


Figure III.9 – *3D representation of the Cap Corse as seen in the model in the DEMO1 (1km) domain.*

While increasing the horizontal resolution helps decrease the effects of this problem, it does not fully remedy the issue. This is seen in figure III.10, where the differences in simulated altitudes in two domains (DEMO10 and DEMO1) have been compared to

	Domains			
	DEMO30	**DEMO10**	**DEMO3**	**DEMO1**
Altitude (m)	48	170	219	365
Bias (m)	-472	-350	-301	-155

Table III.5 – *Simulated altitude of the Ersa site in Cap Corse, as seen in different domains and their difference with the real altitude.*

the real orography of the Cap Corse area. The simulated altitude in the 10km domain (DEMO10) for the cell containing the measurements site (figure III.10, b1 and b2) shows around 170m asl. This is around 350m lower than the real altitude (around 520m asl, figure III.10, a1 and a2). When the horizontal resolution is increased to 1km, the simulated altitude becomes 365m asl (figure III.10 c1 and c2), which is still too low. Bearing in mind that the average boundary layer height in a marine environment might be around 500m, a 200m difference between simulated and real altitude can cause discrepancies when comparing the simulations to measurements. The exact altitudes simulated in all the domains and their difference with the real altitude of the site is shown in table III.5.

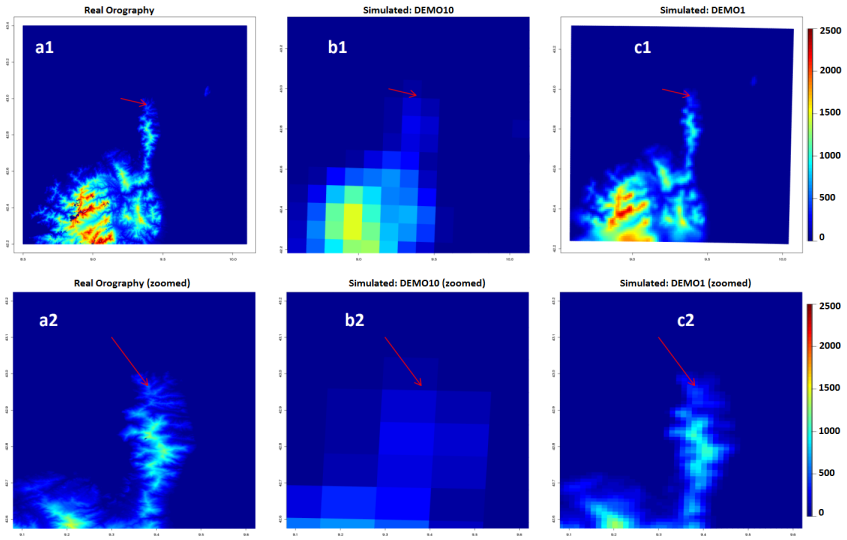


Figure III.10 – *Real orography (left), simulated DEMO10 orography (center) and DEMO1 orography (right). The red arrow points towards the site of the measurements.*

One way to address this issue is to search among neighboring points for a cell with a more appropriate altitude in the simulations. The goal is to find a cell with an average altitude of higher than 500m asl. The hypothesis made here is that the vertical gradient of the pollutants is much stronger compared to the horizontal gradients of said components. This hypothesis is backed up by the fact that at this site, (i) we are far from emission

sources, and (ii) vertical mixing is weak in the marine boundary layer resulting in a rather stratified atmosphere, making the vertical gradient more important than the horizontal one (with the exception of biogenic emissions). This approach would help us adjust the altitude problem in the simulations. Figure III.11 shows the altitudes of the neighboring cells to our in-situ measurements site, showing that there are no cells with the exact characteristics that we are searching for.

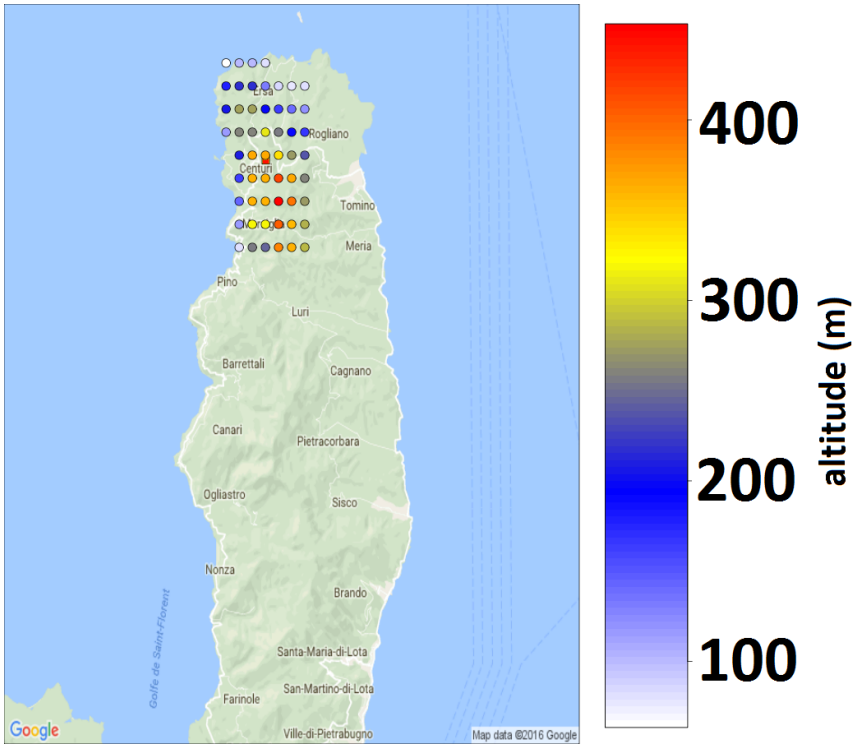


Figure III.11 – *The cell containing the measurements site (square) and its neighbouring cells (round). The colors show the altitude of each site.*

Another possibility is to extrapolate the concentration in measurements site cell towards the altitude of the Ersa site. If this approach is to be taken, a large dataset is necessary containing concentrations and altitudes of neighboring cells for different species. This dataset is then to be used to calculate a regression and at last use this regression to extrapolate towards the desired altitude. The issue that arises here is the fact that there is no unified equation that shows the relationship of different atmospheric species with altitude. All that can be assumed in this regard is its non-linearity and its general shape. To resolve this issue, multiple equations can be used to achieve multiple non-linear regressions. This means that the final goal of this study becomes two-fold: Apart from calculating the extrapolated concentration in the right altitude, a list of concentrations each with a different non-linear regression can be calculated and then using these regressions, an error can be approximated for different components of the atmosphere

with changing altitude.

This approach was taken using neighboring cells to the cell containing the measurements site having a minimum altitude of 100m asl (all the points shown in figure III.11). A total of 9 equations were tested for this purpose (III.1).

$$Eq\ 1.\ y = d + \frac{a-d}{1+\left(\frac{x}{c}\right)^b}, \qquad Eq\ 2.\ y = \left(d + \frac{a-d}{1+\left(\frac{x}{c}\right)^b}\right)^m, \qquad Eq\ 3.\ y = a \times \left(1 - e^{\frac{-x}{b}}\right) + c,$$
$$Eq\ 4.\ y = a \times \left(1 - e^{\frac{-x}{b}}\right) + \log c, \qquad Eq\ 5.\ y = a \times \left(1 - e^{\frac{-x}{b}}\right) + |c|,$$
$$Eq\ 6.\ y = |a| \times \left(1 - e^{\frac{-x}{b}}\right) + |c|, \qquad Eq\ 7.\ y = a \times x^b + c, \qquad Eq\ 8.\ y = a \times x^b,$$
$$Eq\ 9.\ y = a + b \times x + c \times x^2 + d \times x^3 \tag{III.1}$$

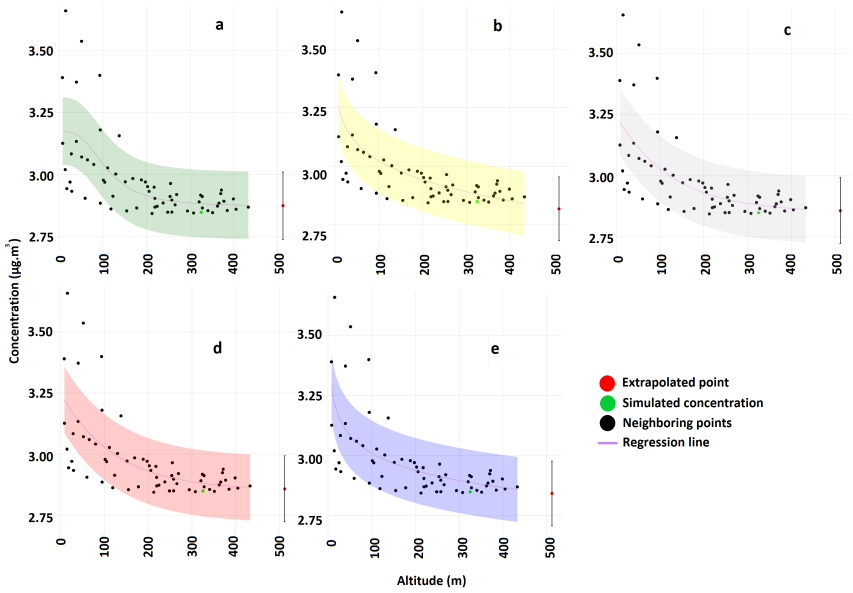


Figure III.12 – *Non-linear regressions performed using concentration of OA and altitude of sites shown in III.11. a→ eq.1, b→ eq.3, c→ eq.5, d→ eq.7, and e→ eq.8 shown in III.1.*

The regression for each of these equations was calculated for the aforementioned points using a least square minimization, if a convergence was achieved for that regression, the calculated extrapolation was used for the error calculation. Bear in mind that this process is repeated for each hourly time-step in the simulation period, resulting in 720 regressions in total for each equation. If for at least more than 40% of the time-steps a convergence was achieved, that equation was used in the error calculation, otherwise the equation was discarded. For the list of equations given above (III.1), 5 were used (eq. 1, 3, 5, 7 and 8, examples shown in figure III.12).

Figure III.12 shows examples of these regressions for the equations that are used for the error calculation at the end of this process, for one time-step for the organic

aerosol. The results are filtered by the correlation coefficient of the regression, only regressions representing a correlation of higher than 0.7 are taken into account. Each regression gives us the corrected concentration for the real altitude and a confidence interval. First interesting fact noticeable in III.12 is a relationship between altitude and concentrations, since concentrations generally decrease with altitude. However, there is a dispersion in the data presented in these figures as well, especially in lower altitudes. Meaning that in lower altitudes (when emission sources such as shipping emissions are nearby) horizontal gradient becomes important, while at higher altitudes the vertical gradient is more important. Secondly, as seen when comparing the extrapolated and the simulated concentrations in III.12, the calculated error interval is higher than the proposed correction to the concentration. This is why we decided that it would be more beneficial to take into account the orographic representativeness error calculated using this approach than the concentration correction calculated by it, which would be too uncertain.

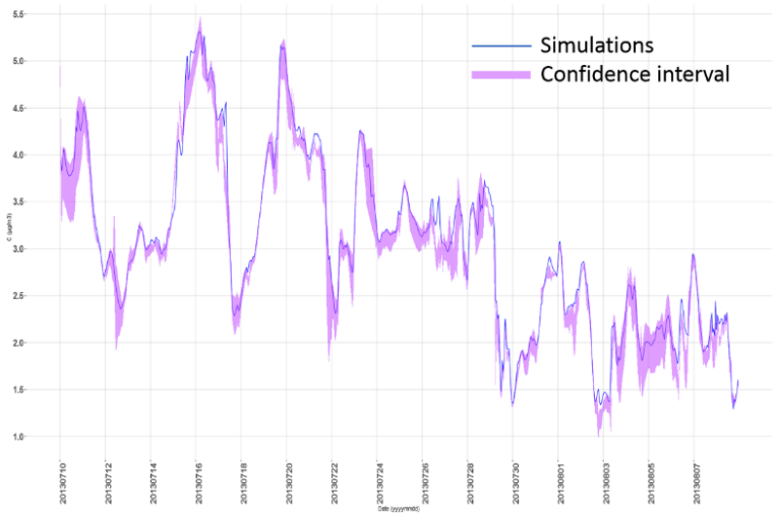


Figure III.13 – *Time series of all confidence intervals for all converged equations for OA.*

Putting together the chosen regressions for all the time-steps, gives us a time series of confidence intervals for each tested atmospheric component. Figure III.13 shows this interval for organic aerosols for all the equations combined. An average of the confidence intervals divided by the simulated average presents a percentage for each species, which can represent the sensitivity of said component to altitude changes in this region. The values obtained for several species are shown in table III.6. The concentration correction calculated for other species were also lower than the error, therefore for all the tested species shown in III.6, only the error is used instead of the concentration correction.

As a result, the orographic sensitivity of different components is calculated for the Cap Corse area. What is concluded from the error calculated here is the fact that this error

Orographic representativeness error							
Pollutant	ORE (%)	Pollutant	ORE (%)	Pollutant	ORE (%)	Parameter	ORE (%)
O_3	4	C_5H_8	85	Mono-terpenes	59	Temperature	0.5
OA	10	BC	26	SO_2	62	Relative humidity	18
SO_{2-}^4	15	NO_x	75	Aromatic species	49		
PM_{10}	9	CO	2	MACR+MVK	60		

Table III.6 – *Orographic representativeness errors (ORE) calculated for different chemical components and meteorological parameters.*

is much higher for primary species or highly reactive secondary species(i.e. NO_x with an error of 75%), while for secondary pollutants with higher life times in the atmosphere the orographic representativeness error is quite low (i.e. ozone with an error of 4%). For organic aerosols this error is calculated to be 10%. For secondary species with high life-times, this error is much smaller than the actual measurement-simulation differences encountered. Therefore, for secondary species, model comparisons with observations are not sensitive to orographic representativeness of the model, while the comparison of primary components is indeed strongly affected.

5 Simulation of dimethyl sulfide in CHIMERE

Dimethyl sulfide (DMS) emissions from the sea surface can increase the SO_2 burden in the atmosphere, which can then be transformed into sulfate particles, increasing the aerosol burden especially over bodies of water. It can also influence the cloud albedo and aerosol condensation nucleus fields. While accounting for a small fraction of sulfur content compared to anthropogenic emissions of this compound from continental areas or from shipping emissions, its effect on the radiative budget of the atmosphere makes it an important subject to study, especially when simulating near bodies of water. Ganor et al. (2000) calculated the contribution of DMS in the production of sulfates to be between 6 and 22% (11% average) over the Eastern Mediterranean basin, showing strong seasonal variations. Others have made estimations in this regard as well, showing around 17% to 28% contribution for sulfate formation for summer months depending on the region.

5.1 Physical dependencies of dimethyl sulfide flux into the atmosphere

The natural emissions originating from the sea surface are generally hard to quantify. They depend on the quantity of the species available close to the water surface or the concentration gradient with the atmosphere, and an exchange speed, depending on near surface turbulent processes, relating in turn on near surface wind speed. In order to get an idea about these fluxes, measurements inside the sea water and at the vicinity of the sea surface have to be performed. While the possibility of measuring in both these environments exists, measurements for both sea surface DMS concentration and its flux into

the atmosphere at the same time are hard to come by. In addition, the formation of DMS in the ocean is related to the plankton activity, which is in turn related to temperature and available nutrients, meaning that in different regions of the world and in different months of the year the concentration of DMS in the ocean is quite variable. Also, the influx of DMS into the atmosphere, apart from the amount of this component available in the ocean, depends on the speed of the wind in contact with the ocean. In conclusion, one could say that the decisive parameters for DMS emissions into the atmosphere are the concentration of DMS in the ocean, the wind speed at the sea surface and the temperature. This is shown in the equation expressed by Liss and Merlivat (1986):

$$F = K_w \Delta C \tag{III.2}$$

Where,

$F \rightarrow$ Flux

$K_w \rightarrow$ Piston velocity

$\Delta C \rightarrow$ Difference of concentration between the air-sea interface

ΔC is expressed by:

$$\Delta C = \frac{C_a}{H} - C_w \tag{III.3}$$

Where,

$C_a \rightarrow$ Concentration in the atmosphere

$C_w \rightarrow$ Concentration in the water

$H \rightarrow$ Henry's constant

In the case of DMS, the atmospheric concentration is negligible compared to what is available in the sea surface (and is at equilibrium with the underlying ocean), therefore:

$$\Delta C = -C_w \tag{III.4}$$

And thus:

$$F = -K_w C_w \tag{III.5}$$

In this equation, the piston velocity is calculated using wind speed and temperature, and the concentration of DMS in the sea can be approximated. In the parts that follow, different methods for the approximation of sea surface concentration of DMS and the calculation of piston velocity will be explained in more detail.

Implementing simulation of DMS in CTMs means that some simplifications have to be made, since CTMs are normally not coupled to an oceanic model that can provide concentrations of this component inside the sea. Meaning that, either emission fluxes have

to be integrated directly into the model as 2D maps or simplified methods of calculating these fluxes have to be identified. Both of these options have been tested in the literature for the influx of DMS into the atmosphere and will be presented in the part that follows.

Kettle, M. Andreae, et al. (1999) assembled a large global database of measurements regarding to not only DMS water surface measurements, but also other related observations such as sea surface salinity temperature, chlorophyll, etc. Using this database that contains around 15000 points, they created climatological 2D fields of sea surface DMS concentration using a complex series of interpolations, extrapolations and iterations. They continued this research by calculating the flux of DMS into the atmosphere using these 2D fields in their next work (Kettle and M. Andreae 2000). Most of the parameterizations used today are based on the dataset collected by Kettle, M. Andreae, et al. (1999), with sometimes addition of newly obtained measurements.

Simó and Dachs (2002) used the same dataset mentioned above, suggesting a procedure, where the DMS sea surface concentration fields are calculated using remotely sensed chlorophyll-α data and climatological mixed layer depth fields. They obtained climatological DMS sea surface concentrations which are then used to calculate the influx of this component into the atmosphere. Another approach is using oceanic models, for example, Chu et al. (2003) implemented a biogeochemical approach in an oceanic model, simulating the gain and loss in DMS, which is then used for the simulation of flux of DMS towards the atmosphere.

Belviso et al. (2004) compared 7 different climatological maps obtained by different studies for the DMS concentration on the sea surface, concluding that different methods were suitable for different regions of the world, for example the method proposed by Simó and Dachs (2002) is more appropriate for the equatorial pacific zone. In this study, the suggested climatological 2D maps by Kettle and M. Andreae (2000) are taken as reference.

In this work, the approach suggested by Lana et al. (2011) is used for the 2D climatological maps of sea surface DMS concentration. The authors based themselves again on the dataset provided by Kettle, M. Andreae, et al. (1999), however, they added around 30000 points to the measurements, assembling a dataset of over 45000 points. They divided the globe into several regions and for each regions temporal interpolation and substitution techniques are used in order to fill the gaps. This gave them a first guess field, which was then smoothed using distance–weighted interpolation methods. The end-point 1° horizontal resolution data is freely available and is used in our work, as DMS sea surface concentration maps. A resolution of 1° is not sufficient for regional simulations, therefore, a re-gridding of this data has been performed in this work, changing the resolution to the resolution used in MEGAN input files, i.e. $0.008^\circ \times 0.008^\circ$. The re-gridding uses the same data provided by the aforementioned source, changing the resolution into a finer one, taking into account a high-resolution land-sea mask (figure III.14). It is important to mention that these fields provide monthly climatological data,

therefore they are not dependent on the actual meteorological conditions used in the model.

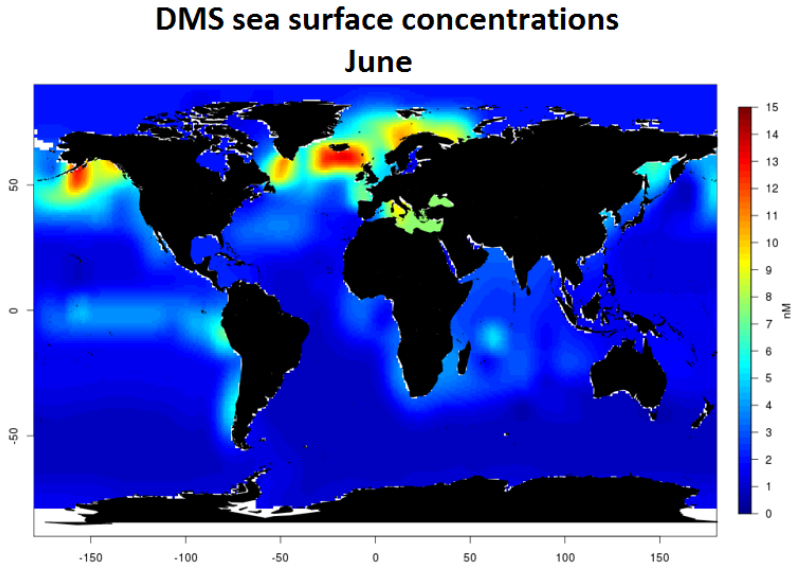


Figure III.14 – *Sea surface concentration of DMS for the month of July according to Lana et al (2011)*

While this resolves the issue of concentration fields for the in-water DMS availability, the flux of DMS into the atmosphere needs to be calculated as well. As mentioned before, this flux depends on the wind speed and temperature. These two parameters are used in the calculation of the piston velocity and the Schmidt number respectively. The Schmidt number is calculated quite easily:

$$Sc = 2674.0 - 147.12T + 3.726T^2 - 0.038T^3 \tag{III.6}$$

Where,

$Sc \rightarrow$ The Schmidt number

$T \rightarrow$ 2m temperature (°C)

However, the piston velocity equation differs depending on the intensity of the wind speed. Several parameterizations exist for the estimation of the piston velocity, four of them are presented in table III.7.

The parameters used in table III.7 are:

$Sc_r \rightarrow$ Reference Schmidt number calculated at reference temperatures (normally calculated for 20°C for freshwater CO_2 or seawater CO_2)

Wind speed range	LM86	W92	N00	B07
$\mathbf{U_{10} < 3.6}$	$e_1 U_{10}(Sc_r/Sc)^{2/3}$	$e_1(U_{10})^2(Sc_r/Sc)^{1/2}$	$e_1 U_{10}(Sc_r/Sc)^{1/2}$ $+e_1 U_{10}{}^2(Sc_r/Sc)^{1/2}$	$e_1(U_{10})^2(Sc_r/Sc)^{1/2}$
$\mathbf{3.6 \leq U_{10} < 5.6}$	$e_2(U_{10}-3.6)(Sc_r/Sc)^{1/2}$ $+e_3(Sc_r/Sc)^{2/3}$	$e_1(U_{10})^2(Sc_r/Sc)^{1/2}$	$e_1 U_{10}(Sc_r/Sc)^{1/2}$ $+e_1 U_{10}{}^2(Sc_r/Sc)^{1/2}$	$e_2(5.6-U_{10})/2.0$ $+e_3(U_{10}-3.6)/2.0$
$\mathbf{5.6 \leq U_{10} < 13}$	$e_2(U_{10}-3.6)(Sc_r/Sc)^{1/2}$ $+e_3(Sc_r/Sc)^{2/3}$	$e_1(U_{10})^2(Sc_r/Sc)^{1/2}$	$e_1 U_{10}(Sc_r/Sc)^{1/2}$ $+e_1 U_{10}{}^2(Sc_r/Sc)^{1/2}$	$e_4(U_{10}-3.6)(Sc_r/Sc)^{1/2}$ $+e_5(Sc_r/Sc)^{2/3}$
$\mathbf{U_{10} \leq 13}$	$e_4(U_{10}-13)(Sc_r/Sc)^{1/2}$ $+e_5(Sc_r/Sc)^{1/2}$ $+e_6(Sc_r/Sc)^{2/3}$	$e_1(U_{10})^2(Sc_r/Sc)^{1/2}$	$e_1 U_{10}(Sc_r/Sc)^{1/2}$ $+e_1 U_{10}{}^2(Sc_r/Sc)^{1/2}$	$e_4(U_{10}-5.6)(Sc_r/Sc)^{1/2}$ $+e_5(Sc_r/Sc)^{2/3}$
Constants	$e_1 = 0.17$ $e_2 = 2.85$ $e_3 = 0.612$ $e_4 = 5.90$ $e_5 = 26.79$ $e_6 = 0.612$ $Sc_r = 600$	$e_1 = 0.31$ $Sc_r = 660$	$e_1 = 0.333$ $e_2 = 0.222$ $Sc_r = 600$	$e_1 = 0.31$ $e_2 = 0.31$ $e_3 = 2.85$ $e_4 = 2.85$ $e_5 = 0.612$ $Sc_r = 600$
Reference	Liss and Merlivat, 1986	Woolf, 1997	Nightingale et al., 2000	Blomquist et al., 2006

Table III.7 – *Four parameterizations for the calculation of piston velocity, all depending on wind speed and temperature. The reference for each configuration is given under the table, an example of the calculated piston velocity with each of these schemes for different temperatures is shown in III.15.*

$U_{10} \rightarrow$ 10m wind speed (m.s^{-1})

$e_i \rightarrow$ Constants for the calculation of each piston velocity

These piston velocity parameterizations are taken from Liss and Merlivat (1986) (LM86), Woolf (1997) (W97), Nightingale et al. (2000)(N00) and Blomquist et al. (2006)(B07). A complete comparison of these methods (and some others) has been provided in Elliott (2009). Figure III.15 shows the calculated piston velocities using different parameterizations for different temperatures. The four parameterizations shown above were implemented in CHIMERE and tested for the Mediterranean domain.

5.2 Chemical processes

The complete chemistry of DMS is extremely complicated, therefore a reduced version of this chemistry has to be used in CHIMERE in order to express the fate of DMS emissions in the atmosphere and their contribution to SO_2 and sulfate. For this purpose, the chemical scheme suggested by Mihalopoulos et al. (2007) has been used here, which contains oxidation reaction of DMS with OH by the means of H abstraction, its oxidation by OH addition and its reaction with NO_3. It includes DMSO (Dimethyl sulfoxide) and

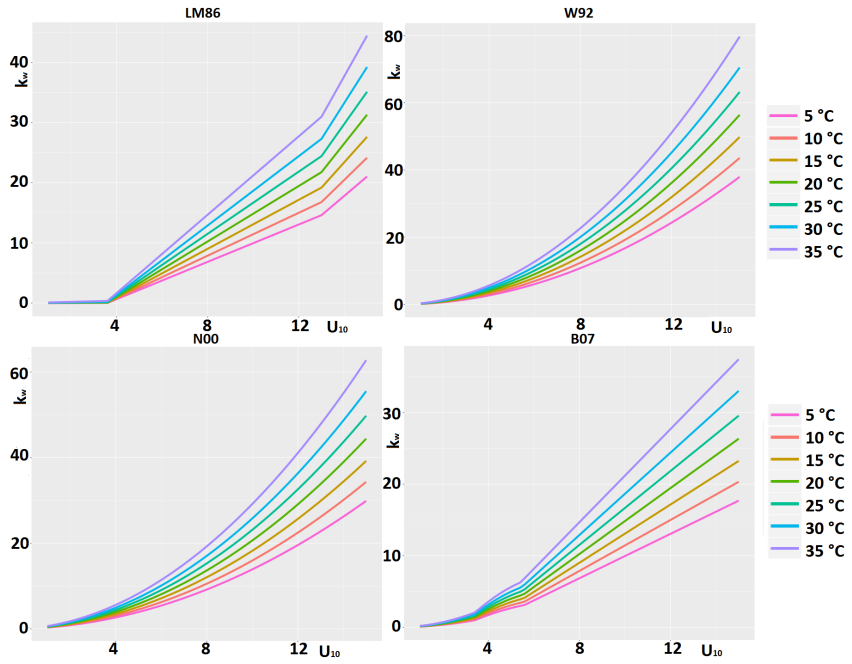


Figure III.15 – *Piston velocities calculated for a range of temperatures using the parameterizations presented in table III.7.Pay attention to the different vertical scales.*

MSIA (Methanesulfinic acid) as intermediate gas-phase chemistry. While the aqueous reactions are also available in this scheme, they were not implemented in CHIMERE, since their importance compared to the gas-phase DMS chemistry is small. The reactions added to CHIMERE for this purpose are presented below.

$$DMS + OH \longrightarrow 0.997(SO_2 + CH_3O_2 + HCHO) + 0.003(MSA + HCHO) \quad \text{(III.7)}$$

$$DMS + OH \longrightarrow DMSO \quad \text{(III.8)}$$

$$DMS + NO_3 \longrightarrow SO_2 + HNO_3 + CH_3O_2 + HCHO \quad \text{(III.9)}$$

$$DMSO + OH \longrightarrow MSIA + CH_3O_2 \quad \text{(III.10)}$$

$$MSIA + OH \longrightarrow CH_3O_2 + SO_2 + H_2O \quad \text{(III.11)}$$

Since MSA (Methanesulfonic acid) has been added to the CHIMERE chemical scheme specifically for the simulation of DMS, the deposition processes for this species has to be added to the model as well. For this purpose, both dry and wet deposition rates were added for this species with information taken from J. Seinfeld and S. Pandis (2016).

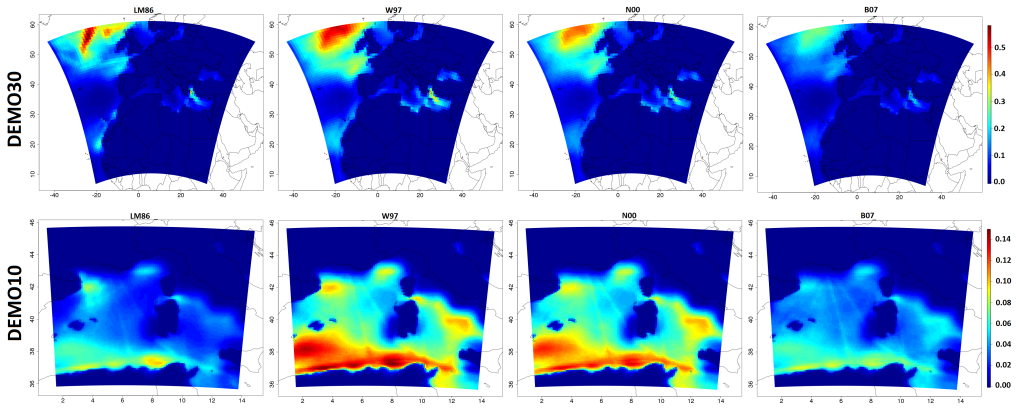


Figure III.16 – *Simulated DMS concentrations in DEMO30 (first row) and DEMO10 (second row). From left to right, each column shows LM86, W97, N00 and B07 parameterizations. Note that color scales are different for the upper and lower row.*

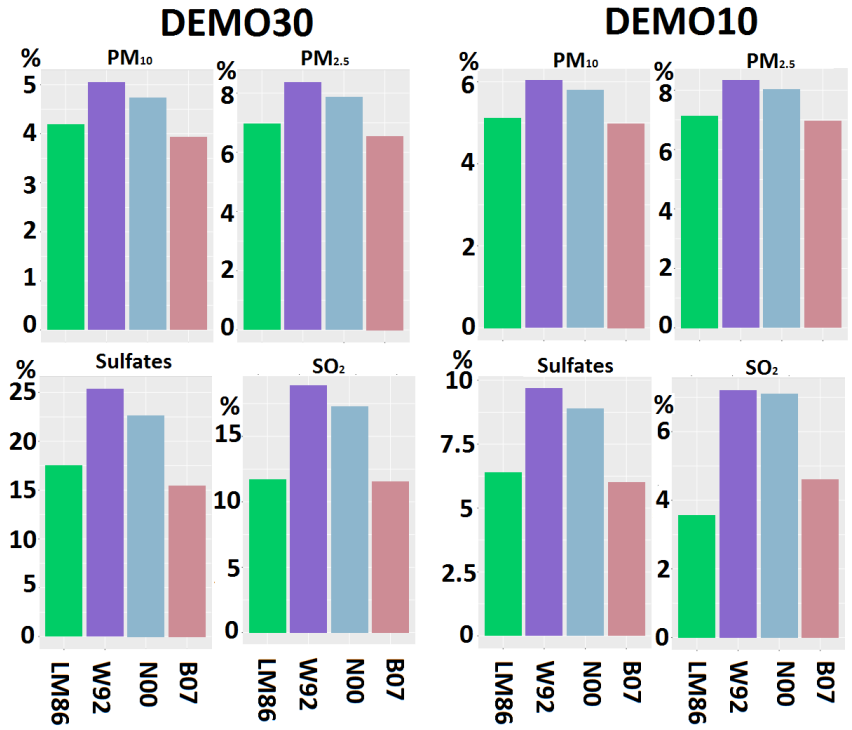


Figure III.17 – *Changes of some components in the four tested parameterizations for DEMO30 (left) and DEMO10 (right) compared to simulations where no DMS simulation scheme has been added. The values are shown in percentage.*

5.3 Simulated DMS fields and its oxidation products

The simulations performed for this part cover exactly the same period and use the exact same input parameters as the ones previously mentioned. The simulations were not performed for the two finest domains (DEMO3 and DEMO1) since no data was available in the Cap Corse area to be compared with the simulations, so the necessity of high resolution simulations is not evident in this case. Figure III.16 presents the 2D maps of DMS simulation in DEMO30 (from Saharian desert to Europe) and DEMO10 (over the Western Mediterranean basin) domains, for all tested parameterizations and figure III.17 shows the percentage changes seen in different parameterizations explained in table III.7 for a number of species that could be affected by DMS emissions. As seen in figure III.16 there are large differences of concentration between the methods used, each of them simulating different amounts of DMS, and also different changes seen in species connected to DMS (figure III.17). It is important to keep in mind that in this section, a land-sea mask has been used to calculate the values that are provided, therefore each value presents concentrations (or percentages) only for the sea surface. In the western mediterranean region for the period of simulations, a maximum of 10% change for sulfate particles is seen in our simulations, while for DEMO30, this change increases to around 25% since the DMS concentrations over the Atlantic Ocean is more important compared to that of the Mediterranean Sea. This is while the SO_2 concentrations show a maximum increase of 20% and 7% and an average increase of 15% and 6% for DEMO30 and DEMO10 respectively. The average change for sulfates for these two regions is 8% and 20%, showing a lower change rate in the western mediterranean compared to what is seen in the literature for the eastern mediterranean. Looking at these values it can be conluded that for the mediterranean region, the formation of sulfates from DMS is a non-negligible but a minor source. The difference between DMS emissions in the eastern and the western mediterranean is also seen in the figure III.17 for DEMO30, where higher concentrations of DMS are simulated for the eastern basin (i.e Ganor et al. (2000)). A maximum of 5% increase in PM_{10} and 8% increase in $PM_{2.5}$ concentrations are seen for DEMO30 and DEMO10 respectively in the same simulations as well (averages are around 4% and 6% respectively). The presence of DMS can change the radical concentrations (OH especially) in the area, which may result in some changes in the concentrations of other normally unimplecated components, but these changes should be minor.

The next step for this work is to compare the aforementioned simulations with measurements of DMS, or its oxidation products such as MSA. While these comparisons are a nessesity in order to validate the schemes used here for the simulation of DMS, no data was available for the simulation period in the ChArMEx campaign. Therefore, no observation-simulation comparisons will be presented in this work.

CHAPTER

IV

Simulation of organic aerosols in the western Mediterranean basin

Contents

1 Summary of article **101**
2 Simulation of organic aerosols in the western Mediterranean basin . . . **103**
3 Abstract **104**
4 Introdution **105**
5 Model setup **106**
5.1 Organic aerosol simulation 107
6 Experimental data set **109**
6.1 ChArMEx measurements 109
6.2 Other measurements 111
7 Model validation **111**
7.1 Orographic representativeness error 111
7.2 Meteorology evaluation 113
7.3 Gaseous species 113
7.4 Particulate species 115
8 Organic aerosol simulation **116**
8.1 Comparison of PM_1 total organic aerosol concentration 117
8.2 Total cabonaceous particle origins based on ^{14}C measurements . 117
8.3 Volatility and oxidation stat comparison with PMF results 119
9 Budget of organic aerosols **120**
10 Conclusion and discussion **121**

11 References **125**

The fourth chapter in this work concentrates on the simulation of OA in the western Mediterranean region. The first goal of the current thesis is to better describe and quantify OA sources in this area. In this regard, an evaluation of the CHIMERE model is necessary before entering into the OA simulation itself. Validation of simulation of different components apart from OA is included in this chapter. Regarding OA itself, an in-depth study of different schemes for the simulation of this component is performed. The modifications made to the model in the previous chapter regarding to meteorological conditions and some other factors dependent to the specific conditions in the western Mediterranean are used in this chapter.

1 Summary of article

The Mediterranean Sea is at the crossroads of multiple emission sources which transport or provide the necessary precursors for the aerosol formation. Dust emissions coming from Northern Africa, anthropogenic and biogenic emissions transported from Europe and local sources such as shipping emissions and salt emissions can contribute directly or indirectly to the aerosol burden in this region. In addition, the geographic situation shows some peculiarities as well: the residence times of pollutants in this region is long due to persistent anticyclonic situations and often high elevation of land in the coastal areas bordering the basin and having a climate between temperate and sub-tropical types, it provides favorable conditions for photo-chemistry.

This strong photo-chemistry triggers processing of biogenic and anthropogenic VOC precursors, leading to a well-known ozone formation, and also to organic aerosol (OA) build-up. The first goal of this thesis is to better describe and quantify OA sources in this area. The method is chemistry- transport modelling.

Therefore, an evaluation of the CTM is necessary in order to improve the model if necessary for this particular domain. This evaluation is based on comparison of simulations to intensive measurements obtained during the ChArMEx campaign. Since one of the regional peculiarities is its OA burden, a dedicated effort is necessary in order to simulate this species in the CTM.

First step in evaluating the model is finding appropriate representation of specific processes occurring over the Mediterranean Sea, this step was discussed in detail in the previous chapter (chapter III). In this chapter, a detailed evaluation of the methods used for the simulation of OA in the CHIMERE CTM is added. Four schemes have been evaluated. The first one is a two-product scheme that is the standard method used in CHIMERE for the simulation of this aerosol. The second and third ones are both VBS schemes, the first one taking into account aging processes by functionalization of SVOCs, for both ASOA and BSOA. The second one only considers the aging processes for ASOA, since it has been shown in the literature that the BSOA aging processes in VBS can result in a strong overestimation of this aerosol (Lane, Donahue, and S. Pandis 2008). Finally,

the fourth scheme is based on VBS as well, but it follows the parameterization proposed by M. Shrivastava, Easter, et al. (2015) and contains fragmentation and formation of non-volatile SOA as part of the aging processes. Month-long simulations covering the SAFMED period were performed for each of the schemes and the results were compared to the measurements from the aforementioned campaign.

Since the goal is to evaluate the CHIMERE CTM as well as to ameliorate the presentation of OA in the model, it is necessary to perform comparisons for other species along with OA. As a matter of fact, we need to make sure that the model well represents gaseous precursors and transport, before specifically evaluating OA schemes. Therefore, comparisons are performed for gaseous species (presented in this article are NO_x, isoprene, mono-terpenes and sum of methyl vinyl ketone and methacrolein) and particulate species (BC and sulfates included in this article). The orographic representativeness error explained in the previous chapter has been taken into account when performing the comparisons, since most of these species show high orographic representativeness errors (i.e. NO_x with 75% orographic representativeness error, which makes less conclusive). These comparisons are performed for two Mediterranean sites: the Ersa supersite and Es Pînar, Mallorca, where measurements for all these parameters were performed for the same period. In general, good correspondence is seen in the model for the simulation of gaseous species, except for mono-terpenes, where an underestimation occurs in both sites. For sulfates and BC, an overestimation for sulfates is observed and a good correlation is shown for BC. The chapter also contains a synthesis of the evaluation of meteorological simulations presented in the last chapter. This is a prerequisite for successful simulation of transport.

Comparisons for the OA have been done for concentration, oxidation state and its origins. For the oxidation state comparisons with three factor PMF results have been performed (LVOOA, SVOOA and HOA), while for the origin of OA, ^{14}C measurements have been used. The orographic representativeness error for OA is around 10%, which means that comparisons for this aerosol in the model are not sensitive to orography. Concentration comparisons show that the standard VBS scheme overestimates the simulated OA, while the CHIMERE standard scheme also overestimates the OA concentrations, but not to the extent of the VBS standard scheme. The other two schemes, the modified VBS scheme and the standard VBS scheme without BSOA aging achieve a good correspondence (bias of -18% and 34% respectively) for the simulated concentration.

Oxidation state comparisons show that the modified VBS scheme presents a good correspondence for all factors and the standard CHIMERE scheme overestimates the SVOOA factor contribution. The schemes based on the standard VBS do not contain particles corresponding to the volatility range of LVOOA, explaining their tendency to overestimate the SVOOA partition. ^{14}C measurements show a good correspondence for the modified VBS scheme as well as the standard CHIMERE scheme. The VBS scheme with BSOA aging overestimates the non-fossil contribution, while the VBS scheme without BSOA aging underestimates the non-fossil part.

2D maps of the western Mediterranean basin simulated with the modified VBS scheme, selected because of its good results, show that the OA with biogenic origins is dominant in the whole basin. In areas between Corsica and Marseille, the Gulf of Genoa and also the northern coast of Africa, the contribution of shipping emissions becomes quite important. At higher altitudes, the contribution of the biogenic sources becomes dominant over the whole basin, while the contribution of POA over the basin drops significantly.

Finally, as a result of this study, we have two OA simulation schemes that correspond well for the simulated concentration, while the modified VBS scheme seems to be able to simulate the oxidation state and the fossil/non-fossil distribution accurately as well. This study gives us an improved version of the CHIMERE model, which will be used in chapter VI for detailed analysis of climate impact on organic aerosol levels.

2 Simulation of organic aerosols in the western Mediterranean basin

This chapter includes the article Cholakian et al. (2018) published in *Atmospheric Chemistry and Physics : "Simulation of fine organic aerosols in the western Mediterranean area during the ChArMEx 2013 summer campaign,18, 7287–7312, doi:10.5194/acp-18-7287-2018, url: Atmospheric chemistry and physics"*.

The article was published the 25 May 2018.

Atmos. Chem. Phys., 18, 7287–7312, 2018
https://doi.org/10.5194/acp-18-7287-2018
© Author(s) 2018. This work is distributed under
the Creative Commons Attribution 4.0 License.



Atmospheric Chemistry and Physics Open Access EGU

Simulation of fine organic aerosols in the western Mediterranean area during the ChArMEx 2013 summer campaign

Arineh Cholakian[1,2], Matthias Beekmann[1], Augustin Colette[2], Isabelle Coll[1], Guillaume Siour[1], Jean Sciare[3,5], Nicolas Marchand[4], Florian Couvidat[2], Jorge Pey[4,a], Valerie Gros[3], Stéphane Sauvage[6], Vincent Michoud[6,b], Karine Sellegri[7], Aurélie Colomb[7], Karine Sartelet[8], Helen Langley DeWitt[4], Miriam Elser[9,c], André S. H. Prévot[9], Sonke Szidat[10], and François Dulac[3]

[1]Laboratoire Inter-Universitaire des Systèmes Atmosphériques (LISA), UMR CNRS 7583, Université Paris Est Créteil et Université Paris Diderot, Institut Pierre Simon Laplace, Créteil, France
[2]Institut National de l'Environnement Industriel et des Risques, Parc Technologique ALATA, Verneuil-en-Halatte, France
[3]Laboratoire des Sciences du Climat et de l'Environnement, LSCE/IPSL, CEA-CNRS-UVSQ, Université Paris-Saclay, Gif-sur-Yvette, France
[4]Aix-Marseille Université, CNRS, LCE FRE 3416, Marseille, 13331, France
[5]The Cyprus Institute, Energy, Environment and Water Research Center, Nicosia, Cyprus
[6]IMT Lille Douai, Univ. Lille, Département Sciences de l'Atmosphère et Génie de l'Environnement, 59000 Lille, France
[7]LAMP, Campus universitaire des Cezeaux, 4 Avenue Blaise Pascal, 63178 Aubière, France
[8]CEREA, Joint Laboratory École des Ponts ParisTech – EDF R and D, Université Paris-Est, 77455 Marne la Vallée, France
[9]Paul Scherrer Institute, 5232 Villigen – PSI, Switzerland
[10]University of Bern, Freiestrasse 3, 3012 Bern, Switzerland
[a]now at: the Spanish Geological Survey, IGME, 50006 Zaragoza, Spain
[b]now at: Laboratoire Inter-Universitaire des Systèmes Atmosphériques (LISA), UMR CNRS 7583, Université Paris Est, France
[c]now at: Laboratory for Advanced Analytical Technologies, Empa, Dübendorf, 8600, Switzerland

Correspondence: Arineh Cholakian (arineh.cholakian@lisa.u-pec.fr)

Received: 26 July 2017 – Discussion started: 23 October 2017
Revised: 6 March 2018 – Accepted: 21 April 2018 – Published: 25 May 2018

Abstract. The simulation of fine organic aerosols with CTMs (chemistry–transport models) in the western Mediterranean basin has not been studied until recently. The ChArMEx (the Chemistry-Aerosol Mediterranean Experiment) SOP 1b (Special Observation Period 1b) intensive field campaign in summer of 2013 gathered a large and comprehensive data set of observations, allowing the study of different aspects of the Mediterranean atmosphere including the formation of organic aerosols (OAs) in 3-D models. In this study, we used the CHIMERE CTM to perform simulations for the duration of the SAFMED (Secondary Aerosol Formation in the MEDiterranean) period (July to August 2013) of this campaign. In particular, we evaluated four schemes for the simulation of OA, including the CHIMERE standard scheme, the VBS (volatility basis set) standard scheme with two parameterizations including aging of biogenic secondary OA, and a modified version of the VBS scheme which includes fragmentation and formation of nonvolatile OA. The results from these four schemes are compared to observations at two stations in the western Mediterranean basin, located on Ersa, Cap Corse (Corsica, France), and at Cap Es Pinar (Mallorca, Spain). These observations include OA mass concentration, PMF (positive matrix factorization) results of different OA fractions, and ^{14}C observations showing the fossil or nonfossil origins of carbonaceous particles. Because of the complex orography of the Ersa site, an original method for calculating an orographic representativeness error (ORE) has been developed. It is concluded that the modified VBS scheme is close to observations in all three aspects mentioned above; the standard VBS scheme without BSOA

(biogenic secondary organic aerosol) aging also has a satisfactory performance in simulating the mass concentration of OA, but not for the source origin analysis comparisons. In addition, the OA sources over the western Mediterranean basin are explored. OA shows a major biogenic origin, especially at several hundred meters height from the surface; however over the Gulf of Genoa near the surface, the anthropogenic origin is of similar importance. A general assessment of other species was performed to evaluate the robustness of the simulations for this particular domain before evaluating OA simulation schemes. It is also shown that the Cap Corse site presents important orographic complexity, which makes comparison between model simulations and observations difficult. A method was designed to estimate an orographic representativeness error for species measured at Ersa and yields an uncertainty of between 50 and 85 % for primary pollutants, and around 2–10 % for secondary species.

1 Introduction

The Mediterranean basin is subject to multiple emission sources; anthropogenic emissions that are transported from adjacent continents or are produced within the basin, local or continental biogenic and natural emissions among which the dust emissions from northern Africa can be considered as an important source (Pey et al., 2013; Vincent et al., 2016). All these different sources, the geographic particularities of the region favoring accumulation of pollutants (Gangoiti et al., 2001), and the prevailing meteorological conditions favorable to intense photochemistry and thus secondary aerosol formation, make the Mediterranean area a region experiencing a heavy burden of aerosols (Monks et al., 2009; Nabat et al., 2012). In the densely populated coastal areas, this aerosol burden constitutes a serious sanitary problem considering the harmful effects of fine aerosols on human health (Martinelli et al., 2013). In addition, studies have shown that the Mediterranean area could be highly sensitive to future climate change effects (Giorgi, 2006; Lionello and Giorgi, 2007). This could affect aerosol formation processes, but in turn the aerosol load also affects regional climate (Nabat et al., 2013). These interactions, the high aerosol burden in the area, and its health impact related to the high population density situated around the basin make this region particularly important to study.

The aforementioned primary emissions can be in the form of gaseous species, as particulate matter, or as semi-volatile species distributed between both phases (Robinson et al., 2007). In the atmosphere, they can subsequently undergo complex chemical processes lowering their volatility, which leads to the formation of secondary particles. These processes are not entirely elucidated especially for the formation of SOAs (secondary organic aerosols) for example (Kroll and Seinfeld, 2008), starting from initially emitted biogenic or anthropogenic VOCs (volatile organic compounds) and SVOCs (semi-volatile organic compounds).

The chemical composition of aerosols has been studied in detail in the eastern Mediterranean area (Lelieveld et al., 2002; Bardouki et al., 2003; Sciare et al., 2005, 2008; Koçak et al., 2007; Koulouri et al., 2008) and to a lesser extent in the western part (Sellegri et al., 2001; Querol et al., 2009; Minguillón et al., 2011; Ripoll et al., 2014; Menut et al., 2015; Arndt et al., 2017). Little focus has been given to the formation of organic aerosol (OA) over the western Mediterranean even if OA can play a significant role in both local and global climate (Kanakidou et al., 2005) and can affect health (Pöschl, 2005; Mauderly and Chow, 2008). Its contribution has been calculated in studies to be nearly 30 % in PM_1 for the eastern Mediterranean area during the FAME 2008 campaign (i.e., Hildebrandt et al., 2010). It is also important to know the contribution of different sources (biogenic, anthropogenic) to the total concentration of OA in the western part of the basin. Such studies have been performed for the eastern Mediterranean basin (e.g., Hildebrandt et al., 2010), while for the western part of the basin, they have been in general restricted to coastal cities such as Marseilles and Barcelona (El Haddad et al., 2011; Mohr et al., 2012; Ripoll et al., 2014).

The ChArMEx (the Chemistry Aerosol Mediterranean Experiment; http://charmex.lsce.ipsl.fr, last access: 17 August 2016) project was organized in this context, with a focus over the western Mediterranean basin during the period of 2012–2014, in order to better assess the sources, formation, transformation, and mechanisms of transportation of gases and aerosols. During this project, detailed measurements were acquired not only for the chemical composition of aerosols but also for a large number of gaseous species from both ground-based and airborne platforms. The project ChArMEx is divided into different sub-projects, each with a different goal; among those, the SAFMED (Secondary Aerosol Formation in the MEDiterranean) project aimed at understanding and characterizing the concentrations and properties of OA in the western Mediterranean (for example Nicolas, 2013; Di Biagio et al., 2015; Chrit et al., 2017; Arndt et al., 2017; Freney et al., 2017). To reach these goals, two intense ground-based and airborne campaigns were organized during July–August of 2013 and also summer of 2014. The focus of the present study is on the SAFMED campaign in summer of 2013, since detailed measurements on the formation of OA and precursors were obtained during this period, namely at Ersa (Corsica) and Es Pinar (Mallorca). Other ChArMEx sub-projects and campaigns included the TRAQA (Transport et Qualité de l'Air) campaign in summer 2012, set up to study the transport and impact of continental air on atmospheric pollution over the basin (Sič et al., 2016), and the ADRIMED (Aerosol Direct Radiative Impact on the regional climate in the MEDiterranean, June–July 2013) campaign aimed at understanding and assessing the radiative impact of various aerosol sources (Mallet et al., 2016).

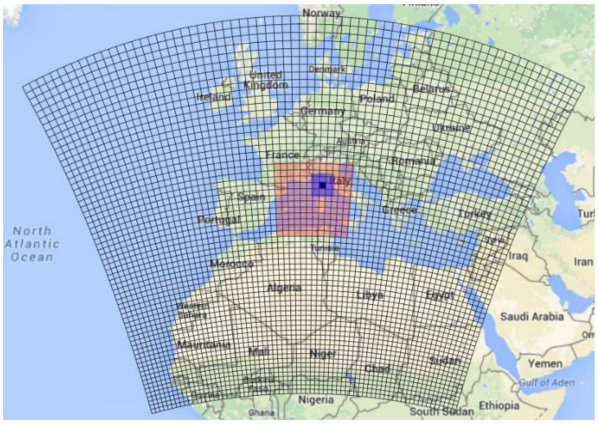
Modeling of aerosol processes and properties is a difficult task. Aside from the lack of knowledge of aerosol formation processes, the difficulty lies in the fact that OAs present an amalgam of thousands of different species that cannot all be represented in a 3-D chemistry–transport model (CTM) due to limits in computational resources. Therefore a small number of lumped species with characteristics that are thought to be representative of all the species in each group are used instead. There are many different approaches that can be used in creating representative groups for OAs (e.g., which characteristics to use to group the species, which species to lump together, physical processes that should be presented for their simulation). It is therefore necessary to test these different simulation schemes for OAs in different regions and compare the results to experimental data to check for their robustness. For example, Chrit et al. (2017) modeled SOA formation in the western Mediterranean area during the ChArMEx summer campaigns, with a surrogate scheme that also contains ELVOCs (extremely low-volatility organic compounds). The simulated concentrations and properties (oxidation and affinity with water) of OAs agree well with the observations performed at Ersa (Corsica), after they had included the formation of extremely low-volatility OAs and organic nitrate from monoterpene oxidation in the model.

The present study focuses on the comparison of different OA formation schemes implemented in the CHIMERE chemistry–transport model for simulation of OA over the western Mediterranean area. Different configurations of the volatility basis set (VBS; Donahue et al., 2006; Robinson et al., 2007; Shrivastava et al., 2013) and the base parameterization of the CHIMERE 3-D model (Bessagnet et al., 2008; Menut et al., 2013) are used for this purpose. Our work takes advantage of the extensive experimental data pool obtained during the SAFMED campaign. This enables us to perform model–observation comparisons with unprecedented detail over this region, including not only the OA concentration but also its origin (^{14}C analyses) and its oxidation state (positive matrix factorization (PMF) method results). In addition, a comparison for meteorological parameters and gaseous or particulate species which could affect the production of OA or could help analyze the robustness of the used schemes has been performed. Moreover, because of the orographic complexity of one of the sites (Ersa, Cap Corse) explored in this work, a novel method is designed to calculate the orographic representativeness error of different species. To the best of our knowledge, this is the first time that the concentrations of precursors, intermediary products, and OA concentrations and properties have been simulated for different OA simulation schemes and compared for each scheme to multiple series of measurements at different stations for the western Mediterranean area. For OA schemes, the paper aims at assessing the robustness of each scheme with regard to different criteria as mass, fossil, and modern fraction and volatility. Section 2 describes the model and the inputs used for the simulations. Also, the evaluated schemes are explained in this section in more detail. The experimental data used for simulation–observation comparisons are discussed in Sect. 3. An overall validation of the model is presented in Sect. 4, together with comparisons of different gaseous and particulate species and meteorological parameters to observations. In Sect. 5, comparison of implemented schemes to measurements regarding concentration, oxidation state, and origin of OA is presented. In Sect. 6, the contribution of different sources to the OA present in the whole basin is explored, before the conclusion in Sect. 7.

2 Model setup

The CHIMERE model (Menut et al., 2013; http://www.lmd.polytechnique.fr/chimere, last access: 9 August 2016) is an offline regional CTM which has been tested rigorously for Europe and France (Zhang et al., 2013; Petetin et al., 2014; Colette et al., 2015; Menut et al., 2015; Rea et al., 2015). It is also widely used in both research and forecasting activities in France, Europe, and other countries (Hodzic and Jimenez, 2011). In this work, a slightly modified version of the CHIMERE 2014b configuration is used to perform the simulations. The modifications concern an updated description of the changes in aerosol size distribution due to condensation and evaporation processes (Mailler et al., 2017). Four domains are used in the simulations: a coarse domain covering all of Europe and northern Africa with a 30 km resolution, and three nested domains inside the coarse domain with resolutions of 10, 3, and 1 km (Fig. 1). The 10 km resolved domain covers the western Mediterranean area and the two smaller domains are centered on the Cap Corse, where the main field observations in SAFMED were performed. Such highly resolved domains are necessary to resolve the complex orography of the Cap Corse ground-based measurement site, which will be discussed in Sect. 4, while for the flatter Es Pinar site, a 10 km resolution is sufficient. The simulations for each domain contain 15 vertical levels starting from 50 m to about 12 km above sea level (a.s.l.) with an average vertical resolution of 400 m within the continental boundary layer and 1 km above. The CHIMERE model needs a set of gridded data as mandatory input: meteorological data, emission data for both biogenic and anthropogenic sources, land use parameters, boundary and limit conditions, and other optional inputs such as dust and fire emissions. Given these inputs, the model produces the concentrations and deposition fluxes for major gaseous and particulate species and also intermediate compounds. The simulations presented in this article cover the period of 1 month from 10 July to 9 August.

Meteorological inputs are calculated with the WRF (Weather Research Forecast) regional model (Wang et al., 2015) forced by NCEP (National Centers of Environmental Predictions) reanalysis meteorological data (http://www.ncep.noaa.gov, last access: 11 September 2016) with a base resolution of 1°. Slightly larger versions of each domain with



Domain name	Cell numbers	Resolution
D30	71×64	30 km×30 km
D10	110×110	10 km×10 km
D3	110×110	3 km×3 km
D1	80×80	1 km×1 km

Figure 1. The four domains used in simulations (D30, D10, D3, D1). The resolution for each domain is given in the table below the image.

the same horizontal resolutions (Fig. 1) are used for the meteorological simulations. The WRF configuration used for this study consists of the single-moment 5 class microphysics scheme (Hong et al., 2004), the Rapid Radiative Transfer model (RRTMG) radiation scheme (Mlawer et al., 1997), the Monin–Obukhov surface layer scheme (Janjic, 2003), and the NOAA Land Surface Model scheme for land surface physics (Chen et al., 2001). Sea surface temperature update, surface grid nudging (Liu et al., 2012; Bowden et al., 2012), ocean physics, and topographic wind options are activated. Also, the feedback option is activated, meaning that the simulation of the nested domains can influence the parent domain. Some observation–simulation comparisons are presented for meteorological parameters in Sect. 4.

Anthropogenic emissions for all but shipping SNAP (Selected Nomenclature for Air Pollution) sectors come from the HTAP-V2 (Hemispheric Transport of Air Pollution; http://edgar.jrc.ec.europa.eu/htap_v2/index.php, last access: 21 August 2016) inventory. The shipping sector in this inventory was judged to overestimate ship traffic around the Cap Corse area, especially on the shipping lines between Marseilles and Corsica, due to overweighing ferries with respect to cargos (Van der Gon, personal communication). This could be explained by the fact that the boat traffic description is based on voluntary information. Therefore HTAP-V2 shipping emissions were replaced by those of the MACC-III inventory (Kuenen et al., 2014). The base resolution of the HTAP inventory is 10 km × 10 km and that of the MACC-III inventory is 7 km × 7 km. For both inventories the emissions for the year 2010 were used since this year was the latest common year in the two inventories.

Biogenic emissions are calculated using MEGAN (Model of Emissions of Gases and Aerosols from Nature; Guenther et al., 2006) including isoprene, limonene, α-pinene, β-pinene, ocimene, and other monoterpenes with a base horizontal resolution of 0.008° × 0.008°. The land use data come from GlobCover (Arino et al., 2008) with a base resolution of 300 m × 300 m. Initial and boundary conditions of chemical species are taken from the climatological simulations of LMDz-INCA3 (Hauglustaine et al., 2014) for gaseous species and GOCART (Chin et al., 2002) for particulate matter.

The chemical mechanism used for the baseline gas-phase chemistry is the MELCHIOR2 scheme (Derognat et al., 2003). This mechanism has around 120 reactions to describe the whole gas-phase chemistry. The reaction rates used in MELCHIOR are constantly updated (last update in 2015); however, the reaction scheme itself has not been updated since 2003. Some reactions have been added to it by Bessagnet et al. (2009) regarding the oxidation of OA precursors, but they do not affect gas-phase chemistry. Also, MELCHIOR has been compared to SAPRC-07A, a more recent scheme (Carter, 2010), and the results show acceptable differences between the two schemes; for example, when compared to EEA (European Economic Area) ozone measurements, both produce a correlation coefficient of 0.71. These comparisons are presented in Menut et al. (2013) and Mailler et al. (2017).

The CHIMERE aerosol module is responsible for the simulation of physical and chemical processes that influence the size distribution and chemical speciation of aerosols (Bessagnet et al., 2008). This module distributes aerosols in a number of size bins; here 10 bins range from 40 nm to 40 µm, in a logarithmic sectional distribution, each bin spanning over a size range of a factor of 2 (40–20, 20–10 µm, etc.). The module also addresses coagulation, nucleation, condensation, and dry and wet deposition processes. The basic chemical speciation includes elemental carbon (EC), sulfate, nitrate, ammonium, SOA, dust, salt, and PPM (primary particulate matter other than ones mentioned above).

2.1 Organic aerosol simulation

The SOA particles are divided, depending on their precursors, into two groups: ASOA (anthropogenic SOA) and BSOA (biogenic SOA). Four schemes were tested to simulate their formation; more detail on each scheme is presented below.

2.1.1 CHIMERE standard scheme

The SOA simulation scheme in CHIMERE (Bessagnet et al., 2008) consists of a single-step oxidation process in which VOC lumped species are directly transformed into SVOCs

with yields that are taken from experimental data (Odum et al., 1997; Griffin et al., 1999; Pun and Seigneur, 2007). These SVOC species are then distributed into gaseous and particulate phases (Fig. 2a) following the partitioning theory of Pankow (Pankow, 1987). The precursors for this scheme are presented in the Supplement (Sect. SI1). A number of 11 semi-volatile surrogate compounds are formed from these precursors, which include six hydrophilic species, three hydrophobic species, and two surrogates for isoprene oxidation. The sum of all 11 species results in the concentration of simulated SOA in this scheme.

2.1.2 VBS scheme

As an alternative to single-step schemes like the one in CHIMERE, the VBS approach was developed. In these types of schemes, SVOCs are divided into volatility bins regardless of their chemical characteristics, but only depending on their saturation concentration. Therefore it becomes possible to add aging processes in the simulation of OA by adding reactions that shift species from one volatility bin to another (Donahue et al., 2006). This scheme was implemented and tested in CHIMERE for Mexico City (Hodzic and Jimenez, 2011) and the Paris region (Zhang et al., 2013). The volatility profile used for this scheme consists of nine volatility bins with saturation concentrations in the range of 0.01 to $10^6\,\mu g\,m^{-3}$ (convertible to saturation pressure using atmospheric standard conditions), across which the emissions of SVOCs and IVOCs are distributed, following a specific aggregation table (Robinson et al., 2007). Four volatility bins are used for ASOA and BSOA ranging from 1 to $1000\,\mu g\,m^{-3}$. SOA yields are taken from the literature (Lane et al., 2008; Murphy and Pandis, 2009) using low-NO_x conditions ($VOC / NO_x > 10\,ppbC\,ppb^{-1}$). The SVOC species can age, by decreasing their volatility by one bin independent of their origin with a given constant rate. SVOC species are either directly emitted or formed from anthropogenic or biogenic VOC precursors. Fragmentation processes and the production of nonvolatile SOAs are ignored in this scheme. In the basic VBS scheme, the BSOA aging processes are usually ignored since they tend to result in a significant overestimation of BSOA (Lane et al., 2008). Although physically present, their kinetic constants for this aging process are considered the same as anthropogenic compounds and seem to be overestimated. However, in Zhang et al. (2013), including BSOA aging was necessary to explain the observed experimental data. Therefore, in this work, the VBS scheme is evaluated both with and without including the BSOA aging processes. Figure 2b shows a simplified illustration for ASOA and BSOA, while the partition for SVOC is presented in the Supplement (Sect. SI2). For all bins, regardless of their origin, the partitioning between gaseous and the particulate phases is performed following Raoult's law and depends on total OA concentration. Under normal atmospheric conditions, SVOC with the volatility range of 0.01 to $10^3\,\mu g\,m^{-3}$ can form aerosols. In total, the sum of 24 species in the model (with 10 size distribution bins each, i.e., 240 species in total) makes up the total concentration of SOA simulated by this scheme.

2.1.3 Modified VBS scheme

The basic VBS scheme does not include fragmentation processes, corresponding to the breakup of oxidized OA compounds in the atmosphere into smaller and thus more volatile molecules (Shrivastava et al., 2011). It also does not include the formation of nonvolatile SOA, where SOA can become nonvolatile after formation (Shrivastava et al., 2015). In this work, these two processes were added to the VBS scheme presented above and tested for the Mediterranean basin. The volatility bins for the VBS model were not changed (ranges presented in the previous section). SOA yields were kept as in the standard VBS scheme; however, instead of using the low-NO_x or the high-NO_x regimes, an interpolation between the yields of these two regimes was added to the model. For this purpose, a parameter is added to the scheme, which calculates the ratio of the reaction rate of RO_2 radicals with NO (high-NO_x regime) with respect to the sum of reaction rates of the reactions with HO_2 and RO_2 (low-NO_x regime). For this purpose, a parameter (α) is added to the scheme, which calculates the ratio of the reaction rate of RO_2 radicals with NO (ν_{NO}; high-NO_x regime) with respect to the sum of reaction rates of the reactions with HO_2 (ν_{HO_2}) and RO_2 (ν_{RO_2}; low-NO_x regime). The parameter α is expressed as follows:

$$\alpha = \frac{\nu_{NO}}{\nu_{NO} + \nu_{HO_2} + \nu_{RO_2}}. \quad (1)$$

This α value represents the part of RO_2 radicals reacting with NO (which leads to applying "high NO_x yields"). It is calculated for each grid cell by using the instantaneous NO, HO_2, and RO_2 concentrations in the model. Then, the following equation is used to calculate an adjusted SOA yield using this α value (Carlton et al., 2009).

$$Y = \alpha \times Y_{highNO_x} + (1-\alpha) \times Y_{lowNO_x} \quad (2)$$

The fragmentation processes for the SVOC start after the third generation of oxidation because fragmentation is favored with respect to functionalization for more oxidized compounds. Therefore, three series of species in different volatility bins were added to present each generation, similar to the approach setup in Shrivastava et al. (2013). For biogenic VOC, fragmentation processes come into effect starting from the first generation, as in Shrivastava et al. (2013), because the intermediate species are considered to be more oxidized. A fragmentation rate of 75 % (with 25 % left for functionalization) is used in this work for each oxidation step following Shrivastava et al. (2015). The formation of nonvolatile SOA is performed by moving a part of each aerosol bin to nonvolatile bins with a reaction constant corresponding to a lifetime of 1 h, similar to Shrivastava et al. (2015).

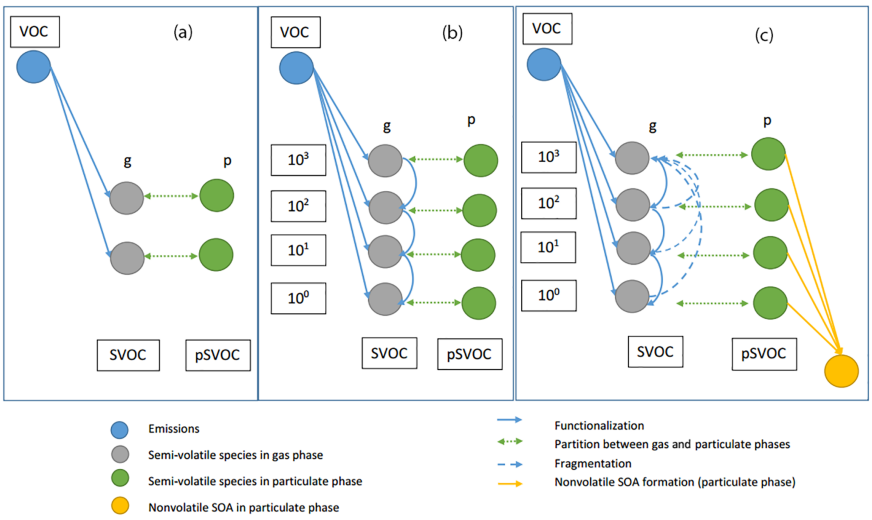


Figure 2. Organic aerosol simulation schemes. **(a)** CHIMERE standard scheme (Bessagnet et al., 2008): from a parent volatile organic compound (VOC), different semi-volatile organic compounds (SVOCs) (only one represented) are formed in a single step by oxidation; they are in equilibrium between gas and aerosol phases (pSVOC); **(b)** VBS standard scheme (Robinson et al., 2007): from a parent VOC, SVOCs with regularly spaced volatility ranges are formed and are in equilibrium with the aerosol phase. Aging of SVOC by functionalization is included by passing species to classes with lower volatility; **(c)** modified VBS scheme (Shrivastava et al., 2015): here SVOC aging also includes fragmentation, leading to transfer of species to classes with higher volatility. In addition, semi-volatile aerosol can be irreversibly transformed into nonvolatile aerosol (yellow-filled circle). For each bin, saturation concentration is shown in micrograms per cubic meter. Note that this schematic represents BSOA and ASOA (biogenic and anthropogenic secondary organic aerosol) where four bins are used; for SVOC and IVOC (semi-volatile and intermediate-volatility organic compounds, where nine bins are used) a schematic is presented in Supplement Sect. SI1.

Figure 2c shows a scheme of the modified VBS for the VOC. In total, 40 species (with 10 size distribution bins each, i.e., 400 species in total) are added together to calculate the total concentration of SOA simulated by this scheme. The resulting model has a total of 740 species in the output files (including gas-phase chemistry), which makes this scheme the most time consuming among the tested schemes. In Sect. 5 of this paper, the results from the three schemes introduced above will be compared to observations.

3 Experimental data set

During the SAFMED sub-project, measurements were made at two major sites, the Ersa, Cap Corse, station and the Cap Es Pinar, Mallorca, station. The geographical characteristics and the measurements performed at each site are presented in the following section.

3.1 ChArMEx measurements

The Ersa supersite (42°58′04.1″, 9°22′49.1″) is located on the northern edge of Corsica, in a rural environment, at an altitude of 530 m a.s.l. The station is located on a crest that dominates the northern part of the cape. It has a direct view of the sea on the western, northern, and eastern sides. Measurements carried out in this station are reported in Table 1. More details about the instrumental setup in Ersa can be found in Michoud et al. (2017) and Arndt et al. (2017).

The Es Pinar supersite (39°53′04.6″, 3°11′40.9″) is located on the northeastern part of Mallorca. The monitoring station was placed in the "Es Pinar" military facilities belonging to the Spanish Ministry of Defense. The environment is a non-urbanized area surrounded by pine forested slopes and is one of the most insulated zones on Mallorca, in between the Alcúdia and Pollença bays, but can still be influenced by local anthropogenic emissions. The site is located at an altitude of 20 m a.s.l. The location of the station and a list of available measurements are presented in Fig. 3 and Table 1, respectively.

At Ersa, NO_x (nitrogen oxides) were measured using a CraNOx analyzer using ozone chemiluminescence with a resolution of 5 min. The photolytic converter in the analyzer allows the conversion of direct measurements of NO_2 into NO in a selective way, thus avoiding interferences with other NO_y species. At Es Pinar, an API Teledyne T200 with molybdenum converter was used; therefore, the measurements are not specific to NO_2 and interferences of NO_y are possible for these measurements. VOCs were monitored at both supersites using a proton-transfer-reaction time-of-flight mass spectrometer (PTR-ToF-MS) (Kore™ second

Table 1. Gas and aerosol and meteorological measurements used for this study.

(1) Ersa, France (42°58′04.1″, 9°22′49.1″) Gases: NO_x (CRANOX), VOCs (PTR-ToF-MS-KORE) Aerosols: PM_{10} total mass (TEOM-FDMS), online (non-refractive) PM_1 Chemistry : OA, SO_4^{2-}, NH_4^+, NO_3^- (ACSM), ^{14}C (PM_1, daily filters), BC ($PM_{2.5}$, MAAP) Meteorology: temperature, wind speed, wind direction, relative humidity
(2) Es Pinar, Spain (39°53′04.6″, 3°11′40.9″) Gases: NO_x (API Teledyne T200), VOCs (PTR-ToF-MS, Ionikon) Aerosols: PM_{10} total mass (BETA corrected by factor obtained after comparison with gravimetric), PM_1 online Chemistry: OA, SO_4^{2-}, NH_3^+, NO_3^- (HR-ToF-AMS), ^{14}C (PM_1, daily filters), BC ($PM_{2.5}$, Aethalometer AE33) Meteorology: temperature, wind speed, wind direction, relative humidity
(3) Palma, Spain (39°36′20.88″, 2°42′23.7594″), (4) Nîmes, France (43°51′21.6″, 4°24′21.5994″), (5) Ajaccio, France (41°55′5.3256″, 8°47′38.0538″) Radiosondes: T, RH, wind speed, wind direction; at 00:00 and 12:00 UTC each day



Figure 3. Experimental data sites, including in situ surface stations (1: Ersa, France; 2: Cap Es Pinar, Spain) and meteorological sounding stations (3: Palma, Spain; 4: Nîmes, France; 5: Ajaccio, France). More details about exact location and measurements performed can be found in Table 1.

generation at Ersa, and Ionikon™ PTR-ToF-MS 8000 at Es Pinar). A detailed procedure of VOC quantification is provided in Michoud et al. (2017) for Ersa. Briefly, both instruments were calibrated daily using gas standard calibration bottles and blanks performed by means of a catalytic converter (stainless steel tubing filled with Pt wool held at 350 °C).

A quadruple aerosol chemical speciation monitor (Q-ACSM, Aerodyne Research Inc.; Ng et al., 2011) was used for the measurements of the chemical composition of non-refractory submicron aerosol at Ersa with a time resolution of 30 min. This instrument has the same general structure of an AMS (aerosol mass spectrometer), with the difference that it was developed specifically for long-term monitoring. A high-resolution time-of-flight AMS (HR-ToF-AMS, Aerodyne Research Inc.; Decarlo et al., 2006) operated under standard conditions (i.e., temperature of the vaporizer set at 600 °C, electronic ionization (EI) at 70 eV) was deployed with a temporal resolution of 8 min to determine the bulk chemical composition of the non-refractory fraction of the aerosol for the Es Pinar site. AMS data were processed and analyzed using the HR-ToF-AMS analysis software SQUIRREL (SeQUential Igor data RetRiEvaL) v.1.52L and PIKA (Peak Integration by Key Analysis) v.1.11L for the IGOR Pro software package (Wavemetrics, Inc., Portland, OR, USA). Q-ACSM and AMS source apportionment results discussed in this work are detailed in Michoud et al. (2017). For both sites, source contributions were obtained from PMF analysis (Paatero and Tapper, 1994) of Q-ACSM and AMS OA mass spectra. PMF was solved using the multilinear engine algorithm (ME-2; Paatero, 1997), using the Source Finder toolkit (SoFi; Canonaco et al., 2013). For the Ersa site, the HOA (hydrocarbon-like organic aerosol) profile was constrained with a reference HOA factor using an a value of 0.1. The a value refers to the extent to which the output HOA factor is allowed to vary from the input HOA reference mass spectra (i.e., 10 % in this case; Canonaco et al., 2013). In such a remote environment, the HOA factor could not be extracted from the OA mass spectral matrix with a classic unconstrained PMF approach. Two other factors were extracted, without any constrains, includ-

ing SVOOA (semi-volatile oxygenated organic aerosol) and LVOOA (low-volatility oxygenated organic aerosol). For the Es Pinar site, HOA has been constrained using an a value of 0.05. Three additional factors were retrieved, including an SVOOA and two LVOOA factors. In addition to HOA, three other factors have been extracted from the PMF analysis: one SVOOA and two LVOOA factors. Differences between these two LVOOA factors are mainly linked to air mass origins and to the probable influence of marine emissions. For the marine LVOOA factor at both sites, a correlation coefficient (R^2) of 0.43 and 0.47 with the main fragment derived from methane sulfonic acid (MSA, fragment $CH_3SO_2^+$) was found for Es Pinar and Ersa, respectively. For the sake of clarity and for the purpose of intercomparison with the model outcomes, we merge the two LVOOA factors into one LVOOA for the Cap Es Pinar site to be compared to the Ersa site results. Online aerosol chemical characterization was complemented by an Aethalometer (AE33, MAGEE; Drinovec et al., 2015) at Es Pinar and a multiangle absorption photometer (MAAP5012, Thermo) for the quantification of black carbon (BC) at Ersa. PM_{10} total mass measurements were taken from TEOM-FDMS (tapered element oscillating microbalance filter dynamic measurement system) at Es Pinar and corrected by a factor obtained after comparison to gravimetric measurements. Finally, daily PM_1 aerosol samples were collected onto 150 mm quartz fiber filters (Tissuquartz, Pall) at both sites. A total of 18 and 8 samples were selected for Ersa and Es Pinar, respectively, for a subsequent analysis of radiocarbon performed on both organic carbon (OC) and EC fractions following the method developed in Zhang et al. (2012).

3.2 Other measurements

For the validation of meteorological parameters, along with the meteorological surface measurements performed at ChArMEx stations, radiosonde data for three stations in the western Mediterranean basin were used for simulation–observation comparisons for meteorological parameters. The radiosondes are performed by Météo France at the two stations of Ajaccio, France (41°55′5″, 8°47′38″), and Nîmes, France (43°51′22″, 4°24′22″), and by AEMet at Palma, Spain (39°36′21″, 2°42′24″). Each day two balloons at about 00:00 and 12:00 UTC are available for each station; a total of 96 balloons are included in the comparisons. Ajaccio and Palma are coastal stations, but Nîmes is farther from the coast compared to the other two stations. Each day two balloons were launched at about 00:00 and 12:00 UTC at each station, and a total of 96 balloons are included in the comparisons for an altitude between the surface and 10 km.

4 Model validation

The CHIMERE model has been previously validated for different parts of the world (Hodzic and Jimenez, 2011; Solazzo et al., 2012; Borrego et al., 2013; Berezin et al., 2013; Petetin et al., 2014; Rea et al., 2015; Konovalov et al., 2015; Mallet et al., 2016). The data set presented in Sect. 3 is used for model validation. First, a representativeness error within simulations is calculated for a list of pollutants, which is necessary to distinguish between uncertainties due to limitations in model resolution and due to other reasons. Then a validation for the meteorological parameters is presented, before comparison of simulation results to gaseous and aerosol measurements.

4.1 Orographic representativeness of Cap Corse simulations

As explained before, during the ChArMEx campaign, an important number of observations were made at Ersa, Cap Corse. In order to use this data set for model evaluation, potential discrepancies due to a crude representation of the complex orography of Cap Corse need to be minimized and quantified since the measurements were performed on the crest line.

For the 10 km domain (D10), we noticed that there was an inconsistency between simulated and real altitude of the cell where the Ersa site is located, altitude being simulated at 360 m a.s.l. below the real altitude of measurements (530 m a.s.l.). Therefore, 1 km horizontally resolved simulations were performed for the inner domain. However, even for the 1 km simulations the simulated altitude remains too low (365 m a.s.l.). This error occurs because the altitude of each cell in CHIMERE is calculated using the average of altitudes of points inside the cell; therefore if the altitude of the ground surface inside a cell happens to vary greatly, the average would be lower than the higher points seen in the cell (which corresponds in our case to the Ersa site located on the crest). In addition, the average of the marine boundary layer height is typically around 500 m (Stull, 1988); therefore a discrepancy in the simulated altitude could cause significant errors in the simulations. These two reasons make it important to explore the representativeness of the simulations regarding this station.

This led us to perform an orographic representativeness test on the 1 km domain (D1) at the Ersa site. A matrix of neighboring cells around the grid cell covering the Ersa station (up to 5 km distance) was taken (Fig. 4a), and species concentrations were plotted against the variation of the altitude of these different cells. The highest altitude reached by one of the cells is about 450 m. Then, the concentration on the exact altitude (530 m) was extrapolated using a nonlinear regression between the altitude and the concentration of the selected cells with several different equations for each time step. In total, nine nonlinear equations were tested, among

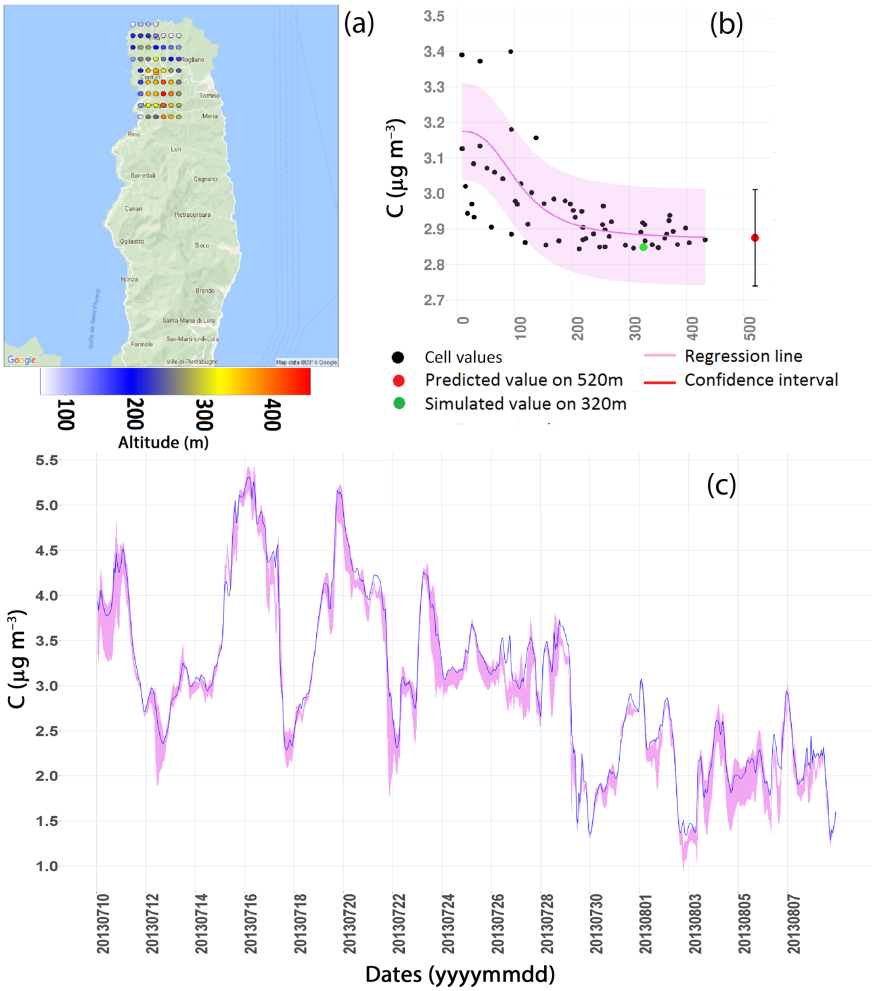


Figure 4. Orographic representativeness error. **(a)** Neighboring cells used in the orographic representativeness test; **(b)** an example of non-linear regressions performed on one time step for organic aerosol (OA, one point corresponds to one grid cell); **(c)** results from all hourly simulations for OA. In **(b)** and **(c)**, the purple ribbon shows the confidence interval of the regression results. In **(c)**, the blue line shows the simulations at the nominal Ersa site grid cell.

which only five were finally used for the calculation of the representativeness error. For the other four equations, convergence problems occurred and no stable solution could be found for some of the hourly time steps (see Supplement Sect. SI3 for details). Regressions were performed separately for each of the 720 hourly time steps of the 1-month simulations. An example of this regression for OAs for one time step and one of the equations is shown in Fig. 4b (Eq. 1 from SI3). The results were filtered using two criteria (convergence of regression for each time step and a correlation coefficient between fitted and simulated points of higher than a threshold) depending on statistical values of the regressions (see Supplement Sect. SI3 for details) and only regressions conforming to these criteria were retained. If at least two converging regressions were not retained for a given time step, the results for that time step were not further used. Figure 4c shows the compiled results for all equations and all simulation times in one time series for total OA concentration. Note that model output was generated with an hourly time step. Using these results, for a list of different species, an orographic representativeness error was calculated using the average of the difference of the upper and lower confidence intervals for all equations. As an example, carbon monoxide, which is a well-mixed and a more stable component in the atmosphere, presents the lowest error among the tested species (2 %). Ozone also presents one of the lowest errors (4 %) and nitrogen oxides one of the highest (75 %). OA, of particular interest for this study, shows a moderate error of 10 %.

In terms of meteorological parameters, relative humidity appears more affected (relative orographic representativeness error of 18 %) than temperature (the relative orographic representativeness error is calculated on values of T in °C). A summary of results of this test is shown in Table 2.

A general conclusion is that secondary pollutants with higher atmospheric lifetimes appear to be well represented from a geographic point of view. Conversely, model–observation comparisons for more reactive primary and secondary pollutants with short lifetimes (primary such as NO_x and reactive secondary such as methyl vinyl ketone and methacrolein, MVK+MACR) should be performed with caution keeping in mind the fact that the simulated altitude is not representative of the orography for this specific station. This is due to the fact that short-lived primary species have not yet had the chance to vertically mix, if emission sources happen to be nearby (which is the case here). Vertical layering of these concentrations then results in significant sensitivity to the simulated altitude of a site. Conversely, secondary species, which have partly been transported from the continental boundary layer, are believed to be better mixed vertically. For those species, differences in the simulated versus observed altitude lead to relatively smaller errors.

The question of which domain should be used for model–measurement comparisons remains. As seen above, D10, despite having a sufficiently fine resolution for most continental areas, is not capable of representing the complex orography of Cap Corse; therefore the D1 simulation results have been used for comparisons, except for meteorological parameters, where all possible domains (and resolutions) are compared. The Es Pinar station does not have the same intense altitudinal gradient seen at Ersa; therefore the aforementioned test was not performed for this station and the D10 simulations are used for comparisons for Es Pinar.

In the following section, the confidence intervals representing the orographic representativeness error derived in this section are considered for the model–observation comparisons.

4.2 Meteorology evaluation

Meteorological output of the mesoscale WRF model at different resolutions has been used as input to the CHIMERE CTM. The meteorological data used by CHIMERE were compared to various meteorological observations such as radiosondes and surface observations at the measurement sites. Detailed results of these comparisons are given in the Supplement (Sect. SI4). Here, a short overview of the results and the implications for the model ability to simulate transport to the measurement sites is given.

Comparisons for temperature, a basic variable to control the quality of meteorological simulations, show a good correlation for radiosonde comparisons (typically from 0.60 to 0.85 for hourly values) and a low bias (typically from −1.16 to −0.39 °C) for the three sites of Palma, Nîmes, and Ajaccio. Wind speed shows a good correlation at higher altitudes, and also near the surface for Nîmes and Palma for radiosonde stations, while for the Ajaccio station the sea–land breezes are probably not well represented in the model. For Es Pinar, the coastal feature of the site is difficult to take into account in a 10 km horizontally resolved simulation and leads to larger errors. Ground-based meteorological measurements were also compared at both sites (SI4). At Ersa, the correlation in finer domains is better than that of D10 for wind speed (typically around 0.66 versus around 0.60). For the E-OBS network (surface data sets provided by European Climate Assessment and Dataset, ECAD) project for monitoring and analyzing climate extremes, (Haylock et al., 2008; Hofstra et al., 2009) comparisons (SI4) also show a good correlation and a low bias for temperature (correlation of 0.79 with a bias of −0.54 °C for mean temperature observed for 71 stations in D10 domain), while the daily minima seem to be underestimated (bias of −3 °C observed for 71 stations).

While the general comparison between the hourly meteorological fields used as input for CHIMERE simulations and observations is in general already satisfying, the correlation becomes higher and the bias lower when daily averages representative for different meteorological conditions are compared instead of hourly values.

4.3 Gaseous species

Among all the gaseous species available in the observations, four were chosen in this study: nitrogen oxides (NO_x), isoprene (C_5H_8), monoterpenes, and the sum of methacrolein and methyl vinyl ketone (hereafter called MACR+MVK). These four species were chosen since isoprene and monoterpenes are the principal precursors for biogenic SOA, MACR+MVK are formed during isoprene oxidation, and NO_x is a good tracer for local pollution. The comparisons for the Ersa and Es Pinar stations are shown in Fig. 5, and statistics of the comparison are shown in Table 3. For Ersa, the orographic representativeness errors derived in Sect. 4.1 are also shown. In all comparisons, the results for the simulations with the modified VBS scheme are used, but the choice of the OA scheme only slightly affects the simulation of gaseous species (mainly via heterogeneous reactions on aerosol surfaces included within CHIMERE).

Results show that there is a good correspondence between the averages of simulated and observed nitrogen oxides at Ersa (Fig. 5a1). The low correlation for nitrogen oxides at Ersa might be partly explained by the high representativeness error (75 %) for this component. This is because the altitude in the simulations is lower and therefore the emission sources are closer in the model than they are in reality. At Es Pinar (Fig. 5a2), since the measurements are not specific to NO_2, the NO_y time series are added to the figure as well. As a consequence, if the model had no error, the NO_x observations would be expected to lie between NO_x and NO_y simulations. This is the case because NO_x observations are on average

Table 2. Calculated relative orographic representativeness error (ORE) for a list of species and meteorological parameters. MACR+MVK presents the sum of methyl vinyl ketone and methacrolein.

Pollutant	ORE (%)	Pollutant	ORE (%)	Pollutant	ORE (%)	Parameter	ORE (%)
O_3	4	C_5H_8	85	Monoterpenes	59	Temperature	0.5
OA	10	BC	26	SO_2	62	Relative humidity	18
SO_4^{2-}	15	NO_x	75	Aromatic species	49		
PM_{10}	9	CO	2	MACR+MVK	60		

Table 3. Statistical data for time series shown in Fig. 5; Mean_obs shows the average of observations. Values in parentheses for Es Pinar NO_x statistics show the comparison of NO_y simulations to NO_x measurements.

		Ersa				Es Pinar			
	ORE	*R*	RMSE	Bias	Mean_obs	*R*	RMSE	Bias	Mean_obs
	%	ppb							
NO_x	75	0.37	0.68	0.16	0.62	0.12 (0.11)	2.76 (2.56)	−1.51 (0.35)	3.53 (3.53)
C_5H_8	85	0.76	0.44	0.24	0.19	0.69	0.10	−0.04	0.17
MACR+MVK	60	0.62	0.22	0.09	0.09	0.41	0.09	0.005	0.10
Monoterpenes	59	0.35	0.69	−0.38	0.52	0.14	0.11	−0.06	0.09

40 % higher than the NO_x simulations and 9 % lower than the NO_y simulations.

For isoprene (Fig. 5b1 and b2), a good correlation (0.76, 0.71) between simulations and observations appears at both sites. However there is an important overestimation (by a factor of 2.5) in the simulations for the Ersa site, which could also be linked to the high orographic representativeness error (85 %), and also to the fact that local emissions sources may not be correctly taken into account in the MEGAN emission model. Conversely, at Es Pinar isoprene is underestimated by about 25 %. The sum of MACR+MVK (Fig. 5c1 and c2) is overestimated by about a factor of 2 at Ersa, following the pattern of overestimation of isoprene at this site, while the bias is small at Es Pinar. Monoterpenes (Fig. 5d1 and d2) show an underestimation by about 70 % at both sites, observations being about 5 times larger at Ersa than at Es Pinar. Again, this could be related to the orographic representativeness error at Ersa and to local vegetation that was not accounted for at both sites.

Daily correlations of 0.35, 0.87, 0.85, and 0.58 (instead of 0.37, 0.76, 0.62, and 0.35 hourly values) are seen at Ersa for nitrogen oxides, isoprene, MACR+MVK, and monoterpenes, respectively. These values change to 0.16, 0.51, 0.72, and 0.10 for daily comparisons (instead of 0.12, 0.69, 0.41, and 0.14 when correlating hourly values) at Es Pinar. Improvements in correlation for daily averages could be related to those in meteorological parameters, at least for Ersa. They show the difficulty to correctly simulate short-term (hourly) variations both in meteorological parameters and chemical species.

A drawback of the comparisons for isoprene, and monoterpenes, contributing respectively to 40 and 60 % of SOA simulated with the modified VBS scheme in the western Mediterranean region, is the measurements' representativeness restricted to local scales. A more regional evaluation of these precursor species would have been necessary since SOA simulated and observed at Ersa and El Pinar was partly formed far away from these sites.

As mentioned before (Sect. 2), isoprene and terpene emissions in our work are generated by the MEGAN model (Guenther et al., 2006). Zare et al. (2012) evaluated isoprene emissions derived from the MEGAN model coupled to the hemispheric DEHM CTM against measurements. On average over 2006, they found a simulated isoprene overestimation at four European sites (between a factor of 2 and 10), good agreement (within ±30 %) at two sites, and an underestimation at two sites (also between factors of 2 and 10). However, none of the sites were located close to the Mediterranean Sea. Curci et al. (2010) performed an inverse modeling study to correct European summer (May to September) 2005 MEGAN isoprene emissions from formaldehyde vertical column OMI measurements (given that isoprene is a major formaldehyde precursor). For the western Mediterranean area, they found an isoprene emissions underestimation using MEGAN of 40 % over Spain, a tendency for an underestimation but with regional differences over Italy, and only small differences over France. This comparison globally lends confidence to MEGAN-derived isoprene emissions. Unfortunately, to our best knowledge, no comparable studies exist in order to validate monoterpene emissions. For the Rome area in Italy, Fares et al. (2013) concluded for a vari-

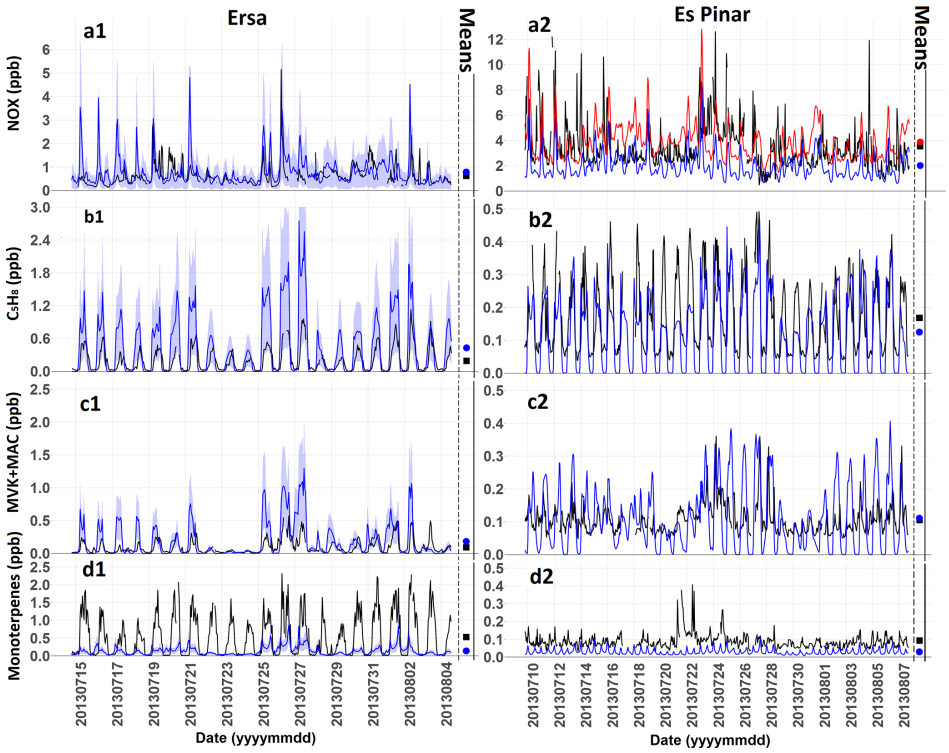


Figure 5. Time series showing the comparison of simulated (in blue) and measured (in black) gaseous species during the ChArMEx/SAFMED campaign period. **(a)** Nitrogen oxides (time series in red for Es Pinar represents NO_y concentrations); **(b)** isoprene; **(c)** MACR+MVK (methyl vinyl ketone+methacrolein); **(d)** monoterpenes. Statistical data for these comparisons are given in Table 2. The ribbon around Ersa simulations presents the orographic representativeness error. On the right side of each time series, two points are shown presenting the average of simulations (blue circle) and observations (black square).

ety of typical Mediterranean tree and vegetation species mix, that MEGAN correctly simulated (within 10 % error) mean observed monoterpene fluxes over the last 2 weeks of August 2007 for a variety of Mediterranean tree and vegetation species mix, as long as a canopy model was included (as in our study).

4.4 Particulate species

Figure 6 shows the comparison between observations and simulations for particulate sulfate and BC in PM_1. These two species are chosen as two important fine aerosol components, before the comparison of OA in Sect. 5. The left panel shows the comparison for Ersa and the right one for Es Pinar. Statistical information for these species is given in Table 4. There is an overestimation for sulfate particles (Fig. 6b1 and b2) by about 45 %, well beyond the representativeness error for this species (15 %). In addition, the short and sharp decreases in the measurements of sulfates correspond to low clouds passing at the level of the station, which are not simulated by the model. Cloud scavenging processes are already taken into account in the model. However, because of the unique geographical characteristics mentioned before for this site, the meteorological inputs did not simulate these fog events and therefore cloud scavenging was not activated in the simulation. Since these decreases concern only a small percentage of the observations, they do not have a major effect on the outcome of these comparisons. While this effect is very visible for sulfates, it is less pronounced for other particulate species such as BC and OA. A large sulfate peak simulated in the morning of 29 July is not present in the observations; it originates in the model from an air mass arriving from Marseille, which is both a busy harbor and an important industrial area with large SO_2 emissions. This is probably due to small errors in the wind fields. In addition, there are two periods of overestimation of this species in the simulations: the period of 18 to 20 July and the period of 29 July to the night of 1 August. During the second period, the ACSM PM_1 observations show concentrations of close to zero, which are consistent with PM_{10} particle-into-liquid sampler ion chromatography (PILS-IC) sulfate measurements. For this period elevated southerly winds are observed in the Corsica area, and the absence of strong SO_2 sources in this sector might explain the lower concentrations that are seen not only for sulfate but

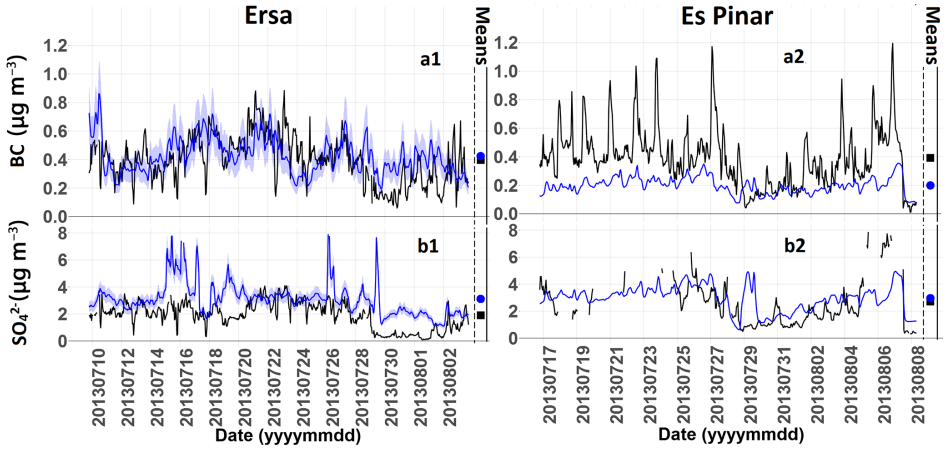


Figure 6. As for Fig. 5, but for particulate matter. **(a)** Black carbon (BC); **(b)** sulfate particles. Statistical data for these comparisons are given in Table 4.

Table 4. Statistical data for time series shown in Fig. 6; Mean_obs column shows the average of observations.

		Ersa				Es Pinar			
	ORE	R	RMSE	Bias	Mean_obs	R	RMSE	Bias	Mean_obs
	%	µg m^{-3}							
BC	26	0.36	0.16	0.02	0.39	0.47	0.22	−0.13	0.39
SO_4^{2-}	15	0.42	1.72	1.21	1.90	0.52	1.93	0.91	2.70

also for BC. The constant overestimation of sulfates during this period may suggest an overestimation of boundary conditions for these species.

A moderate correlation (0.36) between the model and the observations is seen for BC (Fig. 6a1 and a2), but the representativeness error is important for this species (26 %), since one of its primary origins is emission of ships passing nearby the coasts of Cap Corse. The local emissions due to shipping activities at Ersa and anthropogenic activities at Es Pinar are visible in the observations as frequent narrow (in time) peaks. These activities are also visible in the simulations at Ersa. However, at Es Pinar the model does not succeed in simulating them, as already observed to an even larger extent for NO_x. The slight overestimation of BC (5 %) in the model for the Ersa site could be explained by the orographic representativeness error. The same cloud effect seen for the sulfate particles at Ersa is visible to a lesser extent for BC for the Ersa site as well. Correlation between daily observations and the simulations was also calculated. R^2 is 0.51 and 0.56 for the Ersa station (instead of 0.36 and 0.42 for hourly values) and 0.81 and 0.65 for the Es Pinar station (instead of 0.47 and 0.52 for hourly values) for sulfate and BC, respectively. Similar to meteorological parameters, the model can reproduce the daily concentration changes for these two species better than the hourly changes.

5 Organic aerosol simulation

A description of each of the four schemes for the simulation of OAs tested within the CHIMERE model for the Mediterranean area has been given in Sect. 2. These four schemes are the CHIMERE standard scheme, the VBS scheme with BSOA aging (noted as Standard VBS_ba), the VBS scheme without BSOA aging (noted as Standard VBS_nba), and the modified VBS (noted as modified VBS) scheme, which includes fragmentation and formation of nonvolatile OA. For each scheme, four domains were used: one coarse domain and three others nested inside the coarse one with increasing resolutions. As before, the simulations from the finest domain are used for the comparisons. The domain with the finest resolution (1 km) was used for the representativeness tests. For each scheme, meteorological and boundary conditions are the same; hence only the simulation of OAs and subsequently the aggregation of anthropogenic PM emissions differ among simulations.

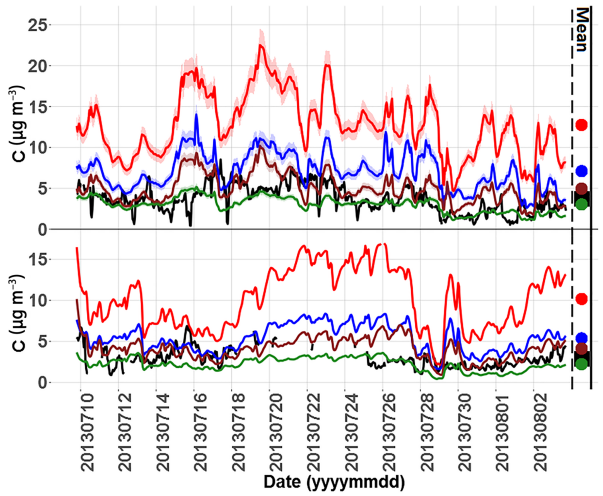


Figure 7. Compared time series of total PM_1 organic aerosol (OA) concentration at Ersa (top) and Es Pinar (bottom) – black: observations; green: modified VBS; brown: standard VBS without BSOA (biogenic secondary organic aerosol) aging; blue: CHIMERE standard; red: standard VBS with BSOA aging. For each site the average of simulations is shown with circles in corresponding colors and the observations with black squares. Shaded area for Ersa presents the orographic representativeness error. Statistical data are shown in Table 5.

5.1 Comparison of PM_1 total organic aerosols concentration

Figure 7 shows the time series of comparison of OAs for these four schemes with the measurements at Ersa and Es Pinar. The circles beside each plot show the average concentration for different time series; in addition Table 5 shows the statistical parameters corresponding to these time series. The observed OA concentration at the Ersa site measured by the ACSM in the PM_1 fraction has an average of 3.71 µg m^{-3} and that of the Es Pinar site measured by the AMS in the PM_1 fraction a somewhat lower average of 2.88 µg m^{-3}. The difference between the two sites may be attributed to the fact that Cap Corse is closer to both local and transported (continental) biogenic sources than Es Pinar. The VBS scheme with BSOA aging greatly overestimates the OA with a bias of more than a factor of 3. As mentioned before, the aging of biogenic aerosols in the VBS scheme usually results in an overestimation in OAs (Lane et al., 2008). With the BSOA aging option turned off, the standard VBS scheme comes much closer to the average of total OA concentration measured at both sites (relative biases of below 50 %). The CHIMERE standard scheme also overestimates the mass concentration of OAs, but to a lesser extent compared to the VBS scheme with BSOA aging (bias of a bit less than a factor of 2). The modified VBS scheme corresponds much better to observations (negative biases about 20 %). The model results agree for both stations in this regard. At Ersa, biases of +244, +91, +34, and −18 %, respectively, are observed for the VBS standard scheme with BSOA aging, the CHIMERE scheme, the standard VBS scheme without BSOA aging, and the VBS modified scheme. The corresponding numbers are of +218, +98, +43, and −23 % for Es Pinar.

The daily correlation for the modified VBS scheme is 0.63 and 0.51 for Ersa and Es Pinar, respectively (instead of 0.50 and 0.29 for hourly values). This shows, again, that the model represents day-to-day changes better than hourly variations. While the concentrations of both the modified VBS scheme and the standard VBS scheme without BSOA aging correspond well with the experimental data, other aspects such as origins of the formed OA and its oxidation state have to be considered before reaching any conclusion about the robustness of these schemes.

The overestimation of secondary OA with the CHIMERE standard scheme is a new feature, not apparent in previous studies (Bessagnet et al., 2008; Hodzic and Jimenez, 2011; Petetin et al., 2014). A previous comparison of CHIMERE with OA simulations using the same scheme and coupled to MEGAN biogenic emissions resulted in a good comparison or underestimation with OC observations over Europe from the CARBOSOL project (Gelencsér et al., 2007) for summer 2003, when biogenic SOA was dominant. However, this comparison included only one site close to the western Mediterranean basin (Montelibretti, Italy). The overestimation of BSOA in the VBS scheme when the BSOA aging is activated was documented for the USA on several occasions (Robinson et al., 2007; Lane et al., 2008). Ultimately, it cannot be excluded that the OA overestimation with both schemes at Ersa and Es Pinar is also due to biogenic VOC (BVOC) overestimation. However, the available material does not support this hypothesis: (i) OA overestimation is observed at two independent, distant sites, (ii) local monoterpene underestimation is observed at both these sites, and (iii) no evidence for MEGAN monoterpene overestimation is available in literature and MEGAN isoprene overestimation over the western Mediterranean area was ruled out by satellite observations (Curci et al., 2010).

5.2 Total carbonaceous particle origins based on ^{14}C measurements

The results of ^{14}C measurements in carbonaceous aerosol filter samples for the PM_1 fraction at the Ersa and Es Pinar sites were used in order to better discriminate between the modern and mostly biogenic versus fossil and anthropogenic origin of OAs, and to compare it to simulations with different OA schemes tested. It must be noted that in the simulations, species are not separated automatically into fossil and nonfossil parts; therefore these fractions need to be calculated as a posttreatment of simulations, affecting each relevant particulate species to both fractions. ASOA is considered to be in the fossil fraction and BSOA in the nonfossil fraction.

Table 5. Statistical data for hourly time series shown in Fig. 7. *R* is the correlation coefficient between model and measurements, RMSE is the root mean square error, mean_sim and mean_obs show the average, and SD_sim and SD_obs show the standard deviation of simulations and observations, respectively.

		CHIMERE standard		Standard VBS ba		Standard VBS nba		Modified VBS	
		Ersa	Es Pinar	Ersa	Es Pinar	Ersa	Es Pinar	Ersa	Es Pinar
R		0.46	0.16	0.50	0.11	0.45	0.22	0.50	0.29
RMSE		3.96	2.65	9.63	7.29	2.17	1.89	1.59	1.49
Bias		3.39	2.49	9.05	7.17	1.26	1.25	−0.68	−0.65
Mean_sim		7.10	5.36	12.76	10.17	4.97	4.13	3.02	2.22
Mean_obs	$\mu g\,m^{-3}$	3.71	2.88	3.71	2.88	3.71	2.88	3.71	2.88
SD_sim		2.21	1.64	3.78	3.62	1.73	1.34	0.95	0.79
SD_obs		1.66	1.16	1.66	1.16	1.66	1.16	1.66	1.16

For carbonaceous aerosol, residential or domestic uses are considered as nonfossil as they are mostly related to wood burning (Sasser et al., 2012). Therefore, they are attributed to the nonfossil bin (3.6 % for BC and 12.3 % for OC; Sasser et al., 2012). The nonfossil contribution of ASOA and primary OA (POA) due to biofuel usage is ignored here, as it is minor (< 5 %). No major biomass burning events were seen in the period of this study, but minor contributions of this source cannot be excluded. It should also be mentioned that the ^{14}C measurements show the mass of carbonaceous particles in each filter and therefore have a unit of $\mu gC\,m^{-3}$, while the simulations show the total OAs in $\mu g\,m^{-3}$. In the comparisons that follow, it is pertinent to use an organic matter (OM) / OC conversion factor to be able to compare the ^{14}C measurements to simulations. For this purpose, an average OM / OC factor of 2 is used for the secondary aerosol fraction (both for the LVOOA and SVOOA factors), while a factor of 1.3 is used for HOA according to Aiken et al. (2008). However, the choice of the OM / OC factor has a small effect on the outcome of general comparisons since HOA values are marginal compared to other factors and we are only interested in the relative contribution of fossil and nonfossil factors.

Figure 8a for Ersa and 8b for Es Pinar show the average of all filters for each scheme compared to the observations, while Fig. 9a and b show the relative distribution of fossil and nonfossil sources at both sites. Among these total averages, the distribution at Ersa is 81 % ± 1.5 % nonfossil and 19 % ± 1.5 % fossil, and 67 % ± 3 % nonfossil versus 33 % ± 3 % fossil at Es Pinar. Apparently, biogenic contributions to OA are dominant at both sites, but larger for the Ersa site.

While the comparison of averages for all schemes with Ersa measurements shows that the modified VBS scheme is the closest in fossil and nonfossil partitioning (19 %/81 % ± 1 %), the CHIMERE standard scheme also performs well when looking at the percentage of distribution for each source (20 %/80 % ± 1 %). The VBS scheme with BSOA aging shows an underestimation in the percentage of fossil carbons (16 %/84 % ± 0.7 %), which can be due to the overestimation of biogenic aging of SOAs in this scheme; conversely, the VBS scheme without BSOA aging shows an important overestimation of the fossil percentage (34 %/66 % ± 2 %).

A distribution of 33 %/67 % ± 3 % of the fossil and nonfossil fractions is observed at Es Pinar. As for the Ersa site, the modified VBS scheme is the closest to the observations (32 %/68 % ± 2.5 %). The CHIMERE standard scheme shows an underestimation of the fossil contribution with a distribution of 28 %/72 % ± 3 %. The standard VBS scheme with BSOA aging underestimates the fossil contribution with a distribution of 21 %/79 % ± 1.5 %, while the standard VBS scheme without BSOA aging largely overestimates the fossil contribution (42 %/58 % ± 2 %). These results show that the two sites differ greatly when taking into account nearby sources and geographical conditions; the Ersa site is an elevated rural station at the interface between the marine boundary layer and the residual boundary layer, and the Es Pinar site is a seaside station closer to anthropogenic sources. These differences should normally be represented in the percentage of fossil carbon concentrations in both observations and simulations. Although this difference is noticeable in observations, and also in the modified VBS scheme, it is less emphasized in the CHIMERE standard scheme and in the VBS standard scheme with either parameterization of aging.

A more detailed look at individual filters for the modified VBS scheme for the Ersa and Es Pinar sites is presented in Fig. 9a and b, respectively. The tendencies from one day to another are in most cases not reproduced correctly for both sites. Therefore while the average mass repartition of modern and fossil sources is well represented by this scheme, the day-to-day variability is not fully consistent with the measurements. This inconsistency is also seen in the other tested schemes.

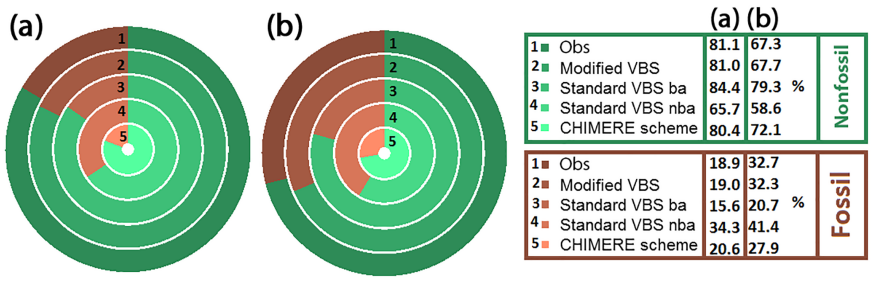


Figure 8. Comparison of simulations to ^{14}C measurements – **(a)** comparison of filters to four schemes for Ersa; **(b)** comparison of filters to four schemes for Es Pinar. For both figures from outer ring to inner ring: observations, modified VBS, standard VBS with BSOA (biogenic secondary organic aerosol) aging, standard VBS without BSOA aging, and CHIMERE standard scheme.

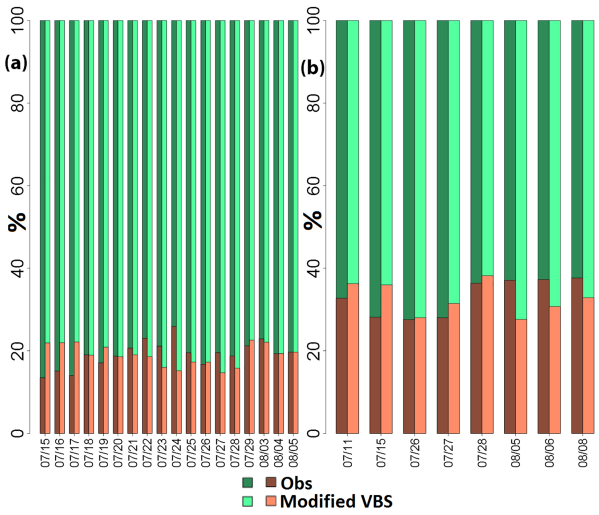


Figure 9. Comparison of simulations to ^{14}C measurements – **(a)** Ersa individual filters; **(b)** Es Pinar individual filters. For each filter, measurements are on the left and modified VBS simulations are on the right. Dark or light brown shows fossil and dark or light green shows nonfossil sources.

5.3 Volatility and oxidation state comparison with PMF results

The PMF results of the ACSM/AMS measurements give us the chance to learn more about the oxidation state of the OAs (Michoud et al., 2017, for Ersa). The PMF analysis allows us to divide PM_1 OA measurements into different groups with distinctive mass spectra corresponding to distinctive oxidation state (Lanz et al., 2010). The most common retrieved factors of such an analysis are HOA, SVOOA, and LVOOA. However, it does not give direct information about the volatility distribution of each group. This makes the PMF output difficult to compare with our model results, which give the volatility distribution of OA but not its oxidative state. Here, we first compare volatility distributions obtained with the four aerosol schemes, and then try to attribute the simulated aerosol to the three factors HOA, SVOOA, and LVOOA, in order to compare it to the observed distributions. The three schemes based on the VBS scheme already distribute aerosols in volatility bins (Robinson et al., 2007). The distribution to LVOOA and SVOOA for these three schemes was performed mainly by taking into account the saturation concentration, with the threshold chosen as a saturation concentration $C^* \geq 1\,\mu g\,m^{-3}$ for SVOOA and $C^* \leq 0.1\,\mu g\,m^{-3}$ for LVOOA (Donahue et al., 2012). Primary OAs were considered to be in the HOA factor regardless of their saturation concentration. For the CHIMERE standard scheme, each surrogate species is associated with a saturation vapor pressure, which was used to calculate the saturation concentration for each component at ambient temperature.

The observations show that at Ersa, the LVOOA factor dominates the PMF results (88 %), with 10 % SVOOA and a minor (only 2 %) contribution of HOA. For the Es Pinar site the contribution of LVOOA drops to 75 % and the contribution of SVOOA and HOA becomes somewhat larger (21 % and 4 %, respectively). As mentioned before, the Es Pinar site is more influenced by local anthropogenic sources. Therefore, more local OA emissions are expected, which corresponds to the increase in the HOA percentage seen in the observations. These emissions are oxidized locally to form SVOCs that fall in the SVOOA group, explaining the rise in the percentage of this group.

Figure 10a and b show the relative distribution of all OAs in seven volatility bins for all tested schemes for the Ersa and Es Pinar sites, respectively, and for all tested schemes. For each scheme, the average for the total period of the simulations was used to calculate the percentage in each bin. The bins shown are in the range of 10^{-3}–$10^{3}\,\mu g\,m^{-3}$; all the aerosols with a volatility higher or lower than the extremes are put in the last high or low bin, respectively.

These figures show that the percentage of aerosols in each volatility bin for the two different sites is relatively similar. The CHIMERE standard scheme distributes most of the aerosol in the three bins in 1–100 $\mu g\,m^{-3}$ volatility ranges,

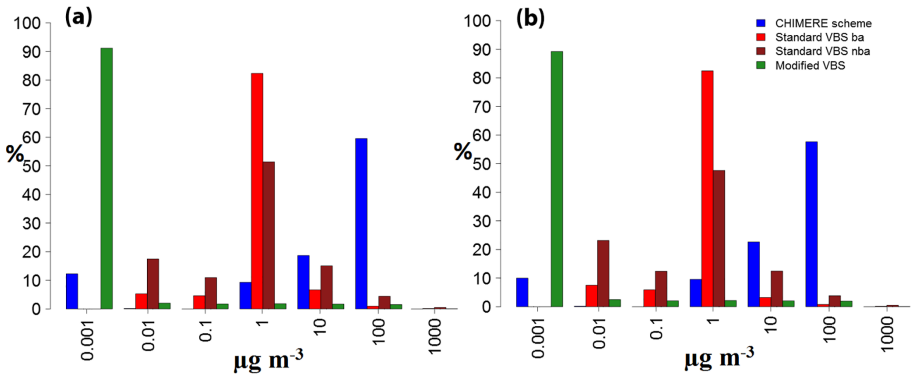


Figure 10. Distribution of simulated organic aerosol (OA) in volatility bins – **(a)** Ersa volatility bins; **(b)** Es Pinar volatility bins.

which falls into the SVOOA group obtained with PMF. This is due to the initial distribution of volatilities of surrogate SVOC species used that best fit chamber measurements, and the fact that there is no aging mechanism in this scheme to make the aerosols less volatile. The $100\,\mu g\,m^{-3}$ volatility bin corresponds to SVOCs produced from isoprene and monoterpene oxidation and presents the highest percentage for this scheme. The standard scheme also produces 16 % of OAs in the LVOOA range (volatilities corresponding to a C^* between 0.001 and $0.1\,\mu g\,m^{-3}$). The standard VBS scheme with BSOA aging has only a small fraction of aerosol in the LVOOA range (from SVOC emission aging) since, by construction of the scheme, the most aged BSOA and ASOA aerosols fall in the $1\,\mu g\,m^{-3}$ volatility bin, which is actually the bin with the highest percentage of OA. The standard VBS scheme without BSOA aging presents relatively similar results to the scheme with biogenic aging, with as expected larger percentages for higher volatilities in the absence of aging. It also shows a larger LVOOA fraction, probably because the lower total OA concentration favors the contribution of lower-volatility SVOCs to the aerosol phase. On the whole, the two schemes yield much too low LVOOA fractions as compared to observations. The modified VBS scheme has a more realistic distribution into the three oxidation groups. In this scheme, the highest percentage of OA falls in the $10^{-3}\,\mu g\,m^{-3}$ volatility bin, which is in the LVOOA range. The rest of the aerosols are distributed almost equally in volatility bins between 10^{-2} and $10^{2}\,\mu g\,m^{-3}$ with a slight decrease in percentage in the higher-volatility bins. The percentage in higher-volatility bins at Ersa are slightly lower than the ones at Es Pinar, which could be explained by the stronger local sources at the Es Pinar site with stronger primary SVOC emissions.

Figure 11a and b show the calculated HOA, LVOOA, and SVOOA groups in simulations compared to the ones in observations at Ersa and at Es Pinar, respectively. At Ersa, the results of the modified VBS scheme are consistent with the observations with a slight underestimation of HOAs, which is more visible at Es Pinar. The standard CHIMERE scheme leads to higher, overestimated HOA values, as primary OA emissions are considered nonvolatile. Only the modified VBS scheme succeeds in reproducing the major contribution of LVOOAs at both sites. However, while staying close to observations at Ersa, it seems to overestimate the formation of LVOOAs at Es Pinar. The standard VBS schemes with or without BSOA aging greatly underestimate the formation of LVOOAs, and as a counterpart overestimate the formation of SVOOAs. Therefore, among the tested schemes, only the modified VBS scheme allows us to represent the distribution of the different PMF factors in a satisfying way.

6 Budget of organic aerosols

In Sect. 5, we have highlighted the best performance of the modified VBS scheme for OA simulation amongst the tested schemes by comparison to observational data at two different sites in the western Mediterranean basin. In the present section, we use this scheme in order to simulate the OA distribution and its anthropogenic and biogenic origins over the western Mediterranean basin during the SAFMED campaign.

Figure 12 shows a series of figures in which the left column always corresponds to simulations near the surface, and the right column shows the same concentration at an altitude of between 300 and 450 m (for marine grid cells; called for simplicity boundary layer, BL). Each row shows a different component, with the first row corresponding to OA concentrations, second row to biogenic OA concentrations, and third row to anthropogenic OA concentrations; the last row presents the sum of POA and all its subsequent oxidation products. The larger part of each figure corresponds to D10 simulations, while the part inside the black rectangle shows the D3 simulations, both showing the average of the OAs for the whole simulation period (1 month from 10 July to 9 August). Figure 13 shows the same type of figures for the percentage of contribution of biogenic OAs, anthropogenic OAs, and the sum of POAs (that is POA and POA oxida-

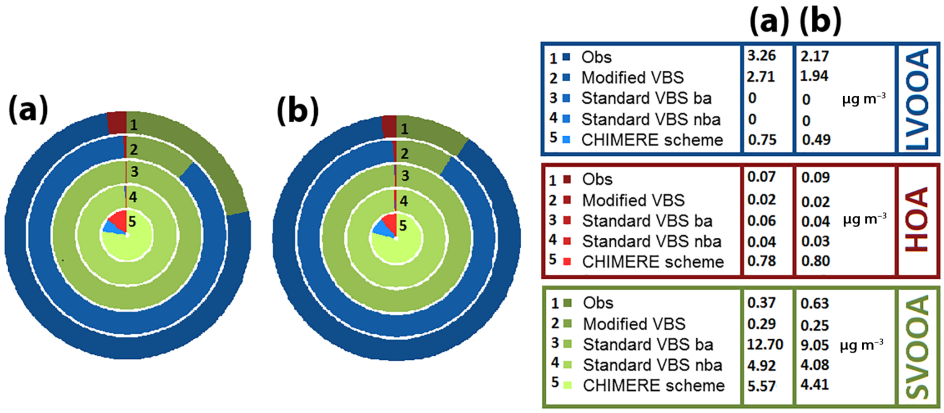


Figure 11. Comparison to PMF results – **(a)** comparison of observed PMF factors to those derived from four schemes for Ersa and **(b)** for Es Pinar. For both figures from outer ring to inner ring: observations, modified VBS, standard VBS with BSOA aging, standard VBS without BSOA (biogenic secondary organic aerosol) aging, and CHIMERE standard scheme. LVOOA refers to low-volatility oxidized organic aerosol, SVOOA to semi-volatile oxidized organic aerosol, and HOA to hydrocarbon-like organic aerosol.

tion products). The small differences at the interface of the two domains is because the CHIMERE model is a one-way chemistry–transport model: the simulations for the parent domain influence the simulations for the nested domain; however, the inverse is not applied; therefore any concentrations observed in the nested domain will not change the concentrations seen in the parent domain.

Examining figures corresponding to OA concentrations (Fig. 12a and b), at the surface level there is a region of high concentration of OA in the Gulf of Genoa (between Genoa and Corsica) reaching nearly 4 µg m^{-3}. The high concentration in this area is less pronounced in the BL (Fig. 12b). The concentration of biogenic OAs (Fig. 12c and d) is high over the basin as well as over Europe, and less important over North Africa. The percentage of contribution of this type of aerosol to the overall OA concentration is shown in Fig. 13a and b. As expected from looking at the total concentration of biogenic OAs, their contribution stays on average around 70 % over the basin, but is lower in the Gulf of Genoa (about 60 % at surface, nearly 70 % at altitude). In this area the secondary anthropogenic OAs show a bit higher contributions compared to their contribution to the rest of the domain (around 14 % instead of 12 %); also, the contribution of POAs (and their subsequent oxidations) is also quite high in this region (around 20 %). The areas between Corsica and Marseilles and also the northern coast of Africa are main shipping routes in the western Mediterranean basin, with high amounts of shipping related emissions. They affect POA and its semi-volatile oxidation products as shown in Fig. 12g and h, with concentrations as high as 0.9 µg m^{-3} around Corsica and near the African coast. This corresponds to a contribution of around 22 % over Corsica and 25 % over the coast of Africa (Fig. 13e and f). These values may actually be upper limits since shipping primary SVOC and IVOC emissions were treated as those from other activity sectors (see Sect. 2.2.3), and recent chamber study data suggest lower SOA yields from shipping emissions (Pieber et al., 2016) than are used here. The influence of shipping emissions is not visible in the BL because vertical mixing within the marine boundary layer is weak, thus in the 300 to 400 m layer the contribution of biogenic OA becomes dominant for the whole basin. Still, in the Gulf of Genoa, some effects of anthropogenic influences are visible in the BL, which could be linked to emissions originating from industrial sites and the harbor of Genoa area, which are apparently better mixed vertically over the continental convective boundary layer (in the coastal region with strong orography). These anthropogenic emissions are visible in figures corresponding to anthropogenic OA, formed from anthropogenic VOCs and especially aromatic compounds (Fig. 12e and f for absolute concentrations and Fig. 13c and d for relative percentages). While the average concentration of anthropogenic OAs stay relatively low over the western Mediterranean basin (an average of 0.30 µg m^{-3} near the surface), they become more pronounced around the Gulf of Genoa and the eastern part of the domain both near the surface and in the BL. A contribution of about 12–15 % both near the surface and in the BL is seen for this component above the Gulf of Genoa and over the highly industrialized and densely populated Po Valley.

7 Conclusion and discussion

Three schemes for the simulation of OA were implemented and tested along with the standard scheme in the CHIMERE chemistry–transport model. The simulations from each of the four schemes were compared to detailed experimental data obtained from two different stations in the western Mediterranean area during the ChArMEx campaign in summer 2013.

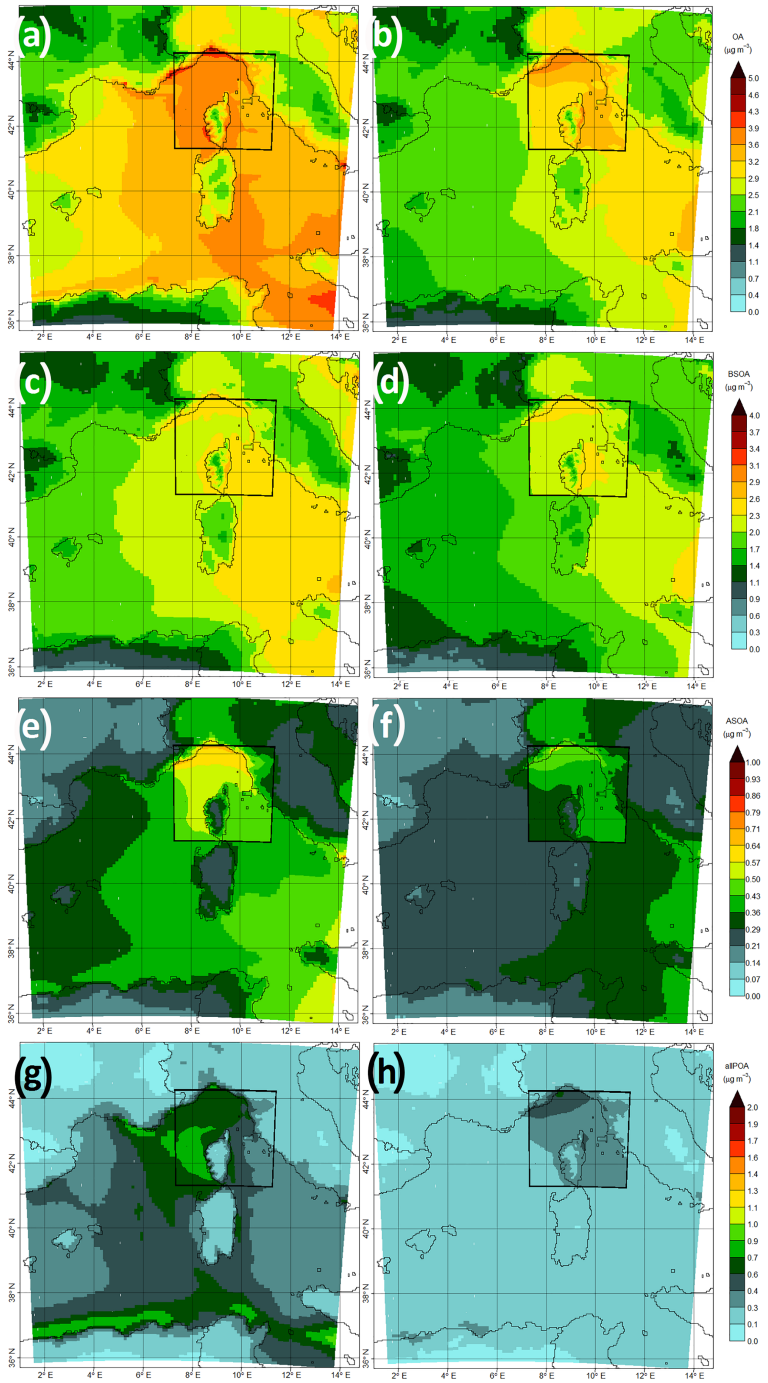


Figure 12. Average organic aerosol (OA) concentrations over the western Mediterranean basin simulated from 10 July to 9 August 2013 with the modified VBS scheme. The left column is near the surface, and the right column is for an altitude between 300 and 450 m a.s.l. From top to bottom: **(a–b)** total organic aerosol concentration ($\mu g\,m^{-3}$); **(c–d)** BSOA (biogenic secondary OA) concentration ($\mu g\,m^{-3}$); **(e–f)** total ASOA (anthropogenic secondary OA) concentration ($\mu g\,m^{-3}$); **(g–h)** sum of POA (primary OA) and its subsequent oxidation products ($\mu g\,m^{-3}$). Results are from the D3 simulation (3 km horizontal resolution) within the framed area and from the D10 simulation outside the framed area (10 km resolution).

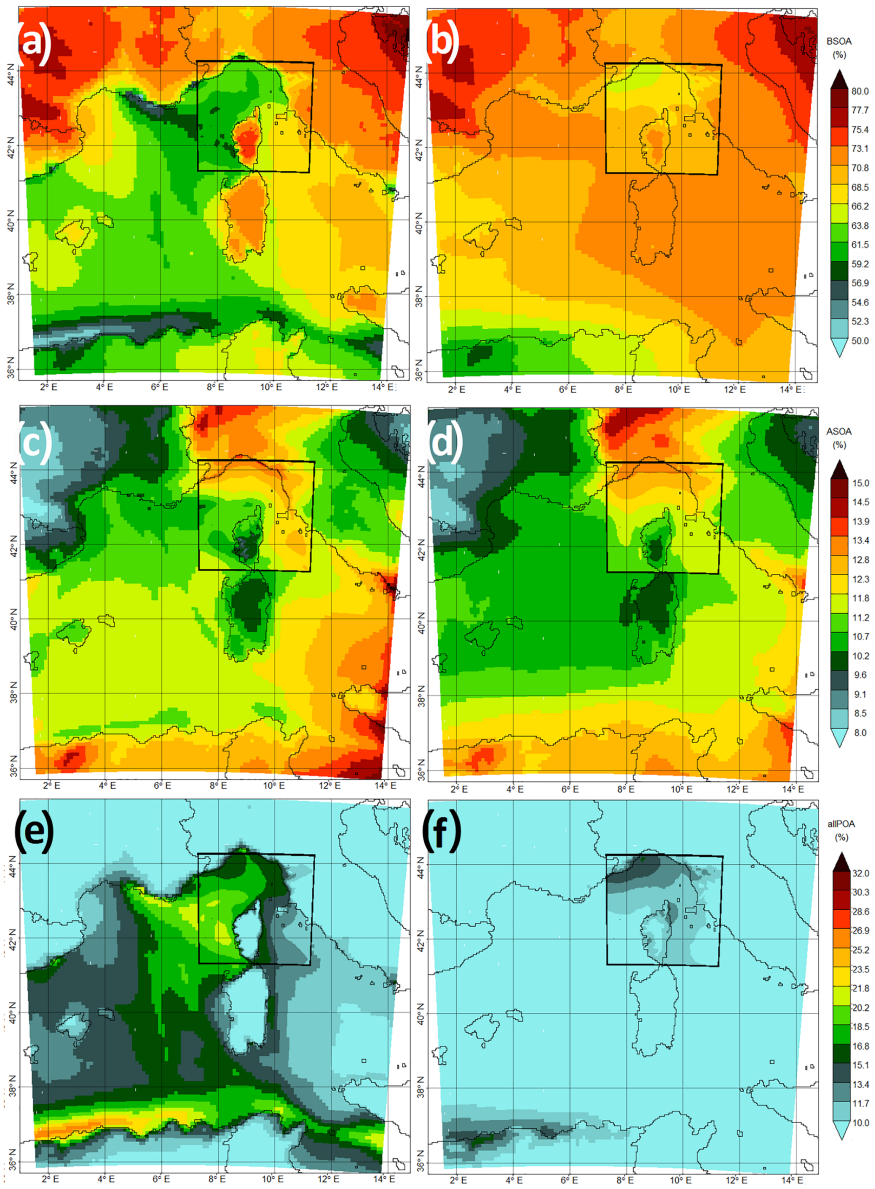


Figure 13. As Fig. 12 but for relative contributions of BSOA, ASOA, and POA to total OA (%). From top to bottom: **(a–b)** biogenic secondary organic aerosol (BSOA); **(c–d)** anthropogenic secondary organic aerosol (ASOA); **(e–f)** POA and its subsequent oxidation products.

The simulations were performed over 1 month in the summer of 2013 on four nested domains with increasing resolutions, the largest one covering Europe and northern Africa with a 30 km horizontal resolution, to the smallest one focused on the Cap Corse area with a 1 km horizontal resolution.

For the comparisons of OA simulated with different schemes to observations, we explored three different aspects: mass concentration, distribution with respect to volatility and oxidative state of OA classes derived using PMF, and ^{14}C measurements discriminating fossil or nonfossil origin. Results show that the modified VBS scheme (i.e., including the fragmentation and formation of nonvolatile OAs), better corresponds to the observations at both sites, and this for all three aspects. The modified VBS scheme succeeds at simulating the average concentration of OA for the 1-month campaign period with low bias (about −20 % at both sites), even if the hourly variability is not perfectly displayed (as for other aerosol components). Comparisons for OA precur-

sors (isoprene and terpenes) and isoprene oxidation products (sum of methyl vinyl ketone and methacroleine) were performed and showed significant differences, which do not, however, necessarily affect the model ability to form BSOA because the BVOC measurements are representative for a local scale, while BSOA formation occurs on a larger regional scale. Chrit et al. (2017) used a two-step surrogate scheme for the simulation of the Ersa site measurements. They found that their modified SOA simulation scheme corresponds well with the data, with a correlation of 0.67 and a mean fractional bias of −0.15 for daily values of the period between June and August 2013. For the period of July to August 2013 for daily values, we find a correlation of 0.52 and a mean fractional bias of −0.03 for the modified VBS scheme, which shows that both these schemes work reasonably well for the simulated area.

Furthermore, the fossil–nonfossil distribution of OA was explored in our different schemes. The modified VBS scheme corresponds better to available data in this regard as well. It is also the only scheme among the four tested that represents the distribution of the different PMF factors in a satisfying way attributing the major OA fraction to LVOOA (but slightly overestimating this part). The differences between the sites, especially the more local anthropogenic character of the Es Pinar site (larger ^{14}C fossil fuel origin, larger SVOOA fraction, higher NO_x concentration, which is a good tracer for anthropogenic pollution) and the lower OA concentration at this site are qualitatively simulated well with this scheme. While the standard VBS scheme without BSOA aging is as close to mass and origin comparisons as the modified VBS scheme, by construction, it does not include the formation of LVOOA, resulting in an important overestimation of the SVOOA at both sites.

A closer look at OA sources over the western Mediterranean basin simulated with the modified VBS scheme, selected because of its good results (at least for the summer of 2013 period and for this given region), shows that the OA with biogenic origins is dominant in the whole basin. In areas between Corsica and Marseilles, the Gulf of Genoa and also the northern coast of Africa, the contribution of biogenic OAs is less than for other parts. This fact points to the influence of shipping emissions for the areas between Marseilles and Corsica and also the northern coast of Africa, which can be seen in the contribution of POA and their oxidation products to the formation of OA over the basin, even if this part may be overestimated in the current simulations. For the Gulf of Genoa, a slightly higher contribution of anthropogenic OAs was observed compared to other parts of the domain. However, at a higher altitude, the contribution of the biogenic sources becomes dominant in the whole basin, with a significant drop in the contribution of POA over the basin and leaving only a small trace of anthropogenic contribution in the Gulf of Genoa. This contribution is attributed to ASOA rather than POA for the industrial area in northern Italy, which is a persistent source of ASOA both near the surface and at higher altitudes.

It would be useful to compare the precursor components for the formation of OA such as isoprene and monoterpenes to multiple stations rather than only two since the measurements for these species tend to have a more local representativeness rather than a regional one; therefore multiple stations spread in the domain would give the needed regional aspect of the comparisons. Longer periods of simulations with comparisons to observations are also necessary since processes leading to the formation of OA can change in other seasons and especially in winter when the biogenic contribution is much lower. Since airborne measurements for OA and biogenic gas-phase precursors were also performed during the summer of 2014 in the SAFMED+ campaign over different forested areas, it would be useful to continue the simulations for this year to compare the results to in situ measurements and airborne measurements at the same time.

Data availability. Access to the data used in this article is restricted to registered users of the ChArMEx project. The data are available on the project website (http://mistrals.sedoo.fr/ChArMEx/, last access: 27 March 2017) and it should be used following the data and publication policies of the ChArMEx project; http://mistrals.sedoo.fr/ChArMEx/Data-Policy/ChArMEx_DataPolicy.pdf.

The Supplement related to this article is available online at https://doi.org/10.5194/acp-18-7287-2018-supplement.

Competing interests. The authors declare that they have no conflict of interest.

Special issue statement. This article is part of the special issue "CHemistry and AeRosols Mediterranean EXperiments (ChArMEx) (ACP/AMT inter-journal SI)". It is not associated with a conference.

Acknowledgements. This research has received funding from the French National Research Agency (ANR) projects SAF-MED (grant ANR-15 12-BS06-0013). This work is part of the ChArMEx project supported by ADEME, CEA, CNRS-INSU, and Météo France through the multidisciplinary programme MISTRALS (Mediterranean Integrated Studies aT Regional And Local Scales). The station at Ersa was partly supported by the CORSiCA project funded by the Collectivité Territoriale de Corse through the Fonds Européen de Développement Régional of the European Operational Program 2007-2013 and the Contrat de Plan Etat-Région. The EEA is acknowledged for air quality data for several stations in Europe which were used for observation–simulation comparisons. The NCEP is acknowledged for the meteorological input data used in the

WRF meteorological model. E-OBS data sets are acknowledged. The thesis work of Arineh Cholakian is supported by ADEME, INERIS (with the support of the French ministry in charge of ecology), and via the ANR SAF-MED project. Eric Hamonou and the ChArMEx team are acknowledged for their great help in organizing the measurement campaign at Ersa, as well as the MISTRALS management and accounting team. Jorge Pey is currently granted with a Ramón y Cajal research contract (RYC-2013-14159) from the Spanish Ministry of Economy, Industry and Competitiveness.

This work was performed using HPC resources from GENCI-CCRT (grant 2017-t2015017232).

Edited by: Jean-Luc Attié
Reviewed by: two anonymous referees

References

Aiken, A. C., DeCarlo, P. F., Kroll, J. H., Worsnop, D. R., Huffman, J. A., Docherty, K. S., Ulbrich, I. M., Mohr, C., Kimmel, J. R., Sueper, D., Sun, Y., Zhang, Q., Trimborn, A., Northway, M., Ziemann, P. J., Canagaratna, M. R., Onasch, T. B., Alfarra, M. R., Prevot, A. S. H., Dommen, J., Duplissy, J., Metzger, A., Baltensperger, U., and Jimenez, J. L.: O/C and OM/OC Ratios of Primary, Secondary, and Ambient Organic Aerosols with High-Resolution Time-of-Flight Aerosol Mass Spectrometry, Environ. Sci. Technol., 42, 4478–4485, https://doi.org/10.1021/es703009q, 2008.

Arino, O., Bicheron, P., Achard, F., Latham, J., Witt, R., and Weber, J.: Globcover: The most detailed protrait of Earth, Eur. Sp. Agency Bull., 36, 24–31, 2008.

Arndt, J., Sciare, J., Mallet, M., Roberts, G. C., Marchand, N., Sartelet, K., Sellegri, K., Dulac, F., Healy, R. M., and Wenger, J. C.: Sources and mixing state of summertime background aerosol in the north-western Mediterranean basin, Atmos. Chem. Phys., 17, 6975–7001, https://doi.org/10.5194/acp-17-6975-2017, 2017.

Bardouki, H., Liakakou, H., Economou, C., Sciare, J., Smolík, J., Ždímal, V., Eleftheriadis, K., Lazaridis, M., Dye, C., and Mihalopoulos, N.: Chemical composition of size-resolved atmospheric aerosols in the eastern Mediterranean during summer and winter, Atmos. Environ., 37, 195–208, https://doi.org/10.1016/S1352-2310(02)00859-2, 2003.

Berezin, E. V., Konovalov, I. B., Ciais, P., Richter, A., Tao, S., Janssens-Maenhout, G., Beekmann, M., and Schulze, E.-D.: Multiannual changes of CO_2 emissions in China: indirect estimates derived from satellite measurements of tropospheric NO_2 columns, Atmos. Chem. Phys., 13, 9415–9438, https://doi.org/10.5194/acp-13-9415-2013, 2013.

Bessagnet, B., Menut, L., Curd, G., Hodzic, A., Guillaume, B., Liousse, C., Moukhtar, S., Pun, B., Seigneur, C., and Schulz, M.: Regional modeling of carbonaceous aerosols over Europe-focus on secondary organic aerosols, J. Atmos. Chem., 61, 175–202, https://doi.org/10.1007/s10874-009-9129-2, 2008.

Borrego, C., Souto, J. A., Dios, M., Monteiro, A., Ferreira, J., Rodriguez, A., Saavedra, S., Casares, J. J., and Miranda, A. I.: The role of transboundary air pollution over galicia and north portugal area, Environ. Sci. Pollut. R., 20, 2924–2936, https://doi.org/10.1007/s11356-012-1201-9, 2013.

Bowden, J. H., Otte, T. L., Nolte, C. G., Otte, M. J., Bowden, J. H., Otte, T. L., Nolte, C. G., and Otte, M. J.: Examining interior grid nudging techniques using two-way nesting in the wrf model for regional climate modeling, J. Climate, 25, 2805–2823, https://doi.org/10.1175/JCLI-D-11-00167.1, 2012.

Canonaco, F., Crippa, M., Slowik, J. G., Baltensperger, U., and Prévôt, A. S. H.: SoFi, an IGOR-based interface for the efficient use of the generalized multilinear engine (ME-2) for the source apportionment: ME-2 application to aerosol mass spectrometer data, Atmos. Meas. Tech., 6, 3649–3661, https://doi.org/10.5194/amt-6-3649-2013, 2013.

Carlton, A. G., Wiedinmyer, C., and Kroll, J. H.: A review of Secondary Organic Aerosol (SOA) formation from isoprene, Atmos. Chem. Phys., 9, 4987–5005, https://doi.org/10.5194/acp-9-4987-2009, 2009.

Carter, W. P. L.: Development of the SAPRC-07 chemical mechanism, Atmos. Environ., 44, 5324–5335, https://doi.org/10.1016/J.ATMOSENV.2010.01.026, 2010.

Chen, F., Dudhia, J., Chen, F., and Dudhia, J.: Coupling an Advanced Land Surface–Hydrology Model with the Penn State–NCAR MM5 Modeling System. Part I: Model Implementation and Sensitivity, Mon. Weather Rev., 129, 569–585, https://doi.org/10.1175/1520-0493(2001)129<0569:CAALSH>2.0.CO;2, 2001.

Chin, M., Ginoux, P., Kinne, S., Torres, O., Holben, B. N., Duncan, B. N., Martin, R. V., Logan, J. A., Higurashi, A., and Nakajima, T.: Tropospheric Aerosol Optical Thickness from the GOCART Model and Comparisons with Satellite and Sun Photometer Measurements, J. Atmos. Sci., 59, 461–483, https://doi.org/10.1175/1520-0469(2002)059<0461:TAOTFT>2.0.CO;2, 2002.

Chrit, M., Sartelet, K., Sciare, J., Pey, J., Marchand, N., Couvidat, F., Sellegri, K., and Beekmann, M.: Modelling organic aerosol concentrations and properties during ChArMEx summer campaigns of 2012 and 2013 in the western Mediterranean region, Atmos. Chem. Phys., 17, 12503–12531, https://doi.org/10.5194/acp-17-12509-2017, 2017.

Colette, A., Andersson, C., Baklanov, A., Bessagnet, B., Brandt, J., Christensen, J. H., Doherty, R., Engardt, M., Geels, C., Giannakopoulos, C., Hedegaard, G. B., Katragkou, E., Langner, J., Lei, H., Manders, A., Melas, D., Meleux, F., Rouïl, L., Sofiev, M., Soares, J., Stevenson, D. S., Tombrou-Tzella, M., Varotsos, K. V., and Young, P.: Is the ozone climate penalty robust in Europe?, Environ. Res. Lett., 10, 84015, https://doi.org/10.1088/1748-9326/10/8/084015, 2015.

Curci, G., Palmer, P. I., Kurosu, T. P., Chance, K., and Visconti, G.: Estimating European volatile organic compound emissions using satellite observations of formaldehyde from the Ozone Monitoring Instrument, Atmos. Chem. Phys., 10, 11501–11517, https://doi.org/10.5194/acp-10-11501-2010, 2010.

Decarlo, P. F., Kimmel, J. R., Trimborn, A., Northway, M. J., Jayne, J. T., Aiken, A. C., Gonin, M., Fuhrer, K., Horvath, T., Docherty, K. S., Worsnop, D. R., and Jimenez, J. L.: Field-Deployable, High-Resolution, Time-of-Flight Aerosol Mass Spectrometer, Anal. Chem., 78, 8281–8289, https://doi.org/10.1021/ac061249n, 2006.

Derognat, C., Beekmann, M., Baeumle, M., Martin, D., and Schmidt, H.: Effect of biogenic volatile organic compound emissions on tropospheric chemistry during the Atmo-

spheric Pollution Over the Paris Area (ESQUIF) campaign in the Ile-de-France region, J. Geophys. Res., 108, 8560, https://doi.org/10.1029/2001JD001421, 2003.

Di Biagio, C., Doppler, L., Gaimoz, C., Grand, N., Ancellet, G., Raut, J.-C., Beekmann, M., Borbon, A., Sartelet, K., Attié, J.-L., Ravetta, F., and Formenti, P.: Continental pollution in the western Mediterranean basin: vertical profiles of aerosol and trace gases measured over the sea during TRAQA 2012 and SAFMED 2013, Atmos. Chem. Phys., 15, 9611–9630, https://doi.org/10.5194/acp-15-9611-2015, 2015.

Donahue, N. M., Robinson, A. L., Stanier, C. O., and Pandis, S. N.: Coupled partitioning, dilution, and chemical aging of semivolatile organics, Environ. Sci. Technol., 40, 2635–2643, https://doi.org/10.1021/es052297c, 2006.

Donahue, N. M., Kroll, J. H., Pandis, S. N., and Robinson, A. L.: A two-dimensional volatility basis set – Part 2: Diagnostics of organic-aerosol evolution, Atmos. Chem. Phys., 12, 615–634, https://doi.org/10.5194/acp-12-615-2012, 2012.

Drinovec, L., Mocnik, G., Zotter, P., Prévôt, A. S. H., Ruckstuhl, C., Coz, E., Rupakheti, M., Sciare, J., Müller, T., Wiedensohler, A., and Hansen, A. D. A.: The "dual-spot" Aethalometer: an improved measurement of aerosol black carbon with real-time loading compensation, Atmos. Meas. Tech., 8, 1965–1979, https://doi.org/10.5194/amt-8-1965-2015, 2015.

El Haddad, I., Marchand, N., Wortham, H., Piot, C., Besombes, J.-L., Cozic, J., Chauvel, C., Armengaud, A., Robin, D., and Jaffrezo, J.-L.: Primary sources of $PM_{2.5}$ organic aerosol in an industrial Mediterranean city, Marseille, Atmos. Chem. Phys., 11, 2039–2058, https://doi.org/10.5194/acp-11-2039-2011, 2011.

Fares, S., Schnitzhofer, R., Jiang, X., Guenther, A., Hansel, A., and Loreto, F.: Observations of diurnal to weekly variations of monoterpene-dominated fluxes of volatile organic compounds from mediterranean forests: implications for regional modeling, Environ. Sci. Technol., 47, 11073–11082, https://doi.org/10.1021/es4022156, 2013.

Freney, E., Sellegri, K., Chrit, M., Adachi, K., Brito, J., Waked, A., Borbon, A., Colomb, A., Dupuy, R., Pichon, J.-M., Bouvier, L., Delon, C., Jambert, C., Durand, P., Bourianne, T., Gaimoz, C., Triquet, S., Féron, A., Beekmann, M., Dulac, F., and Sartelet, K.: Aerosol composition and the contribution of SOA formation over Mediterranean forests, Atmos. Chem. Phys. Discuss., https://doi.org/10.5194/acp-2017-482, in review, 2017.

Gangoiti, G., Millán, M. M., Salvador, R., and Mantilla, E.: Long-range transport and re-circulation of pollutants in the western Mediterranean during the project Regional Cycles of Air Pollution in the West-Central Mediterranean Area, Atmos. Environ., 35, 6267–6276, https://doi.org/10.1016/S1352-2310(01)00440-X, 2001.

Gelencsér, A., May, B., Simpson, D., Sánchez-Ochoa, A., Kasper-Giebl, A., Puxbaum, H., Caseiro, A., Pio, C., and Legrand, M.: Source apportionment of $PM_{2.5}$ organic aerosol over Europe: Primary/secondary, natural/anthropogenic, and fossil/biogenic origin, J. Geophys. Res., 112, D23S04, https://doi.org/10.1029/2006JD008094, 2007.

Giorgi, F.: Climate change hot-spots, Geophys. Res. Lett., 33, 1–4, https://doi.org/10.1029/2006GL025734, 2006.

Griffin, R. J., Cocker, D. R., Flagan, R. C., and Seinfeld, J. H.: Organic aerosol formation from the oxidation of biogenic hydrocarbons, J. Geophys. Res.-Atmos., 104, 3555–3567, https://doi.org/10.1029/1998JD100049, 1999.

Guenther, A., Karl, T., Harley, P., Wiedinmyer, C., Palmer, P. I., and Geron, C.: Estimates of global terrestrial isoprene emissions using MEGAN (Model of Emissions of Gases and Aerosols from Nature), Atmos. Chem. Phys., 6, 3181–3210, https://doi.org/10.5194/acp-6-3181-2006, 2006.

Hauglustaine, D. A., Balkanski, Y., and Schulz, M.: A global model simulation of present and future nitrate aerosols and their direct radiative forcing of climate, Atmos. Chem. Phys., 14, 11031–11063, https://doi.org/10.5194/acp-14-11031-2014, 2014.

Haylock, M. R., Hofstra, N., Klein Tank, A. M. G., Klok, E. J., Jones, P. D., and New, M.: A European daily high-resolution gridded data set of surface temperature and precipitation for 1950–2006, J. Geophys. Res., 113, D20119, https://doi.org/10.1029/2008JD010201, 2008.

Hildebrandt, L., Kostenidou, E., Mihalopoulos, N., Worsnop, D. R., Donahue, N. M., and Pandis, S. N.: Formation of highly oxygenated organic aerosol in the atmosphere: Insights from the Finokalia Aerosol Measurement Experiments, Geophys. Res. Lett., 37, 6–10, https://doi.org/10.1029/2010GL045193, 2010.

Hodzic, A. and Jimenez, J. L.: Modeling anthropogenically controlled secondary organic aerosols in a megacity: a simplified framework for global and climate models, Geosci. Model Dev., 4, 901–917, https://doi.org/10.5194/gmd-4-901-2011, 2011.

Hofstra, N., Haylock, M., New, M., and Jones, P. D.: Testing E-OBS European high-resolution gridded data set of daily precipitation and surface temperature, J. Geophys. Res., 114, D21101, https://doi.org/10.1029/2009JD011799, 2009.

Hong, S.-Y., Dudhia, J., Chen, S.-H., Hong, S.-Y., Dudhia, J., and Chen, S.-H.: A Revised Approach to Ice Microphysical Processes for the Bulk Parameterization of Clouds and Precipitation, Mon. Weather Rev., 132, 103–120, https://doi.org/10.1175/1520-0493(2004)132<0103:ARATIM>2.0.CO;2, 2004.

Janjic, Z. I.: A nonhydrostatic model based on a new approach, Meteorol. Atmos. Phys., 82, 271–285, https://doi.org/10.1007/s00703-001-0587-6, 2003.

Kanakidou, M., Seinfeld, J. H., Pandis, S. N., Barnes, I., Dentener, F. J., Facchini, M. C., Van Dingenen, R., Ervens, B., Nenes, A., Nielsen, C. J., Swietlicki, E., Putaud, J. P., Balkanski, Y., Fuzzi, S., Horth, J., Moortgat, G. K., Winterhalter, R., Myhre, C. E. L., Tsigaridis, K., Vignati, E., Stephanou, E. G., and Wilson, J.: Organic aerosol and global climate modelling: a review, Atmos. Chem. Phys., 5, 1053–1123, https://doi.org/10.5194/acp-5-1053-2005, 2005.

Koçak, M., Mihalopoulos, N., and Kubilay, N.: Chemical composition of the fine and coarse fraction of aerosols in the northeastern Mediterranean, Atmos. Environ., 41, 7351–7368, https://doi.org/10.1016/j.atmosenv.2007.05.011, 2007.

Konovalov, I. B., Beekmann, M., Berezin, E. V., Petetin, H., Mielonen, T., Kuznetsova, I. N., and Andreae, M. O.: The role of semi-volatile organic compounds in the mesoscale evolution of biomass burning aerosol: a modeling case study of the 2010 mega-fire event in Russia, Atmos. Chem. Phys., 15, 13269–13297, https://doi.org/10.5194/acp-15-13269-2015, 2015.

Koulouri, E., Saarikoski, S., Theodosi, C., Markaki, Z., Gerasopoulos, E., Kouvarakis, G., Makela, T., Hillamo, R., and Mihalopoulos, N.: Chemical composition and sources of fine and coarse aerosol particles in the Eastern Mediterranean, Atmos. Environ.,

42, 6542–6550, https://doi.org/10.1016/j.atmosenv.2008.04.010, 2008.

Kroll, J. H. and Seinfeld, J. H.: Chemistry of secondary organic aerosol: Formation and evolution of low-volatility organics in the atmosphere, Atmos. Environ., 42, 3593–3624, https://doi.org/10.1016/j.atmosenv.2008.01.003, 2008.

Kuenen, J. J. P., Visschedijk, A. J. H., Jozwicka, M., and Denier van der Gon, H. A. C.: TNO-MACC_II emission inventory; a multi-year (2003–2009) consistent high-resolution European emission inventory for air quality modelling, Atmos. Chem. Phys., 14, 10963–10976, https://doi.org/10.5194/acp-14-10963-2014, 2014.

Lane, T. E., Donahue, N. M., and Pandis, S. N.: Simulating secondary organic aerosol formation using the volatility basis-set approach in a chemical transport model, Atmos. Environ., 42, 7439–7451, https://doi.org/10.1016/j.atmosenv.2008.06.026, 2008.

Lanz, V. A., Prévôt, A. S. H., Alfarra, M. R., Weimer, S., Mohr, C., DeCarlo, P. F., Gianini, M. F. D., Hueglin, C., Schneider, J., Favez, O., D'Anna, B., George, C., and Baltensperger, U.: Characterization of aerosol chemical composition with aerosol mass spectrometry in Central Europe: an overview, Atmos. Chem. Phys., 10, 10453–10471, https://doi.org/10.5194/acp-10-10453-2010, 2010.

Lelieveld, J., Lelieveld, J., Berresheim, H., Borrmann, S., Crutzen, P. J., Dentener, F. J., Fischer, H., Feichter, J., Flatau, P. J. and Heland, J.: Global Air Pollution Crossroads over the Mediterranean, Science, 794, 794–799, https://doi.org/10.1126/science.1075457, 2002.

Lionello, P. and Giorgi, F.: Winter precipitation and cyclones in the Mediterranean region: future climate scenarios in a regional simulation, Adv. Geosci., 12, 153–158, https://doi.org/10.5194/adgeo-12-153-2007, 2007.

Liu, P., Tsimpidi, A. P., Hu, Y., Stone, B., Russell, A. G., and Nenes, A.: Differences between downscaling with spectral and grid nudging using WRF, Atmos. Chem. Phys., 12, 3601–3610, https://doi.org/10.5194/acp-12-3601-2012, 2012.

Mailler, S., Menut, L., Khvorostyanov, D., Valari, M., Couvidat, F., Siour, G., Turquety, S., Briant, R., Tuccella, P., Bessagnet, B., Colette, A., Létinois, L., Markakis, K., and Meleux, F.: CHIMERE-2017: from urban to hemispheric chemistry-transport modeling, Geosci. Model Dev., 10, 2397–2423, https://doi.org/10.5194/gmd-10-2397-2017, 2017.

Mallet, M., Dulac, F., Formenti, P., Nabat, P., Sciare, J., Roberts, G., Pelon, J., Ancellet, G., Tanré, D., Parol, F., Denjean, C., Brogniez, G., di Sarra, A., Alados-Arboledas, L., Arndt, J., Auriol, F., Blarel, L., Bourrianne, T., Chazette, P., Chevaillier, S., Claeys, M., D'Anna, B., Derimian, Y., Desboeufs, K., Di Iorio, T., Doussin, J.-F., Durand, P., Féron, A., Freney, E., Gaimoz, C., Goloub, P., Gómez-Amo, J. L., Granados-Muñoz, M. J., Grand, N., Hamonou, E., Jankowiak, I., Jeannot, M., Léon, J.-F., Maillé, M., Mailler, S., Meloni, D., Menut, L., Momboisse, G., Nicolas, J., Podvin, T., Pont, V., Rea, G., Renard, J.-B., Roblou, L., Schepanski, K., Schwarzenboeck, A., Sellegri, K., Sicard, M., Solmon, F., Somot, S., Torres, B., Totems, J., Triquet, S., Verdier, N., Verwaerde, C., Waquet, F., Wenger, J., and Zapf, P.: Overview of the Chemistry-Aerosol Mediterranean Experiment/Aerosol Direct Radiative Forcing on the Mediterranean Climate (ChArMEx/ADRIMED) summer 2013 campaign, Atmos. Chem. Phys., 16, 455–504, https://doi.org/10.5194/acp-16-455-2016, 2016.

Martinelli, N., Olivieri, O. and Girelli, D.: Air particulate matter and cardiovascular disease: a narrative review, Eur. J. Intern. Med., 24, 295–302, https://doi.org/10.1016/j.ejim.2013.04.001, 2013.

Mauderly, J. L. and Chow, J. C.: Health Effects of Organic Aerosols, Inhal. Toxicol., 20, 257–288, https://doi.org/10.1080/08958370701866008, 2008.

Menut, L., Bessagnet, B., Khvorostyanov, D., Beekmann, M., Blond, N., Colette, A., Coll, I., Curci, G., Foret, G., Hodzic, A., Mailler, S., Meleux, F., Monge, J.-L., Pison, I., Siour, G., Turquety, S., Valari, M., Vautard, R., and Vivanco, M. G.: CHIMERE 2013: a model for regional atmospheric composition modelling, Geosci. Model Dev., 6, 981–1028, https://doi.org/10.5194/gmd-6-981-2013, 2013.

Menut, L., Rea, G., Mailler, S., Khvorostyanov, D., and Turquety, S.: Aerosol forecast over the Mediterranean area during July 2013 (ADRIMED/CHARMEX), Atmos. Chem. Phys., 15, 7897–7911, https://doi.org/10.5194/acp-15-7897-2015, 2015.

Michoud, V., Sciare, J., Sauvage, S., Dusanter, S., Léonardis, T., Gros, V., Kalogridis, C., Zannoni, N., Féron, A., Petit, J.-E., Crenn, V., Baisnée, D., Sarda-Estève, R., Bonnaire, N., Marchand, N., DeWitt, H. L., Pey, J., Colomb, A., Gheusi, F., Szidat, S., Stavroulas, I., Borbon, A., and Locoge, N.: Organic carbon at a remote site of the western Mediterranean Basin: sources and chemistry during the ChArMEx SOP2 field experiment, Atmos. Chem. Phys., 17, 8837–8865, https://doi.org/10.5194/acp-17-8837-2017, 2017.

Minguillón, M. C., Perron, N., Querol, X., Szidat, S., Fahrni, S. M., Alastuey, A., Jimenez, J. L., Mohr, C., Ortega, A. M., Day, D. A., Lanz, V. A., Wacker, L., Reche, C., Cusack, M., Amato, F., Kiss, G., Hoffer, A., Decesari, S., Moretti, F., Hillamo, R., Teinilä, K., Seco, R., Peñuelas, J., Metzger, A., Schallhart, S., Müller, M., Hansel, A., Burkhart, J. F., Baltensperger, U., and Prévôt, A. S. H.: Fossil versus contemporary sources of fine elemental and organic carbonaceous particulate matter during the DAURE campaign in Northeast Spain, Atmos. Chem. Phys., 11, 12067–12084, https://doi.org/10.5194/acp-11-12067-2011, 2011.

Mlawer, E. J., Taubman, S. J., Brown, P. D., Iacono, M. J., and Clough, S. A.: Radiative transfer for inhomogeneous atmospheres: RRTM, a validated correlated-k model for the longwave, J. Geophys. Res.-Atmos., 102, 16663–16682, https://doi.org/10.1029/97JD00237, 1997.

Mohr, C., DeCarlo, P. F., Heringa, M. F., Chirico, R., Slowik, J. G., Richter, R., Reche, C., Alastuey, A., Querol, X., Seco, R., Peñuelas, J., Jiménez, J. L., Crippa, M., Zimmermann, R., Baltensperger, U., and Prévôt, A. S. H.: Identification and quantification of organic aerosol from cooking and other sources in Barcelona using aerosol mass spectrometer data, Atmos. Chem. Phys., 12, 1649–1665, https://doi.org/10.5194/acp-12-1649-2012, 2012.

Monks, P. S., Granier, C., Fuzzi, S., Stohl, A., Williams, M. L., Akimoto, H., Amann, M., Baklanov, A., Baltensperger, U., Bey, I., Blake, N., Blake, R. S., Carslaw, K., Cooper, O. R., Dentener, F., Fowler, D., Fragkou, E., Frost, G. J., Generoso, S., Ginoux, P., Grewe, V., Guenther, A., Hansson, H. C., Henne, S., Hjorth, J., Hofzumahaus, A., Huntrieser, H., Isaksen, I. S. A., Jenkin, M. E., Kaiser, J., Kanakidou, M., Klimont, Z., Kulmala, M., Laj, P., Lawrence, M. G., Lee, J. D., Liousse, C., Maione, M., McFig-

gans, G., Metzger, A., Mieville, A., Moussiopoulos, N., Orlando, J. J., O'Dowd, C. D., Palmer, P. I., Parrish, D. D., Petzold, A., Platt, U., Pöschl, U., Prévôt, A. S. H., Reeves, C. E., Reimann, S., Rudich, Y., Sellegri, K., Steinbrecher, R., Simpson, D., ten Brink, H., Theloke, J., van der Werf, G. R., Vautard, R., Vestreng, V., Vlachokostas, C., and von Glasow, R.: Atmospheric composition change – global and regional air quality, Atmos. Environ., 43, 5268–5350, https://doi.org/10.1016/j.atmosenv.2009.08.021, 2009.

Murphy, B. N. and Pandis, S. N.: Simulating the Formation of Semivolatile Primary and Secondary Organic Aerosol in a Regional Chemical Transport Model, Environ. Sci. Technol., 43, 4722–4728, https://doi.org/10.1021/es803168a, 2009.

Nabat, P., Solmon, F., Mallet, M., Kok, J. F., and Somot, S.: Dust emission size distribution impact on aerosol budget and radiative forcing over the Mediterranean region: a regional climate model approach, Atmos. Chem. Phys., 12, 10545–10567, https://doi.org/10.5194/acp-12-10545-2012, 2012.

Nabat, P., Somot, S., Mallet, M., Chiapello, I., Morcrette, J. J., Solmon, F., Szopa, S., Dulac, F., Collins, W., Ghan, S., Horowitz, L. W., Lamarque, J. F., Lee, Y. H., Naik, V., Nagashima, T., Shindell, D., and Skeie, R.: A 4-D climatology (1979–2009) of the monthly tropospheric aerosol optical depth distribution over the Mediterranean region from a comparative evaluation and blending of remote sensing and model products, Atmos. Meas. Tech., 6, 1287–1314, https://doi.org/10.5194/amt-6-1287-2013, 2013.

Ng, N. L., Herndon, S. C., Trimborn, A., Canagaratna, M. R., Croteau, P. L., Onasch, T. B., Sueper, D., Worsnop, D. R., Zhang, Q., Sun, Y. L. and Jayne, J. T.: An Aerosol Chemical Speciation Monitor (ACSM) for Routine Monitoring of the Composition and Mass Concentrations of Ambient Aerosol, Aerosol Sci. Tech., 45, 780–794, https://doi.org/10.1080/02786826.2011.560211, 2011.

Odum, J. R., Jungkamp, T. P. W., Griffin, R. J., Forstner, H. J. L., R. C. Flagan, A., and Seinfeld, J. H.: Aromatics, Reformulated Gasoline, and Atmospheric Organic Aerosol Formation, 31, 1890–1897, https://doi.org/10.1021/ES960535L, 1997.

Paatero, P.: Least squares formulation of robust non-negative factor analysis, Chemom. Intell. Lab. Syst., 37, 23–35, https://doi.org/10.1016/S0169-7439(96)00044-5, 1997.

Paatero, P. and Tapper, U.: Positive matrix factorization: A non-negative factor model with optimal utilization of error estimates of data values, Environmetrics, 5, 111–126, https://doi.org/10.1002/env.3170050203, 1994.

Pankow, J. F.: Review and comparative analysis of the theories on partitioning between the gas and aerosol particulate phases in the atmosphere, Atmos. Environ., 21, 2275–2283, https://doi.org/10.1016/0004-6981(87)90363-5, 1987.

Petetin, H., Beekmann, M., Sciare, J., Bressi, M., Rosso, A., Sanchez, O., and Ghersi, V.: A novel model evaluation approach focusing on local and advected contributions to urban $PM_{2.5}$ levels – application to Paris, France, Geosci. Model Dev., 7, 1483–1505, https://doi.org/10.5194/gmd-7-1483-2014, 2014.

Pey, J., Querol, X., Alastuey, A., Forastiere, F., and Stafoggia, M.: African dust outbreaks over the Mediterranean Basin during 2001–2011: PM_{10} concentrations, phenomenology and trends, and its relation with synoptic and mesoscale meteorology, Atmos. Chem. Phys., 13, 1395–1410, https://doi.org/10.5194/acp-13-1395-2013, 2013.

Pieber, S. M., Zhao, Y., Orasche, J., Stengel, B., Czech, H., Corbin, J. C., Haddad, I. El, Klein, F., Kilic, D., Slowik, J. G., Donahue, N., Robinson, A., Zimmermann, R., Baltensperger, U., and Prévôt, A. S. H.: Characterization of organic low-, semi-, intermediate-and volatile organic compounds from four-stroke ship engine emissions: implications for atmospheric processing, EAC Abstr., 2016.

Pöschl, U.: Atmospheric Aerosols: Composition, Transformation, Climate and Health Effects, Angew. Chem. Int. Ed., 44, 7520–7540, https://doi.org/10.1002/anie.200501122, 2005.

Pun, B. K. and Seigneur, C.: Investigative modeling of new pathways for secondary organic aerosol formation, Atmos. Chem. Phys., 7, 2199–2216, https://doi.org/10.5194/acp-7-2199-2007, 2007.

Querol, X., Alastuey, A., Pey, J., Cusack, M., Pérez, N., Mihalopoulos, N., Theodosi, C., Gerasopoulos, E., Kubilay, N., and Koçak, M.: Variability in regional background aerosols within the Mediterranean, Atmos. Chem. Phys., 9, 4575–4591, https://doi.org/10.5194/acp-9-4575-2009, 2009.

Rea, G., Turquety, S., Menut, L., Briant, R., Mailler, S., and Siour, G.: Source contributions to 2012 summertime aerosols in the Euro-Mediterranean region, Atmos. Chem. Phys., 15, 8013–8036, https://doi.org/10.5194/acp-15-8013-2015, 2015.

Ripoll, A., Pey, J., Minguillón, M. C., Pérez, N., Pandolfi, M., Querol, X., and Alastuey, A.: Three years of aerosol mass, black carbon and particle number concentrations at Montsec (southern Pyrenees, 1570 m a.s.l.), Atmos. Chem. Phys., 14, 4279–4295, https://doi.org/10.5194/acp-14-4279-2014, 2014.

Robinson, A. L., Donahue, N. M., Shrivastava, M. K., Weitkamp, E. A., Sage, A. M., Grieshop, A. P., Lane, T. E., Pierce, J. R., and Pandis, S. N.: Rethinking Organic Aerosols: Semivolatile Emissions and Photochemical Aging, Science, 315, 1259–1262, https://doi.org/10.1126/science.1133061, 2007.

Sasser, E., Hemby, J., Adler, K., Anenberg, S., Bailey, C., Brockman, L., Chappell, L., DeAngelo, B., Damberg, R., Dawson, J., Frank, N., Geller, M., Hagler, G., Hemming, B., Jantarasami, L., Luben, T., Mitchell, J., and Moss, J.: Report to Congress on Black Carbon, available at: https://nepis.epa.gov/Exe/ZyPURL.cgi?Dockey=P100EIJZ.TXT (last access: 17 September 2016), EPA, 2012.

Sciare, J., Oikonomou, K., Cachier, H., Mihalopoulos, N., Andreae, M. O., Maenhaut, W., and Sarda-Estève, R.: Aerosol mass closure and reconstruction of the light scattering coefficient over the Eastern Mediterranean Sea during the MINOS campaign, Atmos. Chem. Phys., 5, 2253–2265, https://doi.org/10.5194/acp-5-2253-2005, 2005.

Sciare, J., Oikonomou, K., Favez, O., Liakakou, E., Markaki, Z., Cachier, H., and Mihalopoulos, N.: Long-term measurements of carbonaceous aerosols in the Eastern Mediterranean: evidence of long-range transport of biomass burning, Atmos. Chem. Phys., 8, 5551–5563, https://doi.org/10.5194/acp-8-5551-2008, 2008.

Sellegri, K., Gourdeau, J., Putaud, J.-P., and Despiau, S.: Chemical composition of marine aerosol in a Mediterranean coastal zone during the FETCH experiment, J. Geophys. Res.-Atmos., 106, 12023–12037, https://doi.org/10.1029/2000JD900629, 2001.

Shrivastava, M., Fast, J., Easter, R., Gustafson Jr., W. I., Zaveri, R. A., Jimenez, J. L., Saide, P., and Hodzic, A.: Modeling organic aerosols in a megacity: comparison of simple and complex representations of the volatility basis set approach, At-

mos. Chem. Phys., 11, 6639–6662, https://doi.org/10.5194/acp-11-6639-2011, 2011.

Shrivastava, M., Zelenyuk, A., Imre, D., Easter, R., Beranek, J., Zaveri, R. A., and Fast, J.: Implications of low volatility SOA and gas-phase fragmentation reactions on SOA loadings and their spatial and temporal evolution in the atmosphere, J. Geophys. Res.-Atmos., 118, 3328–3342, https://doi.org/10.1002/jgrd.50160, 2013.

Shrivastava, M., Easter, R. C., Liu, X., Zelenyuk, A., Singh, B., Zhang, K., Ma, P., Chand, D., Ghan, S., Jimenez, J. L., Zhang, Q., Fast, J., Rasch, P. J., and Tiitta, P.: Global transformation and fate of SOA: Implications of low-volatility SOA and gas-phase fragmentation reactions, J. Geophys. Res.-Atmos., 120, 4169–4195, https://doi.org/10.1002/2014JD022563, 2015.

Sič, B., El Amraoui, L., Piacentini, A., Marécal, V., Emili, E., Cariolle, D., Prather, M., and Attié, J.-L.: Aerosol data assimilation in the chemical transport model MOCAGE during the TRAQA/ChArMEx campaign: aerosol optical depth, Atmos. Meas. Tech., 9, 5535–5554, https://doi.org/10.5194/amt-9-5535-2016, 2016.

Solazzo, E., Bianconi, R., Pirovano, G., Matthias, V., Vautard, R., Moran, M. D., Wyat Appel, K., Bessagnet, B., Brandt, J., Christensen, J. H., Chemel, C., Coll, I., Ferreira, J., Forkel, R., Francis, X. V., Grell, G., Grossi, P., Hansen, A. B., Miranda, A. I., Nopmongcol, U., Prank, M., Sartelet, K. N., Schaap, M., Silver, J. D., Sokhi, R. S., Vira, J., Werhahn, J., Wolke, R., Yarwood, G., Zhang, J., and Galmarini, S.: Operational model evaluation for particulate matter in Europe and North America in the context of AQMEII, Atmos. Environ., 53, 75–92, https://doi.org/10.1016/j.atmosenv.2012.02.045, 2012.

Stull, R. B.: Mean Boundary Layer Characteristics, in: An Introduction to Boundary Layer Meteorology, 1–27, Springer Netherlands, Dordrecht, 1988.

Vincent, J., Laurent, B., Losno, R., Bon Nguyen, E., Roullet, P., Sauvage, S., Chevaillier, S., Coddeville, P., Ouboulmane, N., di Sarra, A. G., Tovar-Sánchez, A., Sferlazzo, D., Massanet, A., Triquet, S., Morales Baquero, R., Fornier, M., Coursier, C., Desboeufs, K., Dulac, F., and Bergametti, G.: Variability of mineral dust deposition in the western Mediterranean basin and south-east of France, Atmos. Chem. Phys., 16, 8749–8766, https://doi.org/10.5194/acp-16-8749-2016, 2016.

Wang, W., Bruyère, C., Duda, M., Dudhia, J., Gill, D., Kavulich, M., Keene, K., Lin, H.-C., Michalakes, J., Rizvi, S., Zhang, X., Berner, J., and Smith, K.: WRF ARW Version 3 Modeling System User's Guide, 1–428, https://doi.org/10.1525/jps.2007.37.1.204, 2015.

Zare, A., Christensen, J. H., Irannejad, P., and Brandt, J.: Evaluation of two isoprene emission models for use in a long-range air pollution model, Atmos. Chem. Phys., 12, 7399–7412, https://doi.org/10.5194/acp-12-7399-2012, 2012.

Zhang, Y. L., Perron, N., Ciobanu, V. G., Zotter, P., Minguillón, M. C., Wacker, L., Prévôt, A. S. H., Baltensperger, U., and Szidat, S.: On the isolation of OC and EC and the optimal strategy of radiocarbon-based source apportionment of carbonaceous aerosols, Atmos. Chem. Phys., 12, 10841–10856, https://doi.org/10.5194/acp-12-10841-2012, 2012.

Zhang, Q. J., Beekmann, M., Drewnick, F., Freutel, F., Schneider, J., Crippa, M., Prevot, A. S. H., Baltensperger, U., Poulain, L., Wiedensohler, A., Sciare, J., Gros, V., Borbon, A., Colomb, A., Michoud, V., Doussin, J.-F., Denier van der Gon, H. A. C., Haeffelin, M., Dupont, J.-C., Siour, G., Petetin, H., Bessagnet, B., Pandis, S. N., Hodzic, A., Sanchez, O., Honoré, C., and Perrussel, O.: Formation of organic aerosol in the Paris region during the MEGAPOLI summer campaign: evaluation of the volatility-basis-set approach within the CHIMERE model, Atmos. Chem. Phys., 13, 5767–5790, https://doi.org/10.5194/acp-13-5767-2013, 2013.

CHAPTER

V

Future climatic drivers and their effect on PM_{10} components in Europe and the Mediterranean Sea

Contents

1 Summary of article **133**

2 Future climatic drivers and their effect on PM_{10} components in Europe and the Mediterranean Sea **135**

3 Abstract **136**

4 Introdution **137**

5 Methods **138**

5.1 Modeling framework 138

5.2 CHIMERE chemistry transport model 139

5.3 Climate scenarios 139

5.4 Air pollutant emissions 140

6 Climate impacts **140**

6.1 Meteorological parameters 140

6.2 PM_{10} concentrations 142

6.3 Distribution of PM_{10} chemical components 143

6.4 Dependence of PM_{10} components to meteorological parameters 146

7 Impacts of boundary condition and anthropogenic emissions **151**

7.1 Boundary conditions 152

7.2 Anthropogenic emissions 152

7.3 Cumulative impacts 154

8 Conclusion and discussion **155**

9 References **157**

In the previous chapters, a more suitable parameterization for the simulation of the Mediterranean region was implemented in the CHIMERE model and evaluated. In this chapter, the future changes of the PM and its components in the Mediterranean domain will be explored in multiple future scenarios. A list of scenarios were explored, where, in each one only one driver is changed. Exploring each scenario and comparing it to the historic simulations can give us the effects of that specific driver on the changes seen for the PM in future scenarios. The focus of this chapter will on be three drivers: regional climate, anthropogenic emissions and log-range transport. This study will be continued in the next chapter where the effects of OA simulation scheme change on the future scenarios will be explored.

1 Summary of article

The sensitivity to climate change of different areas in the world depends on the existing local meteorological conditions. Giorgi, (2006) calculated a factor to determine the climate change hotspots in future scenarios to show the sensitivity of different regions when faced with climate change. Using the differences between wet season and dry season historic and future precipitation and temperature for different regions and an ensemble of scenarios and models, he showed that the Mediterranean and the north-eastern European area are more sensitive to climate change than the other examined regions in this study. According to his calculations, European area and the Mediterranean as a whole, are one of the most important hotspots for climate change. This highlights the importance of understanding the changes that might affect these regions. Since PM presents an important factor for the air quality, it becomes interesting and essential to investigate the changes of PM in future scenarios for the Mediterranean area.

Previous works have already addressed the impact of climate change on air quality and PM over Europe (Meleux et al. (2007); Carvalho et al. (2010); Lacressonnière, Foret, et al. (2016); Lacressonnière, Watson, et al. (2017); Fortems-Cheiney et al. (2017)). The work presented here, is original because it addresses different PM components specifically, and it tries to relate observed changes of each component to changes in specific climate variables. It also presents detailed analysis for the Mediterranean region. Finally, it separates analysis of different drivers such as regional climate, anthropogenic emissions and long-range transport.

For this purpose, multiple series of future scenarios, in each one a separate driver being variable, have been explored. These pre-existing simulations were performed with the CHIMERE CTM (version 2013b), covering the European continent and the Mediterranean area. A detailed explication and examination of these scenarios is presented in Colette, Bessagnet, et al. (2013). The regional climate impact simulations contain the period of 1976-2005 for the historic simulations and 2031-2100 for the three future scenarios: RCP2.6, RCP4.5 and RCP8.5. The anthropogenic emission change scenarios are performed for the period of 2046-2055 with CLE2050 and MFR2050 anthropogenic

emissions using RCP4.5. The long-range transport scenario covers the same period as anthropogenic emission scenarios, with CLE2010 emissions, instead the boundary condition inputs change. A more realistic series of scenarios for the 2050s, where all parameters change at the same time (RCP4.5, CLE2050 and future boundary conditions) has been included as well. As explained, in each of the aforementioned series, only one parameter changes, which makes it possible to calculate the effects of each driver separately. A comparison of meteorological conditions in climate scenarios is included in the article.

In general, it is important to bear in mind that compared to the European area, the aerosol burden in the Mediterranean is much higher, because of high salt and dust concentrations. When regional climate is concerned, a decrease is seen in the concentration of PM_{10} in both the Mediterranean and European regions. The reason for this decrease is mainly a strong decrease in the concentration of nitrates. The BSOA shows an increase in concentration, but this increase is overshadowed by the decrease in nitrates. Each of the components of PM_{10} were compared to different meteorological parameters (temperature, relative humidity, precipitation, shortwave radiation, wind speed and PBL height) for the entire 70 year seasonal averages. These comparisons showed us that, for the European region, a high dependency exists between nitrates and BSOA with temperature (an anti-correlation and a correlation respectively), while sulfates and ammonium show a strong correspondence to relative humidity. PM_{10} and $PM_{2.5}$ themselves show the best correlation with the meteorological parameter that is best correlated with their major contributor. For the Mediterranean region, BSOA shows a stronger correlation to wind speed since the BSOA existing on the basin is mostly transported to the area and is not formed locally.

Long-range transport is explored by changing boundary condition inputs in the model. Although future changes in long-range transport do not strongly affect most species, they result in an important increase of dust concentrations.

In terms of anthropogenic emissions, the changes induced by this driver are quite important for most species. Even for BSOA, for which anthropogenic emission changes should not normally have an effect, a decrease in concentration is seen because of anthropogenic emission decreases. This is tentatively attributed to changes in seed aerosol and the changes in oxidant levels because of decrease in anthropogenic emissions and also a direct decrease in anthropogenic COVs, however, more research is needed on the subject to be certain. Dust species are not affected by anthropogenic emission changes as expected (nor are salt species).

Cumulative effects show that for most species, the effects of anthropogenic emission reductions overshadow the effects of other drivers. The exception for this case is the dust species, which is highly affected by long-range transport.

Another point that has been raised in this article is the differences between the European sub-domain and the Mediterranean Sea on one hand and between western and

eastern Mediterranean on the other hand. The behavior of these sub-domains differs when they are exposed to climate change. Meteorological changes in the Mediterranean region show increasing temperatures, increasing PBL height and decreasing humidity. Winters and springs seem to become drier and the other two seasons wetter when regarding to precipitation amount, while rain episodes become more intense and shorter in most cases. Seasonally, in the Mediterranean a maximum of PM_{10} concentrations is seen for spring when dust episodes are more common, contrary to the European sub-domain (maximum at winter for EUR). Emission reduction policies will reduce the concentrations of anthropogenic species in the basin by almost the same percentage as the European sub-domain as shown in this work (for example, for sulfates, anthropogenic emissions reduction results in -29% and -30% for EUR and MED respectively for CLE2050 emissions). While this shows that emission reduction policies will reduce the $PM_{2.5}$ and lower aerosol fraction pollution, they will not lessen the Mediterranean PM_{10} burden as much, since in this area the PM_{10} concentration revolves around dust and salt concentrations.

A continuation of this work is presented in the next chapter, where the effects of changing the OA simulation scheme has been explored on future scenarios (chapter VI). Analysis of population exposure is another perspective of this work, and can be addressed by high resolution simulations on a specific region (chapter VII).

2 Future climatic drivers and their effect on PM_{10} components in Europe and the Mediterranean Sea

This chapter includes the article Cholakian et al. (2019) published in *Atmospheric Chemistry and Physics : "Future climatic drivers and their effect on PM_{10} components in Europe and the Mediterranean Sea,19, 4459–4484, doi:10.5194/acp-19-4459-2019, url: Atmospheric chemistry and physics"*.

The article was published the 18 March 2019.

Atmos. Chem. Phys., 19, 4459–4484, 2019
https://doi.org/10.5194/acp-19-4459-2019
© Author(s) 2019. This work is distributed under
the Creative Commons Attribution 4.0 License.



Atmospheric Chemistry and Physics Open Access EGU

Future climatic drivers and their effect on PM_{10} components in Europe and the Mediterranean Sea

Arineh Cholakian[1,2,a], **Augustin Colette**[2], **Isabelle Coll**[1], **Giancarlo Ciarelli**[1,b], **and Matthias Beekmann**[1]

[1]Laboratoire Interuniversitaire des Systèmes Atmosphériques (LISA), UMR CNRS 7583,
Université Paris Est Créteil et Université Paris Diderot (UPD), Institut Pierre Simon Laplace, Créteil (IPSL), Créteil, France
[2]Institut National de l'Environnement Industriel et des Risques, Parc Technologique ALATA, Verneuil-en-Halatte, France
[a]now at: EPOC, UMR 5805, Université de Bordeaux, Pessac, France
[b]now at: Department of Chemical Engineering, Carnegie Mellon University, Pittsburgh, USA

Correspondence: Arineh Cholakian (arineh.cholakian@lisa.u-pec.fr)

Received: 21 August 2018 – Discussion started: 5 December 2018
Revised: 26 February 2019 – Accepted: 18 March 2019 – Published: 5 April 2019

Abstract. Multiple CMIP5 (Coupled Model Intercomparison Project phase 5) future scenarios run with the CHIMERE chemistry transport model (CTM) are compared to historic simulations in order to study some of the drivers governing air pollution. Here, the focus is on regional climate, anthropogenic emissions and long-range transport. Two major subdomains are explored – the European region and the Mediterranean Basin – with both areas showing high sensitivity to climate change. The Mediterranean area is explored in the context of the ChArMEx (the Chemistry Aerosol Mediterranean Experiment) project, which examines the current and future meteorological and chemical conditions of the Mediterranean area. This climate impact study covers the period from 2031 to 2100 and considers possible future scenarios in comparison with 1976 to 2005 historic simulations using three Representative Concentration Pathways (RCPs; RCP2.6, RCP4.5 and RCP8.5). A detailed analysis of total PM_{10} (particulate matter with a diameter smaller that 10 µm) concentrations is carried out, including the evolution of PM_{10} and changes to its composition. The individual effects of meteorological conditions on PM_{10} components are explored in these scenarios in an effort to pinpoint the meteorological parameter(s) governing each component. The anthropogenic emission impact study covers the period from 2046 to 2055 using current legislation (CLE) and maximum feasible reduction (MFR) anthropogenic emissions for the year 2050 compared with historic simulations covering the period from 1996 to 2005 and utilizing CLE2010 emissions data. Long-range transport is explored by changing the boundary conditions in the chemistry transport model over the same period as the emission impact studies. Finally, a cumulative effect analysis of these drivers is performed, and the impact of each driver on PM_{10} and its components is estimated. The results show that regional climate change causes a decrease in the PM_{10} concentrations in our scenarios (in both the European and Mediterranean subdomains), as a result of a decrease in nitrate, sulfate, ammonium and dust atmospheric concentrations in most scenarios. On the contrary, BSOA (biogenic secondary organic aerosol) displays an important increase in all scenarios, showing more pronounced concentrations for the European subdomain compared with the Mediterranean region. Regarding the relationship of different meteorological parameters to concentrations of different species, nitrate and BSOA show a strong temperature dependence, whereas sulfate is most strongly correlated with relative humidity. The temperature-dependent behavior of BSOA changes when looking at the Mediterranean subdomain, where it displays more dependence on wind speed, due to the transported nature of BSOA existing in this subdomain. A cumulative look at all drivers shows that anthropogenic emission changes overshadow changes caused by climate and long-range transport for both of the subdomains explored, with the exception of dust particles for which long-range transport changes are more influential, especially in the Mediterranean Basin. For certain species (such as sulfates and BSOA), in most of the subdomains explored, the changes caused by anthropogenic emissions are (to a certain

extent) reduced by the boundary conditions and regional climate changes.

1 Introduction

Particulate matter (PM) is one of the most important constituents of air pollution. It can have a variety of adverse effects on air quality (Seinfeld and Pandis, 2016) and, subsequently, on human health (Pope and Dockery, 2006; Kampa and Castanas, 2008; Anderson et al., 2012; Im et al., 2018) and ecosystems (Grantz et al., 2003). Studies have shown that the life expectancy of the population can change drastically in areas densely polluted by atmospheric aerosols (Pope et al., 2009). PM is comprised of a large number of components, with different origins and diverse behaviors with respect to meteorological parameters. Therefore, there are many different ways in which the particles can affect air quality, making their investigation both important and complex.

The intricacy of studying PM increases when coupling its effects with climate change, as air quality and climate change have intertwined interactions (e.g., Kinney, 2008; Wild, 2009; Seinfeld and Pandis, 2016). In other words, changes in meteorological conditions have varied effects on air quality, but at the same time climate change may be affected by the radiative forcing of air pollutants. These effects can, in some cases, be similar in direction, or they may cause inverse outcomes. Thus, when exploring future air quality, it is important to take into account that different drivers can have different impacts while also undergoing nonlinear interactions among themselves. Therefore it is necessary to explore the effects of each driver separately.

Air pollution is mainly governed by four factors: anthropogenic and/or biogenic emissions of primary pollutants and precursors of secondary pollutants, atmospheric chemistry, long-range transport and, of course, meteorology (Jacob and Winner, 2009). While these factors are listed separately, they also undergo interactions among themselves. For example, atmospheric chemistry is directly affected by temperature and radiative forcing. Similarly, parameters such as precipitation, wind speed and wind direction can enhance or reduce dispersion and deposition. Furthermore, meteorological conditions such as temperature and wind speed can indirectly impact the emission of primary pollutants, which may also be precursors of secondary pollutants (EEA, 2004). As a result, the sensitivity of air quality to climate change seems to be crucial, but complex to investigate.

The sensitivity of different areas in the world to climate change depends on the existing local meteorological conditions. Giorgi (2006) calculated a factor to determine climate change hotspots in future scenarios and to establish the sensitivity of different regions when faced with climate change. Using the differences between historic and future precipitation and temperature for different regions and seasons in an ensemble of scenarios and models, he showed that the Mediterranean and northeastern European regions are more sensitive to climate change than other areas of the world, followed by the western Europe. According to his calculations, the European region (both the eastern and western regions on average) and the Mediterranean as a whole, are among the most important hotspots for climate change. This highlights the importance of understanding changes that might affect these regions. Therefore, the focus of this study is on the European area with special attention paid to the Mediterranean Basin, which is why the current work is related to the ChArMEx (the Chemistry Aerosol Mediterranean Experiment; http://charmex.lsce.ipsl.fr, last access: 7 September 2018) project. The goals of ChArMEx are to better assess the sources, formation, transformation and mechanisms of transportation of gases and aerosols in the western Mediterranean Basin and also to better estimate the future composition of the atmosphere over the Mediterranean Sea. The measurement portion of this campaign took place in the western Mediterranean Basin during the period from 2012 to 2014; however, the analysis of the data obtained during the campaign and the assessment of future atmospheric changes for the basin are still ongoing.

A regional chemistry transport model (CTM) was used to explore possible future changes in these regions. Running such regional simulations requires inputs from a global CTM, a global circulation model (GCM) and a regional climate model (RCM), as well as anthropogenic/biogenic emission inputs. Changes made to these inputs make it possible to distinguish the effects of different drivers on air pollution one by one. Modifying RCM inputs allows for the estimation of the effects of meteorology alone, whereas a combined modification of RCM and global CTM inputs allows for the simultaneous assessment of the impacts of meteorology and long-range transport. Conversely, apart from RCM inputs, changes in anthropogenic emissions allow for the exploration of the effects of meteorology and emissions on air pollution.

These kinds of studies naturally already exist for different parts of the world, for one or multiple drivers and for different components. For example, Liao et al. (2006) used a global model to explore the atmospheric changes expected in the year 2100; this was undertaken by comparing a year of historic simulations with a yearlong simulation in 2100, where all factors were changed. The first study that investigated the future atmospheric conditions of a European area only focused on ozone changes and used the two 30-year-long future scenarios compared with a 30-year-long historic period (Meleux et al., 2007). Other studies have used an ensemble of future simulations, each with a different model, in order to compare the results given by each of these models (e.g., Langner et al., 2012). Based on the IMPACT2C project (Jacob, 2017), Lacressonnière et al. (2016, 2017) focused on European regional simulations, exploring the effects of a 2 °C climate change combined with anthropogenic emission changes in an ensemble of four models. Similarly, Fortems-

Cheiney et al. (2017) explored the same scenarios for a 3 °C climate change, with a focus on gaseous species, and Carvalho et al. (2010) conducted a SRES (Special Report on Emission Scenarios) A2 climate change scenario over the end of the 21st century for Europe, zooming on Portugal. The common point of all these studies is that all of the impacting factors were changed simultaneously in a future scenario. A review of existing scenarios is presented in Colette et al. (2015).

Unlike these studies, other papers have investigated the impact of emissions and meteorology on the atmospheric composition in future scenarios separately. Dawson et al. (2007) focused on determining the atmospheric sensitivity to changes in meteorological conditions in the eastern US, over a simulation period of 2 months. Megaritis et al. (2014) used a similar approach to Dawson et al. (2007), exploring the sensitivity of the atmospheric composition to changes in meteorological conditions for Europe over a 3-month-long simulation period. These two studies both conducted sensitivity tests over short (month-long) periods of time. Lemaire et al. (2016) explored climate change effects using the same data set as that used in our work, and developed a statistical method to ascertain the meteorological parameters that affect atmospheric pollutants in future scenarios. Hedegaard et al. (2013) also looked at the relative importance of emissions and meteorological drivers in a hemispheric model. Finally, Colette et al. (2013) explored the same scenarios that we worked on with the aim of analyzing the global effects of the three drivers (meteorology, emissions and boundary conditions) on atmospheric composition, although they only focused on Europe as a whole and did not investigate the individual effects of the drivers on PM composition. Our aim is to complement these previous studies by providing a deeper insight into the respective impacts of climate, atmospheric composition and emission-related forcing. This is why the work described here focuses on simulating a set of future and climatic scenarios over long periods of time, and observing the differences between the drivers discussed above. The chosen approach is to change the drivers one by one and assess the differences induced in PM components in order to investigate the individual effects of the parameters in the simulation. Finally, the simulations are compared with a series of simulations for which all of the aforementioned drivers change at the same time; this can show us the overall impact of all of the drivers, which may be different to the sum of the impacts of individual drivers due to nonlinear effects.

It should be noted that other studies have also explored the dependence of PM components on meteorological conditions (Dawson et al., 2007; Carvalho et al., 2010; Fiore et al., 2012; Jiménez-Guerrero et al., 2012; Juda-Rezler et al., 2012; Hedegaard et al., 2013; Megaritis et al., 2014). However, most of these studies were performed over short time periods, such as 1-year-long simulations (shorter in most cases), and several used sensitivity tests and not actual future scenarios to assess the changes in different meteorological parameters. Conversely, Lemaire et al. (2016) explored the sensitivity of ozone and $PM_{2.5}$ to different meteorological parameters, using 30 years of RCP8.5 scenario simulations; however, they did not consider the relationship between the speciation of PM components and these parameters in detail. To the best of our knowledge, the sensitivity of PM components to meteorological parameters for a data set this extensive containing multiple scenarios and the calculation of the effects of different drivers on same data pool has not been investigated to date.

In this paper, after a brief introduction to the simulations and the modeling framework, the impacts of different drivers are explored. The analysis first deals with climate impacts, before the effects of long-range transport and emission changes are discussed. Finally, the impact of each of these three drivers on the concentration of PM_{10} and its components is calculated. The discussion of the results is divided into two parts corresponding to the geographic area: the European and the Mediterranean subdomains. Finally, a prospective view of what the PM component concentrations in the Mediterranean Basin may be like at the end of the 21st century is given.

2 Method

In this section, we introduce the architecture of the modeling framework, with a focus on the most sensitive component – the chemistry transport model. We also provide references to the input data used by the CHIMERE model in terms of future scenarios and for the various combinations of input parameters.

2.1 Modeling framework

The assessment of the long-term evolution of air quality in the context of a changing climate is performed using a suite of deterministic models following the framework introduced by Jacob and Winner (2009). Global climate projections are obtained from a global circulation model (GCM) that feeds a global chemistry transport model and a regional climate model. Finally, the latter two drive a regional chemistry transport model. The setup used in this study is presented in detail in Colette et al. (2013, 2015).

The global circulation model is the IPSL-CM5A-MR large-scale atmosphere–ocean model (Dufresne et al., 2013). It provides input to the regional climate model and the global chemistry transport model with global meteorological fields. It uses LMDZ (Hourdin et al., 2006) as its meteorological model, ORCHIDEE (Krinner et al., 2005) as its land surface model, and NEMO (Madec and Delecluse, 1998) and LIM (Fichefet and Maqueda, 1999) as the respective oceanic and sea-ice models. The horizontal resolution of this global model is $2.5° \times 1.25°$ with 39 vertical levels. For each scenario, the corresponding RCP is used for the anthropogenic

radiative forcing. The Weather Research and Forecasting model (WRF, Wang et al., 2015) is used as the regional climate model (RCM). The regional climate simulations were part of EURO-CORDEX (Jacob et al., 2014) with a spatial resolution of 0.44°. The historic simulations were evaluated by comparison with experimental data (Menut et al., 2012; Kotlarski et al., 2014; Katragkou et al., 2015). The LMDZ-INCA (Hauglustaine et al., 2014) global CTM is used for the production of chemical initial/boundary conditions for the regional CTM. The LMDZ-INCA runs used in this study have been analyzed in Szopa et al. (2013) and Markakis et al. (2014), and intercomparisons of the same runs with other global chemistry transport models have been analyzed in Shindell et al. (2013) and Young et al. (2013) in the framework of the ACCMIP (Atmospheric Chemistry and Climate Model Intercomparison) experiment. Monthly climatological fields are used as the boundary condition inputs, as the background changes over long periods of time and it was not possible to store hourly global model output to create hourly varying boundary conditions. This induces an unavoidable inconsistency between meteorology and dust fields.

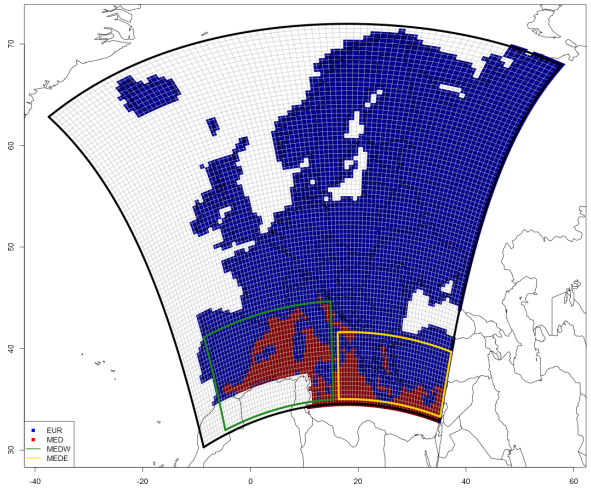


Figure 1. Extension of the main domain and subdomains. Four subdomains are used in this study: EUR – containing only continental Europe (blue cells), MED – containing only the Mediterranean Sea (red cells), MEDW – western Mediterranean region (green rectangle), and MEDE – eastern Mediterranean region (yellow rectangle).

2.2 CHIMERE CTM

The CHIMERE offline regional CTM has been widely used for both future scenarios (Colette et al., 2015; Lacressonnière et al., 2016) and for research activities in France (Zhang et al., 2013; Petetin et al., 2014; Menut et al., 2015; Rea et al., 2015; Cholakian et al., 2018) and abroad (Hodzic and Jimenez, 2011). In this work, the 2013b version of the model was used for all simulations (Menut et al., 2013). The simulations were conducted using the EURO-CORDEX domain with a horizontal resolution of 0.44° and nine vertical levels ranging from the surface to 500 mb. The aerosol module was run with a simple two-product scheme for the simulation of secondary organic aerosols (SOA, Bessagnet et al., 2008) and with the ISORROPIA module for the simulation of inorganic aerosols (Fountoukis and Nenes, 2007). It provides simulated aerosol fields including EC (elemental carbon), sulfate, nitrate, ammonium, SOA, dust, salt and PPM (primary particulate matter other than those mentioned above) considering coagulation, nucleation and condensation processes, as well as wet and dry deposition. The same unchanged land use data from GlobCover (Arino et al., 2008) with a base resolution of 300 m × 300 m have been used in different series of simulations. Dust emissions are taken into account inside the simulation domain based on the method proposed by Marticorena and Bergametti (1995).

The simulation domain has a 0.44° resolution (Fig. 1). The analysis was performed using the subdomains presented in Fig. 1. The EUR subdomain only concerns the European continent (including the British Isles), and a land–sea mask was used to remove other parts of the domain. The MED subdomain was also produced using a land–sea mask, but this time it only contained the Mediterranean Sea. The MEDW and MEDE are the last two subdomains. They refer to the western and eastern Mediterranean areas, respectively. It is important to bear in mind that these two subdomains, contrary to the previous subdomains, contain both land and sea for the purpose of observing the effects of enclosing land on the Mediterranean area. Due to this setup, the sum of MEDW and MEDE is different to that of MED.

2.3 Climate scenarios

Representative concentrations pathway scenarios (RCPs) designed for the fifth IPCC report (Meinshausen et al., 2011; van Vuuren et al., 2011b) are used in this study. Simulations using three of these CMIP5 RCPs (Taylor et al., 2012; Young et al., 2013) are selected: RCP2.6, RCP4.5 and RCP8.5, which consider 2.6, 4.5 and 8.5 $W m^{-2}$ of radiative forcing at the end of the 21st century, respectively. It is worth noting that RCP8.5 includes the least mitigation policies by far compared with the other two scenarios; therefore, RCP8.5 results in a high radiative forcing at the end of the century, with a temperature increase of between 2.6 and 4.8 °C for Europe according to the EEA (European Environmental Agency[1]). On the contrary, the RCP2.6 scenario considers a radiative forcing value that leads to a low-range temperature increase by 2100 (between 0.3 and 1.7 °C). This means that this scenario has to consider ambitious greenhouse gas emission reductions as well as carbon capture and storage. The RCP4.5 is an intermediate scenario with less stringent climate mitiga-

[1] https://www.eea.europa.eu/data-and-maps/indicators/global-and-european-temperature-8/assessment, last access: 21 July 2018.

tion policies, which results in a temperature increase somewhere between the two previously mentioned extreme scenarios.

2.4 Air pollutant emissions

The biogenic emissions input is obtained from the Model of Emissions of Gases and Aerosols from Nature (MEGAN v2.04; Guenther et al., 2006). It is worth mentioning that the emission factors and the leaf area index (LAI) values provided by this model are the same for all simulations; however, as many of the biogenic gases have a temperature-dependent nature, their emissions increase with higher temperatures. The MEGAN version used in CHIMERE takes six biogenic volatile organic compound (BVOC) emissions into account (isoprene, α-pinene, β-pinene, humulene, limonene and ocimene) and their dependence on temperature, solar radiation and the LAI.

Anthropogenic emissions are taken from the ECLIPSE-V4a global emissions projections (Amann et al., 2013; Klimont et al., 2013, 2017). This database covers the 2005–2050 time period with two main prospective pathways: the current legislation emissions (CLE) and the maximum feasible reduction (MFR) scenarios. These two scenarios show the effects of minimum and maximum mitigation efforts that can be expected by 2050, which gives us a spectrum of possible influences of anthropogenic emissions in future scenarios. For both scenarios, the atmospheric emissions of the main anthropogenic pollutants are available as global maps at a resolution of 0.5 °.

The simulations used in this study are summarized in Table 1. As the goal of this study is to separately investigate the regional CTM drivers that can affect the results of future simulations, different series of simulations were performed, with each one allowing for the evaluation of climate, anthropogenic emission and boundary condition impacts on PM concentrations.

As for the climate impact study, RCP2.6, RCP4.5 and RCP8.5 scenarios are used in combination with constant anthropogenic emissions and identical boundary conditions. These scenarios are compared with the historic simulations.

In order to explore the changes induced by boundary conditions on the CTM outputs, RCP4.5 scenarios were conducted using two different sets of boundary conditions from the same global CTM and compared with historic simulations. The difference between these two sets of conditions is the fact that anthropogenic pollutants from the RCP emissions (emissions produced for RCP scenarios exclusively) are used as anthropogenic inputs for one of them (Szopa et al., 2006, 2013), whereas the other one relies on ECLIPSE-V4a emissions as inputs (Markakis et al., 2014).

The emission impact study uses the RCP4.5 climate forcing with CLE 2010, CLE 2050 and MFR 2050 anthropogenic emissions, with each one again being compared with historic simulations.

As seen in Table 1, we simulated different prospective periods in the different series of simulations. In the case of the climate impact studies, a 30-year-long historical simulation and 70-year-long future simulation were used for each future scenario. As for the other simulations, 10 years of historical simulations (1996 to 2005) were compared with 10 years of future scenarios, representing the 2050s (2045 to 2054). This latter period was chosen because it is centered on year 2050, for which CLE/MFR 2050 emissions are available. In the end, a 10-year-long simulation was performed during which all of these factors were simultaneously changed. We have to mention that it would have been numerically too strenuous to perform 70 years of simulations for emission/boundary condition drivers, bearing in mind that the climatic impact simulations already amount to 240 years of simulations.

A validation of our historic simulations is presented in Menut et al. (2012) and Kotlarski et al. (2014) for the meteorological parameters, whereas a validation of some chemical species is presented in the Supplement to this article (Sect. S1). This validation uses an annual profile of 10 years of historic simulations from 1996 to 2005 (with 2010 constant anthropogenic emissions) compared with an annual profile of all available measurements from EEA and air base stations between 2005 and 2015 (EEA, 2016).

3 Climate impacts

This section discusses the comparisons between the simulations using RCP2.6, RCP4.5 and RCP8.5 with historic simulations (simulations 1 to 4 in Table 1). As all of the inputs except the meteorological fields remain identical in these four series of simulations, it is possible to disentangle the effects of climate alone on the PM concentration in different RCPs. While the specific goal of the paper is to focus on the PM changes in the Mediterranean area alone, a general overview of the European domain is also provided. Before exploring PM changes, temperature changes are analyzed as they imply important effects on biogenic volatile organic compound (BVOC) emissions; these emissions are precursors for the production of SOAs and affect gas–particle phase partitioning in simulations. The dependency of total PM_{10} and its components on other meteorological parameters is also discussed in detail in this section.

3.1 Meteorological parameters

The RCP2.6 reaches its maximum radiative forcing ($2.6\,W\,m^{-2}$) in the 2040s (van Vuuren et al., 2011a), meaning that an increase in radiative forcing is seen in this scenario until this decade, whereas afterwards we observe a continuous decrease. Therefore, in the bulk of the RCP2.6 simulations over Europe, a temperature decrease appears from about 2050 onwards, followed by a new increase in temperature over the last 10 years simulated (Fig. 2). As for the

Table 1. The different scenarios used in this work.

	No.	Simulation name	Simulation period	Global chemistry model	Regional climate model	Anthropogenic emissions
Climate	1	Hist	1976–2005	LMDZ-INCA-RCP2.6 ECLIPSE emissions	WRF Historic	ECLIPSE-V4a CLE2010
	2	RCP2.6	2031–2100		WRF RCP2.6	
	3	RCP4.5	2031–2100		WRF RCP4.5	
	4	RCP8.5	2031–2100		WRF RCP8.5	
Boundary conditions	5	RCP4.5-BC	2046–2055	LMDZ-INCA-RCP4.5 RCP emissions	WRF RCP4.5	ECLIPSE-V4a CLE2010
Emissions	6	RCP4.5-CLE2050	2046–2055	LMDZ-INCA-RCP2.6 ECLIPSE emissions	WRF RCP4.5	ECLIPSE-V4a CLE2050
	7	RCP4.5-MFR2050	2046–2055			ECLIPSE-V4a MFR2050
All	8	RCP4.5-BC-CLE2050	2046–2055	LMDZ-INCA-RCP4.5 RCP emissions	WRF RCP4.5	ECLIPSE-V4a CLE2050

RCP4.5 scenario, this maximum radiative forcing is reached in the 2070s (Thomson et al., 2011), whereas such a maximum is not reached for RCP8.5 until the end of the century. As a consequence, the temperature increase levels out after about 2070 in RCP4.5, while the temperature keeps increasing over the whole period in RCP8.5. These elements explain the larger similarities between RCP4.5 and RCP8.5 as well as their structural differences with RCP2.6. The time evolutions are similar for the European (EUR) and Mediterranean (MED) domains, albeit absolute temperatures are nearly 10 °C warmer over the Mediterranean on average (Fig. S2 for 2-D temperature fields).

In the following comparisons, annual average values over each subdomain and for each parameter and time series corresponding to 30 years of historic simulations and 70 years of future scenarios are presented. The uncertainties associated with each value account for the spatial variability of each parameter.

The 2 m temperatures are generally higher for the Mediterranean area than for the European continent; however, the increase in temperature is more pronounced for EUR than for MED (+1.69, +2.63 and +3.62 °C for EUR and +1.06, +1.72 and +2.91 °C for MED for RCP2.6, RCP4.5 and RCP8.5, respectively). In the other two Mediterranean subdomains temperature changes are higher for MEDE than for MEDW (+1.25, +2.05 and +3.38 °C for MEDE and +0.73, +1.77 and +2.88 °C for MEDW for RCP2.6, RCP4.5 and RCP8.5, respectively). While the European subdomain shows a more important temperature increase in winter (+1.86, +3.44 and +4.42 °C for RCP2.6, RCP4.5 and RCP8.5, respectively), the Mediterranean subdomains show a larger increase in summer (for MED +1.40, +2.06 and +3.22 °C for RCP2.6, RCP4.5 and RCP8.5, respectively). Maps of differences in temperature for the different scenarios and seasons are presented in the Supplement (Fig. S2). It should be noted that the average temperature changes discussed here agree with the literature (Knutti and Sedláček, 2012; Vautard et al., 2014).

As seen in Fig. 2, some of the parameters behave differently in the two subdomains. For example, for the amount of precipitation, an increase is simulated in EUR for RCP8.5, whereas a slight decrease is simulated for RCP2.6 after the 2050s, which makes precipitation stronger in RCP8.5 than in RCP2.6 on average for the future period. In the MED area, the opposite behavior is generally noted: precipitation is stronger in RCP2.6 than in RCP8.5. On the contrary, there is a steady decrease in the total duration of rain hours (sum of hours rained each year in each scenario – a threshold that is fixed for each subdomain using the average of 25th percentile for the whole duration of simulations). Therefore, rain events are expected to become more intense (Vautard et al., 2014). Regarding the total duration of rain hours in the Mediterranean region, the same result is obtained as for the EUR region, except for the RCP2.6 scenario where an increase in the number of rainy hours is simulated. This increase corresponds to the western basin of the Mediterranean Sea. For the eastern basin, all scenarios show a decrease in this parameter (Fig. S3 for MEDW and MEDE).

The same type of comparison is performed for wind speed (WS; 10 m wind), relative humidity (RH) and planetary

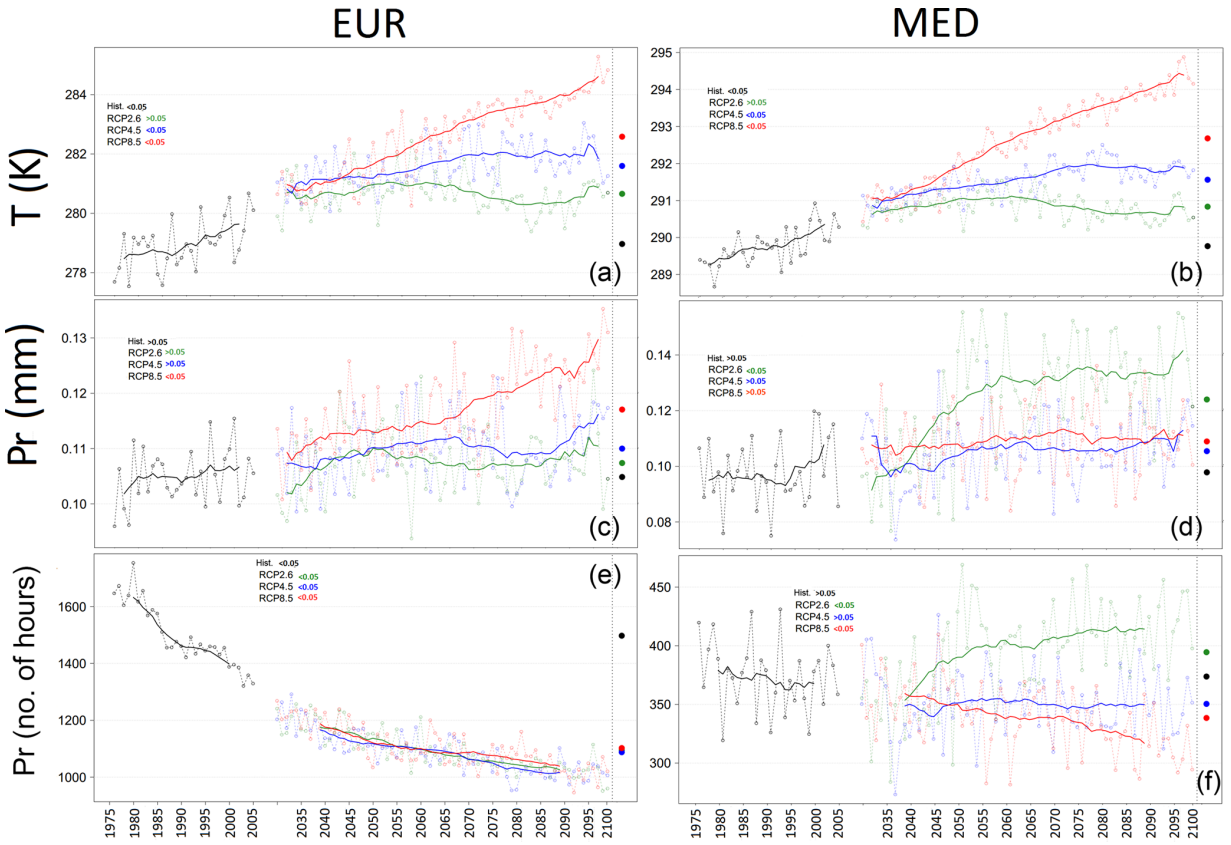


Figure 2. Time series of temperature (K; **a**, **b**), precipitation (mm; **c**, **d**) and number of rainy hours (**e**, **f**) for EUR (**a**, **c**, **e**) and MED (**b**, **d**, **f**) subdomains for all climate change scenarios as well as historic simulations. The average for each scenario is shown by the corresponding point on right side of the plot. The solid lines show the rolling average of 30 years for future scenarios and 20 years for historic scenarios. Numbers in the legend show the p value of the linear regression for each scenario.

boundary layer height (PBLH) in Fig. 3 for the EUR and MED areas. RH remains rather constant without a significant trend over EUR and MED, with the exception of the RCP2.6 scenario for MED which shows a significant decrease. WS mostly shows nonsignificant trends, with the exception of the RCP2.6 scenario over the MED domain. Similar results for WS changes have also been seen in other studies (Dobrynin et al., 2012; de Winter et al., 2013). Finally, PBLH increases are significant for RCP8.5 over EUR and for RCP2.6 over MED.

These meteorological parameters undergo interactions between themselves and show correlations with each other, as they are driven by circulation patterns. The values of correlations between different meteorological parameters examined in this work are shown in Supplement (Sect. S4). The main points that should be taken into account regarding cross-correlations between meteorological parameters are the positive correlations between wind speed and the PBLH, between wind speed and precipitation and also the anti-correlation between wind speed and RH. All of these correlations are above 0.6 as an absolute value.

Also it should be noted that if the GCM used to provide the boundary conditions to the regional climate model was changed, the results seen here might be different (Olesen et al., 2007; Teichmann et al., 2013; Kerkhoff et al., 2015; Lacressonnière et al., 2016).

3.2 PM_{10} concentrations

The simulated PM_{10} concentrations are shown in Fig. 4 for the EUR and MED subdomains. The differences between future (2031–2100) and historical (1976–2005) simulations are presented, with historical simulations being used as a reference. Compared with historical simulations, we observe a decrease in PM_{10} for all scenarios, for both EUR (0 ± 0.95 %, -2.57 ± 0.90 % and -4.40 ± 0.87 % for RCP2.6, RCP4.5 and RCP8.5, respectively) and MED (0.9 ± 0.09 %, -5.65 ± 0.11 % and -8.10 ± 0.12 % for RCP2.6, RCP4.5 and RCP8.5, respectively). The uncertainties shown here and in

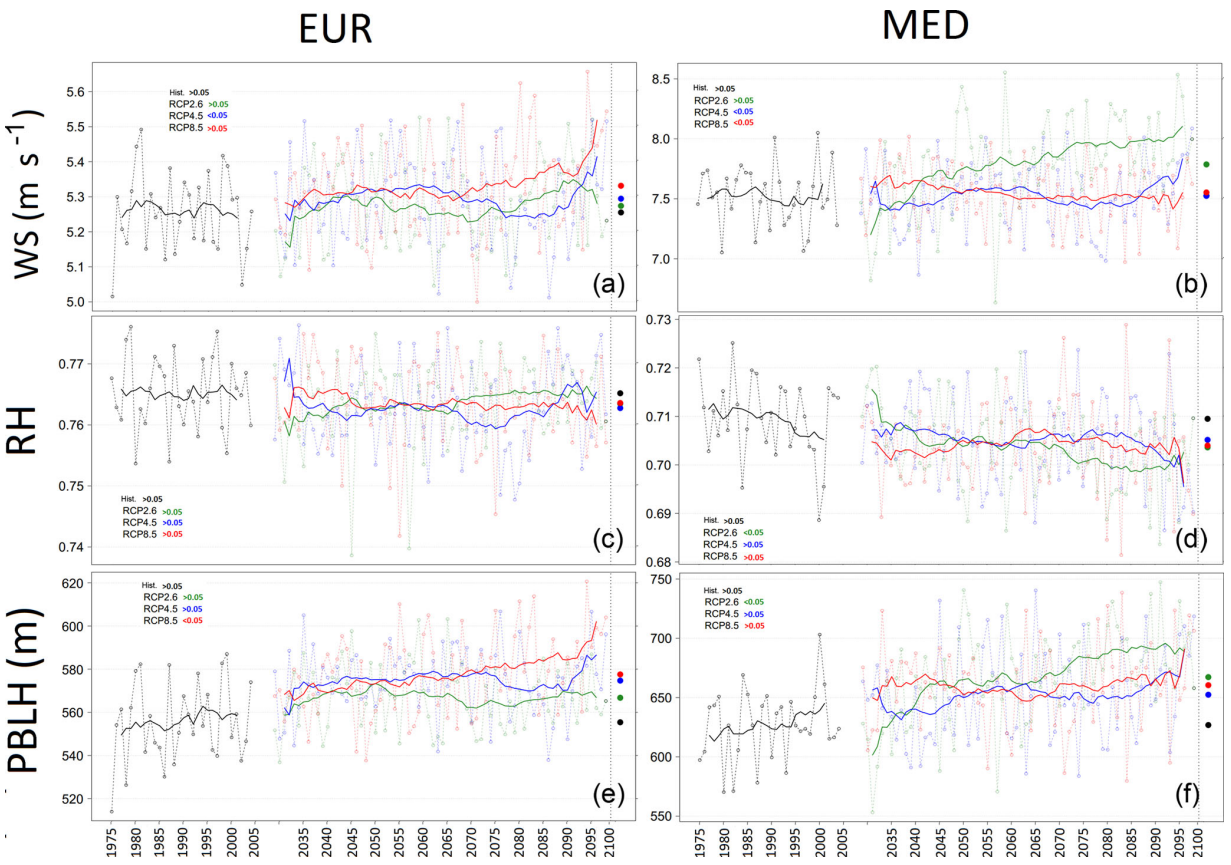


Figure 3. Time series of wind speed (WS; $m\,s^{-1}$; **a, b**), relative humidity (RH; **c, d**) and planetary boundary layer height (PBLH; in meters; **e, f**) for EUR **(a, c, d)** and MED **(b, d, f)** subdomains for all climate change scenarios as well as historic simulations. The average for each scenario is shown by the corresponding point on right side of the plot. The solid lines show the rolling average of 30 years for future scenarios and 20 years for historic scenarios. Numbers in the legend show the p value of the linear regression for each scenario.

the rest of the document refer to spatial 1-sigma intervals. The reasons for these changes in PM_{10} are discussed in the next subsection by analyzing individual PM components.

Alternatively, we also calculate linear trends for the future periods. A statistically significant positive trend is observed for RCP2.6 in the future, whereas it is significantly negative for RCP8.5, and nonsignificant for RCP4.5 (p values are given in Fig. 4 for linear trend lines).

Evidently, PM_{10} has a seasonal variation which is shown in Fig. 5; box plots of PM_{10} for all four seasons and all four subdomains are shown in Fig. 6 (Fig. S5 for $PM_{2.5}$). Interestingly, for EUR, the general PM_{10} decrease noted above for the Hist, RCP2.6, RCP4.5 and RCP8.5 scenarios is reversed in the summer period. We see that elevated concentrations of PM_{10} are simulated over the Mediterranean area for all seasons, reaching their maximum in spring (Fig. 6). Another interesting result in Fig. 5 is the increasing concentrations of PM_{10} over eastern Europe in summer, and over the Scandinavian and eastern European regions both in summer and winter, in RCP4.5 and RCP8.5. This increase for the summer period is due to BVOC emission increases, which are discussed in Sect. 3.4.2. However, the same effect is not seen in RCP2.6 in either of these seasons, highlighting a structural difference between RCP2.6 and the other two scenarios. These results are discussed in the light of PM_{10} components and meteorological parameter covariance in Sect. 3.4. A more general explanation for these structural differences can be found in the nature of the three scenarios, caused by the previously mentioned discriminated changes in meteorological parameters (Sect. 3.1).

3.3 Distribution of chemical PM_{10} components

Figure 7 shows the PM_{10} concentrations and concentration changes for all of different scenarios and subdomains, as well as the contributions of all of the different PM_{10} components (Fig. S6 for $PM_{2.5}$). For each PM component, the relative differences between future scenarios and historical simulations are also reported. Major differences can be seen

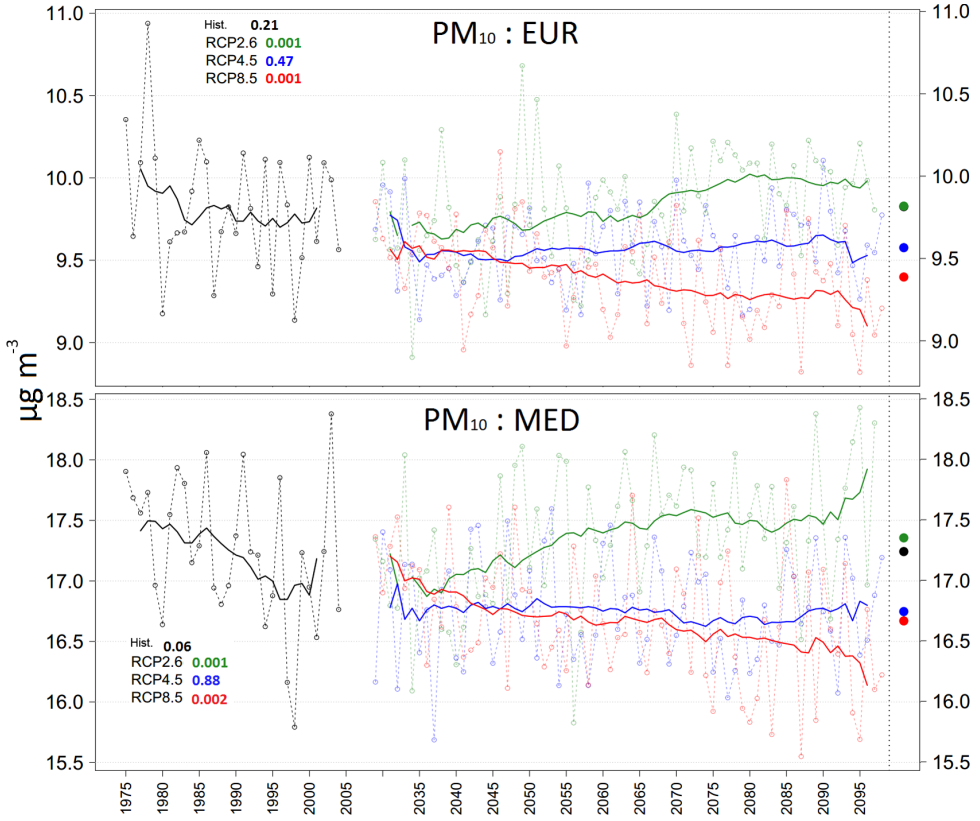


Figure 4. PM_{10} time series for the EUR and MED subdomains for all climate change scenarios and historic simulations. The average for each scenario is shown by the corresponding point on right side of the plot. The solid lines show the rolling average of 30 years for future scenarios and 20 years for historic scenarios. Numbers in the legend indicate the p value of the linear regression for each scenario.

in the distribution of the different PM components: for PM_{10} the major contributors are salt and dust particles in our domains of interest, whereas their contribution to $PM_{2.5}$ is lower. Consequently, secondary inorganics (SO_4^{2-}, NO_3^- and NH_4^+) and carbonaceous aerosol (black carbon, primary organic aerosol, biogenic secondary organic aerosol) are the major contributors to $PM_{2.5}$ (Fig. S6).

Another interesting point from this study is that primary aerosol species such as primary organic aerosols (POA), anthropogenic secondary organic aerosols (ASOA), PPM and black carbon (BC) only change slightly under a future climate (when emissions are kept constant), over both Europe and the Mediterranean Basin (a maximum of $\pm 5\,\%$ change for most of them). It should be noted here that this article deals with annual averages and not extreme events; regional climate changes can have strong effects on primary pollutant peaks as is shown in Vautard et al. (2018). The evolution of these species is again discussed in Sect. 4.2 with respect to anthropogenic emission changes.

The most important changes in the future scenario outputs (with respect to historic simulations) are found to be a decrease in nitrates (for EUR $-11.2 \pm 0.8\,\%$, $-21.4 \pm 0.7\,\%$ and $-28.8 \pm 0.8\,\%$ for RCP2.6, RCP4.5 and RCP8.5, respectively) and an increase in the organic aerosol concentration (for EUR $+15.1 \pm 1.2\,\%$, $+22.7 \pm 1.3\,\%$ and $+34.9 \pm 1.3\,\%$ for RCP2.6, RCP4.5 and RCP8.5, respectively). A slight increase in sea-salt particles (for EUR $+0.8 \pm 0.05\,\%$, $+1.4 \pm 0.06\,\%$ and $+0.2 \pm 0.06\,\%$ for RCP2.6, RCP4.5 and RCP8.5, respectively) and in sulfates (for EUR $+4.50 \pm 0.62\,\%$, $+3.0 \pm 0.6\,\%$ and $+1.6 \pm 0.6\,\%$ for RCP2.6, RCP4.5 and RCP8.5, respectively) is also found. An interesting result regarding sulfates is that the concentration of this species displays an increase in all scenarios compared with historical simulations, although the scenario order for this increase is the inverse of that for the temperature increase (i.e., RCP2.6 > RCP4.5 > RCP8.5). This phenomena is discussed later in this section. While a decrease in dust particles is observed for RCP4.5 and RCP8.5 (for EUR $-5.6 \pm 2.4\,\%$ and $-5.3 \pm 2.2\,\%$, respectively), these particles remain almost constant in RCP2.6. A decrease is seen for the ammonium particles in all scenarios (for EUR $-2.1 \pm 0.2\,\%$, $-6.4 \pm 0.2\,\%$ and $-10.6 \pm 0.2\,\%$ for RCP2.6, RCP4.5 and

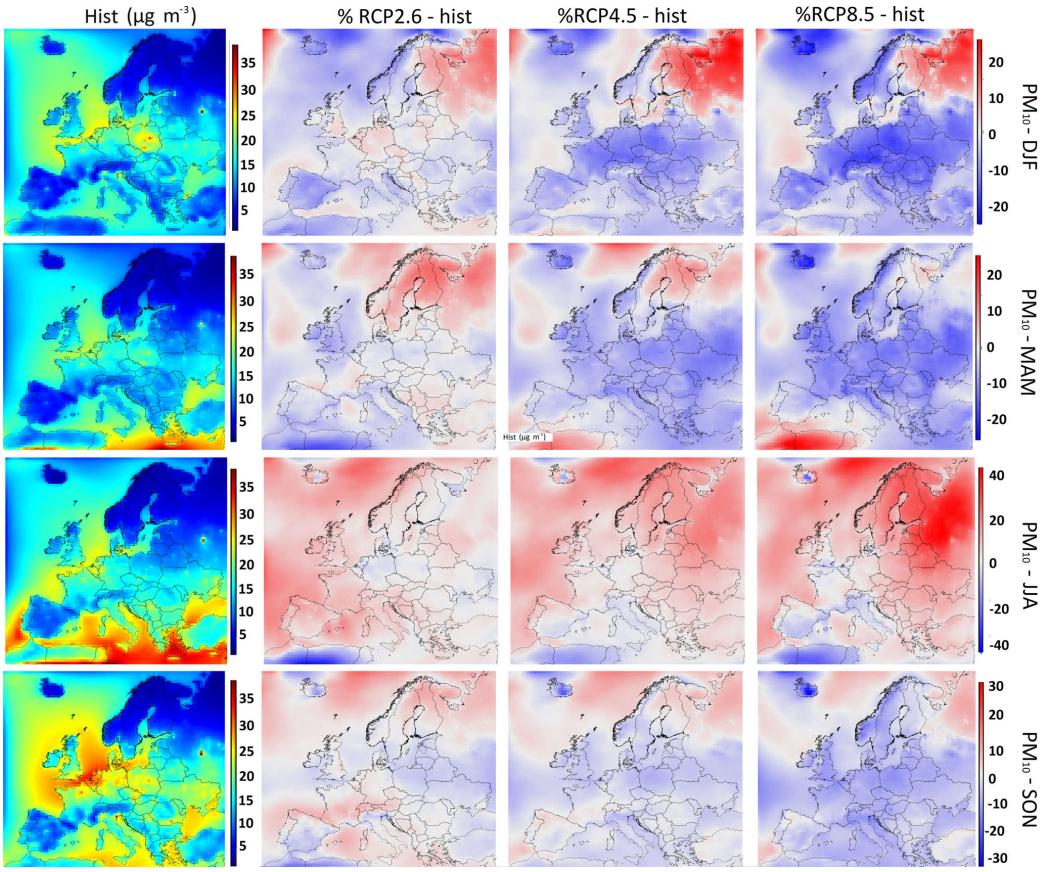


Figure 5. PM_{10} seasonal average concentrations in the historical simulation (first column). Relative differences between the climate simulations (RCP2.6, RCP4.5 and RCP8.5) and the historical simulation (Hist) (second, third and fourth columns, respectively). Rows represents the different seasons (winter, spring, summer and fall, from top to the bottom). Please note that the scale used differs between seasons for the sake of readability.

RCP8.5, respectively). However, the main driving force for the decrease in the concentration of total PM_{10} (seen in Fig. 4) for the RCP4.5 and RCP8.5 scenarios is the decrease of nitrates. The increase in the concentration of other species, especially BSOA, is compensated for by the decrease in nitrate concentrations in the case of the two abovementioned scenarios with a seasonal dependence. As for RCP2.6, as the decrease in nitrates is generally lowest among all future scenarios, the slight increase in BSOA, sulfates, dust and salt particles drives the increase in the PM_{10} concentrations (Fig. 7).

In the Mediterranean area, however, the predictions appears to be quite different: in general, the aerosol burden over the Mediterranean area (MED) is higher than that over the European area (average of 9.8, 9.5 and 9.4 $\mu g\,m^{-3}$ for EUR compared with 17.4, 16.7 and 16.6 $\mu g\,m^{-3}$ for MED for RCP2.6, RCP4.5 and RCP8.5, respectively, Fig. 7). This is mainly due to sea salt (approximately 9 $\mu g\,m^{-3}$ in all scenarios) and dust (nearly 4 $\mu g\,m^{-3}$ in all scenarios). Note that the MED region, by definition, only contains grid cells over sea, which explains the large sea-salt contribution. Conversely, for this area, the concentrations of aerosols that depend on continental emissions are considerably lower (−25 %, −33 % and −32 % for BC, POAs and ammonium, respectively, in MED compared with EUR for the RCP4.5 scenario for PM_{10}). Nitrates also show a significantly lower concentration in this region (from 1.03 $\mu g\,m^{-3}$ for EUR to 0.21 $\mu g\,m^{-3}$, 0.39 $\mu g\,m^{-3}$ and 0.25 $\mu g\,m^{-3}$ for RCP4.5 in PM_{10} for MED, MEDW and MEDE, respectively). Sulfur emissions from maritime shipping lead to high sulfate concentrations over the Mediterranean area, especially over the eastern Mediterranean (2.5 $\mu g\,m^{-3}$ in MEDE compared with 1.99 $\mu g\,m^{-3}$ in EUR for the RCP4.5 scenario for PM_{10}). Finally, it is worth noting that the BSOA fraction is lower over the Mediterranean (−36 %, −31 % and −23 % of BSOA compared with EUR in MED, MEDW and MEDE, respectively). The relative changes in the Mediterranean domain compared with historic simulations are close to those for the

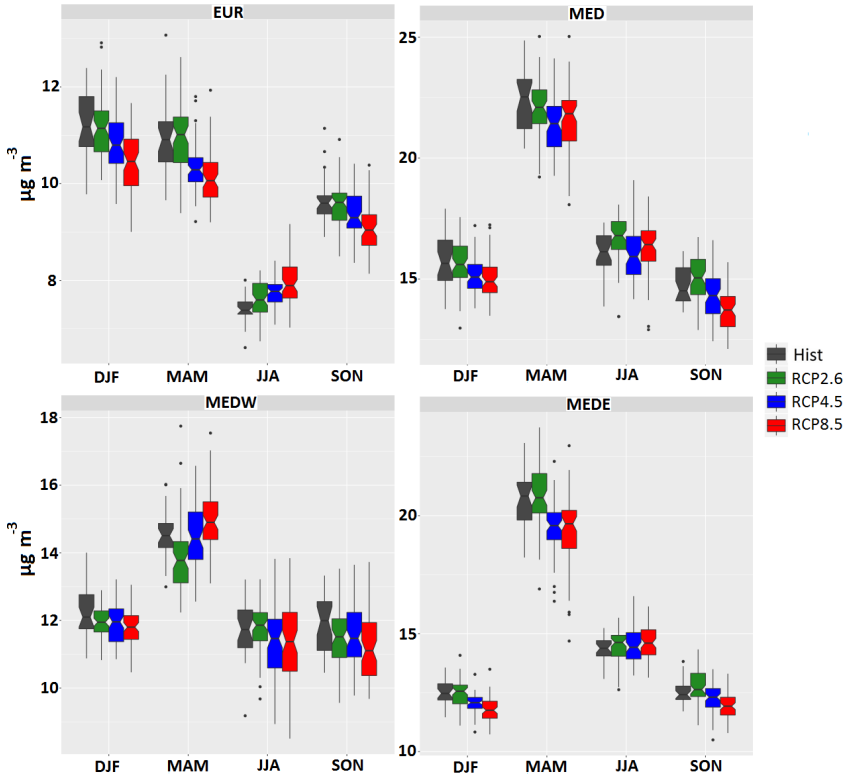


Figure 6. Seasonal box plots for all scenarios for all seasons for PM_{10} (historic simulations are black, RCP2.6 is green, RCP4.5 is blue and RCP8.5 is red) for the different subdomains. Scales are different for different subdomains.

European subdomain for most species, although they show different intensities for most components. An interesting behavior is seen for BSOA, where the increase in the concentration of this component becomes more homogenous between the three future climatic scenarios in the Mediterranean Basin with respect to continental Europe. The reason for this behavior is the origin of BSOA from advection over the Mediterranean subdomain. Also, sulfates, while showing the same general behavior as in the European subdomain, show lower changes between future and historic simulations over the Mediterranean Basin, resulting in a decrease in concentration in the RCP8.5 scenario.

3.4 Dependence of PM_{10} components on meteorological parameters

In order to explain the evolution of PM components under future climate scenarios, they are correlated here with different meteorological parameters. The parameters tested here are temperature, wind speed, precipitation, RH, PBLH and shortwave radiation. Because of the variations in the seasonality of the different PM components, the analysis of their dependencies on meteorological parameters must be conducted for each season separately. Figure 8 shows the seasonal changes for nitrates, sulfates, BSOA and dust particles for all subdomains. The 2-D concentration fields for nitrates, BSOA, sulfates and dust particles are shown in Fig. 9 for the season when each component shows its highest concentration (Fig. 8). The correlations for all seasons and for the five selected meteorological parameters with PM_{10} components are shown in Figs. 10 and 11 for the EUR and MED subdomains for different years. This comprises 30 pairs of values for the historic period and 70 for the future period. Here, a Pearson correlation coefficient of greater than 0.6 is considered to represent a significant relationship. Correlations between the different meteorological parameters are shown in Figs. S7 and S8. Figure S9 shows the 2-D correlations for the same species as Fig. 8, with the parameter that correlates best with them for selected seasons when their concentration is highest (i.e., nitrates, BSOA, sulfates and dust with temperature, temperature, RH and PBLH for winter, summer, summer and spring, respectively).

3.4.1 Inorganic PM components

Particulate nitrate concentrations appear to be strongly anticorrelated with temperature (Fig. 10). Hence, in most regions, they show a decrease in the future scenarios, mainly

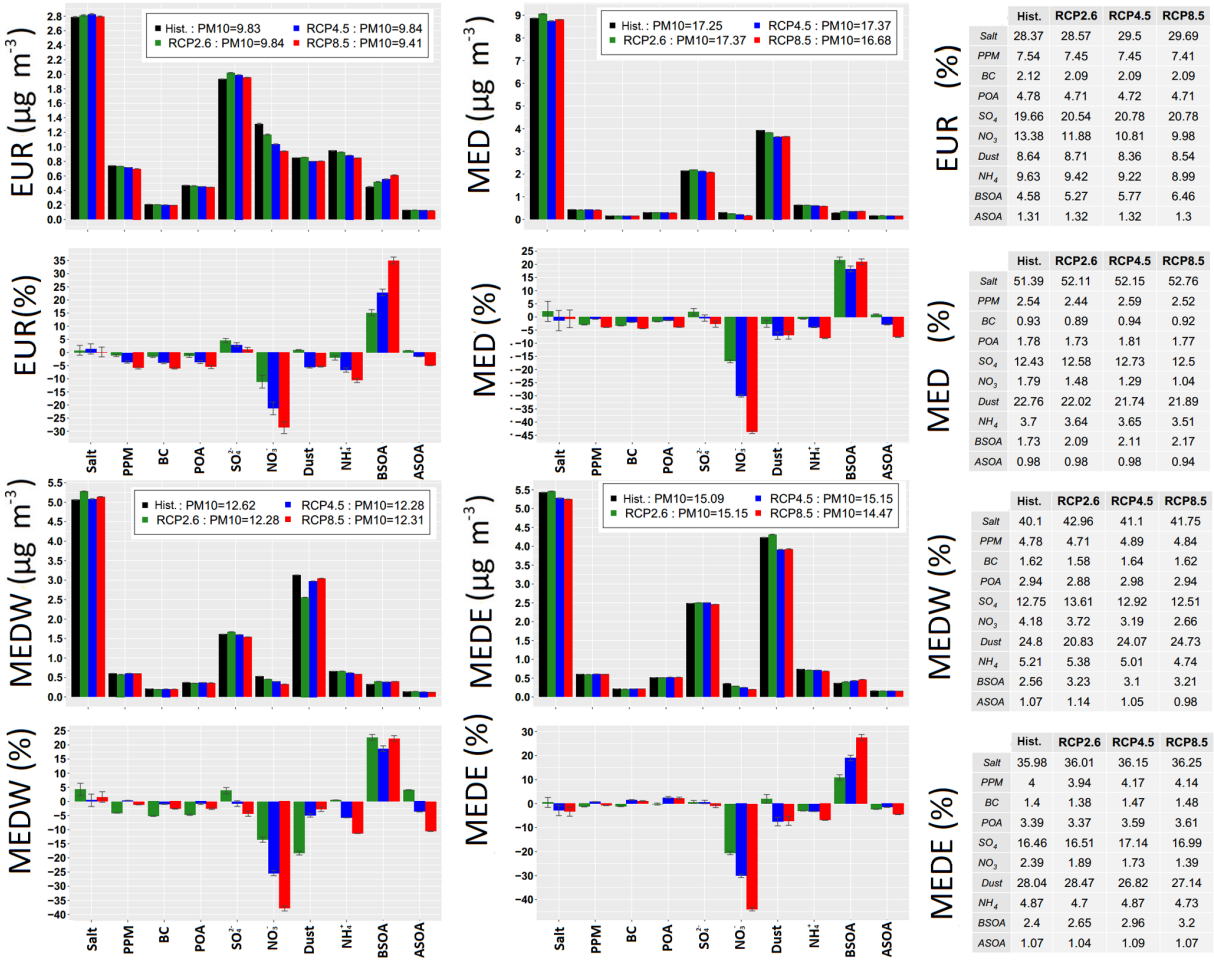


Figure 7. Concentrations and relative changes of PM_{10} components (same color code as in Fig. 6) for all subdomains averaged over the whole period of simulations in climate change scenarios and for the different subdomains. Error bars show the confidence interval calculated for the annual averages for each subdomain. The changes show (future − historic)/historic · 100. Tables report the percentage of each component in each scenario. The concentration of PM_{10} in total is noted in the legend above each figure.

due to the higher temperature predicted in those scenarios, which might lead to a shift in the nitrate gas–aerosol partitioning towards the gaseous phase and more volatilization of already formed nitrate aerosols. Especially during the winter season, anti-correlations are seen with wind speed, precipitation, and PBLH, whereas a correlation is found with surface radiation. This fits with a switch from anticyclonic conditions – characterized by cold continental weather, clear skies and high solar radiation, large vertical stability and a low PBLH – to marine conditions. Continental conditions during this season indeed favor enhanced nitrate concentrations, whereas marine conditions are related to lower concentrations.

The correlation coefficient between nitrates and temperature is the lowest in summer. If we remain in our synoptic-scale framework, hot summer days favor pollution build up and accumulation, but decrease the partitioning in favor of the particle phase, so these effects compensate for each other. In spring, RH shows a high correlation with nitrate alongside temperature as higher RH favors nitrate partitioning into the particulate phase, in particular if it exceeds the deliquescence point of ammonium nitrate (RH > 50 %). These hypotheses are supported by the correlations presented in Sect. S4, which show the correlations between the different meteorological parameters. For the MED region, a strong anti-correlation is still observed, especially for winter and spring. However, the (anti)correlations with other meteorological parameters are less pronounced and not necessarily in the same direction as for EUR, as the distinction between continental and maritime conditions is not valid for this region. Overall, the analysis suggests that the major point to be taken into account

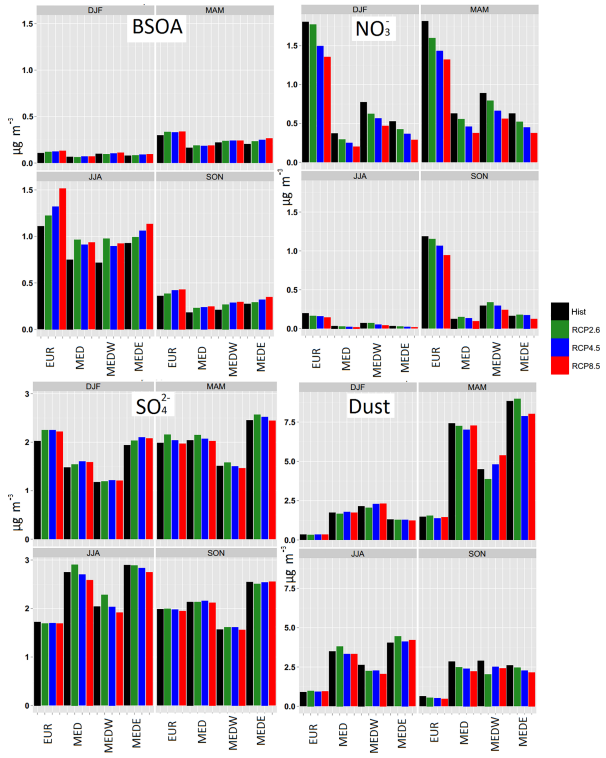


Figure 8. Seasonal absolute concentrations of BSOA, nitrate (NO_3), sulfate (SO_4^{-2}) and dust particles (same color code as in Fig. 5) for the different subdomains. Each panel shows one of the species mentioned above for four scenarios and each subpanel shows one season.

for particle nitrates is their high anti-correlation with temperature (seen in Fig. 10). This confirms the results reported by Dawson et al. (2007), Jiménez-Guerrero et al. (2012) and Megaritis et al. (2014), who conducted sensitivity studies on individual meteorological parameters.

Sulfates are the second most abundant species in Europe after sea salt, and the third most important species after sea salt and dust over the Mediterranean. They show an increase in all of the future scenarios compared with historical simulations, but in the inverse order of the degree of severity projected for temperature increase, i.e., the increase is strongest for RCP2.6 (5 %) and less pronounced for RCP8.5 (1.2 %) as seen in Fig. 7. The spatial distribution of this species varies quite strongly between the RCP2.6 scenario and the RCP4.5 and RCP8.5 scenarios (Fig. 9). For instance, in RCP2.6, sulfate increases with respect to historic in the southwest part of the domain, whereas it decreases for the same area in RCP4.5 and RCP8.5. The 2-D correlation maps of sulfates with RH show a strong correlation between these two parameters, especially for the Mediterranean and the Atlantic, but also for the EUR subdomain in winter and spring periods (Fig. S9). The positive relationship between sulfates and RH could be related to two different processes. First, during the winter season, the major pathway of SO_4^{2-} formation from SO_2 proceeds via aqueous chemistry, and large-scale RH values are a tracer of sub-grid-scale cloud formation (Seinfeld and Pandis, 2016). On the contrary, during summer, over the MED region, gas-phase SO_4^{2-} formation via SO_2 oxidation by OH is dominant, and increased future RH levels, along with increasing temperatures, may lead to increased OH levels (Hedegaard et al., 2008). However for summer and fall, the PBLH shows a higher correlation with sulfate, which is shown in Fig. 10. Another parameter that shows a strong anti-correlation with sulfate concentrations is the wind speed in the spring and winter periods, which can be explained by the correlation between the PBLH and wind speed (Fig. 10).

Ammonium concentrations show a steady decrease in all future scenarios and in all subdomains. The correlations of NH_4^+ with meteorological variables appear to be a combination of those simulated for SO_4^{2-} and NO_3^- with which NH_4^+ forms inorganic aerosol. When looking at correlations, a relationship is seen for ammonium with RH and wind speed, as well as a strong correlation with the PBLH (Fig. 11).

3.4.2 Biogenic SOA

BSOA concentrations show a steady increase in future scenarios for the European subdomain (Figs. 8 and 9). While the increase is seen in all subdomains, the intensity and the scenario dependence are not the same. The formation of the biogenic organic aerosol fraction greatly depends on its precursors (isoprene and monoterpenes), for which emissions increase globally with temperature. In EUR, isoprene emissions increase by 20.3 %, 31.1 % and 52.5 %, and monoterpenes emissions increase by 15.7 %, 24.0 % and 38.1 % for RCP2.6, RCP4.5 and RCP8.5 , respectively. There are many studies that have investigated the changes in BVOC emissions in the future; however, not many of them have only taken the climate effects into account. For example, Lathière et al. (2005) used the full version of MEGAN (which includes CO_2 inhibition and the dependence of isoprene emissions on ozone concentrations) to calculate a 27 % and 51 % increase in isoprene and monoterpenes, respectively, in 2100 compared with the 1990s using a scenario that is close to RCP4.5. Compared with our study, these values are quite similar for isoprene but more than double what we found for monoterpenes. Pacifico et al. (2012) calculated a 69 % increase in isoprene using a RCP8.5 scenario in 2100 compared with the 2000s, Hantson et al. (2017) found a 41 % / 25 % ratio in 2100 compared with 2000 for isoprene/monoterpenes, respectively, using RCP4.5. Langner et al. (2012) explored four different models for the European region (DEHM, EMEP, SILAM and MATCH) finding a 21 %–26 % isoprene increase; the increase in isoprene emissions in our simulations for the same period amounts to 21 %. Therefore, our simulations are consistent with the abovementioned results. In general, isoprene and monoterpene emis-

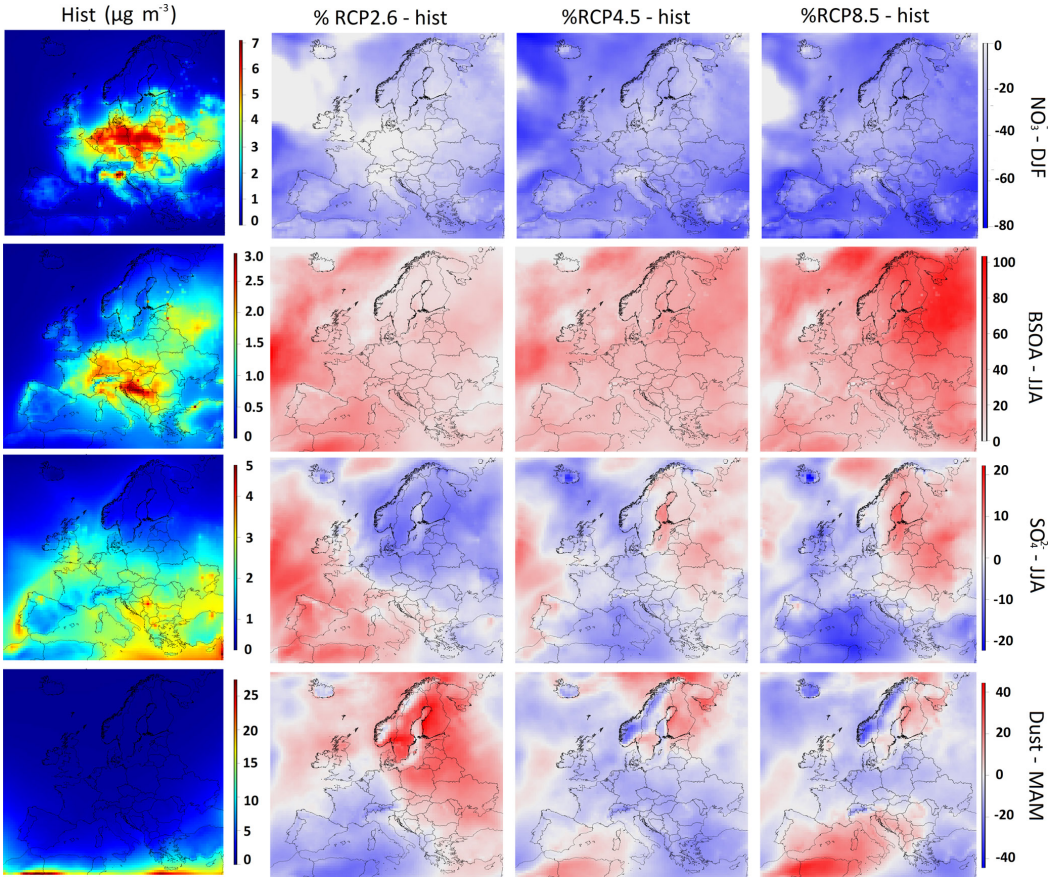


Figure 9. Historic concentrations and relative changes in future scenarios for biogenic SOA (BSOA), nitrates (NO_3^-), sulfate (SO_4^{2-}) and dust particles for selected seasons in which the concentrations were the highest. Figures in the left column show the average concentration of historic simulations, the other three columns show the relative difference of RCP2.6, RCP4.5 and RCP8.5 future scenarios, respectively, to the historic simulations. Each row shows one season, and the scales are different for each row of simulations.

sions show high sensitivity to temperature, CO_2 inhibition (Arneth et al., 2007; Young et al., 2009; Tai et al., 2013) and land use changes, which makes their estimation for future scenarios highly uncertain.

This increase in precursors results in an increase in the concentration of BSOA (for EUR 15.1 %, 22.7 % and 34.9 % for RCP2.6, RCP4.5 and RCP8.5, respectively), with a similar effect having been predicted in other studies (Heald et al., 2008; Megaritis et al., 2014). This increase in BSOA also reflects the summer increase in the PM_{10} mentioned in Sect. 3.2. However, higher temperatures induce higher evaporation for semivolatile organic compounds, and, therefore, lower formation of organic aerosols is to be expected. This fact has been shown in Dawson et al. (2007), where without changing biogenic emissions, the temperature was increased by 5 °C and a decrease of almost 20 % was seen for the SOA concentration over the eastern US. In our simulations, the increase in biogenic precursors resulting due to the formation of BSOA trumps the evaporation effect due to higher temperature, and an increase in biogenic SOA is seen. Figure 10 shows the correlation coefficient of BSOA with temperature for the EUR and MED subdomains (see Fig. S9 for spatial correlations). For the EUR subdomain, statistically significant regressions are seen for all scenarios during summer for temperature and also for shortwave radiation. For the Mediterranean subdomains, no monoterpenes or isoprene are emitted from the sea surface; therefore, the concentration of BSOA in the Mediterranean area is the result of transport from the continental area. This results in low correlations between temperature and BSOA for the Mediterranean subdomains, whereas a high correlation is found between wind speed, RH and PBLH. The correlation of the BSOA concentration with wind speed in the Mediterranean corresponds to the point raised above regarding the advective nature of BSOA concentrations in this subdomain, whereas the high correlations of PBLH and RH with BSOA come from the

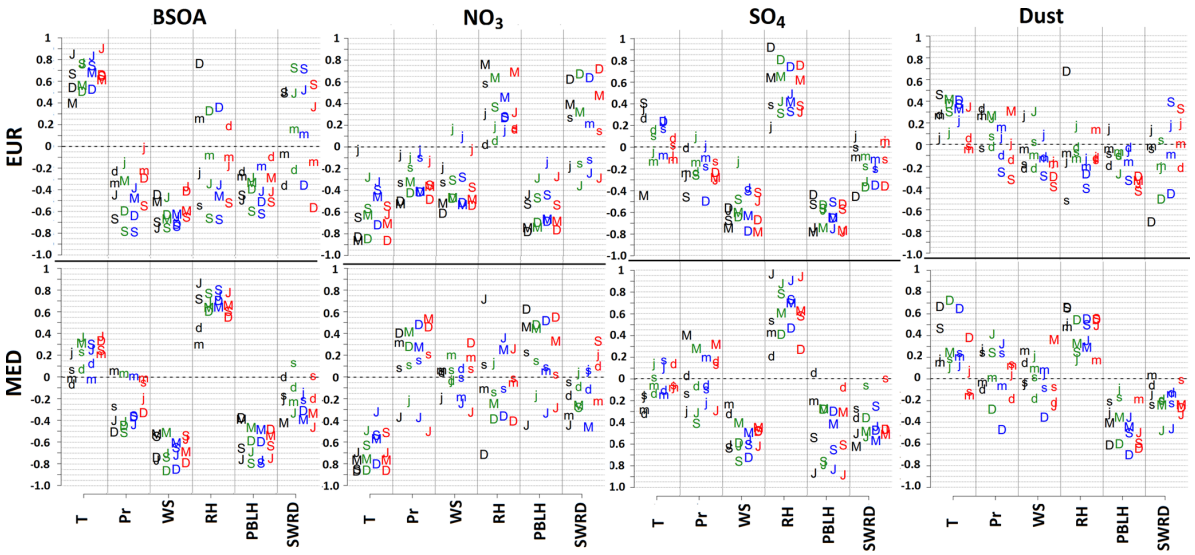


Figure 10. Correlation coefficient between all meteorological parameters tested and BSOA, (NO_3), sulfate (SO_4^{-2}) and dust particles for all seasons and the EUR and MED subdomains. D, M, J and S represent winter, spring, summer and fall, respectively (first letter of the first month of each season). Uppercase letters mean that the correlation between the two parameters is statistically significant, whereas lowercase letters show the contrary. Color coding for different scenarios is the same as in previous figures.

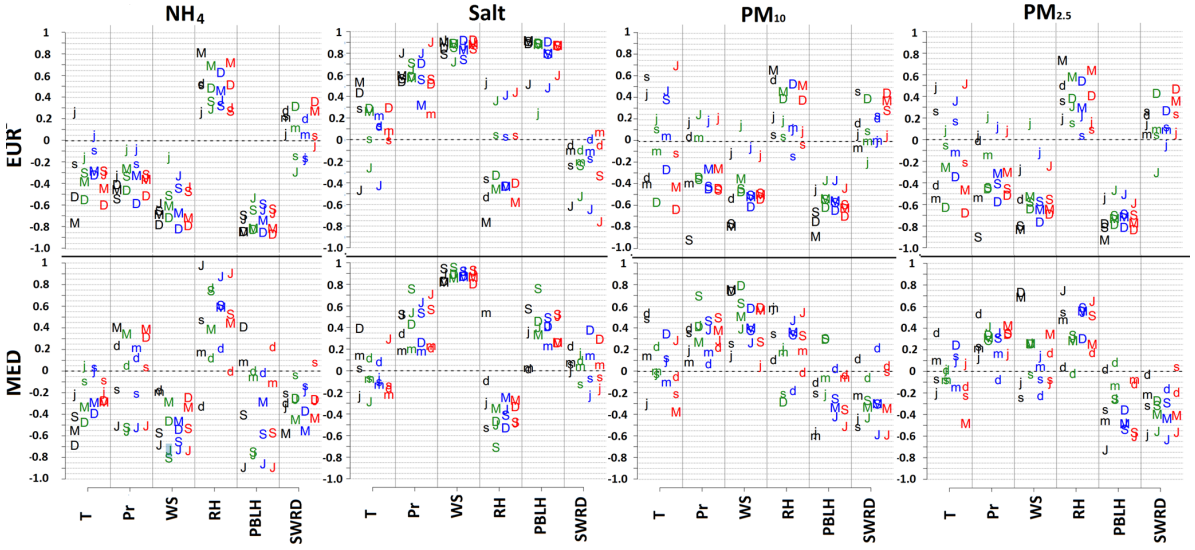


Figure 11. Correlation coefficient between all meteorological parameters tested and ammonium (NH_4^+), salt, PM_{10} and $PM_{2.5}$ particles for all seasons and the EUR and MED subdomains. D, M, J and S represent winter, spring, summer and fall, respectively (first letter of the first month of each season). Uppercase letters mean that the correlation between the two parameters is statistically significant, whereas lowercase letters show the contrary. Color coding for different scenarios is the same as in previous figures. SWRD represents shortwave radiation.

correlation of wind speed with these two parameters. Another notable fact is the percentage of the concentration of BSOA that is formed from isoprene and monoterpenes; year-long sensitivity tests (with the reduction of respective terpene and isoprene emissions by 10 % in two separate 1-year-long simulations) for the year 1998 with historic climate show a distribution of 21 % and 79 % annually and 39 % and 61 % for the summer period for the concentration of BSOA forming from isoprene and monoterpenes, respectively. The isoprene to monoterpene emission ratio was 2.9 annually and

6.1 for the summer. Similar results were reported in Aksoyoglu et al. (2017).

3.4.3 Dust and salt particles

Dust concentrations are predicted to be at their maximum during spring (Fig. 9). This phenomena is also described in the literature for different regions (Werner et al., 2002, and Ginoux et al., 2004 explored global simulations; Laurent et al., 2005, focused on China and Mongolia; and Vincent et al., 2016, studied the western Mediterranean). In our simulations, the spatial maximum in dust particle concentrations normally occurs in the eastern Mediterranean (Figs. 8, 9, 10). While a decrease is observed for RCP4.5 and RCP8.5 (Fig. 7, for EUR $-5.6\,\%$ and $-5.3\,\%$, respectively), these particles do not exhibit any sensible variations in RCP2.6. As dust emissions are not taken into account within the simulated domain in our simulations and boundary conditions are the same in these scenarios, changes in the advection of dust aerosols is responsible for these variations. Therefore only advection plays a role, and cannot be captured by a local correlation analysis by definition.

The reason for the increase in dust particles in RCP2.6 scenarios for MEDE could be the different behavior that is seen in meteorological parameters for this subdomain compared with the others. The temperature decreases in this scenario after the 2040s in contrast with the other two scenarios, and therefore induces changes in RH that are different from the other scenarios. The average RH in RCP2.6 remains higher than the other scenarios, although it is lower than historic simulations for MEDE (Fig. S9). Until this point, we mostly have discussed climate change related modifications in PM sources, some sinks and transport. However, we should also take the effect of climate related changes effecting wet deposition into account. For RCP4.5 and RCP8.5, the amount of precipitation remains rather constant over the MEDW, whereas it increases in RCP2.6 (Fig. S3). The precipitation duration decreases for RCP4.5 and RCP8.5 over this subdomain, whereas it stays quite constant for RCP2.6 for MEDW. Thus, both the amount of precipitation and the precipitation duration are stronger in RCP2.6 than in RCP4.5 or RCP8.5. This could, in addition to different advection patterns, explain the lower MEDW dust concentrations in RCP2.6. However, for MEDE, the amount of precipitation increases as the number of rainy hours decreases; this infers strong but infrequent rain episodes, which would explain the increase in the dust concentration in this subdomain. The impact of changing precipitation frequency/amount is the dominant factor in our simulations when it comes to dust concentration changes, as changes in precipitation patterns result in changes in the amount of wet deposition.

Salt particles show a high concentration in the Mediterranean area and also over the Atlantic Ocean; they are the most important PM species for the EUR and MED subdomains. Sea-salt emissions are very sensitive to wind speed, leading to a correlation between salt concentrations and wind speed (Fig. 11). Therefore, small changes in the salt concentration in future scenarios compared with historic simulations are mostly due to small wind speed changes in future climate.

3.4.4 Total PM_{10} and $PM_{2.5}$ dependencies on meteorological components

Investigating the correlation between PM_{10} and $PM_{2.5}$ and different meteorological parameters, reveals high spatial and temporal variability. For the EUR subdomain, for both PM_{10} and $PM_{2.5}$ the PBLH parameter shows the highest correlation (anti-correlation). For the Mediterranean region, among all of the meteorological parameters investigated, PM_{10} seems to be more affected by wind speed, whereas $PM_{2.5}$ seems to be more affected by more by RH. The analysis of the link between total PM_{10} and total $PM_{2.5}$ with meteorological parameters (Fig. 11) is far less conclusive compared with the individual component analysis. As a generalized conclusion, PM_{10} and $PM_{2.5}$ tend to follow the correlations of their largest contributor.

Finally, precipitation has been pointed out as a crucial, but difficult to model/predict parameter in both current and future meteorological/climatic simulations (Dale et al., 2001). In our study, the correlations of PM or PM components with the amount of annual precipitation are generally weak (and positive correlations are sometimes even seen instead of the expected anti-correlations). It has also been discussed, that total annual precipitation duration could be more impactful on the PM than the total amount of precipitation (Dale et al., 2001). No correlation study was performed with this parameter in this work, but the decreasing total precipitation duration in all scenarios could induce some increase in PM and its components.

4 Impacts of boundary condition and anthropogenic emissions

While climate on its own can have important impacts on the future concentrations of different species, other drivers might have their specific effects on PM concentrations, which can either amplify or compensate for the climate-related effects. This section explores the impacts of two other drivers: boundary conditions and anthropogenic emissions. Five sets of simulations were used to achieve this goal, one where boundary conditions were changed together with climate inputs, and two where anthropogenic emissions were changed alongside climate inputs; these simulations were compared with historic simulations as well as climate simulations with constant boundary conditions and anthropogenic emissions. It should be noted that boundary conditions are taken from a global chemistry transport model; therefore, changing the boundary conditions corresponds to changing the global climate and the global anthropogenic emissions at the same

time. However, comparison between the regional climate change and the BC impact are strong enough for all compounds (see below) to conclude on a major driver, very probably beyond uncertainty. Finally, in an effort to provide a more comprehensive view of what the accumulative effects of all drivers would be, the aforementioned simulations are compared with a series of simulations where all drivers change at the same time. Keep in mind that the series of simulations where all drivers change at the same time show not only the accumulative impacts of all drivers, but also the nonlinear relationships that exist between different drivers. In these simulations, RCP4.5 related climate and boundary conditions are compared with the historic ones, 2050 regional current legislations emissions (CLE) and maximum feasible reductions (MRF) are compared against 2010 emissions. In total, in this section, six series of simulations are presented (the numbers in parenthesis refer to Table 1): historic simulation (simulation 1), climate impact simulation (simulation 3), boundary condition impact (simulation 5), emission impact (simulations 6–7) and accumulative impacts (simulation 8). For each series, 10-year-long simulations are used, between 2046 and 2055 for future scenarios and between 1996 and 2005 for historic simulations. In this way, the effect of boundary conditions, emissions and climate are calculated separately and compared with the overall changes in simulation 8. In Fig. 12 the impact of each driver is shown separately in terms of relative change (Sect. S8 for seasonal changes).

4.1 Boundary conditions

Among PM_{10} components, dust, nitrate, BSOA, POA and sulfates show the highest impact on future PM concentrations when boundary conditions change, with other species showing only minor changes or no change at all (Fig. 12). Among these species, dust particles show the strongest dependence on boundary conditions: an increase of $+77 \pm 2\,\%$, $+30 \pm 10.7\,\%$, $+9 \pm 1.9\,\%$ and $+51 \pm 15.2\,\%$ for EUR, MED, MEDW and MEDE, respectively, for future RCP4.5 with respect to historic boundary conditions. Their simulated dependence on regional climate was indeed much smaller ($-9 \pm 0.3\,\%$, $-4 \pm 1.4\,\%$, $+3 \pm 0.6\,\%$ and $-4 \pm 1.8\,\%$ for EUR, MED, MEDW and MEDE, respectively, for the same period). It is important to bear in mind that the concentration of dusts in the European subdomain in our simulations is $0.8\,\mu g\,m^{-3}$ on average with an important spatial variability, with concentrations dropping significantly as we move further north (Fig. 9). Therefore, the low relative changes simulated for the Mediterranean subdomains have to be considered as a sign of the high absolute sensitivity to the scenario. The reason for the important changes in these species may be due to wind intensity and humidity in source regions or land use changes caused by climate change outside our domain. There are many uncertainties regarding the future changes of dust concentrations (Tegen et al., 2004; Woodward et al., 2005). Changes in climate drivers such as precipitation, wind speed, regional moisture balance in source areas, and land use changes, either resulting from anthropogenic changes or for climatic reasons, can have important effects on dust emissions (Harrison et al., 2001). Projection of changes in land use resulting from both sources are highly uncertain, which results in strong uncertainties in the projections of dust concentration changes in future scenarios (Tegen et al., 2004; Evan et al., 2014). Furthermore, the Mediterranean Sea is located on the southern border of the domain used in this study; therefore, it should be noted that although the results of dust concentration changes seen in this study are consistent with existing literature, the model might not be capable of consistently capturing the relationship between boundary condition changes and the southern parts of the Mediterranean due to the position of the domain. This is not the case for the European subdomain.

Nitrates and BSOA are more affected by climate change impacts than by boundary condition input changes in all subdomains ($-13 \pm 2.6\,\%$, $+14 \pm 0.5\,\%$, $-2 \pm 0.8\,\%$ and $+12 \pm 0.7\,\%$ for RCP4.5 compared with $-6 \pm 2.5\,\%$, $-26 \pm 0.5\,\%$, $-23 \pm 0.9\,\%$ and $-25 \pm 0.7\,\%$ for boundary condition changes for nitrates and $+12 \pm 1.3\,\%$, $+23 \pm 1\,\%$, $+24 \pm 1\,\%$ and $+12 \pm 1.1\,\%$ for RCP4.5 compared with $+6 \pm 1.3\,\%$, $+14 \pm 1.3\,\%$, $+7 \pm 1\,\%$ and $+14 \pm 1.4\,\%$ for BSOA for EUR, MED, MEDW and MEDE, respectively).

Contrary to the species discussed above, sulfates and POA are more sensitive to boundary conditions than to climate effects. Sulfates show a $-2 \pm 1.2\,\%$, $-7 \pm 1.6\,\%$, $-6 \pm 0.9\,\%$ and $-7 \pm 1\,\%$ decrease, whereas POA shows a $-9 \pm 0.7\,\%$, $-26 \pm 0.1\,\%$, $-11 \pm 0.1\,\%$ and $-19 \pm 0.1\,\%$ decrease related to boundary conditions for EUR, MED, MEDW and MEDE, respectively. Climate effects on these particles were smaller.

Ammonium shows a negligible change with regards to boundary conditions in EUR, and an increase in most Mediterranean subdomains ($+12 \pm 0.3\,\%$, $-1 \pm 0.1\,\%$ and $+12 \pm 0.2\,\%$ for MED, MEDW and MEDE), whereas the change in this species was mostly negative for climate impact results.

4.2 Anthropogenic emissions

Changes in anthropogenic emissions in CLE and MFR 2050 inputs are compared with CLE 2010 emissions for different species in the Supplement (Fig. S11). As expected, a decrease is seen for most species in CLE 2050 emissions, but to a higher extent in the MFR 2050 scenario. A simple comparison between CLE and MFR 2050 emission scenarios is shown in Fig. 13. Bear in mind that this figure shows the effects of climate change (RCP4.5) and emission change at the same time, as does every value presented in this paragraph. For CLE simulations, sulfates show a decrease of $-28 \pm 1.2\,\%$, $-29 \pm 1.3\,\%$, $-34 \pm 0.9\,\%$ and $-18 \pm 0.9\,\%$ for EUR, MED, MEDW and MEDE, respectively, with respect to historic simulations, whereas MFR scenarios show

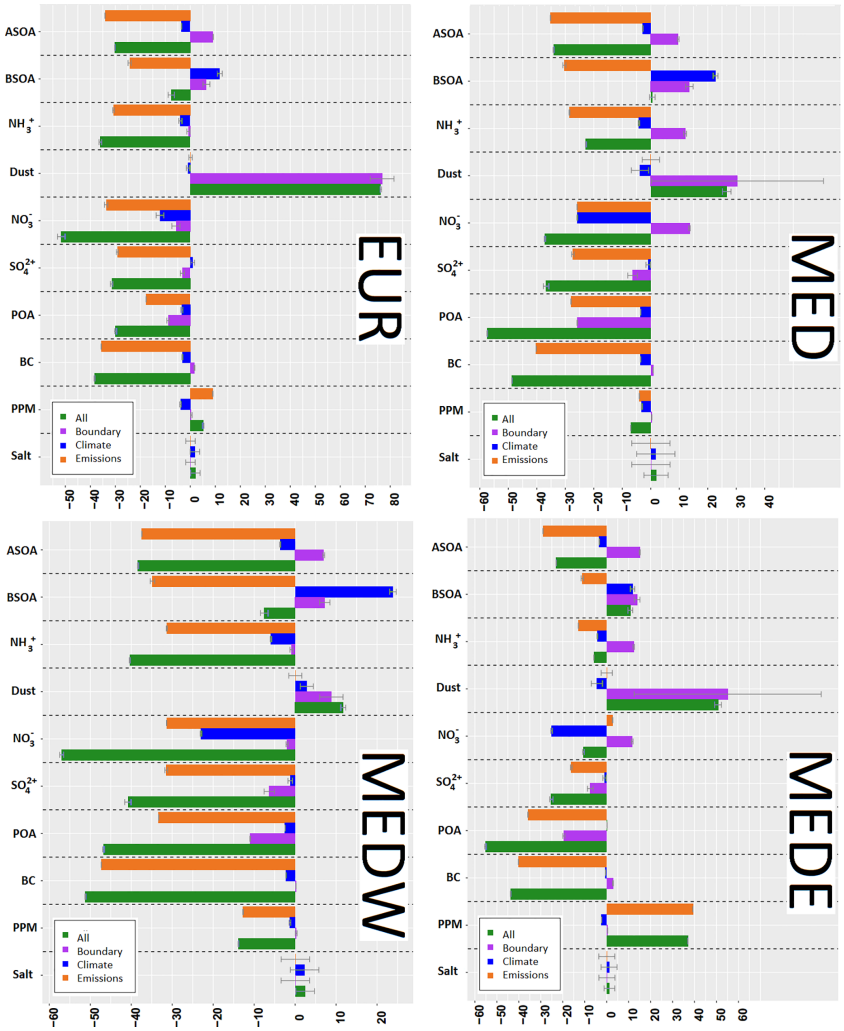


Figure 12. Relative impact of climate, boundary conditions and emission drivers on PM_{10} components for different subdomains. Error bars show the confidence interval calculated on annual averages.

a -60 ± 1 %, -51 ± 1.1 %, -55 ± 0.8 % and -52 ± 0.7 % decrease for the same order of subdomains. The reason for this decrease is the decrease in the emissions of SO_2 (SO_2 emissions reduction of -30 %, -53 %, -52 % and -42 % for CLE and -60 %, -53 %, -57 % and -68 % for MFR for the same order of subdomains). Particulate nitrates also show a strong decrease with the decrease of precursor emissions, presenting -48 ± 2.5 %, -32 ± 0.4 %, -36 ± 0.8 % and -28 ± 0.6 % for CLE and -79 ± 2.2 %, -61 ± 0.4 %, -74 ± 0.8 % and -77 ± 0.5 % for MFR for EUR, MED, MEDW and MEDE, respectively, (NO_x emission reduction of -60 %, -38 %, -48 % and -30 % for CLE and -84 %, -38 %, -76 % and -76 % for MFR for the same order of subdomains). Ammonium displays the same behavior, showing -36 ± 1 %, -55 ± 0.2 %, -56 ± 0.1 % and -18 ± 0.1 % for CLE and -68 ± 0.9 %, -87 ± 0.2 %, -87 ± 0.1 % and -64 ± 0.1 % for MFR for EUR, MED, MEDW and MEDE, respectively. Other components such as BC and POA show a strong decrease, as their concentrations depend directly on the amount of anthropogenic emissions. Interestingly, BSOA concentrations also show a strong decrease related to changes in anthropogenic emissions (contrary to the increase for climate change alone). Values of -7 ± 1.3 %, -34 ± 1.1 %, -39 ± 1.1 % and $+4 \pm 1.3$ % for CLE and -36 ± 1.1 %, -64 ± 1 %, -65 ± 0.9 % and -35 ± 1.1 % for MFR for EUR, MED, MEDW and MEDE are seen, respectively, for this species. The fact that the decrease in anthropogenic emissions overshadows the increase in BSOA when looking at climate and boundary condition effects is an important message to take away from these simulations. The exact mechanism

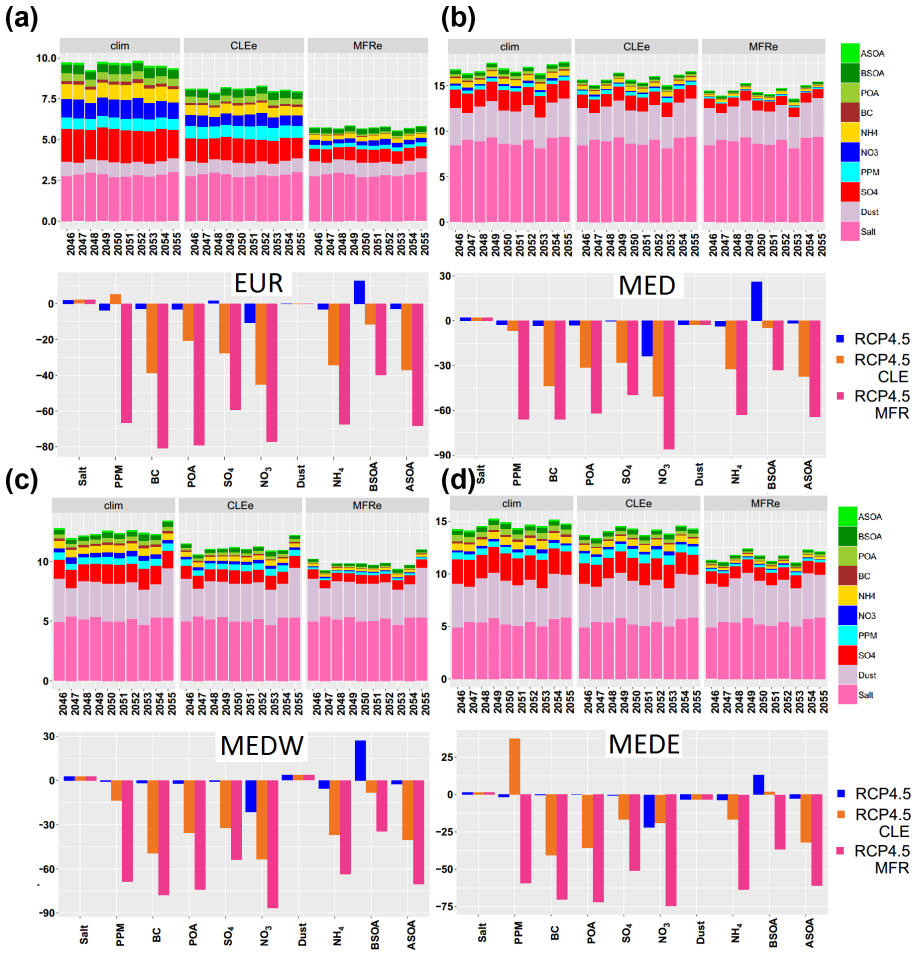


Figure 13. Emission scenario comparisons. Each panel shows one subdomain, the upper subpanels show the PM_{10} components for each scenario, the lower subpanels shows the percentage difference for each scenario ((future − historic)/historic · 100).

for this effect is not clear, although it could be due to the general decrease of seed aerosol in these scenarios modifying the gas–particle equilibrium for SVOCs formed from monoterpenes and isoprene oxidation. Changes in oxidant levels due to a decrease in anthropogenic emissions in addition to a direct decrease in anthropogenic VOCs may be other reasons for this change (i.e., less organic aerosol mass available for oxidation products to condense on).

For the comparison of driver impacts (Fig. 12), only CLE 2050 simulations for emission impact scenarios are used, as CLE 2050 emissions are used in the simulation where all drivers change (presented in Sect. 4.3). Almost all species show strong dependence on emission changes, except dust and salt particles. Quantitative effects vary for the Mediterranean subdomains: the effect of emission changes becomes less pronounced for species without maritime emission sources (such as NH_4^+), whereas they stay high for species like POA, BC and SO_4^{2-} which can be emitted by shipping lines.

4.3 Cumulative impacts

To provide a more complete view of probable atmospheric composition (under the hypotheses of the scenario) in the 2050s, the "All" scenario (Fig. 12) shows the combined effects of all drivers changing at the same time. There are many uncertainties affecting future scenarios as can be surmised; however, with regard to drivers that are explored here, this scenario shows what a more realistic future air composition might look like. As seen in Fig. 12, and with regard to total PM_{10} and PM_{10} components, the changes in emissions set the tone for the future, meaning that a reduction in anthropogenic emissions overshadows the climate and the boundary condition drivers for most of species. This highlights that mitigating air pollution with respect to air quality in the fu-

ture depends greatly on the reduction of anthropogenic emissions.

For PM_{10} for the period from 2046 to 2055 using RCP4.5, the different drivers indicate a decrease of $-15.6\,\%$, $-6.7\,\%$, $-10.5\,\%$ and $+4\,\%$ for EUR, MED, MEDW and MEDE, respectively, mainly driven by anthropogenic emissions. Due to the boundary condition changes, PM increases of $+5.3\,\%$, $+6.8\,\%$, $+1.2\,\%$ and $+15.1\,\%$ for EUR, MED, MEDW and MEDE, respectively, are observed, mainly because of the dust concentration increase. The climate impacts on PM_{10} concentrations for the same period are $-2.9\,\%$, $-0.5\,\%$, $+0.6\,\%$ and $-1.6\,\%$ for EUR, MED, MEDW and MEDE, respectively. The total change for the period from 2046 to 2055 using RCP4.5 (meaning in simulations where all drivers change at the same time) is a decrease which is seen for all subdomains for PM_{10} ($-11.8\,\%$, $-1\,\%$ and $-9.2\,\%$ for EUR, MED MEDW, and MEDE, respectively) except for MEDE where an increase of $+9.1\,\%$ is observed. Thus, for most of the domains, the effect of emission reductions on PM_{10} concentrations around 2050 is reduced to a certain extent by modifications of boundary conditions and regional climate.

5 Conclusion and discussion

We investigated the effect of different drivers on total PM_{10} and PM_{10} components in future scenarios for different subdomains. For this purpose, an exhaustive number of scenarios plus historic simulations were performed. The drivers that were taken into account included climate change, anthropogenic emissions and boundary condition changes. For each driver, simulations were compared against historic simulations and then the effect of a specific factor was calculated separately and compared with a scenario where all drivers changed at the same time. This approach was chosen as, in the existing climate change literature, the effects of different drivers are taken into account either all at once (Lacressonnière et al., 2017), separately but for a single driver and for a short period of time, separately but using sensitivity tests (Dawson et al., 2007; Megaritis et al., 2014), or in the best of cases, separately and for an acceptable period of time but for only one driver (Lemaire et al., 2016). The goal of this work was to explore multiple drivers separately for PM_{10} and its components for a coherent and comparable set of future scenarios, thereby making climate change analysis more comprehensible and more easily finding the drivers with the most impact on the PM_{10} future concentration changes. This work focuses on the Mediterranean area as well as the European region, as to date not many studies have focused on the climate change drivers in the Mediterranean area, although this region might be highly sensitive to climate change; therefore, this study directly responds to one of the major goals of the ChArMEx project, in the context of which the research was performed.

Future scenarios that we performed show that in the 2050s, in the case of an RCP4.5 scenario and CLE 2050 emissions, a general increase in temperature and a decrease of the total average PM_{10} concentration is seen both in the European subdomain ($-12\,\%$) and the Mediterranean subdomain ($-1\,\%$). The diminution of PM_{10} has also been reported in the literature for the European subdomain (e.g., Markakis et al., 2014; Lacressonnière et al., 2014, 2017): the intensity of this decrease changes with the period that is taken into account and the inputs used. The PM changes are far from uniform for different seasons. For the European area a maximum change of $-24\,\%$ for spring and $+9\,\%$ for summer is seen, whereas for the Mediterranean area a maximum change of $+25\,\%$ for winter and $-19\,\%$ for spring is observed. These values seem to indicate different behaviors in the Mediterranean and European areas. The reasons for these changes were explored driver by driver and the effect of each driver was estimated.

Regional climate change alone results in a decrease of PM_{10} in RCP4.5 and RCP8.5, whereas RCP2.6 shows an increase for PM_{10}. Among the PM_{10} components, BSOA and nitrate particles show the most sensitivity to climate change. It appears that, when exploring the impacts of climate change, nitrate decrease governs the decrease of PM_{10} and $PM_{2.5}$ in RCP4.5 and RCP8.5; however, in RCP2.6, the increase in dust, salt and BSOA particles outweighs the decrease in nitrates. In the search for reasons for the changes seen for PM components, correlations of meteorological parameters with individual components were investigated. Nitrates show a strong dependence (anti-correlation) on temperature, especially during winter, when a correlation with shortwave radiation and anti-correlations with wind speed and PBLH are also observed. These relationships seem to suggest a switch to slightly more "marine-type" conditions for a future climate during winter (supported by correlations calculated between different meteorological parameters). BSOA also shows a strong correlation with temperature (and therefore shows a strong increase in future scenarios) in all subdomains, resulting from an increase in BVOC emissions due to higher temperatures. Sulfate particles are seen to have a correlation with RH and PBLH, although the extent of this correlation changes depending on the subdomain explored. The relationship of SO_4^{2-} with RH can be related to either the production of this aerosol from SO_2 or the formation of gas-phase SO_4^{2-} from the oxidation of SO_2 by OH; the dominance of these processes depends on the subdomain and the season in which they are studied. Because of the general RH pattern differences between RCP2.6 compared with RCP4.5 and RCP8.5, sulfates show a particular 2-D structure in RCP2.6, which is different from the general pattern seen for RCP4.5 and RCP8.5. The relationship of ammonium aerosols with meteorological conditions is a combination of the relationships of SO_4^{2-} and NO_3^- with these conditions. Salt particles show a clear correlation with wind speed, whereas dust concentrations present a weak relationship with the meteorological parameters tested, as their changes are re-

lated to advection from outside the model domain and are, therefore, not captured by local correlation analysis.

Future changes in boundary conditions (depicting long-range transport from outside of Europe) greatly affect dust concentrations, especially over the Mediterranean area. In contrast, they only have a limited impact on sulfate, nitrate, ammonium and OA concentrations. It is important to keep in mind that, because of the position of the EURO-CORDEX domain and the fact that the southern part of the Mediterranean is located at the southern borders of the domain, the model might not be able to capture the effects of global climate change and dust activity in a fully consistent way, although the results show an important increase in dust concentrations due to long-range transport.

Emission changes show the largest effect on all non-sea-salt and non-dust PM_{10}/$PM_{2.5}$ components. One of the most interesting cases that was encountered in the emission change scenarios was the decrease in BSOA due to anthropogenic emission changes. This is tentatively attributed to changes in seed aerosol and the changes in oxidant levels because of the decrease in anthropogenic emissions in addition to a direct decrease in anthropogenic COVs. The same impact, with the same important intensity, was seen in a study in preparation by Ciarelli et al. (2019), when looking at an ensemble of simulations in the framework of the EURODELTA multi-model experiment. Sartelet et al. (2012) also noted an important change in SOA concentration in their simulation when changing the anthropogenic emissions. However, the exact mechanism of this relationship still needs further investigation. Compared with the other two drivers, the effects shown by the anthropogenic emission reduction are undeniably more important for most species. This leads us to the conclusion that, according to our study, anthropogenic emission reduction policies (or the lack thereof) will have a strong impact on the concentrations of PM seen in the future; furthermore, the impact of anthropogenic emissions will be more significant than the affects of both regional climate and long-range transport.

Another point that has been raised in this article is the differences between the European subdomain and the Mediterranean Sea and the difference between the eastern and western Mediterranean. The behavior of these subdomains differs when they are exposed to climate change. Meteorological changes in the domain show increasing temperatures, increasing PBLH and decreasing humidity. Winters and springs seem to become drier, while the other two seasons become wetter with respect to the amount of precipitation; rain episodes also become more intense and shorter in most cases (except for RCP2.6). The concentration of PM_{10} is generally higher in the Mediterranean due to higher concentrations of dust and salt particles, whereas its annually averaged changes in the future remain quite similar to what was seen for the European subdomain. Seasonally, in the Mediterranean a maximum for PM_{10} concentrations is seen for spring when dust episodes are more common, contrary to the European subdomain (maximum in winter for EUR). Emission reduction policies will reduce the concentrations of anthropogenic species in the basin by almost the same percentage as the European subdomain shown in this work (for example, for sulfates, anthropogenic emissions reduction results in $-29\,\%$ and $-30\,\%$ for EUR and MED, respectively, for CLE2050 emissions). While this fact shows that emission reduction policies will reduce the $PM_{2.5}$ and lower the aerosol fraction of pollution, they will not lessen the Mediterranean PM_{10} burden by much, as the PM_{10} concentration in this area is dominated by dust and salt concentrations. For the dust concentrations, our scenarios show an increased concentration in the Mediterranean due to long-range transport, especially in the eastern basin. However, changing land use in the northern African area will affect the concentration of dust in the Mediterranean; however, the extent and even the direction of this change is uncertain. Literature suggests that the dust concentrations due to land use changes in future scenarios can decrease or increase depending on the scenario that has been taken into account (Tegen et al., 2004; Woodward et al., 2005).

While exploring the three aforementioned drivers is important for understanding the behavior of PM and PM components in the future, there are other aspects that also need exploring in future studies. Other additions to this study would be, for example, to explore the effects of land use changes, OA simulation scheme changes and BSOA trend changes related to ASOA changes. Land use changes, apart from the previously mentioned effects on dust emission, can affect the emissions of BVOC, which can change the future concentrations of BSOA and can also change the deposition of different species in future scenarios. Additions to inorganic aerosol formation in future scenarios (such as different salt formation schemes, dimethyl sulfide formation from the sea surface and so on) would also be useful additions to the field of climate change study. Furthermore, the driver by driver approach can be taken with each of these parameters in order to explore their effects on future changes of PM concentrations.

Data availability. Access to the data used in this article is restricted to registered users of the ChArMEx project. The data are available from the project website (http://mistrals.sedoo.fr/ChArMEx/, last access: 15 July 2019) and should be used following the data and publication policies of the ChArMEx project: http://mistrals.sedoo.fr/ChArMEx/Data-Policy/ChArMEx_DataPolicy.pdf (last access: 7 August 2018).

Supplement. The supplement related to this article is available online at: https://doi.org/10.5194/acp-19-4459-2019-supplement.

Author contributions. ArC, AuC and MB designed the experiment. AuC performed the simulations, and ArC carried out the post-processing of aforementioned simulations. Article reduction was performed by ArC, and all authors contributed to the text, interpretation of the results and review of the article.

Competing interests. The authors declare that they have no conflict of interest.

Special issue statement. This article is part of the special issue "CHemistry and AeRosols Mediterranean EXperiments (ChArMEx) (ACP/AMT inter-journal SI)". It is not associated with a conference.

Acknowledgements. This research received funding from the French National Research Agency (ANR) projects SAF-MED (grant no. ANR-15 12-BS06-0013). This work is part of the ChArMEx project supported by ADEME, CEA, CNRS-INSU and Météo-France through the multidisciplinary MISTRALS (Mediterranean Integrated Studies aT Regional And Local Scales) program. The work presented here received support from the French Ministry in charge of ecology. This work was performed using HPC resources from GENCI-CCRT (grant no. 2017-t2015017232). Robert Vautard is acknowledged for providing the WRF/IPSL-CM5-MR Cordex simulations, and Didier Hauglustaine and Sophie Szopa are acknowledged for providing the INCA simulations. Zbigniew Klimont is acknowledged for providing the ECLIPSE-v4 emission projections. The thesis work of Arineh Cholakian is supported by ADEME, INERIS (with the support of the French Ministry in charge of Ecology), and via the ANR SAF-MED project. Giancarlo Ciarelli thanks ADEME and the Swiss National Science Foundation (grant no. P2EZP2_175166).

Review statement. This paper was edited by Jean-Luc Attié and reviewed by three anonymous referees.

References

Aksoyoglu, S., Ciarelli, G., El-Haddad, I., Baltensperger, U., and Prévôt, A. S. H.: Secondary inorganic aerosols in Europe: sources and the significant influence of biogenic VOC emissions, especially on ammonium nitrate, Atmos. Chem. Phys., 17, 7757–7773, https://doi.org/10.5194/acp-17-7757-2017, 2017.

Amann, M., Klimont, Z., and Wagner, F.: Regional and Global Emissions of Air Pollutants: Recent Trends and Future Scenarios, Annu. Rev. Env. Resour., 38, 31–55, https://doi.org/10.1146/annurev-environ-052912-173303, 2013.

Anderson, J. O., Thundiyil, J. G., and Stolbach, A.: Clearing the Air: A Review of the Effects of Particulate Matter Air Pollution on Human Health, J. Med. Toxicol., 8, 166–175, https://doi.org/10.1007/s13181-011-0203-1, 2012.

Arino, O., Bicheron, P., Achard, F., Latham, J., Witt, R., and Weber, J.: Globcover: The most detailed protrait of Earth, Eur. Sp. Agency Bull., 36, 24–31, 2008.

Arneth, A., Miller, P. A., Scholze, M., Hickler, T., Schurgers, G., Smith, B., and Prentice, I. C.: CO_2 inhibition of global terrestrial isoprene emissions: Potential implications for atmospheric chemistry, Geophys. Res. Lett., 34, L18813, https://doi.org/10.1029/2007GL030615, 2007.

Bessagnet, B., Menut, L., Curci, G., Hodzic, A., Guillaume, B., Liousse, C., Moukhtar, S., Pun, B., Seigneur, C., and Schulz, M.: Regional modeling of carbonaceous aerosols over Europe – focus on secondary organic aerosols, J. Atmos. Chem., 61, 175–202, https://doi.org/10.1007/s10874-009-9129-2, 2008.

Carvalho, A., Monteiro, A., Solman, S., Miranda, A. I., and Borrego, C.: Climate-driven changes in air quality over Europe by the end of the 21st century, with special reference to Portugal, Environ. Sci. Policy, 13, 445–458, https://doi.org/10.1016/J.ENVSCI.2010.05.001, 2010.

Ciarelli, G., Theobald, M. R., Vivanco, M. G., Beekmann, M., Aas, W., Andersson, C., Bergström, R., Manders-Groot, A., Couvidat, F., Mircea, M., Tsyro, S., Fagerli, H., Mar, K., Raffort, V., Roustan, Y., Pay, M.-T., Schaap, M., Kranenburg, R., Adani, M., Briganti, G., Cappelletti, A., D'Isidoro, M., Cuvelier, C., Cholakian, A., Bessagnet, B., Wind, P., and Colette, A.: Trends of inorganic and organic aerosols and precursor gases in Europe: insights from the EURODELTA multi-model experiment over the 1990–2010 period, Geosci. Model Dev. Discuss., https://doi.org/10.5194/gmd-2019-70, in review, 2019.

Cholakian, A., Beekmann, M., Colette, A., Coll, I., Siour, G., Sciare, J., Marchand, N., Couvidat, F., Pey, J., Gros, V., Sauvage, S., Michoud, V., Sellegri, K., Colomb, A., Sartelet, K., Langley DeWitt, H., Elser, M., Prévot, A. S. H., Szidat, S., and Dulac, F.: Simulation of fine organic aerosols in the western Mediterranean area during the ChArMEx 2013 summer campaign, Atmos. Chem. Phys., 18, 7287–7312, https://doi.org/10.5194/acp-18-7287-2018, 2018.

Colette, A., Bessagnet, B., Vautard, R., Szopa, S., Rao, S., Schucht, S., Klimont, Z., Menut, L., Clain, G., Meleux, F., Curci, G., and Rouïl, L.: European atmosphere in 2050, a regional air quality and climate perspective under CMIP5 scenarios, Atmos. Chem. Phys., 13, 7451–7471, https://doi.org/10.5194/acp-13-7451-2013, 2013.

Colette, A., Andersson, C., Baklanov, A., Bessagnet, B., Brandt, J., Christensen, J. H., Doherty, R., Engardt, M., Geels, C., Giannakopoulos, C., Hedegaard, G. B., Katragkou, E., Langner, J., Lei, H., Manders, A., Melas, D., Meleux, F., Rouïl, L., Sofiev, M., Soares, J., Stevenson, D. S., Tombrou-Tzella, M., Varotsos, K. V., and Young, P.: Is the ozone climate penalty robust in Europe?, Environ. Res. Lett., 10, 084015, https://doi.org/10.1088/1748-9326/10/8/084015, 2015.

Dale, V. H., Joyce, L. A., McNulty, S., Neilson, R. P., Ayres, M. P., Flannigan, M. D., Hanson, P. J., Irland, L. C., Lugo, A. E., Peterson, C. J., Simberloff, D., Swanson, F. J., Stocks, B. J., and Wotton, B. M.: Climate Change and Forest Disturbances: Climate change can affect forests by altering the frequency, intensity, duration, and timing of fire, drought, introduced species, insect and pathogen outbreaks, hurricanes, windstorms, ice storms, or landslides, Bioscience, 51, 723–734, https://doi.org/10.1641/0006-3568(2001)051[0723:ccafd]2.0.co;2, 2001.

Dawson, J. P., Adams, P. J., and Pandis, S. N.: Sensitivity of $PM_{2.5}$ to climate in the Eastern US: a modeling case study, Atmos. Chem. Phys., 7, 4295-4309, https://doi.org/10.5194/acp-7-4295-2007, 2007.

de Winter, R. C., Sterl, A., and Ruessink, B. G.: Wind extremes in the North Sea Basin under climate change: An ensemble study of 12 CMIP5 GCMs, J. Geophys. Res.-Atmos., 118, 1601–1612, https://doi.org/10.1002/jgrd.50147, 2013.

Dobrynin, M., Murawsky, J., and Yang, S.: Evolution of the global wind wave climate in CMIP5 experiments, Geophys. Res. Lett., 39, L18606, https://doi.org/10.1029/2012GL052843, 2012.

Dufresne, J.-L., Foujols, M.-A., Denvil, S., Caubel, A., Marti, O., Aumont, O., Balkanski, Y., Bekki, S., Bellenger, H., Benshila, R., Bony, S., Bopp, L., Braconnot, P., Brockmann, P., Cadule, P., Cheruy, F., Codron, F., Cozic, A., Cugnet, D., de Noblet, N., Duvel, J.-P., Ethé, C., Fairhead, L., Fichefet, T., Flavoni, S., Friedlingstein, P., Grandpeix, J.-Y., Guez, L., Guilyardi, E., Hauglustaine, D., Hourdin, F., Idelkadi, A., Ghattas, J., Joussaume, S., Kageyama, M., Krinner, G., Labetoulle, S., Lahellec, A., Lefebvre, M.-P., Lefevre, F., Levy, C., Li, Z. X., Lloyd, J., Lott, F., Madec, G., Mancip, M., Marchand, M., Masson, S., Meurdesoif, Y., Mignot, J., Musat, I., Parouty, S., Polcher, J., Rio, C., Schulz, M., Swingedouw, D., Szopa, S., Talandier, C., Terray, P., Viovy, N., and Vuichard, N.: Climate change projections using the IPSL-CM5 Earth System Model: from CMIP3 to CMIP5, Clim. Dynam., 40, 2123–2165, https://doi.org/10.1007/s00382-012-1636-1, 2013.

EEA: Air pollution and climate change policies in Europe: exploring linkages and the added value of an integrated approach, European Environment Agency, Copenhagen, available at: https://www.eea.europa.eu/publications/technical_report_2004_5 (last access: 7 December 2017), 2004.

EEA: Air quality in Europe – 2016, European Environment Agency, Copenhagen, available at: https://www.eea.europa.eu//publications/air-quality-in-europe-2016 (last access: 11 December 2017), 2016.

Evan, A. T., Flamant, C., Fiedler, S., and Doherty, O.: An analysis of aeolian dust in climate models, Geophys. Res. Lett., 41, 5996–6001, https://doi.org/10.1002/2014GL060545, 2014.

Fichefet, T. and Maqueda, M. A. M.: Modelling the influence of snow accumulation and snow-ice formation on the seasonal cycle of the Antarctic sea-ice cover, Clim. Dynam., 15, 251–268, https://doi.org/10.1007/s003820050280, 1999.

Fiore, A. M., Naik, V., Spracklen, D. V., Steiner, A., Unger, N., Prather, M., Bergmann, D., Cameron-Smith, P. J., Cionni, I., Collins, W. J., Dalsøren, S., Eyring, V., Folberth, G. A., Ginoux, P., Horowitz, L. W., Josse, B., Lamarque, J.-F., MacKenzie, I. A., Nagashima, T., O'Connor, F. M., Righi, M., Rumbold, S. T., Shindell, D. T., Skeie, R. B., Sudo, K., Szopa, S., Takemura, T., and Zeng, G.: Global air quality and climate, Chem. Soc. Rev., 41, 6663, https://doi.org/10.1039/c2cs35095e, 2012.

Fortems-Cheiney, A., Foret, G., Siour, G., Vautard, R., Szopa, S., Dufour, G., Colette, A., Lacressonniere, G., and Beekmann, M.: A 3C global RCP8.5 emission trajectory cancels benefits of European emission reductions on air quality, Nat. Commun., 8, 89, https://doi.org/10.1038/s41467-017-00075-9, 2017.

Fountoukis, C. and Nenes, A.: ISORROPIA II: a computationally efficient thermodynamic equilibrium model for K^+-Ca^{2+}-Mg^{2+}-NH_4^+-Na^+-SO_4^{2-}-NO_3^--Cl^--H_2O aerosols, Atmos. Chem. Phys., 7, 4639–4659, https://doi.org/10.5194/acp-7-4639-2007, 2007.

Ginoux, P., Prospero, J. M., Torres, O., and Chin, M.: Long-term simulation of global dust distribution with the GOCART model: correlation with North Atlantic Oscillation, Environ. Modell. Softw., 19, 113–128, https://doi.org/10.1016/S1364-8152(03)00114-2, 2004.

Giorgi, F.: Climate change hot-spots, Geophys. Res. Lett., 33, 1–4, https://doi.org/10.1029/2006GL025734, 2006.

Grantz, D., Garner, J. H., and Johnson, D.: Ecological effects of particulate matter, Environ. Int., 29, 213–239, https://doi.org/10.1016/S0160-4120(02)00181-2, 2003.

Guenther, A., Karl, T., Harley, P., Wiedinmyer, C., Palmer, P. I., and Geron, C.: Estimates of global terrestrial isoprene emissions using MEGAN (Model of Emissions of Gases and Aerosols from Nature), Atmos. Chem. Phys., 6, 3181–3210, https://doi.org/10.5194/acp-6-3181-2006, 2006.

Hantson, S., Knorr, W., Schurgers, G., Pugh, T. A. M., and Arneth, A.: Global isoprene and monoterpene emissions under changing climate, vegetation, CO_2 and land use, Atmos. Environ., 155, 35–45, https://doi.org/10.1016/j.atmosenv.2017.02.010, 2017.

Harrison, S. P., Kohfeld, K. E., Roelandt, C., and Claquin, T.: The role of dust in climate changes today, at the last glacial maximum and in the future, Earth-Sci. Rev., 54, 43–80, https://doi.org/10.1016/S0012-8252(01)00041-1, 2001.

Hauglustaine, D. A., Balkanski, Y., and Schulz, M.: A global model simulation of present and future nitrate aerosols and their direct radiative forcing of climate, Atmos. Chem. Phys., 14, 11031–11063, https://doi.org/10.5194/acp-14-11031-2014, 2014.

Heald, C. L., Henze, D. K., Horowitz, L. W., Feddema, J., Lamarque, J.-F., Guenther, A., Hess, P. G., Vitt, F., Seinfeld, J. H., Goldstein, A. H., and Fung, I.: Predicted change in global secondary organic aerosol concentrations in response to future climate, emissions, and land use change, J. Geophys. Res.-Atmos., 113, D05211, https://doi.org/10.1029/2007JD009092, 2008.

Hedegaard, G. B., Brandt, J., Christensen, J. H., Frohn, L. M., Geels, C., Hansen, K. M., and Stendel, M.: Impacts of Climate Change on Air Pollution Levels in the Northern Hemisphere with Special Focus on Europe and the Arctic, in: Air Pollution Modeling and Its Application XIX, 568–576, Springer Netherlands, Dordrecht, 2008.

Hedegaard, G. B., Christensen, J. H., and Brandt, J.: The relative importance of impacts from climate change vs. emissions change on air pollution levels in the 21st century, Atmos. Chem. Phys., 13, 3569–3585, https://doi.org/10.5194/acp-13-3569-2013, 2013.

Hodzic, A. and Jimenez, J. L.: Modeling anthropogenically controlled secondary organic aerosols in a megacity: a simplified framework for global and climate models, Geosci. Model Dev., 4, 901–917, https://doi.org/10.5194/gmd-4-901-2011, 2011.

Hourdin, F., Musat, I., Bony, S., Braconnot, P., Codron, F., Dufresne, J.-L., Fairhead, L., Filiberti, M.-A., Friedlingstein, P., Grandpeix, J.-Y., Krinner, G., LeVan, P., Li, Z.-X., and Lott, F.: The LMDZ4 general circulation model: climate performance and sensitivity to parametrized physics with emphasis on tropical convection, Clim. Dynam., 27, 787–813, https://doi.org/10.1007/s00382-006-0158-0, 2006.

Im, U., Brandt, J., Geels, C., Hansen, K. M., Christensen, J. H., Andersen, M. S., Solazzo, E., Kioutsioukis, I., Alyuz, U., Balzarini, A., Baro, R., Bellasio, R., Bianconi, R., Bieser, J.,

Colette, A., Curci, G., Farrow, A., Flemming, J., Fraser, A., Jimenez-Guerrero, P., Kitwiroon, N., Liang, C.-K., Nopmongcol, U., Pirovano, G., Pozzoli, L., Prank, M., Rose, R., Sokhi, R., Tuccella, P., Unal, A., Vivanco, M. G., West, J., Yarwood, G., Hogrefe, C., and Galmarini, S.: Assessment and economic valuation of air pollution impacts on human health over Europe and the United States as calculated by a multi-model ensemble in the framework of AQMEII3, Atmos. Chem. Phys., 18, 5967–5989, https://doi.org/10.5194/acp-18-5967-2018, 2018.

Jacob, D.: IMPACT2C – An introduction, Clim. Serv., 7, 1–2, https://doi.org/10.1016/J.CLISER.2017.07.006, 2017.

Jacob, D., Petersen, J., Eggert, B., Alias, A., Christensen, O. B., Bouwer, L. M., Braun, A., Colette, A., Déqué, M., Georgievski, G., Georgopoulou, E., Gobiet, A., Menut, L., Nikulin, G., Haensler, A., Hempelmann, N., Jones, C., Keuler, K., Kovats, S., Kröner, N., Kotlarski, S., Kriegsmann, A., Martin, E., van Meijgaard, E., Moseley, C., Pfeifer, S., Preuschmann, S., Radermacher, C., Radtke, K., Rechid, D., Rounsevell, M., Samuelsson, P., Somot, S., Soussana, J.-F., Teichmann, C., Valentini, R., Vautard, R., Weber, B., and Yiou, P.: EURO-CORDEX: new high-resolution climate change projections for European impact research, Reg. Environ. Change, 14, 563–578, https://doi.org/10.1007/s10113-013-0499-2, 2014.

Jacob, D. J. and Winner, D. A.: Effect of Climate Change on Air Quality, Atmos. Environ., 43, 51–63, https://doi.org/10.1016/j.atmosenv.2008.09.051, 2009.

Jiménez-Guerrero, P., Montávez, J. P., Gómez-Navarro, J. J., Jerez, S., and Lorente-Plazas, R.: Impacts of climate change on ground level gas-phase pollutants and aerosols in the Iberian Peninsula for the late XXI century, Atmos. Environ., 55, 483–495, https://doi.org/10.1016/j.atmosenv.2012.02.048, 2012.

Juda-Rezler, K., Reizer, M., Huszar, P., Krüger, B., Zanis, P., Syrakov, D., Katragkou, E., Trapp, W., Melas, D., Chervenkov, H., Tegoulias, I., and Halenka, T.: Modelling the effects of climate change on air quality over Central and Eastern Europe: concept, evaluation and projections, Clim. Res., 53, 179–203, https://doi.org/10.3354/cr01072, 2012.

Kampa, M. and Castanas, E.: Human health effects of air pollution, Environ. Pollut., 151, 362–367, https://doi.org/10.1016/J.ENVPOL.2007.06.012, 2008.

Katragkou, E., García-Díez, M., Vautard, R., Sobolowski, S., Zanis, P., Alexandri, G., Cardoso, R. M., Colette, A., Fernandez, J., Gobiet, A., Goergen, K., Karacostas, T., Knist, S., Mayer, S., Soares, P. M. M., Pytharoulis, I., Tegoulias, I., Tsikerdekis, A., and Jacob, D.: Regional climate hindcast simulations within EURO-CORDEX: evaluation of a WRF multi-physics ensemble, Geosci. Model Dev., 8, 603–618, https://doi.org/10.5194/gmd-8-603-2015, 2015.

Kerkhoff, C., Künsch, H. R., and Schär, C.: A Bayesian Hierarchical Model for Heterogeneous RCM–GCM Multimodel Ensembles, J. Climate, 28, 6249–6266, https://doi.org/10.1175/JCLI-D-14-00606.1, 2015.

Kinney, P. L.: Climate Change, Air Quality, and Human Health, Am. J. Prev. Med., 35, 459–467, https://doi.org/10.1016/j.amepre.2008.08.025, 2008.

Klimont, Z., Smith, S. J., and Cofala, J.: The last decade of global anthropogenic sulfur dioxide: 2000–2011 emissions, Environ. Res. Lett., 8, 014003, https://doi.org/10.1088/1748-9326/8/1/014003, 2013.

Klimont, Z., Kupiainen, K., Heyes, C., Purohit, P., Cofala, J., Rafaj, P., Borken-Kleefeld, J., and Schöpp, W.: Global anthropogenic emissions of particulate matter including black carbon, Atmos. Chem. Phys., 17, 8681–8723, https://doi.org/10.5194/acp-17-8681-2017, 2017.

Knutti, R. and Sedláček, J.: Robustness and uncertainties in the new CMIP5 climate model projections, Nat. Clim. Chang., 3, 369–373, https://doi.org/10.1038/NCLIMATE1716, 2012.

Kotlarski, S., Keuler, K., Christensen, O. B., Colette, A., Déqué, M., Gobiet, A., Goergen, K., Jacob, D., Lüthi, D., van Meijgaard, E., Nikulin, G., Schär, C., Teichmann, C., Vautard, R., Warrach-Sagi, K., and Wulfmeyer, V.: Regional climate modeling on European scales: a joint standard evaluation of the EURO-CORDEX RCM ensemble, Geosci. Model Dev., 7, 1297–1333, https://doi.org/10.5194/gmd-7-1297-2014, 2014.

Krinner, G., Viovy, N., de Noblet-Ducoudré, N., Ogée, J., Polcher, J., Friedlingstein, P., Ciais, P., Sitch, S., and Prentice, I. C.: A dynamic global vegetation model for studies of the coupled atmosphere-biosphere system, Global Biogeochem. Cy., 19, GB1015, https://doi.org/10.1029/2003GB002199, 2005.

Lacressonnière, G., Peuch, V.-H., Vautard, R., Arteta, J., Déqué, M., Joly, M., and Josse, B.: European air quality in the 2030s and 2050s: Impacts of global and regional emission trends and of climate change, Atmos. Environ., 92, 348–358, https://doi.org/10.1016/J.ATMOSENV.2014.04.033, 2014.

Lacressonnière, G., Foret, G., Beekmann, M., Siour, G., Engardt, M., Gauss, M., Watson, L., Andersson, C., Colette, A., Josse, B., Marécal, V., Nyiri, A., and Vautard, R.: Impacts of regional climate change on air quality projections and associated uncertainties, Climatic Change, 136, 309–324, https://doi.org/10.1007/s10584-016-1619-z, 2016.

Lacressonnière, G., Watson, L., Gauss, M., Magnuz, E., Andersson, C. B. M., Augustin, C., Gilles, F., Josse, B., Marécal, V., Nyiri, A., Siour, G., Sobolowski, S., and Vautard, R.: Particulate matter air pollution in Europe in a +2 °C warming world, Atmos. Environ., 154, 129–140, https://doi.org/10.1016/J.ATMOSENV.2017.01.037, 2017.

Langner, J., Engardt, M., Baklanov, A., Christensen, J. H., Gauss, M., Geels, C., Hedegaard, G. B., Nuterman, R., Simpson, D., Soares, J., Sofiev, M., Wind, P., and Zakey, A.: A multi-model study of impacts of climate change on surface ozone in Europe, Atmos. Chem. Phys., 12, 10423–10440, https://doi.org/10.5194/acp-12-10423-2012, 2012.

Lathière, J., Hauglustaine, D. A., De Noblet-Ducoudré, N., Krinner, G., and Folberth, G. A.: Past and future changes in biogenic volatile organic compound emissions simulated with a global dynamic vegetation model, Geophys. Res. Lett., 32, L20818, https://doi.org/10.1029/2005GL024164, 2005.

Laurent, B., Marticorena, B., Bergametti, G., Chazette, P., Maignan, F., and Schmechtig, C.: Simulation of the mineral dust emission frequencies from desert areas of China and Mongolia using an aerodynamic roughness length map derived from the POLDER/ADEOS 1 surface products, J. Geophys. Res., 110, D18S04, https://doi.org/10.1029/2004JD005013, 2005.

Lemaire, V. E. P., Colette, A., and Menut, L.: Using statistical models to explore ensemble uncertainty in climate impact studies: the example of air pollution in Europe, Atmos. Chem. Phys., 16, 2559–2574, https://doi.org/10.5194/acp-16-2559-2016, 2016.

Liao, H., Chen, W.-T., and Seinfeld, J. H.: Role of climate change in global predictions of future tropospheric ozone and aerosols, J. Geophys. Res., 111, D12304, https://doi.org/10.1029/2005JD006852, 2006.

Madec, G. and Delecluse, P.: OPA 8.1 Ocean General Circulation Model Reference Manual, Inst. Pierre Simon Laplace des Sci. l'environnement Glob., available at: https://www.researchgate.net/profile/Gurvan_Madec/publication/243055542_OPA_81_Ocean_General_Circulation_Model_reference_manual/links/02e7e51d1b695c81c5000000/OPA-81-Ocean-General-Circulation-Model-reference-manual.pdf (last access: 26 January 2018), 1998.

Markakis, K., Valari, M., Colette, A., Sanchez, O., Perrussel, O., Honore, C., Vautard, R., Klimont, Z., and Rao, S.: Air quality in the mid-21st century for the city of Paris under two climate scenarios; from the regional to local scale, Atmos. Chem. Phys., 14, 7323–7340, https://doi.org/10.5194/acp-14-7323-2014, 2014.

Marticorena, B. and Bergametti, G.: Modeling the atmospheric dust cycle: 1. Design of a soil-derived dust emission scheme, J. Geophys. Res., 100, 16415, https://doi.org/10.1029/95JD00690, 1995.

Megaritis, A. G., Fountoukis, C., Charalampidis, P. E., Denier van der Gon, H. A. C., Pilinis, C., and Pandis, S. N.: Linking climate and air quality over Europe: effects of meteorology on $PM_{2.5}$ concentrations, Atmos. Chem. Phys., 14, 10283–10298, https://doi.org/10.5194/acp-14-10283-2014, 2014.

Meinshausen, M., Smith, S. J., Calvin, K., Daniel, J. S., Kainuma, M. L. T., Lamarque, J.-F., Matsumoto, K., Montzka, S. A., Raper, S. C. B., Riahi, K., Thomson, A., Velders, G. J. M., and van Vuuren, D. P. P.: The RCP greenhouse gas concentrations and their extensions from 1765 to 2300, Climatic Change, 109, 21–241, https://doi.org/10.1007/s10584-011-0156-z, 2011.

Meleux, F., Solmon, F., and Giorgi, F.: Increase in summer European ozone amounts due to climate change, Atmos. Environ., 41, 7577–7587, https://doi.org/10.1016/J.ATMOSENV.2007.05.048, 2007.

Menut, L., Tripathi, O. P., Colette, A., Vautard, R., Menut, L., Flaounas, E., Tripathi, O. P., Vautard, R., and Bessagnet, B.: Evaluation of regional climate simulations for air quality modelling purposes, Clim. Dynam., 40, 2515–2533, https://doi.org/10.1007/s00382-012-1345-9, 2012.

Menut, L., Bessagnet, B., Khvorostyanov, D., Beekmann, M., Blond, N., Colette, A., Coll, I., Curci, G., Foret, G., Hodzic, A., Mailler, S., Meleux, F., Monge, J.-L., Pison, I., Siour, G., Turquety, S., Valari, M., Vautard, R., and Vivanco, M. G.: CHIMERE 2013: a model for regional atmospheric composition modelling, Geosci. Model Dev., 6, 981–1028, https://doi.org/10.5194/gmd-6-981-2013, 2013.

Menut, L., Rea, G., Mailler, S., Khvorostyanov, D., and Turquety, S.: Aerosol forecast over the Mediterranean area during July 2013 (ADRIMED/CHARMEX), Atmos. Chem. Phys., 15, 7897–7911, https://doi.org/10.5194/acp-15-7897-2015, 2015.

Olesen, J. E., Carter, T. R., Díaz-Ambrona, C. H., Fronzek, S., Heidmann, T., Hickler, T., Holt, T., Minguez, M. I., Morales, P., Palutikof, J. P., Quemada, M., Ruiz-Ramos, M., Rubæk, G. H., Sau, F., Smith, B., and Sykes, M. T.: Uncertainties in projected impacts of climate change on European agriculture and terrestrial ecosystems based on scenarios from regional climate models, Climatic Change, 81, 123–143, https://doi.org/10.1007/s10584-006-9216-1, 2007.

Pacifico, F., Folberth, G. A., Jones, C. D., Harrison, S. P., and Collins, W. J.: Sensitivity of biogenic isoprene emissions to past, present, and future environmental conditions and implications for atmospheric chemistry, J. Geophys. Res.-Atmos., 117, D22302, https://doi.org/10.1029/2012JD018276, 2012.

Petetin, H., Beekmann, M., Sciare, J., Bressi, M., Rosso, A., Sanchez, O., and Ghersi, V.: A novel model evaluation approach focusing on local and advected contributions to urban $PM_{2.5}$ levels – application to Paris, France, Geosci. Model Dev., 7, 1483–1505, https://doi.org/10.5194/gmd-7-1483-2014, 2014.

Pope, C. A. and Dockery, D. W.: Health Effects of Fine Particulate Air Pollution: Lines that Connect, J. Air Waste Manage., 56, 709–742, https://doi.org/10.1080/10473289.2006.10464485, 2006.

Pope, C. A., Ezzati, M., and Dockery, D. W.: Fine-Particulate Air Pollution and Life Expectancy in the United States, N. Engl. J. Med., 360, 376–386, https://doi.org/10.1056/NEJMsa0805646, 2009.

Rea, G., Turquety, S., Menut, L., Briant, R., Mailler, S., and Siour, G.: Source contributions to 2012 summertime aerosols in the Euro-Mediterranean region, Atmos. Chem. Phys., 15, 8013–8036, https://doi.org/10.5194/acp-15-8013-2015, 2015.

Sartelet, K. N., Couvidat, F., Seigneur, C., and Roustan, Y.: Impact of biogenic emissions on air quality over Europe and North America, Atmos. Environ., 53, 131–141, https://doi.org/10.1016/J.ATMOSENV.2011.10.046, 2012.

Seinfeld, J. H. and Pandis, S. N.: Atmospheric chemistry and physics: from air pollution to climate change, John Wiley & Sons, 2016.

Shindell, D. T., Lamarque, J.-F., Schulz, M., Flanner, M., Jiao, C., Chin, M., Young, P. J., Lee, Y. H., Rotstayn, L., Mahowald, N., Milly, G., Faluvegi, G., Balkanski, Y., Collins, W. J., Conley, A. J., Dalsoren, S., Easter, R., Ghan, S., Horowitz, L., Liu, X., Myhre, G., Nagashima, T., Naik, V., Rumbold, S. T., Skeie, R., Sudo, K., Szopa, S., Takemura, T., Voulgarakis, A., Yoon, J.-H., and Lo, F.: Radiative forcing in the ACCMIP historical and future climate simulations, Atmos. Chem. Phys., 13, 2939–2974, https://doi.org/10.5194/acp-13-2939-2013, 2013.

Szopa, S., Hauglustaine, D. A., Vautard, R., and Menut, L.: Future global tropospheric ozone changes and impact on European air quality, Geophys. Res. Lett., 33, L14805, https://doi.org/10.1029/2006GL025860, 2006.

Szopa, S., Balkanski, Y., Schulz, M., Bekki, S., Cugnet, D., Fortems-Cheiney, A., Turquety, S., Cozic, A., Déandreis, C., Hauglustaine, D., Idelkadi, A., Lathière, J., Lefevre, F., Marchand, M., Vuolo, R., Yan, N., and Dufresne, J.-L.: Aerosol and ozone changes as forcing for climate evolution between 1850 and 2100, Clim. Dynam., 40, 2223–2250, https://doi.org/10.1007/s00382-012-1408-y, 2013.

Tai, A. P. K., Mickley, L. J., Heald, C. L., and Wu, S.: Effect of CO_2 inhibition on biogenic isoprene emission: Implications for air quality under 2000 to 2050 changes in climate, vegetation, and land use, Geophys. Res. Lett., 40, 3479–3483, https://doi.org/10.1002/grl.50650, 2013.

Taylor, K. E., Stouffer, R. J., Meehl, G. A., Taylor, K. E., Stouffer, R. J., and Meehl, G. A.: An Overview of CMIP5 and

the Experiment Design, B. Am. Meteorol. Soc., 93, 485–498, https://doi.org/10.1175/BAMS-D-11-00094.1, 2012.

Tegen, I., Werner, M., Harrison, S. P., and Kohfeld, K. E.: Relative importance of climate and land use in determining present and future global soil dust emission, Geophys. Res. Lett., 31, L05105, https://doi.org/10.1029/2003GL019216, 2004.

Teichmann, C., Eggert, B., Elizalde, A., Haensler, A., Jacob, D., Kumar, P., Moseley, C., Pfeifer, S., Rechid, D., Remedio, A., Ries, H., Petersen, J., Preuschmann, S., Raub, T., Saeed, F., Sieck, K., Weber, T., Teichmann, C., Eggert, B., Elizalde, A., Haensler, A., Jacob, D., Kumar, P., Moseley, C., Pfeifer, S., Rechid, D., Remedio, A. R., Ries, H., Petersen, J., Preuschmann, S., Raub, T., Saeed, F., Sieck, K., and Weber, T.: How Does a Regional Climate Model Modify the Projected Climate Change Signal of the Driving GCM: A Study over Different CORDEX Regions Using REMO, Atmosphere, 4, 214–236, https://doi.org/10.3390/atmos4020214, 2013.

Thomson, A. M., Calvin, K. V, Smith, S. J., Page Kyle, G., Volke, A., Patel, P., Delgado-Arias, S., Bond-Lamberty, B., Wise, M. A., Clarke, L. E., and Edmonds, J. A.: RCP4.5: a pathway for stabilization of radiative forcing by 2100, Climatic Change, 109, 77, https://doi.org/10.1007/s10584-011-0151-4, 2011.

Vautard, R., Gobiet, A., Sobolowski, S., Kjellström, E., Stegehuis, A., Watkiss, P., Mendlik, T., Landgren, O., Nikulin, G., Teichmann, C., and Jacob, D.: The European climate under a 2 °C global warming, Environ. Res. Lett., 9, 34006, https://doi.org/10.1088/1748-9326/9/3/034006, 2014.

Vautard, R., Colette, A., van Meijgaard, E., Meleux, F., Jan van Oldenborgh, G., Otto, F., Tobin, I., Yiou, P., Vautard, R., Colette, A., Meijgaard, E. van, Meleux, F., van Oldenborgh, G. J., Otto, F., Tobin, I., and Yiou, P.: Attribution of Wintertime Anticyclonic Stagnation Contributing to Air Pollution in Western Europe, B. Am. Meteorol. Soc., 99, S70–S75, https://doi.org/10.1175/BAMS-D-17-0113.1, 2018.

Vincent, J., Laurent, B., Losno, R., Bon Nguyen, E., Roullet, P., Sauvage, S., Chevaillier, S., Coddeville, P., Ouboulmane, N., di Sarra, A. G., Tovar-Sánchez, A., Sferlazzo, D., Massanet, A., Triquet, S., Morales Baquero, R., Fornier, M., Coursier, C., Desboeufs, K., Dulac, F., and Bergametti, G.: Variability of mineral dust deposition in the western Mediterranean basin and south-east of France, Atmos. Chem. Phys., 16, 8749–8766, https://doi.org/10.5194/acp-16-8749-2016, 2016.

van Vuuren, D. P., Stehfest, E., J den Elzen, M. G., Kram, T., van Vliet, J., Deetman, S., Isaac, M., Klein Goldewijk, K., Hof, A., Mendoza Beltran, A., Oostenrijk, R., and van Ruijven, B.: RCP2.6: exploring the possibility to keep global mean temperature increase below 2 °C, Climatic Change, 109, 95–116, https://doi.org/10.1007/s10584-011-0152-3, 2011a.

van Vuuren, D. P., Edmonds, J., Kainuma, M., Riahi, K., Thomson, A., Hibbard, K., Hurtt, G. C., Kram, T., Krey, V., Lamarque, J.-F., Masui, T., Meinshausen, M., Nakicenovic, N., Smith, S. J., and Rose, S. K.: The representative concentration pathways: an overview, Climatic Change, 109, 5–31, https://doi.org/10.1007/s10584-011-0148-z, 2011b.

Wang, W., Bruyère, C., Duda, M., Dudhia, J., Gill, D., Kavulich, M., Keene, K., Lin, H.-C., Michalakes, J., Rizvi, S., Zhang, X., Berner, J., and Smith, K.: WRF ARW Version 3 Modeling System User's Guide, 1–428, https://doi.org/10.1525/jps.2007.37.1.204, 2015.

Werner, M., Tegen, I., Harrison, S. P., Kohfeld, K. E., Prentice, I. C., Balkanski, Y., Rodhe, H., and Roelandt, C.: Seasonal and interannual variability of the mineral dust cycle under present and glacial climate conditions, J. Geophys. Res., 107, 4744, https://doi.org/10.1029/2002JD002365, 2002.

Wild, M.: Global dimming and brightening: A review, J. Geophys. Res., 114, D00D16, https://doi.org/10.1029/2008JD011470, 2009.

Woodward, S., Roberts, D. L., and Betts, R. A.: A simulation of the effect of climate change-induced desertification on mineral dust aerosol, Geophys. Res. Lett., 32, L18810, https://doi.org/10.1029/2005GL023482, 2005.

Young, P. J., Arneth, A., Schurgers, G., Zeng, G., and Pyle, J. A.: The CO_2 inhibition of terrestrial isoprene emission significantly affects future ozone projections, Atmos. Chem. Phys., 9, 2793–2803, https://doi.org/10.5194/acp-9-2793-2009, 2009.

Young, P. J., Archibald, A. T., Bowman, K. W., Lamarque, J.-F., Naik, V., Stevenson, D. S., Tilmes, S., Voulgarakis, A., Wild, O., Bergmann, D., Cameron-Smith, P., Cionni, I., Collins, W. J., Dalsøren, S. B., Doherty, R. M., Eyring, V., Faluvegi, G., Horowitz, L. W., Josse, B., Lee, Y. H., MacKenzie, I. A., Nagashima, T., Plummer, D. A., Righi, M., Rumbold, S. T., Skeie, R. B., Shindell, D. T., Strode, S. A., Sudo, K., Szopa, S., and Zeng, G.: Preindustrial to end 21st century projections of tropospheric ozone from the Atmospheric Chemistry and Climate Model Intercomparison Project (ACCMIP), Atmos. Chem. Phys., 13, 2063–2090, https://doi.org/10.5194/acp-13-2063-2013, 2013.

Zhang, Q. J., Beekmann, M., Drewnick, F., Freutel, F., Schneider, J., Crippa, M., Prevot, A. S. H., Baltensperger, U., Poulain, L., Wiedensohler, A., Sciare, J., Gros, V., Borbon, A., Colomb, A., Michoud, V., Doussin, J.-F., Denier van der Gon, H. A. C., Haeffelin, M., Dupont, J.-C., Siour, G., Petetin, H., Bessagnet, B., Pandis, S. N., Hodzic, A., Sanchez, O., Honoré, C., and Perrussel, O.: Formation of organic aerosol in the Paris region during the MEGAPOLI summer campaign: evaluation of the volatility-basis-set approach within the CHIMERE model, Atmos. Chem. Phys., 13, 5767–5790, https://doi.org/10.5194/acp-13-5767-2013, 2013.

CHAPTER

VI

Importance of organic aerosol simulation scheme on particulate matter concentrations in climate projections

Contents

1 Summary of article **164**

2 Importance of organic aerosol simulation scheme for particulate matter concentrations in climate projections **166**

3 Abstract **167**

4 Introdution **167**

5 Simulations **169**

5.1 CHIMERE chemistry transport model 169

5.2 OA schemes used for the simulations 169

5.3 Choice of years 170

6 Scheme validation **170**

7 Analysis of the simulations **172**

7.1 Changes in biogenic emissions 172

7.2 European region 173

7.3 Mediterranean region 175

8 Sensitivity of different schemes to temperature changes **177**

9 Conclusions **178**

10 References **181**

In the previous chapter, the future conditions of the Mediterranean region regarding to the changes imposed by different factors were discussed. Many different factors can affect the behavior of each region to climate change, we focused on the climate, long-range transport and anthropogenic emissions previously. Since the Mediterranean region experiences a high burden of aerosols, we concentrated on the changes in PM concentration and also the concentration of its different components when faced with climate change. The results suggested that climate change can cause an increase in the concentration of BSOA, therefore increasing the total concentration of OA in general. This is because an increase in temperature results in an increased emission of BVOCs, major precursors of BSOA. However, the scheme used for the simulation of BSOA can affect its concentration as shown in chapter IV. Therefore, it is interesting to explore the effects of changing this module along with the the drivers mentioned in the previous section. The goal to this section is to see the effects (if any) of changing the scheme used for the simulation of OA to the future concentration of OA and the changes that is seen for each scheme in future scenarios.

1 Summary of article

There are many different schemes that can be used for this purpose in a CTM, some of them were introduced in chapter II. Pun and Seigneur (2007) suggested a molecular single-step oxidation scheme for the formation of SOA. Another possibility is the VBS scheme which includes different volatility bins with interactions among themselves (Donahue, Robinson, et al. 2006; Robinson, Donahue, M. K. Shrivastava, et al. 2007). This scheme includes functionalization for ASOA and BSOA, but fragmentation processes and the formation of non-volatile SOA are not implemented in it. If these two processes were to be added to the basic VBS scheme, the results would be what was proposed by M. Shrivastava, Easter, et al. (2015).

In order to explore the aforementioned hypothesis, a series of historic and future simulations are performed using three different OA simulation schemes. The tested schemes include the three of the four schemes explored in chapter IV: the molecular single scheme (called hereafter SOA2p), the standard VBS scheme without biogenic aging (called hereafter SOAvbs) and the modified VBS scheme containing functionalization, fragmentation and formation of non-volatile SOA (called hereafter SOAmod). Each of these methods has its own merits and also disadvantages. In most future scenarios, a two-product scheme or a molecular single step oxidation scheme is used for the simulation of SOA. While these schemes certainly have their merits (such as simplicity and low computing requirements), other schemes, such as some variations of the VBS scheme, better represent more complex characteristics of SOA, such as its continuous aging.

An evaluation of these schemes is included in this chapter, where a year-long simulation was compared to measurements for the year of 2013. This year was chosen for this purpose since an abundance of measurements for OA are available for this period.

Comparisons for a list of around 30 stations in the European area show 0.42$\mu g.m^{-3}$, 0.64 $\mu g.m^{-3}$ and -0.4$\mu g.m^{-3}$ for the three schemes with a correlation of 0.65, 0.61 and 0.65 respectively. The performance of all schemes is acceptable for this period of time according to the goals and criteria presented by Boylan and Russell (2006).

Long computational times when using the VBS-based schemes make it difficult to simulate long periods of scenarios using these methods, therefore a procedure has to be put into place in order to choose a list of years to simulate for this schemes. Only 10 years of simulations for each scheme can be simulated, five historic simulations and five future scenarios. Using the series of scenarios examined in the previous chapter (see chapter V) using the molecular single-step scheme, an analysis of BSOA and temperature was done for 30 year historic simulations and 70 year future scenarios. For future scenarios, five years were chosen that show the highest BSOA concentration and the highest temperature at the same time, for the historic simulations the years representing the exact opposite conditions were chosen. This analysis was done in an effort to maximize the changes seen between future and historic simulations, therefore, RCP8.5 future scenarios were used. For the simulations for each scheme, only the OA simulation scheme and the regional climate change, the other factors (anthropogenic emissions, boundary conditions, etc.) remain the same.

The analysis of the changes for the European area shows that the modified VBS scheme simulates higher changes in future scenarios compared to historic simulations in summertime (around 122%, 149% and 244% for SOA2p, SOAvbs and SOAmod respectively for the European region). This is due to the increase in BVOC emissions because of the dependence of BVOCs to temperature.

Simulations with the SOAmod scheme show BSOA increases more similar to the BVOC emissions increases, because it includes SVOC aging and formation of non-volatile SOA. On the contrary, in SOA2p and SOAvbs, no aging of biogenic SVOCs is included, so their temperature induced partial shift to gas phase offsets the increase in BVOC emissions to a certain degree. For the Mediterranean area, changes of 80%, 79% and 120% for SOA2p, SOAvbs and SOAmod respectively are seen for summer. This is again, because of the possibility of formation of more aged OA particles in the SOAmod scheme, which makes it possible for more OA aerosols to be transported towards the basin since most of the BSOA that exists in the basin has been transported from the European region towards this area.

In the next chapter (chapter VII) all these points are combined in a regional exploration of the Mediterranean coastline of France (the PACA region) in order to analyze the exposure of the population living in this area to climate change and changes of concentration of atmospheric pollutants and also population changes in future scenarios.

2 Importance of organic aerosol simulation scheme for particulate matter concentrations in climate projections

This chapter includes the article Cholakian et al. (2019b) published in *Atmospheric Chemistry and Physics : "Biogenic secondary organic aerosol sensitivity to organic aerosol simulation schemes in climate projections, 13209–13226, doi:10.5194/acp-19-13209-2019, url: Atmospheric chemistry and physics"*.

The article was published the 25 October 2019.

Atmos. Chem. Phys., 19, 13209–13226, 2019
https://doi.org/10.5194/acp-19-13209-2019
© Author(s) 2019. This work is distributed under
the Creative Commons Attribution 4.0 License.



Atmospheric Chemistry and Physics Open Access EGU

Biogenic secondary organic aerosol sensitivity to organic aerosol simulation schemes in climate projections

Arineh Cholakian[1,2,a], **Matthias Beekmann**[1], **Isabelle Coll**[1], **Giancarlo Ciarelli**[1,b], **and Augustin Colette**[2]

[1]LISA, UMR CNRS 7583, Université Paris Est Créteil et Université de Paris,
Institut Pierre Simon Laplace (IPSL), Créteil, France
[2]Institut National de l'Environnement Industriel et des Risques, Parc Technologique ALATA, Verneuil-en-Halatte, France
[a]now at: EPOC, UMR 5805, Université de Bordeaux, Pessac, France
[b]now at: Department of Chemical Engineering, Carnegie Mellon University, Pittsburgh, USA

Correspondence: Arineh Cholakian (arineh.cholakian@lisa.u-pec.fr)

Received: 10 April 2019 – Discussion started: 11 June 2019
Revised: 30 September 2019 – Accepted: 5 October 2019 – Published: 25 October 2019

Abstract. Organic aerosol (OA) can have important impacts on air quality and human health because of its large contribution to atmospheric fine aerosol and its chemical composition, including many toxic compounds. Simulation of this type of aerosol is difficult, since there are many unknowns in its nature and mechanism and processes involved in its formation. These uncertainties become even more important in the context of a changing climate because different mechanisms, and their representation in atmospheric models, imply different sensitivities to changes in climate variables. In this work, the effects caused by using different schemes to simulate OA are explored. Three schemes are used in this work: (1) a molecular scheme; (2) a standard volatility basis set (VBS) scheme with anthropogenic aging; and (3) a modified VBS scheme containing functionalization, fragmentation and formation of nonvolatile secondary organic aerosol (SOA) for all semi-volatile organic compounds (SVOCs). Five years of historic and five years of future simulations were performed using the RCP8.5 climatic scenario. The years were chosen in a way to maximize the differences between future and historic simulations. The study focuses on biogenic SOA (BSOA), since the contribution of this fraction of BSOA among OA is major in both historic and future scenarios (40 % to 78 % for different schemes in historic simulations). Simulated OA and BSOA concentrations with different schemes are different, with the molecular scheme showing the highest concentrations among the three schemes. The comparisons show that for the European area, the modified VBS scheme shows the highest relative change between future and historic simulations, while the molecular scheme shows the lowest (a factor of 2 lower). These changes are largest over the summer period for BSOA because the higher temperatures increase terpene and isoprene emissions, the major precursors of BSOA. This increase is partially offset by a temperature-induced shift of SVOCs to the gas phase. This shift is indeed scheme dependent, and it is shown that it is the least pronounced for the modified VBS scheme including a full suite of aerosol aging processes, comprising also formation of nonvolatile aerosol. For the Mediterranean Sea, without BVOC emissions, the OA changes are less pronounced and, at least on an annual average, more similar between different schemes. Our results warrant further developments in organic aerosol schemes used for air quality modeling to reduce their uncertainty, including sensitivity to climate variables (temperature).

1 Introduction

Organic aerosol (OA) is an important fraction of fine particulate matter (PM) concentrations. Its production results from both primary emissions of organic aerosols as well as secondary formation from semi-volatile or polar precursor gases in the atmosphere. The mechanisms and pathways of secondary organic aerosol (SOA) formation are in general highly uncertain (Hallquist et al., 2009; Tsimpidi et al., 2017). However, the importance of the concentrations of OA in the atmosphere (Jimenez et al., 2009) and their adverse ef-

fects on human health (Mauderly and Chow, 2008; Lelieveld et al., 2015) make them an important subject to study.

Considering that modeling OA already contains important uncertainties, the uncertainties become even more important for future climate scenarios which account for climate change. These future scenarios present an important number of uncertainties not only due to climate-related parameters but also to the description of how they act on specific processes. As an example, biogenic volatile organic compound (BVOC) emissions, which are the main precursors of biogenic SOA (BSOA), can be affected by, for example, temperature and land use changes, CO_2 inhibition (Heald et al., 2008a), or other factors. Many studies have addressed the effects of these parameters on the BVOC emissions, and a high variability was found in BVOC emissions depending on the factors that were considered in each study. For example, Heald et al. (2009) explored the effects of land use change and CO_2 inhibition on the emission of BVOCs, and they found a 130 % increase in isoprene emission in 2100 compared to 2000, while Pacifico et al. (2012) and Hantson et al. (2017) show a 70 % and 41 % increase for isoprene for the same years with different parameters. Langner et al. (2012) compares four different models for the European region, reporting an isoprene increase in the range of 21 %–26 %. Cholakian et al. (2019), found an increase of 52 % for isoprene for the period of 2031–2100 compared to 1976–2005 because of only temperature change for Europe, amounting to a 12 % increase in BSOA concentrations.

In addition, for the formation of anthropogenic SOA (ASOA), future urbanization, anthropogenic emission and wood-burning emission changes can be mentioned as possible factors. Each one of these parameters represents an uncertainty, which, when coupled with the inherent uncertainty in the simulation of OA, can present important sources of error.

It is mainly to assess the future evolution of tropospheric ozone that BVOC emissions have been quantified at the global scale in chemistry-climate projections (Arneth et al., 2010). Their importance for organic aerosol chemistry has also been considered in global- and regional-scale atmospheric models (Maria et al., 2004; Tsigaridis et al., 2007; Heald et al., 2008b) but to a lesser degree. Several different types of OA simulation schemes can be used in chemistry-transport models (CTMs). Odum et al. (1997) suggested a two-product scheme, where he calculated yields of production of OA from volatile organic compounds (VOCs) from laboratory data. He concluded that two virtual semi-volatile organic compounds were sufficient to represent the formation of OA. Following the partitioning theory of Pankow (1994), these species are distributed between the aerosol and gas phases. Pun and Seigneur (2007) suggested a molecular single-step oxidation scheme for the formation of SOA, based on the Odum scheme. Another approach is the volatility basis set (VBS) scheme, which includes different volatility bins and aging of semi-volatile species, lowering their volatility (Donahue et al., 2006; Robinson et al., 2007). This scheme presents two major versions: one-dimensional (1-D) and two-dimensional (2-D) VBS. 1-D VBS distributes semi-volatile organic compounds (SVOCs) into different bins with regard to their volatility (Robinson et al., 2007). A 2-D VBS scheme takes into account the oxygen-to-carbon (O / C) ratio as well as the volatility (Donahue et al., 2011, 2012). While the 1-D VBS has been tested extensively in different CTMs (i.e Lane et al., 2008; Hodzic and Jimenez, 2011; Zhang et al., 2013; Cholakian et al., 2018), the use of the 2-D VBS is less frequent because of its even more challenging numerical needs. Other variations in the 1-D VBS have been also used for observation–simulation comparisons, each one adding some variables to the basic VBS scheme or building upon its framework. For example, Shrivastava et al. (2015) add fragmentation and formation of nonvolatile SOA mechanisms to the basic 1-D VBS scheme. This scheme was implemented into the CHIMERE chemistry-transport model (CTM) and tested for the Mediterranean region, with good results in terms of the concentration (correlation of 0.55 and a bias of $-0.68\,\mu g\,m^{-3}$ for the summer period of 2013), fossil and non-fossil distribution, and oxidation level of OA (Cholakian et al., 2018). Besides this, Lannuque et al. (2018) provide a new parameterization for the VBS scheme by using a box model based on the GECKO-A modeling tool, which was later implemented in CHIMERE and tested for the European continent, showing a good correspondence between modeled and measured OA (Lannuque et al., 2019).

In addition, the sensitivity of OA schemes to thermodynamic parameters could show large differences due to different processes considered or due to the differences in the parameterization. The formation and partitioning of particulate OA can show various degrees of dependency on temperature in different OA schemes. Therefore, the sensitivity of organic aerosol to climate change, affecting these thermodynamic parameters (mainly temperature), also depends on the OA scheme used. To our knowledge, this issue has not yet been addressed in a dedicated work. In most future scenarios, a two-product scheme is used for the simulation of SOA. However, other schemes, such as different variations in the VBS scheme, could better represent the more complex characteristics of SOA, such as, for example, its oxidation state.

Differences induced by different schemes are also expected to vary regionally, depending on the concentration ranges encountered and ranges and changes in meteorological parameters. In this study, we focus on the European continent and the Mediterranean Basin. The Mediterranean Basin is one of the most sensitive regions to climate change, which makes it important and at the same time interesting to study. However, not much focus has placed on the Mediterranean in the literature, especially on the western side of this basin (Giorgi, 2006). For this reason, the ChArMEx project was put into place in order to study the current chemical characteristics of the atmosphere of the Mediterranean region and its changes in future scenarios.

In this study, future OA concentrations under a climate-change scenario will be quantified using different OA schemes. Three OA simulation schemes are compared, namely (i) a two-product scheme, (ii) a VBS scheme with anthropogenic aging, and (iii) a modified VBS scheme including fragmentation and nonvolatile SOA formation. A representative concentration pathway (RCP) climatic scenario was used. RCP8.5 was chosen in order to maximize future changes and to get a clear climate-change-related signal in our study.

The paper is organized as follows: Section 2 explains the modeling framework for this work. An evaluation of the three schemes against measurements is provided in Sect. 3, while Sect. 4 presents results for the different scenarios. Conclusions are presented in Sect. 5.

2 Simulations

The modeling framework in this study utilizes a chain of models, covering the different compartments of the atmosphere and a global circulation model and a global chemistry-transport model, providing meteorological and chemical conditions of the atmosphere respectively (Fig. 1). In order to downscale the output provided by the global models, a regional climate model and a regional chemistry-transport model are used (Fig. 1). Global circulation data are provided by IPSL-CM5A-MR (Taylor et al., 2012; Dufresne et al., 2013; Young et al., 2013), while the LMDZ-INCA (Hauglustaine et al., 2014) global chemistry-transport model, using simulations from the global circulation model as meteorological input, provides boundary conditions for the regional chemistry-transport model (CTM). The boundary conditions include inputs for organic carbon as well. The global circulation model also provides boundary conditions for the regional climate model, WRF (Weather Research and Forecasting; Wang et al., 2015), which in turn provides meteorological input fields for the regional CTM, CHIMERE (Menut et al., 2013). The WRF simulations were prepared for the EURO-CORDEX project (Jacob et al., 2014) and use RCPs (Meinshausen et al., 2011; van Vuuren et al., 2011) for future simulations. The EURO-CORDEX climatic runs were performed for the period of 1976–2005 for historic simulations and 2031–2100 for future scenarios, for RCP2.6, RCP4.5 and RCP8.5. A detailed analysis of these runs is provided in Vautard et al. (2014) and Jacob et al. (2014). In this work, the RCP8.5 runs are used for a selection of years (Sect. 2.3). Anthropogenic emissions (base year 2010) are taken from the ECLIPSEv4a inventory (Amann et al., 2013; Klimont et al., 2013, 2017), and the biogenic emissions are calculated with MEGAN (Model of Emissions of Gases and Aerosols from Nature; Guenther et al., 2006). The coupling of all these models with the CHIMERE model is done in an offline fashion, except for MEGAN, which is directly coupled with CHIMERE. Since the focus of this article is on the SOA scheme changes in the regional CTM, only this model will be discussed in further detail. More information on the modeling framework in the current study is provided in Colette et al. (2013, 2015).

2.1 CHIMERE chemistry-transport model

The CHIMERE chemistry-transport model has been widely used in different parts of the world (Carvalho et al., 2010; Hodzic and Jimenez, 2011), especially in Europe (Zhang et al., 2013; Petetin et al., 2014; Colette et al., 2015; Menut et al., 2015; Rea et al., 2015), for both forecasting and analysis purposes. It provides a wide range of capabilities; if input information such as anthropogenic and biogenic emissions or meteorological conditions are given, it can simulate an exhaustive list of atmospheric components. Different chemistry schemes are available in the model; in the case of our simulations, the MELCHIOR2 scheme (Derognat et al., 2003) is used, containing around 120 reactions. A sectional logarithmic aerosol size distribution of 10 bins is used, with a range of 40 nm to 40 µm. The aerosol module in CHIMERE includes different chemical and physical processes such as gas–particle partitioning, coagulation, nucleation, condensation, and dry and wet deposition. The chemical speciation contains EC (elemental carbon), sulfate, nitrate, ammonium, SOA and SVOC species, dust, salt, and PPM (primary particulate matter other than that mentioned above). More information on the SOA scheme will be provided in the next section. The simulation domain covers all of Europe with a resolution of 0.44°; the domains used in all the simulations are all the same (the domain approximately covers 30–70° N and 40° W–60° E).

2.2 OA schemes used for the simulations

The CHIMERE model has three SOA simulation schemes with different levels of complexity, all based on a molecular single-step oxidation scheme. In our base simulations, the medium complexity scheme is used (Bessagnet et al., 2008). In this scheme, lumped VOCs can react and form classes of organics with reduced volatility, i.e., SVOCs. Once formed, the model distributes these species between the gaseous and particulate phases according to the mixing theory of Pankow (1987). The yields for the formation of SOA are taken from Odum et al. (1997), Griffin et al. (1999), and Pun and Seigneur (2007). This scheme is referred to as the SOA2p scheme hereafter. A large database of historic and future simulations exists for this scheme, for three RCPs (RCP2.6, RCP4.5 and RCP8.5), each containing 70 years of simulation (2031–2100) and 30 years (1976–2005) of historic simulations. These scenarios are discussed and compared in Colette et al. (2013), Lemaire et al. (2016) and Cholakian et al. (2019) in more detail.

The VBS approach was developed as a general framework to account for the semi-volatile character of organic

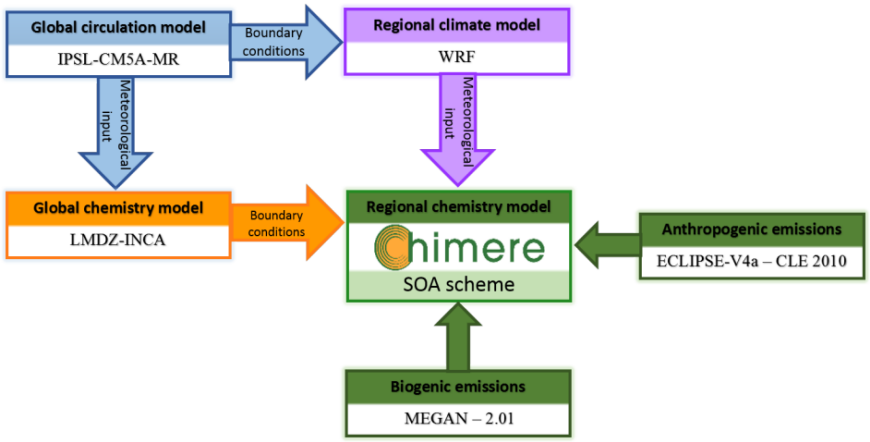


Figure 1. Simulation chain used for this study: the focus of this work is the SOA scheme inside the regional chemistry-transport model.

matter and to allow for changes in volatility over time. In VBS schemes, the SVOCs are partitioned into bins according to their saturation concentrations. Aging processes were included by transferring species from one volatility bin to another (Robinson et al., 2006). This scheme was implemented into CHIMERE and tested for Mexico City (Hodzic and Jimenez, 2011) and the Paris region (Zhang et al., 2013). Nine volatility bins with saturation concentrations in the range of 0.01 to $10^6\,\mu g\,m^{-3}$ are taken into account, and the emissions of SVOCs and IVOCs (intermediate volatility organic compounds) are distributed into these bins using the aggregation proposed by Robinson et al. (2007). Four volatility bins are used for ASOA and BSOA, ranging from 1 to $1000\,\mu g\,m^{-3}$. Since the aging processes of biogenic SOA were reported to overestimate the BSOA concentrations in CTM runs for North America (Robinson et al., 2007; Lane et al., 2008) and the Mediterranean Sea (Cholakian et al., 2018), these processes are not taken into account in this work. Gas–particle partitioning is treated following Raoult's law and depends on total organic aerosol concentrations.

Since the standard VBS scheme does not include fragmentation processes (when molecules break into smaller and more-volatile molecules in the atmosphere) explicitly and the formation of nonvolatile SOA (when SOA, after its formation, becomes irreversibly nonvolatile and therefore cannot be oxidized further), these processes were added to the basic VBS scheme following Shrivastava et al. (2011, 2013, 2015). Another change made to the VBS scheme was to include an interpolation between high-NO_x and low-NO_x regimes (Carlton et al., 2009). Reaction rates for the common species (and generations) do not change between these two schemes, and reaction rates for new species and generations are taken from Shrivastava et al. (2013). The aging processes are all turned on in the modified VBS scheme, and two more oxidation generations are added to primary organic aerosol (POA). BSOA oxidation generation is kept the same (one generation of oxidation). The formation of nonvolatile SOA is added to all the SOA oxidized species (excluding POA), forming a nonvolatile SOA which cannot return to the gaseous phase. The same fragmentation fractions reported by Shrivastava et al. (2015) are used without any change.

Both the standard VBS without biogenic aging (referred to as SOAvbs scheme hereafter) and the modified VBS including fragmentation and formation of nonvolatile aerosol (referred to as SOAmod scheme hereafter) schemes are presented in more detail and compared to experimental data in the western Mediterranean area in Cholakian et al. (2018). In the aforementioned work, it was concluded that these two schemes can reproduce the levels of concentration of organic aerosols in the Mediterranean Basin successfully in regard to concentration of OA, while the oxidation state and fossil and non-fossil repartition is better represented in SOAmod.

2.3 Choice of years

The SOAvbs and the SOAmod schemes are both numerically very resource-consuming; therefore, only 10 years of simulations for each scheme were performed. In order to choose the appropriate years for the simulation, existing long-term sets of simulations were used, containing 30 years of historic simulations (1976–2005) and 70 years of future scenarios (2031–2100). We address results for BSOA, as it makes the major contribution to OA during summer (between 40 % and 78 % for different schemes in the historic scenario, according to our simulation results for the historic period with differences schemes; not shown in figures).

The simulations were performed using the previous version of CHIMERE (CHIMERE 2013b; Menut et al., 2013), the SOA2p scheme and the RCP8.5 scenario. This dataset was used to choose five years of simulations in the historical and future periods each, with the aim of maximizing both the temperature and SOA differences between historic and future

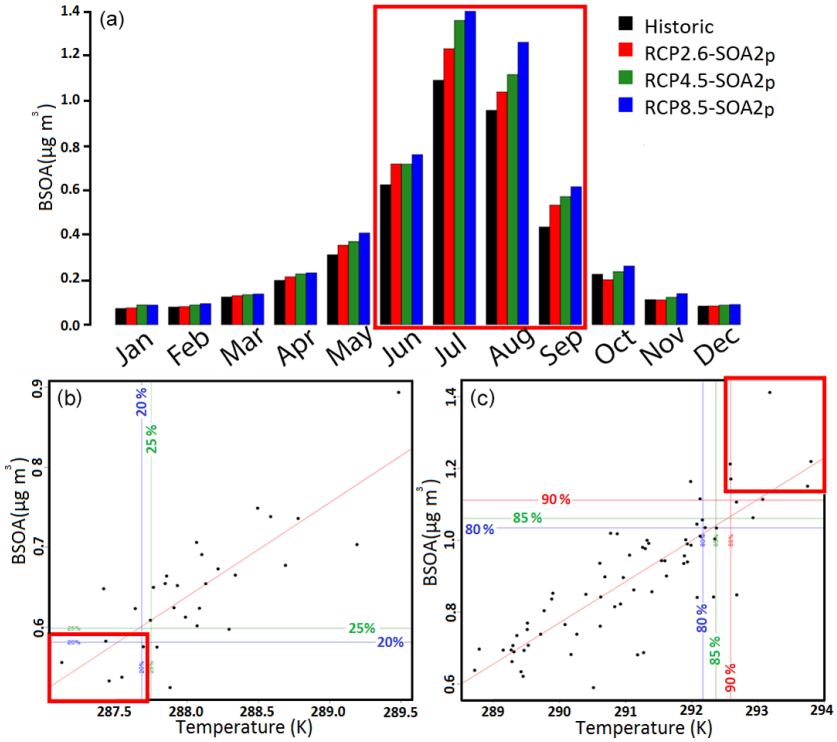


Figure 2. Monthly BSOA concentrations in different RCP scenarios, averaged over 70 years of simulations for future scenarios and 30 years for historic simulations **(a)**. BSOA for the June to September period highlighted in **(a)** was plotted against temperature, and years with the lowest temperature and lowest BSOA concentrations for historic simulations are shown in **(b)**. Those with the highest temperature and BSOA concentrations for future scenarios are shown in **(c)**.

scenarios. Figure 2a shows the monthly average of BSOA concentrations in different RCP scenarios, showing that the production of BSOA reaches its maximum in the period of 4 months of June, July, August and September. During these months BSOA is the major SOA and OA component over Europe, as also discussed in Cholakian et al. (2019).

Figure 2a also shows that the differences of historic and future simulations reach their maximum for RCP8.5 simulations. The concentration of BSOA and the temperature both in historic and RCP8.5 simulations show a strong positive correlation, as seen in Fig. 2b and c, with each point representing the average of the 4 months mentioned previously for 1 year.

For historic simulations, the years representing the lowest temperature and BSOA concentrations are used, which correspond to the years 1980, 1981, 1984, 1985 and 1986, while for future scenarios the years with the highest temperature and BSOA concentrations are used, corresponding to the years 2087, 2092, 2093, 2095 and 2098.

3 Scheme validation

The three schemes show high variability when simulating the concentration and characteristics of OA; therefore, we performed an evaluation to investigate their performances. The schemes are compared to observations for the year 2013, during which an abundance of observational data are available. A year-long simulation for the year 2013 was performed for each of the schemes. The inputs used in these simulations are the same: anthropogenic emissions are taken from EMEP (European Monitoring and Evaluation Programme; http://www.ceip.at, last access: 15 May 2019), meteorological fields are generated using the ECMWF (European Centre for Medium-Range Weather Forecasts) input data (Berrisford et al., 2011), biogenic emissions are provided by MEGAN (Guenther et al., 2006), and boundary and initial conditions are taken from LMDZ-INCA (Hauglustaine et al., 2014).

The observations are mostly accessed from the EBAS database (http://ebas.nilu.no/, last access: 14 June 2019; Tørseth et al., 2012). The used measurements are mostly $PM_{2.5}$ and, in some cases, PM_1. For each type of measurement ($PM_{2.5}$ or PM_1), the corresponding fraction from the simulations was used. In some cases, data were pro-

vided by the lead investigator for a specific station, and the measurements for the two stations of Corsica and Mallorca were added using the ChArMEx (http://mistrals.sedoo.fr/ChArMEx/, last access: 13 April 2019) campaign measurements. In total, 32 stations are compared to simulations. Bear in mind that for some of these stations the available data cover a shorter period than 1 year, or they present weekly measurements rather than daily observations. The list of stations with information about each station and the type of measurement is provided in Appendix A.

Results of these comparisons are shown in Fig. 3, and the statistical information is shown in Table 1. Regarding the concentration of OA, the modified VBS scheme shows a stronger bias ($-0.64\,\mu g\,m^{-3}$ compared to 0.42 and $0.1\,\mu g\,m^{-3}$ for SOAvbs and SOA2p respectively) for the summer period. All compared schemes underestimate the winter period (-1.45, -1.67 and $-1.63\,\mu g\,m^{-3}$ for SOAmod, SOAvbs and SOA2p respectively). The annual biases for the three schemes are -0.91, -0.4 and $-0.65\,\mu g\,m^{-3}$ for SOAmod, SOAvbs and SOA2p respectively. The correlation of determination between observed and simulated OA concentrations for different schemes is the highest for the SOAmod and lowest for the SOAvbs in most seasons; it should also be noted that the differences between the correlations seen for each scheme are rather small (difference of below 0.05). The Taylor diagram in Fig. 3 shows the comparisons of different stations to simulations for each scheme (black for SOA2p, green for SOAmod and red for SOAvbs). The Taylor diagram summarizes some statistical information in one plot: the correlation coefficient, root-mean-square (RMS) difference between observations and simulations, and the standard deviation ratio can be seen. More information about the construction of this diagram is given in Taylor (2001). As seen in this diagram, there is a high variability in the simulation of different stations, and some stations are better represented by the model than the others. This might be because of the geographical placement (altitude, types of emissions in that location, etc.) of stations or because of the nature of the station (urban, rural, etc.).

The three schemes perform reasonably well according to the criteria introduced by Boylan and Russell (2006), with the values for all the schemes falling into in zone 1 for both mean fractional bias (MFB) and mean fractional error (MFE). The goal for these two metrics according to the aforementioned reference is less than or equal to $\pm 30\,\%$ and $+50\,\%$, and the criteria are less than or equal to $\pm 60\,\%$ and $+75\,\%$ respectively. The MFB values for the three schemes are $-19.7\,\%$, $16.5\,\%$ and $26.9\,\%$, while MFE shows $47.9\,\%$, $51.1\,\%$ and $47.2\,\%$ for SOA2p, SOAvbs and SOAvbs respectively. Thus, performance goals are met for nearly all schemes, with a slight exceedance for MFE and the SOAvbs scheme still meeting the criteria. Each one of the schemes performs better for a specific period; the modified VBS performs better in summer, the CHIMERE standard scheme performs better during winter, and the standard VBS scheme shows average performance during the whole year. Looking at Table 1, it is seen that, for example, for the summer period, the SOAmod scheme shows the highest correlation of determination, while SOA2p shows the lowest bias for this season. For spring, SOA2p shows the highest R^2, while SOAvbs shows the lowest bias. For winter and autumn, the performance of the schemes is quite similar. Annually, SOAvbs presents a similar correlation to SOA2p while showing the lowest bias in general. The types of stations have not been filtered in the current study; therefore, all stations, including urban, semi-rural or rural, have been included for the comparisons. This could be responsible for part of the observed negative bias. In conclusion, all three schemes correspond to the performance goals and/or criteria of Boylan and Russell (2006), albeit they show important, and spatially and seasonally dependent, differences with observations. Thus, the three schemes will be retained for the following analysis with equal confidence.

4 Analysis of the simulations

The analysis of the simulations will be presented in the next two sub-sections. First, the changes in BVOC emissions are discussed. Subsequently, the results for the European continent regarding concentration, origins and the oxidation state will be presented. An analysis of these parameters will be performed for the Mediterranean sub-domain, including their origins and the oxidation state. Finally, a general comparison of the spatial distribution will be performed for different schemes. It is important to keep in mind that from this section on, whenever BSOA concentrations are discussed, the PM_1 fraction of this species is used.

4.1 Changes in biogenic emissions

The changes in biogenic emissions are important in the context of this work, since they are highly dependent on temperature changes. For the simulations presented in this work, the biogenic emissions do not change between different schemes; however they change quite a bit between historic and future simulations because of temperature increase in the future. Since the choice of the years was done to maximize future temperature changes, the differences between future and historic simulations are quite remarkable. For the European region, the average historic isoprene emissions are 1.3×10^{11} molecules $cm^{-2}\,yr^{-1}$, and average historical terpene emissions are 3×10^{10} molecules $cm^{-2}\,yr^{-1}$. An increase of 88 % and 82 % for isoprene and terpenes is seen respectively in the future scenarios in response to an average temperature increase of 5.5 °C. For the summer period, the biogenic emission increase raises to 93 % and 92 % for isoprene and terpenes for a temperature increase of 6.4 °C (Fig. 6). The correlation of determination between historic

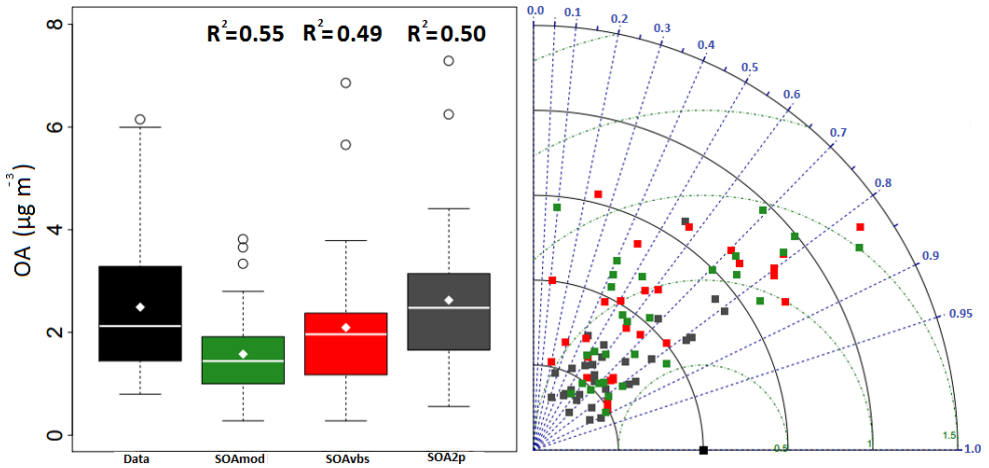


Figure 3. Observation–simulation comparisons for different schemes: the boxplots are presented for the data and the schemes for the annual averages, and the correlation of determination for each scheme is shown above each boxplot. The point on the boxplot shows the average value. Each point in the Taylor diagram shows one station, while each color shows one scheme (black – SOA2p, red – SOAvbs – and green – SOAmod). Table 1 shows statistical information for observed data and the three studied schemes.

Table 1. Statistical information for different schemes in regard to measurements. In this table are the average for the data and each scheme, the bias, standard deviation and root-mean-square error (RMSE; all in $\mu g\,m^{-3}$). R^2 shows the correlation of determination for each scheme. Figure 3 shows the Taylor diagram and the boxplots for these comparisons.

		Average	Bias	Standard deviation	RMSE	R^2
			($\mu g\,m^{-3}$)			
Annual	Data	2.49		0.36		
	SOA2p	1.84	−0.64	1.40	2.21	0.49
	SOAvbs	2.1	−0.4	1.62	2.44	0.50
	SOAmod	1.58	−0.91	1.05	2.11	0.55
DJF	Data	2.55		1.79		
	SOA2p	0.91	−1.63	0.50	2.47	0.51
	SOAvbs	0.89	−1.67	0.65	2.63	0.51
	SOAmod	1.11	−1.45	0.75	2.55	0.56
MAM	Data	2.11		1.33		
	SOA2p	1.88	−0.23	1.3	1.81	0.56
	SOAvbs	2.23	0.11	1.42	1.98	0.50
	SOAmod	1.4	−0.71	0.84	1.64	0.49
JJA	Data	2.48		1.12		
	SOA2p	2.56	0.1	1.71	2.06	0.51
	SOAvbs	2.9	0.42	1.91	2.31	0.54
	SOAmod	1.83	−0.65	1.17	1.69	0.58
SON	Data	2		1.36		
	SOA2p	1.16	−0.84	0.81	1.81	0.47
	SOAvbs	1.28	−0.72	0.92	1.85	0.47
	SOAmod	1.3	−0.7	0.81	1.76	0.45

isoprene and terpene emissions is 0.6 and 0.63, while this correlation is 0.65 and 0.57 for the future simulations.

For the Mediterranean Sea, there are no local biogenic emissions included in the model.

4.2 European region

4.2.1 Changes in BSOA concentration

BSOA concentrations in future scenarios are predicted to increase in all the schemes. However, the intensity of this increase is scheme dependent: while for SOA2p an annually averaged increase of +61 % is calculated, this percentage rises to +80 % for SOAvbs and +98 % for SOAmod for the same period. These changes show that the climate impact on changes of BSOA in the future might have been underestimated until now on a relative scale. This is because most of the future simulations performed in order to explore climate impact use a two-product or a molecular single-step scheme for the simulation of SOA. However, our study shows that using a VBS-based scheme increases the climate-induced effect on the change in BSOA concentration in the future. Reasons for this behavior will be discussed in Sect. 5. However, we would like to emphasize that changes are maximized by the choice of the RCP8.5 scenario and the years chosen for the simulations in this work. Also, it should be noted that there are important differences in absolute concentrations between different schemes (see above).

There is a strong seasonality for the BSOA production. The seasonal changes for BSOA are seen in Fig. 4a1, b1 and c1 for historic simulations, the absolute difference between future and historic simulations, and their relative changes respectively. Summer shows the maximum rela-

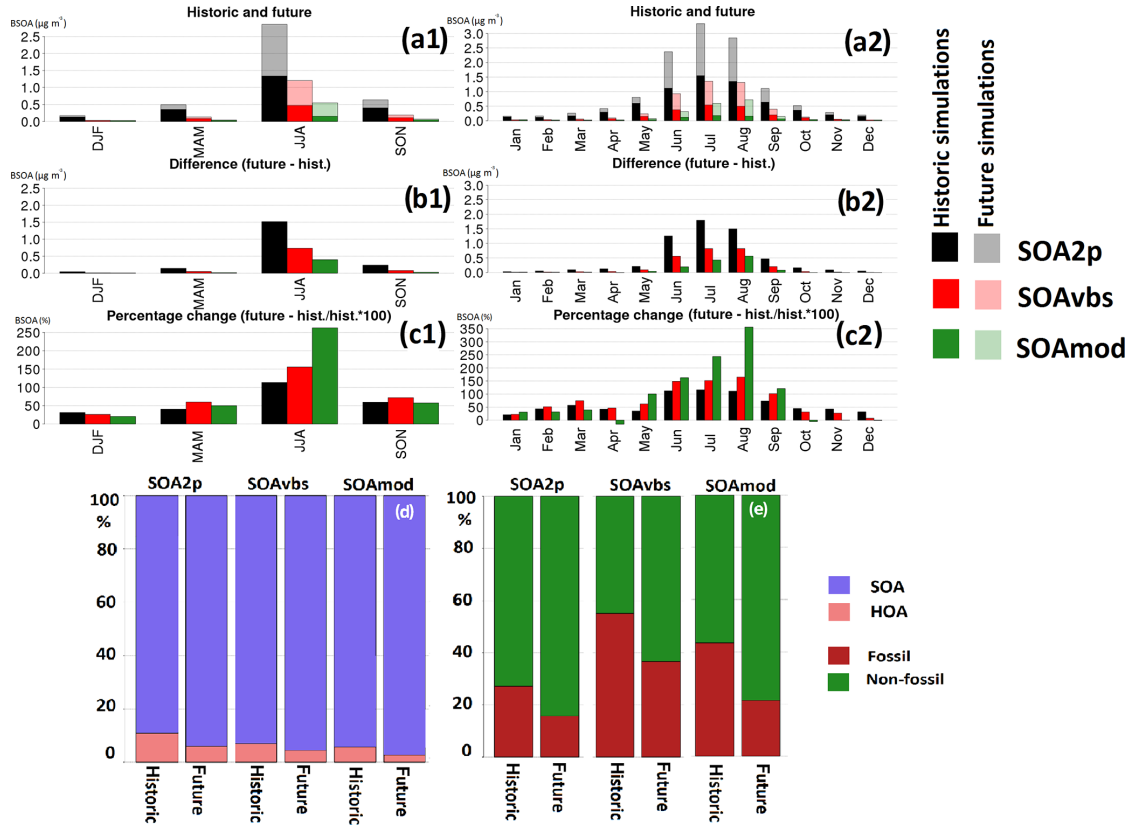


Figure 4. Seasonal and monthly averaged concentrations of BSOA for five years of simulations, and the oxidation state and origins of OA for the European sub-domain. **(a1, a2)** Historic simulations. **(b1, b2)** Absolute changes in future scenarios compared to historic simulations (future–historic). **(c1, c2)** Relative changes in future scenarios; **(d, e)** oxidation state and origins respectively. Lighter colors show future scenarios, and darker colors the historic simulations.

tive increase (+113 %, +155 % and +262 % for SOA2p, SOAvbs and SOAmod respectively) and winter the lowest increase in all schemes (+31.1 %, +26.2 % and +20.5 % for SOA2p, SOAvbs and SOAmod respectively). For autumn and spring SOA2p and SOAmod show similar and intermediate changes, while SOAvbs shows higher relative differences (+59.6 % and +40.3 %, +79.9 % and +60.0 %, and +57.3 % and +50.0 % in autumn and spring respectively for SOA2p, SOAmod and SOAvbs).

For monthly results, as seen in Fig. 4a2, b2 and c2, there is an increase (both in relative and absolute values) in almost all months for all schemes during the year, but the intensity of this increase changes for different months. In July, when the BSOA concentration reaches its maximum, the percentage of change in the future is high as well (+115 %, +151 % and +243 % for SOA2p, SOAvbs and SOAmod respectively). Highest relative changes occur in August for all schemes (+111 %, +165 % and +356 % for SOA2p, SOAvbs and SOAmod respectively), resulting from the seasonal profile of BVOC emissions. For SOAmod, a decreased change is seen for some months in the future scenarios (−11 %, −1.6 % and −0.45 % for April, October and November respectively).

4.2.2 Changes in the origins of OA

Figure 4d shows a simplified distribution for the OA in different schemes: SOA and HOA (hydrocarbon-like organic aerosol) presenting the freshly emitted primary OA. Figure 4d shows that the predicted distribution between HOA and SOA is different for the three schemes. SOA2p indicates a smaller contribution of SOA and a larger one from HOA compared to SOAvbs and SOAmod schemes. This is because POA emissions in SOA2p are considered nonvolatile, while they are volatile in VBS schemes. The relative contribution of HOA decreases in all schemes in the future scenario, since the anthropogenic emissions are kept constant, and the concentration SOA increases. However, the decrease in the relative contribution of HOA is stronger for the SOAmod scheme, since it shows a higher relative increase in the formation of BSOA in future scenarios.

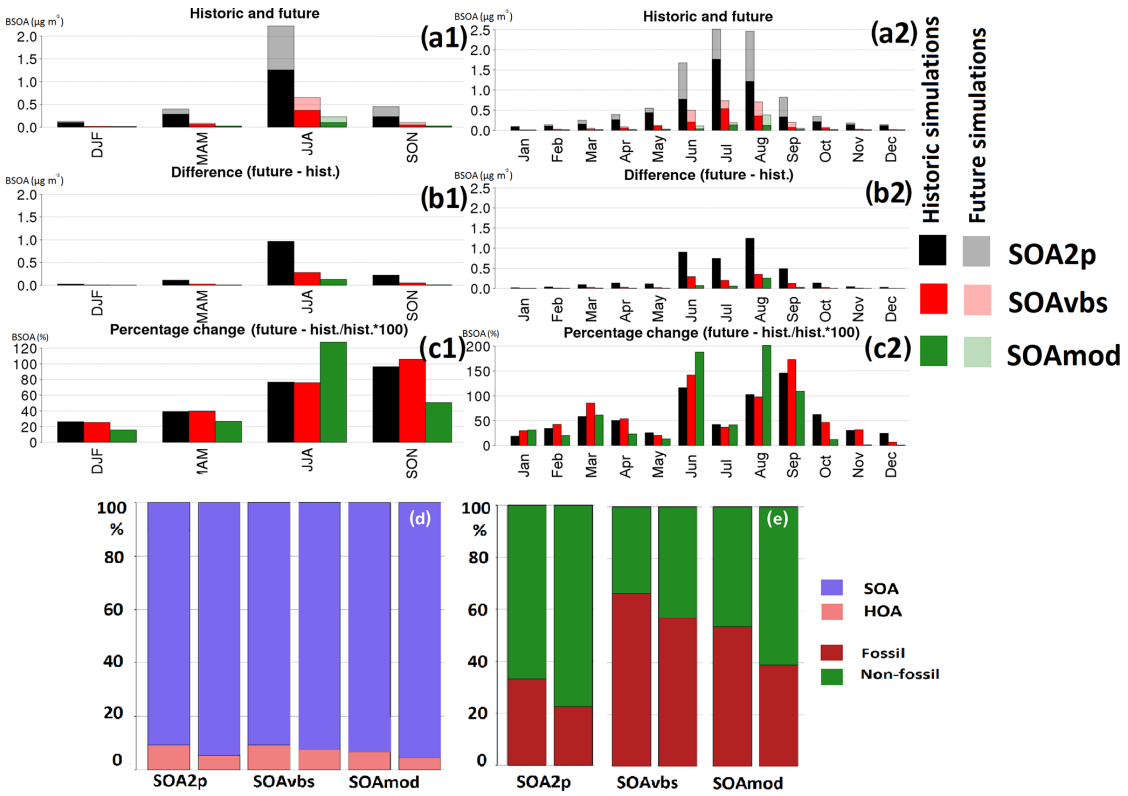


Figure 5. Seasonal and monthly averaged concentrations of BSOA for five years of simulations and the oxidation state and origins of OA for the Mediterranean sub-domain. **(a1, a2)** Historic simulations. **(b1, b2)** Absolute changes in future scenarios compared to historic simulations (future–historic). **(c1, c2)** Relative changes in future scenarios; **(d, e)** oxidation state and origins respectively. Lighter colors show future scenarios, and darker colors the historic simulations.

The schemes behave differently in contributing to different origins in the formation of OA as well; therefore it is interesting to compare this aspect in the tested schemes. Since surrogate species for different sources are present in the outputs, the fossil and non-fossil repartition can be easily calculated. ASOA is considered to be in the fossil fraction (neglecting a small fraction due to biofuels) and BSOA in the non-fossil fraction. For carbonaceous aerosol, residential and domestic uses are considered to be non-fossil, as they are mostly related to wood burning (Sasser et al., 2012). When comparing the simulated fossil and non-fossil fraction, some differences are observed. The SOAvbs scheme predicts more SOA in the fossil fraction mainly because it takes into account aging of anthropogenic SVOCs and not of biogenic SVOCs. On the contrary, the SOAmod scheme takes into account the aging for both biogenic and anthropogenic SVOCs; therefore it simulates more in the non-fossil compartment. All schemes show a relative increase in the contribution of non-fossil sources in the future on an annually averaged basis (10 %, 17 % and 22 % of increase for the non-fossil partition between future and historic simulations for SOA2p, SOAvbs and SOAmod respectively). As already discussed, a strong seasonality is seen for this factor as well. The contribution of non-fossil sources becomes much higher in summer (Fig. 4e), when BVOC emissions are largely abundant. The increase in the contribution of non-fossil sources is logical, since the anthropogenic emissions of OA precursors are kept the same and the biogenic emissions of these species increase with increasing temperature.

4.3 Mediterranean region

While the differences between the schemes for the European area are important to explore in future scenarios, we also focus on the Mediterranean region because of several reasons: high sensitivity to climate change, high burden of OA (and PM in general; Lin et al., 2012, 2014) and also high temperatures in the area. Because of these reasons, we perform a similar analysis as in the previous section. As explained before, a land–sea mask was used in order to separate the Mediterranean Sea; therefore the analysis explained below regards only the sea without any land surface cells.

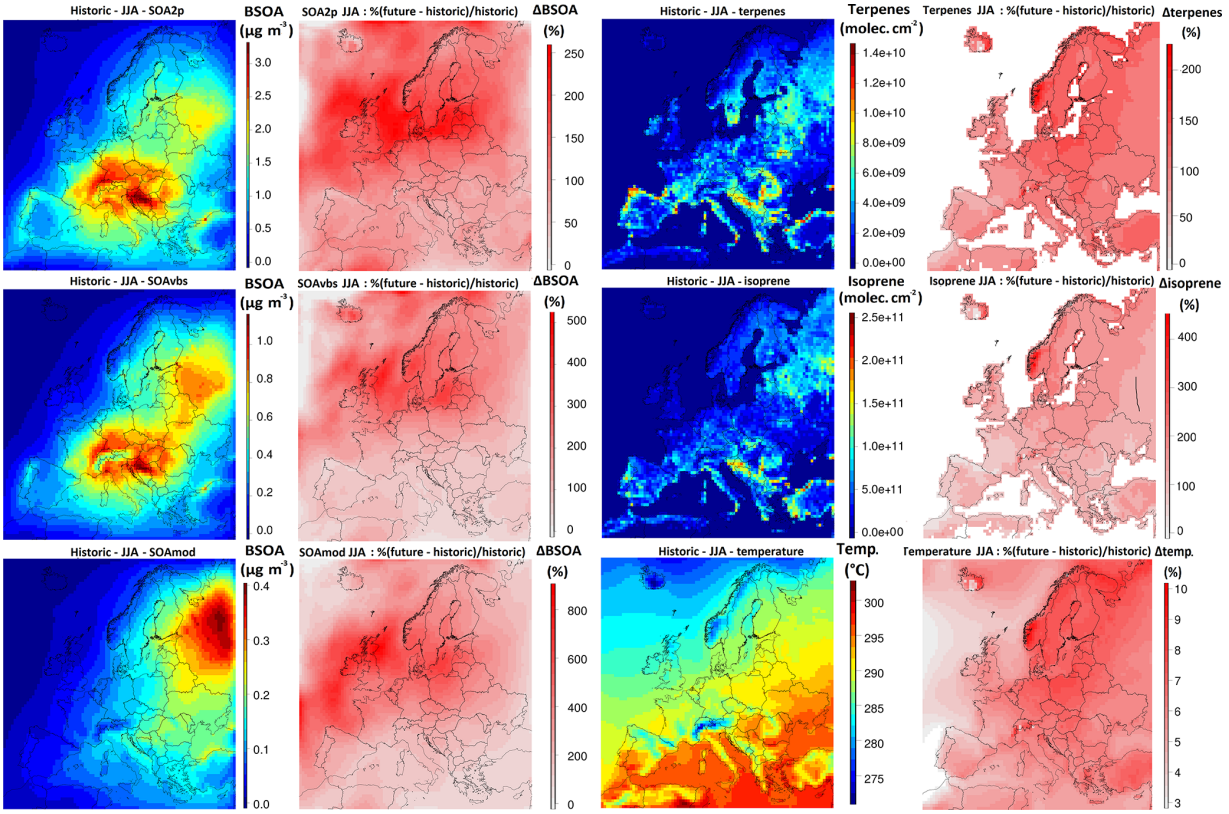


Figure 6. Averaged summer changes in concentrations of BSOA in historic (first column; µg m^{-3}) and their future changes (second column; % (future–historic) / historic) for all three scenarios (SOA2p, SOAvbs and SOAmod in first, second and third rows respectively). Third column shows the emissions of monoterpenes and isoprene (molecules cm^{-2} yr^{-1}; first and second row) and temperature (K; third row)m and the changes of each one of these parameters is seen in fourth column (% (future–historic) / historic). Bear in mind that emissions of BVOCs and the temperature do not change between different schemes, scale for each plot is different, and all the figures are for the summer period.

4.3.1 Changes in BSOA concentration

There are major differences between the concentrations of different aerosol components over the Mediterranean area compared to continental Europe. For example, the concentrations of salt and dust particles are higher for the former because of the marine environment and for the latter because of the northern African dust emissions which are transported to the Mediterranean area. On the contrary, the concentrations of nitrate and BSOA are lower than in the continental area; in the case of nitrate particles, because of higher temperatures, its formation is less efficient than it is in continental Europe, and for the BSOA, this is because of a lack of emission sources over the marine environment. The differences seen for BSOA concentrations in different schemes are presented in Fig. 5 (panels a1, b1 and c1 for seasonal results and a2, b2 and c2 for monthly results). The behavior of different schemes in regard to differences between historic and future simulations differs between the sea and the continental area. For BSOA relative changes, SOAmod still shows the largest relative change in the summer period compared to historic simulations (76 %, 75 % and 127 % for SOA2p, SOAvbs and SOAmod respectively), but the differences between schemes are less pronounced in the Mediterranean area.

4.3.2 Changes in the origins of OA

For all three schemes, the contribution of fossil sources to OA is slightly larger for the Mediterranean sub-domain than for Europe (Fig. 5e). The reason for this difference is the fact that there are local fossil OA formation sources in the Mediterranean Sea, i.e., shipping emissions, while OA originating from non-fossil sources is not directly emitted in this area and is transported from outside. While the contribution of non-fossil sources increases in the future scenarios, fossil sources still contribute more in the Mediterranean area compared to the European area relative to non-fossil sources.

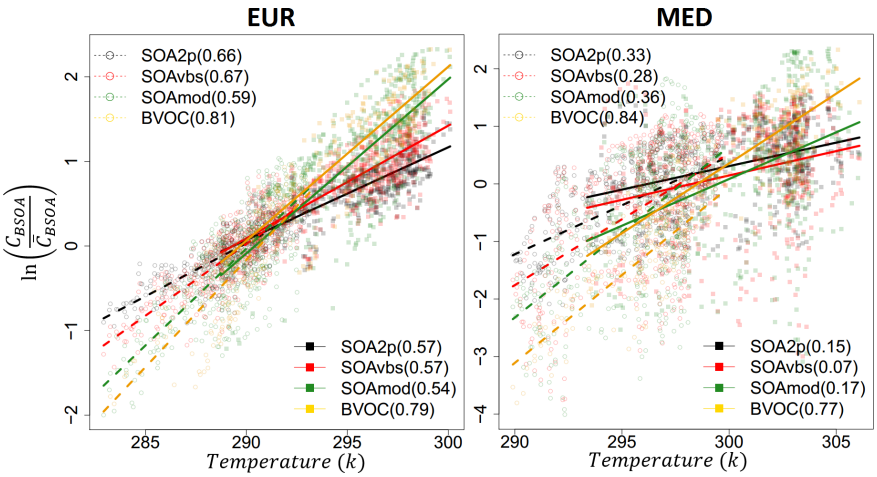


Figure 7. Normalized (divided by the average) concentrations of BSOA versus temperature for the summer period (SOA2p in black, SOAvbs in red and SOAmod in green). Each point represents 1 d of simulation. Empty circles and dashed lines show the historic period, while filled rectangles and filled lines show the future scenarios. The points concerning BVOCs have been added as well (in gold). The regression lines are exponential. The correlation coefficients for each of the schemes are reported in the legend. Emissions of BVOCs are kept constant between different schemes. A different scale is used for each sub-domain to facilitate the comprehension of the panel.

Both for the historic and the future simulations, the HOA and SOA distribution does not change considerably in the Mediterranean area as compared to the European area (Fig. 5d).

4.4 Spatial distribution of future changes

Figure 6 shows the concentration of BSOA in different schemes (in $\mu g\,m^{-3}$; first column), the percentage of differences between historic and future simulations (second column), concentrations of isoprene and monoterpenes and temperature for all schemes (third column), and the changes of these parameters in future scenarios (fourth column). All the panels in Fig. 6 show the summer period. The concentration of BSOA in SOA2p simulations is much higher than that of SOAvbs and even more so than that in SOAmod at the lower end. However, the predicted increase for the future is higher for SOAvbs and SOAmod (Fig. 6, second column), reaching an average 290 % increase over the whole domain for the SOAmod scheme. These increases are most pronounced over Scandinavia for SOAvbs and for central Europe and Scandinavia for SOAmod. The maximum change happens in the summer period, reaching a maximum of 700 % for SOAmod for areas around the British Isles and around 500 % in central Europe, while the differences for SOA2p simulations only show a maximum 70 % and 200 % increase for annual and summer averages respectively for the same area. This fact might suggest that the increase in BSOA concentrations due to climate change might be highly underestimated in future scenarios.

Despite the strong regional variations in the concentrations simulated by different schemes (Fig. 6, column 1), the geographic shape of the differences between historic and future scenarios (Fig. 6, second column) stay similar for all schemes, showing a maximum in the band between the North Sea and Baltic Sea. It is important to keep in mind that some of these differences occur in areas with low concentrations of BSOA, which can lead to large relative changes despite only small absolute ones. This mostly occurs in the oceanic regions of the domain. When a land–sea mask is used, the maximum changes occur on the British Isles, Scandinavia area and central Europe.

Figure 6 also shows the spatial distribution of temperature increase is correlated with that of BSOA increases (for all the schemes). There is an exception for the Mediterranean area, where absolute temperatures are high, but the concentration of BSOA is low mainly because biogenic precursors of BSOA are not emitted in this area.

5 Sensitivity of different schemes to temperature changes

Figure 7 shows the logarithm of normalized concentrations of BSOA for EUR and MED sub-domains plotted against temperature, for the summer period, using daily average values for each scheme for the five considered summer periods. Dashed lines correspond to linear least-square fits for historic simulations, and solid lines correspond to future scenarios. BVOC emissions have been added to the plot as well. Normalization of the data was done by a division by the average of each set of simulations; then the natural logarithm of this ratio is calculated. It is important to bear in mind that as mentioned before, for future scenarios, the years with the

highest temperature and highest BSOA aerosol concentrations are chosen. For the historic scenarios the years with the lowest temperature and lowest BSOA aerosol concentrations are chosen, which explains the high difference between historic and future simulations (Fig. 7). Before entering into the discussion around sensitivity to temperature changes, it is important to keep in mind that the circulation patterns can change between the historic and future periods. Although the average of 5 years of simulations likely filters out part of the noise in these patterns, this could also affect BSOA concentrations in addition to temperature changes, especially over the Mediterranean region being remote with respect to sources.

As seen in Fig. 7, there is a high correlation between BVOC emissions and temperature throughout all the seasons (shown here for summer), showing an exponential behavior with temperature. The relationship between BVOCs and temperature is reported also for the Mediterranean Basin, though the emissions of these species in this area are negligible. Accordingly, the correlation is lower over this area.

When looking at the different schemes, the regression lines show some differences for the future period. Interestingly SOAmod shows a slope rather similar to that of BVOC, while slopes are lower for the SOA2p and SOAvbs. Thus, for SOAmod, the temperature-induced increase in BVOC fully affects BSOA. In contrast, for SOA2p and SOAvbs, less BSOA is formed with a temperature increase, as could be expected from the correspondence of the temperature with BVOC emissions. This negative sensitivity of BSOA formation normalized by BVOC emissions is due to a shift of SVOC species to the gas phase for increasing temperature, as has been mentioned before. Apparently, this effect is much less pronounced or absent for SOAmod, which is probably because it includes, contrary to the other two schemes, formation of nonvolatile SOA. Indeed, the SOAmod scheme shows 80 % of the OA mass in the nonvolatile bins, while the SOAvbs and the SOA2p schemes only show respectively around 10 % and 20 % in these bins. These results suggest that the parameterization of OA schemes might lead to different sensitivity in prediction of the OA load with respect to the variations in the temperature. The same tendencies are observed for the historic period; however they show a lower intensity because of the lower general temperature ranges.

6 Conclusions

In this study, we presented the effect of different OA simulation schemes on future aerosol projections due to climate change. For this purpose, three schemes have been used: a molecular single-step oxidation scheme (SOA2p); a standard VBS scheme with anthropogenic SVOC aging only (SOAvbs); and a modified VBS scheme containing functionalization, fragmentation and formation of nonvolatile SOA for all SVOC species (SOAmod). These schemes were evaluated for the European region for the year 2013. Although showing differences with observations, each OA scheme performs within accepted error ranges. Since VBS schemes are numerically demanding, only 10 years of simulations could be performed for each scheme. In order to maximize the differences between future and historic simulations, the RCP8.5 scenario was used. For the future scenarios, years where the temperature and the BSOA concentration were both at their maximum were chosen, while, for the historic simulations, five years with the lowest temperature and BSOA concentrations were selected. Indeed, climate-change-induced modifications were shown to affect especially the BSOA fraction of organic aerosol. Since BSOA contributes to an important degree to the total concentration of OA, the focus of this article is the evolution of BSOA concentrations in different schemes in future climatic projections.

The results show that the change in concentration indicated by the SOAmod scheme is stronger especially for summertime, showing a difference of +113 %, +155 % and +262 % for SOA2p, SOAvbs and SOAmod respectively for the European area. These changes are mostly due to increased BSOA formation, which is the major SOA fraction during summer. Previous studies investigated the changes in BSOA concentrations for future scenarios using a two-product scheme for the simulation of SOA. Thus, our suggestion is that the relative variation in SOA concentrations predicted with such schemes might be underestimated.

The reason for the augmentation of BSOA concentrations due to climate change in future scenarios is because of the high dependency of BVOC emissions (which are major precursors of the formation of BSOA in summer or warm periods) on temperature. In a future climate, with the increase in temperatures values, the emissions of BVOCs might increase, and in our case, they were predicted to increase by 88 % for terpenes and 82 % for isoprene (over the European domain). The effect on BSOA formation is tempered by the fact that higher temperatures favor the transition of semivolatile organic material in the gas phase. This effect is much more pronounced for the SOA2p and SOAvbs schemes than for the SOAmod scheme, which is the only scheme in our study including aging of biogenic SVOCs and the formation of nonvolatile SOA. The sensitivity of the SOAmod scheme to temperature is the lowest, and its relation to BVOC emissions is the most linear.

The differences were analyzed for the Mediterranean area as well, since organic aerosol and BSOA are transported to this area from continental Europe. While the concentrations in the Mediterranean and changes for future climate are lower for BSOA in general compared to the European area, the changes for this region are stronger in the SOAmod scheme as well (76 %, 75 % and 127 % for SOA2p, SOAvbs and SOAmod respectively for summer).

In conclusion, our study suggests that the BSOA concentration changes are highly sensitive to climate change and the scheme used for their simulation. The changes reported

until now for future scenarios are highly uncertain, both on an absolute and on a relative scale. On a relative scale, these changes might be higher with OA schemes that include formation of nonvolatile SOA (up to a factor of 2).

Future work is necessary in developing more accurate organic aerosol schemes not only in terms of absolute concentrations simulated but also with respect to their temperature sensitivity. The three schemes used in this study can accurately simulate the concentrations of OA each for a specific season and for a specific region, while none of the schemes seem to be able to do so for the whole domain. Therefore, more research is necessary in order to develop OA simulation schemes that are able to represent the concentrations of OA accurately and the temperature sensitivity of this species on a regional scale.

Data availability. Access to the data used in this article is restricted to registered users of the ChArMEx project. The data are available on the project website (http://mistrals.sedoo.fr/ChArMEx/, last access: 13 April 2019) and should be used following the data and publication policies of the ChArMEx project: http://mistrals.sedoo.fr/ChArMEx/Data-Policy/ChArMEx_DataPolicy.pdf (last access: 13 April 2019). The data used for the scheme validation part of the study were downloaded from EBAS (http://ebas.nilu.no/; last access: 14 June 2019).

Appendix A

Table A1. Names and other information about the stations used in scheme validation part of this study.

Country	Station name	Longitude	Latitude	Altitude	Type	Duration	Resolution
Switzerland	CH0001G	7.99	46.55	3578.0 m	PM_1	9 months	1 h
Switzerland	CH0002R	6.94	46.81	489.0 m	$PM_{2.5}$	1 year	1 d
Switzerland	CH0005R	8.46	47.07	1031.0 m	$PM_{2.5}$	1 year	1 d
Switzerland	CH0033R	8.93	46.16	203.0 m	PM_1	18 weeks	1 h
Cyprus	CY0002R	33.06	35.04	520.0 m	$PM_{2.5}$	1 year	1 d
Czech republic	CZ0003R	15.08	49.57	535.0 m	$PM_{2.5}$	1 year	1 d
Germany	DE0002R	10.76	52.80	74.0 m	$PM_{2.5}$	1 year	1 d
Germany	DE0003R	7.91	47.91	1205.0 m	$PM_{2.5}$	1 year	1 d
Germany	DE0007R	13.03	53.17	62.0 m	$PM_{2.5}$	1 year	1 d
Germany	DE0008R	10.77	50.65	937.0 m	$PM_{2.5}$	1 year	1 d
Germany	DE0044R	12.93	51.53	86.0 m	PM_{10}	1 year	1 d
Spain	ES0001R	−4.35	39.55	917.0 m	$PM_{2.5}$	1 year	1 d
Spain	ES0009R	−3.14	41.28	1360.0 m	$PM_{2.5}$	1 year	1 d
Spain	–	3.03	39.84	15.0 m	PM_1	3 months	1 h
Spain	ES1778R	2.35	41.77	700.0 m	PM_1	6 months	1 h
Finland	FI0050R	24.28	61.85	181.0 m	PM_1	9 months	1 h
France	FR0009R	4.63	49.90	390.0 m	$PM_{2.5}$	1 year	6 d
France	FR0013R	0.18	43.62	200.0 m	$PM_{2.5}$	1 year	6 d
France	FR0030R	2.95	45.77	1465.0 m	$PM_{2.5}$	1 year	2 d
France	–	9.38	42.97	520.0 m	PM_1	3 months	1 h
France	–	2.15	48.71	156 m	$PM_{2.5}$	1 year	1 d
Greece	GR0002R	25.67	35.32	250.0 m	PM_{10}	1 year	1 d
Ireland	IE0031R	−9.90	53.33	10.0 m	PM_1	41 weeks	1 h
Italy	IT0004R	8.63	45.80	209.0 m	$PM_{2.5}$	1 year	1 d
Netherlands	NL0644R	4.92	51.97	1.0 m	$PM_{2.5}$	1 year	1 d
Norway	NO0002R	8.25	58.39	219.0 m	PM_1	1 year	1 week
Norway	NO0039R	8.88	62.78	210.0 m	PM_1	1 year	1 week
Norway	NO0056R	11.08	60.37	300.0 m	$PM_{2.5}$	1 year	1 d
Poland	PL0005R	22.07	54.15	157.0 m	PM_{10}	1 year	1 d
Sweden	SE0011R	13.15	56.02	175.0 m	PM_{10}	1 year	1 d
Sweden	SE0012R	17.38	58.80	20.0 m	PM_{10}	1 year	1 d
Slovenia	SI0008R	14.87	45.57	520.0 m	$PM_{2.5}$	1 year	1 d

Author contributions. ArC, AuC and MB designed the experiment. ArC and AuC performed the simulations, and ArC carried out the post-processing of aforementioned simulations. Article reduction was performed by ArC, and all authors contributed to the text, interpretation of the results and review of the article.

Competing interests. The authors declare that they have no conflict of interest.

Special issue statement. This article is part of the special issue "CHemistry and AeRosols Mediterranean EXperiments (ChArMEx) (ACP/AMT inter-journal SI)". It is not associated with a conference.

Acknowledgements. This work was performed using HPC resources from GENCI-CCRT (grant 2018-A0030107232). R. Vautard is acknowledged for providing the WRF/IPSL-CM5-MR CORDEX simulations, and D. Hauglustaine and S. Szopa are acknowledged for providing t he INCA simulations. Z. Klimont is acknowledged for providing ECLIPSE-v4 emission projections. The thesis work of Arineh Cholakian is supported by ADEME, INERIS (with the support of the French Ministry of Ecology), and the ANR SAF-MED project. Giancarlo Ciarelli was supported by ADEME and the Swiss National Science Foundation (grant no. P2EZP2_175166).

Financial support. This research has received funding from the French National Research Agency (ANR) project SAFMED (grant ANR-15 12-BS06-0013). This work is part of the ChArMEx project supported by ADEME, CEA, CNRS-INSU and Météo-France through the multidisciplinary program MISTRALS (Mediterranean Integrated STudies at Regional And Local Scales). The work presented here received support from the French Ministry of Ecology.

Review statement. This paper was edited by Pedro Jimenez-Guerrero and reviewed by three anonymous referees.

References

Amann, M., Klimont, Z., and Wagner, F.: Regional and Global Emissions of Air Pollutants: Recent Trends and Future Scenarios, Annu. Rev. Environ. Resour., 38, 31–55, https://doi.org/10.1146/annurev-environ-052912-173303, 2013.

Arneth, A., Harrison, S. P., Zaehle, S., Tsigaridis, K., Menon, S., Bartlein, P. J., Feichter, J., Korhola, A., Kulmala, M., O'Donnell, D., Schurgers, G., Sorvari, S., and Vesala, T.: Terrestrial biogeochemical feedbacks in the climate system, Nat. Geosci., 3, 525–532, https://doi.org/10.1038/ngeo905, 2010.

Berrisford, P., Kallberg, P., Kobayashi, S., Dee, D., Uppala, S., Simmons, A. J., and Sato, H.: The ERA-Interim archive version 2.0, ERA Rep. Series, Shinfield Park, Reading, 2011.

Bessagnet, B., Menut, L., Curci, G., Hodzic, A., Guillaume, B., Liousse, C., Moukhtar, S., Pun, B., Seigneur, C., and Schulz, M.: Regional modeling of carbonaceous aerosols over Europe–focus on secondary organic aerosols, J. Atmos. Chem., 61, 175–202, https://doi.org/10.1007/s10874-009-9129-2, 2008.

Boylan, J. W. and Russell, A. G.: PM and light extinction model performance metrics, goals, and criteria for three-dimensional air quality models, Atmos. Environ., 40, 4946–4959, https://doi.org/10.1016/j.atmosenv.2005.09.087, 2006.

Carlton, A. G., Wiedinmyer, C., and Kroll, J. H.: A review of Secondary Organic Aerosol (SOA) formation from isoprene, Atmos. Chem. Phys., 9, 4987–5005, https://doi.org/10.5194/acp-9-4987-2009, 2009.

Carvalho, A., Monteiro, A., Solman, S., Miranda, A. I., and Borrego, C.: Climate-driven changes in air quality over Europe by the end of the 21st century, with special reference to Portugal, Environ. Sci. Policy, 13, 445–458, https://doi.org/10.1016/J.ENVSCI.2010.05.001, 2010.

Cholakian, A., Beekmann, M., Colette, A., Coll, I., Siour, G., Sciare, J., Marchand, N., Couvidat, F., Pey, J., Gros, V., Sauvage, S., Michoud, V., Sellegri, K., Colomb, A., Sartelet, K., Langley DeWitt, H., Elser, M., Prévot, A. S. H., Szidat, S., and Dulac, F.: Simulation of fine organic aerosols in the western Mediterranean area during the ChArMEx 2013 summer campaign, Atmos. Chem. Phys., 18, 7287–7312, https://doi.org/10.5194/acp-18-7287-2018, 2018.

Cholakian, A., Colette, A., Coll, I., Ciarelli, G., and Beekmann, M.: Future climatic drivers and their effect on PM_{10} components in Europe and the Mediterranean Sea, Atmos. Chem. Phys., 19, 4459–4484, https://doi.org/10.5194/acp-19-4459-2019, 2019.

Colette, A., Bessagnet, B., Vautard, R., Szopa, S., Rao, S., Schucht, S., Klimont, Z., Menut, L., Clain, G., Meleux, F., Curci, G., and Rouïl, L.: European atmosphere in 2050, a regional air quality and climate perspective under CMIP5 scenarios, Atmos. Chem. Phys., 13, 7451–7471, https://doi.org/10.5194/acp-13-7451-2013, 2013.

Colette, A., Andersson, C., Baklanov, A., Bessagnet, B., Brandt, J., Christensen, J. H., Doherty, R., Engardt, M., Geels, C., Giannakopoulos, C., Hedegaard, G. B., Katragkou, E., Langner, J., Lei, H., Manders, A., Melas, D., Meleux, F., Rouïl, L., Sofiev, M., Soares, J., Stevenson, D. S., Tombrou-Tzella, M., Varotsos, K. V., and Young, P.: Is the ozone climate penalty robust in Europe?, Environ. Res. Lett., 10, 084015, https://doi.org/10.1088/1748-9326/10/8/084015, 2015.

Derognat, C., Beekmann, M., Baeumle, M., Martin, D., and Schmidt, H.: Effect of biogenic volatile organic compound emissions on tropospheric chemistry during the Atmospheric Pollution Over the Paris Area (ESQUIF) campaign in the Ile-de-France region, J. Geophys. Res., 108, 8560, https://doi.org/10.1029/2001JD001421, 2003.

Donahue, N. M., Robinson, A. L., Stanier, C. O., and Pandis, S. N.: Coupled partitioning, dilution, and chemical aging of semivolatile organics, Environ. Sci. Technol., 40, 2635–2643, https://doi.org/10.1021/es052297c, 2006.

Donahue, N. M., Epstein, S. A., Pandis, S. N., and Robinson, A. L.: A two-dimensional volatility basis set: 1. organic-aerosol mixing thermodynamics, Atmos. Chem. Phys., 11, 3303–3318, https://doi.org/10.5194/acp-11-3303-2011, 2011.

Donahue, N. M., Kroll, J. H., Pandis, S. N., and Robinson, A. L.: A two-dimensional volatility basis set – Part 2: Diagnostics of organic-aerosol evolution, Atmos. Chem. Phys., 12, 615–634, https://doi.org/10.5194/acp-12-615-2012, 2012.

Dufresne, J.-L., Foujols, M.-A., Denvil, S., Caubel, A., Marti, O., Aumont, O., Balkanski, Y., Bekki, S., Bellenger, H., Benshila, R., Bony, S., Bopp, L., Braconnot, P., Brockmann, P., Cadule, P., Cheruy, F., Codron, F., Cozic, A., Cugnet, D., de Noblet, N., Duvel, J.-P., Ethé, C., Fairhead, L., Fichefet, T., Flavoni, S., Friedlingstein, P., Grandpeix, J.-Y., Guez, L., Guilyardi, E., Hauglustaine, D., Hourdin, F., Idelkadi, A., Ghattas, J., Joussaume, S., Kageyama, M., Krinner, G., Labetoulle, S., Lahellec, A., Lefebvre, M.-P., Lefevre, F., Levy, C., Li, Z. X., Lloyd, J., Lott, F., Madec, G., Mancip, M., Marchand, M., Masson, S., Meurdesoif, Y., Mignot, J., Musat, I., Parouty, S., Polcher, J., Rio, C., Schulz, M., Swingedouw, D., Szopa, S., Talandier, C., Terray, P., Viovy, N., and Vuichard, N.: Climate change projections using the IPSL-CM5 Earth System Model: from CMIP3 to CMIP5, Clim. Dynam., 40, 2123–2165, https://doi.org/10.1007/s00382-012-1636-1, 2013.

Giorgi, F.: Climate change hot-spots, Geophys. Res. Lett., 33, 1–4, https://doi.org/10.1029/2006GL025734, 2006.

Griffin, R. J., Cocker, D. R., Flagan, R. C., and Seinfeld, J. H.: Organic aerosol formation from the oxidation of biogenic hydrocarbons, J. Geophys. Res. Atmos., 104, 3555–3567, https://doi.org/10.1029/1998JD100049, 1999.

Guenther, A., Karl, T., Harley, P., Wiedinmyer, C., Palmer, P. I., and Geron, C.: Estimates of global terrestrial isoprene emissions using MEGAN (Model of Emissions of Gases and Aerosols from Nature), Atmos. Chem. Phys., 6, 3181–3210, https://doi.org/10.5194/acp-6-3181-2006, 2006.

Hallquist, M., Wenger, J. C., Baltensperger, U., Rudich, Y., Simpson, D., Claeys, M., Dommen, J., Donahue, N. M., George, C., Goldstein, A. H., Hamilton, J. F., Herrmann, H., Hoffmann, T., Iinuma, Y., Jang, M., Jenkin, M. E., Jimenez, J. L., Kiendler-Scharr, A., Maenhaut, W., McFiggans, G., Mentel, Th. F., Monod, A., Prévôt, A. S. H., Seinfeld, J. H., Surratt, J. D., Szmigielski, R., and Wildt, J.: The formation, properties and impact of secondary organic aerosol: current and emerging issues, Atmos. Chem. Phys., 9, 5155–5236, https://doi.org/10.5194/acp-9-5155-2009, 2009.

Hantson, S., Knorr, W., Schurgers, G., Pugh, T. A. M., and Arneth, A.: Global isoprene and monoterpene emissions under changing climate, vegetation, CO_2 and land use, Atmos. Environ., 155, 35–45, https://doi.org/10.1016/j.atmosenv.2017.02.010, 2017.

Hauglustaine, D. A., Balkanski, Y., and Schulz, M.: A global model simulation of present and future nitrate aerosols and their direct radiative forcing of climate, Atmos. Chem. Phys., 14, 11031–11063, https://doi.org/10.5194/acp-14-11031-2014, 2014.

Heald, C. L., Henze, D. K., Horowitz, L. W., Feddema, J., Lamarque, J.-F., Guenther, A., Hess, P. G., Vitt, F., Seinfeld, J. H., Goldstein, A. H., and Fung, I.: Predicted change in global secondary organic aerosol concentrations in response to future climate, emissions, and land use change, J. Geophys. Res. Atmos., 113, D05211, https://doi.org/10.1029/2007JD009092, 2008a.

Heald, C. L., Henze, D. K., Horowitz, L. W., Feddema, J., Lamarque, J.-F., Guenther, A., Hess, P. G., Vitt, F., Seinfeld, J. H., Goldstein, A. H., and Fung, I.: Predicted change in global secondary organic aerosol concentrations in response to future climate, emissions, and land use change, J. Geophys. Res. Atmos., 113, D05211, https://doi.org/10.1029/2007JD009092, 2008b.

Heald, C. L., Wilkinson, M. J., Monson, R. K., Alo, C. A., Wang, G., and Guenther, A.: Response of isoprene emission to ambient CO_2 changes and implications for global budgets, Glob. Chang. Biol., 15, 1127–1140, https://doi.org/10.1111/j.1365-2486.2008.01802.x, 2009.

Hodzic, A. and Jimenez, J. L.: Modeling anthropogenically controlled secondary organic aerosols in a megacity: a simplified framework for global and climate models, Geosci. Model Dev., 4, 901–917, https://doi.org/10.5194/gmd-4-901-2011, 2011.

Jacob, D., Petersen, J., Eggert, B., Alias, A., Christensen, O. B., Bouwer, L. M., Braun, A., Colette, A., Déqué, M., Georgievski, G., Georgopoulou, E., Gobiet, A., Menut, L., Nikulin, G., Haensler, A., Hempelmann, N., Jones, C., Keuler, K., Kovats, S., Kröner, N., Kotlarski, S., Kriegsmann, A., Martin, E., van Meijgaard, E., Moseley, C., Pfeifer, S., Preuschmann, S., Radermacher, C., Radtke, K., Rechid, D., Rounsevell, M., Samuelsson, P., Somot, S., Soussana, J.-F., Teichmann, C., Valentini, R., Vautard, R., Weber, B., and Yiou, P.: EURO-CORDEX: new high-resolution climate change projections for European impact research, Reg. Environ. Chang., 14, 563–578, https://doi.org/10.1007/s10113-013-0499-2, 2014.

Jimenez, J. L., Canagaratna, M. R., Donahue, N. M., Prevot, A. S. H., Zhang, Q., Kroll, J. H., DeCarlo, P. F., Allan, J. D., Coe, H., Ng, N. L., Aiken, A. C., Docherty, K. S., Ulbrich, I. M., Grieshop, A. P., Robinson, A. L., Duplissy, J., Smith, J. D., Wilson, K. R., Lanz, V. A., Hueglin, C., Sun, Y. L., Tian, J., Laaksonen, A., Raatikainen, T., Rautiainen, J., Vaattovaara, P., Ehn, M., Kulmala, M., Tomlinson, J. M., Collins, D. R., Cubison, M. J., Dunlea, E. J., Huffman, J. A., Onasch, T. B., Alfarra, M. R., Williams, P. I., Bower, K., Kondo, Y., Schneider, J., Drewnick, F., Borrmann, S., Weimer, S., Demerjian, K., Salcedo, D., Cottrell, L., Griffin, R., Takami, A., Miyoshi, T., Hatakeyama, S., Shimono, A., Sun, J. Y., Zhang, Y. M., Dzepina, K., Kimmel, J. R., Sueper, D., Jayne, J. T., Herndon, S. C., Trimborn, A. M., Williams, L. R., Wood, E. C., Middlebrook, A. M., Kolb, C. E., Baltensperger, U., Worsnop, D. R., and Worsnop, D. R.: Evolution of organic aerosols in the atmosphere., Science, 326, 1525–1529, https://doi.org/10.1126/science.1180353, 2009.

Klimont, Z., Smith, S. J., and Cofala, J.: The last decade of global anthropogenic sulfur dioxide: 2000–2011 emissions, Environ. Res. Lett., 8, 014003, https://doi.org/10.1088/1748-9326/8/1/014003, 2013.

Klimont, Z., Kupiainen, K., Heyes, C., Purohit, P., Cofala, J., Rafaj, P., Borken-Kleefeld, J., and Schöpp, W.: Global anthropogenic emissions of particulate matter including black carbon, Atmos. Chem. Phys., 17, 8681–8723, https://doi.org/10.5194/acp-17-8681-2017, 2017.

Lane, T. E., Donahue, N. M., and Pandis, S. N.: Simulating secondary organic aerosol formation using the volatility basis-set approach in a chemical transport model, Atmos. Environ., 42, 7439–7451, https://doi.org/10.1016/j.atmosenv.2008.06.026, 2008.

Langner, J., Engardt, M., Baklanov, A., Christensen, J. H., Gauss, M., Geels, C., Hedegaard, G. B., Nuterman, R., Simpson, D., Soares, J., Sofiev, M., Wind, P., and Zakey, A.: A multi-model study of impacts of climate change on sur-

face ozone in Europe, Atmos. Chem. Phys., 12, 10423–10440, https://doi.org/10.5194/acp-12-10423-2012, 2012.

Lannuque, V., Camredon, M., Couvidat, F., Hodzic, A., Valorso, R., Madronich, S., Bessagnet, B., and Aumont, B.: Exploration of the influence of environmental conditions on secondary organic aerosol formation and organic species properties using explicit simulations: development of the VBS-GECKO parameterization, Atmos. Chem. Phys., 18, 13411–13428, https://doi.org/10.5194/acp-18-13411-2018, 2018.

Lannuque, V., Couvidat, F., Camredon, M., Aumont, B., and Bessagnet, B.: Modelling organic aerosol over Europe in summer conditions with the VBS-GECKO parameterization: sensitivity to secondary organic compound properties and IVOC emissions, Atmos. Chem. Phys. Discuss., https://doi.org/10.5194/acp-2018-1244, in review, 2019.

Lelieveld, J., Evans, J. S., Fnais, M., Giannadaki, D., and Pozzer, A.: The contribution of outdoor air pollution sources to premature mortality on a global scale: the example of air pollution in Europe, Nature, 525, 367–371, https://doi.org/10.1038/nature15371, 2015.

Lemaire, V. E. P., Colette, A., and Menut, L.: Using statistical models to explore ensemble uncertainty in climate impact studies: the example of air pollution in Europe, Atmos. Chem. Phys., 16, 2559–2574, https://doi.org/10.5194/acp-16-2559-2016, 2016.

Lin, G., Penner, J. E., Sillman, S., Taraborrelli, D., and Lelieveld, J.: Global modeling of SOA formation from dicarbonyls, epoxides, organic nitrates and peroxides, Atmos. Chem. Phys., 12, 4743–4774, https://doi.org/10.5194/acp-12-4743-2012, 2012.

Lin, G., Sillman, S., Penner, J. E., and Ito, A.: Global modeling of SOA: the use of different mechanisms for aqueous-phase formation, Atmos. Chem. Phys., 14, 5451–5475, https://doi.org/10.5194/acp-14-5451-2014, 2014.

Maria, S. F., Russell, L. M., Gilles, M. K., and Myneni, S. C. B.: Organic Aerosol Growth Mechanisms and Their Climate-Forcing Implications, Science, 306, 1921–1924, https://doi.org/10.1126/science.1103491, 2004.

Mauderly, J. L. and Chow, J. C.: Health Effects of Organic Aerosols, Inhal. Toxicol., 20, 257–288, https://doi.org/10.1080/08958370701866008, 2008.

Meinshausen, M., Smith, S. J., Calvin, K., Daniel, J. S., Kainuma, M. L. T., Lamarque, J.-F., Matsumoto, K., Montzka, S. A., Raper, S. C. B., Riahi, K., Thomson, A., Velders, G. J. M., and van Vuuren, D. P. P.: The RCP greenhouse gas concentrations and their extensions from 1765 to 2300, Clim. Change, 109, 213–241, https://doi.org/10.1007/s10584-011-0156-z, 2011.

Menut, L., Bessagnet, B., Khvorostyanov, D., Beekmann, M., Blond, N., Colette, A., Coll, I., Curci, G., Foret, G., Hodzic, A., Mailler, S., Meleux, F., Monge, J.-L., Pison, I., Siour, G., Turquety, S., Valari, M., Vautard, R., and Vivanco, M. G.: CHIMERE 2013: a model for regional atmospheric composition modelling, Geosci. Model Dev., 6, 981–1028, https://doi.org/10.5194/gmd-6-981-2013, 2013.

Menut, L., Rea, G., Mailler, S., Khvorostyanov, D., and Turquety, S.: Aerosol forecast over the Mediterranean area during July 2013 (ADRIMED/CHARMEX), Atmos. Chem. Phys., 15, 7897–7911, https://doi.org/10.5194/acp-15-7897-2015, 2015.

Odum, J. R., Jungkamp, T. P. W., Griffin, R. J., Forstner, H. J. L., Flagan, R. C., and Seinfeld, J. H.: Aromatics, Reformulated Gasoline, and Atmospheric Organic Aerosol Formation, Environ. Sci. Technol., 31, 1890–1897, https://doi.org/10.1021/es960535l, 1997.

Pacifico, F., Folberth, G. A., Jones, C. D., Harrison, S. P., and Collins, W. J.: Sensitivity of biogenic isoprene emissions to past, present, and future environmental conditions and implications for atmospheric chemistry, J. Geophys. Res. Atmos., 117, D22302, https://doi.org/10.1029/2012JD018276, 2012.

Pankow, J. F.: Review and comparative analysis of the theories on partitioning between the gas and aerosol particulate phases in the atmosphere, Atmos. Environ., 21, 2275–2283, https://doi.org/10.1016/0004-6981(87)90363-5, 1987.

Pankow, J. F.: An absorption model of the gas/aerosol partitioning involved in the formation of secondary organic aerosol, Atmos. Environ., 28, 189–193, https://doi.org/10.1016/1352-2310(94)90094-9, 1994.

Petetin, H., Beekmann, M., Sciare, J., Bressi, M., Rosso, A., Sanchez, O., and Ghersi, V.: A novel model evaluation approach focusing on local and advected contributions to urban $PM_{2.5}$ levels – application to Paris, France, Geosci. Model Dev., 7, 1483–1505, https://doi.org/10.5194/gmd-7-1483-2014, 2014.

Pun, B. K. and Seigneur, C.: Investigative modeling of new pathways for secondary organic aerosol formation, Atmos. Chem. Phys., 7, 2199–2216, https://doi.org/10.5194/acp-7-2199-2007, 2007.

Rea, G., Turquety, S., Menut, L., Briant, R., Mailler, S., and Siour, G.: Source contributions to 2012 summertime aerosols in the Euro-Mediterranean region, Atmos. Chem. Phys., 15, 8013–8036, https://doi.org/10.5194/acp-15-8013-2015, 2015.

Robinson, A. L., Donahue, N. M., and Rogge, W. F.: Photochemical oxidation and changes in molecular composition of organic aerosol in the regional context, J. Geophys. Res., 111, D03302, https://doi.org/10.1029/2005JD006265, 2006.

Robinson, A. L., Donahue, N. M., Shrivastava, M. K., Weitkamp, E. A., Sage, A. M., Grieshop, A. P., Lane, T. E., Pierce, J. R., and Pandis, S. N.: Rethinking Organic Aerosols: Semivolatile Emissions and Photochemical Aging, Science, 315, 1259–1262, https://doi.org/10.1126/science.1133061, 2007.

Sasser, E., Hemby, J., Adler, K., Anenberg, S., Bailey, C., Brockman, L., Chappell, L., DeAngelo, B., Damberg, R., Dawson, J., Frank, N., Geller, M., Hagler, G., Hemming, B., Jantarasami, L., Luben, T., Mitchell, J., and Moss, J.: Report to Congress on Black Carbon, US Environmental Protection Agency, available at: https://nepis.epa.gov/Exe/ZyPURL.cgi?Dockey=P100EIJZ.TXT (last access: 19 December 2018), 2012.

Shrivastava, M., Fast, J., Easter, R., Gustafson Jr., W. I., Zaveri, R. A., Jimenez, J. L., Saide, P., and Hodzic, A.: Modeling organic aerosols in a megacity: comparison of simple and complex representations of the volatility basis set approach, Atmos. Chem. Phys., 11, 6639–6662, https://doi.org/10.5194/acp-11-6639-2011, 2011.

Shrivastava, M., Zelenyuk, A., Imre, D., Easter, R., Beranek, J., Zaveri, R. A., and Fast, J.: Implications of low volatility SOA and gas-phase fragmentation reactions on SOA loadings and their spatial and temporal evolution in the atmosphere, J. Geophys. Res.-Atmos., 118, 3328–3342, https://doi.org/10.1002/jgrd.50160, 2013.

Shrivastava, M., Easter, R. C., Liu, X., Zelenyuk, A., Singh, B., Zhang, K., Ma, P., Chand, D., Ghan, S., Jimenez, J. L., Zhang, Q.,

Fast, J., Rasch, P. J., and Tiitta, P.: Global transformation and fate of SOA: Implications of low-volatility SOA and gas-phase fragmentation reactions, J. Geophys. Res.-Atmos., 120, 4169–4195, https://doi.org/10.1002/2014JD022563.Received, 2015.

Taylor, K. E.: Summarizing multiple aspects of model performance in a Single Diagram, J. Geophys. Res., 106, 7183–7192, https://doi.org/10.1029/2000JD900719, 2001.

Taylor, K. E., Stouffer, R. J., and Meehl, G. A.: An Overview of CMIP5 and the Experiment Design, B. Am. Meteorol. Soc., 93, 485–498, https://doi.org/10.1175/BAMS-D-11-00094.1, 2012.

Tørseth, K., Aas, W., Breivik, K., Fjæraa, A. M., Fiebig, M., Hjellbrekke, A. G., Lund Myhre, C., Solberg, S., and Yttri, K. E.: Introduction to the European Monitoring and Evaluation Programme (EMEP) and observed atmospheric composition change during 1972–2009, Atmos. Chem. Phys., 12, 5447–5481, https://doi.org/10.5194/acp-12-5447-2012, 2012.

Tsigaridis, K., Kanakidou, M., K., T., and Kanakidou, M.: Secondary organic aerosol importance in the future atmosphere, Atmos. Environ., 41, 4682–4692, https://doi.org/10.1016/J.ATMOSENV.2007.03.045, 2007.

Tsimpidi, A. P., Karydis, V. A., Pandis, S. N., and Lelieveld, J.: Global-scale combustion sources of organic aerosols: sensitivity to formation and removal mechanisms, Atmos. Chem. Phys., 17, 7345–7364, https://doi.org/10.5194/acp-17-7345-2017, 2017.

van Vuuren, D. P., Edmonds, J., Kainuma, M., Riahi, K., Thomson, A., Hibbard, K., Hurtt, G. C., Kram, T., Krey, V., Lamarque, J.-F., Masui, T., Meinshausen, M., Nakicenovic, N., Smith, S. J., and Rose, S. K.: The representative concentration pathways: an overview, Clim. Change, 109, 5–31, https://doi.org/10.1007/s10584-011-0148-z, 2011.

Vautard, R., Gobiet, A., Sobolowski, S., Kjellström, E., Stegehuis, A., Watkiss, P., Mendlik, T., Landgren, O., Nikulin, G., Teichmann, C., and Jacob, D.: The European climate under a 2C global warming, Environ. Res. Lett., 9, 34006, https://doi.org/10.1088/1748-9326/9/3/034006, 2014.

Wang, W., Bruyère, C., Duda, M., Dudhia, J., Gill, D., Kavulich, M., Keene, K., Lin, H.-C., Michalakes, J., Rizvi, S., Zhang, X., Berner, J., and Smith, K.: WRF ARW Version 3 Modeling System User's Guide, 37, 204–205, https://doi.org/10.1525/jps.2007.37.1.204, 2015.

Young, P. J., Archibald, A. T., Bowman, K. W., Lamarque, J.-F., Naik, V., Stevenson, D. S., Tilmes, S., Voulgarakis, A., Wild, O., Bergmann, D., Cameron-Smith, P., Cionni, I., Collins, W. J., Dalsøren, S. B., Doherty, R. M., Eyring, V., Faluvegi, G., Horowitz, L. W., Josse, B., Lee, Y. H., MacKenzie, I. A., Nagashima, T., Plummer, D. A., Righi, M., Rumbold, S. T., Skeie, R. B., Shindell, D. T., Strode, S. A., Sudo, K., Szopa, S., and Zeng, G.: Preindustrial to end 21st century projections of tropospheric ozone from the Atmospheric Chemistry and Climate Model Intercomparison Project (ACCMIP), Atmos. Chem. Phys., 13, 2063–2090, https://doi.org/10.5194/acp-13-2063-2013, 2013.

Zhang, Q. J., Beekmann, M., Drewnick, F., Freutel, F., Schneider, J., Crippa, M., Prevot, A. S. H., Baltensperger, U., Poulain, L., Wiedensohler, A., Sciare, J., Gros, V., Borbon, A., Colomb, A., Michoud, V., Doussin, J.-F., Denier van der Gon, H. A. C., Haeffelin, M., Dupont, J.-C., Siour, G., Petetin, H., Bessagnet, B., Pandis, S. N., Hodzic, A., Sanchez, O., Honoré, C., and Perrussel, O.: Formation of organic aerosol in the Paris region during the MEGAPOLI summer campaign: evaluation of the volatility-basis-set approach within the CHIMERE model, Atmos. Chem. Phys., 13, 5767–5790, https://doi.org/10.5194/acp-13-5767-2013, 2013.

CHAPTER

VII

Population exposure in south of France to atmospheric pollutant in future scenarios

Contents

1 Summary of article **187**

2 Population exposure in south of France to atmospheric pollutant in future scenarios **189**

3 Abstract **190**

4 Introdution **191**

5 Materials and methods **192**

5.1 CHIMERE CTM 192

5.2 Simulations 192

5.3 Anthropogenic emissions 193

5.4 Current and future population for the PACA domain 193

6 Results **195**

6.1 Meteorological parameters 195

6.2 Changes in chemical species 196

6.3 Population exposure to atmospheric components in future scenarios 198

6.4 Exposure analysis for the entire PACA region 199

6.5 Spatial analysis of the simulated exposure tendencies 200

6.6 Localization of main risks 200

6.7 County per county analysis 201

7 Summary and conclusions **204**

8 References **205**

During the last three chapters, we have explored the formation and simulation of OA in the Mediterranean area, the sensitivity of this region to climate change and to its different drivers. We also have investigated the sensitivity of different OA simulation schemes to climate change in future scenarios. The conclusion of these sections is that when simulating OA in the Mediterranean area, aging processes and formation of non-volatile SOA present a great importance. Also, we concluded that this basin is sensitive to climate change, anthropogenic emission drivers and long-range transport of pollutants in future scenarios. In addition we have shown that depending on the scheme used for the simulation of OA in the basin, the changes induced by climate change in the region might be underestimated by a factor of two. As a further step forward, we now wish to elucidate the effect of climate change not only on average concentration levels, but also on population exposure. Knowing population exposure will subsequently allow estimating the health impact of air pollution. But, as urban type pollutant concentrations such as NO_x are correlated to population density, calculating exposure requires simulations with high spatial resolutions, much higher than the continental scale simulations performed in the previous two chapters. Therefore, this chapter will focus on a limited region, allowing high resolution simulations. For this purpose, we chose the PACA region in south-eastern France, which shares a long coastline with the Mediterranean Sea. The PACA region, has some specific characteristics: it's highly industrialized, it is densely populated and has major harbor regions, it also has wooded areas which means the emissions of BVOCs can be important as well and finally, being near the Mediterranean, sea-related emissions such as sea salts and shipping emissions play an important role in its atmospheric conditions. The purpose of this chapter is to explore the exposure of the current and future population to changes in air quality caused by climate change. These changes can include mitigation efforts like emission reduction policies as well as climate change itself.

1 Summary of article

We already know that air quality and climate change are intertwined. The adverse effects of air pollution on human health has been proven as well. Combining these two facts makes it important to explore the changes caused by climate change on air quality in order to assess the future exposure of the population to air pollution. Many studies have been performed on the effects of emission reduction policies and climate change on the exposure of the population to air pollutants. However, although it is subject to multiple exposure risks, not many studies have been conducted for the PACA region. First, PACA is located on the coasts of the Mediterranean which have been identified as sensitive to climate change. Second, it has a high population density which is projected to increase in future scenarios. Third, it is at the crossroads of many different emission sources, such as dust emissions from northern Africa which might be exacerbated in the future because of increasing droughts, deforestation and extreme weather patterns. Because of these reasons, we chose to provide a local-scale analysis of the PACA region regarding to

the exposure from climate change, the changes in the exposure of the population in the area and differences seen in this exposure in rural and urban areas.

The goal of this chapter is to explore the changes to air quality on the aforementioned region because of climate change and emission reduction policies at the horizon of 2030s and 2050s. Five years of simulations are conducted. The year 2005 was chosen as a representation of the current state, using CLE 2010 emissions. For future case studies, RCP4.5 and RCP8.5 are used as climate scenarios, and a target year is chosen for each of the two periods of interest, 2030 and 2050. For each future simulation, the emission scenario for the given decade is used. In the end, five years of simulations are obtained, covering the reference situation as well as 4 different yearly future situations crossing the 2030s, 2050s, RCP4.5 and RCP8.5 forcings. For each simulated year, air quality is simulated over a coarse domain which covers the whole of Europe, and over a nested domain which focuses on the PACA region with a horizontal resolution of 5km.

For the purpose of running the high-resolution PACA simulations, rigorous preparation of the forcing data was conducted. Anthropogenic emissions have been prepared using the database from the PACA air quality network (AtmoSud ASQAA), which was re-gridded to be used in our simulations. Also, current population density for this region was obtained from INERIS. In order to calculate the future population scenarios on the area, Shared Socioeconomic Pathway (SSP) scenarios have been used. These scenarios take into account the economic and technologic advances as well as mortality, fertility and migration in the population in the future. Using these factors, O'Neill et al. (2017) suggested five gridded scenarios at the global scale. We used these scenarios in order to project current population of the PACA region to the 2030 and 2050 time horizons.

The air quality analysis we conducted for the PACA region shows that the concentration of PM decreases in all scenarios because of (i) the decrease in nitrate and sulfate concentrations and (ii) the decrease in anthropogenic emissions. The concentration of ozone decreases as well on the average. However, it shows an increase in urban areas during winter in all scenarios. The increase in ozone in urban areas is caused by a reduction of the emissions of NO, which in return results in a decrease in ozone titration. BSOA concentrations also show an increase since the temperature becomes higher in the future scenarios. Finally, dust particle levels show an increase in all scenarios. Other species mostly show a decrease because of emission reduction policies.

Population exposure for this region is then calculated by multiplying the concentration of each pollutant by population density in all grid cells. Therefore it has two drivers that can impose changes: (i) changes in population, and (ii) changes in the concentration of each pollutant. We show that the population mainly increases in urban areas while it decreases in rural areas, with an intensity that depends on the urbanization factor of each SSP scenario. PM exposure (both for $PM_{2.5}$ and PM_{10}) shows a decrease in rural and urban areas, and most of the PM components show a decrease in exposure as well, except for dust and BSOA. As for ozone exposure, it increases in urban areas while it

shows a decrease in the rest of the domain, similarly to BSOA exposure tendencies. The difference between them is the fact that ozone concentration decreases in rural areas, the decrease in rural areas being due both to concentration and population decrease while BSOA concentration shows a moderate increase in the whole domain in all scenarios, therefore the decrease of this exposure in rural areas is solely due to local population decrease. Similarly, dust exposure increases over the whole domain because of the increase in the concentration of this component in future scenarios.

A comparative analysis on an administrative level is also added to this chapter, exploring the six departments of the PACA region separately. Among those six areas are three coastal areas with high population density and large urban zones. Our analysis shows that these departments experience harmful exposure changes to most of the components examined above. For example, in the case of exposure to ozone, it increases in the three coastal departments (Bouches du Rhônes (13), Var (83) and Alpes Maritimes (06)) while showing a decrease in the other three non-coastal ones depending on the SSP scenario.

2 Population exposure in south of France to atmospheric pollutant in future scenarios

This chapter includes the article Cholakian et al. (2021) published in *Atmospheric Environment : "Exposure of the population of southern France to air pollutants in future climate case studies, 264, 118689, doi:10.1016/j.atmosenv.2021.118689, url: Atmospheric environment"*.

Atmospheric Environment 264 (2021) 118689

Contents lists available at ScienceDirect

Atmospheric Environment

journal homepage: www.elsevier.com/locate/atmosenv

Exposure of the population of southern France to air pollutants in future climate case studies

Arineh Cholakian [a,b,c,*,1], Isabelle Coll [a], Augustin Colette [b], Matthias Beekmann [c]

[a] Univ Paris Est Creteil and Université de Paris, CNRS, LISA, F-94010 Créteil, France
[b] Institut National de l'Environnement Industriel et des Risques, Parc Technologique ALATA, Verneuil-en-Halatte, France
[c] Université de Paris and Univ Paris Est Creteil, CNRS, LISA, F-75013 Paris, France

HIGHLIGHTS

- Clarification on the fact that we have chosen to perform case studies and not future scenarios
- Clarification on the choice made for the years simulated and the method used for this choice
- Organization of the sections: separating results from the methodology
- Adding references to corroborate several points raised by the reviewer
- Changes to the visibility of the axes in the images
- Some general proof-reading changes
- Clarification on the county-per-county analysis

ARTICLE INFO

Keywords:
Atmospheric pollution modeling
Future scenarios
Mediterranean
Future atmospheric scenarios

ABSTRACT

Population exposure to air pollutants varies dramatically with time and location on the globe. Taking into account the changing climate, the engaged emission reduction policies and the expected increase in population, the health risks associated with this phenomenon may also change significantly in the near future. In regions such as the Mediterranean, exposed to multiple forms of air pollution and highly sensitive to climate change, it is obviously critical to define trends in human exposure to air pollutants. The objective of this article is to explore the features of population exposure to air pollution in the French Mediterranean coast, under different climatic situations, using distinct emission configurations, and for divergent scenarios of population growth. The use of contrasting situations for these 3 parameters makes it possible to better address the variability of exposure in the different areas of the territory, as a global risk for populations. For this purpose, five 12 month-duration simulations have been carried out as case studies in the Provence Alpes Côtes d'Azur (PACA) region, located in the south-east of France: a 2005 simulation is used as the reference situation, and two more years of simulation are used as samples of time horizons 2030 and 2050, each of which was simulated twice sampling representative future climate years according to representative concentration pathway scenarios RCP4.5 and RCP8.5. Estimates of population change were prepared for the study area, using shared socioeconomic pathways (SSPs) scenarios. The results show that albeit the growing population, the exposure to most atmospheric components decreases because of emission reduction policies. This, however, is not true for all species. The population exposure to dust species increases for spring, when most dust episodes occur. In addition, exposure to ozone – while decreasing on the average - shows an increase in urban areas. Finally, while the concentrations of BSOA (secondary organic aerosol of biogenic origin) increase in the future scenarios, this tendency is not marked enough to offset the population decrease in rural areas in most SSP scenarios. On the reverse, exposure to BSOA does show an increase in urban areas where population is expected to grow. A county per county analysis is conducted, showing that the three coastal counties of the PACA region will experience higher ozone, PM_{10} and $PM_{2.5}$, dust and BSOA exposure. The purpose of our work is to produce a case study in which we compare pollutant concentration changes and population weighed exposure changes on a

* Corresponding author. Univ Paris Est Creteil and Université de Paris, CNRS, LISA, F-94010, Créteil, France.
E-mail address: arineh.cholakian@lmd.ipsl.fr (A. Cholakian).
[1] Now at Laboratoire de Météorologie Dynamique (LMD UMR8539), IPSL, École Polytechnique, Institut Polytechnique de Paris, ENS, Université PSL, Sorbonne Université, CNRS, 91128 Palaiseau, France.

https://doi.org/10.1016/j.atmosenv.2021.118689
Received 31 January 2021; Received in revised form 6 August 2021; Accepted 17 August 2021
Available online 21 August 2021
1352-2310/© 2021 The Authors. Published by Elsevier Ltd. This is an open access article under the CC BY-NC-ND license (http://creativecommons.org/licenses/by-nc-nd/4.0/).

meteorological situation that goes out of the current distribution. For this case study, we propose to distinguish the part of exposure changes due pollutant concentration and population changes. The choice of the study case (weather and horizon) is discussed in the text. This approach differs from the scenario approach, which focuses on the analysis of a trend representative of future years.

1. Introduction

Air quality and climate are intertwined in their effects and their changes, meaning that as a result of mitigating climate change, air quality will improve as well and vice-versa (Jacob and Winner, 2009). Of course, this implies that the climate change mitigation strategy includes an indirect reduction of emission of anthropogenic pollutants into the atmosphere. We already know that atmospheric pollutants can have adverse effects on human health (Pope and Dockery, 2006; Mauderly and Chow, 2008; Anderson et al., 2012). These health effects have been also evaluated for particulate matter, showing that they can, among other conditions, cause commonly cardiovascular diseases such as heart attacks and even more frequently pulmonary diseases ranging from asthma to lung cancer, depending on the size of the particles which determines their depth of penetration into the lungs (Harrison and Yin, 2000). There are also studies suggesting that certain species of PM (specifically dust particles) in addition to the normal cardiovascular effects (De Longueville et al., 2010; Middleton, 2017) can also contribute to the transfer of viral, fungal and bacterial diseases, since some types of these microorganisms are capable of surviving long distance transport (Griffin, 2007). Therefore, mitigation efforts to combat climate change may also help reduce health problems related to exposure to air pollution. However, the very effects of climate change can lead to an exacerbation of emission phenomena, or favor photochemical processes. A future worsening of air quality might be due to (i) increased dust emissions, as a result of drought and land use changes (Mahowald et al., 2010; Mulitza et al., 2010; Lee and Sohn, 2011), (ii) elevated levels of ozone in the atmosphere due to reduced NO_x titration, faster production rates or increased biogenic precursor emissions (Colette et al., 2015; Fortems-Cheiney et al., 2017; Cholakian et al., 2019a), the latter also affecting secondary organic aerosols. Therefore, the analysis of air quality in distant horizons should not only rely on the implementation of emission control and low-carbon policies, but also consider the meteorological expression of climate change.

Such an analysis must also be based on indicators that can be more directly related to health risks, and that integrate more parameters than pollutant concentrations do. Indeed, since the environmental risk is calculated as a cumulative impact on the health of the entire population, the population increase is indeed a mechanical lever to increase the overall risk. Thus, although exposure to atmospheric particles reaches quite high levels in deserts and coastal areas due to the emissions of terrigenous dust and the presence of sea salt, it does not affect the exposure risk, which remains the highest in the world in China and India due to the combination of high population density and elevated pollution levels (Kan et al., 2012; van Donkelaar et al., 2015). Therefore, in the context of climate change, the future impacts of air quality on human health must be assessed by calculating the total population exposure in a given region, taking into account the demographic evolution of this region. In particular, increasing urban population can lead to a redistribution of health issues related to air quality, including local increase of the risk of exposure to primary pollutants in urban areas. As demographic developments may show different features according to socio-economic conditions, scenarios using societal and environmental data should be considered to allow accurate estimates of population growth, aging and distribution across a territory. Such a work has been done for the European area by Tarín-Carrasco et al. (2021), pointing out that the premature mortality is highly correlated with the aging of the population.

Finally, there remains the question of the scale at which air quality simulations must be conducted to produce a relevant analysis of population exposure. Numerous studies have already explored the interrelated effects of emissions control and climate change on air quality, using either global or continental-scale chemistry-transport models. Global models have the advantage of dealing with the Earth system as a whole (Hauglustaine et al., 2014), simulating the connections between global and synoptic meteorological phenomena, and the interactions of the atmosphere with the continental and ocean surfaces. Thus, they can produce estimates of future concentration fields taking into account the multiple drivers of climate change. Continental scale models also have the advantage of being able to take into consideration the transport of air masses over long distances, and to integrate the impact of all sources of gaseous or particulate atmospheric compounds along their path. However, none of them can reproduce fine scale phenomena such as those related to the local topography, or to the heterogeneity of human emitting activities, since for each grid-cell they provide an averaged concentration value that doesn't account for small-scale processes. While it is obviously necessary to have a global vision of atmospheric processes and their consequences, this is not always sufficient to model actual exposure to air pollution as the geography of a site, the local meteorological phenomena, the distribution of human activities and the gradients of population density are needed to produce a better integration of risk across rural and urban areas. Thus, chemistry transport models implemented at high horizontal and vertical resolution and forced by highly resolved data, even on a limited area, provide a more detailed simulation of atmospheric chemistry in complex terrain, and a more realistic representation of concentration field gradients around urban areas. Yet, future climate modeling studies conducted at a high-resolution domain are not reported often in the literature. Therefore, we have decided to conduct a fine-scale study by simulating the exposure of the population on a high-resolution domain over a restricted area, nested into a coarser domain covering a larger area. To the best of our knowledge, these types of studies for this region are not commonly abundant in the literature, especially when exposure of the population and future scenarios are coupled.

This work specifically focuses on air pollution exposure in the Mediterranean area, a region for which the impacts of climate change are expected to be critical. Indeed, not all regions have the same sensitivity to climate change. Some regions can show higher response to a changing climate because of their particular atmospheric and geographic characteristics. Giorgi (2006) calculated a sensitivity factor for climate change depending on precipitation and temperature changes for wet and dry seasons for different regions of the world, concluding that the sensitivity for some regions is much higher than the other ones. In his study, the Mediterranean basin and the north-eastern European region are shown to be more sensitive to climate change than the other studied areas (the study excluded the arctic). Other studies have arrived to the same conclusion as well (Adloff et al., 2015; Ciardini et al., 2016). The Mediterranean region has particulate characteristics, such as presence of orographically high land on its continental surroundings, the longer than usual residence time of atmospheric compounds, the high photochemical potential or the accumulation of local and transported emissions (Lelieveld et al., 2002). Therefore, it is an area in which exposure to pollutants is forced by the geographical configuration, the intensity of solar radiation and the local dynamics of air masses, and therefore, since it has already been shown in the literature that this region is going to experience higher sensitivity to climate change, the Mediterranean can experience a possible exacerbation of a drop in air quality in the future.

Despite this, the future health impacts of air quality in the

Mediterranean region are still partially undetermined. Samoli et al. (2013) explored 10 cities in the Mediterranean region, investigating the particulate matter related mortality for each one. They found that there is a strong correlation between PM2.5 concentrations and air pollution related mortality. The exposure seen in this study is consistent to other city-scaled exposure studies for the US and Europe. The evolution of the composition of the atmosphere –and especially its aerosol content – is therefore critical for this region. However, although studies such as West et al. (2013) found a decrease in future exposure to ozone and PM2.5 at the global scale, few authors investigated the trends of exposure to air pollutants in the Mediterranean basin. This is why we have chosen to focus our study on the provision of new diagnoses on the evolution of air quality in the south of France, on the shores of the Mediterranean. Our target region, called PACA region (Provence Alpes Côtes d'Azur), has a high density of population linked with the presence of multiple urban ports on its coastal boundaries. It has been known for having serious air pollution problems because of high rates of urban and industrial emission and elevated temperature (Sicard et al., 2010). Very high concentrations of PM_{10} have been found in the region using satellite data (Péré et al., 2009). Furthermore, the PACA region is a high-risk area for dust episodes, which constitutes a supplementary concern for human health. A study conducted with the CHIMERE model confirmed the importance of implementing ambitious emission control policies in the area to control oxidizing pollution events (Coll et al., 2009). The combination of demographic and climate scenarios is now needed to provide quantified information on the potential risk of exposure of urban and rural population to air pollution, as well as its sensitivity to climatic factors and emission control strategies.

In this work, we simulated case studies of air quality and population exposure for several scenarios of changes in anthropogenic emissions and climate change (RCP4.5 and RCP8.5) in France, on the southern shores of the Mediterranean. In addition to a baseline year, two years representing respectively the 2030 and 2050 horizons were selected and simulated for each of the two RCP scenarios above. These two years selected have an average annual temperature higher than the median of the distribution over the decade concerned. This choice should make it possible to explore situations with a high impact of climate change on exposure. The simulations were first performed for the European domain, then for a nested domain corresponding to the PACA region - this with a high (5 km) horizontal resolution. The population changes for this region have been estimated from shared socioeconomic pathway (SSP) scenarios, from which the exposure of the current and future population and its changes are discussed.

In the following sections, a brief description of the simulation process is given, then the generation of current and future anthropogenic emissions and population scenarios for the PACA region is explained. Section 4 presents a general assessment of changes in air quality over the studied region, while exposure and its evolution are explored in section 5. Finally, a conclusion on the results of our study is proposed in the last section.

2. Materials and methods

This section provides a brief introduction to the operating principles of the chemistry-transport model (CTM) CHIMERE. The input data used for this study are detailed, in particular the specific inputs used for the high-resolution domain. Finally, the data used for the 2D representation of the current population of the PACA region are presented, and the choice of demographic trends for 2030 and 2050 are discussed.

2.1. CHIMERE CTM

The CHIMERE CTM (Menut et al., 2013) has been used in many studies across Europe and also in other parts of the world, both for research and operational forecasting purposes. Like all CTMs, CHIMERE needs input information in order to perform simulations for a specific region: boundary conditions, meteorological fields, anthropogenic and biogenic emissions as well as chemical reactions and their associated rates have to be provided for the model to operate. Dust emissions are also considered in the model. For African dust emissions, we used the parameterization suggested by Alfaro and Gomes (2001) and the optimizations from Menut et al. (2005). The model proposed by Alfaro and Gomes (2001) is the combination of the saltation flux calculation proposed by Marticorena and Bergametti (1995) and the sandblasting model by Alfaro et al. (1998). For European dust emissions the model follows the method proposed by Zender et al. (2003). Fire emissions can be included in the CHIMERE model as well, but they have not been taken into account in this work because its future evolution was considered as too speculative in this work, depending not only on change in climate variables, but also on forest management practices. For its operation, CHIMERE includes modules that treat horizontal and vertical transport, atmospheric chemistry, formation and size distribution of aerosols and deposition, each one of these parameters being calculated in parallel mode using the related input information. The aerosols simulated in the default version of the model include elemental carbon (EC), sulfate, nitrate, ammonium, SOA (secondary organic aerosols, detailed in the next section), dust, salt and PPM (primary particulate matter other than ones mentioned above). The aerosol module takes into account coagulation, nucleation and absorption; and wet and dry deposition are treated by the deposition module. A sectional logarithmic size distribution is used for the speciation of aerosols into different size bins. More information on the default chemical mechanism, details for the reactions and their kinetic constants are given in Menut et al. (2013).

2.2. Simulations

For a domain covering the entire Europe it would be numerically heavy to use a horizontal resolution that is appropriate for an urban scale (5 km or less). Therefore, the nesting option can be used. In this study, two domains are used: the coarse domain covering continental Europe with a resolution of 0.44° and the nested domain focusing on the PACA region with a horizontal resolution of 5 km being forced by the initial and boundary conditions of the coarse domain (domains shown in Fig. 1). The vertical resolution for both domains is 9 levels ranging from the surface to 500 mb. For aerosols, 10 size distribution bins are used, ranging between 40 nm and 40 μm.

Meteorological fields are taken from the IPSL WRF member of EURO-CORDEX (Jacob et al., 2014) project for both domains; for the coarse domain we used fields with a horizontal resolution of 0.44°, while for the fine domain, more detailed meteorological simulations with a horizontal resolution of 10 km have been used. Biogenic emissions are provided to CHIMERE by the Model of Emissions of Gases and Aerosols from Nature (MEGAN, Guenther et al., 2006): they include isoprene, limonene, α-pinene, β-pinene, ocimene and other mono-terpenes with a base horizontal resolution of $0.008 \times 0.008°$. As CO_2 emissions have a limiting effect on isoprene emissions (HEALD et al., 2009; Tai et al., 2013), the inhibition of isoprene emissions by CO_2 has been added to MEGAN using the parameterization from Wilkinson et al. (2009). Boundary/initial conditions are provided by the LMDZ-INCA global model, specifically ran for the climate scenario used in each test case.

The Mediterranean region presents some challenges when it comes to the simulation of organic aerosols (OA). Most of the biogenic OA existing in the Mediterranean atmosphere is transported from the continental Europe towards the basin, since there are no emissions of precursors for this species at the sea surface. Furthermore, it has been observed that the biogenic OA in the region accounts for the majority of OA, especially during summer. Therefore, since the possibility of aged OA being moved from the continent towards the basin is higher, it is important to integrate a scheme that takes into account the OA aging. This is why we have been modifying the representation of OA in the version of the model used for this study, in order to better account for the specificities of the Mediterranean region. It is based on the VBS (volatility basis set)

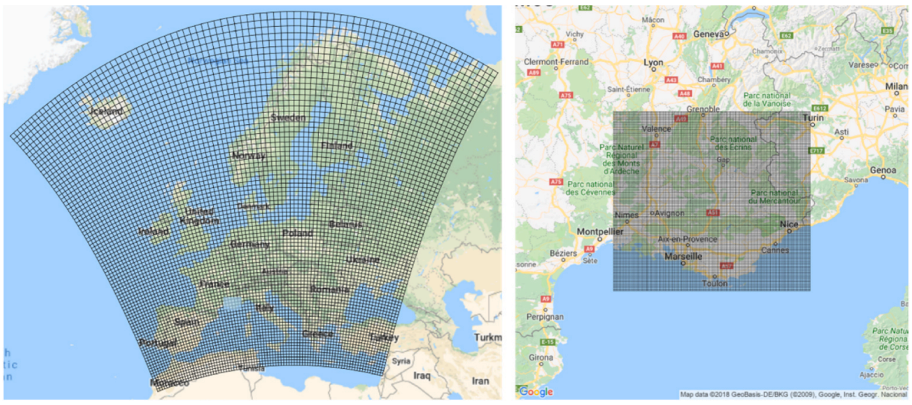


Fig. 1. Domains used in this study. Left: coarse domain with a horizontal resolution of 0.44°. right: nested domain with a horizontal resolution of 5 km.

scheme, which was first proposed by Robinson et al. (2007), and which distributes the organic aerosols in several volatility bins using the saturation concentration (C*), ranging from 10^{-2} μg m^{-3} to 10^{6} μg m^{-3}. In this scheme, the aging processes for biogenic secondary organic aerosols (BSOA) and anthropogenic secondary organic aerosols (ASOA) are taken into account, as well as the emissions of intermediary volatile organic compounds (IVOC) and semi-volatile organic compounds (SVOC). Shrivastava et al. (2013, 2015) proposed some modifications to this scheme, adding fragmentation and formation of non-volatile SOA to the normal VBS scheme. In our study, this last version of VBS has been implemented in the CHIMERE model. The scheme has been previously tested for the Mediterranean region, for the year 2013, using the data obtained during the ChArMEx campaign for two in situ sites (Cap Corse and Mallorca). In this configuration, CHIMERE showed good agreement with the observed mass concentration and oxidation state of the organic aerosol (comparisons performed using the results of the PMF method) and with the origins of this aerosol (comparisons performed using the results of the ^{14}C measurements) for both sites mentioned above. A detailed explication of this validation is given in Cholakian et al. (2018). Also, the model configuration was validated over Europe for around 30 stations, as Cholakian et al. (2019b) found an overall good performance for this scheme, despite some underestimation during winter.

Our work is based on the simulation of 5 target years: one historic year reference year corresponding to the current situation, and four future case studies based on 2030 and 2050 timeframes. The year 2005 was chosen for the baseline simulation and the years 2033 and 2053 were used for the future test cases, as they showed - for the coarse European domain - higher than average temperature increases for the periods 2026 to 2035 and 2046 to 2055, respectively. These years were chosen by plotting the temperature distribution of both decades in the climate runs performed for the European domain, the years representing the 70% quantile were chosen. For each of those future timeframes, two distinct situations corresponding to representative concentration pathways (RCPs, Meinshausen et al., 2011), RCP4.5 (Thomson et al., 2011) and RCP8.5 (Riahi et al., 2011) have been simulated, according to the CMIP5 IPCC (IPCC, 2014) report.

2.3. Anthropogenic emissions

For the coarse domain, emissions provided by ECLIPSE-v4 (Amann et al., 2013; Klimont et al., 2017) have been used. For the historic simulation, baseline emissions of 2010 are used, while current legislation emissions (CLE) for 2030 and 2050 are assigned to the future scenarios. However, the base resolution of the ECLIPSE inventory is 0.5°, which is too coarse for our nested domain. Therefore, local bottom-up emissions dedicated to daily air quality forecasting were collected from the PACA air quality network (AtmoSud, https://www.atmosud.org/), with a base resolution of 1 km. It is important to notice that these emissions correspond to the current period. Thus, 2030, 2050 emission projections have been calculated using the ECLIPSE emission ratio between the reference year and each of the two CLE scenarios, in order to ensure consistency between the coarse domain and the nested domain, on the specific point of the evolution of anthropogenic emissions.

Since the emissions provided by the AtmoSud network are defined on an irregular domain (shapefiles), a formatting process chain was carried out: it consisted of distributing the emissions on a 2D network and re-gridding them on a mesh useable in CHIMERE. Furthermore, AtmoSud emissions being limited to the administrative borders of the PACA region, a third necessary step of our formatting work was to fill the sides of the irregular domain with information provided by a complementary emission inventory (here MACC-III emissions for the same year, with a base resolution of 7 km, Kuenen et al., 2014). Finally, the obtained kilometric anthropogenic emissions had to be aggregated to fit the 5 km-resolution domain that will be used in our simulations. These steps are illustrated in Fig. 2. The emissions corresponding to the scenarios CLE 2030 and 2050 were then calculated from this inventory, using the evolution factors observed on the ECLIPSE inventory, as explained above. As the ECLIPSE inventory provides details of emissions by SNAP sectors (Selective Nomenclature for Air Pollution) for all listed species, evolution factors from 2010 baseline emissions to either CLE 2030 or CLE 2050 emissions were estimated for each snap sector in the PACA region, and applied to the AtmoSud inventory.

2.4. Current and future population for the PACA domain

The current population of the PACA region was calculated by LCSQA (Central Air Quality Monitoring Laboratory, LCSQA, 2015) on the same domain as that used for the current PACA emissions with a resolution of 1 km. So, the same projection and re-gridding procedure was conducted in order to obtain a population density dataset compatible with CHIMERE outputs. The results are shown in Fig. 4-a.

As described in Jones and O'Neill (2016) and O'Neill et al. (2017) several scenarios may be considered for the projection of population density, in order to consider different possible trends for population growth and urbanization. In our study, estimates of the future population density in the PACA region were derived from shared socioeconomic pathways (SSPs) provided at an initial resolution of 0.125°. The scenarios, which are described below, were compared to current situation provided by the same authors for the PACA region, and the factors of differences were applied to the current population density of the PACA region in order to get the 2030 and 2050 population scenarios.

SSPs are future scenarios that take into account energetic, economic and land use changes as well as emissions and radiative forcing changes.

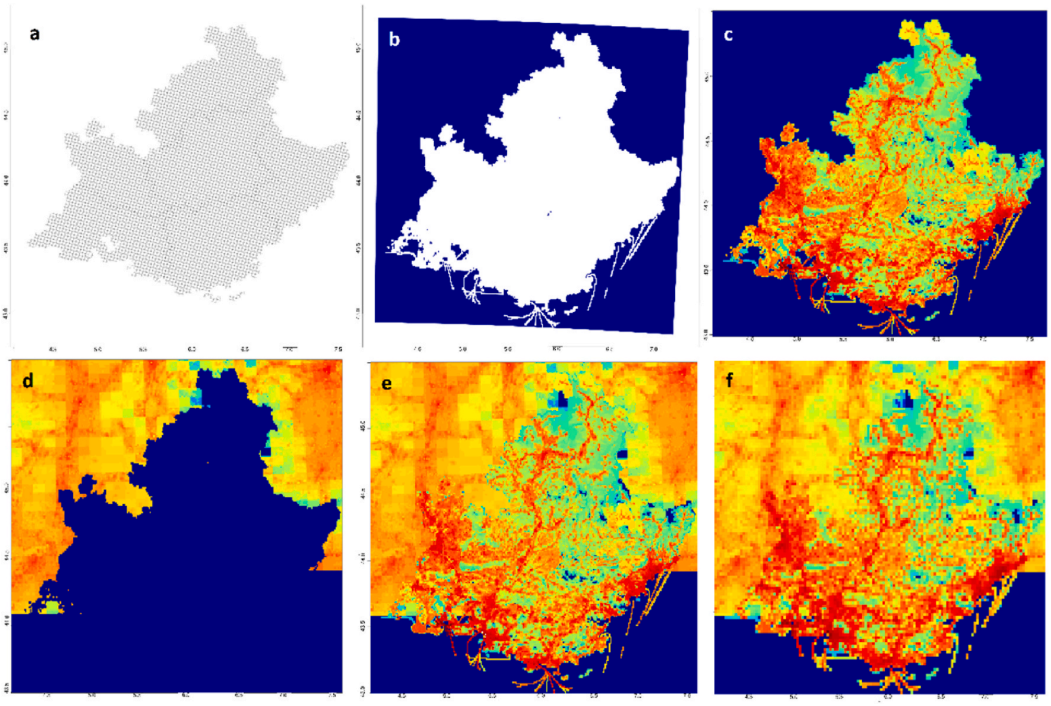


Fig. 2. The procedure of preparation of anthropogenic emissions for the PACA region (here shown the emissions of NO. a: the irregular domain the data was provided on. b: the same domain as a, but distributed regularly on a lambert domain. c: anthropogenic emissions distributed for the PACA region, projection changed from lambert to lan/lot. d: Same as c, but the exterior part of the domain is filled with MACC-III emissions. e: the panels c and d combined to provide the desired results in a 1k horizontal resolution, f: Same domain as d, re-gridded on a 5 km horizontal resolution.

There are five SSP scenarios, each based on a different possible narrative of alternative socio-economic development (Riahi et al., 2017). The population change in each scenario has been projected using mortality, fertility and migration parameters, while urbanization has been estimated only by using current fertility and income conditions. In each scenario there are two concepts that can change: global response to mitigation and to adaptation. All five SSP scenarios will be explained in this section, with an explication of what each of these scenarios could mean for the French population. At the end, a choice of two scenarios will be done in an effort to present the extreme future possibilities for France. The population change trends in SSPs for France are shown in Fig. 3.

SSP1 accounts for the sustainability trend, where environmental boundaries are respected and where the world moves slowly towards low resource and low energy use, also leading reduced inequalities between and within countries. This scenario assumes that there will be low challenges for the sustainable way of life and seems excessively optimistic. In this scenario, population growth seems to slow down in high fertility countries because of more investment in education and health care. High but constrained urbanization is envisioned in this scenario. As for total population, it shows an increase until the 2040s and then starts to follow a decreasing pattern, while urbanization still increases till the end of the century. This scenario assumes low challenges for both mitigation and adaptation.

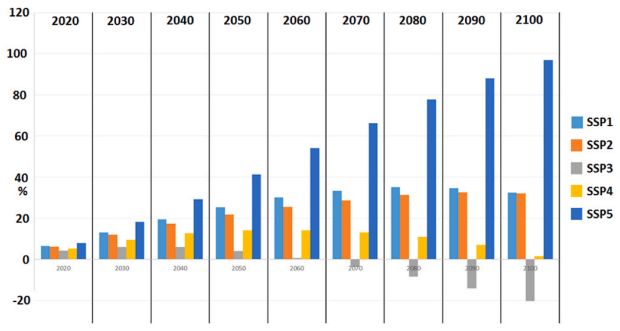


Fig. 3. Population change (in %) in all SSP scenarios for France, compared to 2005.

SSP2 is the "middle of the road" scenario. In this scenario, the patterns of economic and technological growth follow the historical trends: some countries progress very well while others do not. Therefore, inequalities still exist between countries. Finally, international development goals (in economy, renewable energy usage, population stabilization, etc.) are achieved but much more slowly than anticipated. Population increases till the 2070s and then shows a decreasing pattern. Urbanization is moderate in this scenario but it continues till the end of the century. It assumes medium challenges for mitigation and adaptation.

SSP3 is a regional rivalry scenario. Nationalism becomes more important than globalization, conflicts between countries and regions are likely and the policies become more oriented towards national or regional defense than environmental concerns. Economic development is slow and inequalities between countries increase over time. While environmental degradation worsens in many regions, no priority is given to this issue. Population as well as urbanization continue to increase until the end of the century, although the urbanization growth rate is lower compared with the other scenarios. This is a scenario where mitigation and adaptation become extremely difficult.

SSP4 can be defined as an "inequality scenario". It is somewhat similar to SSP3 in terms of slow economic and technological change. The difference between the two is the widening gap of inequalities both country-wide and between different countries, and conflicts become common. Inequalities both in economic opportunities and political power divide the world into two groups: the population majority in bad

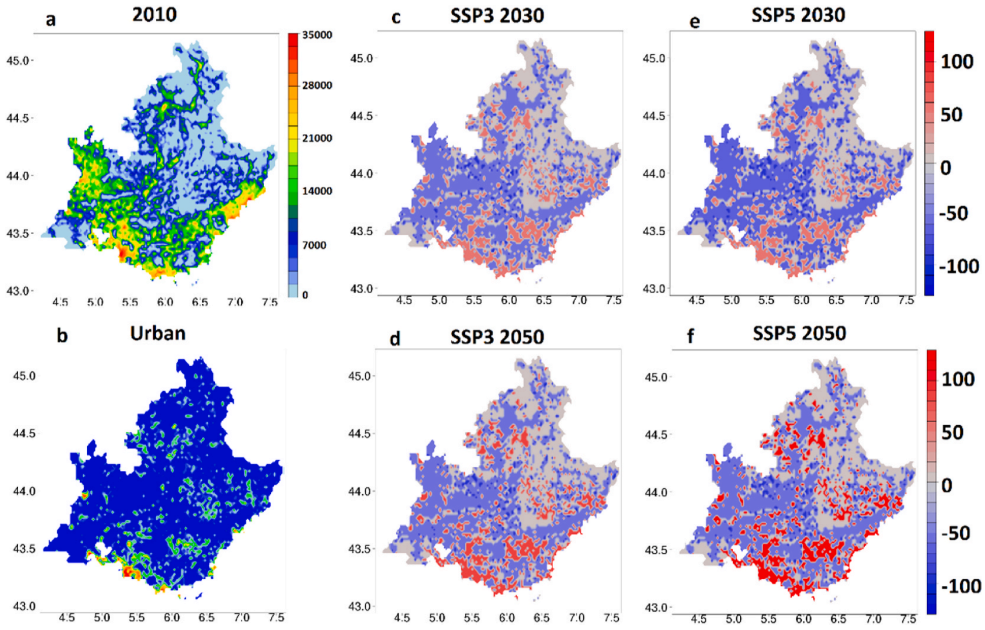


Fig. 4. Re-gridded population for 2005 (a) and its changes in future SSP3 and SSP5 demographic scenarios for 2030 timeframe (first row) and 2050 timeframe (second row) for the PACA region. Panel b shows the urban land use area in the PACA region.

economic conditions and the elite in power. Environmental concerns are treated regionally, in areas where the populations with high income reside. Population in this scenario grows until the 2070s before starting to decrease. Urbanization is strong and comparable to that of SSP1. Mitigation presents low challenges because of the power disparity while adaptation is extremely difficult.

SSP5 is the fossil-fuelled development scenario. In this scenario, the global market remains important and an increasing faith is placed on innovation and participatory societies that encourage fast technology and develop human capital (increased healthcare and education, etc.). These improvements however are performed using fossil fuel and the energy use around the world is intensive. Local environmental problems are solved rapidly, while global ones still remain. The population in this scenario starts decreasing in the 2040s and follows this trend until the end of the century. Urbanization however shows an increase similar to SS1 and SSP4. As expected, mitigation is assumed to be difficult for this scenario, while adaptation challenges are low.

The changes in population induced in each country by a given scenario may be different, due to national specificities such as fertility, mortality, migration and income. France is ranked among the high-income countries (Bank World, 2017), and its gross domestic product (GDP) shows an increasing trend in all SSP scenarios. On this basis, an increase in the population is predicted for SSP1 and SSP2 until the 2050s, and for SSP3 and SSP4 until the 2080s, before decreasing slightly (Fig. 3). In 2100, the SSP3 scenario even results in a lower total population than in 2020. SSP5, on the other hand, predicts a continuous increase of the French population until the end of the century. It is interesting to note that the share of urbanization (i.e. the urban to total population ratio) increases in all scenarios for high-income countries, and can reach as high as 95% by 2100.

In order to study the widest range of exposure variation in the PACA region, we therefore chose to focus our air quality analysis on the SSP3 and SSP5 scenarios, with SSP3 experiencing less population growth and urbanization, in a context of global conflicts and large regional inequalities, and SSP5 showing the highest population growth and the largest urbanization for the region. Thus, although all the demographic scenarios have been simulated, we will only detail here the results obtained with the SSP3 and SSP5 projections. The resulting population changes, when compared with the reference simulation, are shown in Fig. 4 (panels c through f). In summary, in the PACA region, the population decreases in SSP3 in the 2030s and continues to do so until the 2050s. This decrease of population happens in rural areas, urban areas showing an increase in population for this scenario. For SSP5, population decreases in the 2030s, and shows an increase in the 2050s, the rural/urban changes of this population change remain similar to SSP3.

It is important to keep in mind that, although the Eclipse anthropogenic emissions already take into account future demographic changes. SSP scenarios are needed in this work as a best available scenario on future population changes need for exposition calculation. It might also be interesting to keep in mind that while RCPs and SSPs are different sets of future scenario types and were conceived to be complementary of each other, RCP8.5 and SSP5 are quite consistent with each other since both represent a “business as usual” type of scenario.

3. Results

In this section, a thorough analysis of the changes in the meteorological situation between 2005 and the future climatic case studies - as well as a comparative analysis of the simulated chemical concentration fields - is presented as a first step in the analysis of pollutant exposure maps for each future situation.

3.1. Meteorological parameters

Fig. 5 shows box plots of changes in the main simulated meteorological parameters (temperature, wind speed, relative humidity, height of the boundary layer, amount of precipitation and number of rainy hours) between the reference simulation and our prospective case studies. Changes with respect to the regional averages of the historical (2005) period are indicated, so that the box plots show the local spatial climate variability. It is important to keep in mind that the simulations are conducted for different years having their own meteorological specificities, so the inter-annual variability adds to the average impact of the scenario.

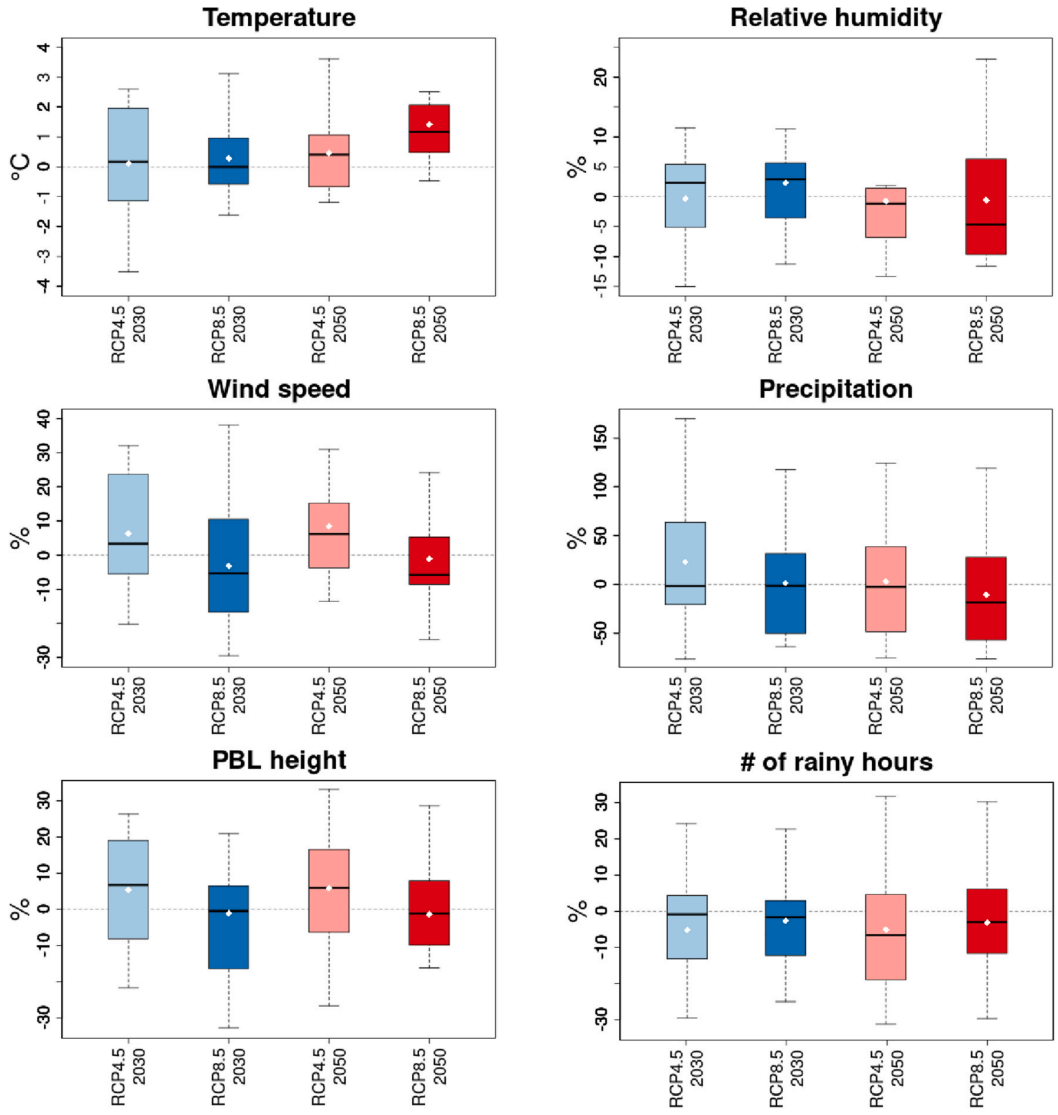


Fig. 5. Changes of meteorological parameters in future scenarios compared to historic simulation for 2005. The values are shown in percentage, except for temperature for which the delta in °C is shown. The boxplots are standard boxplots, the white spot on each boxplot shows the average for each one, the name of the scenarios is given on the x-axis of each grid. The dotted line shows the 0 reference.

Fig. 5 shows changes in average temperature between the 2005 reference simulation and the future case studies. They are small for the 30-RCP4.5 and 30-RCP8.5 scenarios, below 0.1 °C, +0.3 °C for the 50RCP8.5 scenario, and largest for the 50-RCP8.5 scenario, showing a temperature increase of 1.4 °C. Conversely, relative humidity remains on average rather unchanged between the different situations (modifications below 3%), but the median relative humidity and show a stronger decrease (−6%) and the variability is strongest in 50-RCP8.5. Similarly, the average amount of precipitation only shows slight changes from the historic to all the target years (with exception of 50 RCP-8.5), although a large increase is observed in the highest percentiles of all future simulations.

The average number of rainy hours keeps on the average again rather unchanged with stronger decreases in the 30-RCP4.5 and 50 RCP4.5 scenarios (−5%). Average 10m wind speed and boundary layer height most strongly increase for the 30-RCP4.5 50-RCP4.5 scenarios, by respectively (+5 to +9%) and (+5–6%). As a conclusion, largest temperature increase is observed for the 50-RCP8.5 scenario and is correlated to decreases in relative humidity (median), precipitation, and wind speed.

This study should be understood as a case study of 4 different situations, not future scenarios. In this article, the case studies have been noted as "representative of a decade-RCP", reminding that each future simulation has been chosen among a given decade. As an example, the case study simulated for the meteorological year 2033, under the RCP8.5 tendency, is called 30-RCP8.5.

3.2. Changes in chemical species

Our analysis focuses on a restricted series of compounds, whether primary or secondary, that account for species that are predominantly present in urban and suburban smogs, and aerosol fractions that may be sensitive to climate change and environmental policies. Fig. 6 traces the evolution of the simulated seasonal concentrations of ozone (O_3) and nitrogen oxides (NO_x), but also of particulate matter (PM_{10} and $PM_{2.5}$) and its fractions, for the 4 future case studies, as an average over the

nested domain of our study. Note that whenever a Figure is shown for O_3 in this study, it refers to the simulated daily maxima values (based on 8h running means) in order to be consistent with the regulatory threshold for human health protection. In Fig. 6, the changes in the simulated concentrations between the baseline simulation and each of the scenarios result from both the meteorological specificities of the target year and the associated reduction in anthropogenic emissions. Each panel presents the results of a particular pollutant, with case studies being associated with a given color (2033 simulations in blue, 2053 simulations in red, light colors for RCP4.5 scenarios and dark ones for RCP8.5 scenarios). 2D representations of O_3, NO_x, PM_{10}, $PM_{2.5}$, dust and BSOA concentrations are also presented in Fig. 7. These maps show the mean annual concentrations of the pollutants for the reference simulation (in ppb for ozone, in $\mu g.m^{-3}$ for the PM) and the percentage of deviation from these values, for the scenarios. They allow a spatial discrimination of the evolutions of the pollutant concentrations between the reference and the case study. Note also that, for each species, only the season in which it shows the highest average concentration was displayed, summer for ozone. That is, winter for NO_x, spring for PM_{10}, $PM_{2.5}$ and dust, and summer for BSOA.

The concentrations of primary components such as nitrogen oxides depend directly on their related emissions. Thus, predictably, NO_x concentrations (see Fig. 6-b) show a strong diminution in all scenarios – from −20% to −40% – that is mainly the result of anthropogenic emission control at the horizons 2030 and 2050. The same effect can be observed for the gaseous and particulate ammonium concentrations (ammonium particles - not shown in figure – undergo a decrease ranging from −10% to −50%). On the contrary, a large number of parameters – such as the availability of precursors and atmospheric conditions for chemical transformation – affect the evolution of secondary species such as ozone and BSOA. For ozone, a global decrease is observed, which might be explained by the simultaneous decrease in NO_x and volatile organic compounds (VOCs) emissions, thus leading to reduced photochemical production. However, a strong seasonal dependency is expected for this species, as it can be seen in Fig. 6. In winter, meteorological conditions are unfavorable to the production of ozone, therefore the reduction of ozone titration by NO_x in emitting areas (as seen in Fig. 7) becomes a dominant effect, and leads to the lower average decrease of ozone in Fig. 6. In summer, conditions for ozone production are present, and their concentration gets higher than other seasons (annual average of around 40 ppb). Although titration by NO_x also exists at this season, the main impact of the scenario is the fact that ozone production then becomes strongly unfavorable due to the lower availability of NO_x. As a matter of fact, a maximum reduction of −12% means around 4 ppb of decrease on the average. Spatially, ozone concentrations are higher in the north and north-western parts of the domain, probably because of the more rural nature of these areas (for verification of rural areas please refer to Fig. 4 for population of the region and Fig. 10 for the population density of the domain).

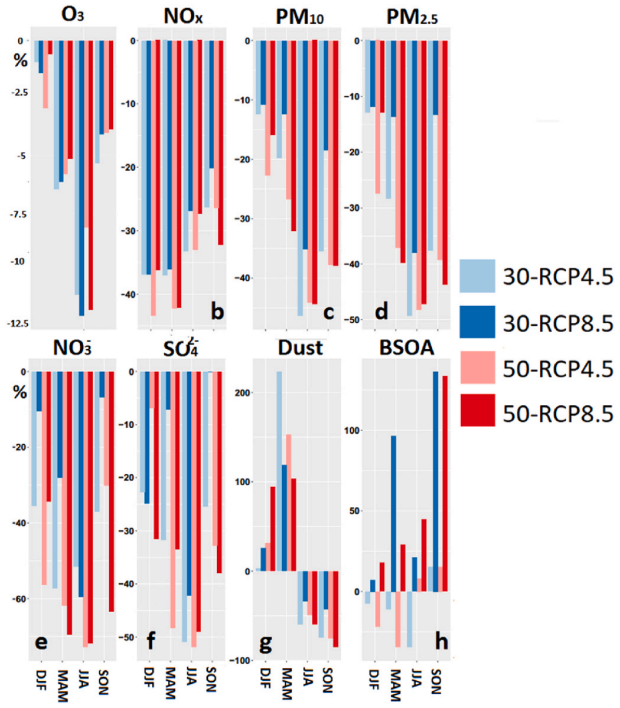


Fig. 6. Seasonal concentration change seen in future scenarios for a number of components (in %). Name of each component is written on the top of the panel. For all future situation, the average changes for all seasons are shown.

As shown in Fig. 6 (panels c and d), PM_{10} and $PM_{2.5}$ each show decreases as well. This tendency is mostly due to a diminution in the concentrations of nitrates and sulfates (see Fig. 6-e and 6-f) in our simulations. The reason for the decrease of these two species is the respective reduction of NO_x and SO_2 emissions (for a decrease of around −40% and −50% for NOx and −30% and −40% for SO_2 for 2030 and 2050 respectively for France), whereas for nitrates there is an additional effect due to the increase in temperature which leads to a greater evaporation of nitrates already formed (Bauer et al., 2007; Hauglustaine et al., 2014; Seinfeld and Pandis, 2016). No significant change in the salt concentrations is seen in the future case studies, while an increase in dust concentrations is observed in most cases (will be discussed in the next section). Seasonally, their trends in both PM_{10} and $PM_{2.5}$ seem similar: showing smaller changes in winter for both PM_{10} and $PM_{2.5}$ and higher changes in summer and autumn. The changes for spring for PM_{10} seem however to be lesser than and $PM_{2.5}$, probably due to the increase in dust concentrations which are mostly in the coarse size fraction. Spatially, PM_{10} shows high concentrations in the southern and south-western coasts of the domain (Fig. 7), notably because of salt emissions from the sea as well as high sulfate concentrations due to the proximity of industries and maritime traffic. Sulfate concentrations show a similar spatial distribution to total PM, both in reference simulation and future changes, higher concentrations in southern coastal areas and a future decrease for all seasons. Nitrates though, show higher concentrations in northern part of the domain, though the spatial variation of the future changes stay quite homogeneous all throughout the domain. The transport of dust particles is another reason for the higher concentrations of PM_{10} near the Mediterranean coasts, this transport has been shown in different studies such as Israelevich et al. (2012); Denjean et al. (2016); Vincent et al. (2016). Its concentration as an average shows a diminution in all test cases (lowest change for 30-RCP8.5), while showing a stronger signal near the coast lines. $PM_{2.5}$ shows a similar spatial distribution to PM_{10}, its changes in future case studies showing a more homogeneous decrease across the domain.

Unlike other major particle fractions, BSOA mass concentrations increase in the majority of our future case studies (Fig. 6-h). This change is attributable to the increase in temperature in the scenarios; because of that, biogenic VOCs (BVOCs) emissions are simulated to step up, resulting in greater production of secondary organic aerosol (Cholakian et al., 2019a). However, opposite effects have to be considered for BSOA. Indeed, higher temperatures may thermodynamically limit the transfer of gaseous semi-volatile VOC (SVOC) to the particulate phase (Cholakian et al., 2019b). Another process that impacts the BSOA budget is the CO_2 inhibition added to MEGAN in this work, where with higher CO_2 concentrations come lower isoprene emissions. In our simulations, the increase of the BSOA particulate mass is the dominant effect in RCP8.5 scenarios (dark colors), while a slight global decrease is simulated in the RCP4.5 scenarios (light colors) for most of the seasons. It therefore seems that the increase of BVOC emissions in the hottest scenarios eclipses the effects of BVOC phase equilibrium, and that the impact of CO_2 on

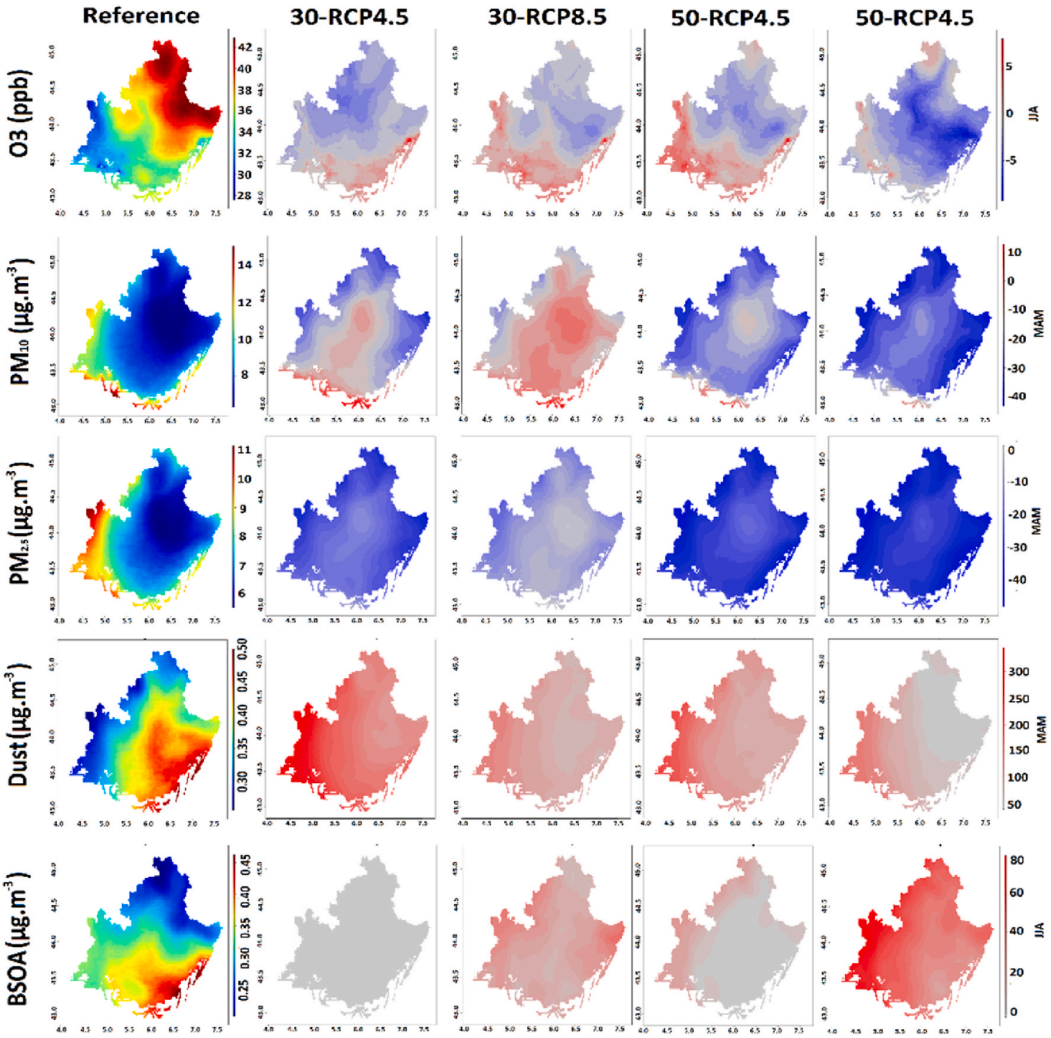


Fig. 7. 2D representations of ozone, PM10, PM2.5, dust and BSOA concentrations for the PACA region. The first column on the left shows the absolute annual concentrations in the historic simulation (2005), while the four right columns show the change in concentrations relative to the historic simulation for each RCP case study. Each row shows one species, for the season in which the concentration shows the highest changes. The name of each scenario is written above each column and the name of each component is written on each row.

isoprene emissions is then of the second order. Quantitatively, the increase in BSOA concentrations become quite high in 50-RCP8.5 (dark red bars), reaching a factor of 2 in spring and exceeding it in fall. It is important to take into account that changes in soil humidity have not been taken into account in the BVOC emission changes.

It seems to be a logical possibility that dust emissions could increase in future scenarios: droughts, land use changes and deforestation will result in broadened dust emissions, all three of which being probable outcomes in future scenarios (Brey et al., 2020); although the uncertainties concerning this species in future scenarios is so high that it is hard to say for certain how its emissions will be affected (Tegen et al., 2004; Evan et al., 2014). As for this study, dust concentrations double in spring in all scenarios (see Fig. 6-g), while they strongly decrease in summer and fall. Spring is the period when the most significant dust episodes take place in the northern African deserts, the dust-rich air masses being transported partly to the Mediterranean, thus affecting the PACA region (Vincent et al., 2016). Dust concentrations are high at the southern coasts of the domain, because of their transport from Northern coasts of Africa towards the south-western coasts of the PACA region. They show an increase in concentration in all case studies, for this area, and especially in spring. This being said, there are major uncertainties when it comes to the simulation of dust concentrations, especially regarding to how they have been taken into account in the global model which has been used as boundary conditions.

Changes in the concentration of the gaseous and particulate species analyzed here, combined with future population projections, result in variations in the exposure of the population to each of these species. Total and spatialized population exposure, in the different scenarios, are explored in the following section.

3.3. Population exposure to atmospheric components in future scenarios

We combined the population density maps and the concentration fields of the main pollutants simulated with CHIMERE, in the current situation and for the years 2033 and 2053, for the RCP4.5 and RCP8.5 scenarios, for each of the different demographic scenarios. As mentioned above, the presentation of the results will be based on the SSP3 and SPP5 projections only.

We first conducted a seasonal analysis of the evolution of exposure from the historic run, and the results are only presented for the least

favorable seasonal situations of each SSP. These data are presented in the form of 2D fields, for each pollutant and demographic/climatic scenario, in order to identify spatial disparities in the evolution of the "exposure" parameter. Finally, in order to address the issue of dense inhabited regions versus rural areas, we have searched for the areas where the model would predict a greater sensitivity to the climatic scenarios and the selected years. To this end, we present plots for each county, an administrative division which allows to distinguish 6 zones in the PACA region. All these results allowed us to define trends in the evolution of the exposure of the population in the PACA region between the current situation and warm future years, and to determine in which situations, in which zone and for which pollutants and seasons the evolution of the exposure was the most unfavorable of all case studies.

3.4. Exposure analysis for the entire PACA region

Fig. 8 shows the results of exposure calculations for the 6 studied species and seasons presented in previous figures, for each climatic scenario and for the SSP3 and SSP5 demographic projections. The values shown in the panels correspond to the percentage of change in total exposure (second and third rows of charts), compared to the baseline population exposure (first row). Each color corresponds to one of the 4 future situations studied: 30-RCP4.5 and 30-RCP8.5 (light and dark blue) and 50-RCP4.5 and 50-RCP8.5 (light and dark red).

On the average, total exposure shows a strong reduction for background nitrogen oxides and for particulate matter in both size fractions. This decrease ranges from −53% to −63% for nitrogen oxides and from −5% to −50% (depending on the case study, season and fraction) for particulate matter, in the selected SSP scenarios. It can be concluded that the reduction of emissions is never offset by the increase in the population, since the total health risk decreases whatever the season and the case study simulated with CHIMERE. Of the 4 simulated future situations, we can see in both figures that the effect on NO_x exposure is very little sensitive to the season and to the considered time frame, and that the difference between the two population scenarios is moderate, showing smaller decrease in exposure when the more densely populated SSP is discussed. It is interesting to note that exposure reduction is quite strong for this species since the NO_x are primary pollutants and future emissions reductions should have a significant impact on their concentrations.

Exposure to ozone appears highly dependent both on the demographic scenario and the time horizon at which the analysis is

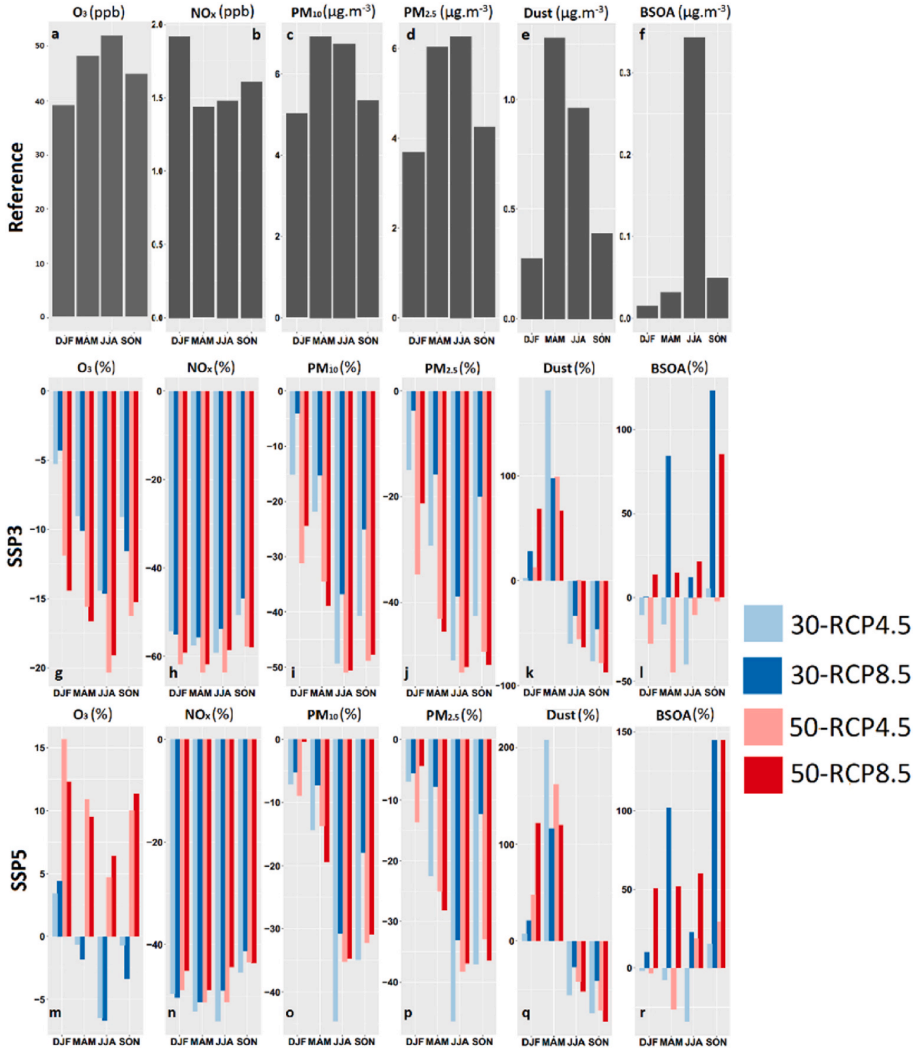


Fig. 8. Population-weighted exposure in the reference simulation and its changes (in %) compared with the reference simulation for the SSP3 and SSP5 demographic scenarios, presented by season and for ozone, nitrogen oxides, particulate matter, dust and BSOA. The name of the species is shown above each panel.

conducted. In the SSP3 (Fig. 8-g) scenario where the population increase is moderate (in particular for urban areas), the general trend is a decrease in total exposure to ozone for all the modeled situations (around −10% on average). The 50-RCP4.5 and 50-RCP8.5 simulations are the most favorable, mostly because they show a decrease in the total population in the region. For SSP5 simulations, on the reverse, CHIMERE predicts a moderate increase in total ozone exposure in the most distant scenarios (from 5 to 15%) and for the whole year, whereas for the 2030 horizon this effect is close to 0 (less than 5% of variation). Interestingly, exposure is always 10–15% lower in 2030 than in 2050, while it is similar for the RCP4.5 and 8.5 pathways.

For both the SSP5 and SSP3 scenarios, we also note that the evolution of exposure is always more favorable in summer (owing to the decrease in the ozone maxima) than in winter (when the reduction of titration by NO is dominant). Largest differences between SSP3 and SSP5 occur in the 2050 scenarios. Reasons for this will be given in the next section.

On the other hand, the signal observed on the particles is much more variable. Two major effects are observed in our case studies. Firstly, the expected decrease in total PM exposure is greater in summer and fall and lower in spring, especially for PM_{10}. This is at least partly an effect of the increased dust particles concentrations in spring. Second, for both PM size fractions, in the short term (2030, blue bars), there is a very high sensitivity of total exposure to the RCP scenario, with a much less favorable situation for the hot 30-RCP8.5 situation (dark blue bars) for both demographic projections. This suggests that climatic conditions play a very important role in particle exposure, in a scenario in which emission inventory is little different from that of today. This is no longer the case in the 2050 simulations, when both RCP scenarios are very favorable, suggesting that the prevailing effect is the long-term reduction of particulate emissions.

It is important to mention that the sensitivity to the demographic scenario is significantly higher for PM_{10} than for $PM_{2.5}$. We have seen in Fig. 7 that the concentration variation in PM_{10} was strongly localized on the Mediterranean coast, a rather highly urbanized area. We can therefore conclude that the demographic scenario (and in particular the increase in the coastal population) is a driving element for PM_{10} exposure in our PACA simulations, in addition to dust concentrations (see below). Since this is highly dependent on the dust fraction, for which the contribution increases in spring (Fig. 8-k and 8-q), it will be interesting to analyze in detail the spatialization of the risk of dust exposure in the different SSP scenarios (see below). Albeit they make up an important part of the PM10 concentration, we didn't consider the role of sea salts in this analysis, as their concentrations were very little variable from one situation to another (as also mentioned before). Conversely, sensitivity to the SSP scenario is lower for $PM_{2.5}$ than PM_{10} in our 4 future situations. Part of this effect is due to the fact that the different components of this fraction (BSOA, nitrates, sulfates) follow very different behaviors in our scenarios. In fact, despite decreasing exposure to nitrate and sulfate fractions, we note that CHIMERE predicts a significant increase in the concentration of the biogenic SOA particulate fraction in the case studies associated with the strongest temperature increases (30-RCP8.5 and 50-RCP8.5). This result generally leads to an increase in total exposure to BSOA in the PACA region, even if the amplitude of the effect is extremely dependent on the climatic conditions. Another reason for the low dependence of $PM_{2.5}$ exposure on the SSP scenario is the fact that some of the $PM_{2.5}$ components are secondary fractions whose formation is strongly climate dependent (BSOA notably). This analysis will be completed in the following section with a 2D-plot of the risk of exposure to $PM_{2.5}$.

3.5. Spatial analysis of the simulated exposure tendencies

As an averaged value does not fully capture changes in population exposure, we conducted a spatial analysis of the results. In Fig. 9 are reported only the species presenting marked spatial tendencies, for the SSP5 scenario.

The 2D maps presented in Fig. 9 represent the evolution of exposure between the historical simulation and each of the future case studies for the SSP5 demographic scenario. In the case of ozone, this Figure shows that urban areas – mainly located on the coast - are subject to increased total exposure, combining both increased concentrations (increased individual exposure) and population growth (increased total risk). These maps are congruent with population growth (Fig. 4-c to 4-f), indicating that population growth is once again the driving parameter of total exposure in our study. However, red areas extend beyond the boundaries of dense urban centers (see the land use map in Fig. 4-b). This indicates that exacerbated ozone exposure also affects the sub-urban areas of the region. Conversely, inland, in the most rural areas, there is a downward overall risk of exposure to ozone, for all the future situations considered in this work. On the average, increased exposures over the coastal areas dominate in absolute terms, which leads to the largest summertime ozone exposure increases for the 2050 SSP scenario.

Spatial patterns are particularly visible for the dust component of PM_{10}. Indeed, there is an increased exposure of at least 40% on all urban grid points (see urban land use in Fig. 4-b). When we cross this map with Fig. 7, which shows that the increase in dust concentrations affects especially the South and West of the domain, we can conclude that – for our scenarios – there is an increased individual (due to concentration rise) and total (due to increased population) risk of exposure to dust on the French Mediterranean coast. We have referred above to the issue of dust as potential vectors of microorganisms such as viruses. In this context, the facilitation of dust transport by favorable climatic conditions (wind, drought) must be considered as a health risk factor for populations over the western Mediterranean basin. However, to better assess the evolution of dust particle sources in future situations, it is necessary to work on the evolution of land use in African source areas. In other words, the land use changes that will occur because of climate change should be considered in order to change the emissions of dust that arrives to the studied domain here (either via changing the land use itself or via changing the boundary conditions used in future test cases), otherwise only the meteorological effects of climate change will be visible on the concentration of dust in the tested future situations.

The same spatial analysis can be conducted for the evolution of the BSOA fraction of PM2.5 particles, as the largest increase in the total exposure risk is observed in areas experiencing the strongest population increase. However, the comparison of case studies that differ greatly in the mean annual temperature (in particular 30-RCP4.5 and 30-RCP8.5) shows that the evolution of exposure to the BSOA fraction remains mainly dependent on climatic conditions.

3.6. Localization of the main risks

As explained above, high spatial variability is seen in the exposure of the population with urban areas showing higher total exposure than rural areas. Also, current air pollution related mortality studies show that the PACA region in general presents high rates of mortality, with very strong relationships between the evolution of respiratory and cardiovascular diseases and that of urban concentrations of pollutants (Sicard et al., 2010, 2011). In order to support health risk management, it is essential to identify the typologies of areas that are most involved in global risk, as well as those where this overall risk evolves most over time.

This is why we propose a first approach to risk management support by looking at the geographical distribution of the risk of exposure, taking into account territorial divisions. We have divided the PACA region into its administrative counties, corresponding to the French sub-regional "*departements*" in France. Our first goal is to determine whether all the geographical zones of the domain show similar total risks related to air pollutant exposure, or if it appears specific zones carrying a greater part of the total risk, or even areas particularly sensitive to future climate and socio-demographic trends, such as those simulated in our case studies.

For these purposes, we used the works of Yao et al. (2014) who

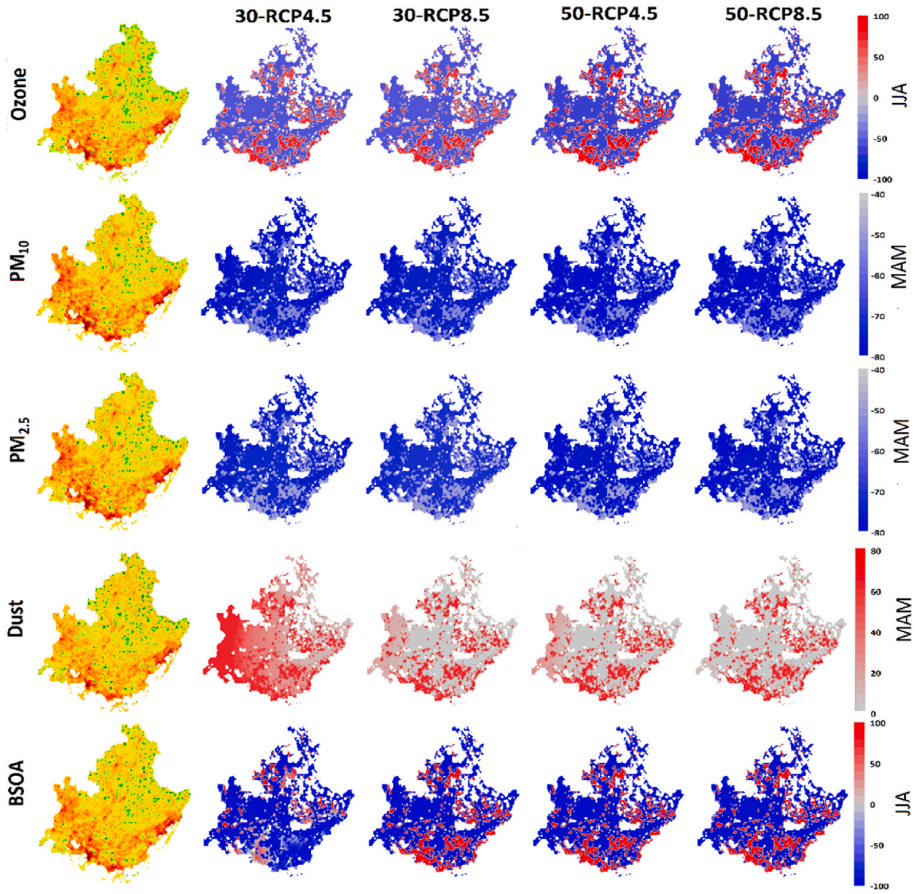


Fig. 9. 2D representations of exposure to ozone, PM10, PM2.5, dust and BSOA for the PACA region for the SSP5 scenario. The first column on the left shows the exposure in the historic simulation (2005), while the four right columns show the changes relative to the historic simulation for each RCP scenario. Each row shows one species, for the season in which the exposure shows the most dramatic changes. The name of each scenario is written above each column and the name of each component is written on each row.

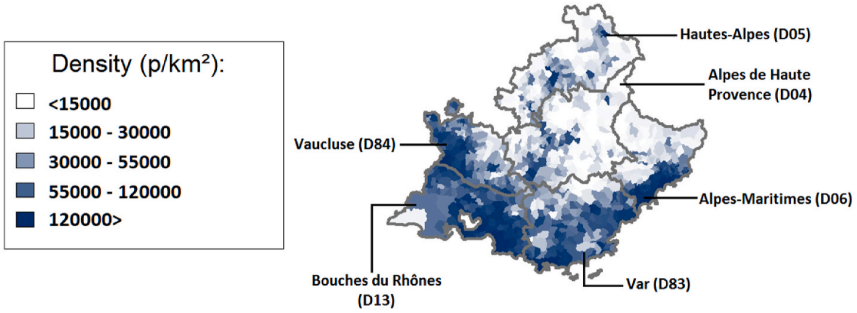


Fig. 10. Counties of the PACA region and associated population density. The region regroupes six counties: D06, D13, D83 and D84 -> dense and urbanized and D04, D05 -> predominantly rural.

developed an exposure index for particulate matter based on a population-weighting calculation (called the WEI index). This index allows us to (take into account the population distribution and) propose a spatialized quantitative assessment of the risk associated with exposure to pollution. It is obtained from the following equation:

$$\text{Weighted exposure} = \sum_{i=1}^{n}\left(C_i \times \frac{P_i}{\sum_{i=1}^{n} P_i}\right)$$

Where.

C_i Concentration in cell i

P_i Population of cell i

$\sum_{i=1}^{n} P_i$ Sum of population in all cells

All the values shown in this section have been calculated using this equation.

3.7. County per county analysis

The six administrative departments of the PACA region are presented in Fig. 10. All have strong gradients of population density, but four of them show an important share of dense urbanized areas (D06, D13, D83

and D84) while the other two (D04, D05) are predominantly rural. In particular, the three counties including a Mediterranean side (Bouches du Rhônes (13), Var (83) and Alpes Maritimes (06)) have a very high density of population because they shelter the large urban areas of Marseille, Toulon and Nice respectively. Taken together, these cities account for about 30% of the total population of the region.

For each of the 6 counties in PACA, we calculated the Weighted Exposure Indicator (WEI) and applied it to all the previously discussed atmospheric components. For a given pollutant in a given department, the calculation consists in multiplying the population of each cell in the sub-domain by the average concentration simulated in this cell, and then divide the result by the total population of said department, all the values obtained for d being finally summed up. Such a process provides the weighted exposure index of the population for this department. The results for this analysis are shown in Fig. 11 (for SSP3) and Fig. 12 (for SSP5). For each component, the weighted exposure calculated for each county in the reference case study is shown in the first column, while the absolute differences between the future situations and the historic simulation have been plotted in the second to fifth columns. For each component, only the season showing the largest changes is shown (written on the side of each line).

In the reference case, the WEI of ozone is high for all coastal counties, which can be explained by their large population, but it is noted that the northern rural county also has a fairly high value, highlighting the accumulation of ozone along the path of the air mass in the region. When exploring the future case studies, a dual behavior is seen for the ozone WEI in SSP3 (decreases everywhere) and SSP5 (increases everywhere). The WEI changes for ozone are dependent on multiple factors: (i) emission reductions, therefore showing a higher change in exposure in the 2050 timeframe simulations when greater emission reductions are achieved, (ii) population increase, therefore showing heightening exposure in SSP5 and lowering exposure in SSP3, (iii) land-use dependency: counties that are home to major cities showing lower exposure reduction in the case of SSP3 and higher exposure increase in the case of SSP5 due to reduced titration and finally (iv) climate change related effects (higher temperature for example). The evolution of the ozone WEI in SSP5 is particularly contrasted between the different counties, since the 3 coastal departments show increases of the index which are up to 4 times stronger than in the rural ones. This increase is not negligible compared to the gap that currently exists between the departments, and it shows that the risk associated with ozone in urban areas must be taken into consideration.

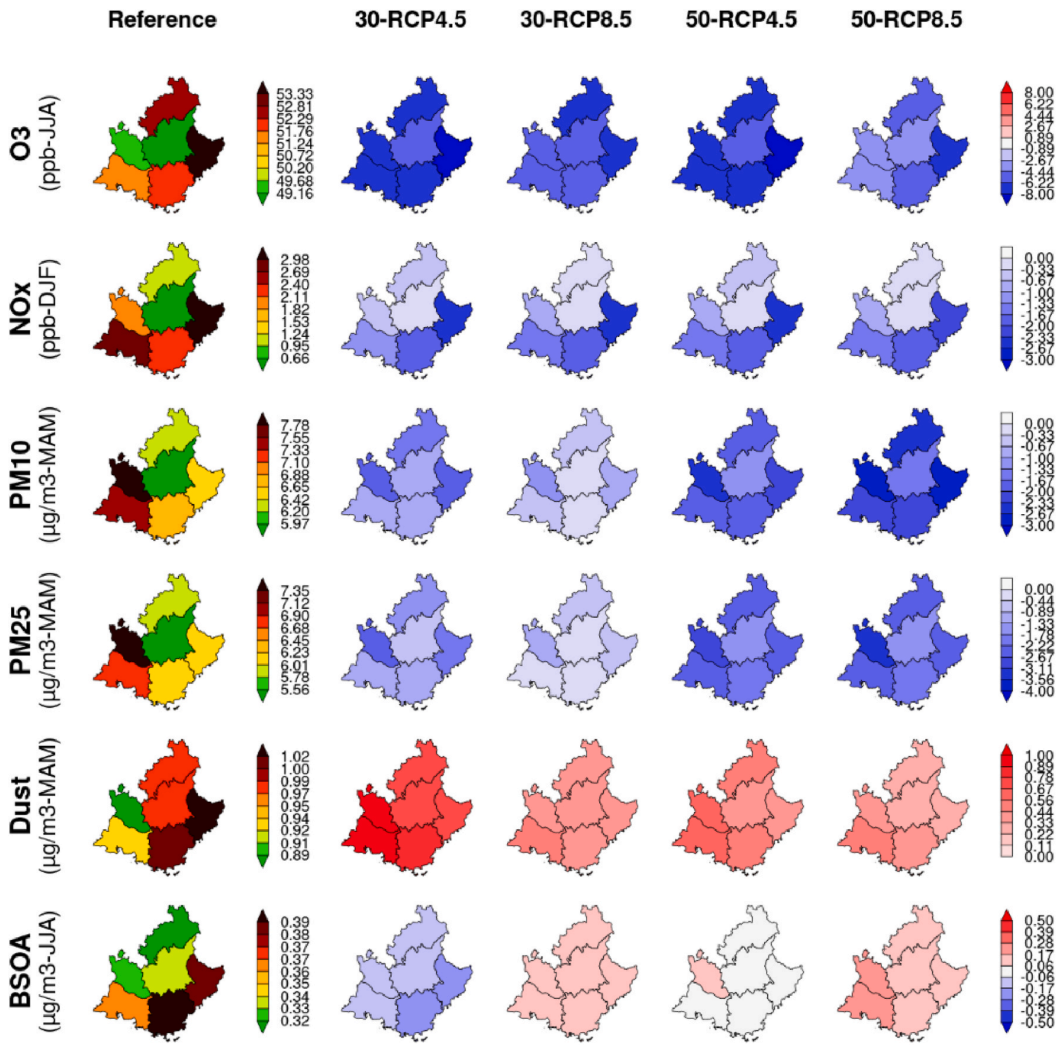


Fig. 11. Population-weighted exposure in different departments for the SSP5 scenario. The historic values are shown in the top panels. The changes between future and historic case studies are shown on the second to fifth columns. The units and the plotted season are written at the left of each row.

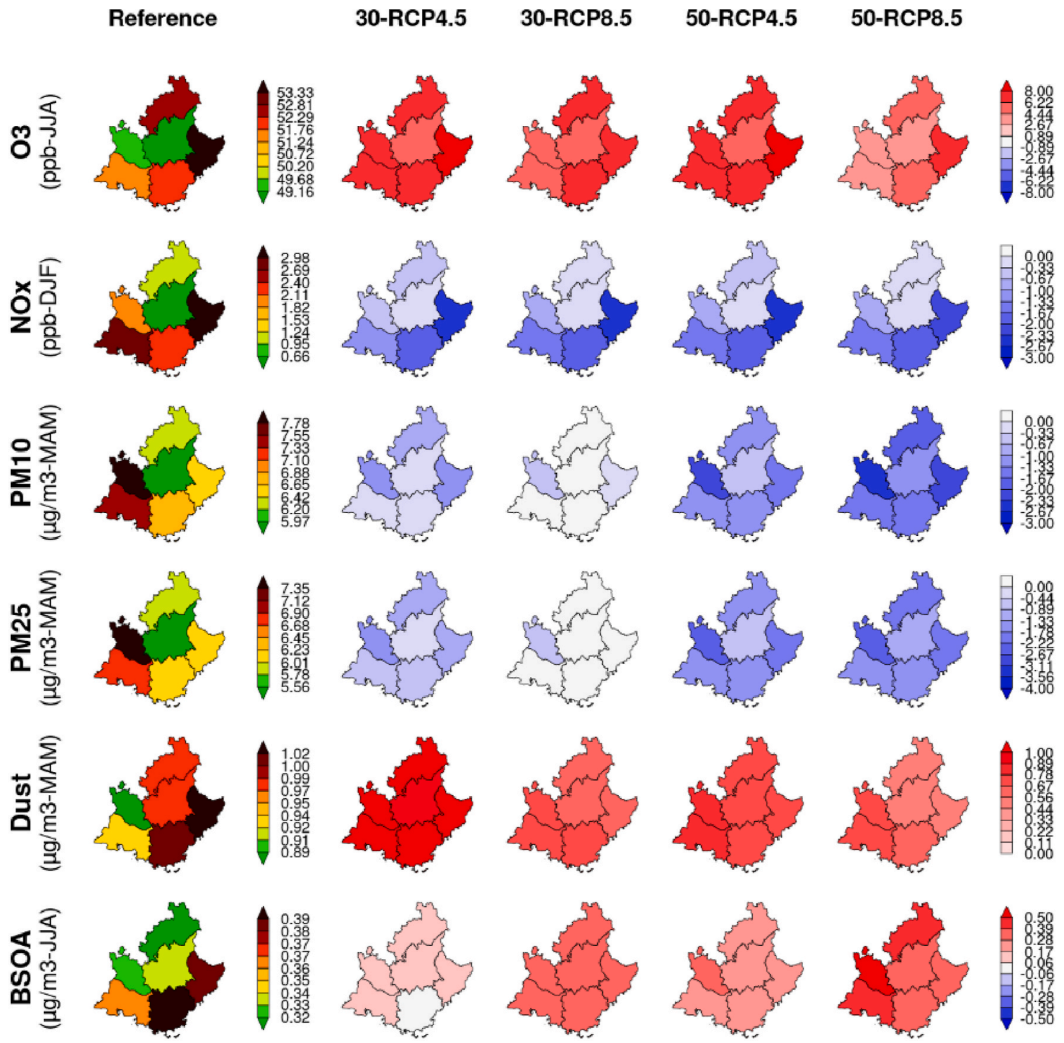


Fig. 12. Population-weighted exposure in different departments for the SSP5 scenario. The historic values are shown in the top panels. The changes between future and historic case studies are shown on the second to fifth columns. The units and the plotted season are written at the left of each row.

As can be seen in Fig. 11, nitrogen oxides show a higher total exposure risk in the coastal, urbanized and industrialized counties (D13, D84 and D06), the exposure for D06 being more than four times that of D04. When exploring the changes in the exposure, the urban and industrial counties show the largest changes, both in SSP3 and SSP5 demographic scenarios, because they house almost all the anthropogenic emissions related to transport, industrial and shipping activities (Figs. 11 and 12) of the region. In the end, the scenarios tend to show a reduction of inequalities between urban and rural departments, since the excess of risk on the current situation in departments D06 and D13 are same order of magnitude as expected gains (up to 2 µg m^{-3}).

Both PM_{10} and $PM_{2.5}$ show higher WEI in D84 and D13, followed by D83 and D06, the 2 remaining counties showing low WEI indexes in the reference simulation. In the future simulations, exposition to both PM size fractions decreases in all subdomains. It is important to note the role of the demographic scenario in the final outcome, since the exposure in SSP5 decreases less (from a factor of 0.75 to a factor of 0.25) than in SSP3 due to a higher expected population growth. In all the simulated scenarios, D84 shows the highest reduction in PM exposure, followed by D05 and D06.

Similarly, to PM, dust particle exposure is rather heterogeneously distributed all around the region, but significantly higher exposure being calculated for western counties (D83 and D06 showing the highest and D13 and D84 showing the lowest exposure) in our baseline simulation. In all our future case studies, dust particles are associated with an increasing exposure level in all counties and quite uniformly across the domain, while showing higher increase in SSP5 rather than SSP3. However, according to CHIMERE, the western fringe of the domain is particularly exposed to dust intrusions, which - together with the increase in population - leads to a greater increase in the weight of the 3 western departments in the total exposure, and calls for greater vigilance on the issue of dusts, as vectors of other contaminants on these regions (Figs. 11 and 12). This is particularly visible for scenario 30-RCP4.5 in SSP3, characterized by large wind speed, while in SSP5 the effect of the increasing population becomes more prevalent. As the order of magnitude of the expected changes is greater than the differences between counties, our results indicate that climate and demographic evolutions are likely to modify very strongly the relative weight of the departments in the total exposure to dust.

As far as BSOA is concerned, it can be seen that the D06, D13 and D83 coastal departments group the highest shares of current exposure, due to the proximity between inhabited urban areas and sub-urban areas where

BSOA-type aerosols can be formed (Figs. 11 and 12). D05 is a remote mountainous area with low population and local pollution conditions do not favor BSOA production, which explains why it shows the lowest exposure for this species. There seems to be a south-north gradient for the BSOA exposure (decreasing towards the north) which corresponds both to the population density and also the predominant anticyclonic condition favorable for the AOS formation. Almost all counties respond in the same way to future case studies, with an increase in the total exposure risk for the 2 hottest situations (30-RCP4.5 and 50-RCP8.5) in SSP3, and an increase in risk in all situations for SSP5 (Figs. 11 and 12). Similarly, to dust, the expected changes can strongly change the relative share of the different counties in exposure. We note that each time, whatever the demographic scenarios, it is the D13 and D84 departments that are most likely to see their total risk worsen.

This territorial analysis shows us that - in our case studies - the evolution of exposure to our target atmospheric pollutants is (in most cases) critical in coastal areas, but this spatial tendency is not the same for all pollutants. In particular dust and BSOA particles show specific evolution depending on the location of their sources, and long-distance transport. These differences underline the importance of spatialized management of health issues.

4. Summary and conclusions

The focus of this article is the exposure of the population in PACA, a densely populated area located in the south-east of France and adjacent to Mediterranean Sea, with respect to future case studies of atmospheric pollutant evolution. For this purpose, five years of simulations were performed, one for the historic simulations and four future case studies chosen from the 2030 and the 2050 decades under RCP4.5 and RCP8.5 climate change trajectories. For each simulation, anthropogenic emissions for the corresponding year have been prepared using the current legislation (CLE) emission scenarios. In order to explore the exposure changes of the population, the current and the future population is needed for the aforementioned region.

The simulations show a decreasing concentration of O_3, NO_x, PM_{10} and $PM_{2.5}$ because of anthropogenic emission reductions of nitrogen oxides, VOC and SO_2. At the same time, an increase in BSOA and dust concentrations is seen in most of the future situations examined in this study, for summer and spring period respectively. The increase in BSOA and dust particles is compensated by the decrease in nitrates and sulfates, resulting in a diminution of total PM_{10} and $PM_{2.5}$ concentrations. Of course, each of these components shows a specific seasonal and spatial behavior. Seasonally, the concentrations of PM_{10}, $PM_{2.5}$ and dust are maximum in spring, while for BSOA this maximum is achieved in summer. In this article, seasons with maximum concentration for each species are explored.

The exposure of the population was analyzed for the species mentioned above, for both historic and future case studies. Spatially, the exposure is maximum in areas where the population density is more important, meaning urban areas. Albeit the increase of the urban population in all future population scenarios, a decrease is seen in population exposure because of the reduction in the concentrations of the pollutants mentioned above. An exception is seen for dust aerosols, where the exposure of the population to this particulate fraction grows in all future situations studied. A decreasing population exposure to PM_{10} and $PM_{2.5}$ pollution means that the effects of this pollutant on the human health can be reduced in the future, albeit increasing populations.

While this is true for PM_{10} and $PM_{2.5}$, the exposure to dust and BSOA fractions becomes higher in spring and summer, respectively, in the future scenarios explored in this work. This is a significant result, since dust particles are one of the species likely to increase exponentially in the future due to land use changes, deforestation and droughts related to climate change. Therefore, an increasing exposure to dust particles can increase the risk of common diseases caused by atmospheric particulate matter as well as the possibility of bacterial, fungal and viral diseases. In addition, the formation of BSOA particles have a high dependence to temperature, which is expected to increase in the future.

Finally, exposure in the administrative counties in the PACA region is analyzed in this work, using a population weighted approach. The PACA contains 6 counties, three of them being highly populated with major urban areas. The exposure to ozone shows a growing trend in these counties (D13, D83 and D06), while diminishing in the other ones (D04, D05 and D84). Exposure to dust and BSOA particles is increasing throughout the region, but the trend is also, to some extent, determined by the population of the urban counties. This means special attention should be given to urbanization and urban area growth since it can result in more exposure to certain atmospheric pollutants for a higher population density.

Our results show that the engaged emission reduction policies may be effective in reducing the total exposure of the PACA region's population to air pollution. This will make it possible to combat primary air pollutants or those formed near the emitting zones, such as nitrogen oxides, sulfates, nitrates and more generally, most of the PM mass. However, this is not true for all atmospheric pollutants. Long-range transport can affect the exposure of the population in this region as well, for example through the transport of dust particles from Northern Africa. Temperature-dependency of the production of species such as BSOA can affect the exposure of the population as well, with an increase in this exposure as the temperature rises. These last two particulate fractions cannot be controlled by local emission reduction policies and a more comprehensive policy is needed to mitigate this exposure.

A future step in this work would be to explore land use changes in this region and include hypotheses on the increase in dust emissions from North Africa, which would lead to changes in dust concentration in the PACA region. Also, boundary/initial condition forcings should be taken into account and studied in more detail specially when it comes to dust emission and transport schemes. Another point would be to explore the exposure based on different age groups and then calculate the mortality for these age groups because of concentration changes in future scenarios. Furthermore, it would be worth doing a similar study on other parts of the Mediterranean area in order to see if the same hypothesis can be made for different types of profiles: dense coasts, rural areas, hotter areas, etc. Finally, it would be interesting to repeat the same experience with longer simulated periods, therefore passing from case studies to future scenario assessment.

CRediT authorship contribution statement

Arineh Cholakian: Conceptualization, Methodology, performing and analyzing the simulations and writing. **Isabelle Coll:** Conceptualization, Methodology, Supervision. **Augustin Colette:** Supervision. **Matthias Beekmann:** Supervision.

Declaration of competing interest

The authors declare that they have no known competing financial interests or personal relationships that could have appeared to influence the work reported in this paper.

Acknowledgements

This research has received funding from the French National Research Agency (ANR) projects SAF-MED (grant ANR-15 12-BS06-0013). This work is part of the ChArMEx project supported by ADEME, CEA, CNRS-INSU and Météo-France through the multidisciplinary program MISTRALS (Mediterranean Integrated Studies aT Regional And Local Scales). The work presented here received support from the French Ministry in charge of ecology. This work was performed using HPC resources from GENCI-CCRT, grant numbers A0030107232 (project number gen6877) and 2017-t2015017232 (project number gen7232). Robert Vautard is acknowledged for providing the WRF/IPSL-CM5-MR

Cordex simulations, and Didier Hauglustaine and Sophie Szopa are acknowledged for providing the INCA simulations. Zbigniew Klimont is acknowledged for providing ECLIPSE-v4 emission projections. INERIS and LCSQA are acknowledged for providing population data for the PACA region. AtmoSud is acknowledged for providing the high-resolution anthropogenic emission data for the PACA region. The thesis work of Arineh Cholakian is supported by ADEME, INERIS (with the support of the French Ministry in charge of Ecology), and via the ANR SAF-MED project.

References

Adloff, F., Somot, S., Sevault, F., Jordà, G., Aznar, R., Déqué, M., Herrmann, M., Marcos, M., Dubois, C., Padorno, E., Alvarez-Fanjul, E., Gomis, D., 2015. Mediterranean Sea response to climate change in an ensemble of twenty first century scenarios. Clim. Dynam. 45 (9–10), 2775–2802. https://doi.org/10.1007/s00382-015-2507-3.

Alfaro, S.C., Gomes, L., 2001. Modeling mineral aerosol production by wind erosion: emission intensities and aerosol size distributions in source areas. J. Geophys. Res. Atmos. 106 (D16), 18075–18084. https://doi.org/10.1029/2000JD900339.

Alfaro, S.C., Gaudichet, A., Gomes, L., Maih, M., 1998. Mineral aerosol production by wind erosion: aerosol particle sizes and binding energies. Geophys. Res. Lett. 25 (1), 991–994. https://doi.org/10.1029/98GL00502.

Amann, M., Klimont, Z., Wagner, F., 2013. Regional and global emissions of air pollutants: recent trends and future scenarios. Annu. Rev. Environ. Resour. 38 (1), 31–55. https://doi.org/10.1146/annurev-environ-052912-173303.

Anderson, J.O., Thundiyil, J.G., Stolbach, A., 2012. Clearing the air: a review of the effects of particulate matter air pollution on human health. J. Med. Toxicol. 8 (2), 166–175. https://doi.org/10.1007/s13181-011-0203-1.

Bank World, 2017. World income classification. Available from: http://www.piscomed.com/wp-content/uploads/2017/03/Income-classification.pdf. (Accessed 26 September 2018). Accessed.

Bauer, S.E., Koch, D., Unger, N., Metzger, S.M., Shindell, D.T., Streets, D.G., 2007. Nitrate aerosols today and in 2030: a global simulation including aerosols and tropospheric ozone. Atmos. Chem. Phys. 7 (19), 5043–5059.

Brey, S.J., Pierce, J.R., Barnes, E.A., Fischer, Emily V., 2020. Estimating the spread in future fine dust concentrations in the Southwest United States. J. Geophys. Res.: Atmosphere 125.

Cholakian, A., Beekmann, M., Colette, A., Coll, I., Siour, G., Sciare, J., Marchand, N., Couvidat, F., Pey, J., Gros, V., Sauvage, S., Michoud, V., Sellegri, K., Colomb, A., Sartelet, K., Langley DeWitt, H., Elser, M., Prévot, A.S.H., Szidat, S., Dulac, F., 2018. Simulation of fine organic aerosols in the western Mediterranean area during the ChArMEx 2013 summer campaign. Atmos. Chem. Phys. 18 (10), 7287–7312. https://doi.org/10.5194/acp-18-7287-2018.

Cholakian, A., Colette, A., Coll, I., Ciarelli, G., Beekmann, M., 2019a. Future climatic drivers and their effect on PM10 components in Europe and the Mediterranean Sea. Atmos. Chem. Phys. 19, 4459–4484. https://doi.org/10.5194/acp-19-4459-2019.

Cholakian, A., Beekmann, M., Coll, I., Ciarelli, G., Colette, A., 2019b. Sensitivity of organic aerosol simulation scheme on biogenic organic aerosol concentrations in climate projections. Atmos. Chem. Phys. 13209–13226. https://doi.org/10.5194/acp-19-13209-2019.

Ciardini, V., Contessa, G.M., Falsaperla, R., Gómez-Amo, J.L., Meloni, D., Monteleone, F., Pace, G., Piacentino, S., Sferlazzo, D., di Sarra, A., 2016. Global and Mediterranean climate change: a short summary. Ann. Ist. Super Sanita 52 (3), 325–337. https://doi.org/10.4415/ANN_16_03_04.

Colette, A., Andersson, C., Baklanov, A., Bessagnet, B., Brandt, J., Christensen, J.H., Doherty, R., Engardt, M., Geels, C., Giannakopoulos, C., Hedegaard, G.B., Katragkou, E., Langner, J., Lei, H., Manders, A., Melas, D., Meleux, F., Rouïl, L., Sofiev, M., Soares, J., Stevenson, D.S., Tombrou-Tzella, M., Varotsos, K.V., Young, P., 2015. Is the ozone climate penalty robust in Europe? Environ. Res. Lett. 10 (8), 084015 https://doi.org/10.1088/1748-9326/10/8/084015.

Coll, I., Lasry, F., Fayet, S., Armengaud, A., Vautard, R., 2009. Simulation and evaluation of 2010 emission control scenarios in a Mediterranean area. Atmos. Environ. 43, 4194–4204. https://doi.org/10.1016/j.atmosenv.2009.05.034.

Denjean, C., Cassola, F., Mazzino, A., Triquet, S., Chevaillier, S., Grand, N., Bourrianne, T., Momboisse, G., Sellegri, K., Schwarzenbock, A., Freney, E., Mallet, M., Formenti, P., 2016. Size distribution and optical properties of mineral dust aerosols transported in the western Mediterranean. Atmos. Chem. Phys. 16, 1081–1104. https://doi.org/10.5194/acp-16-1081-2016.

van Donkelaar, A., Martin, R.V., Brauer, M., Boys, B.L., 2015. Use of satellite observations for long-term exposure assessment of global concentrations of fine particulate matter. Environ. Health Perspect. 123 (2), 135–143. https://doi.org/10.1289/ehp.1408646.

Edenhofer, O., Elgizouli, I., Field, C.B., Howden, M., Pachauri, R.K., Meyer, L., Hallegatte France, S., Bank, W., Hegerl, G., Brinkman, S., van Kesteren, L., Leprince-Ringuet, N., van Boxmeer, F., Seyboth, K., 2014. IPCC. Available from: http://www.ipcc.ch. (Accessed 1 September 2018).

Evan, A.T., Flamant, C., Fiedler, S., Doherty, O., 2014. An analysis of aeolian dust in climate models. Geophys. Res. Lett. 41 (16), 5996–6001. https://doi.org/10.1002/2014GL060545.

Fortems-Cheiney, A., Foret, G., Siour, G., Vautard, R., Szopa, S., Dufour, G., Colette, A., Lacressonniere, G., Beekmann, M., 2017. A 3°C global RCP8.5 emission trajectory cancels benefits of European emission reductions on air quality. Nat. Commun. 8, 1–6. https://doi.org/10.1038/s41467-017-00075-9.

Giorgi, F., 2006. Climate change hot-spots. Geophys. Res. Lett. 33 (8), 1–4. https://doi.org/10.1029/2006GL025734.

Griffin, D.W., 2007. Atmospheric movement of microorganisms in clouds of desert dust and implications for human health. Clin. Microbiol. Rev. 20 (3), 459–477. https://doi.org/10.1128/CMR.00039-06 table of contents.

Guenther, A., Karl, T., Harley, P., Wiedinmyer, C., Palmer, P.I., Geron3, C., 2006. Estimates of global terrestrial isoprene emissions using MEGAN (model of emissions of Gases and aerosols from nature). Atmos. Chem. Phys. 6, 3181–3210. https://doi.org/10.1016/j.cognition.2008.05.007.

Harrison, R.M., Yin, J., 2000. Particulate matter in the atmosphere: which particle properties are important for its effects on health? Sci. Total Environ. 249 (1–3), 85–101. Available from: http://www.ncbi.nlm.nih.gov/pubmed/10813449. (Accessed 30 May 2018).

Hauglustaine, D.A., Balkanski, Y., Schulz, M., 2014. A global model simulation of present and future nitrate aerosols and their direct radiative forcing of climate. Atmos. Chem. Phys. 14 (20), 11031–11063. https://doi.org/10.5194/acp-14-11031-2014.

Heald, C.I., Wilkinson, M.J., Monson, R.K., Alo, C.A., Wang, G., Guenther, A., 2009. Response of isoprene emission to ambient CO 2 changes and implications for global budgets. Global Change Biol. 15 (5), 1127–1140. https://doi.org/10.1111/j.1365-2486.2008.01802.x.

Israelevich, P., Ganor, E., Alpert, P., Kishcha, P., Stupp, A., 2012. Predominant transport paths of saharan dust over the Mediterranean Sea to Europe. J. Geophys. Res.: Atmosphere 117 (D2).

Jacob, D., Petersen, J., Eggert, B., Alias, A., Christensen, O.B., Bouwer, L.M., Braun, A., Colette, A., Déqué, M., Georgievski, G., Georgopoulou, E., Gobiet, A., Menut, L., Nikulin, G., Haensler, A., Hempelmann, N., Jones, C., Keuler, K., Kovats, S., Kröner, N., Kotlarski, S., Kriegsmann, A., Martin, E., van Meijgaard, E., Moseley, C., Pfeifer, S., Preuschmann, S., Radermacher, C., Radtke, K., Rechid, D., Rounsevell, M., Samuelsson, P., Somot, S., Soussana, J.-F., Teichmann, C., Valentini, R., Vautard, R., Weber, B., Yiou, P., 2014. EURO-CORDEX: new high-resolution climate change projections for European impact research. Reg. Environ. Change 14 (2), 563–578. https://doi.org/10.1007/s10113-013-0499-2.

Jacob, D.J., Winner, D.A., 2009. Effect of climate change on air quality. Atmos. Environ. 43 (1), 51–63. https://doi.org/10.1016/j.atmosenv.2008.09.051.

Jones, B., O'Neill, B.C., 2016. Spatially explicit global population scenarios consistent with the Shared Socioeconomic Pathways. Environ. Res. Lett. 11 (8), 084003 https://doi.org/10.1088/1748-9326/11/8/084003.

Kan, H., Chen, R., Tong, S., 2012. Ambient air pollution, climate change, and population health in China. Environ. Int. 42, 10–19. https://doi.org/10.1016/J.ENVINT.2011.03.003.

Klimont, Z., Kupiainen, K., Heyes, C., Purohit, P., Cofala, J., Rafaj, P., Borken-Kleefeld, J., Schöpp, W., 2017. Global anthropogenic emissions of particulate matter including black carbon. Atmos. Chem. Phys. 17 (14), 8681–8723. Available from: https://www.atmos-chem-phys.net/17/8681/2017/. (Accessed 23 May 2017).

Kuenen, J.J.P., Visschedijk, A.J.H., Jozwicka, M., Denier Van Der Gon, H.A.C., 2014. TNO-MACC-II emission inventory; A multi-year (2003-2009) consistent high-resolution European emission inventory for air quality modelling. Atmos. Chem. Phys. 14 (20), 10963–10976. https://doi.org/10.5194/acp-14-10963-2014.

LCSQA, 2015. Mise à disposition des AASQA de données de population spatialisée | LCSQA. Available from: https://www.lcsqa.org/fr/actualite/mise-dispositio n-aasqa-donnees-population-spatialisee. (Accessed 18 October 2018).

Lee, E.-H., Sohn, B.-J., 2011. Recent increasing trend in dust frequency over Mongolia and Inner Mongolia regions and its association with climate and surface condition change. Atmos. Environ. 45 (27), 4611–4616. https://doi.org/10.1016/J.ATMOSENV.2011.05.065.

Lelieveld, J., Lelieveld, J., Berresheim, H., Borrmann, S., Crutzen, P.J., Dentener, F.J., Fischer, H., Feichter, J., Flatau, P.J., Heland, J., 2002. Global Air Pollution Crossroads over the Mediterranean.Pdf, p. 794. https://doi.org/10.1126/science.1075457, 2002.

De Longueville, F., Hountondji, Y.-C., Henry, S., Ozer, P., 2010. What do we know about effects of desert dust on air quality and human health in West Africa compared to other regions? Sci. Total Environ. 409 (1), 1–8. https://doi.org/10.1016/J.SCITOTENV.2010.09.025.

Mahowald, N.M., Kloster, S., Engelstaedter, S., Moore, J.K., Mukhopadhyay, S., McConnell, J.R., Albani, S., Doney, S.C., Bhattacharya, A., Curran, M.A.J., Flanner, M.G., Hoffman, F.M., Lawrence, D.M., Lindsay, K., Mayewski, P.A., Neff, J., Rothenberg, D., Thomas, E., Thornton, P.E., Zender, C.S., 2010. Observed 20th century desert dust variability: impact on climate and biogeochemistry. Atmos. Chem. Phys. 10 (22), 10875–10893. https://doi.org/10.5194/acp-10-10875-2010.

Marticorena, B., Bergametti, G., 1995. Modeling the atmospheric dust cycle: 1. Design of a soil-derived dust emission scheme. J. Geophys. Res. 100 (D8), 16415. https://doi.org/10.1029/95JD00690.

Mauderly, J.L., Chow, J.C., 2008. Health effects of organic aerosols. Inhal. Toxicol. 20, 257–288. https://doi.org/10.1080/08958370701866008.

Meinshausen, M., Smith, S.J., Calvin, K., Daniel, J.S., Kainuma, M.L.T., Lamarque, J.-F., Matsumoto, K., Montzka, S.A., Raper, S.C.B., Riahi, K., Thomson, A., Velders, G.J.M., van Vuuren, D.P.P., 2011. The RCP greenhouse gas concentrations and their extensions from 1765 to 2300. Climatic Change 109 (1–2), 213–241. https://doi.org/10.1007/s10584-011-0156-z.

Menut, L., Schmechtig, C., Marticorena, B., 2005. Sensitivity of the sandblasting flux calculations to the soil size distribution accuracy. J. Atmos. Ocean. Technol. 22 (12), 1875–1884.

Menut, L., Bessagnet, B., Khvorostyanov, D., Beekmann, M., Blond, N., Colette, A., Coll, I., Curci, G., Foret, G., Hodzic, A., Mailler, S., Meleux, F., Monge, J.-L., Pison, I.,

Siour, G., Turquety, S., Valari, M., Vautard, R., Vivanco, M.G., 2013. Chimere 2013: a model for regional atmospheric composition modelling. Geosci. Model Dev. (GMD) 6 (4), 981–1028. https://doi.org/10.5194/gmd-6-981-2013.

Middleton, N.J., 2017. Desert dust hazards: a global review. Aeolian Res 24, 53–63. https://doi.org/10.1016/J.AEOLIA.2016.12.001.

Mulitza, S., Heslop, D., Pittauerova, D., Fischer, H.W., Meyer, I., Stuut, J.-B., Zabel, M., Mollenhauer, G., Collins, J.A., Kuhnert, H., Schulz, M., 2010. Increase in African dust flux at the onset of commercial agriculture in the Sahel region. Nature 466 (7303), 226–228. https://doi.org/10.1038/nature09213.

O'Neill, B.C., Kriegler, E., Ebi, K.L., Kemp-Benedict, E., Riahi, K., Rothman, D.S., van Ruijven, B.J., van Vuuren, D.P., Birkmann, J., Kok, K., Levy, M., Solecki, W., 2017. The roads ahead: narratives for shared socioeconomic pathways describing world futures in the 21st century. Global Environ. Change 42, 169–180. https://doi.org/10.1016/j.gloenvcha.2015.01.004.

Péré, J.-C., Pont, V., Mallet, M., Bessagnet, B., 2009. Mapping of PM10 surface concentrations derived from satellite observations of aerosol optical thickness over South-Eastern France. Atmos. Res. 91 (1), 1–8. https://doi.org/10.1016/J.ATMOSRES.2008.05.001.

Pope, C.A., Dockery, D.W., 2006. Health effects of fine particulate air pollution: lines that connect. J. Air Waste Manag. Assoc. 56 (6), 709–742. https://doi.org/10.1080/10473289.2006.10464485.

Riahi, K., Rao, S., Krey, V., Cho, C., Chirkov, V., Fischer, G., Kindermann, G., Nakicenovic, N., Rafaj, P., 2011. Rcp 8.5—a scenario of comparatively high greenhouse gas emissions. Climatic Change 109 (1–2), 33–57. https://doi.org/10.1007/s10584-011-0149-y.

Riahi, K., van Vuuren, D.P., Kriegler, E., Edmonds, J., O'Neill, B.C., Fujimori, S., Bauer, N., Calvin, K., Dellink, R., Fricko, O., Lutz, W., Popp, A., Cuaresma, J.C., Kc, S., Leimbach, M., Jiang, L., Kram, T., Rao, S., Emmerling, J., Ebi, K., Hasegawa, T., Havlik, P., Humpenöder, F., Da Silva, L.A., Smith, S., Stehfest, E., Bosetti, V., Eom, J., Gernaat, D., Masui, T., Rogelj, J., Strefler, J., Drouet, L., Krey, V., Luderer, G., Harmsen, M., Takahashi, K., Baumstark, L., Doelman, J.C., Kainuma, M., Klimont, Z., Marangoni, G., Lotze-Campen, H., Obersteiner, M., Tabeau, A., Tavoni, M., 2017. The Shared Socioeconomic Pathways and their energy, land use, and greenhouse gas emissions implications: an overview. Global Environ. Change 42, 153–168. https://doi.org/10.1016/j.gloenvcha.2016.05.009.

Robinson, A.L., Donahue, N.M., Shrivastava, M.K., Weitkamp, E.A., Sage, A.M., Grieshop, A.P., Lane, T.E., Pierce, J.R., Pandis, S.N., 2007. Rethinking organic aerosols: semivolatile emissions and photochemical aging. Science (80-.) 315 (5816), 1259–1262. https://doi.org/10.1126/science.1133061.

Samoli, E., Stafoggia, M., Rodopoulou, S., Ostro, B., Declercq, C., Alessandrini, E., Díaz, J., Karanasiou, A., Kelessis, A.G., Le Tertre, A., Pandolfi, P., Randi, G., Scarinzi, C., Zauli-Sajani, S., Katsouyanni, K., Forastiere, F., MED-PARTICLES Study Group, the M.-P. S., 2013. Associations between fine and coarse particles and mortality in Mediterranean cities: results from the MED-PARTICLES project. Environ. Health Perspect. 121 (8), 932–938. https://doi.org/10.1289/ehp.1206124.

Seinfeld, J.H., Pandis, S.N., 2016. Atmospheric Chemistry and Physics : from Air Pollution to Climate Change.

Shrivastava, M., Zelenyuk, A., Imre, D., Easter, R., Beranek, J., Zaveri, R.A., Fast, J., 2013. Implications of low volatility SOA and gas-phase fragmentation reactions on SOA loadings and their spatial and temporal evolution in the atmosphere. J. Geophys. Res. Atmos. 118 (8), 3328–3342. https://doi.org/10.1002/jgrd.50160.

Shrivastava, M., Easter, R.C., Liu, X., Zelenyuk, A., Singh, B., Zhang, K., Ma, P., Chand, D., Ghan, S., Jimenez, J.L., Zhang, Q., Fast, J., Rasch, P.J., Tiitta, P., 2015. Global transformation and fate of SOA: implications of low-volatility SOA and gas-phase fragmentation reactions. J. Geophys. Res. Atmos. 120 (9), 4169–4195. https://doi.org/10.1002/2014JD022563.Received.

Sicard, P., Mangin, A., Hebel, P., Malléa, P., 2010. Detection and estimation trends linked to air quality and mortality on French Riviera over the 1990–2005 period. Sci. Total Environ. 408 (8), 1943–1950. https://doi.org/10.1016/J.SCITOTENV.2010.01.024.

Sicard, P., Lesne, O., Alexandre, N., Mangin, A., Collomp, R., 2011. Air quality trends and potential health effects – development of an aggregate risk index. Atmos. Environ. 45 (5), 1145–1153. https://doi.org/10.1016/J.ATMOSENV.2010.12.052.

Tai, A.P.K., Mickley, L.J., Heald, C.L., Wu, S., 2013. Effect of CO 2 inhibition on biogenic isoprene emission: implications for air quality under 2000 to 2050 changes in climate, vegetation, and land use. Geophys. Res. Lett. 40 (13), 3479–3483. https://doi.org/10.1002/grl.50650.

Tarín-Carrasco, P., Im, U., Geels, C., Palacios-Peña, L., Jiménez-Guerrero, P., 2021. Contribution of fine particulate matter to present and future premature mortality over Europe: a non-linear response. Environ. Int. 153, 106517. https://doi.org/10.1016/j.envint.2021.106517}.

Tegen, I., Werner, M., Harrison, S.P., Kohfeld, K.E., 2004. Relative importance of climate and land use in determining present and future global soil dust emission. Geophys. Res. Lett. 31 (5) https://doi.org/10.1029/2003GL019216 n/a-n/a.

Thomson, A.M., Calvin, K.V., Smith, S.J., Page Kyle, G., Volke, A., Patel, P., Delgado-Arias, S., Bond-Lamberty, B., Wise, M.A., Clarke, L.E., Edmonds, J.A., 2011. RCP4.5: a Pathway for Stabilization of Radiative Forcing by 2100. https://doi.org/10.1007/s10584-011-0151-4.

Vincent, J., Laurent, B., Losno, R., Bon Nguyen, E., Roullet, P., Sauvage, S., Chevaillier, S., Coddeville, P., Ouboulmane, N., di Sarra, A.G., Tovar-Sánchez, A., Sferlazzo, D., Massanet, A., Triquet, S., Morales Baquero, R., Fornier, M., Coursier, C., Desboeufs, K., Dulac, F., Bergametti, G., 2016. Variability of mineral dust deposition in the western Mediterranean basin and south-east of France. Atmos. Chem. Phys. 16 (14), 8749–8766. https://doi.org/10.5194/acp-16-8749-2016.

West, J.J., Smith, S.J., Silva, R.A., Naik, V., Zhang, Y., Adelman, Z., Fry, M.M., Anenberg, S., Horowitz, L.W., Lamarque, J.-F., 2013. Co-benefits of mitigating global greenhouse gas emissions for future air quality and human health. Nat. Clim. Change 3 (10), 885–889. https://doi.org/10.1038/nclimate2009.

Wilkinson, M.J., Monson, R.K., Trahan, N., Lee, S., Brown, E., Jackson, R.B., Polley, H. W., Fay, P.A., Fall, R., 2009. Leaf isoprene emission rate as a function of atmospheric CO2 concentration. Global Change Biol. 15 (5), 1189–1200. https://doi.org/10.1111/j.1365-2486.2008.01803.x.

Yao, L., Lu, N., Yao, L., Lu, N., 2014. Particulate matter pollution and population exposure assessment over mainland China in 2010 with remote sensing. Int. J. Environ. Res. Publ. Health 11 (5), 5241–5250. https://doi.org/10.3390/ijerph110505241.

Zender, C.S., Bian, H., Newman, D., 2003. Mineral dust entrainment and deposition (DEAD) model: description and 1990s dust climatology. J. Geophys. Res. 108 (D14), 4416. https://doi.org/10.1029/2002JD002775.

CHAPTER

VIII

Conclusions and perspectives

Contents

1 Model evaluation and amelioration for the western Mediterranean basin **208**

2 Future conditions of the Mediterranean basin in different scales **211**

3 Perspectives **214**

The Mediterranean region presents several characteristics that make it an important and interesting region to study. Many emission sources enter the Mediterranean area from the European or African continents or can even be transported from Asia and the Americas, apart from the local emission sources. The region is characterized by high photochemical reactivity and high residence times of air masses. In addition, the density of the population is high around the basin. Also, its sensitivity to climate change is expected to be larger than in most other regions. These reasons make the Mediterranean area an interesting and important area to study. However, not many campaigns were carried out in the western Mediterranean region, therefore the ChArMEx project was put into place in order to fill the gaps of some most needed information about the western basin: the current and future conditions of its atmosphere, properties and chemical composition of aerosols in the region and their effects on human health and radiative balance. Because of its particularities, the aerosol burden in this area is high, organic aerosols being an important contributor to this burden. However, the mechanisms of formation of this type of aerosol are not entirely known, therefore, its simulation in CTMs remains difficult. Different schemes can be implemented in atmospheric models in order to simulate this aerosol, each taking into account different processes in a highly parameterized manner. Having obtained detailed and extensive measurements for the western basin of the Mediterranean Sea during the ChArMEx campaign, this project offers the opportunity of evaluating different OA simulation schemes for this region. This first objective completed, we can then use these schemes to evaluate the origins of organic aerosol in the region, and to simulate the impact of future changes on the aerosol load.

In order to achieve the objectives mentioned above, the thesis was divided into two phases. The results obtained from each phase are discussed below.

1 Model evaluation and amelioration for the western Mediterranean basin

The measurements during the ChArMEx campaign were performed in Ersa, Cap Corse, an island in the middle of the Mediterranean with high altitude gradient. In order to simulate this orographical gradient, I used nested domains, the last one a small domain with a horizontal resolution of $1km$ covering only the Northern Corsica. In total, I used four domains with a horizontal resolution of 30km, 10km, 3km and 1km respectively starting from a European scale. Nevertheless, even at the highest model resolution of 1km, the model still underestimated the altitude of the measurements site by about 200m. I put into place a method in order to calculate an orographic representativeness error, corresponding to the dependence of different atmospheric components to altitudinal changes. Non-linear regressions between concentration and the altitude of neighboring cells to the measurement site were used in order to calculate this error, for each time step and using several equations. I put together the confidence intervals from all time steps and all converging equations in order to calculate the orographic repre-

sentativeness error. The major conclusion of this study is the following: for secondary species with higher residence times in the atmosphere, the orographic representativeness error is quite low (10% for OA), thus OA measurements at Cap Corse can indeed be used for evaluation of OA schemes, because the expected error is much larger. On the contrary, for primary species as well as secondary species with low residence times in the atmosphere this error becomes quite high (isoprene and MVK+MACR 85% and 60% respectively). Therefore, comparisons for pollutants with high orographic representativeness error for this site should be carried out with caution and taking into account that the altitude discrepancy in the model can affect the results of the simulation-measurement comparisons.

Since the domain analyzed by this study is a maritime area, it was necessary to add the simulation of naturally occurring emissions from the sea surface to the model. For this purpose, I implemented the emissions of DMS from the sea surface and its subsequent changes in the atmosphere into the model. To this end, it was necessary to prepare the climatological monthly global fields of sea surface DMS concentrations and incorporate them into CHIMERE. Then, the sea to air flux of DMS had to be calculated using the piston velocity: a parameter that depends on the 10m wind speed and the temperature. Several parameterizations exist for the dependence of wind regimes and piston velocity, I implemented four of those in CHIMERE in the current thesis. The resulting simulations show a maximum increase of 25% for the Atlantic region in sulfate concentrations, and 10% for the western Mediterranean region. These values correspond to what is seen in the literature for DMS induced sulfate increases. As a conclusion, DMS emissions in the Mediterranean basin are not a major source for the concentration of sulfates in the area, they are however a non-negligible source that is nonetheless preferred to be included in our simulations.

Subsequently, I performed a complete evaluation of different components of the model for this region, during which meteorological parameters as well as gaseous and particulate species other than OA were compared to measurements. For meteorological simulations, I chose a set of options best representing an extensive meteorological data set. Comparison of NO_x showed a low bias and a good agreement for Ersa (especially taking into account the orographic representativeness error for this species), while for Es Pînar the correlation is low and the bias is high. The urban nature of this site might be the reason for the differences seen in simulated and measured NO_x concentrations. Isoprene and Mono-terpenes are also compared to measurements since they are the major precursors of BSOA, for isoprene showing a good agreement in both sites while an underestimation is seen for Ersa for mono-terpenes, taking into account the orographic representativeness error for this site the error is within expected limits. A more regional look is necessary for the validation of mono-terpene concentrations in the Mediterranean region, however, to the best of our knowledge, such validation was never performed for the MEGAN model. The comparisons done for isoprene in the literature lend credence to the emissions simulated by MEGAN for this species (Curci et al., 2010; Zare et al.,

2012). For other particulate species, a good agreement is seen for BC concentrations in Ersa, which is underestimated in Es Pînar. An overestimation of sulfates is seen in Ersa, while it seems well-simulated in Es Pînar. This evaluation was performed in order to prepare the model for implementation of OA simulation schemes and comparison of each scheme to measurements.

During this thesis, I compared four organic aerosol schemes, including different processes of OA formation, and different representations of them, to the measurements obtained during the ChArMEx campaign for two sites in the Mediterranean: Ersa, Cap Corse and Es Pînar, Mallorca. The first scheme is a molecular single-step oxidation scheme that was implemented in CHIMERE by Bessagnet, Menut, et al. (2008). The second scheme is a standard VBS scheme containing aging processes of BSOA and ASOA which was proposed by Donahue, Robinson, et al. (2006). Next, another parameterization of the same scheme is presented where the aging processes of BSOA is turned off since it causes overestimation of this aerosol in the end (Lane, Donahue, and S. Pandis 2008. The fourth scheme is a VBS based scheme as well, it takes into account all the processes in a standard VBS scheme, as well as fragmentation (where molecules can break in the atmosphere forming more volatile ones) and formation of non-volatile SOA (where SVOC after its formation can pass directly into the particulate phase and become non-volatile). Simulations with these four schemes were compared to measurements exploring the correspondence of the concentration, oxidation state (using the PMF method) and origins (using ^{14}C measurements). This is the first time that such a detailed comparison work could be performed over this region.

The comparisons for OA showed that for the average concentration, the modified VBS and the standard VBS scheme without BSOA aging perform better compared to the other two schemes, which overestimate the concentration of OA (to a much higher extent for the standard VBS scheme with BSOA aging). When comparing PMF results, the modified VBS scheme was the one that comes close to simulating the distribution of LVOOA/SVOOA/HOA in the basin, while the other schemes tended to overestimate the SVOOA partition. Fossil/non-fossil distribution showed that the CHIMERE standard scheme and the modified VBS scheme simulate this distribution quite well, while the other two scheme each overestimated one compartment (fossil for VBS with ASOA aging and non-fossil for VBS with BSOA aging). These results show that for the western Mediterranean basin it is important to take into account the fragmentation and non-volatile SOA production processes.

Once an evaluated OA scheme was obtained, I could use it to evaluate the origin of organic aerosol over the western Mediterranean region: it is evident that OA with biogenic origins is dominant in the basin, both at the surface and at higher altitudes. However, in areas between Corsica and Marseilles, the Gulf of Genoa and the northern coasts of Africa, the contribution of POA and its subsequent oxidation products become quite important because of the shipping lines that pass regularly in these regions. For Northern Italy, where Po valley is located a high concentration of ASOA is seen in the

simulations.

2 Future conditions of the Mediterranean basin in different scales

After modifying the model for a better correspondence to the specific characteristics of the Mediterranean basin and evaluating its performance by comparing it to observations, it became possible to use it in order to assess future scenarios for this region. The goals of this phase were explained in chapter I, the results obtained for each goal will be explained here.

In this part of the thesis I examined an exhaustive list of scenarios in order to know the effects of climate change, anthropogenic emission reduction policies and long-range transport on the changes in the concentration of PM_{10}, $PM_{2.5}$ and their components. For this purpose, I analyzed a list of pre-existing scenarios each helping us to quantify the effects of one driver specifically. For the climatic effects study, three RCP scenarios were used: RCP2.6, RCP4.5 and RCP8.5. For each of these scenarios, 70 years of simulations are investigated, covering the period of 2031 to 2100. These scenarios were compared to 30 years of historic simulations for the period of 1976 to 2005. The results for the effects of regional climate changes showed us a diminution of PM concentration in all scenarios, however, in order to understand the reason for this decrease, different components of PM had to be analyzed separately. This investigation showed that a strong decrease is seen in the concentration of nitrates and dust particles, while the concentration of BSOA and sulfates showed an increase in all scenarios. These results were seen both for the Mediterranean area and for the European continent. The other components of PM did not show strong changes in future scenarios related to regional climate changes. It is also important to notice that although the behavior of PM components regarding climate change seems to be similar in the Mediterranean and European sub-domains, the concentration of PM in the Mediterranean is much higher than what is seen in the European continent because of higher salt, dust and sulfate concentrations.

I then examined the dependencies of PM components to climate variables in detail as well. The meteorological parameters taken into account were temperature, relative humidity, wind speed, short-wave radiation, PBL height and precipitation. Nitrates and BSOA concentrations showed a strong dependence (anti-correlation for nitrates and a correlation for BSOA) to temperature in the European sub-domain. For the latter, the major reason was the positive temperature-dependency of BCOV emissions, triggering enhanced formation of BSOA. For the former, the relationship suggested thermodynamic reasons, higher temperatures shifting the phase equilibrium to gas phase. Sulfates showed high correlation to relative humidity, which is related to either production of this aerosol from SO_2 or formation of gas phase SO_4^{2-} from oxidation of SO_2 by OH, the domination of these processes depend on the sub-domain and the season in which

they are studied. Ammonium showed a combination of the same relationships seen for nitrates and sulfates. Sea salt correlated best with wind speed since the emissions of this species in the model is directly related to this parameter. The overall relationship of PM_{10} and $PM_{2.5}$ to climate variables depended on the component contributing the most to their concentration, for example for the Mediterranean region for PM_{10} and $PM_{2.5}$ wind speed and relative humidity showed the highest correlations because of dominant concentrations of salt and sulfates in PM_{10} and $PM_{2.5}$ respectively.

Future changes in boundary conditions (depicting long range transport from outside of Europe) greatly affected dust concentrations, especially over the Mediterranean area (see below). On the contrary, they had only limited impact on sulfate, nitrate ammonium and OA concentrations.

Analyzing anthropogenic emission changes showed me that they had the largest effect on all $_{10}$/$PM_{2.5}$ components except salt and dust particles. One of the most interesting cases that we encountered in emission change scenarios, was the decrease in BSOA because of anthropogenic emission changes. This was tentatively attributed to changes in seed aerosol and the changes in oxidant levels because of decrease in anthropogenic emissions and also a direct decrease in anthropogenic COVs. However, the exact mechanism of this relationship still needs further investigated. Compared to the other two drivers, the effects shown by the anthropogenic emission reduction were undeniably more important for most species. This gives us the take-away message that, according to this part of the thesis, anthropogenic emission reduction policies (or lack thereof) will have a strong impact on the concentrations of PM seen in the future and also the fact that its impact will be more significant than that of regional climate and long-range transport.

Scenario simulations as presented above are subject to uncertainty in simulations. In my work, I made evident the very different behavior of several OA schemes. Subsequently, I examined the effects of changing the OA simulation schemes in climate impact scenarios. To this end, 10 years of simulations were performed for three OA simulation schemes, 5 historic and 5 future, only changing the regional climate for each series. Afterwards, the changes of BSOA seen in these series of simulations were compared.

The results showed that the modified VBS scheme simulates higher changes compared to the other two schemes in future scenarios for BSOA, showing a difference of 122%, 149% and 244% for CHIMERE standard, standard VBS and modified VBS schemes respectively for the European area. These changes were mostly due to BSOA, which is the major SOA component during summer. I analyzed the differences for the Mediterranean area as well. While the concentrations in the Mediterranean are lower for BSOA in general compared to the European area, the changes for this region seem to be stronger in the VBSmod scheme as well (80%, 79% and 120% for CHIMERE standard, standard VBS and modified VBS schemes respectively for summer). As mentioned before, the reason for the increase in the concentration of BSOA in future scenarios is the increase in the emissions of BVOCs which are temperature dependent. Of course, higher temperatures

mean higher chance of re-volatilization of particulate SVOC. While this explained the reason for the general increase in concentration of BSOA in our future scenarios, the differences simulated in BSOA future changes between different schemes is the sensitivity of each scheme to temperature changes. This is mostly because of taking into account the functionalization, fragmentation and formation of non-volatile SOA in the modified VBS scheme which make this scheme less sensitive to temperature changes and therefore, the formation of BSOA becomes more linear with the increase of BVOCs. The aforementioned processes are not present in the other tested schemes. The lowered sensitivity applies for the Mediterranean region as well, making the transport of BSOA towards this region more feasible and therefore the future simulated BSOA concentration changes higher. These features are not taken into account in OA schemes used for previous studies in the literature. This could lead to an underestimation of the climate impact for BSOA formation by as much as a factor of two in former studies.

Until here, we have examined the changes induced by regional climate, anthropogenic emissions, long-range transport and OA simulation scheme on future concentrations of atmospheric pollutants. Now, we would like to see the effects of these changes on the increasing population in the Mediterranean region. For this purpose, a regional focus is necessary on the coasts of the Mediterranean, in a region where a strong population gradient and large urban areas are seen. The PACA region, in the south-eastern part of France on the western coasts of the Mediterranean was chosen for this purpose.

In order to achieve this objective, I used five years of simulations. The year 2005 was chosen for the current day simulation using CLE 2010 emissions. For future case studies, RCP4.5 and RCP8.5 were used as climate scenarios, for each one a year in the 2030 horizon and a year in 2050 timeframe was simulated. For each year of future situation, a coarse domain was simulated which covers the whole Europe, and then a nested domain was added which is focused on the PACA region with a horizontal resolution of 5km.

Anthropogenic emissions data was obtained from the PACA region air quality control association (AtmoSud ASQAA), which were re-gridded and used in our simulations. Current population density for this region was obtained from INERIS. Shared socioeconomic pathway (SSP) scenarios are used to project the current population of this region to the 2030 and 2050 timeframes. These scenarios take into account the economic, technologic advances as well as mortality, fertility and migration in the population change in future. After a comparison between differences seen in these demographic scenarios (5 in total), 2 of them showing extreme conditions were chosen, one showing a decreasing population for the PACA region starting from the 2040s, the other one showing an increasing trend until the end of the century. Before discussing the results for this study, it is important to mention that these simulations are to be taken as case studies for the eventualities that could happen for this region in the future, they present possibilities of what could change regarding the population exposure in this region and they should not be regarded as an ensemble of future scenarios.

The simulations showed that for the PACA region, the concentration of PM decreased in all case studies because of (i) decrease in nitrate and sulfate concentrations and (ii) decrease in anthropogenic emissions. The concentration of ozone showed an increase in urban areas, which is caused by a reduction of NO emissions, which in return results in a decrease in titration of ozone. BSOA concentrations showed an increase, the reasons for which were already pointed out before. Dust particles also showed an increase in all future situations. Other species mostly showed a decrease because of emission reduction policies.

The population exposure to PM (both $PM_{2.5}$ and PM_{10}) showed a decrease both in rural and urban areas. Most PM components except dust and BSOA showed a decrease in exposure as well. The ozone exposure increased in urban areas while it showed a decrease in the rest of the domain. BSOA showed an increase in exposure in RCP8.5 situations, while showing a decreasing exposure for RCP4.5 ones regardless of the time-frame (2030 or 2050). Its concentration presented an increase in the whole domain in all future situations (the intensity of this increase depends directly to the intensity of the climate scenario used), therefore the decrease of this exposure in rural areas was attributed to be solely because of the population decrease. Dust exposure increased in the western and southern parts of the domain especially, since these particles are normally transported from south side of the domain, their major source being in the Northern parts of Africa.

We also wanted to distinguish exposure evolution in highly populated versus more rural regions. The three coastal densely populated departments (D06, D13 and D83) presented increased exposure risks to all examined species, both in the reference simulation and in future case studies, mainly due to increased population. This exposure becomes quite important for primary components such as nitrogen oxides near the source regions, showing a factor of three between D83 (a coastal county affected by shipping and industrial emissions and also large urban regions) and D05 (a rural and sparsely populated region). This analysis makes it quite obvious that the effects of emission reduction policies in the future are going to be fundamental when it comes to the exposure of the population to primary components especially in coastal areas with high-activity and highly populated ports.

3 Perspectives

My thesis work opens various perspectives in several directions. First, it is important to evaluate the performance of the MEGAN model in simulating isoprene and monoterpene emissions in a more regional look rather than only two stations for the European continent and the Mediterranean region. This means that several stations spread across the domain with measurements for these two species are necessary to be compared to the simulated emissions. For isoprene emissions, a validation using satellite data can be performed as well by using formaldehyde (HCHO) column concentrations. Formalde-

hyde is one of the resulting compounds of isoprene reaction with ozone. For terpenes, an intensive measurement campaign took place in the summer of 2017 in the Landes forest in south-Western France, mainly populated by a highly emitting monoterpenes pines species. During this campaign, measurements of OA and its precursor BVOCs were performed. Measurements in this region can allow us to first, evaluate the emissions of BVOCs (mainly mono-terpenes) taken into account in the CHIMERE model, and secondly, it will help us to evaluate the formation of SOA due to mono-terpenes in the model. This is a region that is close to BVOC sources, remote (so far away from anthropogenic emissions under westerly winds) and orographically flat, helping to remove the source of orographic representativeness error affecting my thesis work.

In addition to the four OA schemes evaluated during my thesis, other recently available OA schemes, showing different functionalities should be tested as well. For example, Lannuque, Camredon, et al. (2018) use the GECKO-A chemical mechanism generator to derive a parameterized OA simulation scheme that was then implemented in CHIMERE. Testing this scheme will allow us to see the performance of an explicitly generated mechanism in the CHIMERE model. One other scheme that can be tested for this region is the SOAP scheme implemented in CHIMERE by Couvidat, Bessagnet, et al. (2018), which may be the future standard scheme incorporated into CHIMERE. Another possibility is the VBS-1.5 scheme (Koo et al. 2014) which has never been implemented in the CHIMERE model. This scheme is a compromise of the VBS-1D and the VBS-2D scheme, containing more details on the oxidation state of OA compared to VBS-1D and being numerically less stringent than the VBS-2D scheme. The comparison between these schemes can help us understand the principal mechanisms that are in play in the Mediterranean region.

This extended set of OA schemes could be evaluated with respect to different data bases showing a large variety of emission situations, starting with the Mediterranean area. In addition, as mentioned before, intensive measurements have been performed for both SOA and its precursors in the Landes region. This will give us the opportunity to explore the performance of these scheme on the simulation of OA formed from mono-terpenes, while removing the errors related to anthropogenic SOA formation to an important degree because of the remoteness of the site. In the long term, the ACROSS project (Atmospheric ChemistRy Of the Suburban forest, planned for 2021) which is a part of the MOGPA (Make Our Planet Great Again) initiative can certainly be of interest for the simulation of OA in the Parisian area. This project will give us an excellent opportunity for comparison against a large number of measurements, both in-situ and airborne, for a forested area near the Paris region, therefore combining both anthropogenic and biogenic source availability for the formation of OA.

Concerning future scenarios, in addition to the effects of emission and climate change other aspects need to be explored as well. For example, scenarios containing land-use changes can be added to the CHIMERE model and then be compared with SSP scenarios for the European area and also the Mediterranean coasts in a regional scale. Land use

changes such as urbanization on the European scale or the deforestation in the African and European area can be important to be taken into account regarding to the future of these two regions.

One of the interesting facts that was seen in this thesis was the effects of anthropogenic emission reduction policies on the concentration of BSOA. This was attributed to the diminution of seed aerosol existing for the formation of more OA, however, a more detailed study is necessary in order to explain this observation completely. Emission reduction sensitivity tests in a climatic setting can be useful in this regard.

In this thesis we have shown that climatic changes can change the exposure of the population to atmospheric pollutants to a large extent. In this work, case studies were performed in order to explore the importance of this change. In the future, complete sets of climatic simulations can be performed, containing at least five years of simulations for each scenario (resulting in at least 25 years of simulations in total for the small domain) in order to explore the average exposure change on a local level. Another addition to this work would be to interpret the exposure calculated in this thesis into mortality rates in future scenarios. This is done by using SSP scenarios: using estimations of natural death in future demographic scenarios along with the population exposure in order to estimate the mortality due to certain atmospheric pollutants. Finally, land use changes are important to explore on an urban level in future scenarios, combining the land use change effect with population change.

Bibliography

Adloff, F., S. Somot, F. Sevault, G. Jordà, R. Aznar, M. Déqué, M. Herrmann, M. Marcos, C. Dubois, E. Padorno, E. Alvarez-Fanjul, and D. Gomis (2015). "Mediterranean Sea response to climate change in an ensemble of twenty first century scenarios". In: *Climate Dynamics* 45.9-10, pp. 2775–2802. ISSN: 0930-7575. DOI: 10.1007/s00382-015-2507-3.

Ahmadov, R., S. A. McKeen, A. L. Robinson, R. Bahreini, A. M. Middlebrook, J. A. de Gouw, J. Meagher, E.-Y. Hsie, E. Edgerton, S. Shaw, and M. Trainer (2012). "A volatility basis set model for summertime secondary organic aerosols over the eastern United States in 2006". In: *Journal of Geophysical Research: Atmospheres* 117.D6, n/a–n/a. ISSN: 01480227. DOI: 10.1029/2011JD016831.

Aiken, A. C., P. F. DeCarlo, J. H. Kroll, D. R. Worsnop, J. A. Huffman, K. S. Docherty, I. M. Ulbrich, C. Mohr, J. R. Kimmel, D. Sueper, Y. Sun, Q. Zhang, A. Trimborn, M. Northway, P. J. Ziemann, M. R. Canagaratna, T. B. Onasch, M. R. Alfarra, A. S. H. Prevot, J. Dommen, J. Duplissy, A. Metzger, U. Baltensperger, and J. L. Jimenez (2008). "O/C and OM/OC Ratios of Primary, Secondary, and Ambient Organic Aerosols with High-Resolution Time-of-Flight Aerosol Mass Spectrometry". In: *Environmental Science & Technology* 42.12, pp. 4478–4485. ISSN: 0013-936X. DOI: 10.1021/es703009q.

Aksoyoglu, S., G. Ciarelli, I. El-Haddad, U. Baltensperger, and A. S. H. Prévôt (2017). "Secondary inorganic aerosols in Europe: sources and the significant influence of biogenic VOC emissions, especially on ammonium nitrate". In: *Atmospheric Chemistry and Physics* 17.12, pp. 7757–7773. ISSN: 1680-7324. DOI: 10.5194/acp-17-7757-2017.

Albert, M. F. M. A., M. Schaap, A. M. M. Manders, C. Scannell, C. D. O'Dowd, and G. de Leeuw (2012). "Uncertainties in the determination of global sub-micron marine organic matter emissions". In: *Atmospheric Environment* 57, pp. 289–300. DOI: 10.1016/j.atmosenv.2012.04.009.

Alfaro, S. C. and L. Gomes (2001). "Modeling mineral aerosol production by wind erosion: Emission intensities and aerosol size distributions in source areas". In: *Journal of Geophysical Research: Atmospheres* 106.D16, pp. 18075–18084. ISSN: 01480227. DOI: 10.1029/2000JD900339.

Alfaro, S., A. Gaudichet, L. Gomes, and M. Maih6 (1998). "Mineral aerosol production by wind erosion: aerosol particle sizes and binding energies". In: *GEOPHYSICAL RESEARCH LETTERS* 25.1, pp. 991–994. DOI: 10.1029/98GL00502.

Amann, M., Z. Klimont, and F. Wagner (2013). "Regional and Global Emissions of Air Pollutants: Recent Trends and Future Scenarios". In: *Annual Review of Environment and Resources* 38.1, pp. 31–55. ISSN: 1543-5938. DOI: 10.1146/annurev-environ-052912-173303.

Ammann, M., R. A. Cox, J. N. Crowley, M. E. Jenkin, A. Mellouki, M. J. Rossi, J. Troe, and T. J. Wallington (2013). "Evaluated kinetic and photochemical data for atmospheric chemistry: Volume VI - Heterogeneous reactions with liquid substrates". In: *Atmospheric Chemistry and Physics* 13.16, pp. 8045–8228. ISSN: 16807316. DOI: 10.5194/acp-13-8045-2013.

Anderson, J. O., J. G. Thundiyil, and A. Stolbach (2012). "Clearing the Air: A Review of the Effects of Particulate Matter Air Pollution on Human Health". In: *Journal of Medical Toxicology* 8.2, pp. 166–175. ISSN: 1556-9039. DOI: 10.1007/s13181-011-0203-1.

Andreae, M. O. and P. Merlet (2001). "Emission of trace gases and aerosols from biomass burning". In: *Global Biogeochemical Cycles* 15.4, pp. 955–966. ISSN: 08866236. DOI: 10.1029/2000GB001382.

Arakawa and A. (1972). *Design of the UCLA general circulation model*. Tech. rep. Los angeles: UCLA.

Arino, O., P. Bicheron, F. Achard, J. Latham, R. Witt, and J. Weber (2008). "Globcover: The most detailed protrait of Earth". In: *European Space Agency Bulletin* 36, pp. 24–31.

Arndt, J., J. Sciare, M. Mallet, G. C. Roberts, N. Marchand, K. Sartelet, K. Sellegri, F. Dulac, R. M. Healy, and J. C. Wenger (2017). "Sources and mixing state of summertime background aerosol in the northwestern Mediterranean basin". In: *ACPD Atmos. Chem. Phys. Discuss* 17.11. DOI: 10.5194/acp-2016-1044.

Arneth, A., P. A. Miller, M. Scholze, T. Hickler, G. Schurgers, B. Smith, and I. C. Prentice (2007). "CO ₂ inhibition of global terrestrial isoprene emissions: Potential implications for atmospheric chemistry". In: *Geophysical Research Letters* 34.18, p. L18813. ISSN: 0094-8276. DOI: 10.1029/2007GL030615.

Arrhenius, S. (1896). "On the Influence of Carbonic Acid in the Air upon the Temperature of the Ground". In: *Philosophical Magazine and Journal of Science Series* 5.41, pp. 237–276.

Aumont, B., A. Jaecker-Voirol, B. Martin, and G. Toupance (1996). "Tests of some reduction hypotheses made in photochemical mechanisms". In: *Atmospheric Environment* 30.12, pp. 2061–2077. ISSN: 1352-2310. DOI: 10.1016/1352-2310(95)00279-0.

Aumont, B., S. Szopa, and S. Madronich (2005). "Modelling the evolution of organic carbon during its gas-phase tropospheric oxidation: development of an explicit model based on a self generating approach". In: 5, pp. 2497–2517. DOI: 10.5194/acp-5-2497-2005.

Bank World (2017). *World income classification*. Tech. rep. World Bank.

Bardouki, H., H. Liakakou, C. Economou, J. Sciare, J. Smolík, V. Ždímal, K. Eleftheriadis, M. Lazaridis, C. Dye, and N. Mihalopoulos (2003). "Chemical composition of size-resolved atmospheric aerosols in the eastern Mediterranean during summer and winter". In: *Atmospheric Environment* 37.2, pp. 195–208. DOI: 10.1016/S1352-2310(02)00859-2.

Barsanti, K. C., J. N. Smith, and J. F. Pankow (2011). "Application of the np+ mP modeling approach for simulating secondary organic particulate matter formation from alpha-pinene oxidation". In: *Atmospheric environment* 45.37, pp. 6812–6819.

Bauer, S. E., D. Koch, N. Unger, S. M. Metzger, D. T. Shindell, and D. G. Streets (2007). "Nitrate aerosols today and in 2030: a global simulation including aerosols and tropospheric ozone". In: *Atmospheric Chemistry and Physics* 7.19, pp. 5043–5059. DOI: 10.5194/acp-7-5043-2007.

Belviso, S., L. Bopp, C. Moulin, J. C. Orr, T. R. Anderson, O. Aumont, S. Chu, S. Elliott, M. E. Maltrud, and R. Simó (2004). "Comparison of global climatological maps of sea surface dimethyl sulfide". In: *Global Biogeochemical Cycles* 18.3. ISSN: 08866236. DOI: 10.1029/2003GB002193.

Berezin, E. V., I. B. Konovalov, P. Ciais, A. Richter, S. Tao, G. Janssens-Maenhout, M. Beekmann, and E.-D. Schulze (2013). "Multiannual changes of CO 2 emissions in China: indirect estimates derived from satellite measurements of tropospheric NO 2 columns". In: *Atmos. Chem. Phys* 13, pp. 9415–9438. DOI: 10.5194/acp-13-9415-2013.

Bergström, R., H. A. C. Denier van der Gon, A. S. H. Prévôt, K. E. Yttri, and D. Simpson (2012). "Modelling of organic aerosols over Europe (2002–2007) using a volatility basis set (VBS) framework: application of different assumptions regarding the formation of secondary organic aerosol". In: *Atmospheric Chemistry and Physics* 12.18, pp. 8499–8527. ISSN: 1680-7324. DOI: 10.5194/acp-12-8499-2012.

Bernstein, L., P. Bosch, O. Canziani, Z. Chen, R. Christ, O. Davidson, W. Hare, S. Huq, D. Karoly, V. Kattsov, Z. Kundzewicz, J. Liu, U. Lohmann, M. Manning, T. Matsuno, B. Menne, B. Metz, M. Mirza, N. Nicholls, L. Nurse, R. Pachauri, J. Palutikof, M. Parry, D. Qin, N. Ravindranath, A. Reisinger, J. Ren, K. Riahi, C. Rosenzweig, M. Rusticucci, S. Schneider, Y. Sokona, S. Solomon, P. Stott, R. Stouffer, T. Sugiyama, R. Swart, D. Tirpak, C. Vogel, G. Yohe, T. Barker, A. Allali, R. Bojariu, S. Diaz, I. Elgizouli, D. Griggs, D. Hawkins, O. Hohmeyer, P. Jallow, L. 4ka Kajfez 4-Bogataj, N. Leary, H. Lee, and D. Wratt (2007). *Climate Change 2007, Synthesis report*. Tech. rep.

Berrisford, P., P. Kallberg, S. Kobayashi, D. Dee, S. Uppala, A. J. Simmons, and H. Sato (2011). *The ERA-Interim archive version 2.0. ERA Rep. Series*. Tech. rep. Shinfield Park, Reading: ECMWF.

Bessagnet, B., A. Hodzic, R. Vautard, M. Beekmann, S. Cheinet, C. Honoré, C. Liousse, and L. Rouil (2004). "Aerosol modeling with CHIMERE—preliminary evaluation at the continental scale". In: *Atmospheric Environment* 38.18, pp. 2803–2817. ISSN: 1352-2310. DOI: 10.1016/J.ATMOSENV.2004.02.034.

Bessagnet, B., G. Pirovano, M. Mircea, C. Cuvelier, A. Aulinger, G. Calori, G. Ciarelli, A. Manders, R. Stern, S. Tsyro, M. García Vivanco, P. Thunis, M.-T. Pay, A. Colette, F. Couvidat, F. Meleux, L. Rouïl, A. Ung, S. Aksoyoglu, J. M. Baldasano, J. Bieser, G. Briganti, A. Cappelletti, M. D'Isodoro, S. Finardi, R. Kranenburg, C. Silibello, C. Carnevale, W. Aas, J.-C. Dupont, H. Fagerli, L. Gonzalez, L. Menut, A. S. H. Prévôt, P. Roberts, and L. White (2016). "Presentation of the EURODELTA III inter-comparison exercise – Evaluation of the chemistry transport models performance on criteria pollutants and joint analysis with meteorology". In: *Atmospheric Chemistry and Physics Discussions* January, pp. 1–61. ISSN: 1680-7375. DOI: 10.5194/acp-2015-736.

Bessagnet, B., L. Menut, G. Curci, A. Hodzic, B. Guillaume, C. Liousse, S. Moukhtar, B. Pun, C. Seigneur, M. M. Schulz, G. Curd, A. Hodzic, B. Guillaume, C. Liousse, S. Moukhtar, B. Pun, C. Seigneur, and M. M. Schulz (2008). "Regional modeling of carbonaceous aerosols over Europe-focus on secondary organic aerosols". In: *Journal of Atmospheric Chemistry* 61.3, pp. 175–202. ISSN: 01677764. DOI: 10.1007/s10874-009-9129-2.

Bicheron, P., V. Amberg, L. Bourg, D. Petit, M. Huc, B. Miras, C. Brockmann, O. Hagolle, S. Delwart, F. Ranera, M. Leroy, and O. Arino (2011). "Geolocation Assessment of MERIS GlobCover Orthorectified Products". In: *IEEE Transactions on Geoscience and Remote Sensing* 49.8, pp. 2972–2982. ISSN: 0196-2892. DOI: 10.1109/TGRS.2011.2122337.

Bjerknes, V. (1902). "Cirkulation relativ zu der Erde." In: *Meteor. Z.* 19, pp. 97–108.

Blomquist, B. W., C. W. Fairall, B. J. Huebert, D. J. Kieber, and G. R. Westby (2006). "DMS sea-air transfer velocity: Direct measurements by eddy covariance and parameterization based on the NOAA/COARE gas transfer model". In: *Geophysical Research Letters* 33.7, p. L07601. ISSN: 0094-8276. DOI: 10.1029/2006GL025735.

Borrego, C., J. A. Souto, A. Monteiro, M. Dios, A. Rodríguez, J. Ferreira, S. Saavedra, J. J. Casares, and A. I. Miranda (2013). "The role of transboundary air pollution over Galicia and North Portugal area". In: *Environmental Science and Pollution Research* 20.5, pp. 2924–2936. ISSN: 0944-1344. DOI: 10.1007/s11356-012-1201-9.

Boucher, O., D. Randall, P. Artaxo, C. Bretherton, G. Feingold, P. Forster, V.-M. Kerminen, Y. Kondo, H. Liao, U. Lohmann, P. Rasch, S. Satheesh, S. Sherwood, B. Stevens, and X.-Y. Zhang (2013). *Clouds and Aerosols. In: Climate Change 2013: The Physical Science Basis*. Tech. rep. Cambridge University Press, Cambridge, United Kingdom and New York, NY, USA, pp. 571–658.

Bouchlaghem, K., B. Nsom, N. Latrache, and H. Haj Kacem (2009). "Impact of Saharan dust on PM10 concentration in the Mediterranean Tunisian coasts". In: *Atmospheric Research* 92.4, pp. 531–539. ISSN: 01698095. DOI: 10.1016/j.atmosres.2009.02.009.

Bowden, J. H., T. L. Otte, C. G. Nolte, M. J. Otte, J. H. Bowden, T. L. Otte, C. G. Nolte, and M. J. Otte (2012). "Examining interior grid nudging techniques using two-way nesting in the wrf model for regional climate modeling". In: *Journal of Climate* 25.8, pp. 2805–2823. ISSN: 0894-8755. DOI: 10.1175/JCLI-D-11-00167.1.

Boylan, J. W. and A. G. Russell (2006). "PM and light extinction model performance metrics, goals, and criteria for three-dimensional air quality models". In: *Atmospheric Environment* 40.26, pp. 4946–4959. ISSN: 13522310. DOI: 10.1016/j.atmosenv.2005.09.087.

Brey, S. J., J. R. Pierce, E. A. Barnes, and E. V. Fischer (2020). "Estimating the spread in future fine dust concentrations in the Southwest United States". In: *Journal of Geophysical Research: Atmospheres* 125.21, e2019JD031735.

Brunekreef, B. and S. T. Holgate (2002). "Air pollution and health". In: *The Lancet* 360.9341, pp. 1233–1242. ISSN: 01406736. DOI: 10.1016/S0140-6736(02)11274-8.

Byun, D. W., C.-K. Song, P. B. Percell, J. Pleim, T. Otte, J. Young, and R. Mathur (2006). "Linkage between WRF/NMM and CMAQ Models". In:

Callendar, G. S. (1938). "The artificial production of carbon dioxide and its influence on temperature". In: *Quarterly Journal of the Royal Meteorological Society* 64.275, pp. 223–240. ISSN: 00359009. DOI: 10.1002/qj.49706427503.

Calori, G., C. SiIibello, and G. Marras (2014). *FARM(Flexible Air quality Regional Model) Model formulation and user's Manual*. Tech. rep. Milano: ARIANET.

Camredon, M. and B. Aumont (2007). "I – L'ozone troposphérique : production/consommation et régimes chimiques". In: *Pollution atmosphérique* N193. ISSN: 2268-3798. DOI: 10.4267/pollution-atmospherique.1404.

Camredon, M., J. Hamilton, M. Alam, K. Wyche, T. Carr, I. White, P. Monks, A. Rickard, and W. Bloss (2010). "Distribution of gaseous and particulate organic composition during dark alpha-pinene ozonolysis". In: *Atmospheric Chemistry and Physics* 10.6, pp. 2893–2917.

Canonaco, F., M. Crippa, J. G. Slowik, U. Baltensperger, and A. S. H. Prévôt (2013). "No Title". In: 6.

Cappa, C. and J. Jimenez (2010). "Quantitative estimates of the volatility of ambient organic aerosol". In: *Atmospheric Chemistry and Physics* 10.12, pp. 5409–5424. ISSN: 1680-7324. DOI: 10.5194/acp-10-5409-2010.

Cappa, C., X. Zhang, C. Loza, J. Craven, Y. Lee, and J. Seinfeld (2013). "Application of the Statistical Oxidation Model (SOM) to Secondary Organic Aerosol formation from photooxidation of C_ (12) alkanes". In: *Atmospheric Chemistry and Physics* 13.3, pp. 1591–1606.

Cappa, C. D., S. H. Jathar, M. J. Kleeman, K. S. Docherty, J. L. Jimenez, J. H. Seinfeld, and A. S. Wexler (2016). "Simulating secondary organic aerosol in a regional air quality model using the statistical oxidation model – Part 2: Assessing the influence of vapor wall losses: Simulating Secondary Organic Aerosol in a Regional Air Quality Model". In: *Atmos. Chem. Phys* 16, pp. 3041–3059. DOI: 10.5194/acp-16-3041-2016.

Cappa, C. D. and K. R. Wilson (2012). "Multi-generation gas-phase oxidation, equilibrium partitioning, and the formation and evolution of secondary organic aerosol". In: *Atmospheric Chemistry and Physics* 12.20, pp. 9505–9528.

Carlton, A. G., C. Wiedinmyer, and J. H. Kroll (2009). "A review of Secondary Organic Aerosol (SOA) formation from isoprene". In: *Atmospheric Chemistry and Physics* 9.14, pp. 4987–5005. ISSN: 1680-7324. DOI: 10.5194/acp-9-4987-2009.

Carter, W. (2010). "Development of the SAPRC-07 chemical mechanism". In: *Atmospheric Environment* 44.40, pp. 5324–5335. ISSN: 1352-2310. DOI: 10.1016/J.ATMOSENV.2010.01.026.

Carter, W. (2015). "Development of a database for chemical mechanism assignments for volatile organic emissions". In: *Journal of the Air & Waste Management Association* 65.10, pp. 1171–1184. DOI: 10.1080/10962247.2015.1013646.

Carter, W. P. (1990). "A detailed mechanism for the gas-phase atmospheric reactions of organic compounds". In: *Atmospheric Environment. Part A. General Topics* 24.3, pp. 481–518. ISSN: 0960-1686. DOI: 10.1016/0960-1686(90)90005-8.

Carvalho, A., A. Monteiro, S. Solman, A. Miranda, and B. C. (2010). "Climate-driven changes in air quality over Europe by the end of the 21st century, with special reference to Portugal". In: *Environmental Science & Policy* 13.6, pp. 445–458. ISSN: 1462-9011. DOI: 10.1016/J.ENVSCI.2010.05.001.

Cassee, F. R., M.-E. Héroux, M. E. Gerlofs-Nijland, and F. J. Kelly (2013). "Particulate matter beyond mass: recent health evidence on the role of fractions, chemical constituents and sources of emission." In: *Inhalation toxicology* 25.14, pp. 802–12. ISSN: 1091-7691. DOI: 10.3109/08958378.2013.850127.

Cécile Honoré, Robert Vautard, and Matthias Beekmann (2000). "Low and high NOx chemical regimes in an urban environment". In: *Environmental Modelling & Software* 15.6-7, pp. 559–564. DOI: 10.1016/S1364-8152(00)00043-8.

Charney, J. G. and A. Eliassen (1949). "A Numerical Method for Predicting the Perturbations of the Middle Latitude Westerlies". In: *Tellus* 1.2, pp. 38–54. ISSN: 00402826. DOI: 10.1111/j.2153-3490.1949.tb01258.x.

Chen, F., J. Dudhia, F. Chen, and J. Dudhia (2001). "Coupling an Advanced Land Surface–Hydrology Model with the Penn State–NCAR MM5 Modeling System. Part I: Model Implementation and Sensitivity". In: *Monthly Weather Review* 129.4, pp. 569–585. ISSN: 0027-0644. DOI: 10.1175/1520-0493(2001)129<0569:CAALSH>2.0.CO;2.

Chin, M., P. Ginoux, S. Kinne, O. Torres, B. N. Holben, B. N. Duncan, R. V. Martin, J. a. Logan, A. Higurashi, and T. Nakajima (2002). "Tropospheric Aerosol Optical Thickness from the GOCART Model and Comparisons with Satellite and Sun Photometer Measurements". In: *Journal of the Atmospheric Sciences* 59.3, pp. 461–483. ISSN: 0022-4928. DOI: 10.1175/1520-0469(2002)059<0461:TAOTFT>2.0.CO;2.

Cholakian, A., M. Beekmann, A. Colette, I. Coll, G. Siour, J. Sciare, N. Marchand, F. Couvidat, J. Pey, V. Gros, S. Sauvage, V. Michoud, K. Sellegri, A. Colomb, K. Sartelet, H. Langley DeWitt, M. Elser, A. S. H. Prévot, S. Szidat, and F. Dulac (2018). "Simulation of fine organic aerosols in the western Mediterranean area during the ChArMEx 2013

summer campaign". In: *Atmospheric Chemistry and Physics* 18.10, pp. 7287–7312. ISSN: 1680-7324. DOI: 10.5194/acp-18-7287-2018.

Cholakian, A., M. Beekmann, I. Coll, G. Ciarelli, and A. Colette (2019). "Biogenic secondary organic aerosol sensitivity to organic aerosol simulation schemes in climate projections". In: *Atmospheric Chemistry and Physics* 19.20, pp. 13209–13226.

Cholakian, A., A. Colette, I. Coll, G. Ciarelli, and M. Beekmann (2019). "Future climatic drivers and their effect on PM10 components in Europe and the Mediterranean Sea". In: *Atmospheric Chemistry and Physics* 19.7, pp. 4459–4484.

Chrit, M., K. Sartelet, J. Sciare, M. Majdi, J. Nicolas, J.-E. Petit, and F. Dulac (2018). "Modeling organic aerosol concentrations and properties during winter 2014 in the northwestern Mediterranean region". In: *Atmospheric Chemistry and Physics Discussions* 2018, pp. 1–28. DOI: 10.5194/acp-2018-149.

Chrit, M., K. Sartelet, J. Sciare, J. Pey, N. Marchand, F. Couvidat, K. Sellegri, and M. Beekmann (2017). "Modelling organic aerosol concentrations and properties during ChArMEx summer campaigns of 2012 and 2013 in the western Mediterranean region". In: *Atmospheric Chemistry and Physics Discussions*, pp. 1–33. ISSN: 1680-7375. DOI: 10.5194/acp-2017-312.

Chu, S., S. Elliott, and M. E. Maltrud (2003). "Global eddy permitting simulations of surface ocean nitrogen, iron, sulfur cycling". In: *Chemosphere* 50.2, pp. 223–235. ISSN: 0045-6535. DOI: 10.1016/S0045-6535(02)00162-5.

Chuang, W. and N. Donahue (2016). "A two-dimensional volatility basis set – Part 3: Prognostic modeling and NO x dependence". In: *Atmos. Chem. Phys* 16, pp. 123–134. DOI: 10.5194/acp-16-123-2016.

Ciardini, V., G. M. Contessa, R. Falsaperla, J. L. Gómez-Amo, D. Meloni, F. Monteleone, G. Pace, S. Piacentino, D. Sferlazzo, and A. di Sarra (2016). "Global and Mediterranean climate change: a short summary." In: *Annali dell'Istituto superiore di sanita* 52.3, pp. 325–337. ISSN: 2384-8553. DOI: 10.4415/ANN_16_03_04.

Ciarelli, G., S. Aksoyoglu, M. Crippa, J.-L. Jimenez, E. Nemitz, K. Sellegri, M. Äijälä, S. Carbone, C. Mohr, C. O'Dowd, L. Poulain, U. Baltensperger, and A. S. H. Prévôt (2016). "Evaluation of European air quality modelled by CAMx including the volatility basis set scheme". In: *Atmospheric Chemistry and Physics* 16.16, pp. 10313–10332. ISSN: 1680-7324. DOI: 10.5194/acp-16-10313-2016.

Colella, P. and P. R. Woodward (1984). "The Piecewise Parabolic Method (PPM) for gas-dynamical simulations". In: *Journal of Computational Physics* 54.1, pp. 174–201. ISSN: 0021-9991. DOI: 10.1016/0021-9991(84)90143-8.

Colette, A., B. Bessagnet, R. Vautard, S. Szopa, S. Rao, S. Schucht, Z. Klimont, L. Menut, G. Clain, F. Meleux, G. Curci, and L. Roul (2013). "Geoscientific Instrumentation Methods and Data Systems European atmosphere in 2050, a regional air quality and climate perspective under CMIP5 scenarios". In: *Atmos. Chem. Phys* 13, pp. 7451–7471. DOI: 10.5194/acp-13-7451-2013.

Colette, A., C. Andersson, A. Baklanov, B. Bessagnet, J. Brandt, J. H. Christensen, R. Doherty, M. Engardt, C. Geels, C. Giannakopoulos, G. B. Hedegaard, E. Katragkou, J. Langner, H. Lei, A. Manders, D. Melas, F. Meleux, L. Rouïl, M. Sofiev, J. Soares,

D. S. Stevenson, M. Tombrou-Tzella, K. V. Varotsos, and P. Young (2015). "Is the ozone climate penalty robust in Europe?" In: *Environmental Research Letters* 10.8, p. 084015. ISSN: 1748-9326. DOI: 10.1088/1748-9326/10/8/084015.

Coll, I., F. Lasry, S. Fayet, A. Armengaud, and R. Vautard (2009). "Simulation and evaluation of 2010 emission control scenarios in a Mediterranean area". In: *Atmospheric Environment* 43.27, pp. 4194–4204. ISSN: 13522310. DOI: 10.1016/j.atmosenv.2009.05.034.

Couvidat, F., Y. Kim, K. Sartelet, C. Seigneur, N. Marchand, and J. Sciare (2013). "Modeling secondary organic aerosol in an urban area: application to Paris, France". In: *Atmospheric Chemistry and Physics* 13.2, pp. 983–996. ISSN: 1680-7324. DOI: 10.5194/acp-13-983-2013.

Couvidat, F., B. Bessagnet, M. Garcia-Vivanco, E. Real, L. Menut, and A. Colette (2018). "Development of an inorganic and organic aerosol model (CHIMERE 2017β; v1.0): seasonal and spatial evaluation over Europe". In: *Geoscientific Model Development* 11.1, pp. 165–194. ISSN: 1991-9603. DOI: 10.5194/gmd-11-165-2018.

Couvidat, F., É. Debry, K. Sartelet, and C. Seigneur (2012). "A hydrophilic/hydrophobic organic (H2O) aerosol model: Development, evaluation and sensitivity analysis". In: *Journal of Geophysical Research: Atmospheres* 117.D10, n/a–n/a. ISSN: 01480227. DOI: 10.1029/2011JD017214.

Couvidat, F. and K. Sartelet (2015). "The Secondary Organic Aerosol Processor (SOAP v1.0) model: a unified model with different ranges of complexity based on the molecular surrogate approach". In: *Geosci. Model Dev* 8, pp. 1111–1138. DOI: 10.5194/gmd-8-1111-2015.

Crippa, M., P. F. Decarlo, J. G. Slowik, C. Mohr, M. F. Heringa, R. Chirico, L. Poulain, F. Freutel, J. Sciare, J. Cozic, C. F. Di Marco, M. Elsasser, J. B. Nicolas, N. Marchand, E. Abidi, A. Wiedensohler, F. Drewnick, J. Schneider, S. Borrmann, E. Nemitz, R. Zimmermann, J.-L. Jaffrezo, A. S. H. Prévôt, and U. Baltensperger (2013). "Wintertime aerosol chemical composition and source apportionment of the organic fraction in the metropolitan area of Paris". In: *Atmos. Chem. Phys. Atmospheric Chemistry and Physics* 13, pp. 961–981. DOI: 10.5194/acp-13-961-2013.

Crippa, M., I. E. Haddad, J. G. Slowik, P. F. Decarlo, C. Mohr, M. F. Heringa, R. Chirico, N. Marchand, J. Sciare, U. Baltensperger, and A. S. H. Prévôt (2013). "Identification of marine and continental aerosol sources in Paris using high resolution aerosol mass spectrometry". In: *J. Geophys. Res. Atmos* 118, pp. 1950–1963. DOI: 10.1002/jgrd.50151.

Curci, G., P. I. Palmer, T. P. Kurosu, K. Chance, and G. Visconti (2010). "Estimating European volatile organic compound emissions using satellite observations of formaldehyde from the Ozone Monitoring Instrument". In: *Atmos. Chem. Phys. Atmospheric Chemistry and Physics* 10, pp. 11501–11517. DOI: 10.5194/acp-10-11501-2010.

Dale, V. H., L. A. Joyce, S. McNulty, R. P. Neilson, M. P. Ayres, M. D. Flannigan, P. J. Hanson, L. C. Irland, A. E. Lugo, C. J. Peterson, D. Simberloff, F. J. Swanson, B. J. Stocks, and B. M. Wotton (2001). "Climate Change and Forest Disturbances:Climate change can affect forests by altering the frequency, intensity, duration, and timing of fire,

drought, introduced species, insect and pathogen outbreaks, hurricanes, windstorms, ice storms, or landslides". In: *BioScience* 51.9, pp. 723–734. ISSN: 0006-3568. DOI: 10.1641/0006-3568(2001)051[0723:ccafd]2.0.co;2.

Dawson, J. P., P. J. Adams, and S. N. Pandis (2007). "Sensitivity of PM2.5 to climate in the Eastern US: a modeling case study". In: *Atmospheric Chemistry and Physics* 7.16, pp. 4295–4309. ISSN: 1680-7324. DOI: 10.5194/acp-7-4295-2007.

De Longueville, F., Y.-C. Hountondji, S. Henry, and P. Ozer (2010). "What do we know about effects of desert dust on air quality and human health in West Africa compared to other regions?" In: *Science of The Total Environment* 409.1, pp. 1–8. ISSN: 0048-9697. DOI: 10.1016/J.SCITOTENV.2010.09.025.

Decarlo, P. F., J. R. Kimmel, A. Trimborn, M. J. Northway, J. T. Jayne, A. C. Aiken, M. Gonin, K. Fuhrer, T. Horvath, K. S. Docherty, D. R. Worsnop, and J. L. Jimenez (2006). "Field-Deployable, High-Resolution, Time-of-Flight Aerosol Mass Spectrometer". In: *Analytical Chemistry* 78, pp. 8281–8289. DOI: 10.1021/ac061249n.

Denjean, C., F. Cassola, A. Mazzino, S. Triquet, S. Chevaillier, N. Grand, T. Bourrianne, G. Momboisse, K. Sellegri, A. Schwarzenbock, E. Freney, M. Mallet, and P. Formenti (2016). "Size distribution and optical properties of mineral dust aerosols transported in the western Mediterranean". In: *Atmospheric Chemistry and Physics* 16.2, pp. 1081–1104. DOI: 10.5194/acp-16-1081-2016.

Derognat, C., M. Beekmann, M. Baeumle, D. Martin, and H. Schmidt (2003). "Effect of biogenic volatile organic compound emissions on tropospheric chemistry during the Atmospheric Pollution Over the Paris Area (ESQUIF) campaign in the Ile-de-France region". In: *Journal of Geophysical Research* 108.D17, p. 8560. ISSN: 0148-0227. DOI: 10.1029/2001JD001421.

Di Biagio, C., L. Doppler, C. Gaimoz, N. Grand, G. Ancellet, J.-C. Raut, M. Beekmann, A. Borbon, K. Sartelet, J.-L. Attié, F. Ravetta, and P. Formenti (2015). "Continental pollution in the western Mediterranean basin: vertical profiles of aerosol and trace gases measured over the sea during TRAQA 2012 and SAFMED 2013". In: *Atmospheric Chemistry and Physics* 15.16, pp. 9611–9630. ISSN: 1680-7324. DOI: 10.5194/acp-15-9611-2015.

Dobrynin, M., J. Murawsky, and S. Yang (2012). "Evolution of the global wind wave climate in CMIP5 experiments". In: *Geophysical Research Letters* 39.18. ISSN: 00948276. DOI: 10.1029/2012GL052843.

Donahue, N., W. Chuang, S. Epstein, J. Kroll, D. Worsnop, A. Robinson, P. Adams, and S. Pandis (2013). "Why do organic aerosols exist? Understanding aerosol lifetimes using the two-dimensional volatility basis set". In: *Environmental Chemistry* 10.3, pp. 151–157.

Donahue, N., W. Chuang, P. Ye, S. Schobesberger, F. Bianchi, F. Riccobono, J. Dommen, U. Baltensperger, M. Kulmala, and D. R. Worsnop (2013). "Two-dimensional volatility basis set modeling of pinanediol oxidation in the CLOUD experiment". In: *AIP Conference Proceedings*. Vol. 1527. 1. AIP, pp. 334–338.

Donahue, N., S. Epstein, S. Pandis, and A. L. Robinson (2011). "A two-dimensional volatility basis set: 1. organic-aerosol mixing thermodynamics". In: *Atmospheric Chemistry and Physics* 11.7, pp. 3303–3318.

Donahue, N., J. Kroll, S. Pandis, and A. L. Robinson (2012). "A two-dimensional volatility basis set–Part 2: Diagnostics of organic-aerosol evolution". In: *Atmospheric Chemistry and Physics* 12.2, pp. 615–634.

Donahue, N., A. Robinson, C. Stanier, and S. N. Pandis (2006). "Coupled partitioning, dilution, and chemical aging of semivolatile organics". In: *Environmental Science and Technology* 40.8, pp. 2635–2643. ISSN: 0013936X. DOI: 10.1021/es052297c.

Donkelaar, A. van, R. V. Martin, M. Brauer, and B. L. Boys (2015). "Use of Satellite Observations for Long-Term Exposure Assessment of Global Concentrations of Fine Particulate Matter". In: *Environmental Health Perspectives* 123.2, pp. 135–143. ISSN: 0091-6765. DOI: 10.1289/ehp.1408646.

Drinovec, L., G. Močnik, P. Zotter, A. S. H. Prévôt, C. Ruckstuhl, E. Coz, M. Rupakheti, J. Sciare, T. Müller, A. Wiedensohler, and A. D. A. Hansen (2015). "The " dual-spot " Aethalometer: an improved measurement of aerosol black carbon with real-time loading compensation". In: *Atmos. Meas. Tech* 8, pp. 1965–1979. DOI: 10.5194/amt-8-1965-2015.

Dudhia, J. (2011). "WRF Physics Options". In: *NCAR WRF basic tutorial*, p. 129.

Dudhia, J. (2010). "Microphysics Options in WRF". In: *11th WRF Users' Workshop*.

Dufresne, J.-L., M.-A. Foujols, S. Denvil, A. Caubel, O. Marti, O. Aumont, Y. Balkanski, S. Bekki, H. Bellenger, R. Benshila, S. Bony, L. Bopp, P. Braconnot, P. Brockmann, P. Cadule, F. Cheruy, F. Codron, A. Cozic, D. Cugnet, N. de Noblet, J.-P. Duvel, C. Ethé, L. Fairhead, T. Fichefet, S. Flavoni, P. Friedlingstein, J.-Y. Grandpeix, L. Guez, E. Guilyardi, D. Hauglustaine, F. Hourdin, A. Idelkadi, J. Ghattas, S. Joussaume, M. Kageyama, G. Krinner, S. Labetoulle, A. Lahellec, M.-P. Lefebvre, F. Lefevre, C. Levy, Z. X. Li, J. Lloyd, F. Lott, G. Madec, M. Mancip, M. Marchand, S. Masson, Y. Meurdesoif, J. Mignot, I. Musat, S. Parouty, J. Polcher, C. Rio, M. Schulz, D. Swingedouw, S. Szopa, C. Talandier, P. Terray, N. Viovy, and N. Vuichard (2013). "Climate change projections using the IPSL-CM5 Earth System Model: from CMIP3 to CMIP5". In: *Climate Dynamics* 40.9-10, pp. 2123–2165. ISSN: 0930-7575. DOI: 10.1007/s00382-012-1636-1.

Edenhofer, O., R. Pichs-Madruga, and Y. Sokona (2014). *Climate Change 2014: Mitigation of Climate Change: Working Group III Contribution to the Fifth Assessment Report of the Intergovernmental Panel on*. ISBN: 9781107654815.

Edenhofer, O., I. Elgizouli, C. B. Field, M. Howden, R. K. Pachauri, L. Meyer, S. Hallegatte France, W. Bank, G. Hegerl, S. Brinkman, L. van Kesteren, N. Leprince-Ringuet, F. van Boxmeer, and K. Seyboth (2014). *IPCC*. Tech. rep.

EEA (2014). *Air pollution by ozone across Europe during the summer 2013. Technical report No 3/2014*. Tech. rep. 3. Copenhagen: European Environmental Agency, p. 32. DOI: 10.2800/77390.

Ehn, M., J. A. Thornton, E. Kleist, M. Sipilä, H. Junninen, I. Pullinen, M. Springer, F. Rubach, R. Tillmann, B. Lee, F. Lopez-Hilfiker, S. Andres, I.-H. Acir, M. Rissanen, T.

Jokinen, S. Schobesberger, J. Kangasluoma, J. Kontkanen, T. Nieminen, T. Kurtén, L. B. Nielsen, S. Jørgensen, H. G. Kjaergaard, M. Canagaratna, M. D. Maso, T. Berndt, T. Petäjä, A. Wahner, V.-M. Kerminen, M. Kulmala, D. R. Worsnop, J. Wildt, and T. F. Mentel (2014). "A large source of low-volatility secondary organic aerosol". In: *Nature* 506.7489, pp. 476–479. ISSN: 0028-0836. DOI: 10.1038/nature13032.

El Haddad, I., N. Marchand, H. Wortham, C. Piot, J.-L. Besombes, J. Cozic, C. Chauvel, A. Armengaud, D. Robin, and J.-L. Jaffrezo (2011). "Primary sources of PM_{2.5} organic aerosol in an industrial Mediterranean city, Marseille". In: *Atmospheric Chemistry and Physics* 11.5, pp. 2039–2058. ISSN: 1680-7324. DOI: 10.5194/acp-11-2039-2011.

Eliassen, A., J. Saltbones, F. Stordal, Ø. Hov, I. S. A. Isaksen, F. Stordal, A. Eliassen, J. Saltbones, F. Stordal, Ø. Hov, I. S. A. Isaksen, and F. Stordal (1982). "A Lagrangian Long-Range Transport Model with Atmospheric Boundary Layer Chemistry". In: *Journal of Applied Meteorology* 21.11, pp. 1645–1661. ISSN: 0021-8952. DOI: 10.1175/1520-0450(1982)021<1645:ALLRTM>2.0.CO;2.

Elliott, S. (2009). "Dependence of DMS global sea-air flux distribution on transfer velocity and concentration field type". In: *Journal of Geophysical Research: Biogeosciences* 114.2, pp. 1–18. DOI: 10.1029/2008JG000710.

European Environment Agency (2016). *Air quality in Europe - 2016*. Tech. rep. Copenhagen: European Environment Agency.

European Environmental Agency (2004). *Air pollution and climate change policies in Europe: exploring linkages and the added value of an integrated approach — European Environment Agency*. Tech. rep. Copenhagen: European Environmental Agency.

Evan, A. T., C. Flamant, S. Fiedler, and O. Doherty (2014). "An analysis of aeolian dust in climate models". In: *Geophysical Research Letters* 41.16, pp. 5996–6001.

Fares, S., R. Schnitzhofer, X. Jiang, A. Guenther, A. Hansel, and F. Loreto (2013). "Observations of diurnal to weekly variations of monoterpene-dominated fluxes of volatile organic compounds from mediterranean forests: implications for regional modeling." In: *Environmental science & technology* 47.19, pp. 11073–82. ISSN: 1520-5851. DOI: 10.1021/es4022156.

Fichefet, T. and M. A. M. Maqueda (1999). "Modelling the influence of snow accumulation and snow-ice formation on the seasonal cycle of the Antarctic sea-ice cover". In: *Climate Dynamics* 15.4, pp. 251–268. ISSN: 0930-7575. DOI: 10.1007/s003820050280.

Fiore, A. M., V. Naik, D. V. Spracklen, A. Steiner, N. Unger, M. Prather, D. Bergmann, P. J. Cameron-Smith, I. Cionni, W. J. Collins, S. Dalsøren, V. Eyring, G. A. Folberth, P. Ginoux, L. W. Horowitz, B. Josse, J.-F. Lamarque, I. A. MacKenzie, T. Nagashima, F. M. O'Connor, M. Righi, S. T. Rumbold, D. T. Shindell, R. B. Skeie, K. Sudo, S. Szopa, T. Takemura, and G. Zeng (2012). "Global air quality and climate". In: *Chemical Society Reviews* 41.19, p. 6663. ISSN: 0306-0012. DOI: 10.1039/c2cs35095e.

Fortems-Cheiney, A., G. Foret, G. Siour, R. Vautard, S. Szopa, G. Dufour, A. Colette, G. Lacressonniere, and M. Beekmann (2017). "A 3C global RCP8. 5 emission trajectory cancels benefits of European emission reductions on air quality". In: *Nature communications* 8.1, p. 89.

Fountoukis, C. and A. Nenes (2007). "ISORROPIA II: a computationally efficient thermodynamic equilibrium model for K –H 2 O aerosols". In: *Atmos. Chem. Phys. Atmospheric Chemistry and Physics* 7, pp. 4639–4659.

Freney, E., K. Sellegri, M. Chrit, K. Adachi, J. Brito, A. Waked, A. Borbon, A. Colomb, R. Dupuy, J.-M. Pichon, L. Bouvier, C. Delon, C. Jambert, P. Durand, T. Bourianne, C. Gaimoz, S. Triquet, A. Féron, M. Beekmann, F. Dulac, and K. Sartelet (2017). "Aerosol composition and the contribution of SOA formation over Mediterranean forests". In: *Atmospheric Chemistry and Physics Discussions*, pp. 1–25. ISSN: 1680-7375. DOI: 10.5194/acp-2017-482.

Fuch, N., A. (1964). "The Mechanics of Aerosols." In: *Science* 146.3647, pp. 1033–1034. DOI: 10.1126/science.146.3647.1033-b.

Gangoiti, G., M. M. Millán, R. Salvador, and E. Mantilla (2001). "Long-range transport and re-circulation of pollutants in the western Mediterranean during the project Regional Cycles of Air Pollution in the West-Central Mediterranean Area". In: *Atmospheric Environment* 35.36, pp. 6267–6276. ISSN: 1352-2310. DOI: 10.1016/S1352-2310(01)00440-X.

Ganor, E., H. Foner, H. Bingemer, R. Udisti, and I. Setter (2000). "Biogenic sulphate generation in the Mediterranean Sea and its contribution to the sulphate anomaly in the aerosol over Israel and the Eastern Mediterranean". In: *Atmospheric Environment* 34.20, pp. 3453–3462. ISSN: 1352-2310. DOI: 10.1016/S1352-2310(00)00077-7.

Garcia, R. R. and S. Solomon (1983). "A numerical model of the zonally averaged dynamical and chemical structure of the middle atmosphere". In: *Journal of Geophysical Research* 88.C2, p. 1379. ISSN: 0148-0227. DOI: 10.1029/JC088iC02p01379.

Garratt, J. (1994). "Review: the atmospheric boundary layer". In: *Earth-Science Reviews* 37.1-2, pp. 89–134. ISSN: 0012-8252. DOI: 10.1016/0012-8252(94)90026-4.

Gelbard, F. and J. H. Seinfeld (1980). "Simulation of multicomponent aerosol dynamics". In: *Journal of Colloid and Interface Science* 78.2, pp. 485–501. ISSN: 0021-9797. DOI: 10.1016/0021-9797(80)90587-1.

Gelencsér, A., B. May, D. Simpson, A. Sánchez-Ochoa, A. Kasper-Giebl, H. Puxbaum, A. Caseiro, C. Pio, and M. Legrand (2007). "Source apportionment of PM2.5 organic aerosol over Europe: Primary/secondary, natural/anthropogenic, and fossil/biogenic origin". In: *Journal of Geophysical Research* 112.D23, D23S04. ISSN: 0148-0227. DOI: 10.1029/2006JD008094.

Ginoux, P., J. M. Prospero, O. Torres, and M. Chin (2004). "Long-term simulation of global dust distribution with the GOCART model: correlation with North Atlantic Oscillation". In: *Environmental Modelling & Software* 19, pp. 113–128. DOI: 10.1016/S1364-8152(03)00114-2.

Giorgi, F. (2006). "Climate change hot-spots". In: *Geophysical Research Letters* 33.8, pp. 1–4. DOI: 10.1029/2006GL025734.

Goldstein, A. H. and I. E. Galbally (2007). "Known and Unexplored Organic Constituents in the Earth's Atmosphere". In: *Environmental Science & Technology* 41.5, pp. 1514–1521. ISSN: 0013-936X. DOI: 10.1021/es072476p.

Granier, C., B. Bessagnet, T. Bond, A. D'Angiola, H. Denier van der Gon, G. J. Frost, A. Heil, J. W. Kaiser, S. Kinne, Z. Klimont, S. Kloster, J.-F. Lamarque, C. Liousse, T. Masui, F. Meleux, A. Mieville, T. Ohara, J.-C. Raut, K. Riahi, M. G. Schultz, S. J. Smith, A. Thompson, J. van Aardenne, G. R. van der Werf, and D. P. van Vuuren (2011). "Evolution of anthropogenic and biomass burning emissions of air pollutants at global and regional scales during the 1980–2010 period". In: *Climatic Change* 109.1-2, pp. 163–190. ISSN: 0165-0009. DOI: 10.1007/s10584-011-0154-1.

Grantz, D., J. Garner, and D. Johnson (2003). "Ecological effects of particulate matter". In: *Environment International* 29.2-3, pp. 213–239. ISSN: 0160-4120. DOI: 10.1016/S0160-4120(02)00181-2.

Grell, G. A., S. E. Peckham, R. Schmitz, S. A. McKeen, G. Frost, W. C. Skamarock, and B. Eder (2005). "Fully coupled "online" chemistry within the WRF model". In: *Atmospheric Environment* 39.37, pp. 6957–6975. DOI: 10.1016/j.atmosenv.2005.04.027.

Grieshop, A., N. Donahue, and A. L. Robinson (2009). "Laboratory investigation of photochemical oxidation of organic aerosol from wood fires 2: analysis of aerosol mass spectrometer data". In: *Atmospheric Chemistry and Physics* 9.6, pp. 2227–2240. ISSN: 1680-7324. DOI: 10.5194/acp-9-2227-2009.

Grieshop, A., J. Logue, N. Donahue, and A. Robinson (2009). "Laboratory investigation of photochemical oxidation of organic aerosol from wood fires 1: measurement and simulation of organic aerosol evolution". In: *Atmos. Chem. Phys. Atmospheric Chemistry and Physics* 9, pp. 1263–1277.

Griffin, D. W. (2007). "Atmospheric movement of microorganisms in clouds of desert dust and implications for human health." In: *Clinical microbiology reviews* 20.3, 459–77, table of contents. ISSN: 0893-8512. DOI: 10.1128/CMR.00039-06.

Griffin, R. J., D. R. Cocker, R. C. Flagan, and J. H. Seinfeld (1999). "Organic aerosol formation from the oxidation of biogenic hydrocarbons". In: *Journal of Geophysical Research: Atmospheres* 104.D3, pp. 3555–3567. ISSN: 01480227. DOI: 10.1029/1998JD100049.

Guenther, A., T. Karl, P. Harley, C.Wiedinmyer, P. I. Palmer, and C. Geron3 (2006). "Estimates of global terrestrial isoprene emissions using MEGAN (Model of Emissions of Gases and Aerosols from Nature)". In: *Atmospheric Chemistry and Physics* 6, pp. 3181–3210. ISSN: BMC Genomics. DOI: 10.1016/j.cognition.2008.05.007. arXiv: arXiv:1011.1669v3.

Hallquist, M., J. Wenger, U. Baltensperger, Y. Rudich, D. Simpson, M. Claeys, J. Dommen, N. M. Donahue, C. George, A. H. Goldstein, J. F. Hamilton, H. Herrmann, T. Hoffmann, Y. Iinuma, M. Jang, M. E. Jenkin, J. L. Jimenez, A. Kiendler-Scharr, W. Maenhaut, G. McFiggans, T. F. Mentel, A. Monod, A. S. H. Prévôt, J. H. Seinfeld, J. D. Surratt, R. Szmigielski, and J. Wildt (2009). "The formation, properties and impact of secondary organic aerosol: current and emerging issues". In: *Atmospheric Chemistry and Physics* 9.14, pp. 5155–5236. ISSN: 1680-7324. DOI: 10.5194/acp-9-5155-2009.

Hantson, S., W. Knorr, G. Schurgers, T. A. M. Pugh, and A. Arneth (2017). "Global isoprene and monoterpene emissions under changing climate, vegetation, CO 2 and land use". In: DOI: 10.1016/j.atmosenv.2017.02.010.

Harrison, R. M. and J. Yin (2000). "Particulate matter in the atmosphere: which particle properties are important for its effects on health?" In: *The Science of the total environment* 249.1-3, pp. 85–101. ISSN: 0048-9697.

Harrison, S. P., K. E. Kohfeld, C. Roelandt, and T. Claquin (2001). "The role of dust in climate changes today, at the last glacial maximum and in the future". In: *Earth-Science Reviews* 54.1-3, pp. 43–80. ISSN: 0012-8252. DOI: 10.1016/S0012-8252(01)00041-1.

Hauglustaine, D. A., Y. Balkanski, and M. Schulz (2014). "A global model simulation of present and future nitrate aerosols and their direct radiative forcing of climate". In: *Atmospheric Chemistry and Physics* 14.20, pp. 11031–11063. ISSN: 1680-7324. DOI: 10.5194/acp-14-11031-2014.

Haylock, M. R., N. Hofstra, A. M. G. Klein Tank, E. J. Klok, P. D. Jones, and M. New (2008). "A European daily high-resolution gridded data set of surface temperature and precipitation for 1950–2006". In: *Journal of Geophysical Research* 113.D20, p. D20119. ISSN: 0148-0227. DOI: 10.1029/2008JD010201.

Heald, C. L., D. K. Henze, L. W. Horowitz, J. Feddema, J.-F. Lamarque, A. Guenther, P. G. Hess, F. Vitt, J. H. Seinfeld, A. H. Goldstein, and I. Fung (2008). "Predicted change in global secondary organic aerosol concentrations in response to future climate, emissions, and land use change". In: *Journal of Geophysical Research: Atmospheres* 113.D5, n/a–n/a. ISSN: 01480227. DOI: 10.1029/2007JD009092.

Heald, C. L., J. H. Kroll, J. L. Jimenez, K. S. Docherty, P. F. DeCarlo, A. C. Aiken, Q. Chen, S. T. Martin, D. K. Farmer, and P. Artaxo (2010). "A simplified description of the evolution of organic aerosol composition in the atmosphere". In: *Geophysical Research Letters* 37.8. ISSN: 00948276. DOI: 10.1029/2010GL042737.

Heald, C., M. Wilkinson, R. Monson, C. A. Alo, G. Wang, and A. Guenther (2009). "Response of isoprene emission to ambient CO2 changes and implications for global budgets". In: *Global Change Biology* 15.5, pp. 1127–1140.

Hedegaard, G. B., J. H. Christensen, and J. Brandt (2013). "No Title". In: 13, pp. 3569–3585.

Hedegaard, G. B., J. Brandt, J. H. Christensen, L. M. Frohn, C. Geels, K. M. Hansen, and M. Stendel (2008). "Impacts of Climate Change on Air Pollution Levels in the Northern Hemisphere with Special Focus on Europe and the Arctic". In: *Air Pollution Modeling and Its Application XIX*. Dordrecht: Springer Netherlands, pp. 568–576. DOI: 10.1007/978-1-4020-8453-9_62.

Hildebrandt, L., G. J. Engelhart, C. Mohr, E. Kostenidou, V. A. Lanz, A. Bougiatioti, P. F. Decarlo, A. S. H. Prevot, U. Baltensperger, N. Mihalopoulos, N. M. Donahue, and S. N. Pandis (2010). "Aged organic aerosol in the Eastern Mediterranean: the Finokalia Aerosol Measurement Experiment – 2008". In: *Atmos. Chem. Phys. Atmospheric Chemistry and Physics* 10, pp. 4167–4186. DOI: 10.5194/acp-10-4167-2010.

Hildebrandt, L., E. Kostenidou, N. Mihalopoulos, D. R. Worsnop, N. M. Donahue, and S. N. Pandis (2010). "Formation of highly oxygenated organic aerosol in the atmosphere: Insights from the Finokalia Aerosol Measurement Experiments". In: *Geophysical Research Letters* 37.23, pp. 6–10. ISSN: 00948276. DOI: 10.1029/2010GL045193.

Hodzic, A. and J. Jimenez (2011). "Modeling anthropogenically controlled secondary organic aerosols in a megacity: a simplified framework for global and climate models". In: *Geoscientific Model Development* 4.4, pp. 901–917. ISSN: 1991-9603. DOI: 10.5194/gmd-4-901-2011.

Hofstra, N., M. Haylock, M. New, and P. D. Jones (2009). "Testing E-OBS European high-resolution gridded data set of daily precipitation and surface temperature". In: *Journal of Geophysical Research* 114.D21, p. D21101. ISSN: 0148-0227. DOI: 10.1029/2009JD011799.

Holloway, J. L., S. Manabe, and JR. (1971). "Simulation of climate by a global general circulation model". In: *Monthly Weather Review* 99.5, pp. 335–370. ISSN: 0027-0644. DOI: 10.1175/1520-0493(1971)099<0335:SOCBAG>2.3.CO;2.

Hong, S.-Y., J. Dudhia, S.-H. Chen, S.-Y. Hong, J. Dudhia, and S.-H. Chen (2004). "A Revised Approach to Ice Microphysical Processes for the Bulk Parameterization of Clouds and Precipitation". In: *Monthly Weather Review* 132.1, pp. 103–120. ISSN: 0027-0644. DOI: 10.1175/1520-0493(2004)132<0103:ARATIM>2.0.CO;2.

Hourdin, F., I. Musat, S. Bony, P. Braconnot, F. Codron, J.-L. Dufresne, L. Fairhead, M.-A. Filiberti, P. Friedlingstein, J.-Y. Grandpeix, G. Krinner, P. LeVan, Z.-X. Li, and F. Lott (2006). "The LMDZ4 general circulation model: climate performance and sensitivity to parametrized physics with emphasis on tropical convection". In: *Climate Dynamics* 27.7-8, pp. 787–813. ISSN: 0930-7575. DOI: 10.1007/s00382-006-0158-0.

Im, U., J. Brandt, C. Geels, K. M. Hansen, J. H. Christensen, M. S. Andersen, E. Solazzo, I. Kioutsioukis, U. Alyuz, A. Balzarini, R. Baro, R. Bellasio, R. Bianconi, J. Bieser, A. Colette, G. Curci, A. Farrow, J. Flemming, A. Fraser, P. Jimenez-Guerrero, N. Kitwiroon, C.-K. Liang, U. Nopmongcol, G. Pirovano, L. Pozzoli, M. Prank, R. Rose, R. Sokhi, P. Tuccella, A. Unal, M. G. Vivanco, J. West, G. Yarwood, C. Hogrefe, and S. Galmarini (2018). "Assessment and economic valuation of air pollution impacts on human health over Europe and the United States as calculated by a multi-model ensemble in the framework of AQMEII3". In: *Atmospheric Chemistry and Physics* 18.8, pp. 5967–5989. ISSN: 1680-7324. DOI: 10.5194/acp-18-5967-2018.

Ipcc (2000). "Summary for Policymakers: Emissions Scenarios. A Special Report of Working Group III of the Intergovernmental Panel on Climate Change". In: *Group*, p. 20. ISSN: 00280836. DOI: 92-9169-113-5. arXiv: arXiv:1011.1669v3.

Israelevich, P., E. Ganor, P. Alpert, P. Kishcha, and A. Stupp (2012). "Predominant transport paths of Saharan dust over the Mediterranean Sea to Europe". In: *Journal of Geophysical Research: Atmospheres* 117.D2.

Jacob, D. J. and D. A. Winner (2009). "Effect of Climate Change on Air Quality". In: *Atmospheric Environment* 43.1, pp. 51–63. DOI: 10.1016/j.atmosenv.2008.09.051.

Jacob, D. (2017). "IMPACT2C – An introduction". In: *Climate Services* 7, pp. 1–2. ISSN: 2405-8807. DOI: 10.1016/J.CLISER.2017.07.006.

Jacob, D., J. Petersen, B. Eggert, A. Alias, O. B. Christensen, L. M. Bouwer, A. Braun, A. Colette, M. Déqué, G. Georgievski, E. Georgopoulou, A. Gobiet, L. Menut, G. Nikulin, A. Haensler, N. Hempelmann, C. Jones, K. Keuler, S. Kovats, N. Kröner, S. Kotlarski, A. Kriegsmann, E. Martin, E. van Meijgaard, C. Moseley, S. Pfeifer, S. Preuschmann,

C. Radermacher, K. Radtke, D. Rechid, M. Rounsevell, P. Samuelsson, S. Somot, J.-F. Soussana, C. Teichmann, R. Valentini, R. Vautard, B. Weber, and P. Yiou (2014). "EURO-CORDEX: new high-resolution climate change projections for European impact research". In: *Regional Environmental Change* 14.2, pp. 563–578. ISSN: 1436-3798. DOI: 10.1007/s10113-013-0499-2.

Janjic, Z. I. (2003). "A nonhydrostatic model based on a new approach". In: *Meteorology and Atmospheric Physics* 82.1-4, pp. 271–285. ISSN: 0177-7971. DOI: 10.1007/s00703-001-0587-6.

Jathar, S. H., C. D. Cappa, A. S. Wexler, J. H. Seinfeld, and M. J. Kleeman (2016). "Simulating secondary organic aerosol in a regional air quality model using the statistical oxidation model – Part 1: Assessing the influence of constrained multi-generational ageing". In: *Atmos. Chem. Phys* 16, pp. 2309–2322. DOI: 10.5194/acp-16-2309-2016.

Jimenez-Guerrero, P., J. Montávez, J. Gómez-Navarro, S. Jerez, and R. Lorente-Plazas (2012). "Impacts of climate change on ground level gas-phase pollutants and aerosols in the Iberian Peninsula for the late XXI century". In: 55, pp. 483–495.

Jimenez, J., M. Canagaratna, N. Donahue, A. S. H. Prevot, Q. Zhang, J. H. Kroll, P. F. DeCarlo, J. D. Allan, H. Coe, N. L. Ng, A. C. Aiken, K. S. Docherty, I. M. Ulbrich, A. P. Grieshop, A. L. Robinson, J. Duplissy, J. D. Smith, K. R. Wilson, V. A. Lanz, C. Hueglin, Y. L. Sun, J. Tian, A. Laaksonen, T. Raatikainen, J. Rautiainen, P. Vaattovaara, M. Ehn, M. Kulmala, J. M. Tomlinson, D. R. Collins, M. J. Cubison, E. J. Dunlea, J. A. Huffman, T. B. Onasch, M. R. Alfarra, P. I. Williams, K. Bower, Y. Kondo, J. Schneider, F. Drewnick, S. Borrmann, S. Weimer, K. Demerjian, D. Salcedo, L. Cottrell, R. Griffin, A. Takami, T. Miyoshi, S. Hatakeyama, A. Shimono, J. Y. Sun, Y. M. Zhang, K. Dzepina, J. R. Kimmel, D. Sueper, J. T. Jayne, S. C. Herndon, A. M. Trimborn, L. R. Williams, E. C. Wood, A. M. Middlebrook, C. E. Kolb, U. Baltensperger, D. R. Worsnop, and D. R. Worsnop (2009). "Evolution of organic aerosols in the atmosphere." In: *Science (New York, N.Y.)* 326.5959, pp. 1525–9. ISSN: 1095-9203. DOI: 10.1126/science.1180353.

Johansson, L., J.-P. Jalkanen, and J. Kukkonen (2017). "Global assessment of shipping emissions in 2015 on a high spatial and temporal resolution". In: *Atmospheric Environment* 167, pp. 403–415. ISSN: 1352-2310. DOI: 10.1016/J.ATMOSENV.2017.08.042.

Johnson, B. T., K. P. Shine, and P. M. Forster (2004). "The semi-direct aerosol effect: Impact of absorbing aerosols on marine stratocumulus". In: 130, pp. 1407–1422. DOI: 10.1256/qj.03.61.

Jones, B. and B. C. O'Neill (2016). "Spatially explicit global population scenarios consistent with the Shared Socioeconomic Pathways". In: *Environmental Research Letters* 11.8, p. 084003. ISSN: 1748-9326. DOI: 10.1088/1748-9326/11/8/084003.

Joseph Fourier (1827). "Mémoire sur la température du globe terrestre et des espaces planétaires". In: *Mémoires de l'Académie Royale des Sciences de l'Institute de France* 7, pp. 570–604.

Juda-Rezler, K., M. Reizer, P. Huszar, B. Krüger, P. Zanis, D. Syrakov, E. Katragkou, W. Trapp, D. Melas, H. Chervenkov, I. Tegoulias, and T. Halenka (2012). "Modelling the effects of climate change on air quality over Central and Eastern Europe: concept,

evaluation and projections". In: *Climate Research* 53.3, pp. 179–203. ISSN: 0936-577X. DOI: 10.3354/cr01072.

Kampa, M. and E. Castanas (2008). "Human health effects of air pollution". In: *Environmental Pollution* 151.2, pp. 362–367. ISSN: 0269-7491. DOI: 10.1016/J.ENVPOL.2007.06.012.

Kan, H., R. Chen, and S. Tong (2012). "Ambient air pollution, climate change, and population health in China". In: *Environment International* 42, pp. 10–19. ISSN: 0160-4120. DOI: 10.1016/J.ENVINT.2011.03.003.

Kanakidou, M., J. H. Seinfeld, S. N. Pandis, I. Barnes, F. J. Dentener, M. C. Facchini, R. Van Dingenen, B. Ervens, A. Nenes, C. J. Nielsen, E. Swietlicki, J. P. Putaud, Y. Balkanski, S. Fuzzi, J. Horth, G. K. Moortgat, R. Winterhalter, C. E. L. Myhre, K. Tsigaridis, E. Vignati, E. G. Stephanou, and J. Wilson (2005). "Organic aerosol and global climate modelling:a review". In: *Atmospheric Chemistry and Physics* 5.4, pp. 1053–1123. DOI: 10.5194/acp-5-1053-2005.

Karydis, V. A., A. P. Tsimpidi, and S. N. Pandis (2007). "Evaluation of a three-dimensional chemical transport model (PMCAMx) in the eastern United States for all four seasons". In: *Journal of Geophysical Research* 112.D14, p. D14211. ISSN: 0148-0227. DOI: 10.1029/2006JD007890.

Katragkou, E., M. García-Díez, R. Vautard, S. Sobolowski, P. Zanis, G. Alexandri, R. M. Cardoso, A. Colette, J. Fernandez, A. Gobiet, K. Goergen, T. Karacostas, S. Knist, S. Mayer, P. M. M. Soares, I. Pytharoulis, I. Tegoulias, A. Tsikerdekis, and D. Jacob (2015). "Regional climate hindcast simulations within EURO-CORDEX: evaluation of a WRF multi-physics ensemble". In: 8.3, pp. 603–618. ISSN: 1991-9603. DOI: 10.5194/gmd-8-603-2015.

Kavouras, I. G., N. Mihalopoulos, and E. G. Stephanou (1998). "Formation of atmospheric particles from organic acids produced by forests". In: *Nature* 395.6703, pp. 683–686. ISSN: 0028-0836. DOI: 10.1038/27179.

Kettle, A. and M. Andreae (2000). "Flux of dimethylsulfide from the oceans : A comparison of updated data sets and flux models". In: *Journal of Geophysical Research* 105, pp. 26, 793–26, 808. ISSN: 0148-0227. DOI: 10.1029/2000JD900252.

Kettle, A., M. Andreae, D. Amouroux, T. W. Andreae, T. S. Bates, H. Berresheim, H. Bingemer, R. Boniforti, M. A. J. Curran, G. R. DiTullio, G. Helas, G. B. Jones, M. D. Keller, R. P. Kiene, C. Leek, M. Levasseur, G. Malin, M. Maspero, P. Matrai, A. R. McTaggart, N. Mihalopoulos, B. C. Nguyen, A. Novo, J. P. Putaud, S. Rapsomanikis, G. Roberts, G. Schebeske, S. Sharma, R. Sim??, R. Staubes, S. Turner, and G. Uher (1999). "A global database of sea surface dimethylsulfide (DMS) measurements and a procedure to predict sea surface DMS as a function of latitude, longitude, and month". In: *Global Biogeochemical Cycles* 13.2, pp. 399–444. ISSN: 19449224. DOI: 10.1029/1999GB900004.

Kim, Y. (2011). "Modélisation de la qualité de l'air: Évaluation des paramétrisations chimiques et météorologiques". PhD thesis. Paris-Est.

Kim, Y., F. Couvidat, K. Sartelet, and C. Seigneur (2011). "Comparison of Different Gas-Phase Mechanisms and Aerosol Modules for Simulating Particulate Matter For-

mation". In: *Journal of the Air & Waste Management Association* 61.11, pp. 1218–1226. ISSN: 1047-3289. DOI: 10.1080/10473289.2011.603999.

Kinney, P. L. (2008). "Climate Change, Air Quality, and Human Health". In: *American Journal of Preventive Medicine* 35.5, pp. 459–467. ISSN: 07493797. DOI: 10.1016/j.amepre.2008.08.025.

Klimont, Z., S. J. Smith, and J. Cofala (2013). "The last decade of global anthropogenic sulfur dioxide: 2000–2011 emissions". In: *Environmental Research Letters* 8.1, p. 014003. ISSN: 1748-9326. DOI: 10.1088/1748-9326/8/1/014003.

Klimont, Z., K. Kupiainen, C. Heyes, P. Purohit, J. Cofala, P. Rafaj, J. Borken-Kleefeld, and W. Schöpp (2017). "Global anthropogenic emissions of particulate matter including black carbon". In: *Atmospheric Chemistry and Physics* 17.14, pp. 8681–8723. ISSN: 1680-7324.

Knutti, R. and J. Sedláček (2012). "Robustness and uncertainties in the new CMIP5 climate model projections". In: *Nature Climate Change* 3. DOI: 10.1038/NCLIMATE1716.

Koçak, M., N. Mihalopoulos, N. N. Kubilay, M. Ko??ak, N. Mihalopoulos, and N. N. Kubilay (2007). "Chemical composition of the fine and coarse fraction of aerosols in the northeastern Mediterranean". In: *Atmospheric Environment* 41.34, pp. 7351–7368. DOI: 10.1016/j.atmosenv.2007.05.011.

Konovalov, I. B., M. Beekmann, E. V. Berezin, H. Petetin, T. Mielonen, I. N. Kuznetsova, and M. O. Andreae (2015). "The role of semi-volatile organic compounds in the mesoscale evolution of biomass burning aerosol: a modeling case study of the 2010 mega-fire event in Russia". In: *Atmos. Chem. Phys* 15, pp. 13269–13297. DOI: 10.5194/acp-15-13269-2015.

Konovalov, I. B., M. Beekmann, E. V. Berezin, and H. Petetin (2014). "Top-down constraints to aerosol emissions from open biomass burning : the role of gas-particle partitioning and secondary organic aerosol formation". In: 16, pp. 9–10. DOI: 10.5194/bg-9-527-2012.

Koo, B., E. Knipping, and G. Yarwood (2014). "1.5-Dimensional volatility basis set approach for modeling organic aerosol in CAMx and CMAQ". In: *Atmospheric Environment* 95, pp. 158–164. ISSN: 1352-2310. DOI: https://doi.org/10.1016/j.atmosenv.2014.06.031.

Korontzi, S., J. McCarty, T. Loboda, S. Kumar, and C. Justice (2006). "Global distribution of agricultural fires in croplands from 3 years of Moderate Resolution Imaging Spectroradiometer (MODIS) data". In: *Global Biogeochemical Cycles* 20.2, n/a–n/a. ISSN: 08866236. DOI: 10.1029/2005GB002529.

Kotlarski, S., K. Keuler, O. B. Christensen, A. Colette, M. Déqué, A. Gobiet, K. Goergen, D. Jacob, D. Lüthi, E. Van Meijgaard, G. Nikulin, C. Schär, C. Teichmann, R. Vautard, K. Warrach-Sagi, and V. Wulfmeyer (2014). "Regional climate modeling on European scales: a joint standard evaluation of the EURO-CORDEX RCM ensemble". In: *Geosci. Model Dev* 7, pp. 1297–1333. DOI: 10.5194/gmd-7-1297-2014.

Koulouri, E., S. Saarikoski, C. Theodosi, Z. Markaki, E. Gerasopoulos, G. Kouvarakis, T. Makela, R. Hillamo, and N. Mihalopoulos (2008). "Chemical composition and sources

of fine and coarse aerosol particles in the Eastern Mediterranean". In: *Atmospheric Environment* 42.26, pp. 6542–6550. DOI: 10.1016/j.atmosenv.2008.04.010.

Krinner, G., N. Viovy, N. de Noblet-Ducoudré, J. Ogée, J. Polcher, P. Friedlingstein, P. Ciais, S. Sitch, and I. C. Prentice (2005). "A dynamic global vegetation model for studies of the coupled atmosphere-biosphere system". In: *Global Biogeochemical Cycles* 19.1. ISSN: 08866236. DOI: 10.1029/2003GB002199.

Kroll, J. H. and J. H. Seinfeld (2008). "Chemistry of secondary organic aerosol: Formation and evolution of low-volatility organics in the atmosphere". In: *Atmospheric Environment* 42.16, pp. 3593–3624. ISSN: 13522310. DOI: 10.1016/j.atmosenv.2008.01.003.

Kroll, J., N. Donahue, J. L. Jimenez, S. H. Kessler, M. R. Canagaratna, K. R. Wilson, K. E. Altieri, L. R. Mazzoleni, A. S. Wozniak, H. Bluhm, et al. (2011). "Carbon oxidation state as a metric for describing the chemistry of atmospheric organic aerosol". In: *Nature Chemistry* 3.2, p. 133.

Kuenen, J. J. P., A. J. H. Visschedijk, M. Jozwicka, and H. A. C. Denier Van Der Gon (2014). "TNO-MACC-II emission inventory; A multi-year (2003-2009) consistent high-resolution European emission inventory for air quality modelling". In: *Atmospheric Chemistry and Physics* 14.20, pp. 10963–10976. ISSN: 16807324. DOI: 10.5194/acp-14-10963-2014.

Kulmala, M., A. Laaksonen, and L. Pirjola (1998). "Parameterizations for sulfuric acid/water nucleation rates". In: *Journal of Geophysical Research: Atmospheres* 103.D7, pp. 8301–8307. ISSN: 01480227. DOI: 10.1029/97JD03718.

Kurt, O. K., J. Zhang, and K. E. Pinkerton (2012). "Pulmonary health effects of air pollution." In: *Current opinion in pulmonary medicine* 22.2, pp. 138–43. ISSN: 1531-6971. DOI: 10.1097/MCP.0000000000000248.

Lacressonnière, G., G. Foret, M. Beekmann, G. Siour, M. Engardt, M. Gauss, L. Watson, C. Andersson, A. Colette, B. Josse, V. Marécal, A. Nyiri, and R. Vautard (2016). "Impacts of regional climate change on air quality projections and associated uncertainties". In: *Climatic Change* 136.2, pp. 309–324. ISSN: 0165-0009. DOI: 10.1007/s10584-016-1619-z.

Lacressonnière, G., V.-H. Peuch, R. Vautard, J. Arteta, M. Déqué, M. Joly, and B. Josse (2014). "European air quality in the 2030s and 2050s: Impacts of global and regional emission trends and of climate change". In: *Atmospheric Environment* 92, pp. 348–358. ISSN: 1352-2310. DOI: 10.1016/J.ATMOSENV.2014.04.033.

Lacressonnière, G., L. Watson, M. Gauss, E. Magnuz, C. B. M. Andersson, C. Augustin, F. Gilles, B. Josse, V. Marécal, A. Nyiri, G. Siour, S. Sobolowski, and R. Vautard (2017). "Particulate matter air pollution in Europe in a +2 C warming world". In: *Atmospheric Environment* 154, pp. 129–140. ISSN: 1352-2310. DOI: 10.1016/J.ATMOSENV.2017.01.037.

Lana, A., T. G. Bell, R. Simó, S. M. Vallina, J. Ballabrera-Poy, A. J. Kettle, J. Dachs, L. Bopp, E. S. Saltzman, J. Stefels, J. E. Johnson, and P. S. Liss (2011). "An updated climatology of surface dimethlysulfide concentrations and emission fluxes in

the global ocean". In: *Global Biogeochemical Cycles* 25.1, pp. 1–17. ISSN: 08866236. DOI: 10.1029/2010GB003850.

Lane, T., N. Donahue, and S. N. Pandis (2008). "Effect of NOx on Secondary Organic Aerosol Concentrations". In: *Environmental Science & Technology* 42.16, pp. 6022–6027. ISSN: 0013-936X. DOI: 10.1021/es703225a.

Lane, T., N. Donahue, and S. Pandis (2008). "Simulating secondary organic aerosol formation using the volatility basis-set approach in a chemical transport model". In: *Atmospheric Environment* 42.32, pp. 7439–7451. ISSN: 13522310. DOI: 10.1016/j.atmosenv.2008.06.026.

Langner, J., M. Engardt, A. Baklanov, J. H. Christensen, M. Gauss, C. Geels, G. B. Hedegaard, R. Nuterman, D. Simpson, J. Soares, M. Sofiev, P. Wind, and A. Zakey (2012). "A multi-model study of impacts of climate change on surface ozone in Europe". In: *Atmospheric Chemistry and Physics* 12.21, pp. 10423–10440. ISSN: 1680-7324. DOI: 10.5194/acp-12-10423-2012.

Lannuque, V., F. Couvidat, M. Camredon, B. Aumont, and B. Bessagnet (2019). "Modelling organic aerosol over Europe in summer conditions with the VBS-GECKO parameterization: sensitivity to secondary organic compound properties and IVOC emissions". In: *Atmospheric Chemistry and Physics Discussions* 2019, pp. 1–40. DOI: 10.5194/acp-2018-1244.

Lannuque, V., M. Camredon, F. Couvidat, A. Hodzic, R. Valorso, S. Madronich, B. Bessagnet, and B. Aumont (2018). "Exploration of the influence of environmental conditions on secondary organic aerosol formation and organic species properties using explicit simulations: development of the VBS-GECKO parameterization". In: *Atmospheric Chemistry and Physics Discussions*, pp. 1–33. ISSN: 1680-7375. DOI: 10.5194/acp-2018-233.

Lanquar, R. (2011). *Tourism in the Mediterranean: Scenarios up to 2030*. Tech. rep.

Lanz, V. A., A. S. H. Prévôt, M. R. Alfarra, S. Weimer, C. Mohr, P. F. DeCarlo, M. F. D. Gianini, C. Hueglin, J. Schneider, O. Favez, B. D'Anna, C. George, and U. Baltensperger (2010). "Characterization of aerosol chemical composition with aerosol mass spectrometry in Central Europe: an overview". In: *Atmospheric Chemistry and Physics* 10.21, pp. 10453–10471. ISSN: 1680-7324. DOI: 10.5194/acp-10-10453-2010.

Lathière, J., D. A. Hauglustaine, N. De Noblet-Ducoudré, G. Krinner, and G. A. Folberth (2005). "Past and future changes in biogenic volatile organic compound emissions simulated with a global dynamic vegetation model". In: *Geophysical Research Letters* 32.20, p. L20818. ISSN: 0094-8276. DOI: 10.1029/2005GL024164.

Lattuati, M. (1997). "Impact des emissions europeennes sur le bilan de l'ozone troposperique a l'interface de l'europe et de l'atlantique nord : apport de la modelisation lagrangienne et des mesures en altitude". PhD thesis.

Laurent, B., B. Marticorena, G. Bergametti, P. Chazette, F. Maignan, and C. Schmechtig (2005). "Simulation of the mineral dust emission frequencies from desert areas of China and Mongolia using an aerodynamic roughness length map derived from the POLDER/ADEOS 1 surface products". In: *Journal of Geophysical Research* 110.D18, D18S04. ISSN: 0148-0227. DOI: 10.1029/2004JD005013.

LCSQA (2015). *Mise à disposition des AASQA de données de population spatialisée | LCSQA*.

Lee, E.-H. and B.-J. Sohn (2011). "Recent increasing trend in dust frequency over Mongolia and Inner Mongolia regions and its association with climate and surface condition change". In: *Atmospheric Environment* 45.27, pp. 4611–4616. ISSN: 1352-2310. DOI: 10.1016/J.ATMOSENV.2011.05.065.

Leer, B. van (1979). "Towards the ultimate conservative difference scheme. V. A second-order sequel to Godunov's method". In: *Journal of Computational Physics* 32.1, pp. 101–136. ISSN: 0021-9991. DOI: 10.1016/0021-9991(79)90145-1.

Lelieveld, J., J. Lelieveld, H. Berresheim, S. Borrmann, P. J. Crutzen, F. J. Dentener, H. Fischer, J. Feichter, P. J. Flatau, and J. Heland (2002). "Global Air Pollution Crossroads over the Mediterranean.pdf". In: 794.2002. ISSN: 00368075. DOI: 10.1126/science.1075457.

Lemaire, V. E. P., A. Colette, and L. Menut (2016). "Using statistical models to explore ensemble uncertainty in climate impact studies: the example of air pollution in Europe". In: *Atmos. Chem. Phys* 16.4, pp. 2559–2574. ISSN: 1680-7324. DOI: 10.5194/acp-16-2559-2016.

Liao, H., W.-T. Chen, and J. H. Seinfeld (2006). "Role of climate change in global predictions of future tropospheric ozone and aerosols". In: *Journal of Geophysical Research* 111.D12, p. D12304. ISSN: 0148-0227. DOI: 10.1029/2005JD006852.

Lionello, P. and F. Giorgi (2007). "Winter precipitation and cyclones in the Mediterranean region: future climate scenarios in a regional simulation". In: *Advances in Geosciences* 12, pp. 153–158. ISSN: 1680-7359. DOI: 10.5194/adgeo-12-153-2007.

Liss, P. S. and L. Merlivat (1986). "Air-Sea Gas Exchange Rates: Introduction and Synthesis". In: *The Role of Air-Sea Exchange in Geochemical Cycling*. Dordrecht: Springer Netherlands, pp. 113–127. DOI: 10.1007/978-94-009-4738-2_5.

Liu, P., A. P. Tsimpidi, Y. Hu, B. Stone, A. G. Russell, and A. Nenes (2012). "Differences between downscaling with spectral and grid nudging using WRF". In: *Atmospheric Chemistry and Physics* 12.8, pp. 3601–3610. ISSN: 1680-7324. DOI: 10.5194/acp-12-3601-2012.

Loosmore, G. A. and R. T. Cederwall (2004). "Precipitation scavenging of atmospheric aerosols for emergency response applications: testing an updated model with new real-time data". In: *Atmospheric Environment* 38.7, pp. 993–1003. ISSN: 1352-2310. DOI: 10.1016/J.ATMOSENV.2003.10.055.

Lynch, P. (2006). *The emergence of numerical weather prediction : Richardson's dream*. Cambridge University Press, p. 279. ISBN: 0521857295.

Madec, G. and P. Delecluse (1998). "OPA 8.1 Ocean General Circulation Model Reference Manual". In: *Institut Pierre Simon Laplace des sciences de l'environnement global (IPSL)*.

Mahowald, N. M., S. Kloster, S. Engelstaedter, J. K. Moore, S. Mukhopadhyay, J. R. McConnell, S. Albani, S. C. Doney, A. Bhattacharya, M. A. J. Curran, M. G. Flanner, F. M. Hoffman, D. M. Lawrence, K. Lindsay, P. A. Mayewski, J. Neff, D. Rothenberg, E. Thomas, P. E. Thornton, and C. S. Zender (2010). "Observed 20th century desert dust variability: impact on climate and biogeochemistry". In: *Atmospheric Chemistry and*

Physics 10.22, pp. 10875–10893. ISSN: 1680-7324. DOI: 10.5194/acp-10-10875-2010.

Mailler, S., L. Menut, D. Khvorostyanov, M. Valari, F. Couvidat, G. Siour, S. Turquety, R. Briant, P. Tuccella, B. Bessagnet, A. Colette, L. Létinois, K. Markakis, and F. Meleux (2017). "CHIMERE-2017: from urban to hemispheric chemistry-transport modeling". In: *Geoscientific Model Development* 10.6, pp. 2397–2423. ISSN: 1991-9603. DOI: 10.5194/gmd-10-2397-2017.

Mallet, M. et al. (2016). "Overview of the Chemistry-Aerosol Mediterranean Experiment/Aerosol Direct Radiative Forcing on the Mediterranean Climate (ChArMEx/ADRIMED) summer 2013 campaign". In: *Atmospheric Chemistry and Physics* 16.2, pp. 455–504. ISSN: 16807324. DOI: 10.5194/acp-16-455-2016.

Mallet, V., D. Quélo, B. Sportisse, M. Ahmed de Biasi, É. Debry, I. Korsakissok, L. Wu, Y. Roustan, K. Sartelet, M. Tombette, and H. Foudhil (2007). "Technical Note: The air quality modeling system Polyphemus". In: *Atmospheric Chemistry and Physics* 7.20, pp. 5479–5487. DOI: 10.5194/acp-7-5479-2007.

Manders-Groot, A., A. Segers, S. Jonkers, M. Schaap, R. Timmermans, C. Hendriks, F. Sauter, R. W. Kruit, E. van der Swaluw, H. Eskes, et al. (2016). *LOTOS-EUROS v2. 0 reference guide*. Tech. rep.

Maria, S. F., L. M. Russell, M. K. Gilles, and S. C. Myneni (2004). "Organic aerosol growth mechanisms and their climate-forcing implications". In: *Science* 306.5703, pp. 1921–1924.

Markakis, K., M. Valari, A. Colette, O. Sanchez, O. Perrussel, C. Honore, R. Vautard, Z. Klimont, and S. Rao (2014). "Air quality in the mid-21st century for the city of Paris under two climate scenarios; from the regional to local scale". In: *Atmos. Chem. Phys* 14, pp. 7323–7340. DOI: 10.5194/acp-14-7323-2014.

Marmer, E., F. Dentener, J. V. Aardenne, F. Cavalli, E. Vignati, K. Velchev, J. Hjorth, F. Boersma, G. Vinken, N. Mihalopoulos, and F. Raes (2009). "What can we learn about ship emission inventories from measurements of air pollutants over the Mediterranean Sea?" In: *Atmospheric Chemistry and Physics Discussions* 9.2, pp. 7155–7211. DOI: 10.5194/acpd-9-7155-2009.

Marticorena, B. and G. Bergametti (1995). "Modeling the atmospheric dust cycle: 1. Design of a soil-derived dust emission scheme". In: *Journal of Geophysical Research* 100.D8, p. 16415. ISSN: 0148-0227. DOI: 10.1029/95JD00690.

Martinelli, N., O. Olivieri, and D. Girelli (2013). "Air particulate matter and cardiovascular disease: A narrative review". In: *European Journal of Internal Medicine* 24.4, pp. 295–302. ISSN: 0953-6205. DOI: 10.1016/J.EJIM.2013.04.001.

Matthias, V., A. Aulinger, and M. Quante (2008). "Adapting CMAQ to investigate air pollution in North Sea coastal regions". In: *Environmental Modelling & Software* 23.3, pp. 356–368. ISSN: 1364-8152. DOI: 10.1016/J.ENVSOFT.2007.04.010.

Mauderly, J. and J. Chow (2008). "Health Effects of Organic Aerosols". In: *Inhalation Toxicology* 20.3, pp. 257–288. ISSN: 0895-8378. DOI: 10.1080/08958370701866008.

Megaritis, A. G., C. Fountoukis, P. E. Charalampidis, H. A. C. Denier Van Der Gon, C. Pilinis, and S. N. Pandis (2014). "Linking climate and air quality over Europe: effects

of meteorology on PM 2.5 concentrations". In: *Atmos. Chem. Phys* 14, pp. 10283–10298. DOI: 10.5194/acp-14-10283-2014.

Meier, H. E. M., E. Kjellström, and L. P. Graham (2006). "Estimating uncertainties of projected Baltic Sea salinity in the late 21st century". In: *Geophysical Research Letters* 33.15, p. L15705. ISSN: 0094-8276. DOI: 10.1029/2006GL026488.

Meinshausen, M., S. J. Smith, K. Calvin, J. S. Daniel, M. Kainuma, J.-F. Lamarque, K. Matsumoto, S. Montzka, S. Raper, K. Riahi, et al. (2011). "The RCP greenhouse gas concentrations and their extensions from 1765 to 2300". In: *Climatic change* 109.1-2, p. 213.

Meleux, F., F. Solmon, and F. Giorgi (2007). "Increase in summer European ozone amounts due to climate change". In: *Atmospheric Environment* 41.35, pp. 7577–7587. ISSN: 1352-2310. DOI: 10.1016/J.ATMOSENV.2007.05.048.

Memmesheimer, M., E. Friese, A. Ebel, H. Jakobs, H. Feldmann, C. Kessler, and G. Piekorz (2004). "Long-term simulations of particulate matter in Europe on different scales using sequential nesting of a regional model." In: *Int. J. of Environment and Pollution.* 22, pp. 108–132. DOI: 10.1504/IJEP.2004.005530..

Menut, L., B. Bessagnet, D. Khvorostyanov, M. Beekmann, N. Blond, A. Colette, I. Coll, G. Curci, G. Foret, A. Hodzic, S. Mailler, F. Meleux, J.-L. Monge, I. Pison, G. Siour, S. Turquety, M. Valari, R. Vautard, and M. G. Vivanco (2013). "CHIMERE 2013: a model for regional atmospheric composition modelling". In: *Geoscientific Model Development* 6.4, pp. 981–1028. ISSN: 1991-9603. DOI: 10.5194/gmd-6-981-2013.

Menut, L., G. Rea, S. Mailler, D. Khvorostyanov, and S. Turquety (2015). "Aerosol forecast over the Mediterranean area during July 2013 (ADRIMED/CHARMEX)". In: *Atmospheric Chemistry and Physics* 15.14, pp. 7897–7911. ISSN: 16807324. DOI: 10.5194/acp-15-7897-2015.

Menut, L., R. Vautard, C. Flamant, C. Abonnel, M. Beekmann, P. Chazette, P. H. Flamant, D. Gombert, D. Guédalia, D. Kley, M. P. Lefebvre, B. Lossec, D. Martin, G. Mégie, P. Perros, M. Sicard, and G. Toupance (2000). "Measurements and modelling of atmospheric pollution over the Paris area: an overview of the ESQUIF Project". In: *Annales Geophysicae* 18.11, pp. 1467–1481. ISSN: 1432-0576. DOI: 10.1007/s00585-000-1467-y.

Menut, L., C. Schmechtig, and B. Marticorena. (2005). "Sensitivity of the sandblasting flux calculations to the soil size distribution accuracy". In: *Journal of Atmospheric and Oceanic Technology* 22.12, pp. 1875–1884.

Menut, L., O. P. Tripathi, A. Colette, R. Vautard, L. Menut, E. Flaounas, O. P. Tripathi, R. Vautard, and B. Bessagnet (2012). "Evaluation of regional climate simulations for air quality modelling purposes". In: *Climate Dynamics* 40.9-10, pp. 2515–2533. ISSN: 0930-7575. DOI: 10.1007/s00382-012-1345-9.

Michoud, V., J. Sciare, S. Sauvage, S. Dusanter, T. Léonardis, V. Gros, C. Kalogridis, N. Zannoni, A. Féron, J.-E. Petit, V. Crenn, D. Baisnée, R. Sarda-Estève, N. Bonnaire, N. Marchand, H. L. DeWitt, J. Pey, A. Colomb, F. Gheusi, S. Szidat, I. Stavroulas, A. Borbon, and N. Locoge (2017). "Organic carbon at a remote site of the western Mediterranean Basin: composition, sources and chemistry during the ChArMEx SOP2

field experiment". In: *Atmospheric Chemistry and Physics Discussions*, pp. 1–63. ISSN: 1680-7375. DOI: 10.5194/acp-2016-955.

Middleton, N. (2017). "Desert dust hazards: A global review". In: *Aeolian Research* 24, pp. 53–63. ISSN: 1875-9637. DOI: 10.1016/J.AEOLIA.2016.12.001.

Mihalopoulos, N., V. M. Kerminen, M. Kanakidou, H. Berresheim, and J. Sciare (2007). "Formation of particulate sulfur species (sulfate and methanesulfonate) during summer over the Eastern Mediterranean: A modelling approach". In: *Atmospheric Environment* 41.32, pp. 6860–6871. ISSN: 13522310. DOI: 10.1016/j.atmosenv.2007.04.039.

Minguillón, M. C., N. Perron, X. Querol, S. Szidat, S. M. Fahrni, A. Alastuey, J. L. Jimenez, C. Mohr, A. M. Ortega, D. A. Day, V. A. Lanz, L. Wacker, C. Reche, M. Cusack, F. Amato, G. Kiss, A. Hoffer, S. Decesari, F. Moretti, R. Hillamo, K. Teinilä, R. Seco, J. Peñuelas, A. Metzger, S. Schallhart, M. Müller, A. Hansel, J. F. Burkhart, U. Baltensperger, and A. S. H. Prévôt (2011). "Fossil versus contemporary sources of fine elemental and organic carbonaceous particulate matter during the DAURE campaign in Northeast Spain". In: *Atmospheric Chemistry and Physics* 11.23, pp. 12067–12084. ISSN: 1680-7324. DOI: 10.5194/acp-11-12067-2011.

Mlawer, E. J., S. J. Taubman, P. D. Brown, M. J. Iacono, and S. A. Clough (1997). "Radiative transfer for inhomogeneous atmospheres: RRTM, a validated correlated-k model for the longwave". In: *Journal of Geophysical Research: Atmospheres* 102.D14, pp. 16663–16682. ISSN: 01480227. DOI: 10.1029/97JD00237.

Mohr, C., P. F. DeCarlo, M. F. Heringa, R. Chirico, J. G. Slowik, R. Richter, C. Reche, A. Alastuey, X. Querol, R. Seco, J. Peñuelas, J. L. Jiménez, M. Crippa, R. Zimmermann, U. Baltensperger, and A. S. H. Prévôt (2012). "Identification and quantification of organic aerosol from cooking and other sources in Barcelona using aerosol mass spectrometer data". In: *Atmospheric Chemistry and Physics* 12.4, pp. 1649–1665. ISSN: 1680-7324. DOI: 10.5194/acp-12-1649-2012.

Monahan, E. C. (1986). "The Ocean as a Source for Atmospheric Particles". In: *The Role of Air-Sea Exchange in Geochemical Cycling*. Dordrecht: Springer Netherlands, pp. 129–163. DOI: 10.1007/978-94-009-4738-2_6.

Monks, P. S., C. Granier, S. Fuzzi, A. Stohl, M. L. Williams, H. Akimoto, M. Amann, A. Baklanov, U. Baltensperger, I. Bey, N. Blake, R. S. Blake, K. Carslaw, O. R. Cooper, F. Dentener, D. Fowler, E. Fragkou, G. J. Frost, S. Generoso, P. Ginoux, V. Grewe, A. Guenther, H. C. Hansson, S. Henne, J. Hjorth, A. Hofzumahaus, H. Huntrieser, I. S. A. Isaksen, M. E. Jenkin, J. Kaiser, M. Kanakidou, Z. Klimont, M. Kulmala, P. Laj, M. G. Lawrence, J. D. Lee, C. Liousse, M. Maione, G. McFiggans, A. Metzger, A. Mieville, N. Moussiopoulos, J. J. Orlando, C. D. O'Dowd, P. I. Palmer, D. D. Parrish, A. Petzold, U. Platt, U. Pöschl, A. S. H. Prévôt, C. E. Reeves, S. Reimann, Y. Rudich, K. Sellegri, R. Steinbrecher, D. Simpson, H. ten Brink, J. Theloke, G. R. van der Werf, R. Vautard, V. Vestreng, C. Vlachokostas, and R. von Glasow (2009). "Atmospheric composition change - global and regional air quality". In: *Atmospheric Environment* 43.33, pp. 5268–5350. ISSN: 13522310. DOI: 10.1016/j.atmosenv.2009.08.021.

Mulitza, S., D. Heslop, D. Pittauerova, H. W. Fischer, I. Meyer, J.-B. Stuut, M. Zabel, G. Mollenhauer, J. A. Collins, H. Kuhnert, and M. Schulz (2010). "Increase in African dust flux at the onset of commercial agriculture in the Sahel region". In: *Nature* 466.7303, pp. 226–228. ISSN: 0028-0836. DOI: 10.1038/nature09213.

Murphy, B. and S. Pandis (2010). "Exploring summertime organic aerosol formation in the eastern United States using a regional-scale budget approach and ambient measurements". In: *Journal of Geophysical Research: Atmospheres* 115.D24. DOI: 10.1029/2010JD014418.

Murphy, B. and S. Pandis (2009). "Simulating the Formation of Semivolatile Primary and Secondary Organic Aerosol in a Regional Chemical Transport Model". In: *Environmental Science & Technology* 43.13, pp. 4722–4728. ISSN: 0013-936X. DOI: 10.1021/es803168a.

Murphy, B., N. Donahue, C. Fountoukis, and S. N. Pandis (2011). "Simulating the oxygen content of ambient organic aerosol with the 2D volatility basis set". In: *Atmos. Chem. Phys. Atmospheric Chemistry and Physics* 11, pp. 7859–7873. DOI: 10.5194/acp-11-7859-2011.

Murphy, B., N. Donahue, A. Robinson, and S. N. Pandis (2014). "A naming convention for atmospheric organic aerosol". In: *Atmos. Chem. Phys* 14, pp. 5825–5839. DOI: 10.5194/acp-14-5825-2014.

Nabat, P., S. Somot, M. Mallet, I. Chiapello, J. J. Morcrette, F. Solmon, S. Szopa, F. Dulac, W. Collins, S. Ghan, L. W. Horowitz, J. F. Lamarque, Y. H. Lee, V. Naik, T. Nagashima, D. Shindell, and R. Skeie (2013). "A 4-D climatology (1979–2009) of the monthly tropospheric aerosol optical depth distribution over the Mediterranean region from a comparative evaluation and blending of remote sensing and model products". In: *Atmospheric Measurement Techniques* 6.5, pp. 1287–1314. ISSN: 1867-8548. DOI: 10.5194/amt-6-1287-2013.

Nabat, P., F. Solmon, M. Mallet, J. F. Kok, and S. Somot (2012). "Atmospheric Chemistry and Physics Discussions Dust emission size distribution impact on aerosol budget and radiative forcing over the Mediterranean region: a regional climate model approach". In: *ACPD Atmos. Chem. Phys. Discuss* 12.12, pp. 17835–17886. DOI: 10.5194/acpd-12-17835-2012.

Ng, N. L., S. C. Herndon, A. Trimborn, M. R. Canagaratna, P. L. Croteau, T. B. Onasch, D. Sueper, D. R. Worsnop, Q. Zhang, Y. L. Sun, and J. T. Jayne (2011). "An Aerosol Chemical Speciation Monitor (ACSM) for Routine Monitoring of the Composition and Mass Concentrations of Ambient Aerosol". In: *Aerosol Science and Technology* 45.7. DOI: 10.1080/02786826.2011.560211.

Nicolas, J. (2013). "Caractérisation physico-chimique de l'aérosol troposphérique en Méditerranée : Sources et Devenir". In: *http://www.theses.fr*.

Nightingale, P. D., G. Malin, C. S. Law, A. J. Watson, P. S. Liss, M. I. Liddicoat, J. Boutin, and R. C. Upstill-Goddard (2000). "In situ evaluation of air-sea gas exchange parameterizations using novel conservative and volatile tracers". In: *Global Biogeochemical Cycles* 14.1, pp. 373–387. ISSN: 19449224. DOI: 10.1029/1999GB900091.

O'Neill, B. C., E. Kriegler, K. L. Ebi, E. Kemp-Benedict, K. Riahi, D. S. Rothman, B. J. van Ruijven, D. P. van Vuuren, J. Birkmann, K. Kok, M. Levy, and W. Solecki (2017). "The roads ahead: Narratives for shared socioeconomic pathways describing world futures in the 21st century". In: *Global Environmental Change* 42, pp. 169–180. ISSN: 0959-3780. DOI: https://doi.org/10.1016/j.gloenvcha.2015.01.004.

Odum, J., T. Jungkamp, R. Griffin, R. Flagan, and J. Seinfeld (1997). "The atmospheric aerosol-forming potential of whole gasoline vapor". In: *Science* 276.5309, pp. 96–99.

Owens, A. J., C. H. Hales, D. L. Filkin, C. Miller, J. M. Steed, and J. P. Jesson (1985). "A coupled one-dimensional radiative-convective, chemistry-transport model of the atmosphere: 1. Model structure and steady state perturbation calculations". In: *Journal of Geophysical Research* 90.D1, p. 2283. ISSN: 0148-0227. DOI: 10.1029/JD090iD01p02283.

Paatero, P. (1997). "Least squares formulation of robust non-negative factor analysis". In: *Chemometrics and Intelligent Laboratory Systems* 37.1, pp. 23–35. ISSN: 01697439. DOI: 10.1016/S0169-7439(96)00044-5.

Paatero, P. and U. Tapper (1994). "Positive matrix factorization: A non-negative factor model with optimal utilization of error estimates of data values". In: *Environmetrics* 5.2, pp. 111–126. ISSN: 11804009. DOI: 10.1002/env.3170050203.

Pacifico, F., G. A. Folberth, C. D. Jones, S. P. Harrison, and W. J. Collins (2012). "Sensitivity of biogenic isoprene emissions to past, present, and future environmental conditions and implications for atmospheric chemistry". In: *Journal of Geophysical Research: Atmospheres* 117.D22, n/a–n/a. ISSN: 01480227. DOI: 10.1029/2012JD018276.

Pankow, J. F. (1987). "Review and comparative analysis of the theories on partitioning between the gas and aerosol particulate phases in the atmosphere". In: *Atmospheric Environment (1967)* 21.11, pp. 2275–2283. ISSN: 00046981. DOI: 10.1016/0004-6981(87)90363-5.

Pankow, J. F. and K. C. Barsanti (2009). "The carbon number-polarity grid: A means to manage the complexity of the mix of organic compounds when modeling atmospheric organic particulate matter". In: *Atmospheric Environment* 43.17, pp. 2829–2835. DOI: 10.1016/J.ATMOSENV.2008.12.050.

Pankow, J. F. and E. I. Chang (2008). "Variation in the sensitivity of predicted levels of atmospheric organic particulate matter (OPM)". In: *Environmental science & technology* 42.19, pp. 7321–7329.

Péré, J.-C., V. Pont, M. Mallet, and B. Bessagnet (Jan. 2009). "Mapping of PM10 surface concentrations derived from satellite observations of aerosol optical thickness over South-Eastern France". In: *Atmospheric Research* 91.1, pp. 1–8. ISSN: 0169-8095. DOI: 10.1016/J.ATMOSRES.2008.05.001.

Petetin, H., M. Beekmann, J. Sciare, M. Bressi, A. Rosso, O. Sanchez, and V. Ghersi (2014). "A novel model evaluation approach focusing on local and advected contributions to urban PM2.5 levels - Application to Paris, France". In: *Geoscientific Model Development* 7.4, pp. 1483–1505. ISSN: 19919603. DOI: 10.5194/gmd-7-1483-2014.

Pey, J., X. Querol, A. Alastuey, F. Forastiere, and M. Stafoggia (2013). "African dust outbreaks over the Mediterranean Basin during 2001–2011: PM₁₀

concentrations, phenomenology and trends, and its relation with synoptic and mesoscale meteorology". In: *Atmospheric Chemistry and Physics* 13.3, pp. 1395–1410. ISSN: 1680-7324. DOI: 10.5194/acp-13-1395-2013.

Pieber, S., Y. Zhao, J. Orasche, B. Stengel, H. Czech, J. C. Corbin, I. E. Haddad, F. Klein, D. Kilic, J. G. Slowik, N. Donahue, A. Robinson, R. Zimmermann, U. Baltensperger, and A. S. H. Prévôt (2016). "Characterization of organic low-, semi-, intermediate- and volatile organic compounds from four-stroke ship engine emissions: implications for atmospheric processing". In: *EAC abstract*.

Pope, C. A. and D. W. Dockery (2006). "Health Effects of Fine Particulate Air Pollution: Lines that Connect". In: *Journal of the Air & Waste Management Association* 56.6, pp. 709–742. ISSN: 1096-2247. DOI: 10.1080/10473289.2006.10464485.

Pope, C. A., M. Ezzati, and D. W. Dockery (2009). "Fine-Particulate Air Pollution and Life Expectancy in the United States". In: *New England Journal of Medicine* 360.4, pp. 376–386. ISSN: 0028-4793. DOI: 10.1056/NEJMsa0805646.

Pöschl, U. (2005). "Atmospheric Aerosols: Composition, Transformation, Climate and Health Effects". In: *Angewandte Chemie International Edition* 44.46, pp. 7520–7540. ISSN: 1433-7851. DOI: 10.1002/anie.200501122.

Pouliot, G., T. Pierce, H. Denier van der Gon, M. Schaap, M. Moran, and U. Nopmongcol (2012). "Comparing emission inventories and model-ready emission datasets between Europe and North America for the AQMEII project". In: *Atmospheric Environment* 53, pp. 4–14. ISSN: 1352-2310. DOI: 10.1016/J.ATMOSENV.2011.12.041.

Pun, B. K. and C. Seigneur (2007). "Investigative modeling of new pathways for secondary organic aerosol formation". In: *Atmos. Chem. Phys. Atmospheric Chemistry and Physics* 7, pp. 2199–2216.

Pun, B. K., C. Seigneur, and L. Kristen (2006). "Modeling Secondary Organic Aerosol Formation via Multiphase Partitioning with Molecular Data". In: DOI: 10.1021/ES0522736.

Pun, B. K., C. Seigneur, and K. Lohman (2006). "Modeling Secondary Organic Aerosol Formation via Multiphase Partitioning with Molecular Data". In: DOI: 10.1021/ES0522736.

Pun, B. K., R. J. Griffin, C. Seigneur, and J. H. Seinfeld (2001). "Secondary organic aerosol 2. Thermodynamic model for gas/particle partitioning of molecular constituents". In: *J. Geophys. Res* 107.433310. DOI: 10.1029/2001JD000542.

Pun, B. K. and C. Seigneur (2008). "Organic aerosol spatial/temporal patterns: perspectives of measurements and model". In: *Environmental science & technology* 42.19, pp. 7287–7293.

Pun, B. K., S.-Y. Wu, C. Seigneur, J. H. Seinfeld, R. J. Griffin, and S. N. Pandis (2003). "Uncertainties in modeling secondary organic aerosols: Three-dimensional modeling studies in Nashville/Western Tennessee". In: *Environmental Science & Technology* 37.16, pp. 3647–3661.

Querol, X., a. Alastuey, J. Pey, M. Cusack, N. Pérez, N. Mihalopoulos, C. Theodosi, E. Gerasopoulos, N. Kubilay, and M. Koçak (2009). "Variability in regional background

aerosols within the Mediterranean". In: *Atmospheric Chemistry and Physics Discussions* 9.2, pp. 10153–10192. ISSN: 1680-7324. DOI: 10.5194/acpd-9-10153-2009.

Rea, G., S. Turquety, L. Menut, R. Briant, S. Mailler, and G. Siour (2015). "Source contributions to 2012 summertime aerosols in the Euro-Mediterranean region". In: *Atmospheric Chemistry and Physics* 15.14, pp. 8013–8036. ISSN: 16807324. DOI: 10.5194/acp-15-8013-2015.

Riahi, K., S. Rao, V. Krey, C. Cho, V. Chirkov, G. Fischer, G. Kindermann, N. Nakicenovic, and P. Rafaj (2011). "RCP 8.5—A scenario of comparatively high greenhouse gas emissions". In: *Climatic Change* 109.1-2, pp. 33–57. ISSN: 0165-0009. DOI: 10.1007/s10584-011-0149-y.

Riahi, K., D. P. van Vuuren, E. Kriegler, J. Edmonds, B. C. O'Neill, S. Fujimori, N. Bauer, K. Calvin, R. Dellink, O. Fricko, W. Lutz, A. Popp, J. C. Cuaresma, S. KC, M. Leimbach, L. Jiang, T. Kram, S. Rao, J. Emmerling, K. Ebi, T. Hasegawa, P. Havlik, F. Humpenöder, L. A. Da Silva, S. Smith, E. Stehfest, V. Bosetti, J. Eom, D. Gernaat, T. Masui, J. Rogelj, J. Strefler, L. Drouet, V. Krey, G. Luderer, M. Harmsen, K. Takahashi, L. Baumstark, J. C. Doelman, M. Kainuma, Z. Klimont, G. Marangoni, H. Lotze-Campen, M. Obersteiner, A. Tabeau, and M. Tavoni (2017). "The Shared Socioeconomic Pathways and their energy, land use, and greenhouse gas emissions implications: An overview". In: *Global Environmental Change* 42, pp. 153–168. ISSN: 0959-3780. DOI: https://doi.org/10.1016/j.gloenvcha.2016.05.009.

Ripoll, A., J. Pey, M. C. Minguillón, N. Pérez, M. Pandolfi, X. Querol, and A. Alastuey (2014). "Three years of aerosol mass, black carbon and particle number concentrations at Montsec (southern Pyrenees, 1570 m a.s.l.)" In: *Atmospheric Chemistry and Physics* 14.8, pp. 4279–4295. ISSN: 1680-7324. DOI: 10.5194/acp-14-4279-2014.

Robert Vautard, Matthias Beekmann, and Laurent Menut (2000). "Applications of adjoint modelling in atmospheric chemistry: sensitivity and inverse modelling". In: *Environmental Modelling & Software* 15.6-7, pp. 703–709. DOI: 10.1016/S1364-8152(00)00058-X.

Robinson, A., N. Donahue, M. K. Shrivastava, E. A. Weitkamp, A. M. Sage, A. P. Grieshop, T. E. Lane, J. R. Pierce, and S. N. Pandis (2007). "Rethinking Organic Aerosols: Semivolatile Emissions and Photochemical Aging". In: *Science* 315.5816, pp. 1259–1262. ISSN: 0036-8075. DOI: 10.1126/science.1133061.

Robinson, A., N. Donahue, and W. Rogge (2006). "Photochemical oxidation and changes in molecular composition of organic aerosol in the regional context". In: *Journal of Geophysical Research* 111.D3, p. D03302. ISSN: 0148-0227. DOI: 10.1029/2005JD006265.

Rohling, E. J. and H. L. Bryden (1992). "Man-Induced Salinity and Temperature Increases in Western Mediterranean Deep Water". In: *Journal of Geophysical Research* 97.C7, pp. 11191–11198. ISSN: 0148-0227. DOI: 10.1029/92JC00767.

Samoli, E., M. Stafoggia, S. Rodopoulou, B. Ostro, C. Declercq, E. Alessandrini, J. Díaz, A. Karanasiou, A. G. Kelessis, A. Le Tertre, P. Pandolfi, G. Randi, C. Scarinzi, S. Zauli-Sajani, K. Katsouyanni, F. Forastiere, and t. M.-P. S. MED-PARTICLES Study Group (2013). "Associations between fine and coarse particles and mortality in Mediter-

ranean cities: results from the MED-PARTICLES project." In: *Environmental health perspectives* 121.8, pp. 932–8. ISSN: 1552-9924. DOI: 10.1289/ehp.1206124.

Sartelet, K. N., F. Couvidat, C. Seigneur, and Y. Roustan (2012). "Impact of biogenic emissions on air quality over Europe and North America". In: *Atmospheric Environment* 53, pp. 131–141. ISSN: 1352-2310. DOI: 10.1016/J.ATMOSENV.2011.10.046.

Sasser, E., J. Hemby, K. Adler, S. Anenberg, C. Bailey, L. Brockman, L. Chappell, B. DeAngelo, R. Damberg, J. Dawson, N. Frank, M. Geller, G. Hagler, B. Hemming, L. Jantarasami, T. Luben, J. Mitchell, and J. Moss (2012). *Report to Congress on Black Carbon*. Tech. rep. March. U.S. Environmental Protection Agency, EPA–450/R–12–001.

Schell, B., I. J. Ackermann, H. Hass, F. S. Binkowski, and A. Ebel (2001). "Modeling the formation of secondary organic aerosol within a comprehensive air quality model system". In: *Journal of Geophysical Research: Atmospheres* 106.D22, pp. 28275–28293. ISSN: 01480227. DOI: 10.1029/2001JD000384.

Schwier, A. N., K. Sellegri, S. Mas, B. Charrière, J. Pey, C. Rose, B. Temime-Roussel, J.-L. Jaffrezo, D. Parin, D. Picard, M. Ribeiro, G. Roberts, R. Sempéré, N. Marchand, and B. D'Anna (2017). "Primary marine aerosol physical flux and chemical composition during a nutrient enrichment experiment in mesocosms in the Mediterranean Sea". In: *Atmospheric Chemistry and Physics* 17.23, pp. 14645–14660. ISSN: 1680-7324. DOI: 10.5194/acp-17-14645-2017.

Sciare, J., K. Oikonomou, H. Cachier, N. Mihalopoulos, M. O. Andreae, W. Maenhaut, and R. Sarda - Es eve (2005). "Aerosol mass closure and reconstruction of the light scattering coefficient over the Eastern Mediterranean Sea during the MINOS campaign". In: *Atmos. Chem. Phys* 5, pp. 2253–2265.

Sciare, J., K. Oikonomou, O. Favez, E. Liakakou, Z. Markaki, H. Cachier, and N. Mihalopoulos (2008). "Long-term measurements of carbonaceous aerosols in the Eastern Mediterranean: evidence of long-range transport of biomass burning". In: *Atmos. Chem. Phys. Atmospheric Chemistry and Physics* 8, pp. 5551–5563.

Seinfeld, J. and S. Pandis (2016). *Atmospheric chemistry and physics : from air pollution to climate change*, p. 1120. ISBN: 9781118947401.

Sellegri, K., J. Gourdeau, J.-P. Putaud, and S. Despiau (2001). "Chemical composition of marine aerosol in a Mediterranean coastal zone during the FETCH experiment". In: *Journal of Geophysical Research: Atmospheres* 106.D11, pp. 12023–12037. ISSN: 01480227. DOI: 10.1029/2000JD900629.

Shrivastava, M., J. Fast, R. Easter, W. I. Gustafson, R. A. Zaveri, J. L. Jimenez, P. Saide, and A. Hodzic (2011). "Modeling organic aerosols in a megacity: Comparison of simple and complex representations of the volatility basis set approach". In: *Atmospheric Chemistry and Physics* 11.13, pp. 6639–6662. ISSN: 16807316. DOI: 10.5194/acp-11-6639-2011.

Shrivastava, M., R. C. Easter, X. Liu, A. Zelenyuk, B. Singh, K. Zhang, P.-l. Ma, D. Chand, S. Ghan, J. L. Jimenez, Q. Zhang, J. Fast, P. J. Rasch, and P. Tiitta (2015). "Global transformation and fate of SOA: Implications of low-volatility SOA and gas-phase

fragmentation reactions". In: *Journal of Geophysical Research : Atmospheres* 120.9, pp. 4169–4195. ISSN: 2169897X. DOI: 10.1002/2014JD022563.Received.

Shrivastava, M., A. Zelenyuk, D. Imre, R. Easter, J. Beranek, R. A. Zaveri, and J. Fast (2013). "Implications of low volatility SOA and gas-phase fragmentation reactions on SOA loadings and their spatial and temporal evolution in the atmosphere". In: *Journal of Geophysical Research Atmospheres* 118.8, pp. 3328–3342. ISSN: 21698996. DOI: 10.1002/jgrd.50160.

Shrivastava, M., T. Lane, N. Donahue, S. Pandis, and L. Robinson (2008). "Effects of gas particle partitioning and aging of primary emissions on urban and regional organic aerosol concentrations". In: *Journal of Geophysical Research* 113.D18, p. D18301. ISSN: 0148-0227. DOI: 10.1029/2007JD009735.

Sič, B., L. El Amraoui, A. Piacentini, V. Marécal, E. Emili, D. Cariolle, M. Prather, and J.-L. Attié (2016). "Aerosol data assimilation in the chemical transport model MOCAGE during the TRAQA/ChArMEx campaign: aerosol optical depth". In: *Atmospheric Measurement Techniques* 9.11, pp. 5535–5554. ISSN: 1867-8548. DOI: 10.5194/amt-9-5535-2016.

Sicard, P., O. Lesne, N. Alexandre, A. Mangin, and R. Collomp (Feb. 2011). "Air quality trends and potential health effects – Development of an aggregate risk index". In: *Atmospheric Environment* 45.5, pp. 1145–1153. ISSN: 1352-2310. DOI: 10.1016/J.ATMOSENV.2010.12.052.

Sicard, P., A. Mangin, P. Hebel, and P. Malléa (Mar. 2010). "Detection and estimation trends linked to air quality and mortality on French Riviera over the 1990–2005 period". In: *Science of The Total Environment* 408.8, pp. 1943–1950. ISSN: 0048-9697. DOI: 10.1016/J.SCITOTENV.2010.01.024.

Simó, R. and J. Dachs (2002). "Global ocean emission of dimethylsulfide predicted from biogeophysical data". In: *Global Biogeochemical Cycles* 16.4, p. 1078. ISSN: 0886-6236. DOI: 10.1029/2001GB001829.

Solazzo, E., R. Bianconi, G. Pirovano, V. Matthias, R. Vautard, M. D. Moran, K. Wyat Appel, B. Bessagnet, J. Brandt, J. . Christensen, C. Chemel, I. Coll, J. Ferreira, R. Forkel, X. V. Francis, G. Grell, P. Grossi, A. B. Hansen, A. I. Miranda, U. Nopmongcol, M. Prank, K. N. Sartelet, M. Schaap, J. D. Silver, R. S. Sokhi, J. Vira, J. Werhahn, R. Wolke, G. Yarwood, J. Zhang, and S. Galmarini (2012). "Operational model evaluation for particulate matter in Europe and North America in the context of AQMEII". In: *Atmospheric Environment* 53, pp. 75–92. ISSN: 13522310. DOI: 10.1016/j.atmosenv.2012.02.045.

Stern, R. and R. Yamartino (2006). *Analyzing the response of a chemical transport model to emissions reductions utilizing various grid resolutions*. Tech. rep. Berlin.

Stone, E. A., C. J. Hedman, J. Zhou, M. Mieritz, and J. J. Schauer (2010). "Insights into the nature of secondary organic aerosol in Mexico City during the MILAGRO experiment 2006". In: *Atmospheric Environment* 44.3, pp. 312–319. ISSN: 1352-2310. DOI: 10.1016/J.ATMOSENV.2009.10.036.

Szopa, S., D. A. Hauglustaine, R. Vautard, and L. Menut (2006). "Future global tropospheric ozone changes and impact on European air quality". In: *Geophysical Research Letters* 33.14, p. L14805. ISSN: 0094-8276. DOI: 10.1029/2006GL025860.

Szopa, S., Y. Balkanski, M. Schulz, S. Bekki, D. Cugnet, A. Fortems-Cheiney, S. Turquety, A. Cozic, C. Déandreis, D. Hauglustaine, A. Idelkadi, J. Lathière, F. Lefevre, M. Marchand, R. Vuolo, N. Yan, and J.-L. Dufresne (2013). "Aerosol and ozone changes as forcing for climate evolution between 1850 and 2100". In: *Climate Dynamics* 40.9-10, pp. 2223–2250. ISSN: 0930-7575. DOI: 10.1007/s00382-012-1408-y.

Tai, A. P., L. Mickley, C. Heald, and S. Wu (2013). "Effect of CO ₂ inhibition on biogenic isoprene emission: Implications for air quality under 2000 to 2050 changes in climate, vegetation, and land use". In: *Geophysical Research Letters* 40.13, pp. 3479–3483. ISSN: 00948276. DOI: 10.1002/grl.50650.

Tarin-Carrasco, P., U. Im, C. Geels, L. Palacios-Pena, and P. Jimenez-Guerrero (2021). "Contribution of fine particulate matter to present and future premature mortality over Europe: A non-linear response". In: *Environment International* 153, p. 106517.

Taylor, K. E., R. J. Stouffer, G. A. Meehl, K. E. Taylor, R. J. Stouffer, and G. A. Meehl (2012). "An Overview of CMIP5 and the Experiment Design". In: *Bulletin of the American Meteorological Society* 93.4, pp. 485–498. ISSN: 0003-0007. DOI: 10.1175/BAMS-D-11-00094.1.

Tegen, I., M. Werner, S. P. Harrison, and K. E. Kohfeld (2004). "Relative importance of climate and land use in determining present and future global soil dust emission". In: *Geophysical Research Letters* 31.5. ISSN: 00948276. DOI: 10.1029/2003GL019216.

Thomson, A. M., K. V. Calvin, S. J. Smith, G. Page Kyle, A. Volke, P. Patel, S. Delgado-Arias, B. Bond-Lamberty, M. A. Wise, L. E. Clarke, and J. A. Edmonds (2011). "RCP4.5: a pathway for stabilization of radiative forcing by 2100". In: DOI: 10.1007/s10584-011-0151-4.

Thorpe, A. J., H. Volkert, and M. J. Ziemiański (2003). *The Bjerknes' circulation theorem: A historical perspective*. DOI: 10.1175/BAMS-84-4-471.

Tie, X., D. Wu, and G. Brasseur (2009). "Lung cancer mortality and exposure to atmospheric aerosol particles in Guangzhou, China". In: *Atmospheric Environment* 43.14, pp. 2375–2377. ISSN: 1352-2310. DOI: 10.1016/J.ATMOSENV.2009.01.036.

Troen, I. B. and L. Mahrt (Oct. 1986). "A simple model of the atmospheric boundary layer; sensitivity to surface evaporation". In: *Boundary-Layer Meteorology* 37.1, pp. 129–148. ISSN: 1573-1472. DOI: 10.1007/BF00122760.

Tsigaridis, K., M. Kanakidou, T. K., and M. Kanakidou (2007). "Secondary organic aerosol importance in the future atmosphere". In: *Atmospheric Environment* 41.22, pp. 4682–4692. ISSN: 1352-2310. DOI: 10.1016/J.ATMOSENV.2007.03.045.

Tsimpidi, A. P., V. A. Karydis, M. Zavala, W. Lei, L. Molina, I. M. Ulbrich, J. L. Jimenez, and S. N. Pandis (2010). "Evaluation of the volatility basis-set approach for the simulation of organic aerosol formation in the Mexico City metropolitan area". In: *Atmospheric Chemistry and Physics* 10.2, pp. 525–546. ISSN: 1680-7324. DOI: 10.5194/acp-10-525-2010.

Tsimplis, M. N. and M. Rixen (2002). "Sea level in the Mediterranean Sea: The contribution of temperature and salinity changes". In: *Geophysical Research Letters* 29.23, pp. 51–1–51–4. ISSN: 00948276. DOI: 10.1029/2002GL015870.

Tsyro, S. (2002). *First estimates of the effect of aerosol dynamics in the calculation of PM10 and PM2. 5*. Tech. rep. EMEP.

Turquety, S., L. Menut, B. Bessagnet, A. Anav, N. Viovy, F. Maignan, and M. Wooster (2014). "APIFLAME v1.0: high-resolution fire emission model and application to the Euro-Mediterranean region". In: *Geoscientific Model Development* 7.2, pp. 587–612. ISSN: 1991-9603. DOI: 10.5194/gmd-7-587-2014.

Vautard, R., C. Honoré, M. Beekmann, and L. Rouil (2005). "Simulation of ozone during the August 2003 heat wave and emission control scenarios". In: *Atmospheric Environment* 39.16, pp. 2957–2967. ISSN: 1352-2310. DOI: 10.1016/J.ATMOSENV.2005.01.039.

Vautard, R., A. Gobiet, S. Sobolowski, E. Kjellström, A. Stegehuis, P. Watkiss, T. Mendlik, O. Landgren, G. Nikulin, C. Teichmann, et al. (2014). "The European climate under a 2 C global warming". In: *Environmental Research Letters* 9.3, p. 034006.

Vestreng, V., G. Myhre, H. Fagerli, S. Reis, and L. Tarrasón (2007). "Twenty-five years of continuous sulphur dioxide emission reduction in Europe". In: *Atmospheric Chemistry and Physics* 7.13, pp. 3663–3681. ISSN: 1680-7324. DOI: 10.5194/acp-7-3663-2007.

Vincent, J., B. Laurent, R. Losno, E. Bon Nguyen, P. Roullet, S. Sauvage, S. Chevaillier, P. Coddeville, N. Ouboulmane, A. G. di Sarra, A. Tovar-Sánchez, D. Sferlazzo, A. Massanet, S. Triquet, R. Morales Baquero, M. Fornier, C. Coursier, K. Desboeufs, F. Dulac, and G. Bergametti (2016). "Variability of mineral dust deposition in the western Mediterranean basin and south-east of France". In: *Atmospheric Chemistry and Physics* 16.14, pp. 8749–8766. ISSN: 1680-7324. DOI: 10.5194/acp-16-8749-2016.

Volkamer, R., J. L. Jimenez, F. S. Martini, K. Dzepina, Q. Zhang, D. Salcedo, L. T. Molina, D. R. Worsnop, M. J. Molina, J. L. Jimenez, F. S. Martini, K. Dzepina, Q. Zhang, D. Salcedo, L. T. Molina, D. R. Worsnop, and M. J. Molina (2006). "Secondary organic aerosol formation from anthropogenic air pollution: Rapid and higher than expected". In: DOI: 10.1029/2006GL026899.

Vuuren, D. P. van, E. Stehfest, M. G. J den Elzen, T. Kram, J. van Vliet, S. Deetman, M. Isaac, K. Klein Goldewijk, A. Hof, A. Mendoza Beltran, R. Oostenrijk, and B. van Ruijven (2011). "RCP2.6: exploring the possibility to keep global mean temperature increase below 2C". In: *Climatic Change* 109, pp. 95–116. DOI: 10.1007/s10584-011-0152-3.

Vuuren, D. P. van, J. Edmonds, M. Kainuma, K. Riahi, A. Thomson, K. Hibbard, G. C. Hurtt, T. Kram, V. Krey, J.-F. Lamarque, T. Masui, M. Meinshausen, N. Nakicenovic, S. J. Smith, and S. K. Rose (2011). "The representative concentration pathways: an overview". In: *Climatic Change* 109.1-2, pp. 5–31. ISSN: 0165-0009. DOI: 10.1007/s10584-011-0148-z.

Vuuren, D. P. van, E. Stehfest, M. G. J. den Elzen, T. Kram, J. van Vliet, S. Deetman, M. Isaac, K. Klein Goldewijk, A. Hof, A. Mendoza Beltran, R. Oostenrijk, and B. van Ruijven (2011). "RCP2.6: exploring the possibility to keep global mean temperature

increase below 2C". In: *Climatic Change* 109.1-2, pp. 95–116. ISSN: 0165-0009. DOI: 10.1007/s10584-011-0152-3.

Wang, W., C. Bruyère, M. Duda, J. Dudhia, D. Gill, M. Kavulich, K. Keene, H.-C. Lin, J. Michalakes, S. Rizvi, X. Zhang, J. Berner, and K. Smith (2015). "WRF ARW Version 3 Modeling System User's Guide". In: January, pp. 1–428. DOI: 10.1525/jps.2007.37.1.204.

Werner, M., I. Tegen, S. P. Harrison, K. E. Kohfeld, I. C. Prentice, Y. Balkanski, H. Rodhe, and C. Roelandt (2002). "Seasonal and interannual variability of the mineral dust cycle under present and glacial climate conditions". In: *Journal of Geophysical Research* 107.D24, p. 4744. ISSN: 0148-0227. DOI: 10.1029/2002JD002365.

Wesely, M. (1989). "Parameterization of surface resistances to gaseous dry deposition in regional-scale numerical models". In: *Atmospheric Environment (1967)* 23.6, pp. 1293–1304. ISSN: 0004-6981. DOI: 10.1016/0004-6981(89)90153-4.

West, J. J., S. J. Smith, R. A. Silva, V. Naik, Y. Zhang, Z. Adelman, M. M. Fry, S. Anenberg, L. W. Horowitz, and J.-F. Lamarque (2013). "Co-benefits of mitigating global greenhouse gas emissions for future air quality and human health". In: *Nature Climate Change* 3.10, pp. 885–889. ISSN: 1758-678X. DOI: 10.1038/nclimate2009.

Wild, M. (2009). "Global dimming and brightening: A review". In: *Journal of Geophysical Research* 114.D10, p. D00D16. ISSN: 0148-0227. DOI: 10.1029/2008JD011470.

Wilkinson, M., R. Monson, N. Trahan, S. Lee, E. Brown, R. B. Jackson, H. W. Polley, P. A. Fay, and R. Fall (2009). "Leaf isoprene emission rate as a function of atmospheric CO2 concentration". In: *Global Change Biology* 15.5, pp. 1189–1200.

Winter, R. C. de, A. Sterl, and B. G. Ruessink (2013). "Wind extremes in the North Sea Basin under climate change: An ensemble study of 12 CMIP5 GCMs". In: *Journal of Geophysical Research: Atmospheres* 118.4, pp. 1601–1612. ISSN: 2169897X. DOI: 10.1002/jgrd.50147.

Woodward, S., D. L. Roberts, and R. A. Betts (2005). "A simulation of the effect of climate change-induced desertification on mineral dust aerosol". In: *Geophysical Research Letters* 32.18, n/a–n/a. ISSN: 00948276. DOI: 10.1029/2005GL023482.

Woolf, D. (1997). "Bubbles and their role in gas exchange." In: *The sea surface and global change*.

World health organisation (2018). *WHO*.

Yao, L. and N. Lu (2014). "Particulate Matter Pollution and Population Exposure Assessment over Mainland China in 2010 with Remote Sensing". In: *International Journal of Environmental Research and Public Health* 11.5, pp. 5241–5250. ISSN: 1660-4601. DOI: 10.3390/ijerph110505241.

Young, P. J., A. T. Archibald, K. W. Bowman, J.-F. Lamarque, V. Naik, D. S. Stevenson, and S. Tilmes (2013). "Geoscientific Instrumentation Methods and Data Systems Preindustrial to end 21st century projections of tropospheric ozone from the Atmospheric Chemistry and Climate Model Intercomparison Project (ACCMIP)". In: *Atmos. Chem. Phys* 13, pp. 2063–2090. DOI: 10.5194/acp-13-2063-2013.

Young, P. J., A. Arneth, G. Schurgers, G. Zeng, and J. A. Pyle (2009). "The CO2 inhibition of terrestrial isoprene emission significantly affects future ozone projections". In:

Atmospheric Chemistry and Physics 9.8, pp. 2793–2803. ISSN: 1680-7324. DOI: 10.5194/acp-9-2793-2009.

Zare, A., J. H. Christensen, P. Irannejad, and J. Brandt (2012). "Evaluation of two isoprene emission models for use in a long-range air pollution model". In: *Atmos. Chem. Phys. Atmospheric Chemistry and Physics* 12, pp. 7399–7412. DOI: 10.5194/acp-12-7399-2012.

Zender, C. S., H. Bian, and D. Newman (2003). "Mineral Dust Entrainment and Deposition (DEAD) model: Description and 1990s dust climatology". In: *Journal of Geophysical Research* 108.D14, p. 4416. ISSN: 0148-0227. DOI: 10.1029/2002JD002775.

Zhang, L., J. R. Brook, and R. Vet (2003). *Atmospheric Chemistry and Physics A revised parameterization for gaseous dry deposition in air-quality models*. Tech. rep.

Zhang, Q. J., M. Beekmann, F. Drewnick, F. Freutel, J. Schneider, M. Crippa, A. S. H. Prevot, U. Baltensperger, L. Poulain, A. Wiedensohler, J. Sciare, V. Gros, A. Borbon, A. Colomb, V. Michoud, J. F. Doussin, H. A. C. Denier Van Der Gon, M. Haeffelin, J. C. Dupont, G. Siour, H. Petetin, B. Bessagnet, S. N. Pandis, A. Hodzic, O. Sanchez, C. Honor??, and O. Perrussel (2013). "Formation of organic aerosol in the Paris region during the MEGAPOLI summer campaign: Evaluation of the volatility-basis-set approach within the CHIMERE model". In: *Atmospheric Chemistry and Physics* 13.11, pp. 5767–5790. ISSN: 16807324. DOI: 10.5194/acp-13-5767-2013.

Zhang, Y. L., N. Perron, V. G. Ciobanu, P. Zotter, M. C. Minguillón, L. Wacker, A. S. H. Prévôt, U. Baltensperger, and S. Szidat (2012). "On the isolation of OC and EC and the optimal strategy of radiocarbon-based source apportionment of carbonaceous aerosols". In: *Atmospheric Chemistry and Physics* 12.22, pp. 10841–10856. ISSN: 1680-7324. DOI: 10.5194/acp-12-10841-2012.

Zhao, B., S. Wang, N. Donahue, W. Chuang, L. Hildebrandt Ruiz, N. L. Ng, Y. Wang, and J. Hao (2015). "Evaluation of One-Dimensional and Two-Dimensional Volatility Basis Sets in Simulating the Aging of Secondary Organic Aerosol with Smog-Chamber Experiments". In: *Environmental Science & Technology* 49.4, pp. 2245–2254. ISSN: 0013-936X. DOI: 10.1021/es5048914.

APPENDIX

A Acronyms

Contents

1 Acronyms 251

Acronyms

aci aerosol-cloud interactions.

ari aerosol-radiation interactions.

ASOA Anthropogenic Secondary Organic Aerosol.

AVOC Anthropogenic Volatile Organic Compound.

BC Black Carbon.

BSOA Biogenic secondary Organic Aerosol.

BVOC Biogenic Volatile Organic Compound.

ChArMEx Chemistry Aerosol Mediterranean Experiment.

CLE Current Legislation Emissions.

CMIP5 Coupled Model Intercomparison Project, Phase 5.

CTM Chemistry-Transport Model.

DJF December, January, February (Winter).

DMS DiMethyl Sulfide.

EC Elemental Carbon.

ECMWF European Centre for Medium-Range Weather Forecasts.

EMEP European Monitoring and Evaluation Programme.

ERFaci Effective Radiative Forcing from aerosol-cloud interactions.

ERFari Effective Radiative Forcing from aerosol-radiation interactions.

GCM Global Circulation Model.

GLCF Global Land Cover Facility.

GOCART The Goddard Chemistry Aerosol Radiation and Transport.

HOA Hydrogen-like Organic Aerosol.

HTAP Hemispheric Transport of Air Pollution.

IPCC Intergovernmental panel to climate change.

IVOC Intermediate-Volatility Organic Compound.

JJA June, July, August (Summer).

LVOOA Low Volatility Oxygenated Organic Aerosol.

MACC Monitoring Atmospheric Composition and Climate.

MAM March, April, May (Spring).

MEGAN Model of Emissions of Gases and Aerosols from Nature.

MFR Maximum Feasible Reduction emissions.

MISTRALS Mediterranean Integrated Studies aT Regional And Local Scales.

MSA MethaneSulfonic Acid.

NCEP National Centers for Environmental Prediction.

NMVOC Non Methanic Volatile Organic Compound.

NO_x Nitrogen oxides, sum of NO and NO_2.

OA Organic Aerosol.

OM Organic Matter.

PBL Planetary Boundary Layer.

PM Particulate Matter.

PM_1 Particles with a diameter less than $1\mu m$.

PM_{10} Particles with a diameter less than $10\mu m$.

$PM_{2.5}$ Particles with a diameter less than $2.5\mu m$.

PMF Positive Matrix Factorization.

POA Primary Organic Aerosol.

PPM Primary Particulate Matter.

RCCI Regional Climate Change Index.

RCP Representative Concentration Pathways.

RCP2.6 Representative Concentration Pathway, 2100 maximum radiative forcing reached: 2.6Watt.m^{-2}.

RCP4.5 Representative Concentration Pathway, 2100 maximum radiative forcing reached: 4.5Watt.m^{-2}.

RCP8.5 Representative Concentration Pathway, 2100 maximum radiative forcing reached: 8.5Watt.m^{-2}.

rCTM regional Chemistry Transport Model.

SAFMED Secondary Aerosol Formation in the MEDiterranean.

SNAP Selected Nomenclature for Air Pollution.

SOA Secondary Organic Aerosol.

SON September, October, November (Autumn).

SOP Special Observation Period.

SSP Shared Socioeconomic Pathway.

SST Sea Surface Temperature.

SVOC Semi-Volatile Organic Compound.

SVOOA Semi Volatile Oxygenated Organic Aerosol.

VBS Volatility Basis Set.

VOC Volatile Organic Compound.

WRF Weather Research and Forecast.

APPENDIX

B Supplementary materials for articles

Contents

1 OA simulation schemes in CHIMERE article - SI **256**

2 Climate scenarios and PM concentration changes in CHIMERE article - SI **265**

1 OA simulation schemes in CHIMERE article - SI

Supplementary information

SI1

The gaseous VOC precursors for organic aerosol (OA) formation in different chemical schemes used in this work are presented in table SI-1. Species with an L after their name are lumped species, meaning that they are surrogates for a group of species; in this case, a representative compound is given in the table. Note that the precursors for both the standard VBS schemes (with and without BSOA aging) and modified VBS scheme are the same.

	CHIMERE standard		VBS (standard and modified)	
Anthropogenic	TOL	Toluene (L)	TOL	Toluene (L)
	TMB	Trimethylbenzene (L)	TMB	Trimethylbenzene (L)
	NC4H10	n-butane (L)*	NC4H10	n-butane (L)
			OLE1	C4-C13 terminal alkenes (L)
			OLE2	C4-C13 internal alkenes (L)
			ARO1	Toluene (L)
			ARO2	Xylenes (L)
			ALK4	Branched C5-C6 alkanes (L)
			ALK5	C7-C13 n-alkanes
Biogenic	APINEN	α-pinene	APINEN	α-pinene
	BPINEN	β-pinene	BPINEN	β-pinene
	LIMON	Limonene	LIMON	Limonene
	OCIMEN	Ocemene (L)	OCIMEN	Ocemene (L)
	C5H8	Isoprene	C5H8	Isoprene
	HUMULE	Humulene (L)	HUMULE	Humulene (L)

Table SI-1. Precursors for used schemes: name used in the model and the name of the species. For lumped species which are signified with an L after their model name, an example of species lumped in that group is given.

*: only higher weight alkanes which are included in the lumped nCH_4H_{10} species form organic aerosol.

SI2

A simplified diagram of OA formation schemes from VOCs was presented in the main article; here, the same type of diagrams are shown for OA formation from semi-volatile primary OA for the VBS standard scheme and modified VBS scheme.

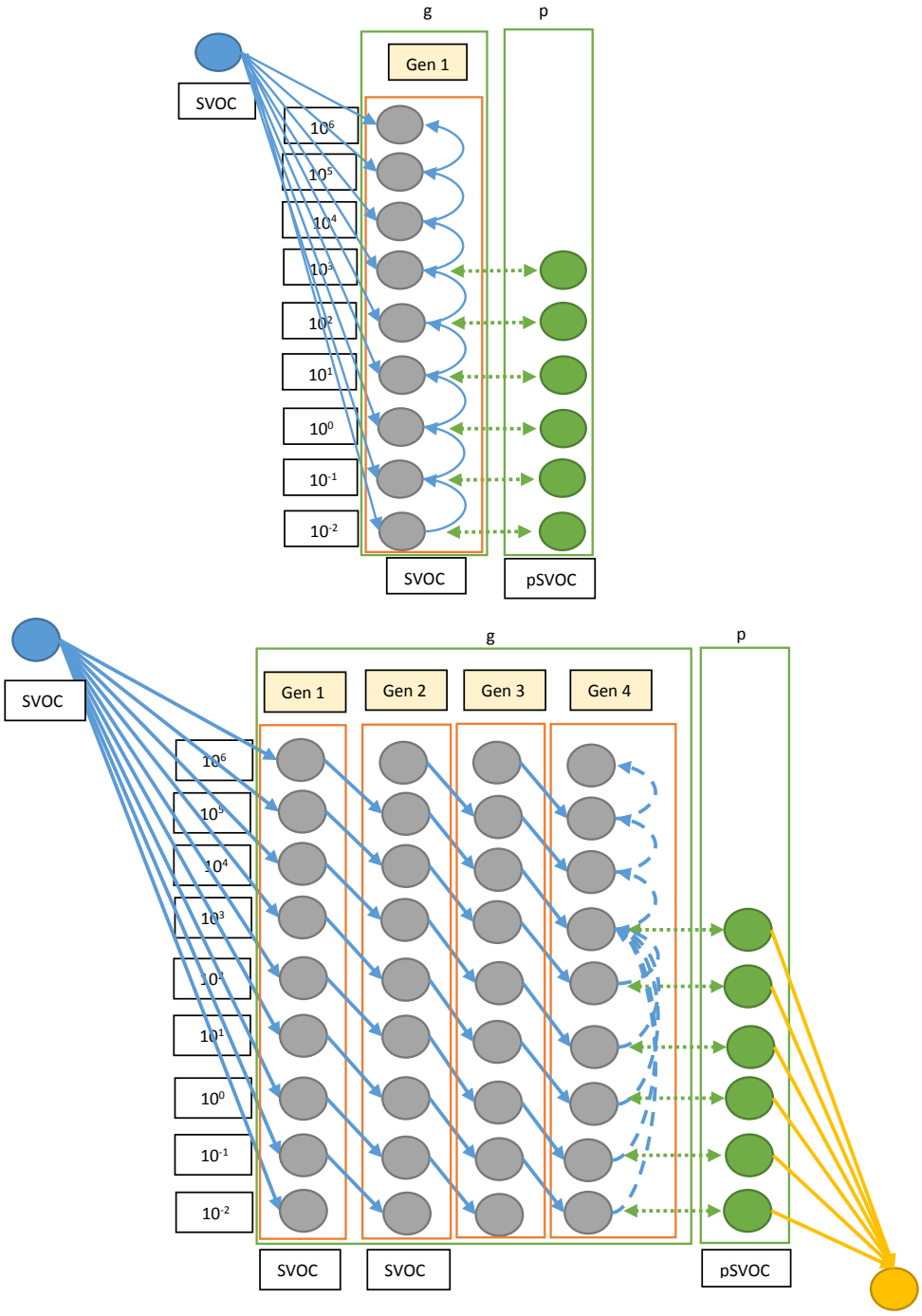


Figure SI-1. Schematic of oxidation of POAs in the Standard VBS scheme (upper panel) and modified VBS scheme (lower panel). POA and IVOC (intermediate volatility organic carbon) emissions are distributed into 9 SVOC/IVOC bins of saturation concentration ranging from 10^{-2} to 10^{6} µg.m^{-3}. In the standard VBS scheme (a), they undergo functionalization transferring species to classes with lower volatility. SVOC species are in equilibrium between the gas and condensed phase (SI-SOA); in the modified VBS scheme (b), the number of functionalization steps is accounted for (GEN). Highly functionalized SVOC's (starting from fourth generation) can undergo fragmentation, leading to transfer of species to classes with higher volatility. In addition, semi-volatile aerosol can be irreversibly transformed into non-volatile one (yellow-filled circle).

SI3

In the procedure to estimate a representativeness error described in section 4-1 of the article, a panel of 9 equations including 2 – 4 open parameters was tested for the non-linear regressions of simulated species concentration versus model altitude. Estimated species concentrations were required to be positive.

$$Eq\ 1.\ y = d + \frac{a-d}{1+\left(\frac{x}{c}\right)^b}, \qquad Eq\ 2.\ y = \left(d + \frac{a-d}{1+\left(\frac{x}{c}\right)^b}\right)^m, \qquad Eq\ 3.\ y = a \times \left(1 - e^{\frac{-x}{b}}\right) + c,$$

$$Eq\ 4.\ y = a \times \left(1 - e^{\frac{-x}{b}}\right) + \log c\ , \qquad Eq\ 5.\ y = a \times \left(1 - e^{\frac{-x}{b}}\right) + |c|\ ,$$

$$Eq\ 6.\ y = |a| \times \left(1 - e^{\frac{-x}{b}}\right) + |c|\ , \qquad Eq\ 7.\ y = a \times x^b + c\ , \qquad Eq\ 8.\ y = a \times x^b\ ,$$

$$Eq\ 9.\ y = a + b \times x + c \times x^2 + d \times x^3$$

The results for several equations were not used since the number of hourly time-steps for which convergence was not achieved were too frequent (more than 40% of all time-steps), and thus the results have been judged as not representative. Finally, the results for five equations were retained (eq. 1, 3, 5, 7 and 8).

For each of the five equations, regressions for all time steps were calculated. The results for each equation for different simulation times were filtered, by two factors: first convergence for a given simulation time step; second correlation coefficient of higher than 50% between the fitted data and the original points. If these two criteria were met, the results were retained. Then the results for all equations were put together and means, lower and upper confidence intervals calculated (intervals were calculated by using the maximum and minimum values seen for different equations, and the mean presents the average of all equations). Only simulation times with at least two converged equations were used in the calculation of orographic representativeness error.

SI4

Meteorological output of the mesoscale WRF model at different resolutions has been used as input to the CHIMERE CTM. The meteorological data used by CHIMERE was compared to various meteorological observations such as radiosoundings and surface observations at the measurement sites. Detailed results of these comparisons are given in this supplementary material (SI4), in addition to the short overview given in the main article.

First, we present here a comparison of simulations with observations from the European gridded dataset of daily meteorological data (E-Obs; Haylock et al., 2008; Hofstra et al., 2009) for all available stations in the European D10 domain. In addition, individual stations where data was available (EMEP stations in Europe, ChArMEx stations of Ersa and Es Pinar, QualitairCorse stations in Corsica) were also used for meteorological comparisons; among them, Ersa, France, Es Pinar, Spain, Corsica Isl., France (42°14'09.6", 9°10'46.1") stations are presented in this study since they are closest to sites where measurements for pollutants were done.

All available stations from E-Obs were compared to model results starting from the D10 domain. In the two smaller domains (D3 and D1) no station is available. In D10, statistical results of the comparisons as well as the number of stations for each parameter are shown in table SI-2. Note that the E-OBS stations were not filtered with respect their orographic caracteristics, which might not well be taken into account by the model. The correlation between simulations and observations for average daily temperature and the daily maximum of temperature is high (0.82 with a +2.1°C bias), while it is lower for the daily minima is underestimated (correlation of 0.55 with a -3.3°C bias) in the model. Note that the model quite overestimates the daily dynamics of temperature by more than 5°C. The correlation for relative humidity is also acceptable, since this parameter is also very sensitive to altitude changes. The other parameters (wind speed, WS; wind direction, WD; and precipitation, P) are not very well correlated (r <0.5).

For the E-OBS network (Datasets provided by European Climate Assessment & Dataset project for monitoring and analyzing climate extremes, Haylock et al., 2008; Hofstra et al., 2009) comparisons also show a good correlation and a low bias for temperature (correlation of 0.79 with a bias of -0.54°C for mean temperature observed for 71 stations in D10), while the daily minima seems to be underestimated (bias of -3°C for daily minima observed for 71 stations).

	D10				
	stations	R	RMSE	Bias	Mean_obs
T_{max} (°C)	71	0.82	3.39	2.18	29.51
T_{min} (°C)	71	0.48	3.64	-3.17	17.14
T_{mean} (°C)	62	0.79	1.71	-0.54	22.85
RH (%)	59	0.63	11.15	4.7	64.13
WS ($m.s^{-1}$)	59	0.50	1.34	-0.91	2.39
WD(deg)	58	0.30	72.29	0.95	184.7
P ($mm.d^{-1}$)	71	0.35	4.86	1.83	1.88

Table SI-2. Statistical data for E-OBS dataset compared to D10 simulations over the 1-month simulation period from 10 July to 8 August 2013. Mean_obs shows the average of observations in all stations.

An example of radiosounding comparisons for the balloons launched on the afternoon of 25 july 2013 is shown in figure SI-2. The red line shows the observations while the blue one shows the simulations. A good correlation is seen for this day for all three stations for all parameters. Only the Ajaccio station is located in a smaller domain (D3): for the balloon of 25 July, a correlation of 0.99, 0.98 and 0.91 and a bias of -2, -18 and -9% is seen for temperature, wind speed and relative humidity respectively.

The radiosounding measurements stations have been listed in table 2. In figure SI-2, an example of model-observation comparisons is shown for D10, for all the three stations and for the three parameters, temperature, relative humidity and wind speed for the balloons of the afternoon radiosounding of 25 July 2013. There is an excellent correlation with respect to altitude and an acceptable bias (a minimum correlation of 0.8 and a maximum bias of less than -20%) for the compared parameters for all stations in this example. In figure SI-3, vertical profiles of the same variables are shown. In addition, for each vertical level of simulations, two boxplots show the whole variability of the measurements (in red) and simulations (in blue, for Ajaccio D10 in dark blue and D3 in light blue). The small white dot on the boxes shows the average for each level. The altitudes correspond to the average altitude represented in each vertical level. For temperature, bias at different sites and altitude levels is in general small, being on average -1.16, -0.61 and -0.39°C over the different altitudes for Palma, Nimes and Ajaccio respectively. Correlation is on average 0.65, 0.80 and 0.80, for Palma, Nimes and Ajaccio respectively. Looking at the box plots for each altitude, there is not much variation in the values seen in each level neither in the model nor in observations.

In figure SI-3, vertical profiles of the same variables are shown, but for a total of 32 balloon launches at each site in the period of 10 july to 30 july (32 ballons for each site when data was available for all three sites). In addition, for each vertical level of simulations, two boxplots show the variability of the 32 measurements (in red) and corresponding simulations (in blue, for Ajaccio D10 in dark blue and D3 in light blue). The small white dot on the boxes shows the average for each level. The altitudes correspond to the average altitude represented in each vertical level. For temperature, bias at different sites and altitude levels is in general small, being on average -1.16, -0.61 and -0.39°C over the different altitudes for Palma, Nimes and Ajaccio respectively. Correlation (with respect to sounding time), is on average 0.65, 0.80 and 0.80, for Palma, Nimes and Ajaccio respectively. Looking at the box plots for each altitude, there is not much variation in the values seen in each level neither in the model nor in observations.

For wind speed, the correlation coefficients become better in many cases at higher levels, where the variability is also larger . General bias of 0.44%, -0.83% and -1.19% is seen for a general correlation of 0.55, 0.65 and 0.56 in Palma, Nimes and Ajaccio respectively. This bias drops to 5%, 0.2% and -7% if only altitudes above 3000 m are considered, thus lower layers are more biased. A reasonable explanation for the strong general bias observed at the Ajaccio station may be because of incorrect sea/land breezes representation in the model, however this cannot explain the bias for Nimes, since it is not close enough to the sea. Model errors in wind speed might directly affect advection to the measurement sites.

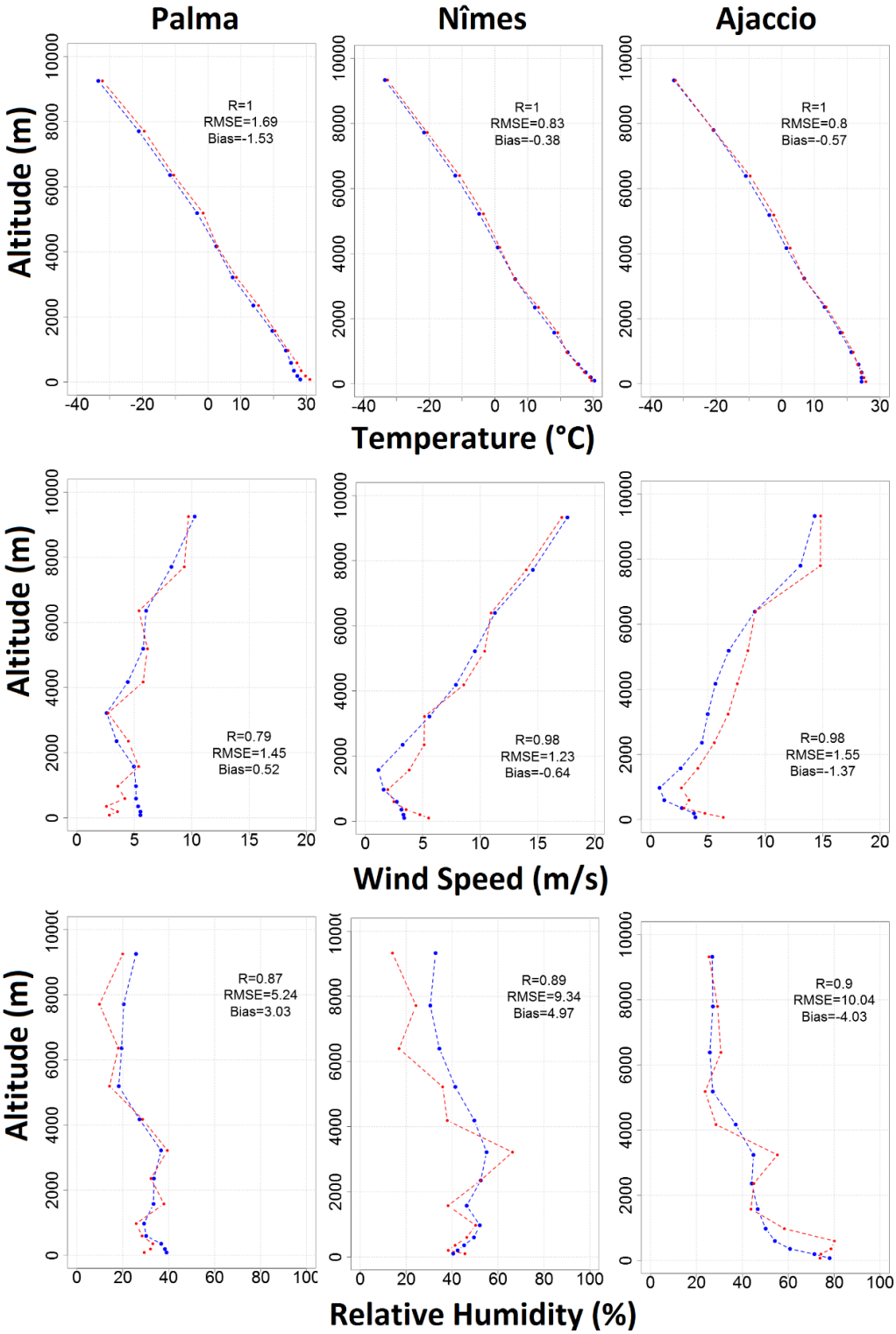


Figure SI-2. Comparison of radio sounding measurements for balloon soundings on the noon of 25 July. In each panel, the blue line shows the simulations and the red line shows the observations, points on each line show the vertical levels in CHIMERE.

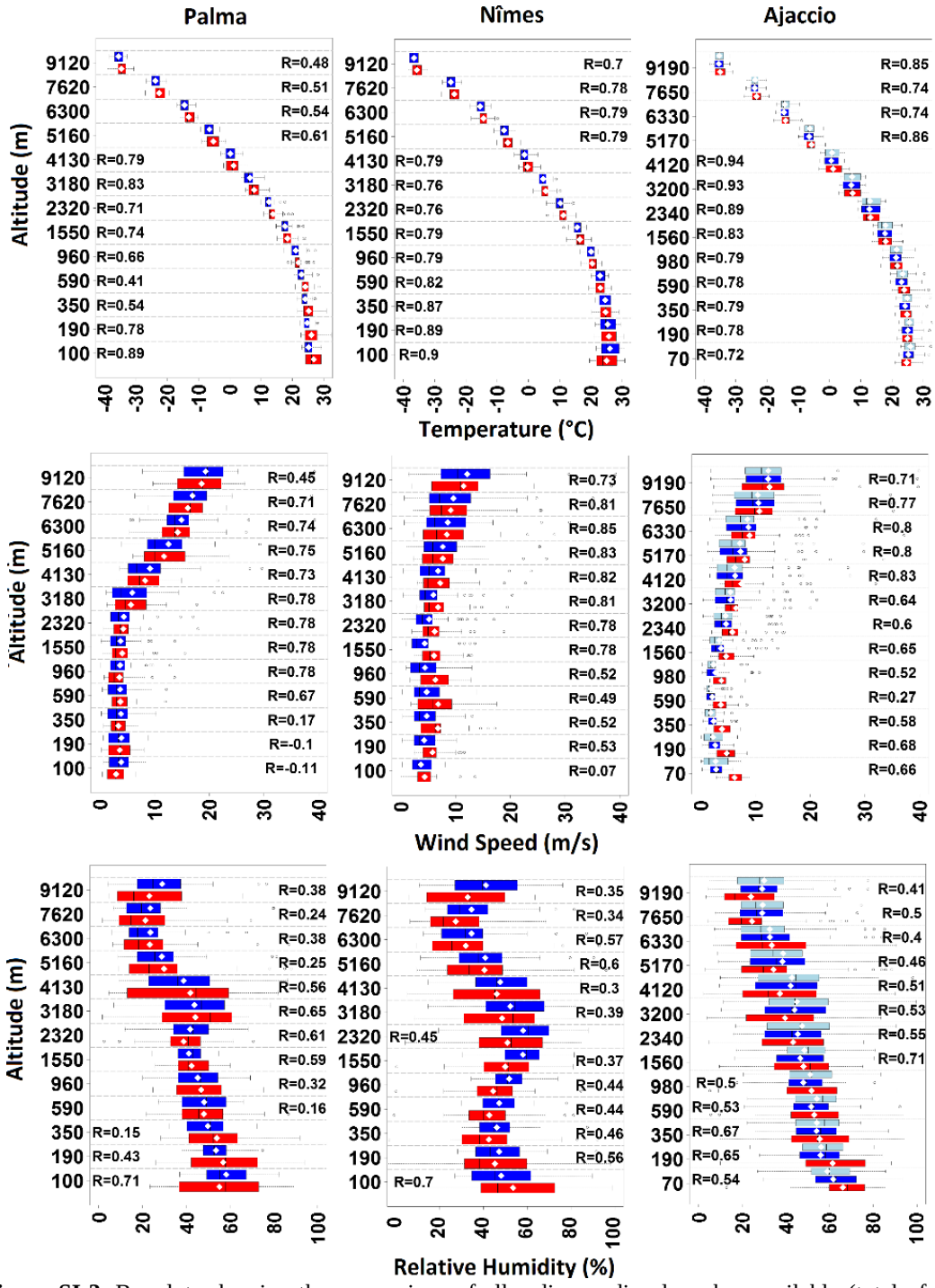


Figure SI-3. Boxplots showing the comparison of all radiosounding launches available (total of 32 balloons for each site) in the period of 10 to 30 july. Each row of figure represents a parameter, each column a station. The Y axis shows the altitude and the X axis shows temperature (°C), wind speed ($m.s^{-1}$) and relative humidity (%). The blue box shows the simulations and the red box the observations. If possible, both D10 (dark blue) and D3 (light blue) simulations are displayed, else only the D10 one. On each box the white dot shows the average over 32 soundings, the bars the variability (minimum and maximum with outliers shown with dots). R values represent the correlation coefficient between measurements and observation for each level.

For relative humidity, there is no apparent relation between the correlation and the vertical levels. For this parameter, general correlation of 0.42, 0.46 and 0.45 is seen at Palma, Nimes and Ajaccio respectively, for a general relative bias of -0.1%, 9% and -0.4%. Contrary to wind speed, the bias becomes stronger at altitudes higher than 3000m (2%, 10% and 11% respectively).

Available comparisons of meteorological parameters at the two supersites for chemical measurements are presented in table 4 (for the three domains D10, D3, and D1 at Ersa and for D10 at Es Pinar). In general, the results for these comparisons become more accurate when the domain has a higher resolution (Table 4). Figure 5 shows the simulation-observation comparisons for these two stations for four parameters including temperature (T), relative humidity (RH), wind speed (WS) and wind direction (WD). For Ersa, the correlation and the bias become better for domains with higher resolution. As illustrated in figure 5, the comparison for temperature and relative humidity (figures 5-a1 5-b1) for this station show excellent results for the D1 domain. For wind speed (figure 5-c1), while longer-lasting synoptic scale events such as the strong wind conditions between 22 to 26 July and also 28 to 30 July are well-represented by the model, some short term variability (lasting one or several hours) is disregarded. It is interesting to notice that in both of these two strong wind periods, the wind direction shows little variation which is also seen by the model. For Es Pinar, the comparisons are less satisfying. An overestimation in the simulation of daily minima of the temperature is seen for this station, which could be explained by the fact that this is a coastal station and the corresponding cell in the simulations is half covered by land and half by sea. The slight overestimation in relative humidity daily maxima could also be attributed to this reason. Wind speed is overestimated in the simulations, here probably again due to local features not depicted by the 10-km resolved fields are determining.

		Ersa				Es Pinar			
		R	RMSE	Bias	Mean_obs	R	RMSE	Bias	Mean_obs
D10	T (°C)	0.79	2.30	1.48	23.17	0.55	2.72	-2.01	28.49
	RH (%)	0.48	17.29	3.91	70.22	0.48	10.24	-1.03	70.10
	WS (m/s)	0.60	1.88	-0.39	3.71	0.60	2.27	1.97	1.13
	WD (°)	0.13	117.5	46.9	194.2	0.13	124.1	-35.8	165.6
D3	T (°C)	0.81	2.52	1.99	23.17				
	RH (%)	0.48	17.59	-4.56	70.22				
	WS (m/s)	0.69	1.63	0.05	3.71				
	WD (°)	0.27	101.3	36.10	194.2				
D1	T (°C)	0.86	1.54	0.70	23.17				
	RH (%)	0.54	16.51	-1.67	70.22				
	WS (m/s)	0.66	1.90	0.61	3.71				
	WD (°)	0.37	92.0	25.0	194.2				

Table SI-3. Comparison of hourly meteorological parameters at the two ChArMEx supersites of Ersa and Es Pinar from 10 July to 5 August, 2013. R is the correlation coefficient, RMSE, the root mean square error and Mean_obs the average of observations.

The model succeeds in catching the different regimes and the general changes of the wind speed while overestimating its intensity. This fact is also seen in wind rose diagrams shown in figures SI-4-d1 and SI-4-d2. The prevalent wind direction is correctly simulated in both sites, however, wind directions with less occurrences are sometimes not seen by the model.

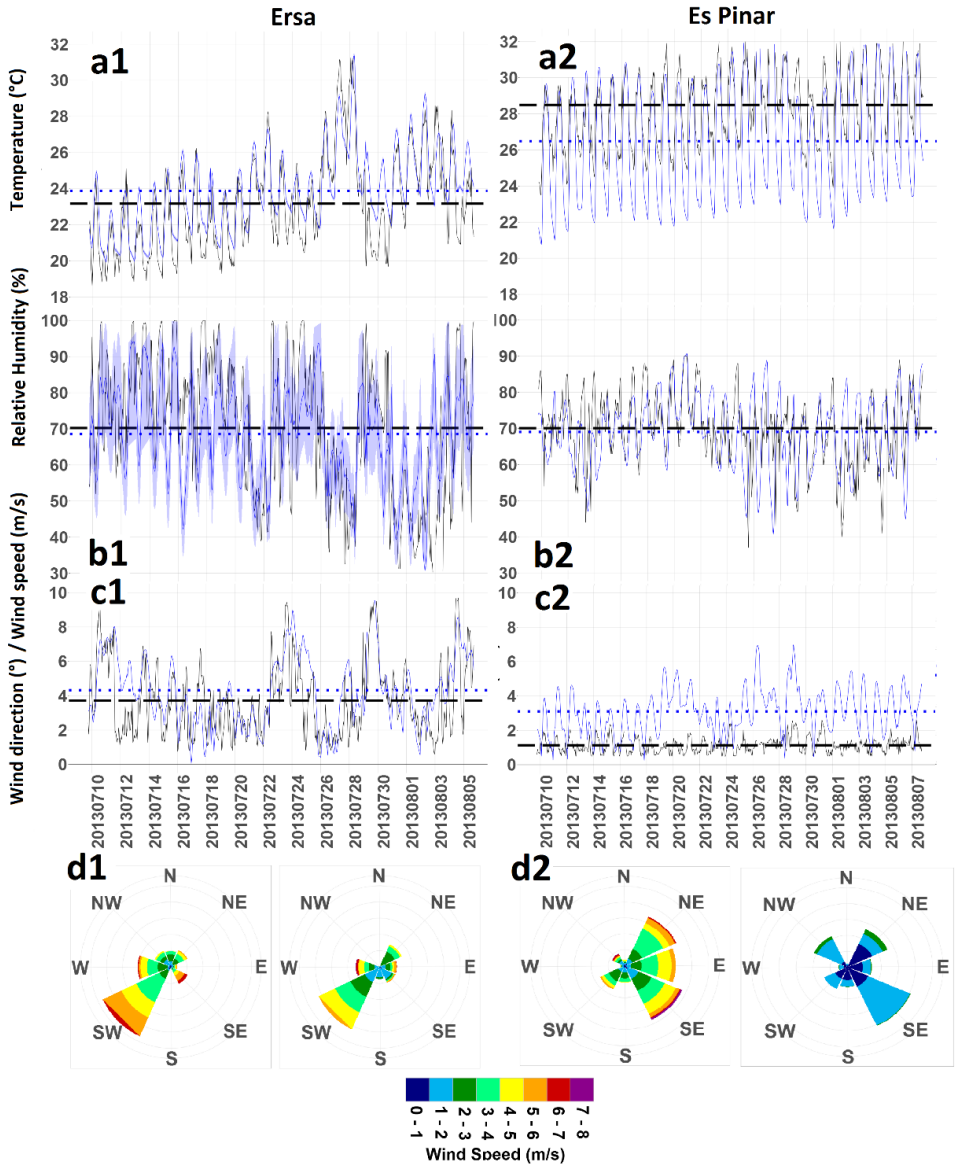


Figure SI-4. Comparison of observed and simulated coincident meteorological parameters for at Ersa (left) and Es Pinar (right) stations. For Ersa D1 simulations and for Es Pinar D10 simulations are shown. In plots a to c, simulations are in blue and observations in black. For relative humidity at Ersa, the envelope corresponding to the spatial representativeness is given. In figures d1 and d2, simulations are shown at the left side, and observations on the right.

2 Climate scenarios and PM concentration changes in CHIMERE article - SI

Supplementary Information

SI1: Comparison of historic simulations to EEA stations for certain species

Since we are using historic simulations and not hindcast simulations as the reference for our future scenarios, they are not directly comparable to measurements, since they are prepared with climatological meteorological inputs and not reanalyzed meteorological inputs. Also, the emissions in our simulations don't change and are always ECLIPSE CLE 2010 emissions, which could also produce discrepancies. Therefore, a yearlong profile was prepared from an average of historic simulations between the years 1996 and 2005. Another annual profile was prepared with all available EEA e-reporting stations for key species for the period of 2005-2015. These two profiles were compared in annual and monthly comparisons, the results for which are provided in figures SI1 fig.1 and SI1 fig.2 for O_3, NO_2, PM_{10} and $PM_{2.5}$. The results shown below were filtered to only include rural and remute stations. Table SI1 shows statistic information for these comparisons.

	Mean_S	Mean_M	% Bias	Sd_S	Sd_M	R
O3	65.4	61.9	5.9	20.6	12.2	0.69
NO2	6.9	11.3	-38.9	7.8	4.3	0.55
PM2.5	9.5	11.9	-20.7	8.2	3.9	0.49
PM10	12.5	18.9	-33.5	7.2	4.6	0.34

Table SI1 1. Statistical parameters for the comparisons performed using EEA stations and our historic simulations. A monthly profile of EEA data covering the period of 2006 to 2015 is compared to a monthly profile of historic simulations covering the period of 1996 to 2005. Mean_S and Mean_M show simulation and measurement averages respectively, Sd_S and SD_M show the standard deviation of simulations and measurements respectively.

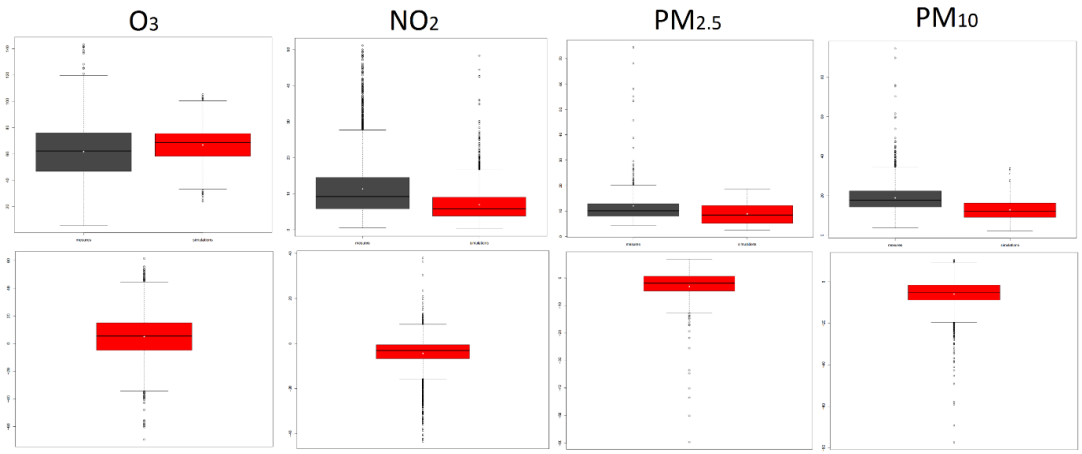


Figure SI1 1. Comparison of the same data introduced in table 1 to historic simulations. First row shows the average of the comparisons in black for measurements and in red for historic simulations. Second row shows the boxplot for the biases between the two.

SI 2: 2D temperature images for different seasons

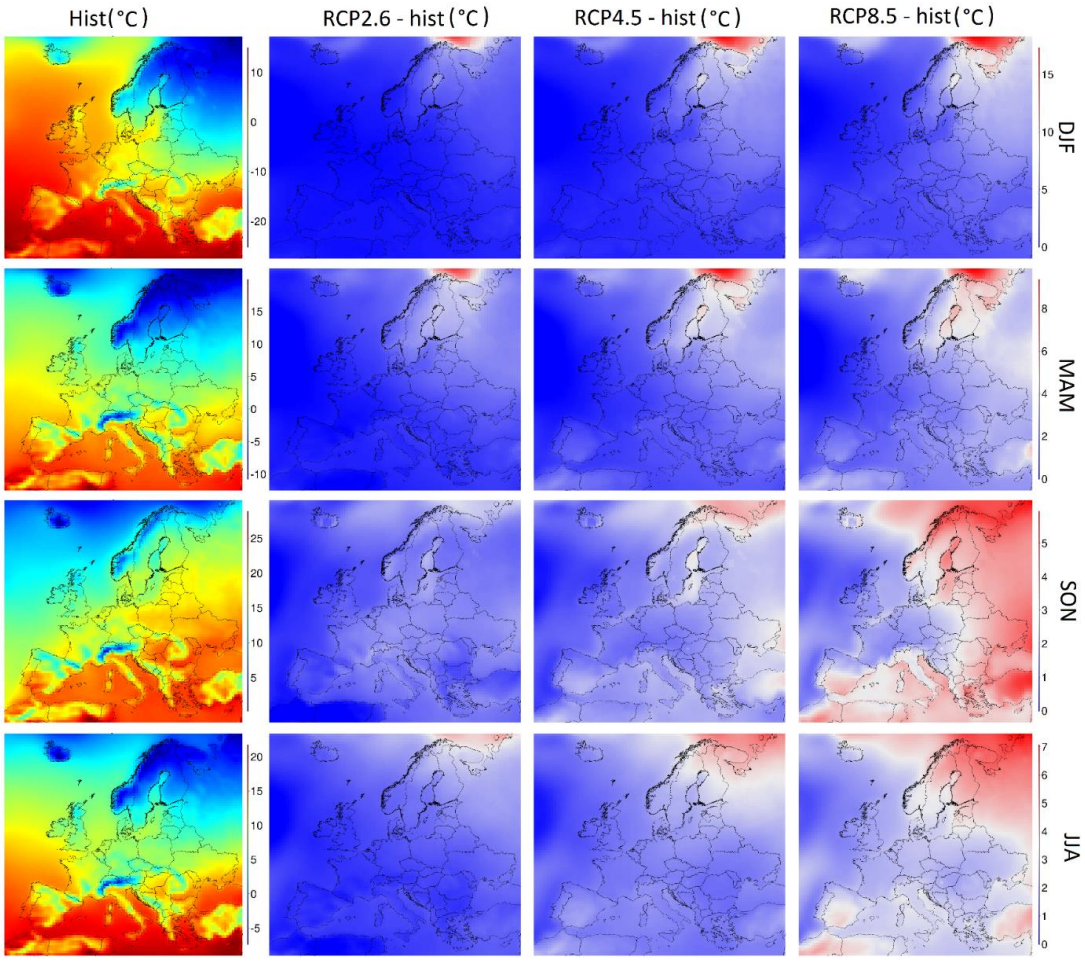


Figure SI2 1. Seasonal temperature maps for historic simulations (in °C, first column from the left), and the difference between RCP2.6, RCP4.5 and RCP8.5 (in °C, second to fourth columns from the left). Each row shows one season, from the top DJF, MAM, SON and JJA respectively.

SI 3: Meteorological parameters for different scenarios for MEDW and MEDE sub-domains

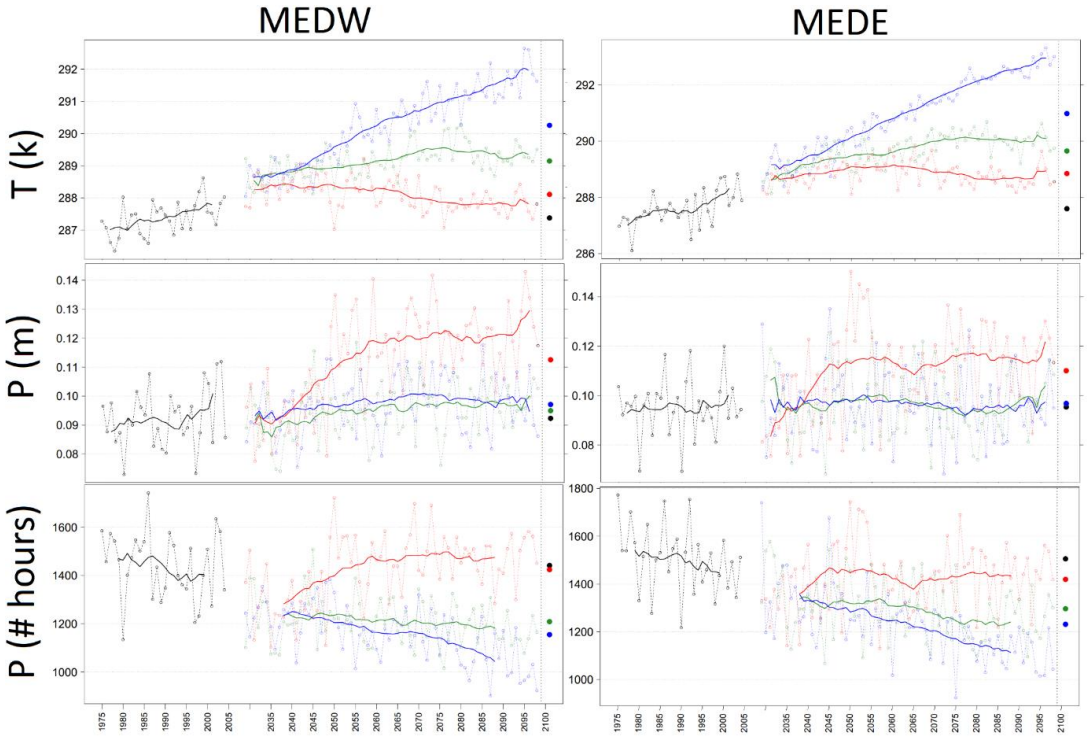


Figure SI3 1. Same as figure 2, but for MEDE and MEDW.

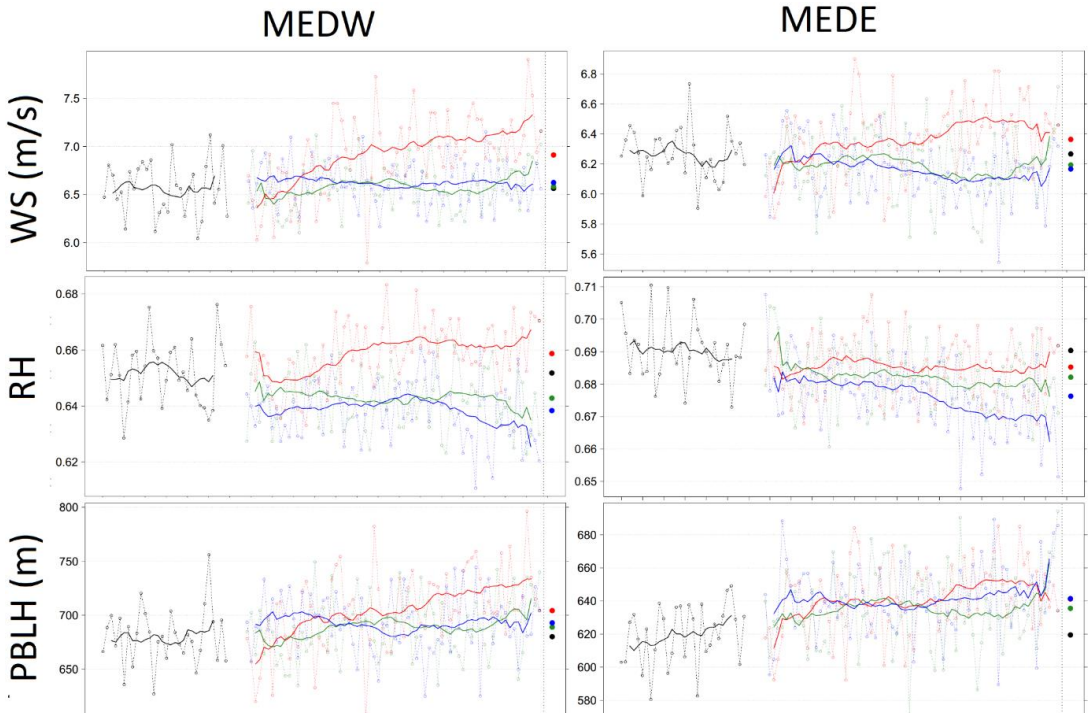


Figure SI3 2. Same as figure 2, but for MEDE and MEDW.

SI4: Correlations of meteorological parameters to each other

EUR

	T	P	RH	WS	PBLH	SWRD
T	**1**	0.05	-0.03	0.09	0.37	-0.72
P	-0.28	**1**	-0.26	0.76	0.72	0.26
RH	-0.40	0.60	**1**	-0.60	-0.60	-0.21
WS	-0.55	0.72	0.30	**1**	0.94	0.01
PBLH	-0.33	0.33	-0.38	0.64	**1**	-0.18
SWRD	0.50	-0.75	-0.80	-0.62	-0.05	**1**

MED

	T	P	RH	WS	PBLH	SWRD
T	**1**	-0.55	0.53	-0.28	-0.66	-0.01
P	0.36	**1**	-0.70	0.62	0.80	-0.19
RH	0.01	0.38	**1**	-0.80	-0.95	-0.34
WS	-0.01	0.76	-0.61	**1**	0.77	0.30
PBLH	-0.01	0.53	-0.95	0.70	**1**	0.14
SWRD	-0.43	-0.60	-0.38	-0.18	0.17	**1**

Table SI4. Correlations of meteorological parameters to each other, red values show the correlation for winter and green values for summer, on the left for EUR and on the right for MED.

SI 5: Information regarding to $PM_{2.5}$

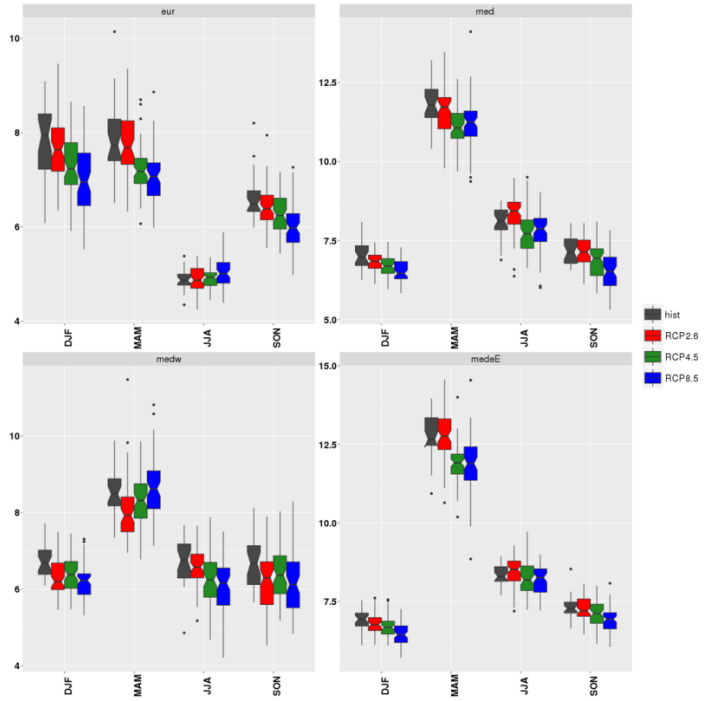
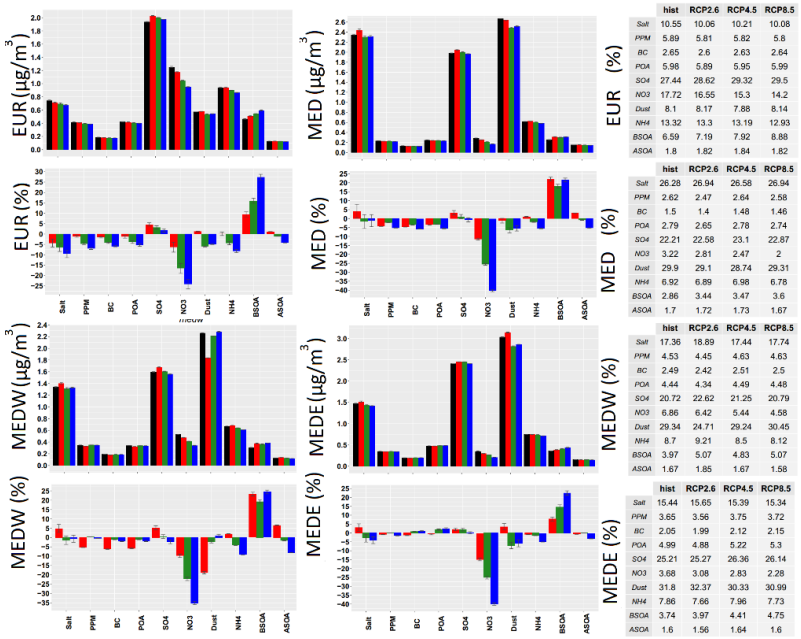


Figure SI5 1. Seasonal concentrations of $PM_{2.5}$ for all subdomains.



	hist	RCP2.6	RCP4.5	RCP8.5
Salt	10.55	10.06	10.21	10.08
PPM	5.89	5.81	5.82	5.8
BC	2.65	2.6	2.63	2.64
POA	5.98	5.89	5.95	5.99
SO4	27.44	28.62	29.32	29.5
NO3	17.72	16.55	15.3	14.2
Dust	8.1	8.17	7.88	8.14
NH4	13.32	13.3	13.19	12.93
BSOA	6.59	7.19	7.92	8.88
ASOA	1.8	1.82	1.84	1.82

	hist	RCP2.6	RCP4.5	RCP8.5
Salt	26.28	26.94	26.58	26.94
PPM	2.62	2.47	2.64	2.58
BC	1.5	1.4	1.48	1.46
POA	2.79	2.65	2.78	2.74
SO4	22.21	22.58	23.1	22.87
NO3	3.22	2.81	2.47	2
Dust	29.9	29.1	28.74	29.31
NH4	6.92	6.89	6.98	6.78
BSOA	2.86	3.44	3.47	3.6
ASOA	1.7	1.72	1.73	1.67

	hist	RCP2.6	RCP4.5	RCP8.5
Salt	17.36	18.89	17.44	17.74
PPM	4.53	4.45	4.63	4.63
BC	2.49	2.42	2.51	2.5
POA	4.44	4.34	4.49	4.48
SO4	20.72	22.62	21.25	20.79
NO3	6.86	6.42	5.44	4.58
Dust	29.34	24.71	29.24	30.45
NH4	8.7	9.21	8.5	8.12
BSOA	3.97	5.07	4.83	5.07
ASOA	1.67	1.85	1.67	1.58

	hist	RCP2.6	RCP4.5	RCP8.5
Salt	15.44	15.65	15.39	15.34
PPM	3.65	3.56	3.75	3.72
BC	2.05	1.99	2.12	2.15
POA	4.99	4.88	5.22	5.3
SO4	25.21	25.27	26.36	26.14
NO3	3.68	3.08	2.83	2.28
Dust	31.8	32.37	30.33	30.99
NH4	7.86	7.66	7.96	7.73
BSOA	3.74	3.97	4.41	4.75
ASOA	1.6	1.56	1.64	1.6

Figure SI5 2. Same as figure 7, but for $PM_{2.5}$

SI 6: Regressions for different seaosns and different components

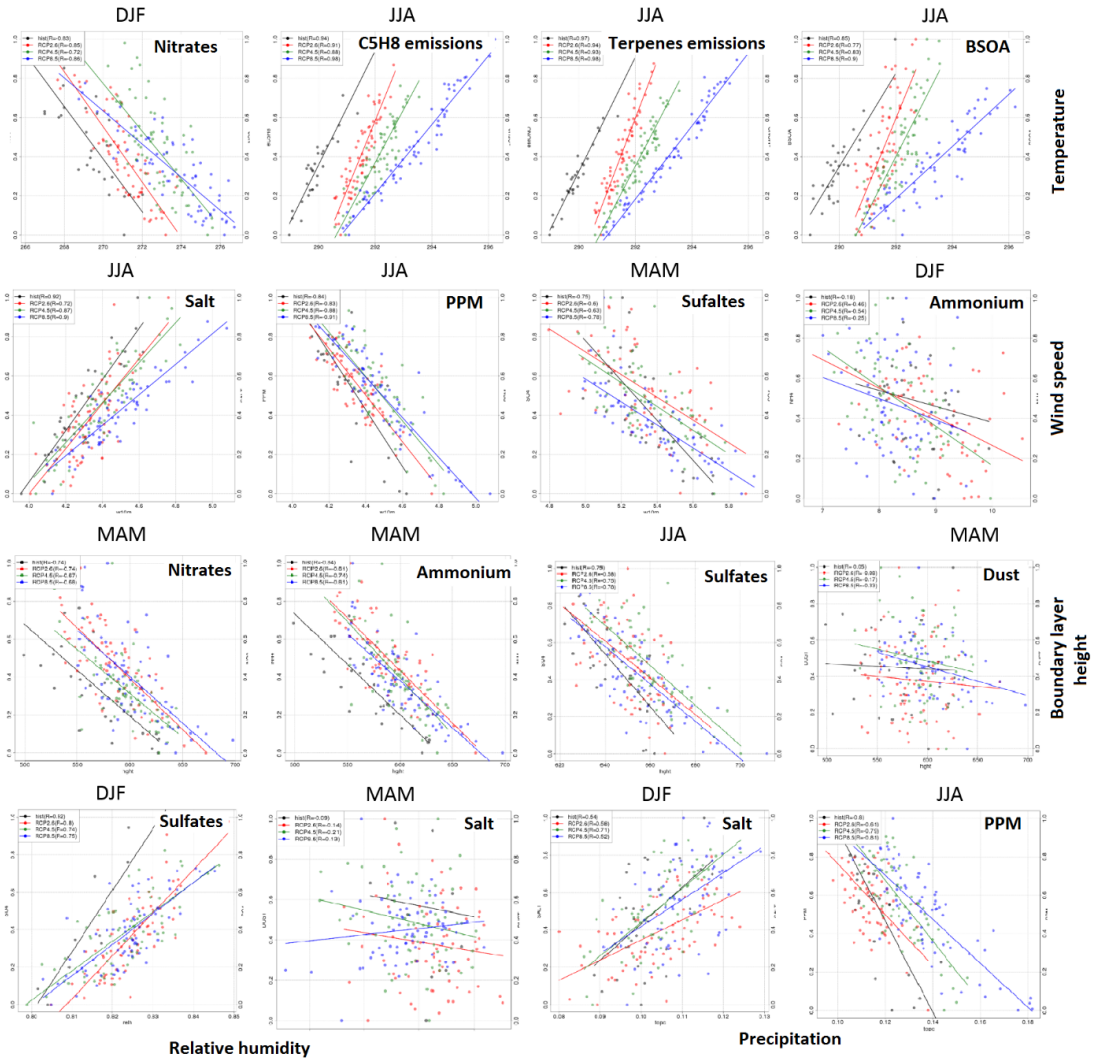


Figure SI6 1. Individual correlations for all scenarios with different components for EUR sub-domain: the name of the component, season and the meteorological parameter is written on each figure.

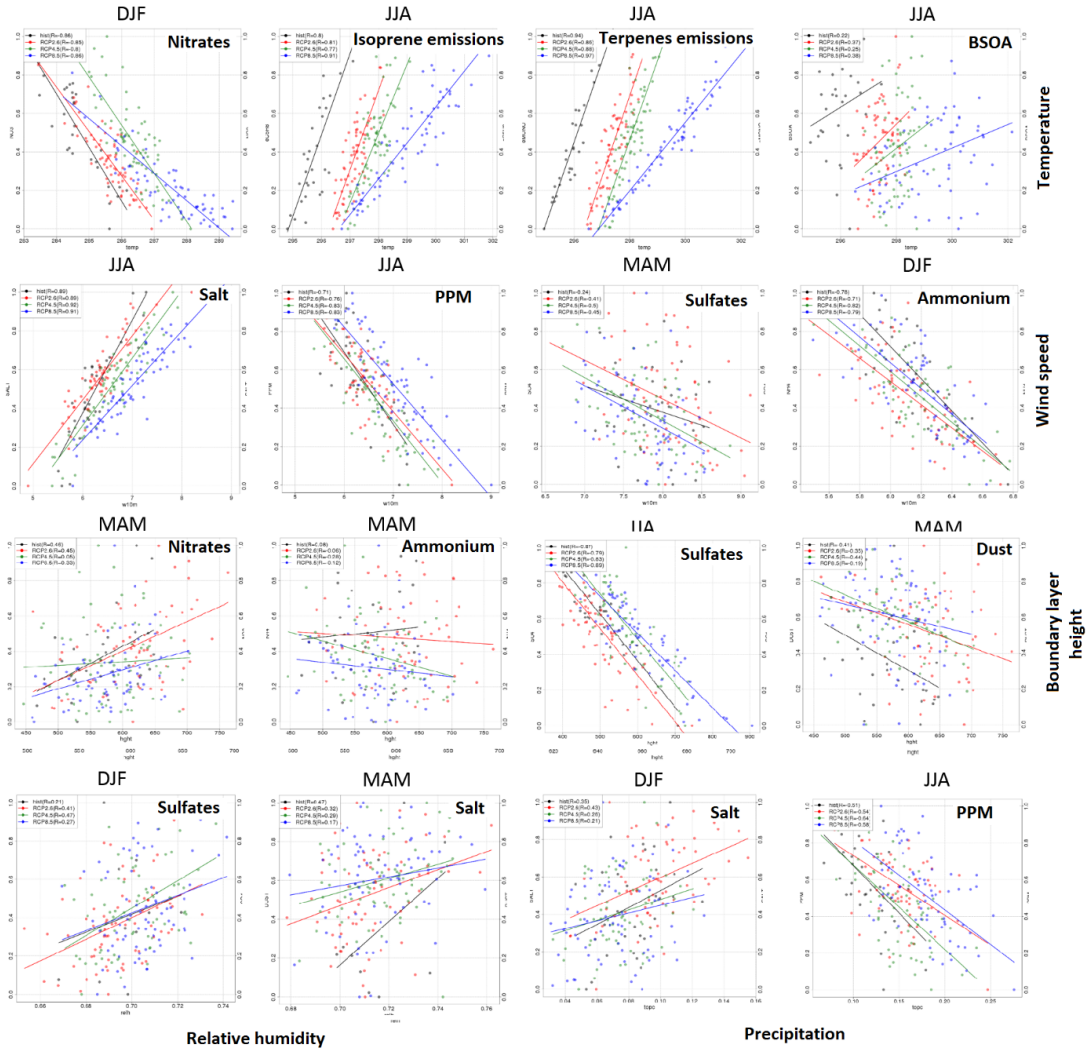


Figure SI6 2. Individual correlations for all scenarios with different components for EUR sub-domain: the name of the component, season and the meteorological parameter is written on each figure.

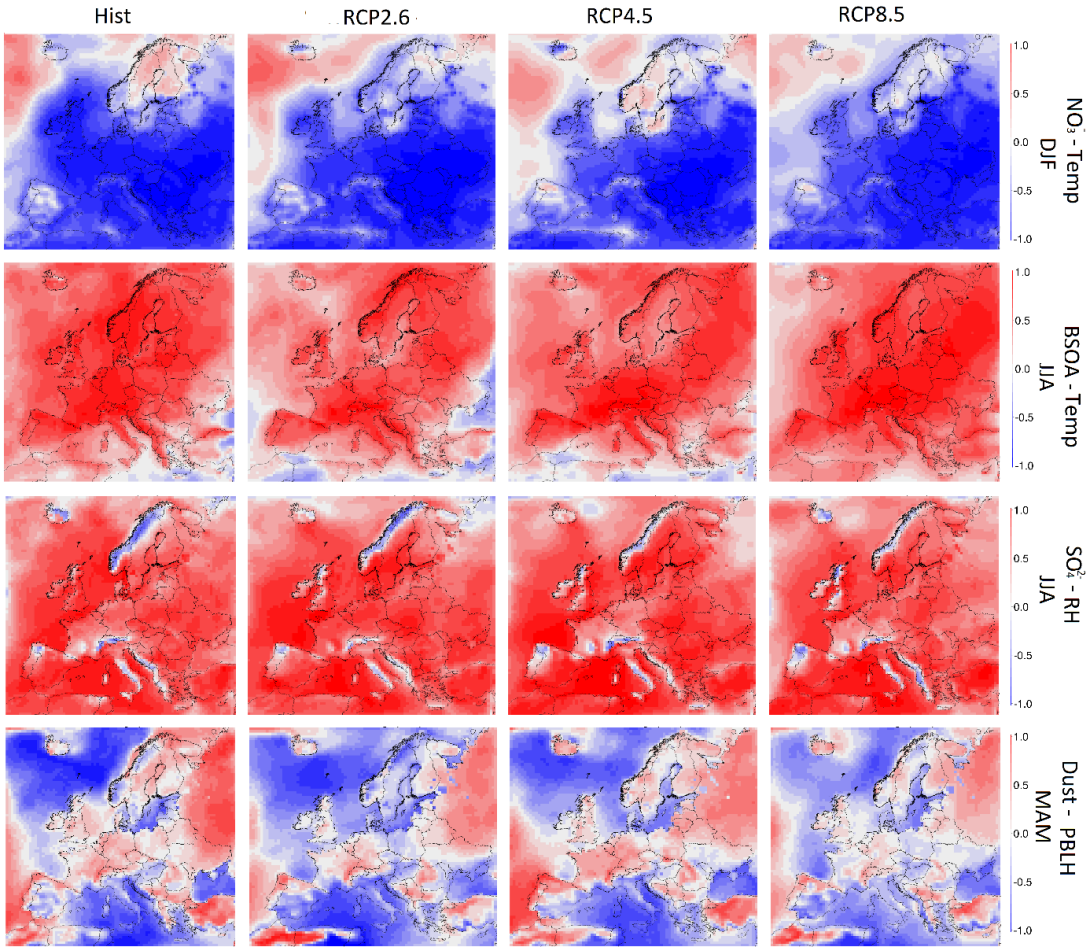


Figure SI6 3. Correlations of historic and future scenarios for BSOA, nitrate, sulfate and dust with temperature, temperature, relative humidity and PBL height respectively for the season in which the concentration of the pollutant is highest. Each column corresponds to one scenario (name above column). Each row shows the correlation of one pollutant with one meteorological parameter on a scale of -1 to 1.

SI7: Seasonal absolute and relative

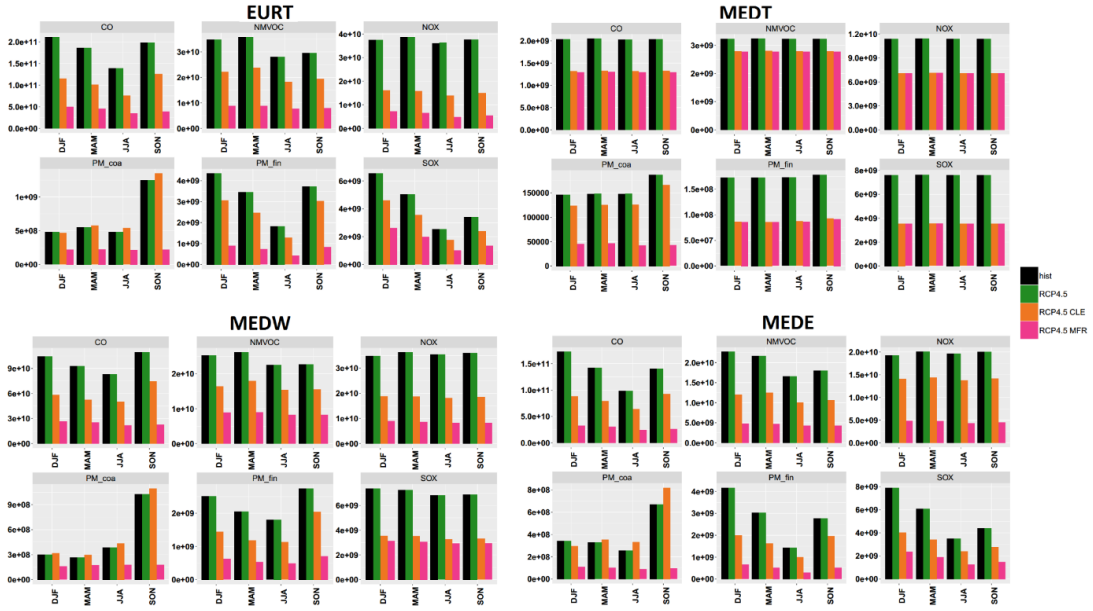


Figure SI7 1. Anthropogenic emissions for CLE-2010, CLE 2050 and MFR 2050 emissions

SI8: Seasonal comparison for the impact of each driver on PM_{10} components

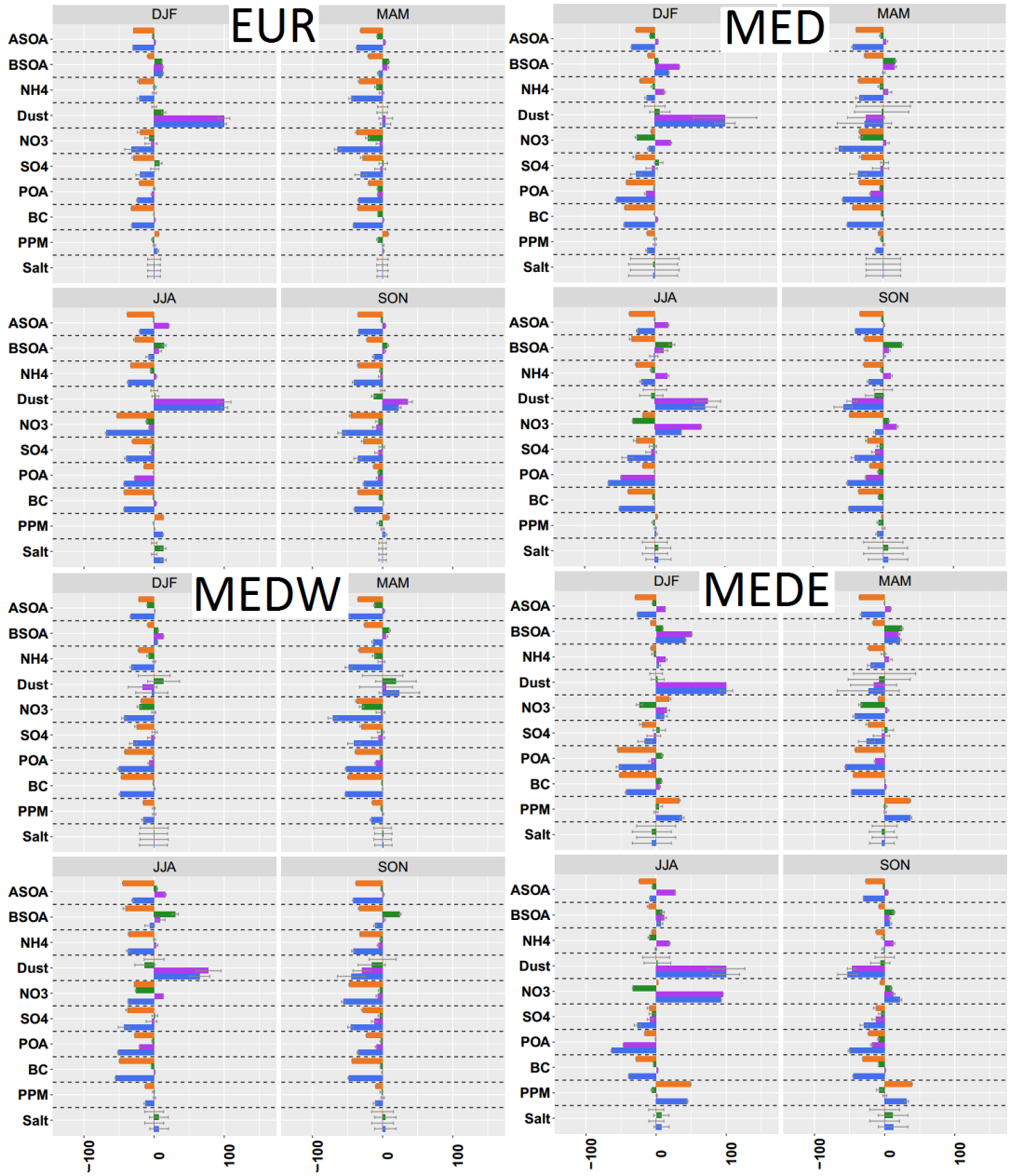


Figure SI8 1. Seasonal relative impact of climate, BC and emission drivers on PM_{10} components for different sub-domains, the name of the sub-domains is written on each panel. Each sub-panel shows one season. Error bars show the confidence interval calculated by annual averages.

APPENDIX

C

MELCHIOR2 Chemical scheme and meteorological parameters used in CHIMERE

Contents

1 MELCHIOR2 Chemical scheme and meteorological parameters used in CHIMERE 277

Model species	Name
Inorganic species	
O_3	Ozone
H_2O_2	Hydrogene Peroxyde
OH	Hydroxyl radical
HO_2	Hydroperoxyl radical
NO	Nitrogen oxide
NO_2	Nitrogen dioxide
NO_3	Nitrate radical
N_2O_5	Dinitrogen pentoxide
HONO	Nitrous acid
HNO_3	Nitric acid
CO	Carbone monoxyde
SO_2	Sulfur dioxide
H_2SO_4	Sulfuric acid
hydrocarbons	
CH_4	Methane
C_2H_6	Ethane
NC_4H_{10}	n-butane
C_2H_4	Ethene
C_3H_6	Propene
OXYL	o-xylene
C_5H_8	Isoprene
APINEN	α-pinene
BPINEN	β-pinene
LIMONE	Limonene
TERPEN	Lumped terpenes
HUMULE	Lumped humulene
OCIMEN	Lumped ocimene
Carbonyls	
HCHO	Formaldheyde
CH_3CHO	Acetaldehyde
CH_3COE	Methyl ethyl ketone
GLYOX	Glyoxal
MGLYOX	Methylglyoxal
CH_3COY	Dimethyl glyoxal
MEMALD	Unsaturated reactive dicarbonyls like 4-oxo-2-pentanal
MVK	Methyl Vinyl ketone
MAC	Methacroleine
Nitrates Organiques	
PAN	Peroxyacetyl nitrate
CARNIT	Carbonyl nitrate like α-nitroxy actetone
ISNI	Unsaturated nitrogen produced by C_5H_8
Organic peroxyls	
CH_3O_2H	Hydroperoxymethane
PPA	peracetic acid
Peroxyl radicals	
CH_3O_2	Methyl peroxyl radical
CH_3COO	Peroxyl actethyl radical
Chemical operators	
oRO_2	Peroxyl radical produced by OH+COV
oROOH	Hydroperoxyle radical produced by oRO_2
obio	Biogenic peroxyl radical produced by OCIMEN, APINEN, BPINEN, LIMONE,TERPEN, HUMULE et C_5H_8
obioH	Biogenic hydroperoxyl radical produced by obio
oPAN	Representes PAN analogs
PANH	Produced by oPAN+HO_2
toPAN	Produced by oPAN+NO_2
oRN1	Organic nitrates produit par C_2H_4,C_3H_6, C_5H_8, APINEN, BPINEN, LIMONE, TERPEN, HUMULE, OCIMEN et ISNI

Table 1: List of species in the MELCHIOR2 scheme

Reaction	Kinetic constants
Inorganic chemistry	
O3+NO →NO2	k(T)=Aexp(-B/T),A=1.8e-12,B=1370
O3+NO2 →NO3	k(T)=Aexp(-B/T),A=1.2e-13,B=2450
O3+OH →HO2	k(T)=Aexp(-B/T),A=1.9e-12,B=1000
O3+HO2 →OH	k(T)=Aexp(-B/T),A=1.4e-14,B=600
NO+HO2 →OH+NO2	k(T)=Aexp(-B/T),A=3.7e-12,B=-240
NO2+OH+M →HNO3	k(T,M)=mtroe(3.4e-30,0,3.2,4.77e-11,0,1.4,0.30)
HO2+OH →H2O	k(T)=Aexp(-B/T),A=4.8e-11,B=-250
H2O2+OH →HO2	k(T)=Aexp(-B/T),A=2.9e-12,B=160
HNO3+OH →NO3	k(T)=Aexp(-B/T),A=5.5e-15,B=-985
CO+OH →HO2+CO2	k(T)=Aexp(-B/T)(300/T)**N,A=2e-13,B=0,N=1
HO2+HO2 →H2O2	k(T)=Aexp(-B/T),A=2.2e-13,B=-740
HO2+HO2+H2O →H2O2	k(T)=Aexp(-B/T),A=4.52e-34,B=-2827
NO3+HO2 →NO2+OH	k=4e-12
NO3+H2O2 →HNO3+HO2	k=2e-15
NO3+NO →2*NO2	k(T)=Aexp(-B/T),A=1.8e-11,B=-110
NO2+NO3 →NO+NO2	k(T)=Aexp(-B/T),A=4.5e-14,B=1260
NO2+NO3+M →N2O5	k(T,M)=troe(2.7e-30,0,3.4,2e-12,0,-0.2,0.33)
N2O5+M →NO3+NO2	k(T,M)=troe(1e-3,11000,3.5,9.7e14,11080,-0.1,0.33)
NO+OH+M →HONO	k(T,M)=troe(7.e-31,0,2.6,1.5e-11,0,0.5,0.6)
HONO+OH →NO2	k(T)=Aexp(-B/T),A=1.8e-11,B=390
NO+NO+O2 →2*NO2	k(T)=Aexp(-B/T),A=3.30E-39,B=-530.0
N2O5+H2O →2*HNO3	k=2.6e-22
N2O5+H2O+H2O →2*HNO3	k=2e-39
Surface reaction, Aumont et *al.*, 2002.	
NO2 →HONO+NO2	ks=0.5*depo(NO2)
Chemistry of SO_X	
SO2+CH3O2 →H2SO4+HCHO+HO2	k=4e-17
SO2+OH+M →H2SO4+HO2	k(T,M)=troe(4e-31,0,3.3,2e-12,0,0,0.45)
Biogenic VOC operators	
obio+NO →0.86*NO2+0.78*HO2+0.14*ISNI	k(T)=Aexp(-B/T),A=1.6e-11,B=180
obio+HO2 →obioH	k(T)=Aexp(-B/T),A=2.7e-13,B=-1000
obio+NO3 →NO2+HO2	k=1.2e-12
CH3O2+obio →0.8*HO2+0.5*HCHO	k(T)=Aexp(-B/T),A=2.44e-11,B=223
CH3COO+obio →0.5*HCHO+1.5*HO2+0.7*CO2	k(T)=Aexp(-B/T),A=1.18e-11,B=127
obioH+OH →OH	k=8e-11
oRO_2 Operator	
oRO2+NO →NO2+HO2	k=4e-12
oRO2+HO2 →oROOH	k(T)=Aexp(-B/T),A=2.7e-13,B=-1000
oRO2+oRO2 →1.3*HO2	k=6.4e-14
oRO2+NO3 →NO2+HO2	k=1.2e-12
CH3O2+oRO2 →0.65*HCHO+0.8*HO2+0.35*CH3OH	k(T)=Aexp(-B/T),A=1.5e-13,B=-220
CH3COO+oRO2 →0.8*CH3O2+0.8*CO2+0.8*HO2	k(T)=Aexp(-B/T),A=8.6e-13,B=-260

continued...

Reaction	Kinetic constants
continued	*continued*
oROOH+OH →0.8*OH+0.2*oRO2	k(T)=Aexp(-B/T),A=4.35e-12,B=-455
PAN Operator	
MAC+OH →0.5*CH3COE+0.5*CO2+0.5*oPAN	k(T)=Aexp(-B/T),A=1.86e-11,B=-175
oPAN+NO →NO2+HO2	k=1.4e-11
oPAN+NO3 →NO2+HO2	k=4e-12
oPAN+HO2 →PANH	k(T)=Aexp(-B/T),A=2.7e-13,B=-1000
PANH+OH →0.2*oPAN	k=1.64e-11
oPAN+CH3O2 →HCHO+0.5*HO2	k(T)=Aexp(-B/T),A=7.9e-12,B=-140
oPAN+CH3COO →CH3O2+CO2+HO2	k(T)=Aexp(-B/T),A=5.6e-12,B=-530
oPAN+NO2+M →toPAN	k(T,M)=troe(2.7e-28,0,7.1,1.2e-11,0,0.9,0.3)
toPAN+M →oPAN+NO2	k(T,M)=troe(4.9e-3,12100,0,5.4e16,13830,0,0.3)
toPAN+OH →NO3+CO2	k(T)=Aexp(-B/T),A=3.25e-13,B=-500
Nitrate operators	
C2H4+NO3 →0.5*CARNIT+HCHO+oRN1	k=2e-16
C3H6+NO3 →0.5*CARNIT+1.5*HCHO+	...
0.5*CH3CHO+0.5*HO2+oRN1	k=9.45e-15
ISNI+OH →oRN1+0.95*CH3CHO+0.475*CH3COE+	...
0.475*MGLYOX+0.05*ISNI+0.05*HO2	k=3.4e-11
C5H8+NO3 →oRN1+0.85*ISNI+0.1*MAC+	...
0.05*MVK+0.15*HCHO+0.8*HO2	k=7.8e-13
oRN1+NO →1.5*NO2	k=4e-11
oRN1+NO3 →1.5*NO2	k=1.2e-12
oRN1+HO2 →X	k(T)=Aexp(-B/T),A=2.7e-13,B=-1000
Hydrocarbon oxidation with OH radical	
CH4+OH →CH3O2	k(T)=Aexp(-B/T),A=2.3e-12,B=1765
C2H6+OH →CH3CHO+oRO2	k(T)=Aexp(-B/T),A=7.9e-12,B=1030
C2H4+OH+M →2*HCHO+oRO2	k(T,M)=troe(7e-29,0,3.1,9e-12,0,0,0.7)
C3H6+OH+M →HCHO+CH3CHO+oRO2	k(T,M)=troe(8e-27,0,3.5,3e-11,0,0,0.5)
NC4H10+OH →0.9*CH3COE+0.1*CH3CHO+	...
0.1*CH3COO+0.9*oRO2	k(T)=Aexp(-B/T)(300/T)**N,A=1.36e-12,B=-190,N=-2
OXYL+OH →MEMALD+MGLYOX+oRO2	k=1.37e-11
Oxidation of cabonyls and peroxyls OH	
HCHO+OH →CO+HO2	k(T)=Aexp(-B/T),A=8.6e-12,B=-20
CH3CHO+OH →CH3COO	k(T)=Aexp(-B/T),A=5.6e-12,B=-310
MEMALD+OH →GLYOX+MGLYOX+oRO2	k=5.6e-11
CH3COE+OH →CH3COY+oRO2	k(T)=Aexp(-B/T)(300/T)**N,A=2.92e-13,B=-414,N=-2
GLYOX+OH →2*CO+HO2	k=1.1e-11
MGLYOX+OH →CH3COO+CO	k=1.5e-11
MVK+OH →0.266*MGLYOX+0.266*HCHO+0.684*CH3CHO+	...
0.684*CH3COO+0.05*ISNI+0.95*oRO2	k(T)=Aexp(-B/T),A=4.1e-12,B=-453
CH3O2H+OH →CH3O2	k(T)=Aexp(-B/T),A=1.9e-12,B=-190
PPA+OH →CH3COO	k(T)=Aexp(-B/T),A=1.9e-12,B=-190

continued...

Reaction	Kinetic constants
continued	*continued*
CH3O2H+OH →HCHO+OH	k(T)=Aexp(-B/T),A=1.e-12,B=-190
Oxidation by NO_3 radical	
HCHO+NO3 →CO+HNO3+HO2	k=5.8e-16
CH3CHO+NO3 →CH3COO+HNO3	k=2.8e-15
CH3O2+NO3 →HCHO+HO2+NO2	k=1.2e-12
CH3COO+NO3 →CH3O2+NO2+CO2	k=4e-12
Ozonolysis	
C2H4+O3 →HCHO+0.12*HO2+0.13*H2+0.44*CO	k(T)=Aexp(-B/T),A=9.1e-15,B=2580
C3H6+O3 →0.53*HCHO+0.5*CH3CHO+0.31*CH3O2+	...
0.28*HO2+0.15*OH+0.065*H2+0.4*CO+0.7*CH4	k(T)=Aexp(-B/T),A=5.5e-15,B=1880
C5H8+O3 →0.67*MAC+0.26*MVK+0.55*OH+0.07*C3H6+	...
0.8*HCHO+0.06*HO2+0.05*CO+0.3*O3	k(T)=Aexp(-B/T),A=1.2e-14,B=2013
MAC+O3 →0.8*MGLYOX+0.7*HCHO+0.215*OH+	...
0.275*HO2+0.2*CO+0.2*O3	k(T)=Aexp(-B/T),A=5.3e-15,B=2520
MVK+O3 →0.82*MGLYOX+0.8*HCHO+0.04*CH3CHO+	...
0.08*OH+0.06*HO2+0.05*CO+0.2*O3	k(T)=Aexp(-B/T),A=4.3e-15,B=2016
Conversion of organic radicals	
CH3O2+NO →HCHO+NO2+HO2	k(T)=Aexp(-B/T),A=4.2e-12,B=-180
CH3COO+NO →CH3O2+NO2+CO2	k=2e-11
Recombination of organic radicals	
CH3O2+HO2 →CH3O2H	k(T)=Aexp(-B/T),A=4.1e-13,B=-790
CH3COO+HO2 →0.67*PPA+0.33*O3	k(T)=Aexp(-B/T),A=4.3e-13,B=-1040
CH3O2+CH3O2 →1.35*HCHO+0.7*HO2	k(T)=Aexp(-B/T),A=1.13e-13,B=-356
CH3COO+CH3O2 →0.5*CH3O2+0.5*CO2+	...
HCHO+0.5*HO2	k(T)=Aexp(-B/T),A=3.34e-12,B=-400
CH3COO+CH3COO →2.*CH3O2+2.*CO2	k(T)=Aexp(-B/T),A=2.8e-12,B=-530
Organic nitrates	
CH3COO+NO2+M →PAN	k(T,M)=troe(2.7e-28,0,7.1,1.2e-11,0,0.9,0.3)
PAN+M →CH3COO+NO2	k(T,M)=troe(4.9e-3,12100,0,5.4e16,13830,0,0.3)
PAN+OH →HCHO+NO3+CO2	k(T)=Aexp(-B/T),A=9.5e-13,B=650
CARNIT+OH →CH3CHO+CO+NO2	k(T)=Aexp(-B/T),A=5.6e-12,B=-310
Photolysis reactions	
O3 →2*OH	J(T,Z,H2O)=photorate(O3)
NO2 →NO+O3	J(Z)=photorate(NO2)
NO3 →NO	J(Z)=photorate(NO3-1)
NO3 →NO2+O3	J(Z)=photorate(NO3-2)
H2O2 →2*OH	J(Z)=photorate(H2O2)
HNO3 →NO2+OH	J(Z)=photorate(HNO3)
HONO →NO+OH	J(Z)=photorate(HONO)
HCHO →CO+2*HO2	J(Z)=photorate(HCHO-1)
HCHO →CO+H2	J(Z)=photorate(HCHO-2)
CH3CHO →CH3O2+HO2+CO	J(Z)=photorate(CH3CHO)

continued...

Reaction	Kinetic constants
continued	*continued*
CH3COY →2*CH3COO	J(Z)=photorate(CH3COY)
MGLYOX →CH3COO+HO2+CO	J(Z)=photorate(MGLYOX)
GLYOX →0.6*HO2+2*CO+1.4*H2	J(Z)=photorate(GLYOX)
MEMALD →0.5*MVK+0.5*MALEIC+0.5*oPAN+	...
0.5*HCHO+0.5*HO2	J(Z)=photorate(MEMALD)
CH3COE →CH3COO+CH3CHO+oRO2	J(Z)=photorate(CH3COE)
N2O5 →NO2+NO3	J(Z)=photorate(N2O5)
CH3O2H →HCHO+OH+HO2	J(Z)=photorate(CH3O2H)
PPA →CH3O2+CO2+OH	J(Z)=photorate(PPA)
PAN →CH3COO+NO2	J(Z)=photorate(PAN)
PANH →OH+HO2	J(Z)=photorate(PANH)
oROOH →OH+HO2	J(Z)=photorate(oROOH)
obioH →OH+HO2	J(Z)=photorate(obioH)
Biogenic chemistry	
APINEN+NO3 →CH3CHO+CH3COE+oRN1	k(T)=Aexp(-B/T),A=1.19e-12,B=-490
BPINEN+NO3 →CH3CHO+CH3COE+oRN1	k(T)=Aexp(-B/T),A=1.19e-12,B=-490
LIMONE+NO3 →CH3CHO+CH3COE+oRN1	k(T)=Aexp(-B/T),A=1.19e-12,B=-490
OCIMEN+NO3 →CH3CHO+CH3COE+oRN1	k(T)=Aexp(-B/T),A=1.19e-12,B=-490
TERPEN+NO3 →CH3CHO+CH3COE+oRN1	k(T)=Aexp(-B/T),A=1.19e-12,B=-490
HUMULE+NO3 →CH3CHO+CH3COE+oRN1	k(T)=Aexp(-B/T),A=1.19e-12,B=-490
APINEN+OH →0.8*CH3CHO+0.8*CH3COE+obio	k(T)=Aexp(-B/T),A=1.21e-11,B=-444
BPINEN+OH →0.8*CH3CHO+0.8*CH3COE+obio	k(T)=Aexp(-B/T),A=1.21e-11,B=-444
LIMONE+OH →0.8*CH3CHO+0.8*CH3COE+obio	k(T)=Aexp(-B/T),A=1.21e-11,B=-444
OCIMEN+OH →0.8*CH3CHO+0.8*CH3COE+obio	k(T)=Aexp(-B/T),A=1.21e-11,B=-444
TERPEN+OH →0.8*CH3CHO+0.8*CH3COE+obio	k(T)=Aexp(-B/T),A=1.21e-11,B=-444
HUMULE+OH →0.8*CH3CHO+0.8*CH3COE+obio	k(T)=Aexp(-B/T),A=1.21e-11,B=-444
APINEN+O3 →1.27*CH3CHO+0.53*CH3COE+0.14*CO+	...
0.62*oRO2+0.42*HCHO+0.85*OH+0.1*HO2	k(T)=Aexp(-B/T),A=1.0e-15,B=736
BPINEN+O3 →1.27*CH3CHO+0.53*CH3COE+0.14*CO+	...
0.62*oRO2+0.42*HCHO+0.85*OH+0.1*HO2	k(T)=Aexp(-B/T),A=1.0e-15,B=736
LIMONE+O3 →1.27*CH3CHO+0.53*CH3COE+0.14*CO+	...
0.62*oRO2+0.42*HCHO+0.85*OH+0.1*HO2	k(T)=Aexp(-B/T),A=1.0e-15,B=736
TERPEN+O3 →1.27*CH3CHO+0.53*CH3COE+0.14*CO+	...
0.62*oRO2+0.42*HCHO+0.85*OH+0.1*HO2	k(T)=Aexp(-B/T),A=1.0e-15,B=736
OCIMEN+O3 →1.27*CH3CHO+0.53*CH3COE+0.14*CO+	...
0.62*oRO2+0.42*HCHO+0.85*OH+0.1*HO2	k(T)=Aexp(-B/T),A=1.0e-15,B=736
HUMULE+O3 →1.27*CH3CHO+0.53*CH3COE+0.14*CO+	...
0.62*oRO2+0.42*HCHO+0.85*OH+0.1*HO2	k(T)=Aexp(-B/T),A=1.0e-15,B=736
C5H8+OH →0.32*MAC+0.42*MVK+0.74*HCHO+obio	k(T)=Aexp(-B/T),A=2.55e-11,B=-410

Table 2: MELCHIOR2 chemical scheme

Name	Variable	Dimension	Unit
winz	Zonal wind component	3D	$m.s^{-1}$
winm	Meridional wind component	3D	$m.s^{-1}$
temp	Temperature	3D	K
sphu	Specific humidity	3D	$kg.kg^{-1}$
alti	Altitude of half layer	3D	m.s
pres	Pressure	3D	Pa
cliq	Water content of clouds	3D	$kg.kg^{-1}$
tem2	2m temperature	2D	k
rh2m	2m relative humidity	2D	0-1
swrd	Short wave radiation	2D	$W.m^{-2}$
lwrd	Long wave radiation	2D	$W.m^{-2}$
copc	Convective precipitation	2D	$kg.m^{-2}.h^{-1}$
lspc	Large-scale precipitation	2D	$kg.m^{-2}.h^{-1}$
psfc	Surface pressure	2D	Pa
	Optional variables		
rain	Precipitation [1]	3D	$kg.kg^{-1}$
cice	Ice [1]	3D	$kg.kg^{-1}$
sshf	Sensible heat flux [2]	2D	$W.m^{-2}$
slhf	Latent heat flux [2]	2D	$W.m^{-2}$
usta	Friction speed [2]	2D	$m.s^{-1}$
hght	PBL height [2]	2D	m
lowc	Low cloud fraction [1]	2D	m
medc	Low cloud fraction [1]	2D	m
higc	Low cloud fraction [1]	2D	m

Table 3: Meteorological parameters in CHIMERE when using ECMWF

1 : Used for the attenuation of photolysis parameters.
2 : Might be recalculated by the model